INSTITUTE OF SPACE AND ASTRONAUTICAL SCIENCE
YOSHINODAI, CHUO, SAGAMIHARA, KANAGAWA 252-5210

ISAS RESEARCH NOTE

ISAS RN 876

An X-ray and Near-Infrared Study of the Galactic Ridge X-ray Emission

Kumiko MORIHANA[1,2]

February 2013

1 : Institute of Space and Astronautical Science, Japan Aerospace Exploration Agency
2 : Department of Astronomy, Graduate School of Science, University of Tokyo

An X-ray and Near-Infrared Study of the Galactic Ridge X-ray Emission

Kumiko Morihana

Reproduced from the thesis submitted to
the Department of Astronomy,
Graduate School of Science, University of Tokyo
December 22, 2011

An X-ray and Near-Infrared Study of the Galactic Ridge X-ray Emission

Kumiko Morihana

Department of Astronomy, Graduate School of Science, The University of Tokyo
7-3-1 Hongo, Bunkyo-ku, Tokyo, 113-0033, Japan
morihana@astro.isas.jaxa.jp

December 2011

Abstract

The Galactic Ridge X-ray Emission (GRXE) is an apparently extended X-ray emission along the Galactic Plane, which has a thermal spectrum with characteristic Fe K line emission. The origin of the GRXE, whether it is a truly diffuse plasma or a sum of numerous dim X-ray point sources, had been a mystery for a long time. Recently, $\sim$80% of the GRXE was finally resolved into dim X-ray point sources at around the Fe K-line energy band by the deepest observation using *Chandra X-ray Observatory* (Revnivtsev et al. 2009). Thus, it is now elucidated that the GRXE is primarily composed of dim point sources. There are some candidates of the point sources (cataclysmic variables [CVs] or late-type stars), but it is extremely difficult to constrain the nature of these sources from X-rays alone, because most of the sources have only a limited number of X-ray photons.

Thus, we combine near-infrared (NIR) data with the X-ray data in this thesis. We focus on revealing the nature of the Galactic X-ray point sources that primarily contribute to the GRXE Fe K-line emission, since Fe K-line is one of the most important parameters to characterize X-ray emission mechanisms. So far, two Galactic fields have been intensively studied, which are the "Revnivtsev field" ($l = 0.^\circ1$, $b = -1.^\circ4$) and the "Ebisawa field" ($l = 28.^\circ5$, $b = 0.^\circ0$). We use the both fields, but primarily the Revnivtsev field, since it is the most deeply exposed Galactic field by *Chandra X-ray Observatory* to date.

We divided all the detected sources in the Revnivtsev field into four sub-groups (Aa: hard and bright, Ab: hard and dim, B1: soft, and B2: medium) by their spectral colors and X-ray fluxes. We studied composite spectra of these groups, as well as individual spectra and variabilities of the bright sources. We found most bright sources in the group Aa have non-thermal spectra with *weak* Fe K line. On the other hand, composite spectra of the group Ab and B2 have *strong* Fe K lines, whereas iron line emission is hardly seen in B1. More than half the variable sources belong to the group B2. We obtained fractions of each population contributing to the total point-source flux in the Fe K band as follows (fractions to the 4–8 keV continuum and to the iron line): Aa ($\sim$44%, $\sim$18%), Ab ($\sim$38%, $\sim$52%), B1 ($\sim$2%, $\sim$0%) and B2 ($\sim$16%, $\sim$30%).

Combining the 2MASS (Two Micron All Sky Survey) and our data taken at the Infra-Red Survey Facility telescope in South Africa, we identified $\sim$11% of the X-ray sources in the Revnivtsev field with NIR. None of the group Aa sources have NIR counterparts in K_s band, which suggests that most of the group Aa sources are background AGNs attenuated by a

large Galactic extinction. Most NIR identified sources in the group Ab have large extinction, which indicates that these sources are located rather at large distances, suggesting that they are intrinsically X-ray bright accreting white dwarfs. On the other hand, NIR identified sources in the groups B1 and B2 show a wide range of extinction, suggesting that these sources are located at various distances, including X-ray faint nearby late-type stars.

We obtained the NIR spectra of the sources in groups Ab, B1 and B2 in $K_{\rm s}$ band using the Multi-Object Infrared Camera and Spectrograph (MOIRCS) of Subaru telescope both in the Revnivtsev field and the Ebisawa field. The NIR spectra are classified into the following three types: spectra with (1) HI (Brγ) and CO absorption lines, (2) CO absorption lines, and (3) HI (Brγ) and HeII emission lines. (1) and (2) are signatures of the late-type stars and type (3) is a signature of the accretion disk in CVs. Most Ab sources are in type (1) or (2), and only 2 Ab sources are in type (3). From these results, we propose that most sources in the group Ab are detached systems consisting of a white dwarf that does not have a NIR line emitting accretion disk (pre-CVs), while a small number of CVs are included. All the sources in B1 and B2 are in type (1) and (2), thus they are considered to be late-type stars.

From these X-ray and NIR results, we propose nature of the sources in each group as follows: (Aa) mainly background AGNs, (Ab) mainly pre-CVs and a small fraction of CVs, (B2) mainly late-type stars on *flare*, and (B1) mainly late-type stars on *quiescence*.

We have confirmed that the GRXE is primarily explained with superposition of the X-ray point sources, and propose that these point sources consist of background AGNs, CVs, detached systems consisting of a white dwarf (pre-CVs), late-type stars on *flare*, and late-type stars on *quiescence*. Pre-CVs are the primary contributor to the GRXE iron line emission, and late-type stars on *flare* are the secondary. X-ray properties of the pre-CVs are currently hardly understood, but our study suggests that such dim, unknown X-ray sources are filling the Galactic plane, constituting a major part of the GRXE.

Contents

List of Figures

List of Tables

Chapter 1

Introduction

Electro-magnetic emission from the Galactic Plane (GP) in our Galaxy has been observed in various wavelengths. In the 1980's, X-ray emission from the GP was discovered, which is called the Galactic Ridge X-ray Emission (GRXE; Worrall et al. 1982). The GRXE is apparently extended emission of low surface brightness along the inner part of the GP ($|l| < \pm 45°$, $|b| < \pm 1°$: Figure 1.1). It has a thermal spectrum below $\sim$10 keV with a strong 6.7 keV Fe emission line (Koyama et al. 1986, Koyama 1989a), and a power-law spectrum above $\sim$10 keV (e.g., Yamasaki et al. 1997).

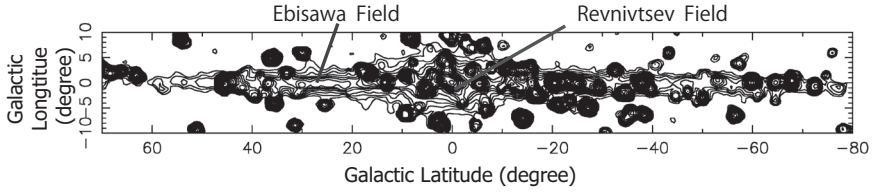

Figure 1.1: X-ray intensity contour map at the GP in 3–20 keV by the *Rossi X-ray Timing Explorer satellite* (Revnivtsev et al. 2006). This map shows that there are many bright sources and underlying unresolved emission. The total luminosity of the GRXE is about $\sim 10^{38}$ ergs cm^{-2} s^{-1}.

Origin of the GRXE has been a mystery for a long time. A long-standing debate has been whether it is a truly diffuse plasma or the sum of unresolved X-ray point sources. If the GRXE is a diffuse plasma, the GP is filled with a thermal plasma of $\sim 10^7$ K. However, our Galaxy does not have enough gravity to bound such a high-temperature thermal plasma (Warwick et al. 1985). Thus, it requires a mechanism to maintain the thermal plasma in our

Galaxy. On the other hand, if the GRXE is the sum of unresolved X-ray point sources, it suggests that there are numerous dim point-like X-ray sources that have not been resolved yet.

In order to answer the question, many X-ray observations have been carried out. Two fields are intensively studied : the Revnivtsev field ($l = 0.^\circ1$, $b = -1.^\circ4$; Revnivtsev et al. 2009) and the Ebisawa field ($l = 28.^\circ5$, $b = 0.^\circ0$; Ebisawa et al. 2005). Recently, the *Chandra* X-ray Observatory brought a revolution in the study of the GRXE with its unprecedented spatial resolution of $0.6''$ at the on-axis position. Deep X-ray observations were made in both the Ebisawa ($\sim$100 ks$\times$2; Ebisawa et al. 2001, 2005) and Revnivtsev ($\sim$900 ks; Revnivtsev et al. 2009) fields. In the latter study, which is the deepest X-ray observations ever made in the GP, Revnivtsev et al. (2009) claimed that $\sim$80% of the Fe line emission was resolved into point-like sources, which strongly favors the scenario that the GRXE is made up of numerous unresolved point-like sources.

If the GRXE is composed of unresolved point-like sources, new questions arise. What are the populations of these dim X-ray point sources? Which class of sources contribute to the Fe emission lines of the GRXE most? These are the questions that we attempt to address in this thesis. We do not know the nature of the majority of the dim X-ray point-like sources resolved in the *Chandra* observations because most of these sources produce only a limited number of photons. Thus, we combine near infrared (NIR) data with the X-ray data in this thesis. The NIR emission has almost the same transmission power as the X-rays into the deep interstellar extinction toward the GP and yields a much larger number of photons to reveal the nature of these dim X-ray sources.

In this thesis, we focus on the two regions, the Revnivtsev field and the Ebisawa field, but mainly on the Revnivtsev field, since it is the deepest exposed Galactic field. In the two fields, we assemble both the X-ray and NIR data, many of which were taken as the original data of this thesis. We refer to Ebisawa et al. (2005) for the X-ray and NIR imaging data in the Ebisawa field. Table 1.1 shows the dataset and observatory/instruments used in this thesis.

The plan of this thesis is as follows. We review the GRXE and set the historical context of this thesis in Chap. 2. In Chap. 3, the basic features of the X-ray and NIR telescopes and instruments used in this thesis are presented. The observations and the data reduction are described in Chap. 4 and the data analysis and results are in Chap. 5. In Chap. 6, we discuss population of the dim X-ray sources constituting the GRXE based on the X-ray and

Table 1.1: Study fields and data sets

	Revnivtsev field	Ebisawa field
X-ray	*Chandra*/ACIS[a]	*Chandra*/ACIS[b]
NIR imaging	IRSF/SIRIUS[a]	NTT/SofI[b]
NIR spectroscopy	Subaru/MOIRCS[a]	Subaru/MOIRCS[a]

[a] The data presented in this work.
[b] The data presented in Ebisawa et al. (2005).

NIR results. Finally, we summarize major findings of this study in Chap. 7.

Chapter 2

Review

In this chapter, we review historical background of the study of the GRXE. We also review X-ray and NIR properties of major Galactic point source populations that might contribute to the GRXE.

Contents

2.1 Galactic Ridge X-ray Emission

2.1.1 Discovery of the GRXE and its Properties

The GRXE was discovered soon after the beginning of the X-ray astronomy by the *HEAO-1* satellite (Worrall et al. 1982). After the discovery, the *EXOSAT* satellite carried out a Galactic Plane (GP) survey, and found that the GRXE extends along the GP ($|l| < 40°$, $|b| < 10°$) with a total luminosity of 2×10^{38} ergs s^{-1} in 2–6 keV (Warwick et al. 1985). The *Temma* satellite found that the GRXE spectrum has a strong Fe K line around 6.7 keV, which indicates the existence of thermal plasma of $k_{\rm B}T$ = 5–10 keV (Koyama et al. 1986, Koyama 1989b). The *Ginga* satellite mapped the intensity of the Fe K line and found that the GRXE distribution is represented by the sum of an exponential disk and spiral arm components (Koyama et al. 1989, Yamauchi et al. 1990; Figure 2.1). The scale height of the disk component is ∼100 pc with a radius of ∼4 kpc. The spiral arm component is extended from $l = -30°$ to $l = 30°$ (Yamauchi & Koyama 1993). The *Ginga* satellite also carried out GRXE observations above 10 keV from $l = -20°$ to $l = 40°$. It has a power-law spectrum and its luminosity in 3–16 keV is 2×10^{38} ergs s^{-1} (Yamasaki et al. 1997).

After that, many X-ray satellites performed observations of the GRXE. The *Suzaku* satellite carried out observations (∼100 ks) in the Ebisawa field. Thanks to the low background and modest spectral resolution of *Suzaku*, it resolved the Fe K line into three narrow Kα emission lines for the first time, which are neutral or low-ionized Fe (6.4keV), He-like Fe XXV (6.67 keV), and H-like Fe XXVI (7.0 keV) as shown in Figure 2.2. While He-like and H-like Fe K lines can be explained by collisional ionization equilibrium, the neutral 6.4 keV Fe K line is not expected from thermal plasma but from fluorescence by low-ionized optically thick matter. The equivalent widths of Fe K lines are 80±20 eV (the neutral), 330±40 eV (He-like), and 70±30 eV (H-like), respectively (Ebisawa et al. 2005).

2.1.2 Proposed Origin of the GRXE

In order to know origin of the GRXE, two approaches have been taken: (a) shallow and wide field observations like the *ASCA* GP survey programs (e.g., Sugizaki et al. 2001) and (b) deep and narrow field observations (Ebisawa et al. 2001, 2005, Revnivtsev et al. 2009). Despite these intensive studies, origin of the GRXE has been a mystery for a long time since its discovery. There have been two qualitative ideas to explain the origin of the GRXE:

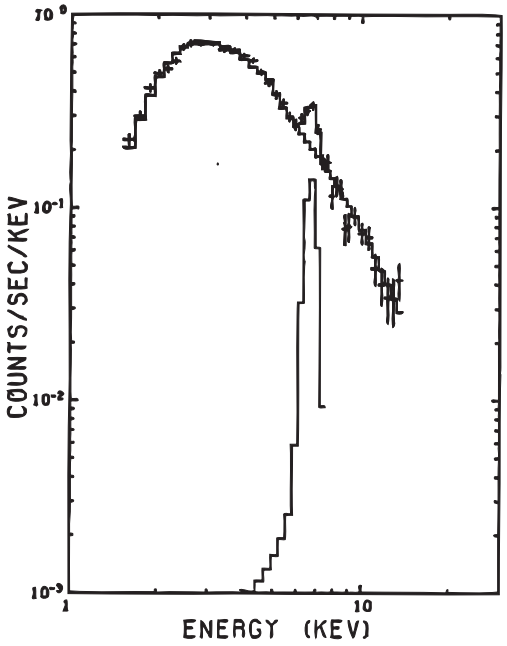

Figure 2.1: GRXE spectrum by stacking eight observations at the GP ($280° < l < 340°$, $-5° < b < 5°$) with *Temma* (Koyama et al. 1986). Crosses show the observed data and curves shows the best-fit continuum (bremsstrahlung) and the Fe K line at 6.7 keV.

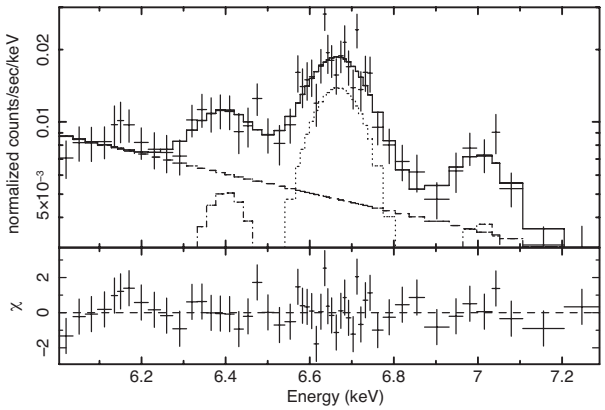

Figure 2.2: GRXE spectrum around the Fe K lines in the Ebisawa field with the *Suzaku* satellite (Ebisawa et al. 2008). The spectrum was fitted by a power-law continuum and three narrow Gaussian lines.

(1) diffuse scenario (Ebisawa et al. 2001, Ebisawa et al. 2005) and (2) point source scenario (Revnivtsev et al. 2006, Revnivtsev et al. 2009). The former is that the GRXE is diffuse X-ray-emitting plasma that fills the interstellar space. The latter is that the GRXE is composed of unresolved dim X-ray point sources. Below, we describe each scenario in more detail.

Diffuse Scenario

As a shallow and wide field observation, the *ASCA* satellite carried out the GP survey ($|l| \leq 45°$, $|b| \leq 0.4°$) and detected more than 200 new X-ray point sources brighter than $2{\times}10^{-13}$ ergs cm^{-2} s^{-1} in 2–10 keV. In addition, the the cumulative source number versus flux ($\log N$–$\log S$) curve was made to study the contribution of X-ray point sources to the GRXE, which was found unaccountable only by X-ray point sources above the flux limit. After that, the *XMM-Newton* satellite carried out a GP survey and made a $\log N$–$\log S$ curve brighter than 10^{-14} ergs cm^{-2} s^{-1} in 2–10 keV (Hands et al. 2004). It detected more X-ray point sources than the *ASCA* survey, but the GRXE was not explained entirely by the detected point sources.

Under such circumstances, the *Chandra* X-ray observatory was launched, which is an ideal tool to investigate even fainter X-ray point sources with its unprecedented spatial resolution of $\sim$0.6″ at the optical axis (Weisskopf et al. 2002). Using *Chandra*, long GRXE observations of two overlapping regions with a 100 ks exposure each were carried out at $(l, b) = (28.°5, 0.°0)$ by Ebisawa et al. (2001), which we call the Ebisawa field (Figure 2.3). In the observations, *Chandra* detected 274 new X-ray point sources down to $\sim 3{\times}10^{-15}$ ergs cm^{-2} s^{-1} in 2–10 keV. The $\log N$–$\log S$ curve was made, which revealed that the integrated flux of all the detected X-ray point source can only explain $\sim$10% of the total flux of the GRXE in 2-10 keV (Ebisawa et al. 2001, Ebisawa et al. 2005, Figure 2.4). If this $\log N$–$\log S$ curve is extrapolated toward the fainter end below the detection limit, it could not explain 100% of the GRXE. Therefore, they concluded that at least a part of the GRXE was a truly diffuse plasma.

If the GRXE is a truly diffuse plasma, it raises a new question. As the GRXE is thermal plasma of $k_{\rm B}T = 5$–10 keV, its energy density is $\sim$10 eV cm^{-3}, which is higher by an order than that of the interstellar medium, cosmic-rays, and Galactic magnetic field. Such a high-temperature plasma cannot be maintained by the gravity of our Galaxy. Thus, if the diffuse scenario is correct, we need a mechanism to continuously refill such hot plasma. Supernova explosions are such candidates to generate high-temperature plasmas. However, a required

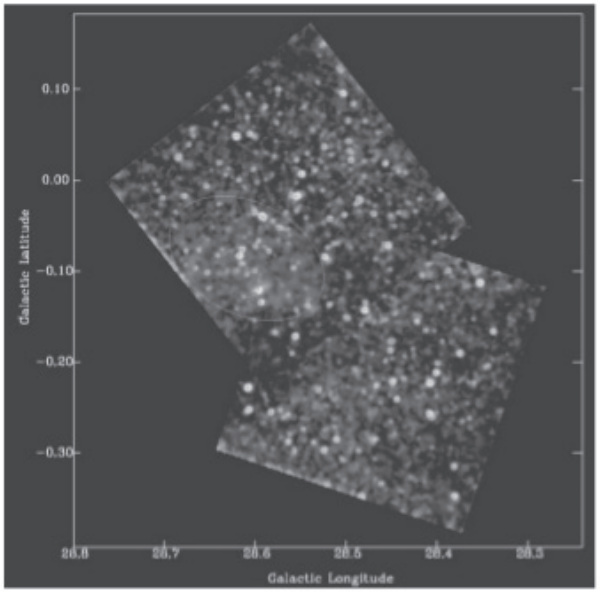

Figure 2.3: X-ray image of two *Chandra* observations in the Ebisawa field (200 ks in total). The pseudo-color image shows soft X-rays in 0.5–2 keV (red), medium X-rays in 2–4 keV (green), and hard X-rays in 4–8 keV (blue). The image was smoothed to show X-ray point sources and diffuse emission clearly (Ebisawa et al. 2005).

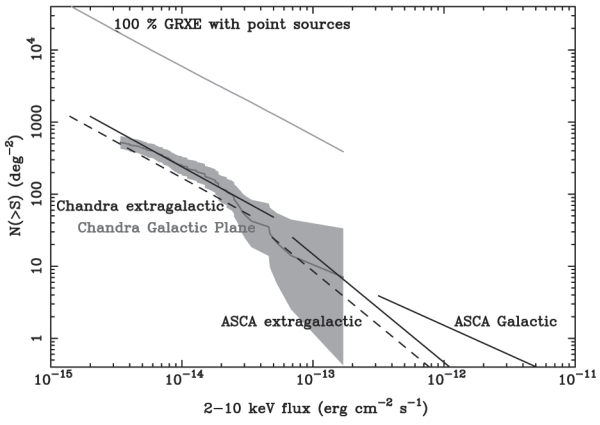

Figure 2.4: The $\log N$–$\log S$ curves of the sources constituting the GRXE with *Chandra* (black histogram) and the detected sources in the Ebisawa field (red) in 2–10 keV (Ebisawa et al. 2005). The 90% error regions are shown in gray. The number of hypothetical point sources that would account for 100% of the GRXE is shown.

number of supernovae to maintain the GRXE is 1 per several decades in our Galaxy (Yamasaki et al. 1997), which exceeds our understanding of the rate of the supernova explosion. Another proposed candidate is magnetic activity in the interstellar medium (Tanuma et al. 1999). This model explains the thermal plasma is heated by magnetic reconnection in the interstellar space. Yet another mechanism is the charge exchange process between cosmic-ray and interstellar medium. In this model, Fe emission lines are produced Fe ions undergoing charge exchange when they impinge upon the interstellar medium (Tanaka 2002).

Point Source Scenario

On the other hand, point source scenario claims that the GRXE consists mostly of faint X-ray point sources; e.g., cataclysmic variables (CVs), and X-ray active late type stars. CVs are binary systems that consist of a white dwarf and a late-type star (details in § 2.2). X-ray active late type stars include active binaries consisting of two late-type stars such as RS CVn, as well as single late-type stars. Such X-ray active stars often contain rapidly rotating stars that cause frequent flaring.

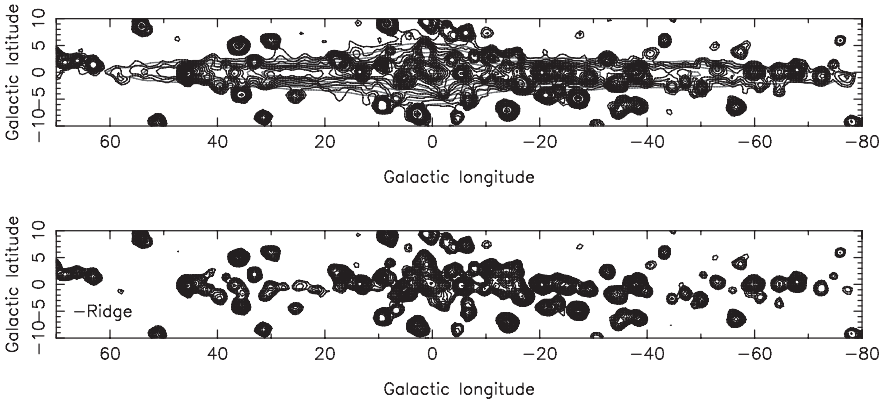

Figure 2.5: (Top) *RXTE*/PCA X-ray intensity map of the sky around the GP (3–20 keV, Revnivtsev et al. 2006). The GRXE is seen along the GP with bright point sources. Contours show *COBE* NIR 3.5 μm map; the lowest contour level corresponds to an X-ray intensity of 10^{-11} ergs cm^{-2} s^{-1} deg^{-2}. (Bottom) the same *RXTE*/PCA map in which rescaled NIR intensity is subtracted. Only bright NIR sources remain.

The *RXTE* satellite carried out extensive scan observations of the Galactic plane, which yielded an intensity map of the GRXE in 3–20 keV (Figure 2.5 top). As shown in Figure 2.5 bottom, only bright X-ray sources remain after subtracting a rescaled NIR 3.5 μm map from

the observed X-ray brightness map. It shows that the GRXE intensity is proportional to the NIR 3.5 μm intensity distribution. Since the NIR 3.5 μm emission is considered to represent the stellar population (mainly late-type main-sequence stars), this correlation suggests the stellar origin of the GRXE. Revnivtsev et al. (2006) proposed that the GRXE is resolved into X-ray point sources at $\sim 10^{-16}$–$10^{-16.5}$ ergs cm^{-2} s^{-1} in 2–10 keV.

After that, the *Chandra* satellite carried out the longest observation ($\sim$900 ks) at $(l, b) = (0.^\circ 0, -1.^\circ 4)$ (Revnivtsev et al. 2009), which we call the Revnivtsev field. They detected 473 X-ray point sources in the central (circle of radius 2.56 arcmin) of the field and revealed that $\sim$80% of the GRXE flux around the Fe K line was explained by X-ray faint point sources (Revnivtsev et al. 2009, Figure 2.6).

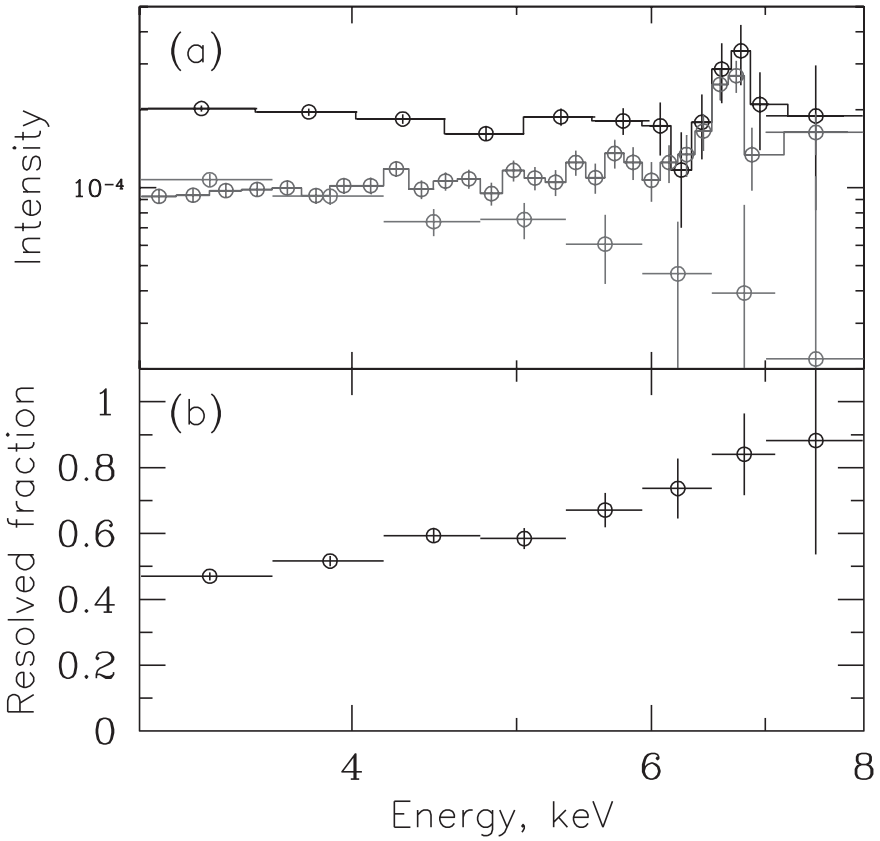

Figure 2.6: (Top) The GRXE spectrum extracted in the center region of the Revnivtsev field. Symbols from the top to the down indicate the total, resolved, and unresolved emission. (Bottom) Fraction of the detected X-ray point sources.

Wide-band GRXE spectra by 18 pointing observations of *Suzaku* (exposure time : $\sim 10^6$ s) were studied in (Yuasa 2011). The spectrum is represented by two thermal plasma models, in which soft X-ray emission has a plasma temperature of 1.2–1.5 keV and hard X-ray emission (Figure 2.7). The former is typical for X-ray active late-type stars. This result suggests that the wide-band GRXE spectrum can be explained by a combination of late-type stars and WD.

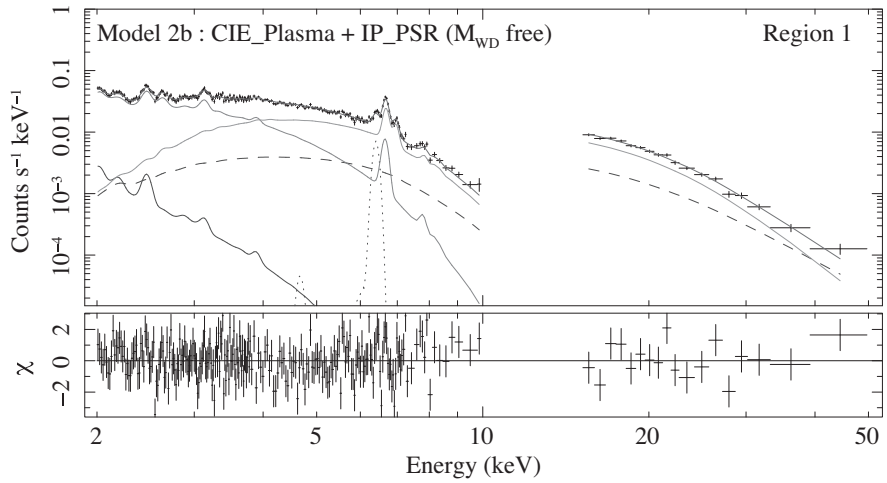

Figure 2.7: Wide-band GRXE spectrum by *Suzaku* in 2–50 keV. Black crosses are observed spectrum. The spectrum was fitted with optically-thin thermal model (magenta) and the Intermediate Polar model (orange). Red curves are the sum of all the model components. Solid, dashed, and dotted gray curves show the foreground diffuse soft X-ray emission, the cosmic X-ray background, and Kα emission line from neutral 6.4 keV Fe K line (Yuasa 2011).

As seen above, the point source scenario is recently considered more likely for the origin of the GRXE. If the origin of the GRXE is mostly point sources, it raises a new question: *What are the major populations of these faint X-ray point sources?* In this thesis, we study individual faint X-ray point source in order to know their populations.

2.2 X-ray and NIR Properties of the Major Source Populations

In this subsection, we review general X-ray and NIR properties of the major source populations that are considered to contribute to the GRXE. They are late-type stars, cataclysmic variables, detached systems including white dwarfs, and active galactic nuclei.

2.2.1 Late-type Stars

In general, stars are classified into two types: the early-type and the late-type stars. The former has a relatively high mass (>10 solar mass) and a short life, while the latter has a low mass (< 1 solar mass) and a long life. We focus on the late-type stars because stars of this type are overwhelmingly numerous compared to the early-type ones. The energy source is the nuclear fusion in the core. The late-type stars spend billions of years fusing hydrogen to helium via the proton-proton chain. When a star evolves and its core-supply of the hydrogen disappears, the core begins to collapse and the outer layer expands (the luminosity begins to increase). Such stars are called giants.

Late-type stars exist alone or in binary systems. By the stellar size and distance between the two stars, binaries are classified into three types: detached binary systems (both stars are smaller than the Roche lobe), semi-detached binary systems (one star fills its Roche lobe but the other does not), and contact binary systems (both stars fill their Roche lobe and essentially in contact), as shown in Figure 2.8. In this thesis, we do not distinguish X-ray emitting *single* late-type stars and *binary* late-type stars.

X-ray Emission

X-rays of late-type stars are emitted by hot corona. Late type stars in X-rays have two states, *flare* state and *quiescence* state. *Flare* occurs by a sudden release of energy via magnetic reconnection on the stellar surface. The flare releases a large amount of energies in X-rays, making an X-ray luminosity of 10^{30}–10^{31} ergs s^{-1} (Strassmeier et al. 1993). On *quiescence*, on the other hand, X-ray luminosities are in 10^{29}–10^{30} ergs s^{-1} (Pandey & Singh 2012).

X-ray spectra from late-type stars are characterized by a thermal, optically thin plasma

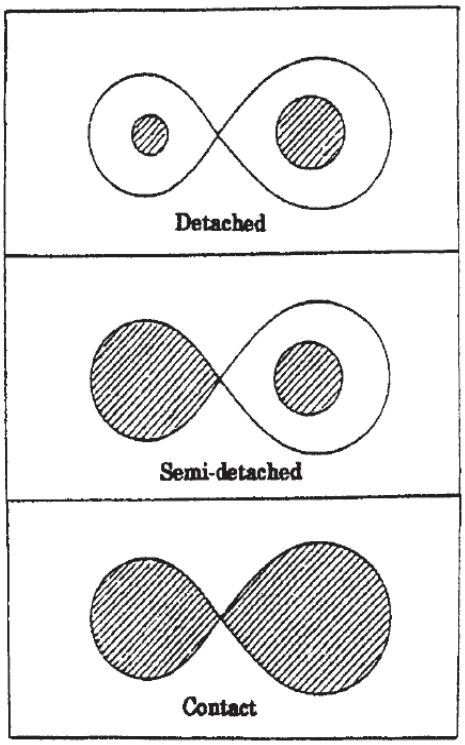

Figure 2.8: Three types of close binaries, classified by stellar and Roche lobe sizes (Kopal 1959).

model with two (or multi–) temperatures. On *flare*, the late-type stars can have high temperatures from several keV to >10 keV. Such hot, thermal plasma spectra necessarily accompany prominent Fe K emission lines (6.7 keV line from He-like and 7.0 keV line from H-like ions, respectively). Figure 2.9 shows X-ray spectra of UX Ari on *quiescence* and on *flare*. On *flare*, they have a strong Fe K line (6.7 keV), and the highest temperature is ∼18.9 keV (Güdel et al. 1999). Such a high temperature on *flare* is common for other late-type stars. For example, II Peg, too, has a temperature as high as ∼18 keV on *flare* (Osten et al. 2007). On *quiescence*, the late-type star spectra have lower temperatures than several keV, and the Fe K-lines are insignificant (Figure 2.9). For example, equivalent width of the Fe K line (6.7 keV and 7.0 keV lines merged) is ∼560 eV on *flare* and less than ∼270 eV on *quiescence* in the case of UX Ari (Tsuru et al. 1989).

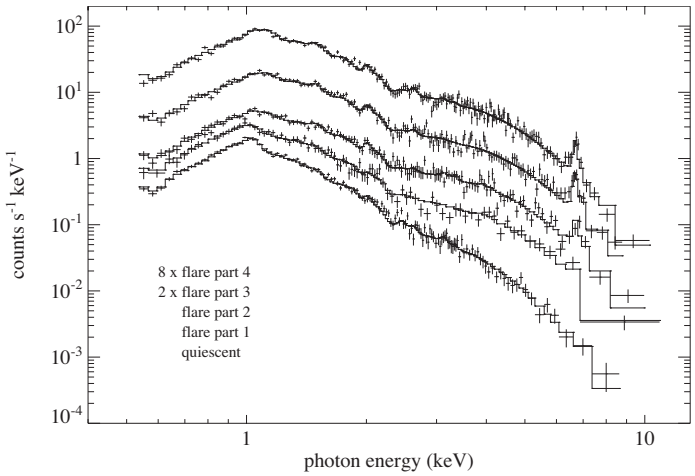

Figure 2.9: X-ray spectra of a late-type star (UX Ari) with *ASCA* (Güdel et al. 1999). The bottom spectrum is on *quiescence* and the others are on *flare*.

NIR Emission

Figure 2.10 shows examples of medium resolution NIR (2.15–2.35 μm) spectra of late-type stars (from F-type to M-type; Ali et al. 1995). Each spectrum has different absorption lines based on surface temperatures. Major absorption lines are listed in Table 2.1.

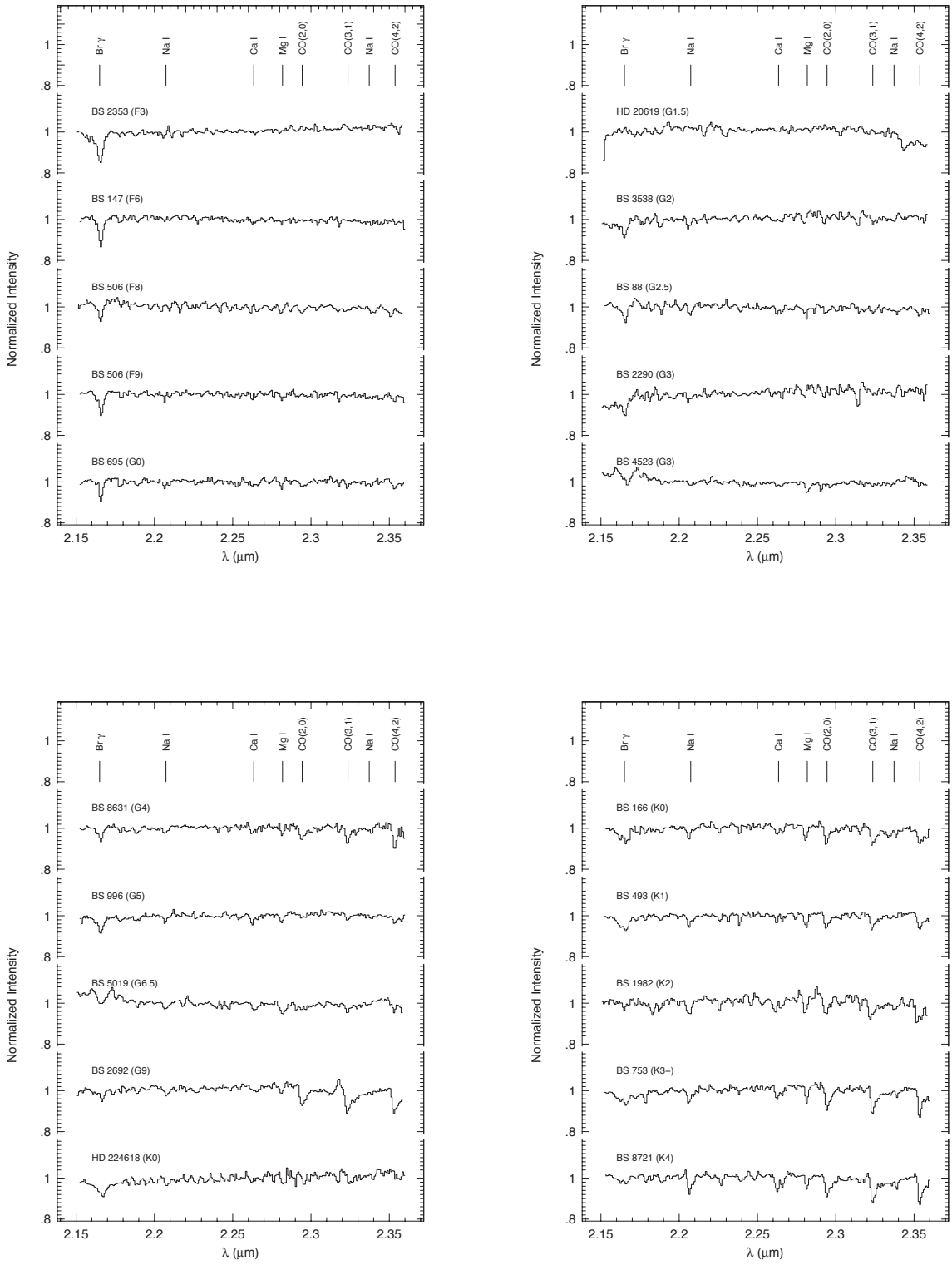

Figure 2.10: Examples of normalized K-band spectra of late-type stars (spectral type F, G, K, and M). All prominent features are shown in the top (Ali et al. 1995).

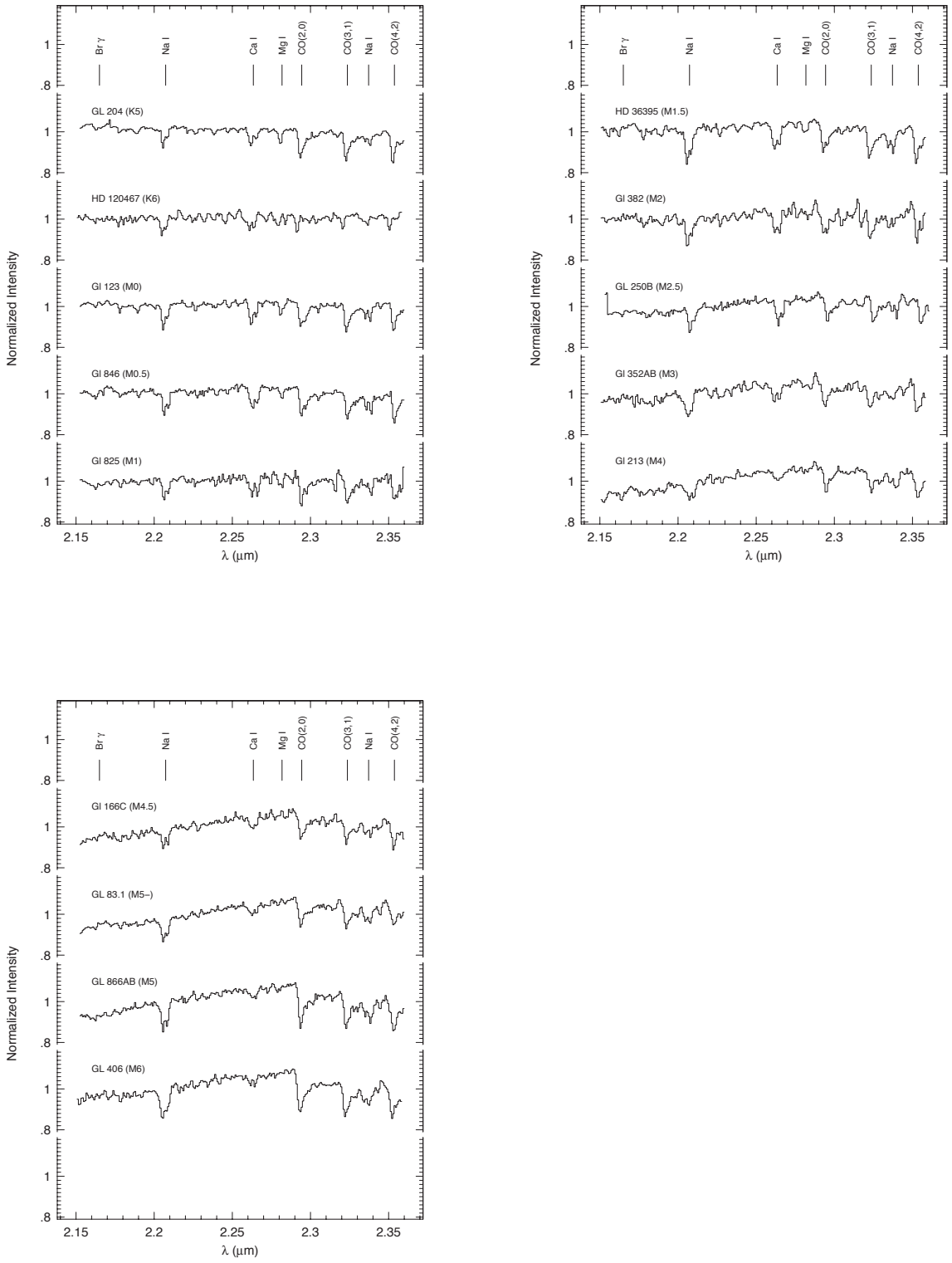

Figure 2.10: *Continued.*

Table 2.1: Spectral features in K band.

Spectral type	Absorption lines
F	HI Brγ (2.16 μm)
G	HI Brγ (2.16 μm)
K	HI Brγ (2.16 μm), CaI (2.26 μm; triplet),
	MgI (2.28 μm), CO (2.29 μm, 2.32 μm, 2.35 μm, 2.38 μm)
M	NaI (2.20 μm; doublet), Ca I (2.26 μm; triplet),
	MgI (2.28 μm), CO (2.29 μm, 2.32 μm, 2.35 μm, 2.38 μm)

2.2.2 Cataclysmic Variables

Cataclysmic variables (CVs) are thought to be one of the population constituting the GRXE in the hard band. CVs are in semi-detached binary systems consisting of a white dwarf (WD) as the primary and a late-type star as the secondary. In the binary systems, when the late-type star fills its Roche lobe, the gas around the late-type star overflows to the WD via the Lagrange point, then mass accelerates to the WD (Figure 2.11). This process is called Roche lobe overflow. Accreting matter with significant angular momentum is considered to form an accretion disk.

Based on the strength of the magnetic field of the WD, CVs are divided into two subclasses: (1) non-magnetic CVs and (2) magnetic CVs. Non-magnetic CVs do not have sufficiently strong magnetic field to dominate the accretion flow. Thus, the accretion materials form an accretion disk which reaches to the white dwarf surfaces (Warner 1995). In addition, non-magnetic CVs have strong variability. They are further classified into several sub-groups according to their properties. For examples, one of the sub-groups, dwarf novae, show two states: the quiescent state and the outburst state. The former state is that the accretion disk is mostly made by neutral H. The latter state is that the accretion disk in mostly made by ionized H, which shows high surface density, mass accretion rate, and viscosity. On the other hand, magnetic CVs have strong magnetic fields, which dominates the accretion flow, so that the accretion disks are considered to be truncated before reaching the white dwarf surfaces. When accretion flow falls into a WD, a strong shock occurs at the WD surface. Then, the accretion materials turn into a hot plasma of 10^8 K. Magnetic CVs are also further classified into two subclasses (intermediate polars and Polars) based on the difference of the magnetic field strength. The intermediate polars (IPs) have 10^5–10^7 G and

polars have 10^7–10^9 G. Non-magnetic CVs and magnetic CVs can be observed by X-rays.

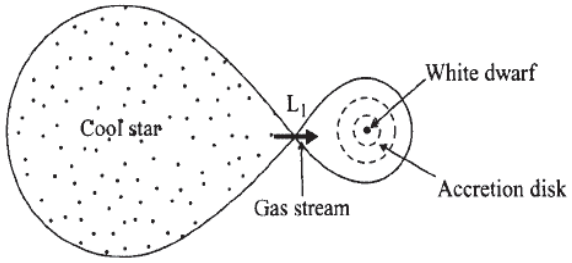

Figure 2.11: Schematic picture of CVs in the orbital plane. Cool star fills its Roche lobe, and a gas stream flows on to the accretion disk of the WD (Hoffmeister & Kholopov 1985).

X-ray Emission

In non-magnetic CVs, when the gas transfers from the secondary to the primary, it carries angular momentum and makes an accretion disk around the WD. The accretion disk extends to the surface of the WD, then optically-thin plasma of $\sim 10^8$ K is created due to a strong frictional force at the boundary layer, emitting hard X-rays. Non-magnetic CVs have thermal spectra with three Fe K lines from neutral or low-ionized ions (6.4 keV), from He-like ions (6.7 keV), and from H-like ions (7.0 keV). Typical equivalent widths of the three Fe lines are $\sim$50 eV (a neutral), $\sim$130 eV (He-like), and $\sim$60 eV (H-like), respectively (Rana et al. 2006). Typical luminosity of non-magnetic CVs is $\sim 10^{30}$–10^{32} ergs s^{-1} (Verbunt et al. 1997). Figure 2.12 shows a sample spectrum of non-magnetic CVs in the quiescent phase.

In magnetic CVs, materials can not accrete on the surface of the WD directly due to the magnetic strength. When a pressure of gas equals to a pressure of magnetic pressure, materials fall to the WD along lines of magnetic flux. Since the accretion flow exceeds sound velocity, a strong shock occurs close to the WD, and accretion materials turn into a hot plasma of $\sim 10^8$ K. We can observe the hard X-ray emission with Fe K lines, which are He-like Fe K line (6.7 keV) and H-like Fe K line (7.0 keV). Furthermore, since a hot plasma reflects on the surface of the WD, it emits a neutral Fe K line (6.4 keV). In Hellier & Mukai (2004), the equivalent width of these three Fe lines are $\sim$120 eV, $\sim$160 eV, and $\sim$110 eV, respectively. Typical luminosity of magnetic CVs is $\sim 10^{32}$–10^{34} ergs s^{-1}. *Suzaku* satellite. Figure 2.13 and 2.14 show examples of X-ray spectra of IPs and Polars, respectively.

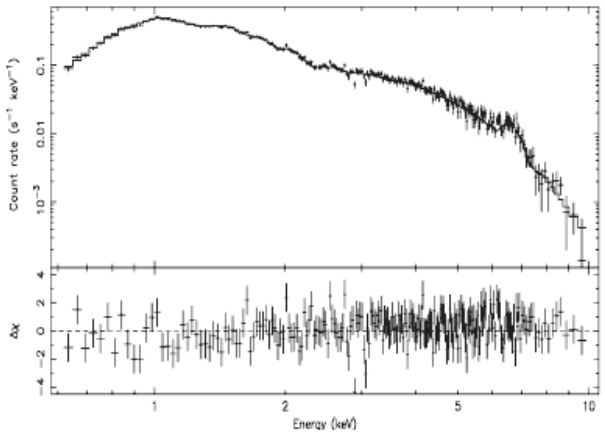

Figure 2.12: A typical spectrum of non-magnetic CVs (V603 Aql) by the *ASCA* satellite. The spectrum is fitted with a thermal plasma model. The lower panel shows residuals from the fit (Baskill et al. 2005).

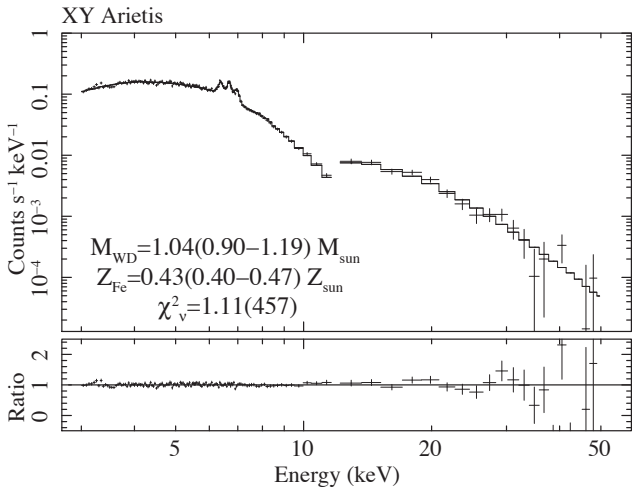

Figure 2.13: X-ray spectrum of IPs XY Arietis by *Suzaku* (crosses) with the best-fit model (solid line). The lower panel shows the ratio of the data to the model (Yuasa et al. 2010).

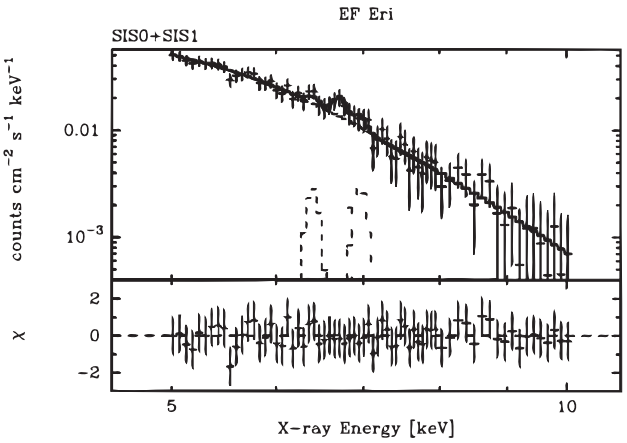

Figure 2.14: Example spectrum of polars (EF Eri) in 5–10 keV observed by the *ASCA* satellite (Ezuka & Ishida 1999). In the upper plot, crosses and histograms show data points and model components of thermal continuum with three Gaussian lines. The lower panel shows spectral fit residuals.

NIR Emission

We can observe CVs in NIR. The emission mainly from cool regions of the accretion disk (Dhillon et al. 1997), as well as from the late-type companions. NIR spectra of CVs show prominent HI (Brγ) and HeI emission lines from the accretion disks, CO and neutral metal absorption lines from the companion stars. Figures 2.15 and 2.16 show NIR spectra of CVs in the K band.

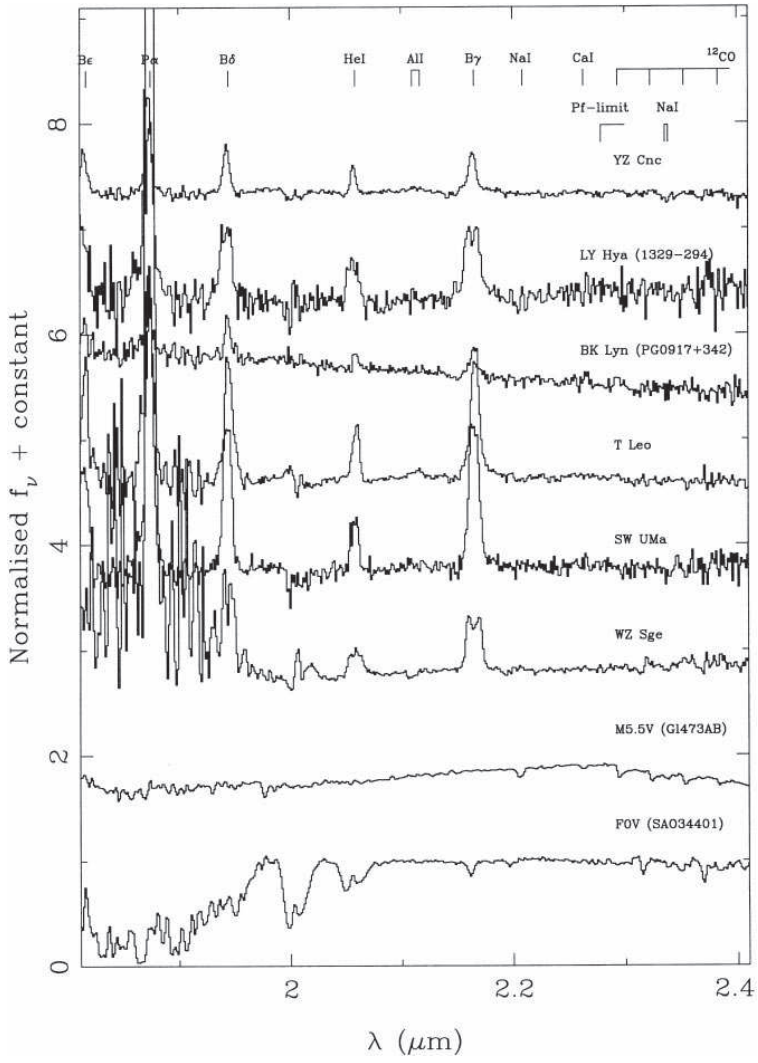

Figure 2.15: NIR spectra of non-magnetic CVs (from the top, YZ Cne, LY Hya, BK Lyn, T Leo, SW UMa, WZ Sge), as well as reference spectra of M and F stars (bottomo two). These spectra are normalized at 2.24 μm. The F0V spectrum indicates the location of telluric absorption features (Dhillon et al. 1997).

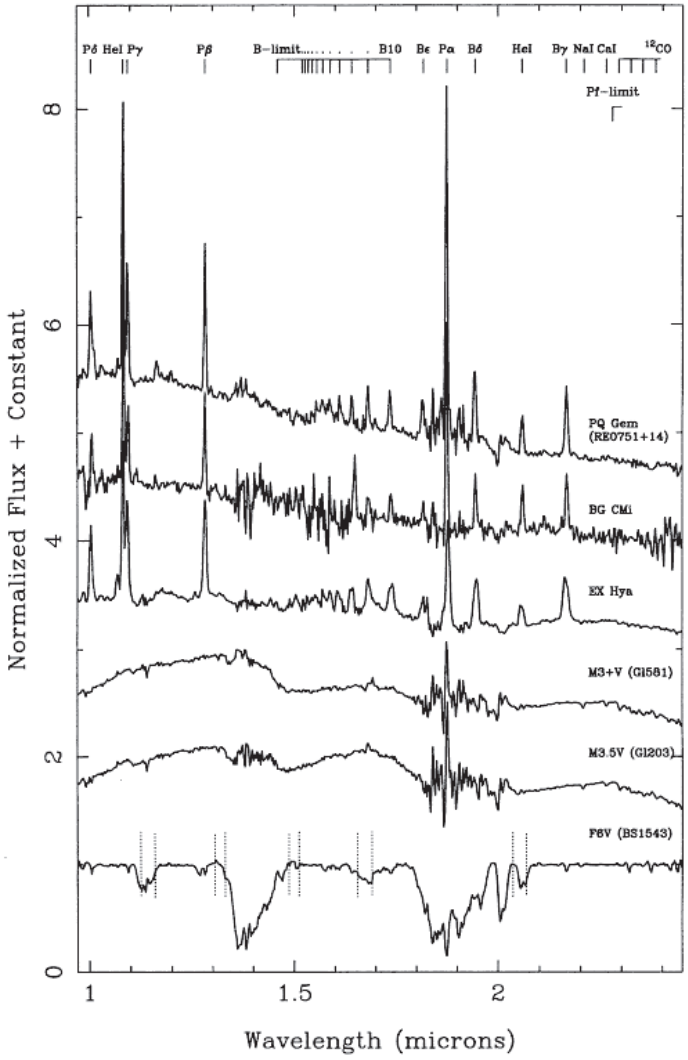

Figure 2.16: NIR spectra of IPs (PQ Gem, BG GMi and EX Hya). These spectra are normalized at 2.24 μm (Dhillon et al. 1997).

2.2.3 Detached Systems Consisting a White Dwarf

There are detached binary systems consisting of a white dwarfs (WD) and late-type stars. They are in a different population from CVs, and called pre-cataclysmic variables (pre-CVs). Pre-CVs are considered to be progenitors of CVs. Pre-CVs are composed of a WD primary star and a late type secondary star. Figure 2.17 shows an X-ray spectrum of pre-CVs. This population has not been recognized widely, so there are not many X-ray observations so far. NIR spectra of pre-CVs are shown in Figure 2.18. In NIR spectra of pre-CVs, there are absorption lines of CaI, NaI and CO, which are from the secondary stars. In contrast to the NIR spectra of CVs, pre-CVs do not show prominent Brγ lines. The fact that most pre-CVs do not have NIR emission lines indicate that pre-CVs do not have accretion disks.

,

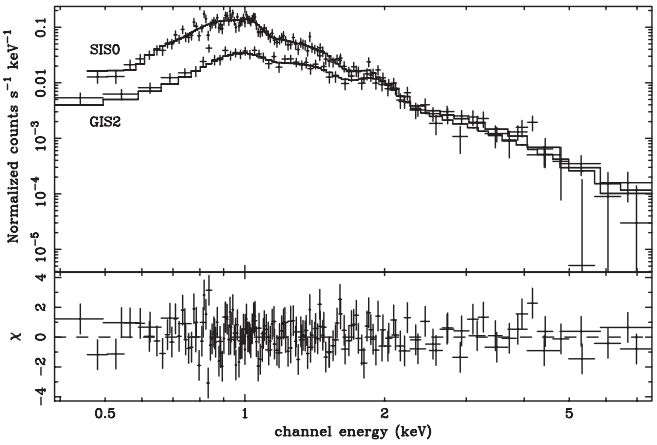

Figure 2.17: X-ray spectrum of a detached system consisting a WD (V471 Tau) by the *ASCA* satellite (Martin et al. 1997).

2.2.4 Active Galactic Nuclei

Active galactic nuclei (AGN) are massive black holes at the center of galaxies. The luminosity is $\sim 10^{44}$–10^{46} ergs s^{-1}. Its energy comes from a mass accretion to the back hole in the center. The emission of AGNs are observed from radio to X-ray wavelengths.

The X-ray emission of AGNs has the following properties: The X-ray spectra are approximated with a power-law model of a photon index $\sim$–1.7 above $\sim$ 2 keV. In addition, soft X-ray excess component and Fe K lines are observed. The Fe K line is at $\sim$6.4 keV,

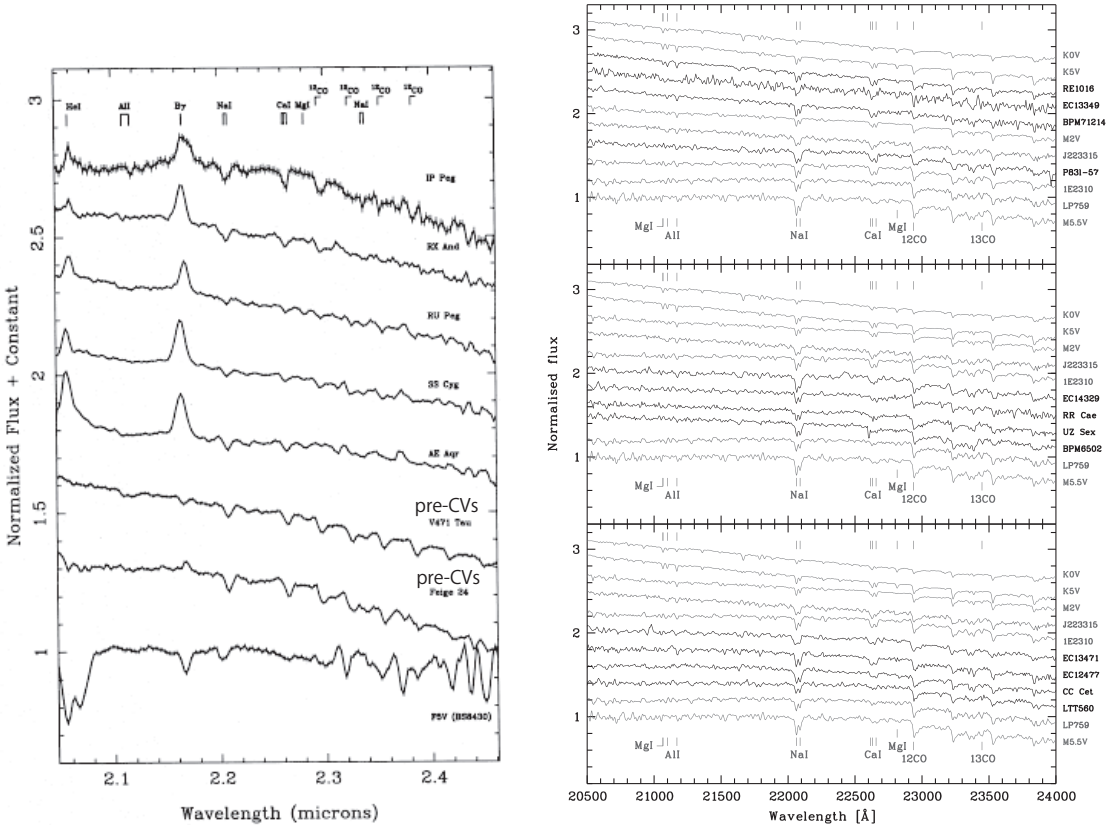

Figure 2.18: (Left) NIR spectra of CVs and pre-CVs. Top five are those ofCVs, and the sixth and seventh are those of pre-CVs (V471 Tau and Feige 24). These spectra are normalized by dividing by the flux at 2.24 μm (Dhillon et al. 1997). V471 Tau is the same source as we show in Figure 2.17. (Right) Normalized NIR spectra of four pre-CVs, together with three comparison stars (J223315, 1E2310, and LP759) and four late-type star templates (K0V, K5V, M2V, and M5.5V). Source names and the spectral types shown on the right (Tappert et al. 2007).

which is due to fluorescence by neutral or low-ionized accretion disks, and may be gravitationally red-shifted and broadened by relativistic effects. Figure 2.19 shows an example of X-ray spectrum of AGNs. In the GP, we may observe power-law spectra of the background AGNs with $\sim$ 6.4 keV Fe K lines affected by significant Galactic absorptions.

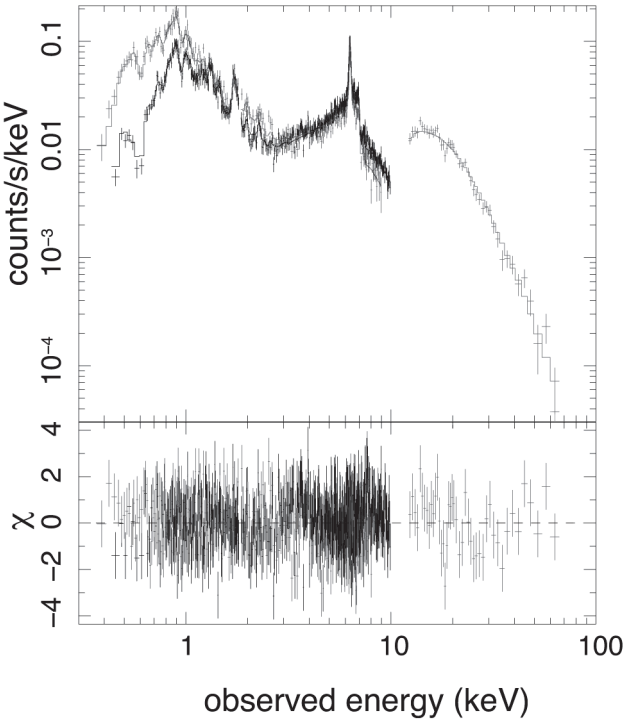

Figure 2.19: Example wide-band spectrum of AGNs (Mrk3) with the *Suzaku* satellite (Awaki et al. 2008). The black, red and green crosses are spectra obtained by XIS-BI, XIS-FI, and HXD-PIN of *Suzaku*, respectively.

2.3 Scope, Purpose, and Strategy of this thesis

The strong Fe K emission line complex is the feature that characterizes the GRXE spectrum most, and has been debated intensively in the past. In this thesis, we focus on the origin of the hard band (2–8 keV) X-ray emission of the GRXE, which includes the Fe K complex feature in 6–7 keV. The soft band (<2 keV) emission of the GRXE, which may have different origins, is out of the scope of this thesis. In particular, we are interested in the nature of the dim point sources that contribute to the Fe line emission.

From two circumstantial lines of evidence, we are almost certain that there is an unknown X-ray point source population that contributes significantly to the Fe line emission of the GRXE. The first evidence is from the result of the deepest X-ray observation of GRXE by Revnivtsev et al. (2009) with a limiting sensitivity of $F_{\rm X} = 10^{-16}$ ergs cm^{-2} s^{-1}. The authors demonstrated that 80% of the Fe emission was resolved into point sources. However, as we shall show in § 5.1, the X-ray spectra of almost all bright point sources do not exhibit Fe emission line. They are mostly described as a power-law spectrum contributing only to the continuum emission. This infers the presence of a different point source population, which is fainter but contributes much more to the line emission than these bright power-law sources. The second evidence is from the result of the second deepest X-ray observation by Ebisawa et al. (2005) with a limiting sensitivity of $F_{\rm X} = 3 \times 10^{-15}$ ergs cm^{-2} s^{-1}. They showed that only 10% of the hard band emission of GRXE was resolved into point sources. They constructed a $\log N$–$\log S$ curve and decomposed the curve into an extra-Galactic population and two Galactic X-ray point source populations of different luminosity functions: one is a high $L_{\rm X}$ population mostly for the low-mass X-ray binaries; i.e., semi-detached binary systems containing a neutron star or a black hole, and the other is a low $L_{\rm X}$ population mostly for the CVs; i.e., semi-detached binary systems containing a white dwarf (Figure 2.4). Assuming a Galactic distribution of the two populations, they extrapolated the $\log N$–$\log S$ curve of each component and found that the integrated emission below the limiting sensitivity accounts only for a 50% of the hard band emission of the GRXE at most. The apparently contradicting results of the two studies (Revnivtsev et al. 2009 and Ebisawa et al. 2005) infers the presence of another point source population that are dominant in the flux range in between the limiting sensitivities of the two studies.

The speculation above has not been extensively discussed in the community before, but seems reasonable enough for us to pursue the theme. The aim of this thesis is to classify nature of the numerous anonymous X-ray point sources and to identify the new faint class of X-ray point sources yet to be recognized as a major contributor to the GRXE emission.

In this thesis, we did the following steps; (1) Detect X-ray point sources, (2) Identify X-ray point sources with NIR imaging, and (3) Spectroscopy of the identified X-ray sources with NIR. About (1) and (2) steps of the Ebisawa field, we used the results of Ebisawa et al. (2005).

Chapter 3

Observing Facilities

In this chapter, we review one X-ray and two NIR observing facilities: *Chandra* (§ 3.1), IRSF (§ 3.2), and Subaru (§ 3.3). We present the overview of the telescopes and the instruments used in this study.

Contents

3.1 *Chandra*/ACIS

3.1.1 Spacecraft–*Chandra*

The *Chandra* X-ray Observatory (Weisskopf et al. 2002) was launched on 1999 July 23 by the National Aeronautics and Space Administration (NASA) using the space shuttle Colombia. The satellite was placed into a highly elliptical orbit with an apogee of 140,000 km and a perigee of 100,000 km with a period of ∼63.5 hr. The high and elliptical orbit allows for uninterrupted observing intervals at the maximum of ∼170 ks. Thus, *Chandra* has a high observing efficiency (∼80%).

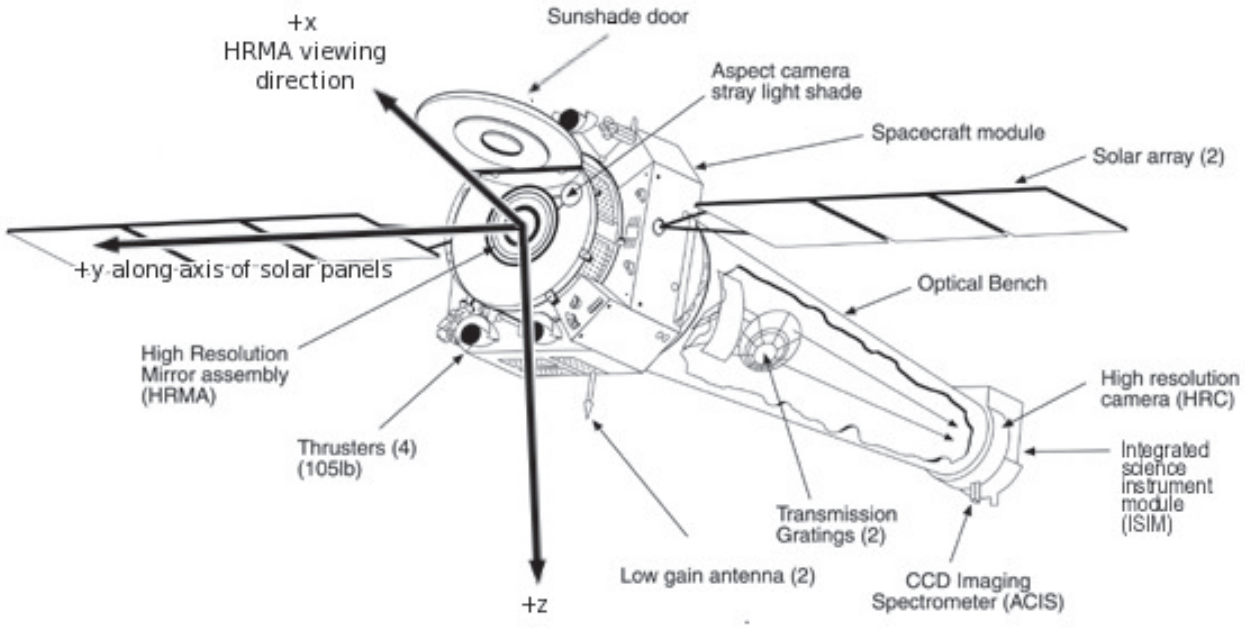

Figure 3.1: Schematic view of the *Chandra* satellite (*Chandra* Proposers' Observatory Guide 2010).

The outline of *Chandra* is shown in Figure 3.1. *Chandra* has the following sub-systems. X-ray telescope (High Resolution Mirror Assembly; HRMA: Jerius et al. 2004), the objective transmission gratings (OTGs), and two focal plane instruments; the High-Resolution Camera (HRC-I and HRC-S; Murray et al. 2000) and the Advanced CCD Imaging Spectrometer (ACIS-I and ACIS-S; Garmire et al. 2003). ACIS-I and -S are X-ray CCD arrays and HRC-I and -S are micro channel plate arrays. The ACIS-I and -S can obtain images and medium-resolution spectra and the HRC-I and -S can obtain images. The OTGs have two types,

the Low-Energy Transmission Grating (LETG: Brinkman et al. 2000) and the High-Energy Transmission Grating (HETG: Canizares et al. 2005). The ACIS and HRC arrays can obtain high resolution spectra with a combination of either of the two gratings elements (LETG, HETG). The details are given in the *Chandra* Proposer's Observatory Guide (2010).

The *Chandra*'s optical axis is kept dithered during an observation. It is intended to prevent bad pixels ruining an entire observation, to smooth over CCD chip gaps, and to reduce pixel-to-pixel variation of the quantum efficiency. The dithering pattern is a Lissajous figure with a period of ∼1000 s. The *Chandra*'s pointing and dithering are controlled by the Pointing Control and Aspect Determination System (PCAD).

3.1.2 Telescope — High Resolution Mirror Assembly (HRMA)

Configuration

The High Resolution Mirror Assembly (HRMA) is an X-ray telescope assembly carried on *Chandra*. The HRMA adopts a grazing incidence X-ray optics (Figure 3.2) and consists of four sets of nested Wolter-I type thick mirrors as shown in Figure 3.2. The mirrors are coated with iridium. The diameter of mirrors range from 0.65 m to 1.23 m, and the focal length is about 10 m.

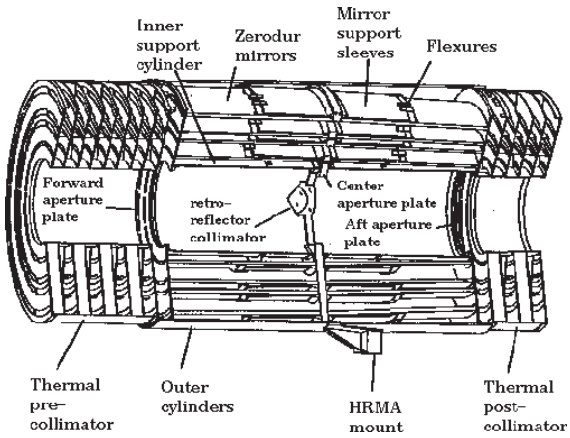

Figure 3.2: Four nested HRMA mirror sets and associated structures (*Chandra* Proposers' Observatory Guide 2010).

Effective Area

The effective area of the telescope depends on both X-ray energy and off-axis angle, which is the angular distance from the optical axis. Figure 3.3 (a) shows the on-axis effective area, which is about 800 cm^2 at 0.25 keV, 400 cm^2, and 100 cm^2 at 8.0 keV. Above 10 keV, no X-ray photons can be reflected by the mirrors. Figure 3.3 (b) shows the off-axis effective area, which decreases as the off-axis angles increases. This is due to the vignetting effect of the mirror.

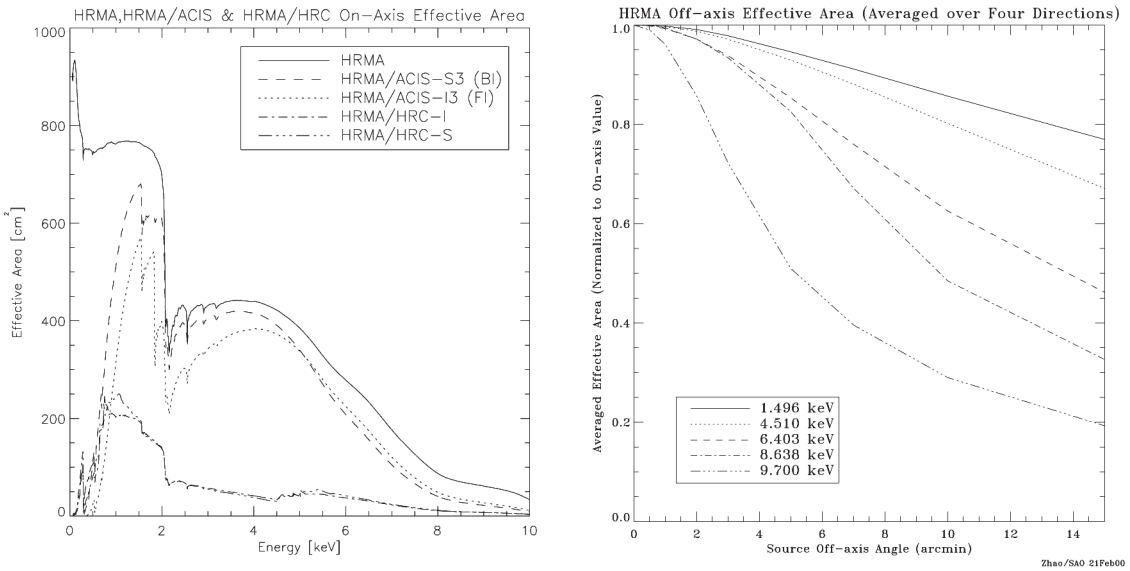

(a) (b)

Figure 3.3: (a) HRMA effective areas versus X-ray energy at the optical axis. The structure near 2 keV is from the iridium M-edge used for mirror coating. The solid line shows the total effective area. The other lines show the expected effective area convolved with the detector quantum efficiency. (b) HRMA effective areas versus off-axis angle. The curves show the profiles at five selected energies (*Chandra* Proposers' Observatory Guide 2010).

Point Spread Function

Point Spread Function (PSF) is a spatial distribution function for a point-like source for imaging detectors. In HRMA, it depends on both the energy and off-axis angle. At on-axis, most X-ray photons are collected within a 1″ radius circle. Figure 3.4 (a) shows the encircled

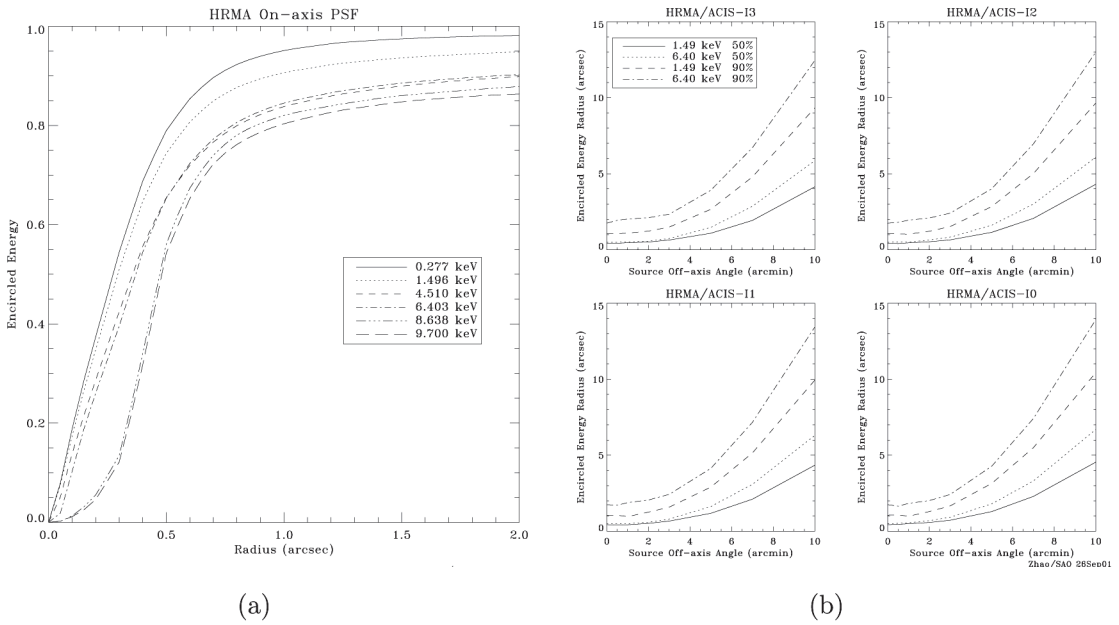

(a) (b)

Figure 3.4: (a) Encircled energy fraction as a function of radius at the optical axis. (b) HRMA/ACIS-I encircled energy radii for circles enclosing 50% and 90% of the power at 1.49 and 6.40 keV as a function of off-axis angle (*Chandra* Proposers' Observatory Guide 2010).

energy function at on-axis. For example, 50% photons are encircled in about 0.35″ radius at 4.510 keV, which is called the half-power radius. Figure 3.4 (b) shows the dependence of PSFs at several off-axis angles.

3.1.3 Instrument — Advanced CCD Imaging Spectrometer (ACIS)

Configuration

The Advanced CCD Imaging Spectrometer (ACIS) consists of 10 charge coupled devices (CCDs). Four of them comprise the ACIS-I (ACIS-I0, I1, I2, and I3) with a 2×2 array, while six of them comprise the ACIS-S (ACIS-S0, S1, S2, S3, S4, and S5) with a 1×6 array (Figure 3.5). Each CCD has a format of 1024×1024 pixels. The pixel scale is 0.492″ pixel^{-1}. ACIS-S1 and S3 are back-illuminated (BI) CCDs, which is useful for detecting soft X-ray photons, and the others are front-illuminated (FI) CCDs. Any combination of up to six CCDs can be used simultaneously. The aim points of ACIS-I and ACIS-S are on ACIS-I3 and ACIS-S3, respectively (Figure 3.5).

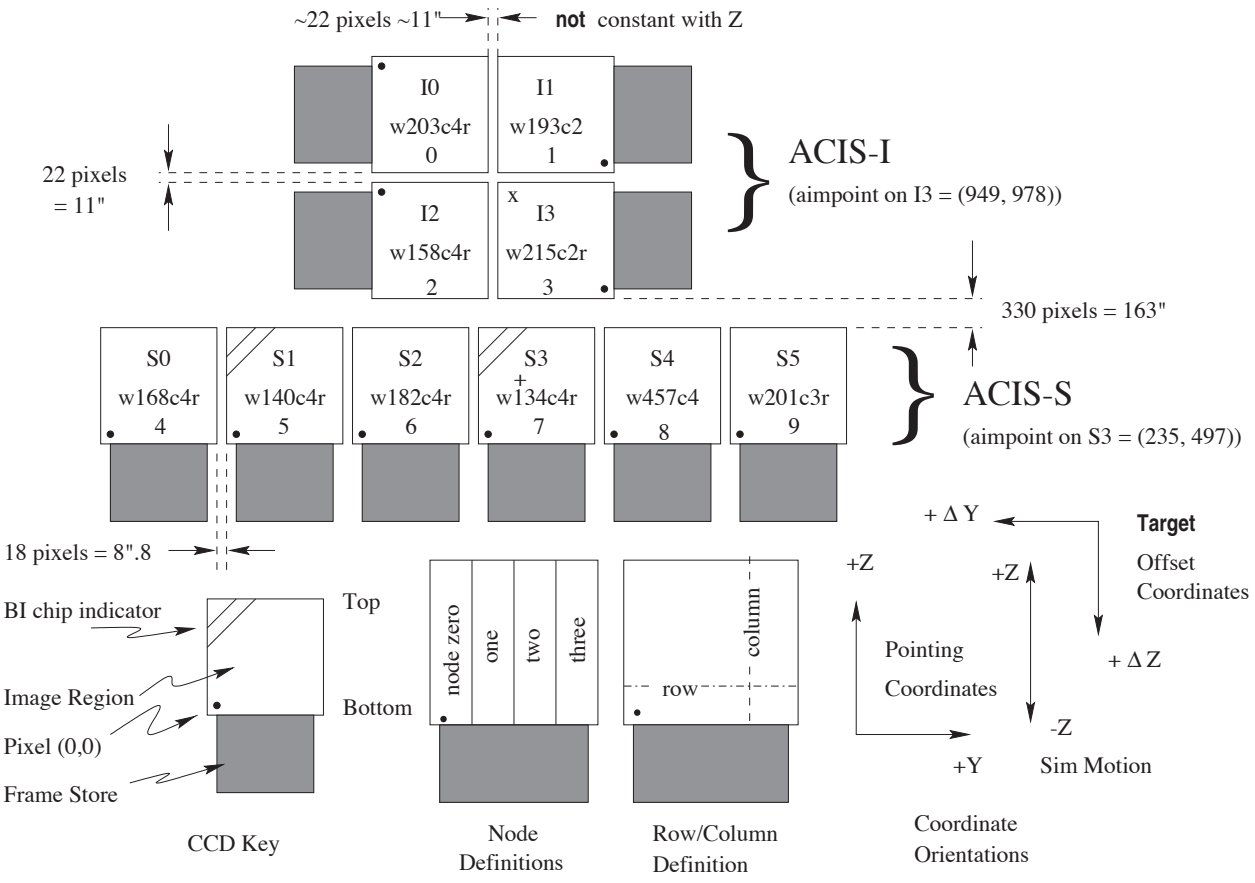

Figure 3.5: Configuration of the ACIS array. The top 2×2 array is ACIS-I and the bottom 1×6 array are ACIS-S. (*Chandra* Proposers' Observatory Guide 2010).

Quantum efficiency

Figure 3.8 (a) shows the effective area of HRMA/ACIS. The edge at 1.838 keV is due to the K-edge of SI. Low energy photons are absorbed by optical blocking filter (OBF). For the FI CCDs, the gate structure can absorb low energy photons too. The ACIS-I and ACIS-S have the OBF to block photons in the optical and the ultraviolet wavelengths. The OBF is composed of polymide sandwiched between two thin aluminum layers. The thickness of them are shown in Table 3.1.

Table 3.1: Nominal Optical Blocking Filter composition and thickness.

ACIS-I	Al/Polymide/Al	1200 Å 2000 Å 400 Å
ACIS-S	Al/Polymide/Al	1000 Å 2000 Å 300 Å

As the gate structure of the BI chips is at the opposite side of the HRMA, the quantum efficiency of the BI is larger than that of the FI at the low energy band. On the other hand, at high energies, the FI chips are more sensitive than the BI as the depletion layer is thicker than that of the BI (Figure 3.8 b).

Energy Resolution

Figure 3.7 (a) shows energy resolution of the ACIS estimated by ground calibrations. The FI CCDs have a good energy resolution near the theoretical limit ($\sim$ 120 eV at 5.9 keV), but the BI CCDs have a slightly worse resolution. After the launch, energy resolution was degraded due to damage by low energy protons when the satellite went through the earth radiation belt. These protons made many charge traps, which caused an increase of the charge transfer inefficiency (CTI).

Correction algorithm of the energy resolution has been developed by the ACIS instrument team. The algorithm was incorporated in the *Chandra* Interactive Analysis of Observations (CIAO) tool, `acis_process_events`. From December 2006, data for the two BI (S1 and S3) chips can be corrected using the same way. For the FI chips, the increase of the CTI is substantial in Figure 3.7 (b). They measured the resolution using the Al (1.29 keV) and Mn (5.9 keV) Kα lines.

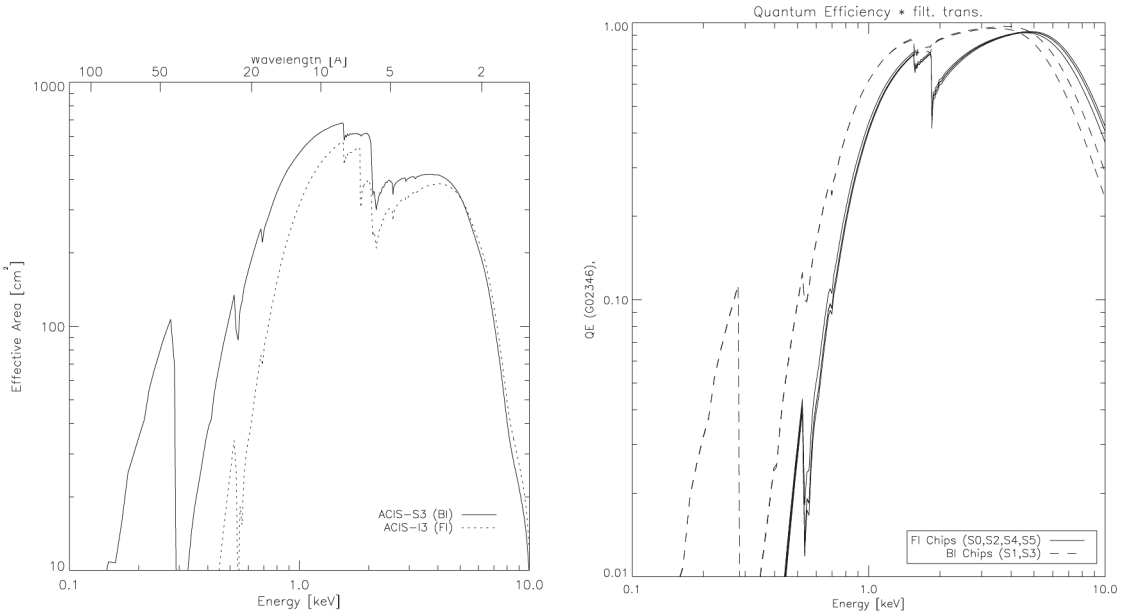

(a) (b)

Figure 3.6: (a) Quantum efficiency convolved with the the quantum efficiency of the detector. (b) HRMA effective area convolved with the ACIS efficiency as a function of energy. The solid curve shows the FI CCDs, and the dashed curve shows the BI CCDs (*Chandra* Proposers' Observatory Guide 2010).

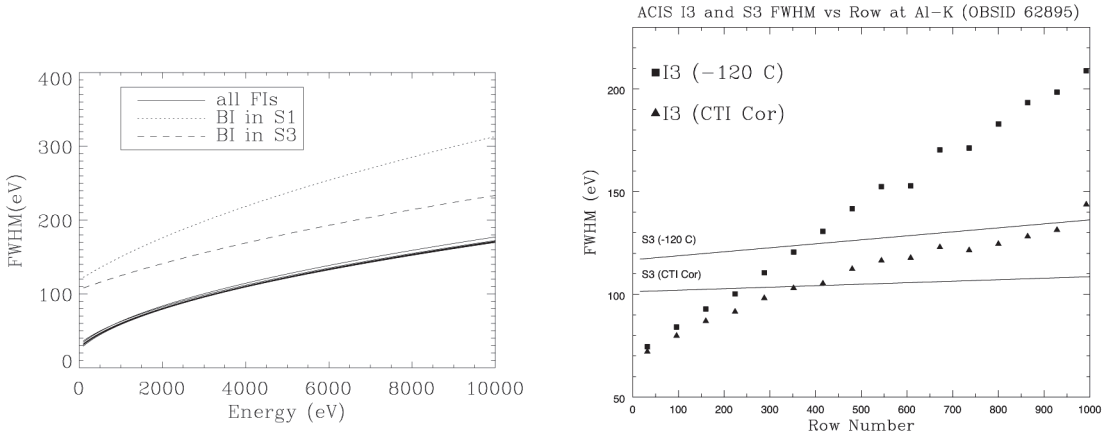

(a) (b)

Figure 3.7: (a) ACIS pre-launch energy resolution as a function of energy. (b) The energy resolution of chip I3 and S3 as a function of a raw number, after proton damage in the orbit. Data were taken from I3 node 3, and S3 node 0 (where the aim points are located) from May through July of 2009 (*Chandra* Proposers' Observatory Guide 2010).

Event Grades

Events are detected when they satisfy two criteria: the bias-subtracted pulse height exceeds the event threshold, and also the pulse height is the highest among the surrounding 3×3 pixels.

To distinguish X-ray events from non X-ray events due to cosmic-rays, the grade filtering is adopted, which was originally developed for ASCA SIS. A number is specified for each pixel around the center pixel. The grade is calculated by summing up those pixel numbers around the center pixel. For example, an event with all 3×3 pixels above the threshold is grade 255. From the number, we distinguish X-ray events from non X-ray events. A single pixel event is grade 0. The ASCA grade 0, 2, 3, 4 and 6 are recognized as X-ray events. The other grades (ASCA grade 1 and 7) are regarded as non X-ray events.

Telemetry Format

The following three telemetry formats are available, Faint, Very Faint, and Graded. The Faint format includes detector coordinates, arrival time and event amplitudes. This carries

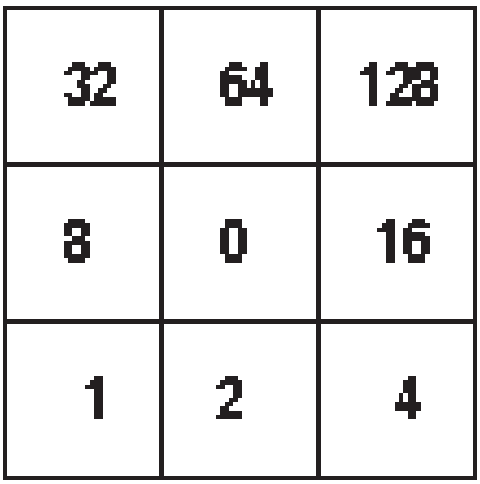

(a)

ACIS Grades	*ASCA* Grade	Description
0	0	Single pixel events
64 65 68 69	2	Vertical Split Up
2 34 130 162	2	Vertical Split Down
16 17 48 49	4	Horizontal Split Right
8 12 136 140	3	Horizontal Split Left
72 76 104 108	6	"L" & Quad, upper left
10 11 138 139	6	"L" & Quad, down left
18 22 50 54	6	"L" & Quad, down right
80 81 208 209	6	"L" & Quad, up right
1 4 5 32 128	1	Diagonal Split
33 36 37 129	1	
132 133 160 161	1	
164 165	1	
3 6 9 20 40	5	"L"-shaped split with corners
96 144 192 13 21	5	
35 38 44 52 53	5	
97 100 101 131	5	
134 137 141 145	5	
163 166 168 172	5	
176 177 193 196	5	
197	5	
24	7	3-pixel horizontal split
66	7	3-pixel vertical split
255	7	All pixels
All other grades	7	

(b)

Figure 3.8: (a) Concept for determining the grade of an event. (b) ACIS and ASCA Grades (*Chandra* Proposers' Observatory Guide 2010).

pulse height values of 3×3 pixels around the event pixel. The Very Faint format includes detector coordinates, arrival time, and pulse height of all events. This contains pulse height values of 5×5 pixels around the event pixels. A better background rejection is thus possible for the Very Faint mode than the Faint mode. The Graded format includes detector coordinates, arrival time, and event grades, but the pulse height of pixels are not include.

3.2 IRSF/SIRIUS

3.2.1 Telescope — InfraRed Survey Facility (IRSF) 1.4 m Telescope

For NIR imaging observations, we used the Simultaneous Infrared Imager for Unbiased Survey (SIRIUS, Nagashima et al. 1999; Nagayama et al. 2003) on the Infrared Survey Facility (IRSF) 1.4 m telescope (Figure 3.9).

The IRSF is located in the Sutherland observing station of the South African Astronomical Observatory (SAAO), which is about 370 km north-east of Cape Town, South Africa. It is at the latitude 32° 22′ 48″ south and longitude 20° 45′ 38″ east. The altitude is 1761 m, and the average ratio of clear skies is about 50%.

The facility was constructed under an agreement between Nagoya University and the SAAO. Nagoya University provided the telescope and the SIRIUS camera, while the SAAO provided the location, dome, and logistical supports. The IRSF construction was started in 1999, and celebrated the first light in November 2000. One of the main objectives is the NIR surveys in the Southern hemisphere with a depth 2–3 mag deeper than the 2MASS (Two Micron All-Sky Survey; Skrutskie et al. 2006). A comparison of the SIRIUS and the 2MASS camera is shown in Table 3.2.

The IRSF telescope is a 1.4 m classical Cassegrain telescope on an altazimuth mount. The mirror was coated with aluminum. It was made by Nagoya University in collaboration with the Nishimura Telescope Company. The pointing and tracking accuracies are 10″ rms and 0.3″ per 30 s, respectively.

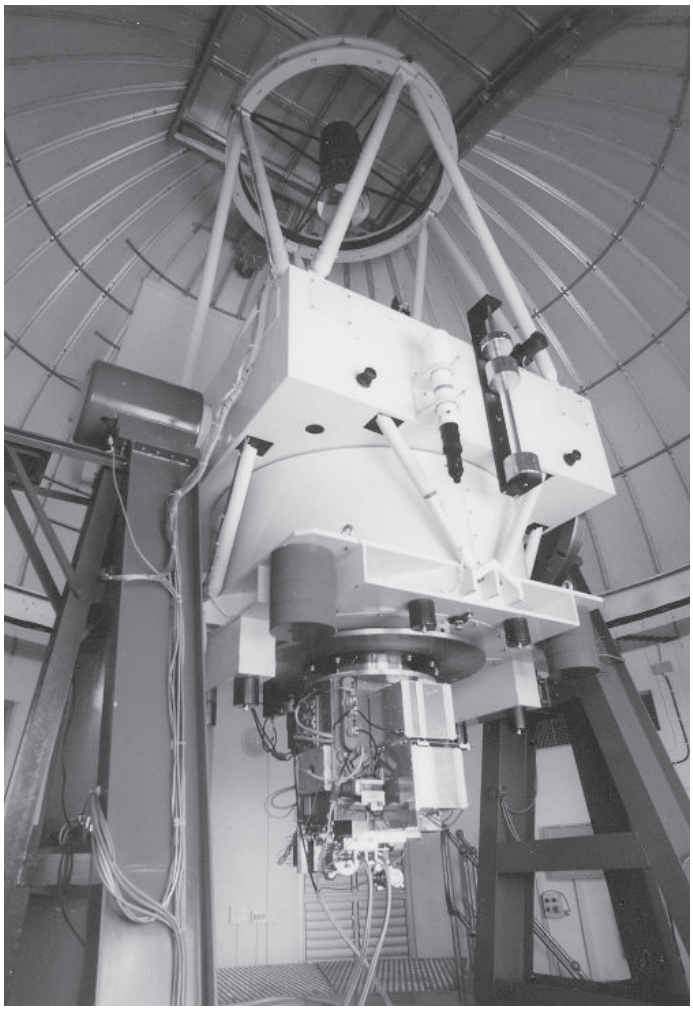

Figure 3.9: IRSF 1.4 m telescope (`http://www.z.phys.nagoya-u.ac.jp/~telescope/`).

Table 3.2: Comparison of SIRIUS and 2MASS.

	SIRIUS	2MASS
Wavelength [μm]	1.25 1.65 2.14	1.25 1.65 2.16
Band	J H $K_{\rm s}$	J H $K_{\rm s}$
Field of view	$7.7' \times 7.7'$	$8.5' \times 8.5'$
Telescope	IRSF1.4 m	Mt. Hopkins 1.3 m
		CTIO[a] 1.3 m

[a] Cerro Tololo Inter-American Observatory.

3.2.2 Instrument — Simultaneous InfraRed Imager for Unbiased Survey (SIRIUS)

The SIRIUS is mounted on the Cassegrain focus of the IRSF telescope, which can obtain J-(1.25 μm), H-(1.65 μm), and K_s-(2.14 μm) band images simultaneously using two dichroic mirrors and three HAWAII arrays (HgCdTe arrays). Each array has a format of 1024 × 1024 pixels with a pixel scale of 0.45″ pixel^{-1}, corresponding to a 7.7′×7.7′ field of view. The pixel scale matches with the on-axis spatial resolution of *Chandra*. The specification of the SIRIUS is shown in Figure 3.10 (a). The 5σ limiting magnitude of the SIRIUS is 20.6 (J), 19.4 (H), and 19.1 (K_s) magnitude, respectively with a 15 minute exposure and a seeing of 1.0″.

detectors	three 1024 × 1024 HgCdTe (HAWAII) science-grade arrays
wavelengths	J, H, Ks broad-band filters ("Filter consortium" standard)
pixel scale	0.45 arcsec/pixel
field of view	7.8 arcmin/frame
limiting mag.*	Ks=19.1, H=19.4, J=20.6
survey efficiency	~ 1 degree^2 / 6 nights

*900sec, 5 σ

(a)

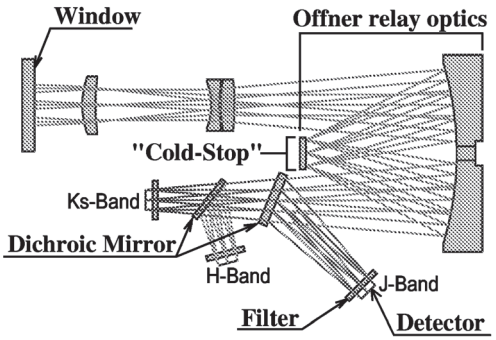

(b)

Figure 3.10: (a) Specification of SIRIUS. (b) Optical layout of SIRIUS (Nagashima et al. 1999).

The optical layout of SIRIUS is shown in Figure 3.10 (b). Using a cold stop, we can avoid radiations from the telescope and the sky. The transmission rate of each bandpass filter is shown in Figure 3.11. The readout noise is less than 15 e ADU^{-1}.

The detector is operated at 60 K. The detectors and optical components are cooled with a Gifford-McMahon (GM) cycle refrigerator. The optical bench temperature is kept at ∼100 K.

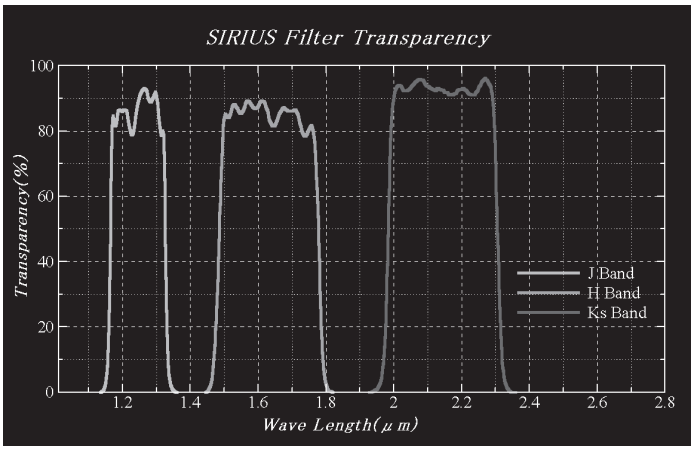

Figure 3.11: Transmission rate of the J-, H-, and K_s-band filters (`http://www.z.phys.nagoya-u.ac.jp/~sirius/tech/index.html`).

3.3 Subaru/MOIRCS

3.3.1 Telescope — Subaru

The Subaru telescope is at the summit of Mauna Kea, Hawai. The altitude is 4139 m. The primary mirror has a diameter of 8.2 m and a focal length of 15 m. It achieved the first light in 1999, and it has been operated by the National Astronomical Observatory in Japan (NAOJ).

The telescope is altazimuth with four foci: the prime focus, the Cassegrain focus, and the optical and the infrared Nasmyth foci (Figure 3.12 a). The Subaru Prime Focus Camera (Suprime-Cam; Miyazaki et al. 2002) is mounted at the prime focus. At the Cassegrain focus, one of the four instruments is installed: Multi-Object Infrared Camera and Spectrograph (MOIRCS; Ichikawa et al. 2006), Faint Object Camera And Spectrograph (FOCAS; Kashikawa et al. 2002), Cooled Mid-Infrared Camera and Spectrograph (COMICS; Kataza et al. 2000), and Fiber Multi Object Spectrograph (FMOS; Kimura et al. 2010). High Dispersion Spectrograph (HDS; Noguchi et al. 2002) and the Infrared Camera and Spectrograph (IRCS; Tokunaga et al. 1998) are installed at the optical and the infrared Nasmyth foci, respectively (Figure 3.12 b).

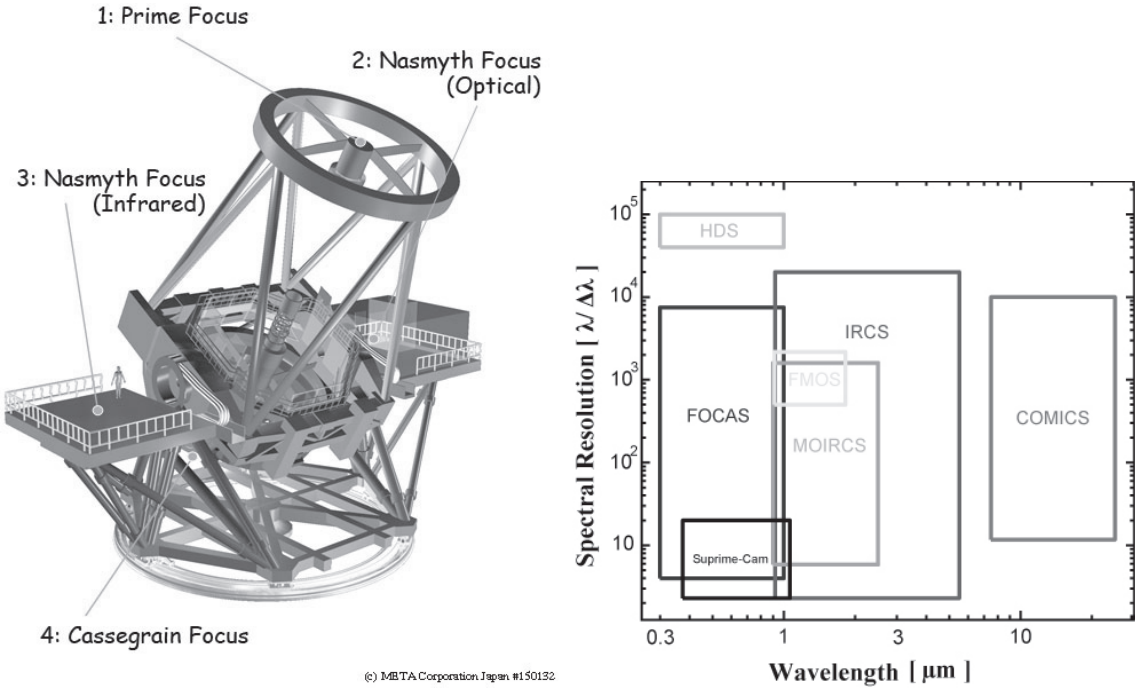

(a) (b)

Figure 3.12: (a) Schematic view of the Subaru telescope. MOIRCS is mounted on the Cassegrain focus. (b) Plot of wavelength versus the spectral resolution of each instrument (`http://www.naoj.org/Observing/Telescope/index.html`).

3.3.2 Instrument—Multi-Object InfraRed Camera and Spectrograph (MOIRCS)

The MOIRCS (Ichikawa et al. 2006; Suzuki et al. 2008) is a wide-field imager and a multi-object spectrometer in the 0.8–2.5 μm band. It has been constructed by the Institute of Astronomy, Tohoku University and the NAOJ. The design started in 1999 and the first light was achieved in September 2004. The schematic structure is shown in Figure 3.13 (b). The MOIRCS provides a $4' \times 7'$ field of view with HAWAII arrays with a format of 2048 $\times$ 2048 pixels with a pixel scale of $0.117''$ pixel^{-1}. In the multi-object spectroscopy mode, we can conduct spectroscopy of multiple objects at a time using exchangeable masks that are custom-made for each observing field. Users can choose a slit of a resolution of low (R $\sim$500), medium (R $\sim$1300), and high (R $\sim$3000). The 5σ limiting magnitude of the MOIRCS are $J\sim$ 23.8, $H\sim$ 22.7, and $K_{\rm s}\sim$ 22.7 magnitude with one hour exposure time and with a $1''$ aperture under typical seeing conditions.

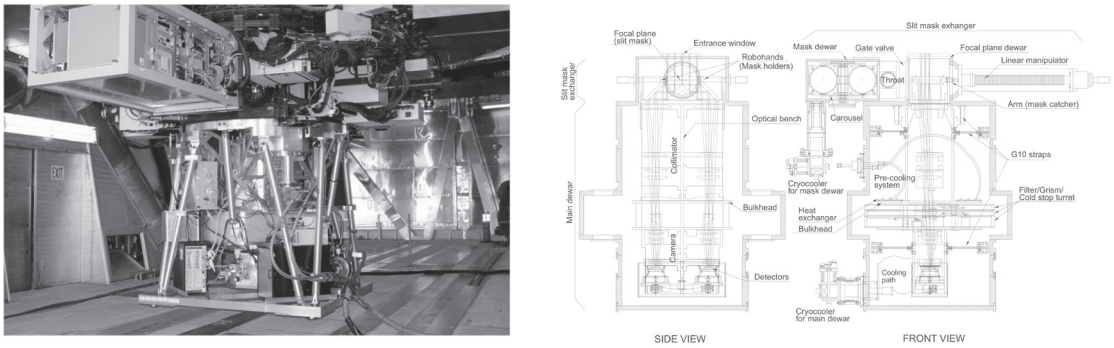

(a) (b)

Figure 3.13: (a) Picture of the MOIRCS. (b) Schematic view of the MOIRCS (Ichikawa et al. 2006).

Chapter 4

Observations and Data Reduction

In this chapter, we describe X-ray and NIR observations and their data reduction.

Contents

4.1 X-ray Imaging and Spectroscopy

In order to investigate X-ray source populations in the GP in detail, we focus on two fields: the Revnivtsev field (l = 0.°1, b=−1.°4; Revnivtsev et al. 2009) and the Ebisawa field (l = 28.°5, b = 0.°0; Ebisawa et al. 2005). This is because these fields have been observed with a very long exposure time with *Chandra* (∼900 ks for the former and ∼200 ks for the latter). The results of the Ebisawa field is published in Ebisawa et al. (2005). Those of the Revnivtsev field have been published only for its central region to achieve the lowest detection limit (Revnivtsev et al. 2009). On the other hand, it is important for us to detect as many as NIR counterparts. We therefore analyze the entire region of the Revnivtsev field in this thesis.

4.1.1 Observations

We retrieved all the archived data of the Revnivtsev field taken with the *Chandra*/ACIS-I array. The observations were carried out from 2008 May to 2008 August with a total integration time of ∼900 ks. The CCDs were operated with a frame time of 3.2 s and the data were down-linked with the Very Faint telemetry mode. Their basic information (observation ID, date, coordinate, exposure time, and roll angle) are shown in Table 4.1. Figure 4.1 shows the combined ACIS-I images of the study field. Throughout this thesis, we used events in the 0.5–8 keV band.

4.1.2 Data Reduction

We retrieved pipeline products and reduced the data sets using the *Chandra* Interactive Analysis of Observations (CIAO) software package version 4.2. We used the level2 event files reprocessed at the *Chandra* X-ray Center (CXC). In the pipeline process, a background events by cosmic-rays were removed based on event grades (only *ASCA* grades 0, 2, 3, 4, and 6) and filtering of good time intervals and energy band was applied. We merged the ten event files into one.

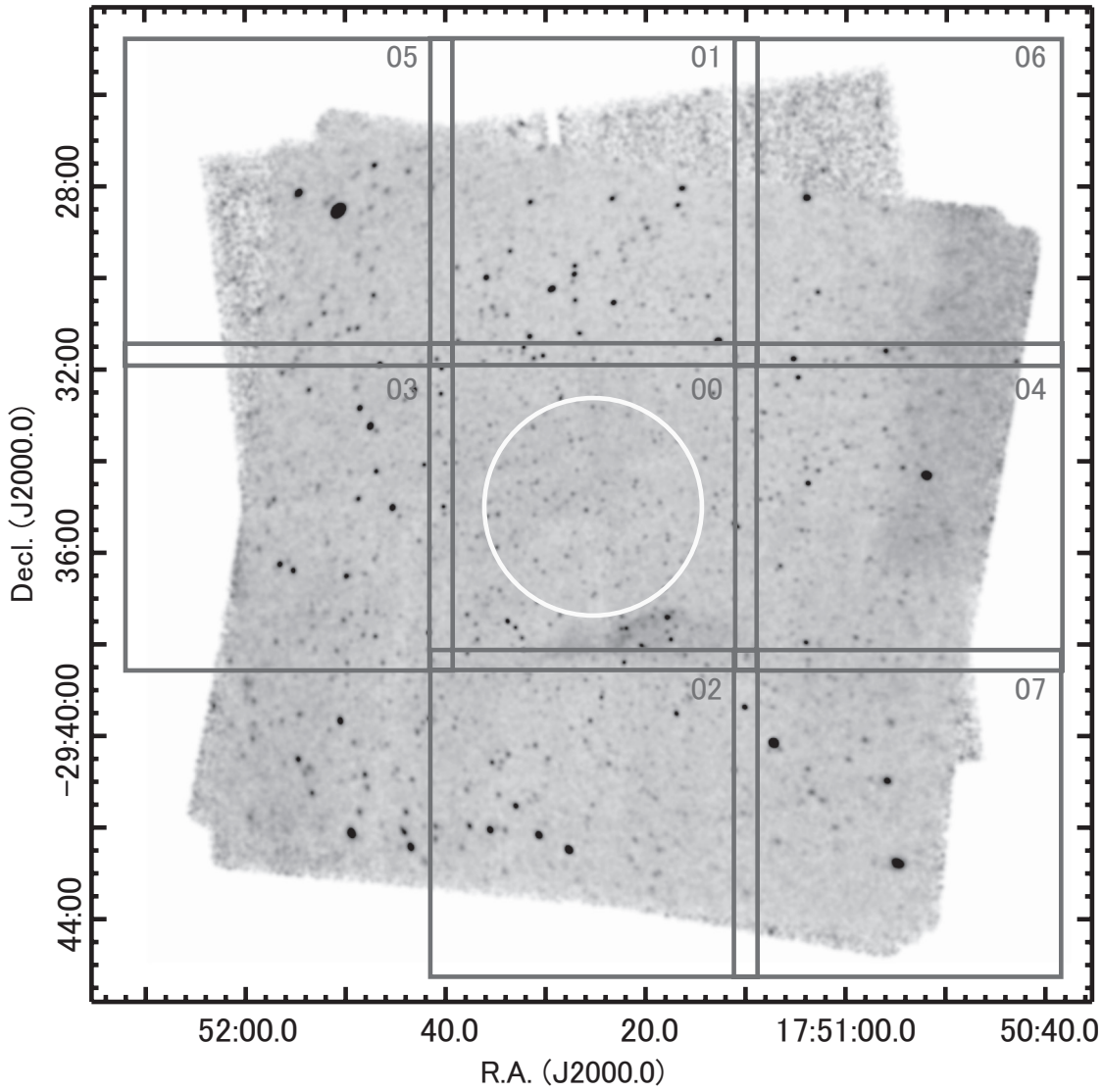

Figure 4.1: Smoothed and exposure-corrected X-ray image of the study field (0.5–8.0 keV). The field of view of the SIRIUS (NIR) observations are shown by squares with region numbers (see Table 4.2 in detail.) The white circle shows the region, the result of which was published in Revnivtsev et al. (2009).

Table 4.1: X-ray Observation Log

ObsID	Date	Coordinate (J2000.0)		$t_{\rm exp}$[a]	Roll
		R.A.	Decl.	(ks)	(degree)
9500	2008-07-20	17:54:38.5	−29:35:47	162.56	279.99
9501	2008-07-23	17:54:39.1	−29:35:53	131.01	278.91
9502	2008-07-17	17:54:39.8	−29:35:58	164.12	281.16
9503	2008-07-28	17:54:40.2	−29:36:60	102.31	275.21
9504	2008-08-02	17:54:40.8	−29:36:12	125.42	275.21
9505	2008-05-07	17:54:37.5	−29:34:47	10.72	82.22
9854	2008-07-27	17:54:41.5	−29:36:17	22.78	277.72
9855	2008-05-08	17:54:37.5	−29:34:47	55.94	82.22
9892	2008-07-31	17:54:40.2	−29:36:60	65.79	275.21
9893	2008-08-01	17:54:40.8	−29:36:12	42.16	275.21

[a] Exposure time.

4.2 NIR Imaging

4.2.1 Observations

X-ray sources in the Ebisawa field were correlated with NIR sources (Ebisawa et al. 2005). On the other hand, NIR imaging observation deeper than all sky surveys has not been available yet in the Revnivtsev field. We thus carried out NIR three-color simultaneous observation (J, H, and $K_{\rm s}$ band) in the Revnivtsev field with SIRIUS to identify those X-ray point sources.

We divided the *Chandra* field of view (FoV) into nine SIRIUS FoVs (Figure 4.1) and observed eight of them up to several times in three runs in 2009 July, 2010 February, and 2010 September. The observation information (data label, date, coordinate, exposure time, and air mass) are shown in Table 4.2. Each frame was exposed for 30 s, and sets of 10-dithered frames were taken repeatedly with a dithering amplitude of 15″. We only used data taken in photometric nights with a seeing of less than 1.2″. The typical seeing was 1.8″. We could not obtain NIR data in the bottom left corner of the SIRIUS layout because of the lack of time. In this region, we only have a shallower NIR coverage than the others. However, as the number of X-ray sources in this region is only 2% of the total, this does not make much difference in our results.

Table 4.2: NIR (SIRIUS) Observation Log

Data label	Date	Coordinate (J2000.0)		$t_{\rm exp}$[a] (min)	Air mass (arcsec)
		R.A.	Decl.		
00-a	2009-06-26	17:51:27.1	−29:35:05	60.0	1.08–1.27
00-b	2010-09-01	17:51:27.0	−29:35:05	60.0	1.25–1.33
00-c	2010-09-02	17:51:27.0	−29:35:05	59.5	1.18–1.50
00-d	2010-09-02	17:51:27.0	−29:35:05	60.0	1.01–1.02
00-e	2010-09-03	17:51:27.0	−29:35:05	60.0	1.01–1.01
00-f	2010-09-03	17:51:27.1	−29:35:04	60.0	1.37–1.92
00-g	2010-09-04	17:51:27.0	−29:35:05	59.5	1.34–1.85
00-h	2010-09-04	17:51:27.0	−29:35:05	60.0	1.01–1.01
00-i	2010-09-06	17:51:27.0	−29:35:04	60.0	1.36–1.92
01	2010-09-01	17:51:27.0	−29:27:54	60.0	1.01–1.02
02	2010-09-01	17:51:27.0	−29:42:18	60.0	1.17–1.49
03	2010-09-02	17:52:00.0	−29:35:05	60.0	1.01–1.11
04	2010-09-02	17:50:54.0	−29:35:05	60.0	1.11–1.34
05	2010-09-03	17:52:00.0	−29:27:54	59.0	1.11–1.33
06	2010-09-03	17:50:54.1	−29:27:55	60.0	1.01–1.11
07	2010-09-04	17:50:54.1	−29:42:18	60.0	1.11–1.35

[a] Exposure time.

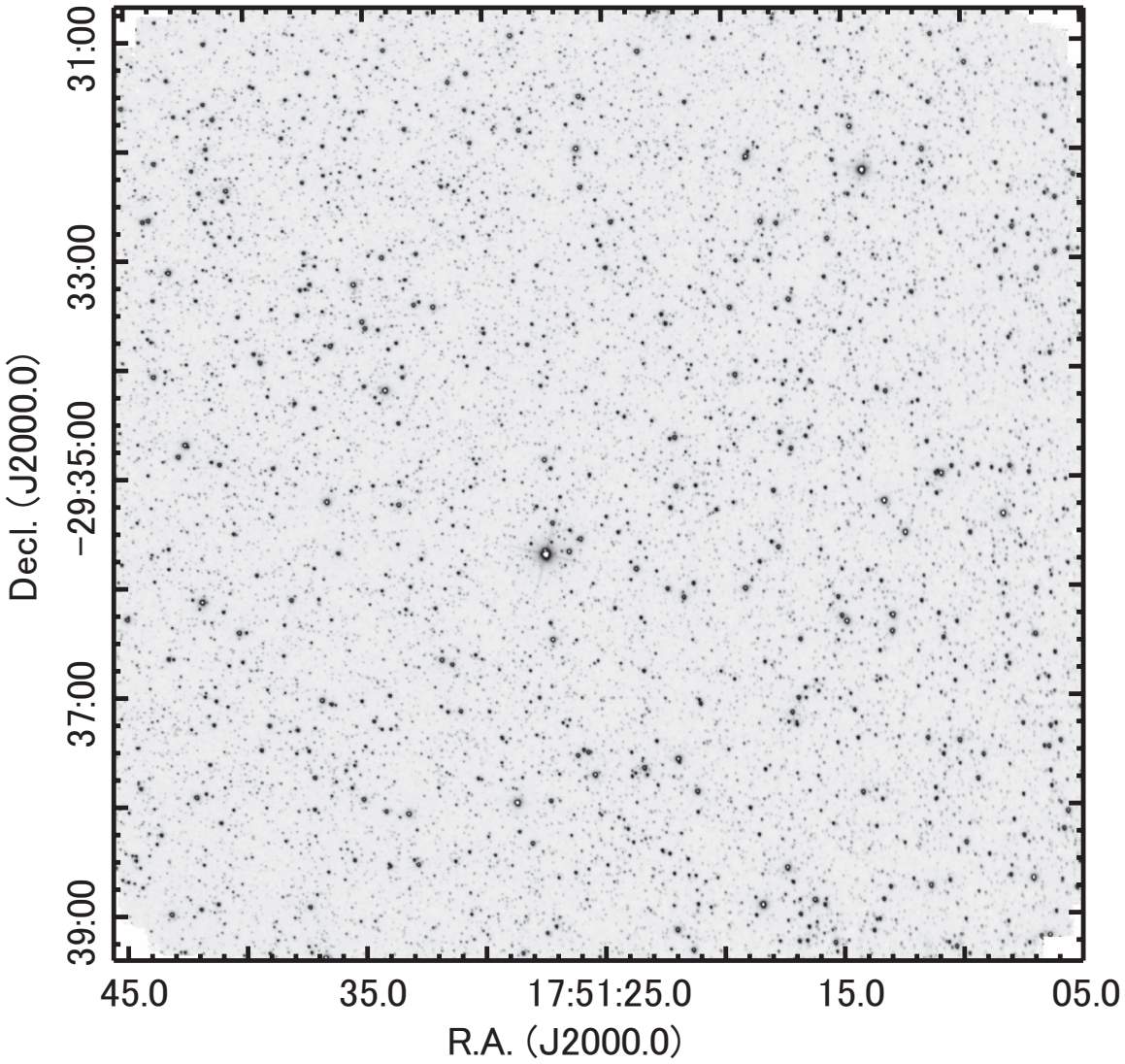

Figure 4.2: Sample SIRIUS K_s-band image of the data 00-a.

4.2.2 Data Reduction

Using the SIRIUS pipeline version sirius09[1] developed for the Imaging Reduction and Analysis Facility (IRAF) software package, we processed all the SIRIUS data sets by applying the standard procedures, including dark frame subtraction, flat fielding, and median-sky subtraction. The flat-field images were constructed from twilight skies. Finally, the dithered frames of each region were merged into one separately for the J, H, and $K_{\rm s}$ bands. Figure 4.2 shows the $K_{\rm s}$-band image of the data 00-a as an example.

4.3 NIR Spectroscopy

We conducted NIR spectroscopy observations for some selected objects in both the Revnivtsev field and the Ebisawa field with Subaru/MOIRCS.

4.3.1 Target Selection

We have nearly 150 X-ray sources identified in the NIR in both the Revnivtsev and Ebisawa fields, which are potential targets of the NIR spectroscopy. Even with the high efficiency of multi-object spectroscopy, we cannot obtain spectra for all of them. Also, in the multi-object spectroscopy using masks, we cannot select arbitrary sets of targets in a mask. Indeed, we need a careful selection of targets so that all of them are within a detector field of view and no two sources have overlapping dispersed spectra. We thus prioritized the NIR-identified X-ray sources to select the targets of our NIR spectroscopy observations.

As our interest is in the point sources contributing to the hard band emission of the GRXE, we biased toward hard X-ray sources. Some assumed populations (active binaries) are characterized by the presence of X-ray flux variability such as flares, so we added the variability information for prioritization in the observations of the Revnivtsev field, which took place after the observations of the Ebisawa were finished. We designed the mask patterns to include the largest possible number of hard (and variable for the Revnvtsev field) X-ray sources and then filled in the remaining part of the mask with low priority, soft sources. These soft sources serve as a comparison data set.

[1]See http://www.z.phys.nagoya-u.ac.jp/nakajima/sirius/software/software.html for detail

Revnivtsev Field

We found 222 NIR identified X-ray sources in the Revnivtsev field (See § 5.2). From them, we selected 52 sources for spectroscopy in K_s band. The sources were selected based on the X-ray hardness as well as the X-ray flux variability. We used the Median Energy (ME) for the X-ray hardness (details are shown in § 5.1). We defined the ME as background-corrected median photon energy in 0.5–8 keV. We separated X-ray sources into three hardness ranges: (1) hard (ME $\geq$ 2.3 keV), (2) medium (1.5 keV $\leq$ ME $<$ 2.3 keV), and (3) soft (ME $<$ 1.5 keV). For X-ray flux variability (see § 5.1 in detail), we performed the Kolmogorov-Smirnov test for all X-ray source light curves and classified them into three groups: (a) non variable (the probability of the null hypothesis of being a constant flux $\geq$ 0.05), (b) marginally variable (0.005 $<$ the probability of the null hypothesis $<$0.05), and (c) variable (the probability of the null hypothesis $\leq$ 0.005). Based on these two quantities, we prioritized in the target source list (Table 4.3).

Table 4.3: Source Priority in the Revnivtsev field

Priority	Conditions
1	(1) hard and (c) variable
2	(1) hard and (b) marginally variable, (2) medium, and (c) variable
3	(1) hard and (a) nonvariable, (2) medium and (b) marginally variable, and (3)soft and (c)variable
4	Others

As a result, we selected 23 sources that satisfied the conditions above with a separation between X-ray and NIR sources below $<$1.1″ (Table 4.4). These sources are considered X-ray and NIR counterpart sources (details in § 5.2). In addition, we selected 28 sources with relaxed conditions, which have a separation to the closest X-ray counterpart from 1.1″ to 2.0″. These sources satisfied at least one condition of Table 4.4. Table 4.5 shows the list of the additional 28 sources.

Table 4.4: Target sources in the Revnivtsev field

ID[1]	Position (J2000.0)		K_s[2]	Flux variability[3]	Median
	R. A.	Decl.			Energy
	(deg)	(deg)	(mag)		(keV)
464	267.81160	−29.50197	9.78	b	1.3
500	267.81786	−29.54719	13.45	b	4.1
505	267.81805	−29.57942	13.99	b	2.2
532	267.82113	−29.68663	13.51	b	1.9
538	267.82172	−29.63984	12.00	a	1.1
599	267.82738	−29.50417	11.06	c	1.7
631	267.83006	−29.65494	13.32	a	1.3
647	267.83166	−29.54233	13.90	b	1.1
874	267.85251	−29.49210	12.32	b	2.1
997	267.86679	−29.58130	13.51	a	1.2
1000	267.86726	−29.61758	10.92	a	1.1
1151	267.88242	−29.56410	12.72	b	1.9
1299	267.89563	−29.54132	14.92	c	1.6
1399	267.90693	−29.55152	11.53	a	1.1
1424	267.90987	−29.62817	13.11	a	1.6
1456	267.91221	−29.59669	14.08	b	1.1
1494	267.91565	−29.59643	14.73	a	1.1
1495	267.91571	−29.61957	13.25	a	1.1
1577	267.92534	−29.59347	13.12	b	2.1
1667	267.93675	−29.61987	13.01	c	1.7
1706	267.94245	−29.54876	13.81	a	1.1
1729	267.94483	−29.56681	13.53	b	1.1
1774	267.95390	−29.56919	12.49	b	1.7

[1]Source number in Table A.1.

[2]NIR magunitude by SIRIUS and 2MASS.

[3]Source variability of Table A.1.

Table 4.5: Target source list in relaxed conditions in the Revnivtsev field

ID[1]	Position (J2000.0)		K_s[2]	Flux variability[3]	Median
	R. A.	Decl.			Energy
	(deg)	(deg)	(mag)		(keV)
311	267.78829	−29.66079	11.70	a	2.6
350	267.79477	−29.69453	11.84	b	1.7
357	267.79567	−29.52500	12.77	a	2.6
397	267.80199	−29.51229	13.24	b	1.6
421	267.80567	−29.49183	13.87	b	2.9
452	267.80922	−29.63941	14.19	b	1.7
461	267.81168	−29.64702	12.95	c	3.0
553	267.82278	−29.55812	14.34	a	2.6
564	267.82364	−29.57847	11.84	c	1.8
640	267.83046	−29.60208	12.44	a	2.6
661	267.83300	−29.72787	12.30	c	1.3
684	267.83490	−29.64442	10.54	c	2.7
700	267.83710	−29.47912	13.61	c	2.4
758	267.84190	−29.66176	12.73	a	2.0
782	267.84399	−29.71494	13.27	a	3.1
786	267.84508	−29.67205	12.44	b	1.6
974	267.86452	−29.56408	11.36	c	1.2
1023	267.86947	−29.60903	12.73	c	1.4
1039	267.87128	−29.57880	12.47	c	2.8
1053	267.87252	−29.62947	10.84	a	2.0
1277	267.89382	−29.60241	13.83	a	3.5
1339	267.90147	−29.53818	13.08	c	1.9
1349	267.90122	−29.62964	11.83	b	2.0
1493	267.91594	−29.55509	11.65	b	1.7
1560	267.92314	−29.57608	12.62	c	1.6
1571	267.92382	−29.53683	13.02	c	2.0
1690	267.94001	−29.59841	13.09	a	2.9
1745	267.94807	−29.55173	12.54	b	1.9

[1]Source number in Table A.1.

[2]NIR magunitude by SIRIUS and 2MASS.

[3]Source variability of Table A.1.

Ebisawa Field

There are 142 NIR identified X-ray sources in the Ebisawa field (Ebisawa et al. 2005). In Ebisawa et al. (2005), X-ray sources were classified into three based on Hardness Ratio (HR). The X-ray spectral hardness is defined as HR ≡ (H-S)/(H+S), where H is the count rate in the hard band (2–8 keV) and S is the count rate in the soft band (0.5–2 keV). The sources were grouped into (1) hard (HR $\geq$ 0.1), (2) medium ($-0.6 <$ HR < 0.1), and (3) soft (HR ≤ -0.6). We selected targets for NIR spectroscopy so that the sources cover a wide range

of X-ray spectral hardness. Based on these groups, we selected 98 X-ray sources for NIR spectroscopy (Table 4.6).

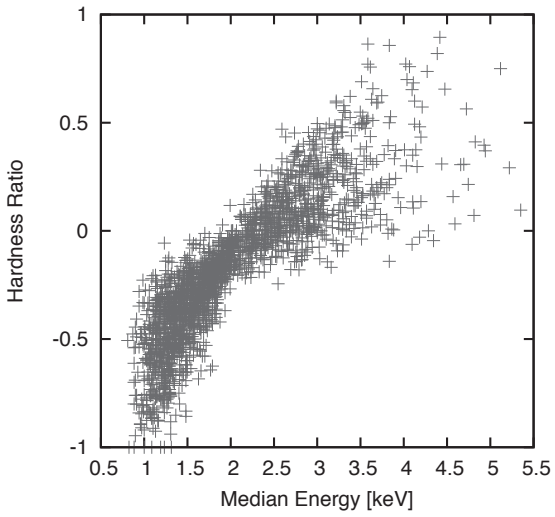

Figure 4.3: The relation between ME and HR in the Revnivtsev field. We used 2–8 keV and 0.5–2 keV as the hard band range and soft band range.

Since the observation in the Ebisawa field were carried out in the beginning of this study, we selected target sources only based on the X-ray hardness. Figure 4.3 shows the relation between ME and HR. For example, ME = 2.3 corresponds to HR$\sim$0.1.

Table 4.6: Target Sources in the Ebisawa field

ID[1]	Position		Hardness	F_x	Separation	J[2]	H[2]	K_s[2]
	R. A.	Decl.	$(H-S)/(H+S)$	0.5–2 keV/2–10 keV				
	(J2000.0)			(ergs s^{-1} cm^{-2})	(arcsec)	(mag)	(mag)	(mag)
21	18:43:13.77	−03:57:07.4	−0.99±0.11	6e−16/2e−16	0.28	13.66	13.07	12.73
29	18:43:17.43	−03:56:00.2	−0.16±0.30	1e−16/4e−15	0.90	12.48	12.10	11.96
30	18:43:17.43	−03:57:32.7	−0.92±0.11	5e−16/2e−16	0.13	16.54	15.25	15.13
35	18:43:18.59	−03:58:52.1	−1.00±0.11	5e−16/2e−16	0.36	15.86	15.08	14.77
36	18:43:18.73	−03:54:25.2	−0.20±0.31	7e−17/2e−15	0.22	17.07	16.20	–
37	18:43:18.95	−03:53:27.3	−0.81±0.21	4e−16/2e−16	0.74	14.98	14.42	14.24
39	18:43:19.22	−03:57:31.9	−0.74±0.21	3e−16/1e−15	0.73	15.24	–	–
41	18:43:19.61	−03:55:02.1	−0.93±0.22	2e−16/9e−17	0.81	16.44	15.53	–
46	18:43:21.11	−03:54:30.0	0.69±0.26	6e−18/5e−15	0.21	–	14.60	–
47	18:43:21.22	−03:49:31.2	−0.76±0.10	1e−15/4e−15	0.97	14.74	13.87	12.85
50	18:43:21.76	−04:00:39.6	−0.94±0.12	6e−16/3e−16	0.73	14.88	14.24	13.93
51	18:43:21.81	−03:53:03.3	−0.77±0.17	4e−16/2e−15	0.24	13.94	13.49	13.29
52	18:43:22.09	−03:54:26.4	−0.83±0.17	6e−16/3e−16	0.34	16.20	15.28	15.33
54	18:43:22.98	−03:57:53.0	−0.89±0.11	6e−16/2e−16	0.47	13.92	13.48	13.25
55	18:43:23.03	−03:57:25.3	−0.63±0.27	3e−16/1e−15	0.66	17.0	15.77	15.17
56	18:43:23.30	−03:48:51.7	−1.00±0.03	3e−15/1e−15	0.47	14.78	14.09	13.81
58	18:43:23.62	−03:53:14.1	−0.39±0.30	3e−16/1e−15	0.13	15.57	14.57	14.38
59	18:43:23.68	−03:51:40.6	−0.86±0.19	5e−16/2e−16	0.09	15.71	14.97	14.69
62	18:43:23.96	−03:57:58.9	−0.38±0.15	9e−16/4e−15	0.65	16.87	15.96	15.31
64	18:43:24.47	−03:53:49.8	−0.67±0.07	2e−15/9e−15	0.05	13.72	12.64	12.21
67	18:43:25.25	−03:59:15.3	−0.55±0.19	6e−16/2e−15	0.55	15.96	15.23	14.88
68	18:43:26.14	−03:56:49.7	−0.51±0.18	7e−16/3e−15	0.42	16.51	15.61	15.21
72	18:43:28.67	−03:56:22.8	−0.62±0.30	2e−16/7e−16	0.27	17.29	14.81	14.70
73	18:43:28.91	−03:57:33.3	−0.78±0.14	5e−16/2e−15	0.04	14.41	13.50	13.16
74	18:43:29.11	−03:59:42.3	0.26±0.27	8e−17/2e−15	0.69	17.85	15.39	15.76
79	18:43:29.70	−03:50:15.1	0.71±0.17	1e−17/8e−15	0.30	–	12.90	–
80	18:43:30.20	−03:51:18.2	−0.70±0.28	3e−16/1e−15	–	–	–	–
81	18:43:30.21	−03:53:44.3	−0.90±0.19	3e−16/1e−16	0.33	15.37	14.73	14.50
82	18:43:30.27	−03:54:11.4	−0.60±0.08	4e−15/1e−14	0.39	13.11	12.07	11.67
84	18:43:30.52	−04:03:50.3	−0.53±0.17	7e−16/3e−15	-	–	–	–
85	18:43:30.63	−03:53:52.0	−1.00±0.18	3e−16/1e−16	0.29	11.93	11.26	11.00
86	18:43:30.75	−04:01:02.5	−0.97±0.03	2e−15/9e−16	0.41	9.67	9.40	9.27
87	18:43:30.80	−04:00:45.9	−1.00±0.13	6e−16/2e−16	0.35	15.51	14.83	–
91	18:43:31.59	−03:56:49.4	−0.62±0.11	5e−16/2e−15	0.18	14.23	13.53	13.30
94	18:43:31.75	−03:51:26.7	−0.53±0.17	6e−16/2e−15	0.55	15.21	14.20	13.41

(*cont.*)

Table 4.6: Target Sources in the Ebisawa field

ID[1]	Position		Hardness	F_x	Separation	J[2]	H[2]	K_s[2]
	R. A.	Decl.	$(H-S)/(H+S)$	0.5–2 keV/2–10 keV				
	(J2000.0)			(ergs s^{-1} cm^{-2})	(arcsec)	(mag)	(mag)	(mag)
98	18:43:32.41	−04:00:50.4	−0.85±0.18	4e−16/2e−16	0.70	15.78	15.04	–
100	18:43:32.58	−04:04:18.7	0.11±0.07	2e−15/5e−14	0.32	15.14	12.55	11.14
104	18:43:33.47	−04:03:54.3	−0.38±0.21	6e−16/3e−15	0.52	11.62	10.71	10.35
105	18:43:33.94	−03:52:53.0	0.77±0.30	4e−18/3e−15	0.08	–	14.89	13.09
106	18:43:34.12	−03:55:23.8	−1.00±0.15	3e−16/1e−16	0.45	15.25	14.47	14.10
107	18:43:34.13	−03:50:47.5	−0.82±0.21	2e−16/9e−17	0.24	16.95	16.15	–
110	18:43:35.33	−04:00:44.7	−0.66±0.13	5e−16/2e−15	0.48	15.61	14.66	14.44
112	18:43:35.41	−03:57:14.8	−0.96±0.19	3e−16/1e−16	0.08	16.42	15.38	14.93
113	18:43:35.45	−04:01:12.7	0.53±0.10	2e−16/5e−15	0.35	16.40	15.69	13.51
114	18:43:35.48	−03:58:46.1	−0.07±0.25	6e−17/2e−15	0.27	14.74	14.01	13.68
116	18:43:35.82	−03:58:54.4	−0.72±0.20	2e−16/6e−16	0.68	14.35	13.66	13.34
119	18:43:36.18	−04:01:54.2	−1.00±0.16	4e−16/2e−16	0.94	16.09	15.59	–
122	18:43:36.74	−03:57:47.9	−0.82±0.11	5e−16/2e−16	0.32	15.52	14.71	14.38
130	18:43:38.63	−03:57:32.7	−0.86±0.14	3e−16/1e−16	0.38	16.06	15.13	14.84
143	18:43:41.02	−03:58:02.3	−0.80±0.18	4e−16/1e−15	0.27	12.20	11.18	10.73
148	18:43:42.37	−03:55:07.4	−0.91±0.15	3e−16/1e−16	0.24	17.84	16.60	16.11
149	18:43:42.57	−03:59:41.1	−0.32±0.17	4e−16/2e−15	0.70	15.46	14.64	14.45
150	18:43:42.73	−03:54:24.7	−0.64±0.17	5e−16/2e−15	0.21	17.76	15.88	15.61
156	18:43:45.35	−03:53:16.7	−0.32±0.24	4e−16/2e−15	0.60	14.67	14.02	13.75
158	18:43:46.06	−03:53:51.8	−0.95±0.12	5e−16/2e−16	0.12	15.75	14.74	14.44
161	18:43:46.43	−03:54:11.6	−1.00±0.15	5e−16/2e−16	0.33	14.21	13.53	13.36
164	18:43:46.72	−03:54:43.5	−0.51±0.29	2e−16/8e−16	0.06	15.42	14.14	13.38
169	18:43:47.11	−03:53:18.3	−0.58±0.15	7e−16/3e−15	0.11	15.65	14.60	14.23
172	18:43:47.63	−03:56:10.3	−0.44±0.12	1e−15/4e−15	0.20	15.70	14.84	14.66
176	18:43:48.67	−04:01:36.1	−0.82±0.05	2e−15/7e−16	0.13	14.42	13.61	13.37
178	18:43:49.03	−03:59:57.1	−0.35±0.12	4e−16/2e−15	0.92	16.55	14.65	13.68
183	18:43:50.42	−04:02:29.5	−1.00±0.22	3e−16/1e−16	0.11	13.87	13.21	12.95
185	18:43:50.67	−03:58:52.1	−0.84±0.24	3e−16/1e−16	0.62	14.97	14.37	14.13
187	18:43:51.09	−03:52:39.1	−0.98±0.02	2e−15/1e−15	0.29	–	10.90	–
188	18:43:51.81	−03:59:22.3	−0.62±0.10	9e−16/4e−15	0.03	14.93	14.01	13.54
190	18:43:52.78	−03:53:59.3	−0.60±0.18	4e−16/2e−15	–	–	–	–
191	18:43:52.78	−04:00:50.1	−0.49±0.13	5e−16/2e−15	0.67	16.39	15.19	14.62
193	18:43:53.11	−03:57:59.8	−0.57±0.14	5e−16/2e−15	0.48	13.47	12.93	12.71
195	18:43:54.18	−03:58:44.0	−0.59±0.18	3e−16/1e−15	0.37	16.28	15.41	15.09
198	18:43:54.65	−03:53:36.5	−0.77±0.16	6e−16/2e−15	0.34	15.67	14.70	14.23

(*cont.*)

Table 4.6: Target Sources in the Ebisawa field

ID[1]	Position		Hardness	F_x	Separation	J[2]	H[2]	K_s[2]
	R. A.	Decl.	$(H-S)/(H+S)$	0.5–2 keV/2–10 keV				
	(J2000.0)			(ergs s^{-1} cm^{-2})	(arcsec)	(mag)	(mag)	(mag)
199	18:43:54.83	−04:07:42.0	−0.88±0.06	2e−15/8e−16	0.42	14.31	13.57	13.32
204	18:43:55.70	−03:52:50.2	0.18±0.15	4e−16/1e−14	0.93	17.37	16.05	15.34
212	18:43:57.68	−03:51:57.1	−0.14±0.19	2e−16/6e−15	0.90	16.90	15.44	14.77
214	18:43:57.87	−04:07:37.7	−0.95±0.05	3e−15/1e−15	0.37	12.82	12.12	11.95
217	18:43:58.30	−04:03:21.2	−0.65±0.26	3e−16/1e−15	0.35	16.81	15.44	14.80
221	18:43:59.67	−03:55:18.3	−0.86±0.08	2e−15/7e−16	0.21	9.30	8.93	8.76
223	18:44:00.31	−04:05:59.2	−0.73±0.17	5e−16/2e−15	0.81	13.59	12.37	11.91
226	18:44:02.16	−04:05:23.7	−0.99±0.04	2e−15/7e−16	0.93	14.18	13.41	13.15
233	18:44:03.95	−04:02:57.6	0.32±0.11	6e−16/2e−14	0.43	14.22	13.40	–
235	18:44:05.05	−04:04:36.9	0.03±0.13	7e−16/2e−14	0.80	17.40	15.35	–
237	18:44:05.56	−04:05:39.1	−0.39±0.26	4e−16/2e−15	0.52	14.98	14.31	14.07
238	18:44:05.91	−04:06:12.2	−0.65±0.11	1e−15/5e−15	0.53	16.59	15.28	14.87
246	18:44:11.90	−04:06:30.7	−0.45±0.22	6e−16/2e−15	0.55	–	15.35	13.97
249	18:44:13.72	−04:02:32.8	−0.42±0.32	3e−16/1e−15	–	–	–	–
252	18:44:15.62	−04:03:56.9	0.14±0.24	2e−16/5e−15	0.55	16.96	14.59	13.60
255	18:44:18.54	−04:06:02.5	−0.47±0.16	9e−16/4e−15	0.35	13.54	12.59	12.11
257	18:44:21.60	−04:04:53.2	0.03±0.21	3e−16/1e−14	0.25	–	15.35	14.57
260	18:44:22.61	−04:03:51.0	−0.76±0.09	1e−15/6e−15	0.85	14.80	13.52	13.57
262	18:44:22.67	−04:00:17.4	−0.55±0.15	7e−16/3e−15	0.30	14.36	13.39	12.52
264	18:44:24.09	−03:59:11.9	−0.59±0.09	2e−15/7e−15	0.86	13.59	12.69	12.37
265	18:44:24.24	−04:01:35.1	−0.70±0.16	8e−16/3e−15	0.72	16.00	14.70	13.83
269	18:44:26.71	−04:03:27.3	−0.75±0.10	1e−15/5e−15	–	–	–	–
272	18:44:28.87	−04:01:03.9	−0.20±0.09	8e−16/2e−14	0.60	13.29	11.83	11.11

[1]Source number in Ebisawa et al. (2005).

[2]NIR magunitude by NIR identification in Ebisawa et al. (2005).

4.3.2 Observations

Before spectroscopy observations, we first took pre-images (an exposure time of ∼5 min) of the Revnivtsev field and the Ebisawa field based on positions of target list sources. Based on these pre-images, we made multi-object spectroscopy masks using the Mask Design Program[2]. We arranged target sources to each mask in the order of the source priorities. The slit width of target sources were set to ∼0.8″. Bright stars were used as alignment stars. We created square alignment holes for the alignment stars with a side of ∼3.5″. Figure 4.4 shows four designed masks of the Revnivtsev field. About the Ebisawa field, we did the same method for the mask design.

The observations were performed on 2011 June 23–24 (the Revnivtsev field), and 2007 June 07–10 and 2008 June 27–28 (the Ebisawa field). The visibility plots of the two fields are shown in Figure 4.5. We used the $R \sim 1300$ grism in the K_s-band (2.0–2.3 μm) with a dispersion scale of $\sim$ 3.88 Å pixel^{-1}. We used OH night emission lines for wavelength calibration in the Revivtsev field and Th-Ar lump for the Ebisawa field. Dome flat images were taken for flat-fielding. The atmosphere of the Earth introduces absorption into ground-based NIR spectra, which needs to be corrected. For this telluric correction, we used A0V stars as standard stars because A0V stars do not have any emission and absorption features except for the Brγ absorption in the wavelengths of interestx. In each night, we took standard stars several times, so that one of them has almost the same airmass with the target objects. The observation information (mask ID, date, coordinate, exposure time, number of slits, airmass, seeing) is shown in Table 4.7. In our study, we used the A-B-B-A dithering pattern, in which A and B indicate two different positions along the slits, with different dithering amplitude for each mask in order to avoid having another source at the position B by chance. This is not negligible as our regions are very crowded.

4.3.3 Data Reduction

We reduced all the data taken with MOIRCS using the IRAF software package[3]. We describe two-dimentional data reduction in this subsection and one-dimentional reduction in § 5.3. First, we subtracted a dark frame from each object frame and standard star frame. The dark frames were taken with the same exposure time of each object and standard star frame

[2]See http://subarutelescope.org/Observing/Instruments/MOIRCS/wmdp_moircs.html
[3]http://iraf.noao.edu/

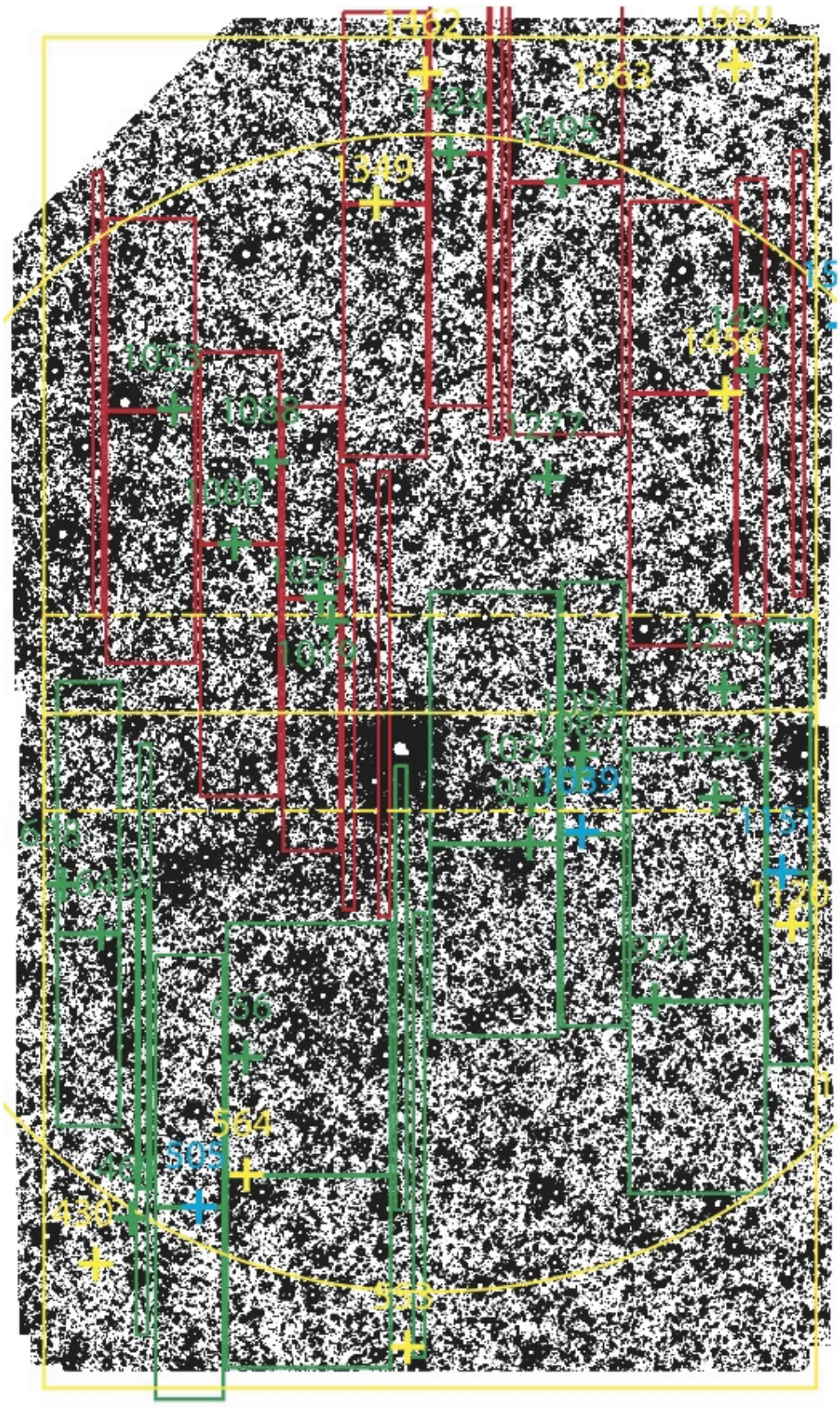

Figure 4.4: Mask designs in R1–R4 (Table 4.7) in the Revnivtsev field. Green and red boxes show slits and their dispersion area in the chip 1 and chip 2, respectively. Cross points indicate target sources and the difference of color shows source priority (Cyan: first priority sources, magenta: second priority sources, green: third priority sources, and yellow: fourth priority sources in Table 4.3). We arranged slits in order to take as many high priority sources as possible.

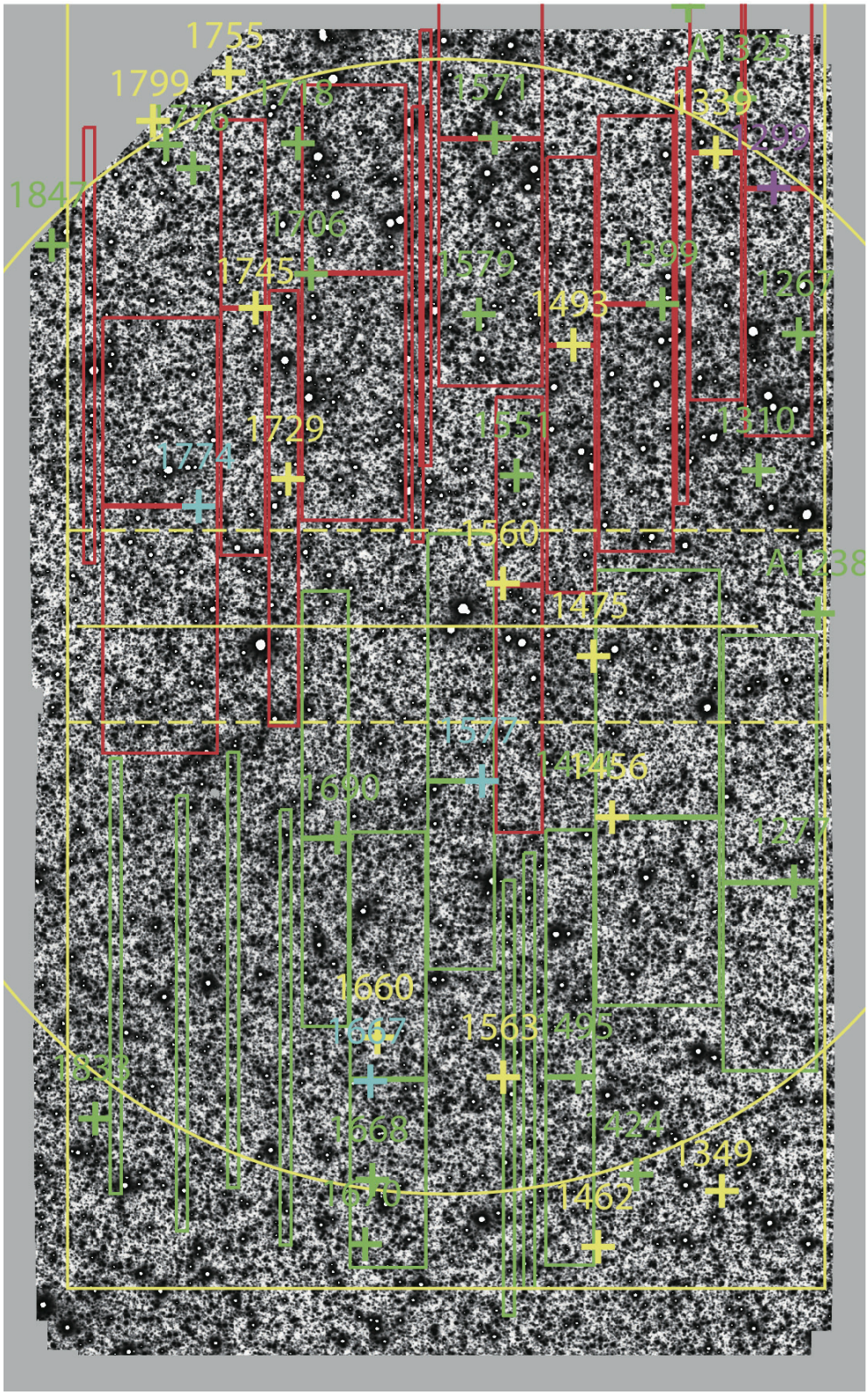

Figure 4.4: *Continued.*

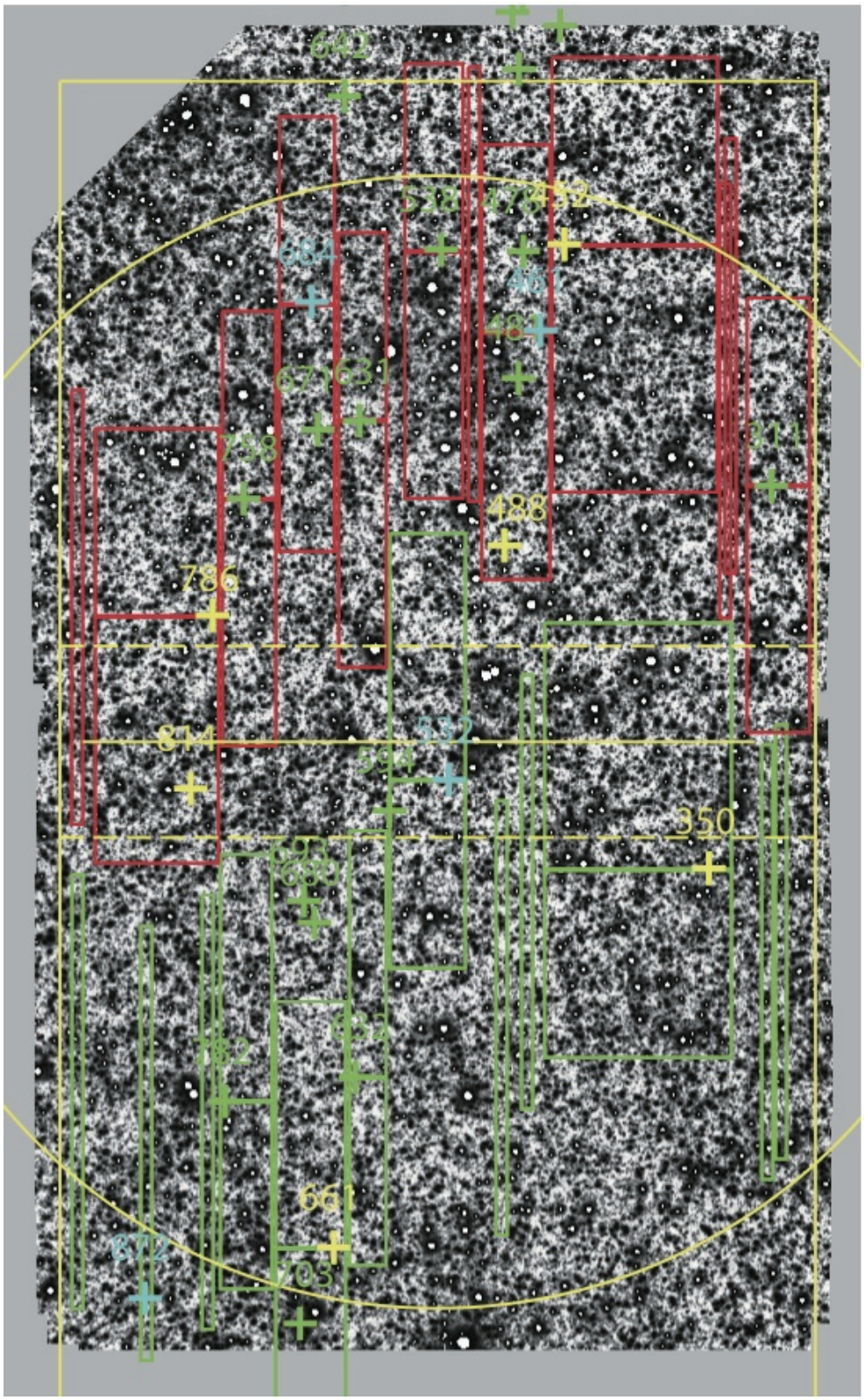

Figure 4.4: *Continued.*

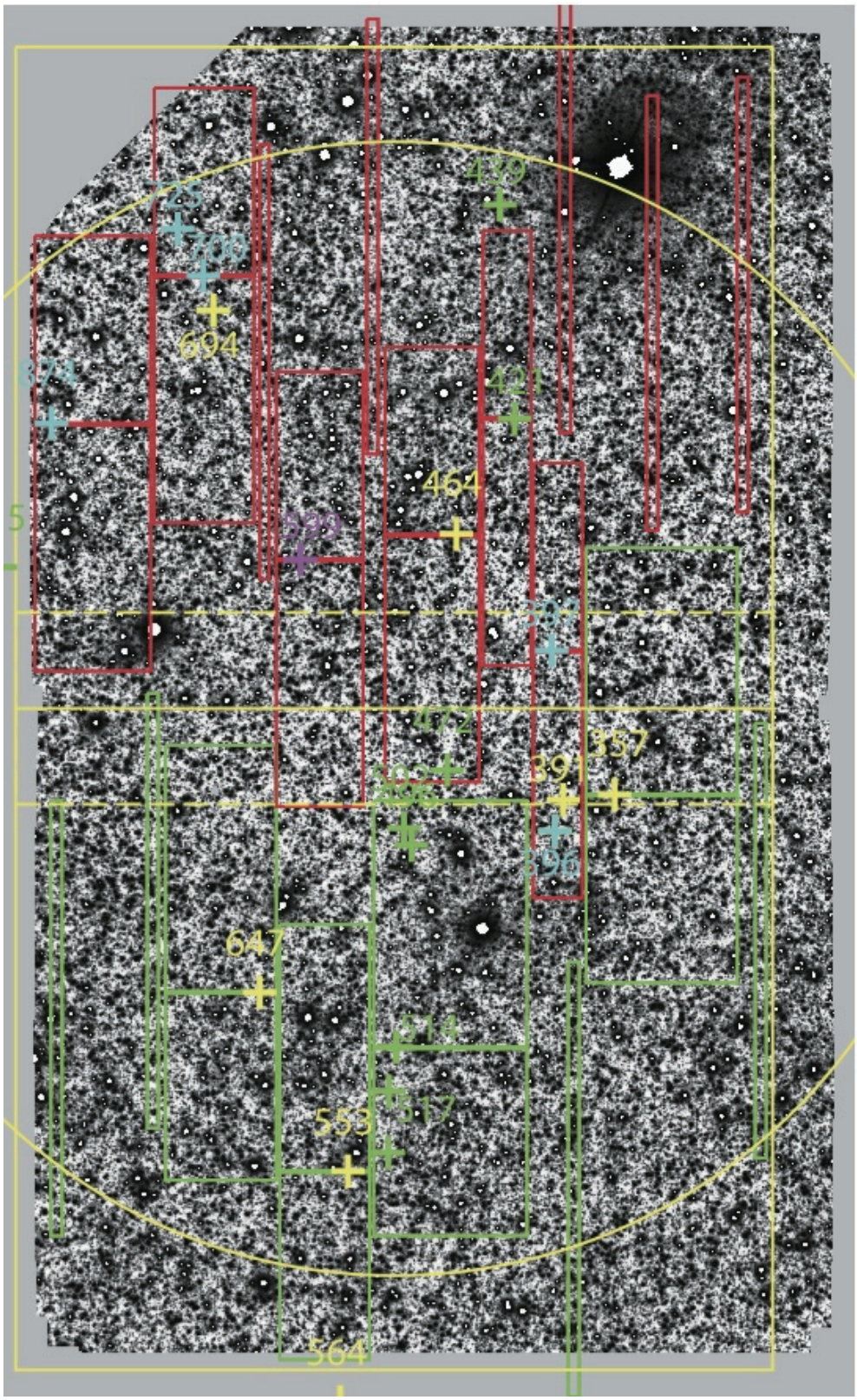

Figure 4.4: *Continued.*

Table 4.7: Subaru observation log

Mask[a] ID	Date	Coordinate (J2000.0)		t_{exp}[b] (s)	Num. of slits	Airmass	Seeing[c] (arcsec)
		R. A.	Decl.				
R1	2011-06-23	17:51:29	−29:35:43	10800	15	1.55–1.97	0.8
R2	2011-06-24	17:51:43	−29:34:47	9900	15	1.63–2.02	1.3
R3	2011-06-23	17:51:17	−29:40:60	8400	13	1.55–1.83	0.7
R4	2011-06-24	17:51:16	−29:31:02	9600	10	1.53–1.85	0.9
E1	2007-06-07	18:42:52	−03:53:29	720	7	1.00–1.62	0.3
E2	2007-06-08	18:47:53	−03:52:01	1440	7	1.09–1.29	0.3
E3	2007-06-08	18:44:24	−04:02:01	1920	14	1.47–1.73	0.5
E4	2007-06-09	18:43:50	−03:53:40	1440	14	1.23–1.88	0.5
E5	2007-06-10	18:43:30	−04:01:26	1080	9	1.09–1.32	0.3
E6	2007-06-10	18:43:45	−03:58:20	1440	11	1.22–1.52	0.7
E7	2007-06-10	18:43:50	−03:53:39	1800	12	1.09–1.14	0.3
E8	2008-06-27	18:43:40	−04:01:48	2700	7	1.21–1.60	0.3
E9	2008-06-27	18:43:25	−03:56:55	2400	11	1.09–1.12	0.4
E10	2008-06-27	18:43:57	−04:01:37	2400	6	1.18–1.49	0.4
E11	2008-06-28	18:43:21	−03:51:41	2700	9	1.21–1.68	0.4
E12	2008-06-28	18:43:51	−03:54:20	2700	9	1.09–1.12	0.5
E13	2008-06-28	18:44:05	−04:06:26	2400	11	1.20–1.59	0.9

[a] "E" shows the Ebisawa field, and "R" shows the Revnivtsev field.
[b] Exposure time.
[c] Average seeing of all images in each mask.

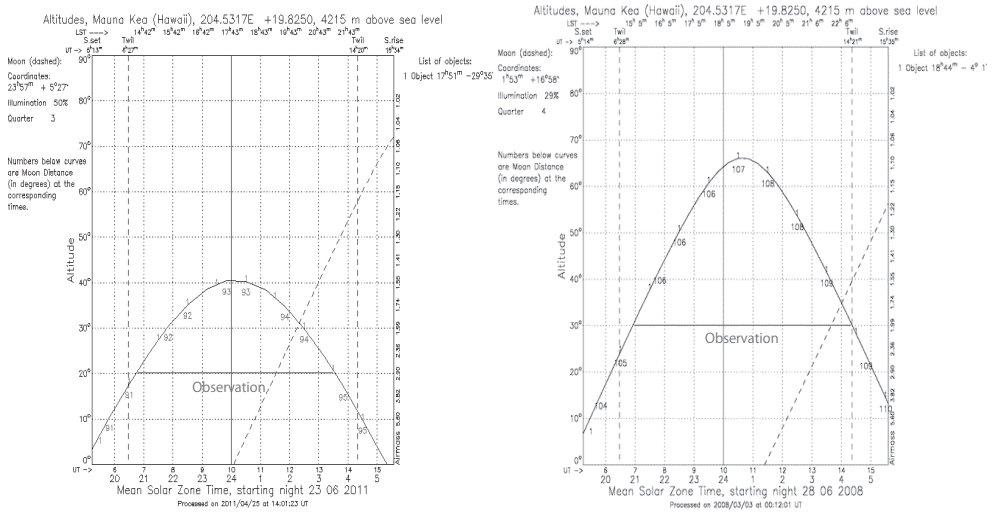

Figure 4.5: Visibility plot in the Revnivtsev field (left) and the Ebisawa field (right). The observations were carried out at an airmass < 2 (solid lines).

(Figure 4.8). The dark frames were taken at the end of each night.

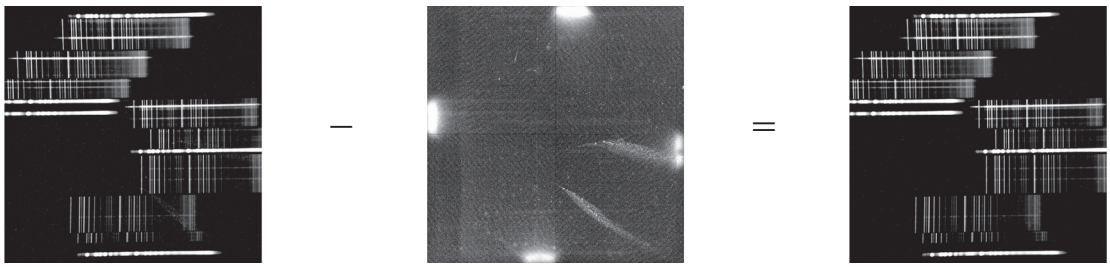

Figure 4.8: Example of a raw data (left), a dark frame (middle), and dark subtracted frame (right) of the mask R1 chip 2.

Second, we conducted flat-fielding using the normalized dome flat frames (Figure 4.9). The flat frames were taken for each mask.

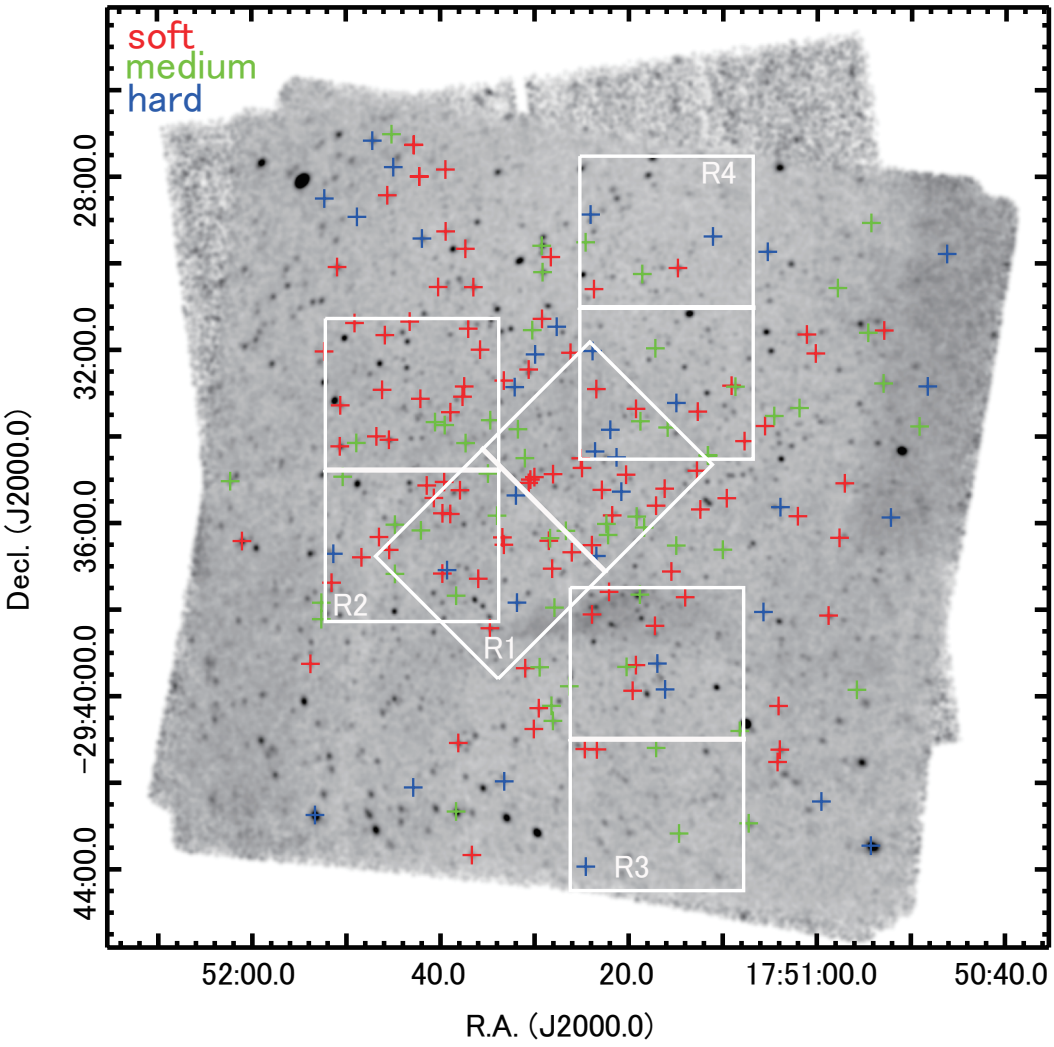

Figure 4.6: MOIRCS mask layout in the Revnivtsev field (white). Each field number corresponds to the mask ID in Table 4.7. The background is a mosaicked and smoothed X-ray image in 0.5–8.0 keV. Red, green, and blue plusses show soft, medium, and hard X-ray sources identified with NIR, respectively.

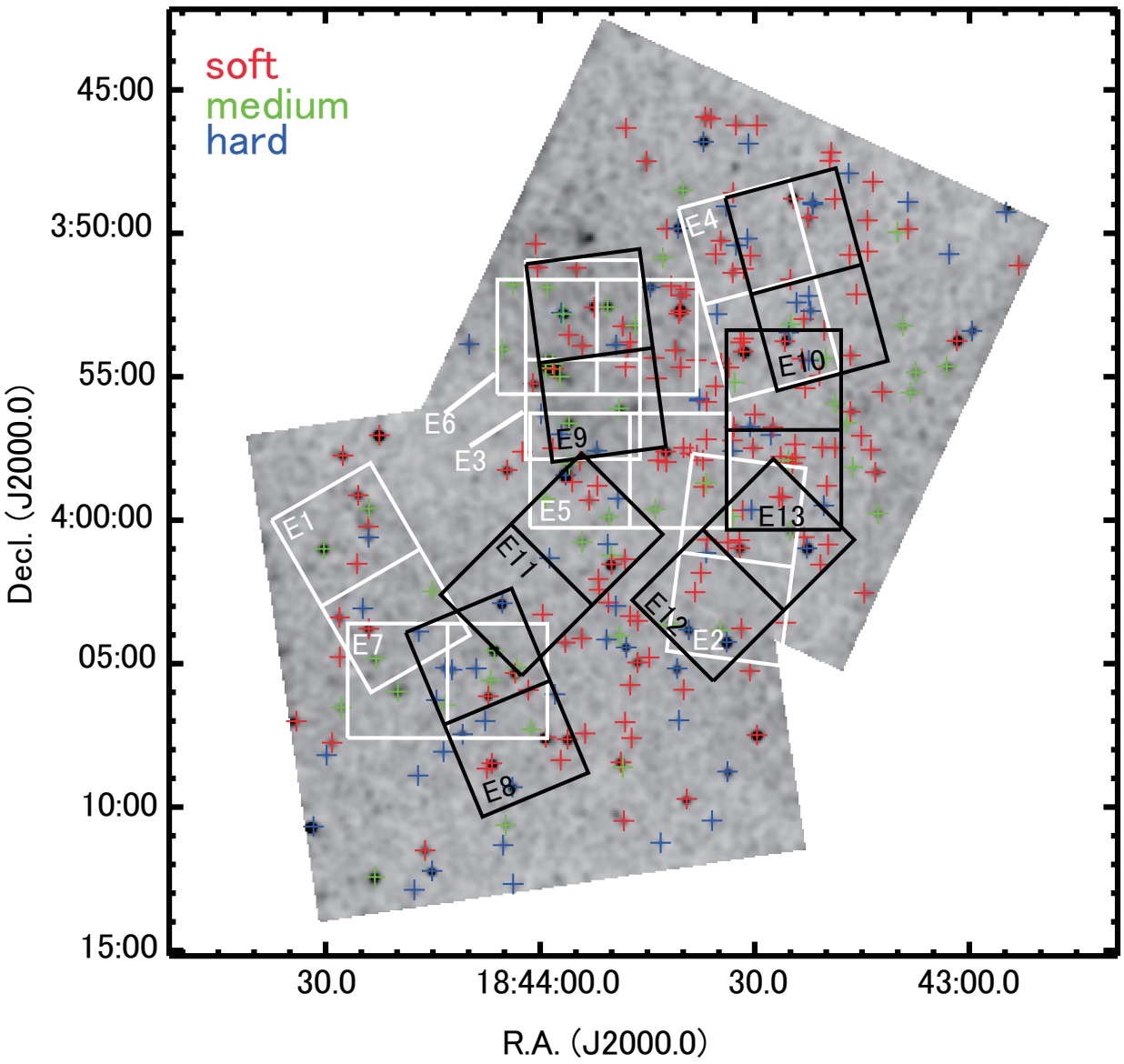

Figure 4.7: MOIRCS mask layout in the Ebisawa field. The symbols follow Figure 4.6.

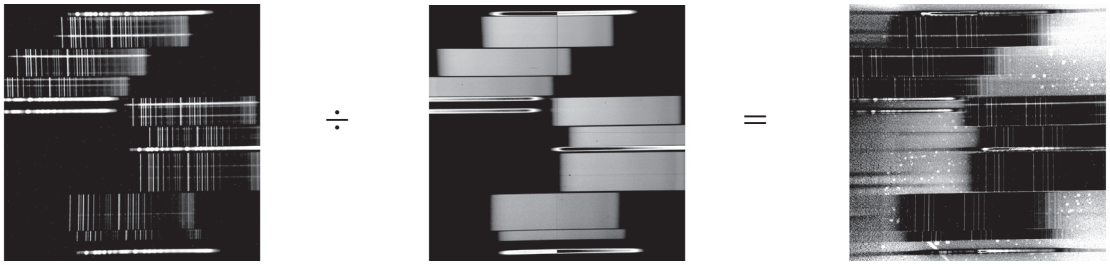

Figure 4.9: Example of a dark subtracted frame (left), a flat frame (middle), and flat-fielded frame (right) of mask R1 chip2.

Third, night-sky emission was subtracted by using the other frame in the A and B pairs: A–B to extract spectra taken at the position A (Figure 4.11) and B–A for the position B.

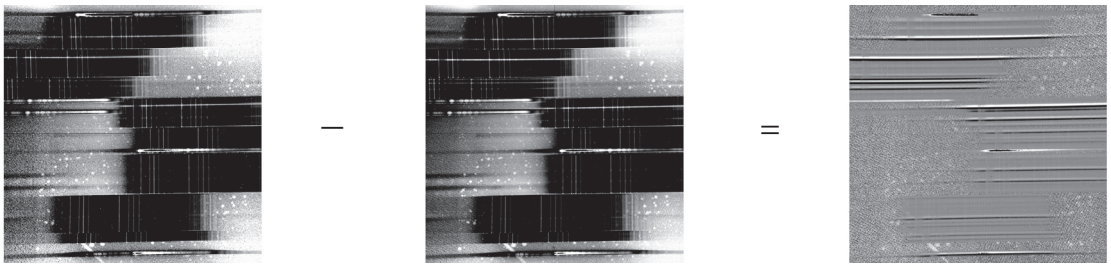

Figure 4.10: Example of frame A (left), frame B (middle), and A–B frame (right) of mask R1 chip2. The frames were dithered in the vertical direction in this figure.

Fourth, we removed bad pixels using the bad pixel map provided by the MOIRCS team.[4] This map includes dead and hot pixels. We interpolated the value in bad pixels by the values around them using the `fixpix` tool in the IRAF package. We also removed cosmic rays using the `craverage` tool.

Fifth, we correlated the distortion of all frames using the `geotran` tool. We finally stacked all the frames taken with the same chip with the same mask, resulting in 4 (mask) $\times$ 2 (chips) $\times$ 2 (A–B and B–A combinations) stacked frames. Our target sources are so faint that some sources are difficult to extract from each "A–B" and "B–A". Thus, in order to get enough signal-to-noise ratio, we combined "A–B" and "B–A" frames into one image for each mask using the `imcombine` tool. Hereafter, we used these the combined "A–B" and "B–A" images.

[4]See http://subarutelescope.org/staff/ichi/MOIRCS/OPEN/mcsbadpix_20110416.tar.gz

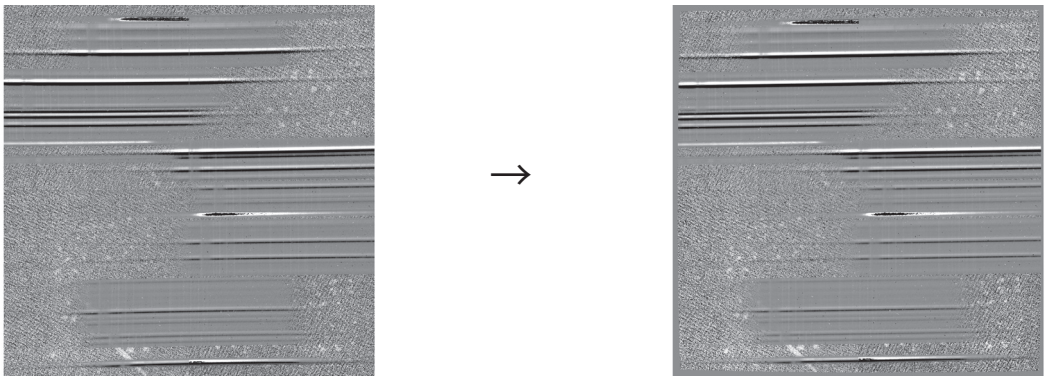

Figure 4.11: Example of A–B before (left) and after (right) the correction of bad pixels, cosmic-rays and distortion of mask R1 chip2.

Chapter 5

Data Analysis and Results

In this chapter, we describe X-ray and NIR analysis and their results. We analyzed the data taken with the deep-exposure *Chandra* ACIS observation, and extracted ∼2,000 sources, and derived their X-ray photometric and spectroscopic properties (§ 5.1). From NIR imaging data with IRSF, we searched for NIR (J, H, and K_s) counterparts of the *Chandra* X-ray sources (§ 5.2), and studied their NIR photometric properties. In order to constrain nature of the NIR-identified X-ray sources, we obtained NIR spectra of some selected NIR sources using the Subaru telescope (§ 5.3). Hereafter, errors correspond to 90% confidence unless stated otherwise.

Contents

5.1 X-ray Imaging and Spectroscopy

5.1.1 Source Extraction

As we show in § 2.1, Revnivtsev et al. (2009) used only the center of the Revnivtsev field, because they aimed to reach the deepest detection limit. On the other hand, in order to study as many as X-ray and NIR counterpart sources, we extract X-ray point sources using the entire field of view of the ACIS-I.

We first extracted X-ray point source candidates using the `wavdetect` software. We set the significance threshold at 2.5×10^{-5}, implying that one false positive detection would be expected at every 4×10^4 cells. As a result, 2,596 X-ray source candidates were found. For all the source candidates, we extracted source and background events using the ACIS Extract (AE; Broos et al. 2010)[1] package version 4.2. Point sources events were extracted from a region encircling ∼90% of photons of each source, while background events were from an annulus around each source.

To select significant X-ray point sources from the candidates, we examined their validity based on their photometric significance (PS) and the probability of no source ($P_{\rm B}$). The PS is defined as the background-subtracted source counts value ($C_{\rm net}$) divided by its background counts normalized by the area. $P_{\rm B}$ is the probability that the source is attributable to a background fluctuation. We recognized the source to be valid if they satisfy both two criteria: PS ≥ 1.0 and $P_{\rm B} \leq 1.0 \times 10^{-2}$. Consequently, we found 2,002 valid X-ray point sources. Table A.1 shows the basic properties of the detected 2,002 X-ray sources. The X-ray sources can be referred following the International Astronomical Union (IAU) convention; e.g., CXOU J175044.88–292837.6 for the source sequence number in Table A.1. Figure 5.1 shows a radial profile of the surface number densities of all the detected X-ray point sources.

[1]See the ACIS Extract User's Guide at http://www.astro.psu.edu/xray/docs/TARA/aeusersguide.html for details.

We can see that the number of detected sources decrease as the off-axis angle increases, that is a vignetting effect of the mirror as we have shown in § 3.1.2.

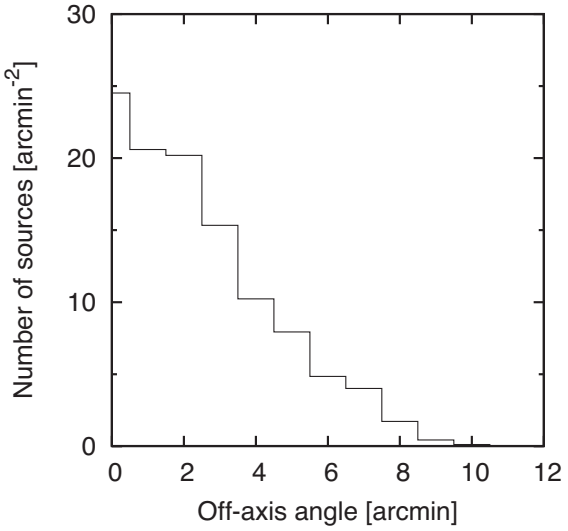

Figure 5.1: Radial profile of the surface number densities of the detected X-ray point sources in 0.5–8 keV.

Detection Rate

We estimated the detection rate of the *Chandra* data in the following method. First, we embedded random 400 artificial X-ray sources into the actual image (assuming the same exposure time, $\sim$ 900ksec) with a flux of $\sim 10^{-13} - 10^{-17}$ ergs cm^{-2} s^{-1} in 0.5–8 keV. We assumed that these artificial sources have the same spectral shape as the GRXE spectrum. The source detection method described in § 5.1.1 was employed to detect the artificial sources, and detection rates of the sources in $10^{-13} - 10^{-17}$ ergs cm^{-2} s^{-1} were derived in 0.5–8 keV. The same procedure was used to derive the detection rate in 2–8 keV. Figure 5.2 shows the detection rates of *Chandra* data thus calculated. The 100% detection rate corresponds to the 0.5–8 keV flux $\sim 10^{-15.2}$ ergs cm^{-2} s^{-1}. About 2–8 keV, the detection rate of 100% corresponds to $\sim 10^{-14.8}$ ergs cm^{-2} s^{-1}.

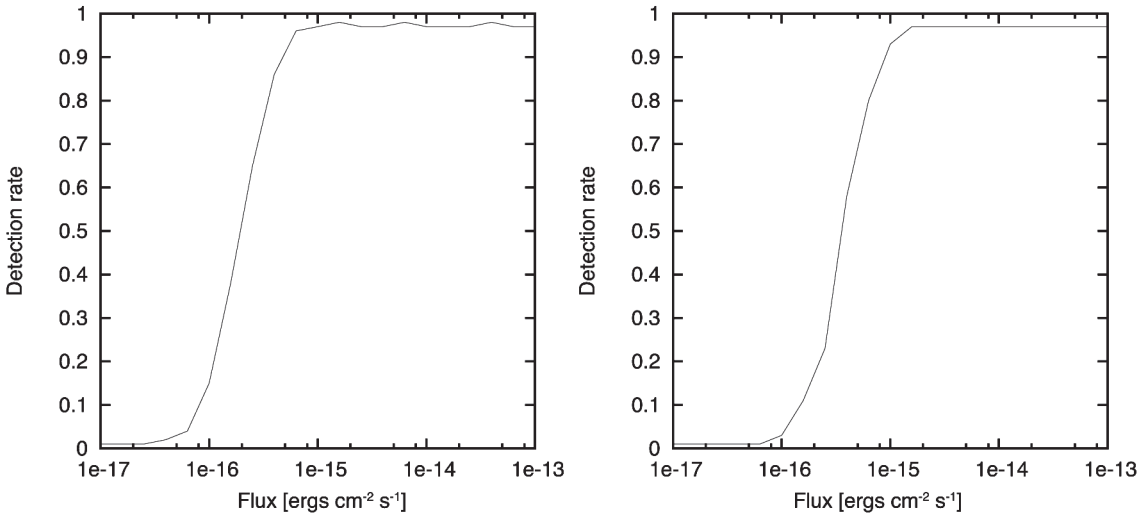

Figure 5.2: Detection rates of the point sources in the Revnivtsev fields in 0.5–8 keV (left) and in 2–8 keV (right).

5.1.2 Photometry

We calculated the median energy (ME), which represents the spectral hardness of all the detected sources. The value is defined as the median photon energy of detected photons when sorted with energy. The number distribution of calculated ME is shown in Figure 5.3 left.

Most detected X-ray sources are too faint (less than 100 counts) to determine the flux by spectral fitting. Thus, we estimated the X-ray flux by photometric information (hereafter called the "photometric flux"). The photometric flux is defined as the median energy $\times$ count rate $\times$ effective area^{-1}. The number distribution of photometric flux is shown in Figure 5.3 right. The consistency between the flux determined by the spectral fitting and the photometric flux was checked for relatively bright 335 sources (with more than 100 counts), for which flux determination by spectral fitting was possible. They are in a good agreement (Figure 5.4). Hereafter, we use the photometric flux for all the detected X-ray sources.

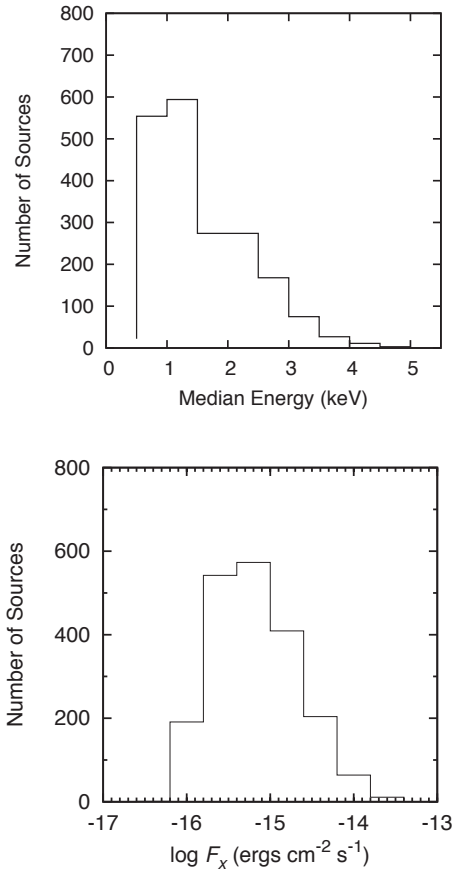

Figure 5.3: Histogram of the median energies for all the detected X-ray sources (left). Histogram of the photometric fluxes for all the detected X-ray sources in 0.5–8 keV (right).

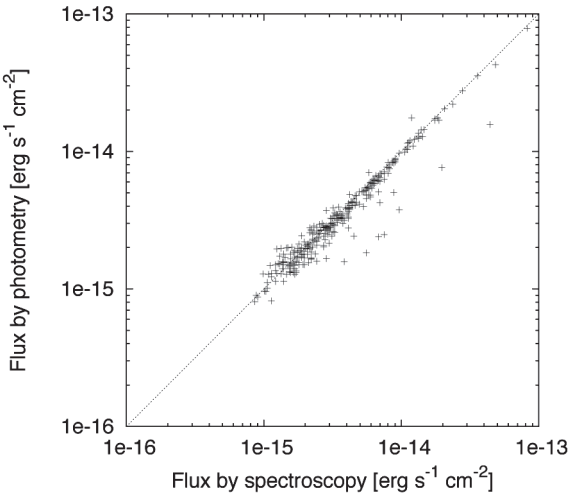

Figure 5.4: Relation between the two X-ray flux estimations in 0.5–8.0 keV for bright 335 sources. The vertical and horizontal axes represent the X-ray flux estimated by the photometric method and the spectral fitting, respectively. The dotted line represents equal values between the two estimates.

5.1.3 Variability

In order to examine time variability of the flux, we applied the Kolmogorov-Smirnov (KS) test, which examines the degree of non-uniformity in the distribution of photon arrival times against a uniform distribution (or constant flux) with χ^2-statistics. The test was not performed for sources in chip gaps or on the field edge, where *Chandra* satellite dithering can cause artificial variability. Thus we tested the time variability of 1,097 X-ray sources. Using a null hypothesis probability ($P_{\rm KS}$) derived from the KS test, we classified sources into three groups: (a) $P_{\rm KS} \geq 5 \times 10^{-2}$ for non-variable sources (680 sources), (b) $5 \times 10^{-3} \leq P_{\rm KS} < 5 \times 10^{-2}$ for marginally variable sources (316 sources), and (c) $P_{\rm KS} < 5 \times 10^{-3}$ for variable sources (101 sources, Appendix D.1). These results are shown in the column (15) in Table A.1. We plotted concatenated light curves of each source concatenating the ten observations (Appendix D.1). The light curves show variation in photon flux and median energy.

5.1.4 Spectroscopy

For the 2,002 sources, we constructed source and background spectra and generated instrumental response files; i.e., redistribution matrix functions (RMFs) of the detector and auxiliary response files (ARFs) of the telescope. We used the X-ray spectral fitting package XSPEC version 12.6.0 for the spectral analysis. We derived best-fit parameters of bright sources (counts > 100) by using the χ^2-statistics.

Table 5.1: Thermal fittings for the X-ray sources with source counts over 500

Source[1]				Spectral Fit[2]			X-ray Flux[3]					Notes[4]
Seq. #	CXOU J	$C_{\rm t,net}$	Signif.	$\log N_{\rm H}$ ($\rm cm^{-2}$)	kT (keV)	$\log EM$ ($\rm cm^{-3}$)	$F_{\rm s}$	$F_{\rm h}$	$F_{\rm h,c}$	$F_{\rm t}$	$F_{\rm t,c}$	
								($\rm ergs\ s^{-1}\ cm^{-2}$)				
(1)	(2)	(3)	(4)	(5)	(6)	(7)		(8)				(9)
33	175051.16−293419.5	1469.3	34.5	$22.4^{+0.07}_{-0.10}$	$8.8^{\cdots}_{-2.7}$	$55.5^{+0.06}_{-0.05}$	3.3e-13	3.9e-12	4.6e-12	4.2e-12	7.1e-12	...
241	175105.50−293135.4	520.5	20.4	$22.6^{+0.1}_{-0.2}$	$5.8^{\cdots}_{-2.5}$	$55.2^{+0.2}_{-0.1}$	...	1.5e-12	1.9e-12	1.6e-12	...	...
287	175107.66−294037.3	3252.3	55.1	20.0	3.2	55.6	2.9e-12	2.9e-12	2.9e-12	5.8e-12	5.8e-12	...
371	175111.58−293532.6	783.6	26.7	$22.3^{+0.08}_{-0.10}$	$8.6^{\cdots}_{-2.9}$	$55.2^{+0.07}_{-0.05}$	2.0e-13	1.9e-12	2.2e-12	2.1e-12	3.3e-12	...
385	175112.04−293527.7	633.8	23.8	$22.3^{+0.08}_{-0.09}$	$6.4^{+5.7}_{-1.9}$	$55.1^{+0.08}_{-0.08}$	1.7e-13	1.4e-12	1.6e-12	1.6e-12	2.7e-12	...
1049	175129.23−292936.2	818.9	26.7	$21.9^{+0.09}_{-0.09}$	$4.9^{+1.9}_{-1.3}$	$55.1^{+0.07}_{-0.06}$	3.4e-13	1.2e-12	1.3e-12	1.6e-12	2.3e-12	...
1077	175129.85−294307.9	824.9	26.0	20.0	1.8	55.2	1.4e-12	7.3e-13	7.3e-13	2.1e-12	2.1e-12	...
1083	175130.06−293613.4	643.2	24.3	$22.4^{+0.08}_{-0.07}$	$11.^{\cdots}_{-4.9}$	$55.1^{+0.08}_{-0.04}$	1.4e-13	1.6e-12	1.9e-12	1.7e-12	2.8e-12	...
1111	175130.80−293736.5	722.1	25.8	$22.1^{+0.08}_{-0.07}$	$5.8^{+2.6}_{-1.7}$	$55.1^{+0.08}_{-0.06}$	2.7e-13	1.4e-12	1.5e-12	1.6e-12	2.5e-12	...
1252	175134.06−293103.9	1390.3	36.0	$22.1^{+0.06}_{-0.06}$	$11.^{\cdots}_{-3.4}$	$55.3^{+0.04}_{-0.03}$	4.6e-13	2.8e-12	3.0e-12	3.3e-12	4.6e-12	...
1320	175135.60−293754.8	509.6	21.4	$22.2^{+0.1}_{-0.1}$	$8.1^{\cdots}_{-3.3}$	$54.9^{+0.10}_{-0.07}$	1.6e-13	1.1e-12	1.2e-12	1.3e-12	1.9e-12	...
1425	175138.33−294240.3	614.2	21.2	$21.8^{+0.2}_{-0.2}$	$4.6^{+3.0}_{-1.6}$	$55.0^{+0.11}_{-0.08}$	3.3e-13	9.8e-13	1.0e-12	1.3e-12	1.8e-12	...
1670	175144.97−293802.0	667.6	24.3	$22.1^{+0.1}_{-0.1}$	$13.^{\cdots}_{-6.4}$	$55.0^{+0.06}_{-0.04}$	1.9e-13	1.5e-12	1.6e-12	1.7e-12	2.4e-12	...
1732	175146.92−294304.3	704.5	21.8	$22.5^{+0.1}_{-0.1}$	$14.^{\cdots}_{-8.4}$	$55.3^{+0.09}_{-0.05}$	1.4e-13	2.4e-12	2.8e-12	2.5e-12	4.1e-12	...
1775	175148.91−293505.6	1779.1	40.7	$21.6^{+0.07}_{-0.07}$	$1.5^{+0.1}_{-0.1}$	$55.5^{+0.03}_{-0.03}$	1.3e-12	9.8e-13	1.0e-12	2.3e-12	3.6e-12	...
1805	175150.23−293143.7	527.5	20.6	$22.4^{+0.09}_{-0.10}$	$5.5^{+5.6}_{-1.9}$	$55.1^{+0.1}_{-0.1}$	1.3e-13	1.4e-12	1.6e-12	1.5e-12	2.7e-12	...
1893	175154.54−294006.3	561.9	19.8	$22.6^{+0.1}_{-0.1}$	$5.9^{+8.9}_{-2.5}$	$55.3^{+0.2}_{-0.1}$	...	1.8e-12	2.3e-12	1.9e-12	...	...
1895	175154.71−292806.1	6440.6	77.1	$22.3^{+0.03}_{-0.03}$	$9.4^{+2.9}_{-1.5}$	$56.1^{+0.02}_{-0.02}$	2.0e-12	1.7e-11	2.0e-11	1.9e-11	3.0e-11	...

[1]For convenience, cols. (1)–(4) reproduce the source identification, net counts, and photometric significance data from Table A.1. [2]All fits used the *source* model "tbabs*vapec" in XSPEC abundances frozen at the values relative to Anders & Grevesse (1989), scaled to Wilms et al. (2000), using the tbabs absorption code in XSPEC. Cols. (5) and (6) present the best-fit values for the extinction column density and plasma temperature parameters. Col. (7) presents the emission measure derived from the model spectrum, assuming a distance of 8.5 kpc. Quantities marked with an asterisk (*) were frozen in the fit. Uncertainties represent 90% confidence intervals. More significant digits are used for uncertainties <0.1 in order to avoid large rounding errors; for consistency, the same number of significant digits is used for both lower and upper uncertainties. Uncertainties are missing when XSPEC was unable to compute them or when their values were so large that the parameter is effectively unconstrained. Fits lacking uncertainties, fits with large uncertainties, and fits with frozen parameters should be viewed merely as splines to the data to obtain rough estimates of luminosities; the listed parameter values are not robust. [3] X-ray flux derived from the model spectrum are presented in cols. (8)–(12): (s) soft band (0.5–2 keV); (h) hard band (2–8 keV); (t) total band (0.5–8 keV). Cols. (8) and (12) are omitted when $\log N_{\rm H} > 22.5$ $\rm cm^{-2}$ since the soft band emission is essentially unmeasurable.

Table 5.2: Power-law fitting for the X-ray sources with source counts over 500

Source[1]				Spectral Fit[2]			X-ray Flux[3]				
Seq.	CXOU J	$C_{\rm t,net}$	Signif.	$\log N_{\rm H}$	Γ	$\log N_\Gamma$	$F_{\rm s}$	$F_{\rm h}$	$F_{\rm h,c}$	$F_{\rm t}$	$F_{\rm t,c}$
#				($\rm cm^{-2}$)			($\rm ergs\ s^{-1}\ cm^{-2}$)				
33	175051.16-293419.5	1469.3	34.5	$22.4^{+0.09}_{-0.09}$	$1.7^{+0.3}_{-0.2}$	$-4.92^{+0.2}_{-0.2}$	3.3e-13	3.9e-12	4.7e-12	4.3e-12	8.0e-12
203	175103.96-293431.0	670.9	24.0	$22.2^{+0.1}_{-0.2}$	$1.2^{+0.3}_{-0.3}$	$-5.61^{+0.2}_{-0.2}$	1.5e-13	2.1e-12	2.3e-12	2.2e-12	3.0e-12
371	175111.58-293532.6	783.6	26.7	$22.3^{+0.1}_{-0.1}$	$1.7^{+0.3}_{-0.3}$	$-5.29^{+0.2}_{-0.2}$	2.0e-13	1.9e-12	2.2e-12	2.1e-12	3.6e-12
385	175112.04-293527.7	633.8	23.8	$22.4^{+0.09}_{-0.09}$	$1.9^{+0.3}_{-0.3}$	$-5.27^{+0.2}_{-0.2}$	2.0e-13	1.9e-12	2.2e-12	2.1e-12	3.6e-12
438	175113.70-293110.1	4325.4	64.4	$22.5^{+0.04}_{-0.04}$	$1.5^{+0.1}_{-0.1}$	$-4.53^{+0.08}_{-0.08}$	...	1.4e-11	1.6e-11	1.4e-11	...
888	175125.00-293016.1	610.9	22.9	$22.1^{+0.1}_{-0.2}$	$1.4^{+0.3}_{-0.3}$	$-5.62^{+0.2}_{-0.2}$	1.7e-13	1.4e-12	1.5e-12	1.6e-12	2.2e-12
1049	175129.23-292936.2	818.9	26.7	$22.0^{+0.09}_{-0.10}$	$2.0^{+0.2}_{-0.2}$	$-5.29^{+0.1}_{-0.1}$	3.5e-13	1.2e-12	1.4e-12	1.6e-12	2.7e-12
1077	175129.85-294307.9	824.9	26.0	21.2	2.8	-5.08	1.5e-12	7.5e-13	7.6e-13	2.3e-12	3.1e-12
1083	175130.06-293613.4	643.2	24.3	$22.4^{+0.09}_{-0.09}$	$1.7^{+0.3}_{-0.3}$	$-5.34^{+0.2}_{-0.2}$	1.5e-13	1.6e-12	1.9e-12	1.7e-12	3.1e-12
1111	175130.80-293736.5	722.1	25.8	$22.2^{+0.08}_{-0.09}$	$2.0^{+0.3}_{-0.2}$	$-5.25^{+0.1}_{-0.1}$	2.8e-13	1.3e-12	1.5e-12	1.6e-12	3.0e-12
1149	175131.68-292957.0	2908.3	52.5	$22.4^{+0.06}_{-0.06}$	$1.3^{+0.1}_{-0.1}$	$-4.87^{+0.10}_{-0.09}$	5.5e-13	9.2e-12	1.1e-11	9.8e-12	1.4e-11
1207	175133.05-294247.6	790.6	24.7	$22.2^{+0.1}_{-0.1}$	$1.5^{+0.3}_{-0.3}$	$-5.37^{+0.2}_{-0.2}$	2.4e-13	2.2e-12	2.4e-12	2.4e-12	3.5e-12
1252	175134.06-293103.9	1390.3	36.0	$22.1^{+0.08}_{-0.08}$	$1.6^{+0.2}_{-0.2}$	$-5.18^{+0.10}_{-0.09}$	4.6e-13	2.9e-12	3.1e-12	3.3e-12	4.9e-12
1320	175135.60-293754.8	509.6	21.4	$22.2^{+0.1}_{-0.1}$	$1.8^{+0.3}_{-0.3}$	$-5.47^{+0.2}_{-0.2}$	1.6e-13	1.1e-12	1.2e-12	1.3e-12	2.2e-12
1425	175138.33-294240.3	614.2	21.2	$21.9^{+0.2}_{-0.2}$	$2.0^{+0.3}_{-0.3}$	$-5.40^{+0.2}_{-0.2}$	3.3e-13	1.0e-12	1.1e-12	1.3e-12	2.2e-12
1670	175144.97-293802.0	667.6	24.3	$22.2^{+0.1}_{-0.1}$	$1.6^{+0.3}_{-0.3}$	$-5.47^{+0.2}_{-0.2}$	2.0e-13	1.5e-12	1.6e-12	1.7e-12	2.5e-12
1732	175146.92-294304.3	704.5	21.8	$22.5^{+0.1}_{-0.1}$	$1.7^{+0.4}_{-0.4}$	$-5.18^{+0.3}_{-0.3}$	...	2.3e-12	2.8e-12	2.5e-12	...
1805	175150.23-293143.7	527.5	20.6	$22.5^{+0.1}_{-0.1}$	$2.0^{+0.4}_{-0.4}$	$-5.18^{+0.3}_{-0.2}$	1.3e-13	1.4e-12	1.7e-12	1.5e-12	3.5e-12
1831	175151.29-293310.3	1447.3	36.3	$22.3^{+0.09}_{-0.10}$	$0.65^{+0.2}_{-0.2}$	$-5.51^{+0.1}_{-0.1}$	1.9e-13	5.5e-12	6.1e-12	5.8e-12	7.1e-12
1869	175153.33-294245.0	1202.7	30.0	$22.4^{+0.1}_{-0.1}$	$1.0^{+0.3}_{-0.3}$	$-5.30^{+0.2}_{-0.2}$	2.3e-13	5.0e-12	5.7e-12	5.3e-12	7.1e-12
1893	175154.54-294006.3	561.9	19.8	$22.7^{+0.1}_{-0.2}$	$2.1^{\cdots}_{-0.5}$	$-4.98^{+0.4}_{-0.3}$	...	1.8e-12	2.4e-12	1.9e-12	...

[1]For convenience, cols. (1)–(4) reproduce the source identification, net counts, and photometric significance data from Appendix A.1. [2]All fits used the *source* model "tbabs (powerlaw)" in XSPEC. Cols. (5) and (6) present the best-fit values for the extinction column density and power law photon index parameters. Col. (7) presents the power law normalization for the model spectrum. Quantities marked with an asterisk (*) were frozen in the fit. Uncertainties represent 90% confidence intervals. More significant digits are used for uncertainties <0.1 in order to avoid large rounding errors; for consistency, the same number of significant digits is used for both lower and upper uncertainties. Uncertainties are missing when XSPEC was unable to compute them or when their values were so large that the parameter is effectively unconstrained. Fits lacking uncertainties, fits with large uncertainties, and fits with frozen parameters should be viewed merely as splines to the data to obtain rough estimates of luminosities; the listed parameter values are unreliable. [3]X-ray Flux derived from the model spectrum, assuming a distance of 8 kpc, are presented in cols. (8)–(12): (s) = soft band (0.5–2 keV); (h) hard band (2–8 keV); (t) total band (0.5–8 keV). Absorption-corrected luminosities are subscripted with a *c*. Cols. (8) and (12) are omitted when $\log N_{\rm H} > 22.5\ \rm cm^{-2}$ since the soft band emission is essentially unmeasurable.

For the spectral models, we used an interstellar absorption model (`tbabs`; Wilms et al. 2000) convolved with either of the two continuum models: an optically-thin thermal plasma model with the solar abundance (`apec`; Smith et al. 2001) and a power-law model to represent the thermal and non-thermal spectra, respectively. The free parameters in the thermal model are absorption ($N_{\rm H}$), plasma temperature ($k_{\rm B}T$), and X-ray flux ($F_{\rm X}$). On the other hand, the free parameters in power-law model are absorption ($N_{\rm H}$), photon index (Γ), and flux ($F_{\rm X}$). First, we selected the sources that have the reduced χ^2 of the fitting < 1.5. Second, we removed results with unphysical best-fit values; i.e., $\Gamma > 3$ in the power-law fitting and $k_{\rm B}T$ >15 keV in the `apec` fitting. As a result, 200 sources were fitted with the thermal model and 360 sources were fitted with the non-thermal model. Appendix B.1 and C.1 show the best-fit model and spectra of thermal and non-thermal fitting for the bright sources, respectively. Tables 5.1, 5.2 show the best-fit model parameters.

5.1.5 Total and All Point Source combined spectra

In order to compare with Revnivtsev et al. (2009), we extracted total X-ray spectra in the Revnivtsev field as follows. (1) Using the CIAO tool `specextract`, we extracted X-ray spectra and build associated weighted ARFs and RMFs for each CCD chip (chip 0–3) on each observation (ten ObsIDs). We combined each spectrum, each ARF and each RMF to one total spectra using `mathpha`, `addarf`, and `addrmf`, respectively. (2) The CIAO/ACIS observation in the Revnivtsev field have a lot of point sources in the image, thus we could not estimate the background from the image. Thus, we used the non-X-ray background database (blank-sky database[2]) provided by *Chandra* X-ray Center (CXC). The blank sky lies at high Galactic latitude, which away from soft bright features such as North Polar spur. We chose the background database matching to our data using the CIAO tool`acis_bkg_lookup`. The background files were projected to match the coordinates of the Revnivtsev field pointing using the real aspect solution files. (3) Using the non-X-ray background thus created, we have made background subtracted total spectra (including both point source and diffuse X-rays) for the Revnivtsev field (Figure 5.5).

Meanwhile, we made the combined point source spectrum of 2,002 point sources using the CIAO tool`combine_spectra`. Figure 5.5 shows the total spectrum and the combined point source spectrum in the Revnivtsev field. In Revnivtsev et al. (2009), the total surface brightness in 3–7 keV is $(4.2\pm0.4)\times10^{-11}$ ergs cm^{-2} s^{-1} deg^{-2}. The surface brightness of

[2]http://cxc.cfa.harvard.edu/contrib/maxim/acisbg/

our total spectrum in 3–7 keV is $(5.0\pm0.4)\times10^{-11}$ ergs cm^{-2} s^{-1} deg^{-2}. Figure 5.5 bottom shows the point source resolved fraction. We measured the flux and resolved fraction with a bin size of 1 keV. In 6–7 keV, the resolved fraction is $\sim$89%, which is consistent with the fraction of Revnivtsev et al. (2009) as we show in § 2.1.

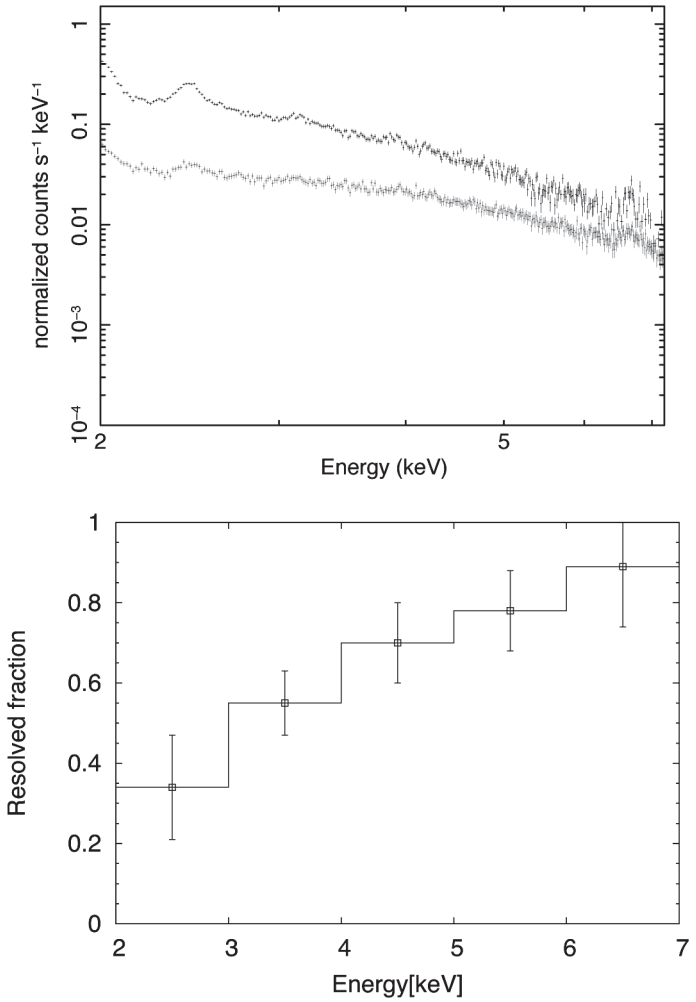

Figure 5.5: (Top) Comparison of the GRXE total spectrum and point source combined spectrum. (Bottom) Resolved fraction of the GRXE total spectrum. The errorbars give 1σ error.

5.2 NIR Imaging

5.2.1 Source Extraction

In this section, we used the SIRIUS data with the best seeing in each region (Table 4.1). We extracted NIR sources with a 3σ level from the eight regions by using the SExtractor version 2.8.6 (Bertin & Arnouts 1996). We applied a convolution mask of 3×3 pixel binning plus 1.5 pixel Gaussian smoothing. Consequently, we detected 52,312 (J), 61,188 (H), and 65,061 ($K_{\rm s}$) sources. Detected NIR sources in each region are given in Table 5.3. We note that the SIRIUS sources include duplicated counts in overlapped regions.

Table 5.3: NIR detected sources

Data [a]	Number of sources		
label	J	H	$K_{\rm s}$
00-c	6794	8959	8252
01	7066	6287	8493
02	6248	8163	7506
03	5587	8425	6929
04	7026	4920	8600
05	6211	8103	8219
06	6956	8951	9230
07	6424	7380	7832
total	52,312	61,188	65,051

[a] Data labels are same as Table 4.1.

5.2.2 Astrometry

We calibrated the position of the SIRIUS sources by referring to the Two Micron All Sky Survey (2MASS; Skrutskie et al. 2006) point source catalogue. For the astrometry correction, we used software provided by Dr. Matsunaga at the Kiso Observatory, which is based on the optimistic pattern matching algorithm advocated by Tabur (2007). The software calculates coordinate transformation between the SIRIUS and the 2MASS catalogs, and corrects the SIRIUS astrometry. In Figure 5.6, we plotted the difference between the corrected SIRIUS

and 2MASS positions both in R.A. and Decl.. We found that ΔR.A. = $0.08'' \pm 0.29''$ (1σ) and ΔDecl. = $0.11'' \pm 0.25''$ (1σ). This indicates that SIRIUS positions are determined at an accuracy of the pixel size of SIRIUS, and the systematic error between SIRIUS and 2MASS is negligible.

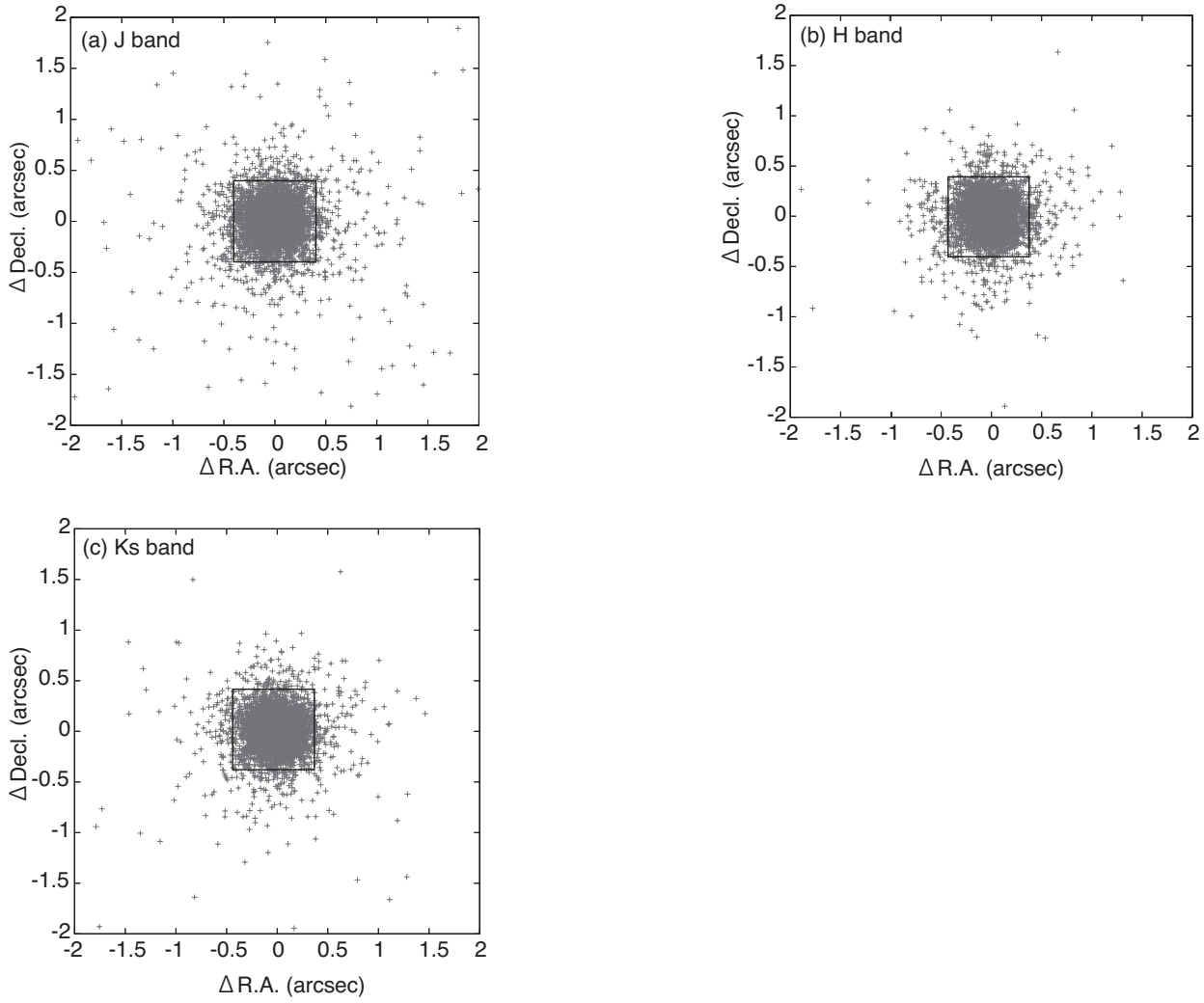

Figure 5.6: Astrometric consistency between the SIRIUS and the 2MASS sources in the (a) J, (b) H, and (c) K_s bands. The black boxes at the center is the SIRIUS pixel size.

5.2.3 Photometry

We also calibrated the photometry of the SIRIUS sources by referring to 2MASS. We identified the 2MASS counterparts to SIRIUS sources only using 2MASS sources with a signal-to-noise ratio of >10 (flag A) and in the magnitude range of 12–14 mag (see § 5.2.4 for the detailed procedure). The SIRIUS magnitudes were shifted to match those by 2MASS. Figure 5.7 shows the relative photometry between SIRIUS and 2MASS. The data deviate from the linear relations (2MASS magnitudes equal to SIRIUS magnitudes) brighter than ∼10 mag (J), ∼10.5 mag ($H$and $K_{\rm s}$) due to the saturation of SIRIUS sources. Thus, we used SIRIUS sources fainter than ∼10 mag (J), ∼10.5 mag (H and $K_{\rm s}$) for the derivation of SIRIUS photometric zero point of each observation in each band.

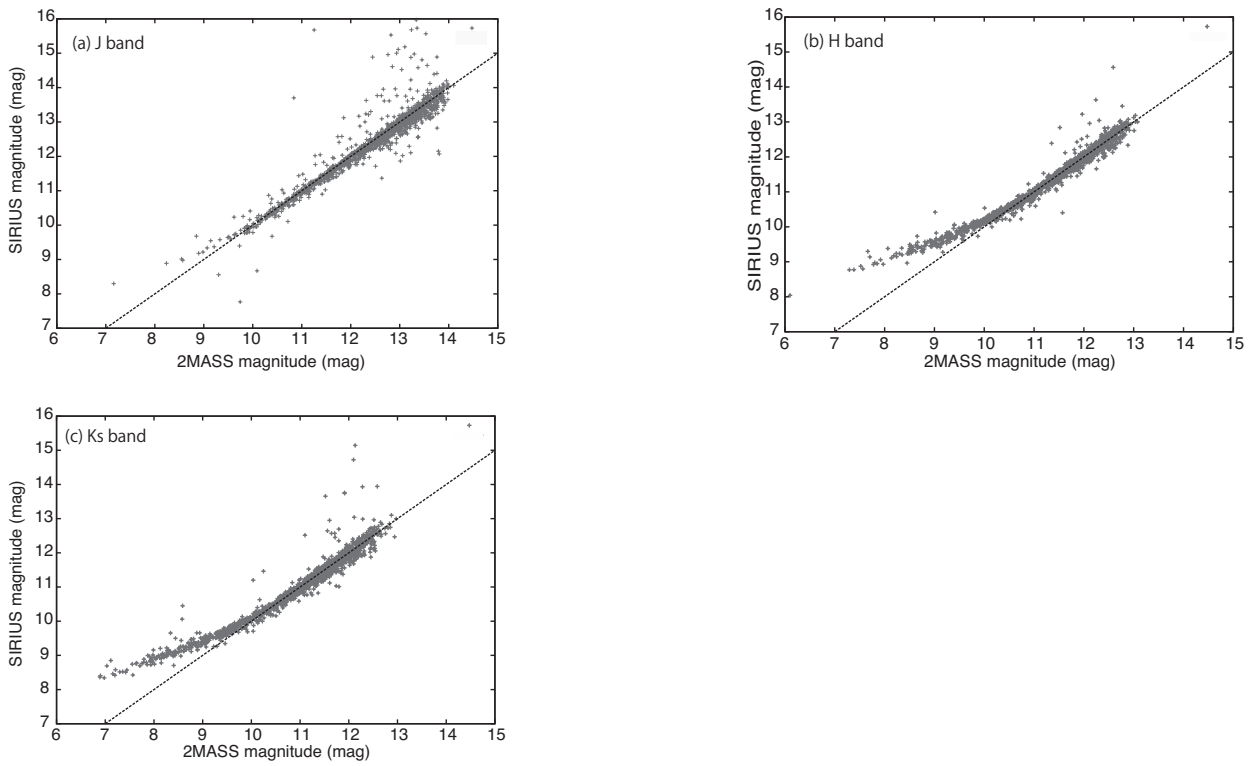

Figure 5.7: Photometric consistency between the SIRIUS and 2MASS sources. The corrected SIRIUS and the 2MASS magnitudes are plotted separately for the (a) J, (b) H, (c) $K_{\rm s}$ bands. The dotted line in each panel shows that the 2MASS magnitude being equal to the SIRIUS magnitudes.

5.2.4 X-ray and NIR Correlation

We search for possible NIR counterparts for all the X-ray sources using the 2MASS and SIRIUS source list. Here, we used 2MASS sources brighter than 10.0 (J), 10.5 (H), and 10.5 (K_s) magnitudes and SIRIUS sources fainter than these values due to the saturation of SIRIUS sources. To identify X-ray sources with the NIR, we used NIR sources within 5″ radius around each X-ray source. First, we selected counterpart candidates for each X-ray source, which are NIR sources within 5″ radius. Each X-ray sources have some NIR counterpart candidates. Second, we measured residual displacements of the candidate pairs, the rms (1σ) of the displacement is 1.3″ (X-ray-2MASS source) and 1.2″ (X-ray-SIRIUS source). Then, we recognized 222 X-ray sources (2MASS; 6 sources, SIRIUS; 216 sources) to have NIR counterpart within 1σ circle (about 12% of all X-ray sources). When there are two or more sources within the 1σ circle, we assumed the closest one to be the counterpart. Table E.1 shows X-ray–NIR counterparts pairs. In this criteria, the rate of false positive (unrelated pairs identified as counterparts) and false negative (unidentified pairs as counterpart) is to be around 13% of the identified pairs. For all and NIR identified X-ray sources, Figure 5.8 shows histogram of the median energies.

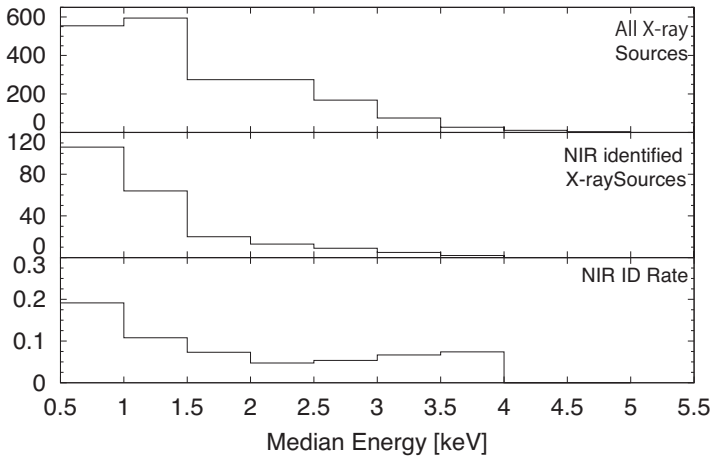

Figure 5.8: Histogram of the median energies separately for all the X-ray sources (top) and NIR identified X-ray sources (middle). The rate of NIR identification at each ME bin is shown at the bottom.

5.3 NIR Spectroscopy

5.3.1 Spectral Extraction

In the Revnivtsev field, we did the following steps to extract one-dimensional spectra from all the processed frames. From the combined image for each mask, we defined aperture to trace spectra for each slit in each mask using the `apall` tool and extracted (Figure 5.9). We registered wavelength for the dispersed spectra using OH night-sky emission line spectra extracted from the same aperture with the source (Figure 5.10; Rousselot et al. 2000). For this purpose, we used A+B frames because the OH emission is cancelled out in the A–B frames. Then, we identified the OH night-sky emission lines using the `identify` tool for the extracted spectrum of A and B images. Using the pixel coordinates of the sky emission lines, we derived a chebyshev polynomial function to convert pixel position to wavelength. Using this function for each slit, we made wavelength calibrated spectra for each slit using the `dispcor` tool (Figure 5.10 (d)). In the Ebisawa field, we did almost the same steps as the Revnivtsev field. Since we had comparison data taken with Th-Ar in the Ebisawa field, we used it for the wavelength calibration. The same procedure was taken also for the standard stars.

After the wavelength calibration, we corrected for telluric features of the objects. The telluric feature was derived from the standard star spectra after removing the Br γ feature by fitting with a Voigt profile and flattening continuum emission using a blackbody emission of a temperature of 9790 K for A0V stars. The OH emission features are sparse in the longer wavelength in the $K_{\rm s}$-band (Figure 5.11), in which we suffer degraded calibration accuracy. In the last, we combined A–B and B–A spectra of the same aperture using the `scombine` tool.

5.3.2 Line Identification

Table 5.4 shows the $K_{\rm s}$-band spectral features that we used to investigated the nature of each source. Most spectra show absorption features indicating that they are stars. Figure 5.12 and 5.13 show spectra of the sources in the Revnivtsev field and the Ebisawa field, respectively.

In order to find their spectra types, we compared each spectra with the published NIR late-type star spectra (Ali et al. 1995, Ivanov et al. 2004). There are mainly two types of

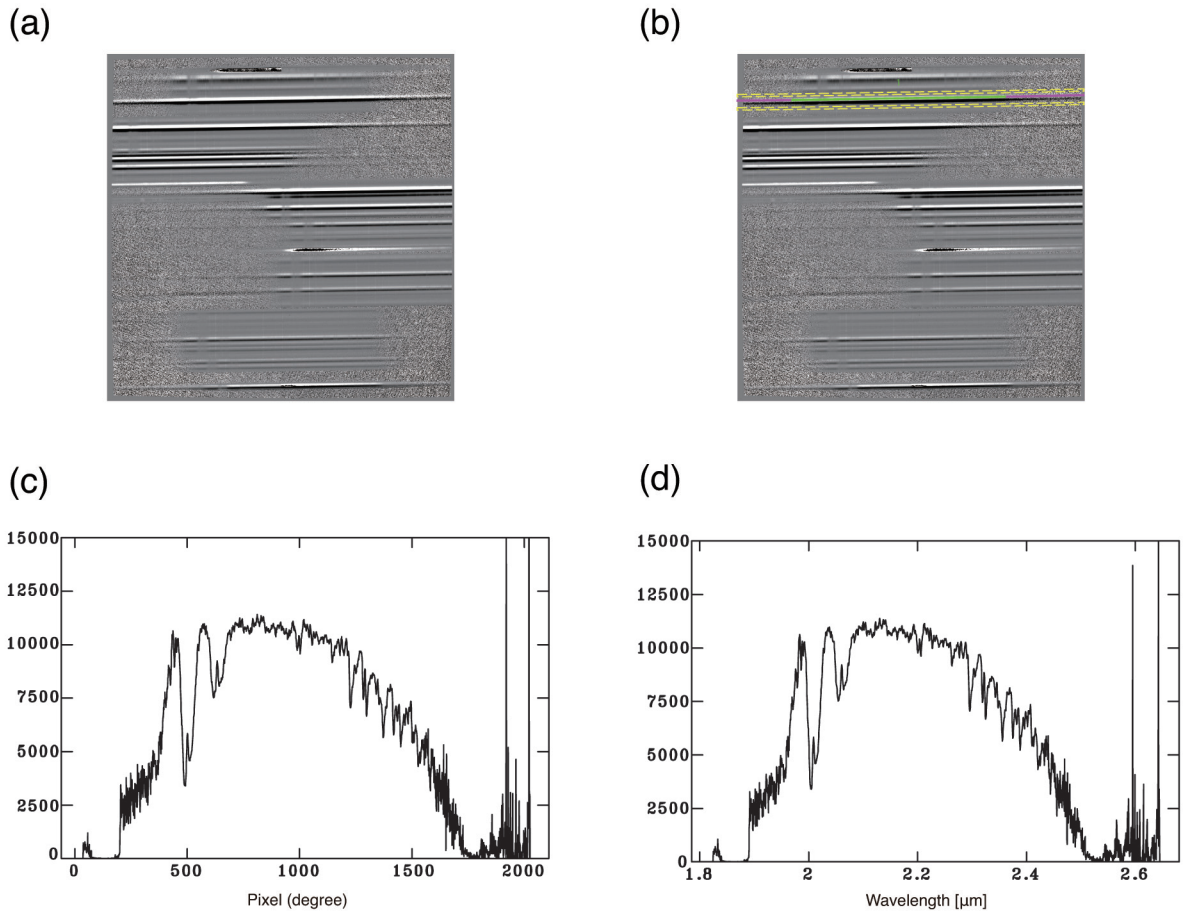

Figure 5.9: Example of extraction of one-dimensional spectrum (mask R1 slit 1). (a) Combined A–B image. (b) Source and background apertures. Green curves show the source region, yellow dashed curves show the background region, and magenta curves show noisy region, which were not used to derive traces. (c) Extracted spectrum. (d) Wavelength–calibrated spectrum.

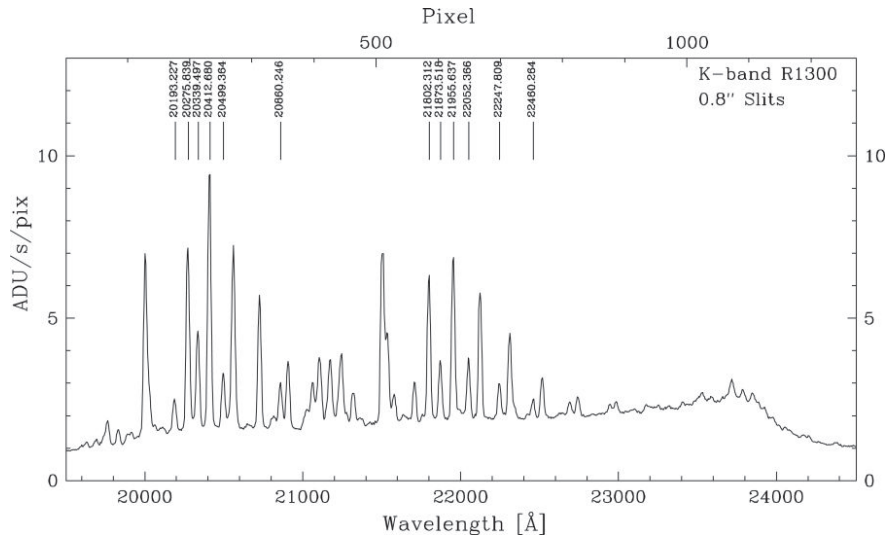

Figure 5.10: Night-sky OH spectra for R1300 grism of MOIRCS in K_s band. The top and bottom horizontal axes are in the unit of pixels and wavelengths, respectively, and which the vertical axis is the intensity with 0.8″ long slit.

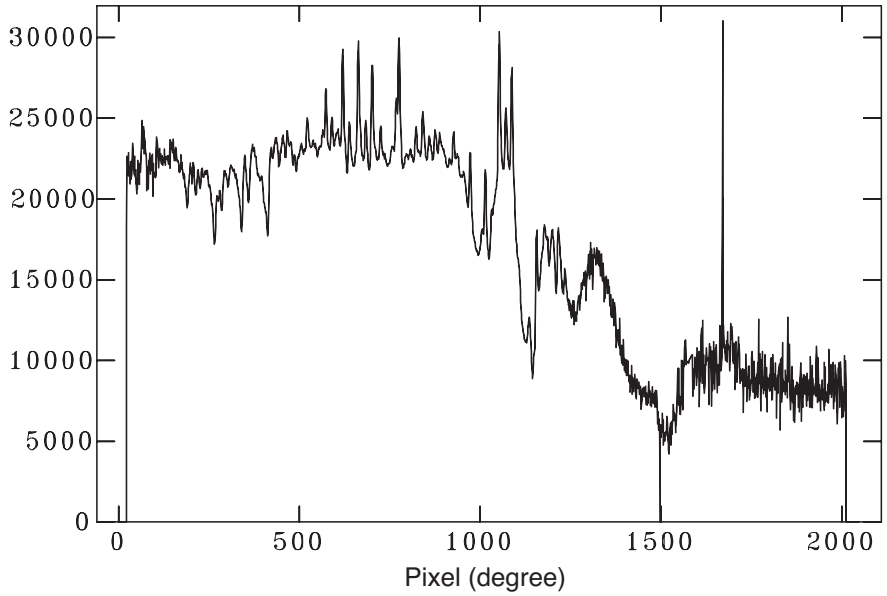

Figure 5.11: Example of the night-sky OH emission features in our data, which are found mainly in ∼500–1000 pixels.

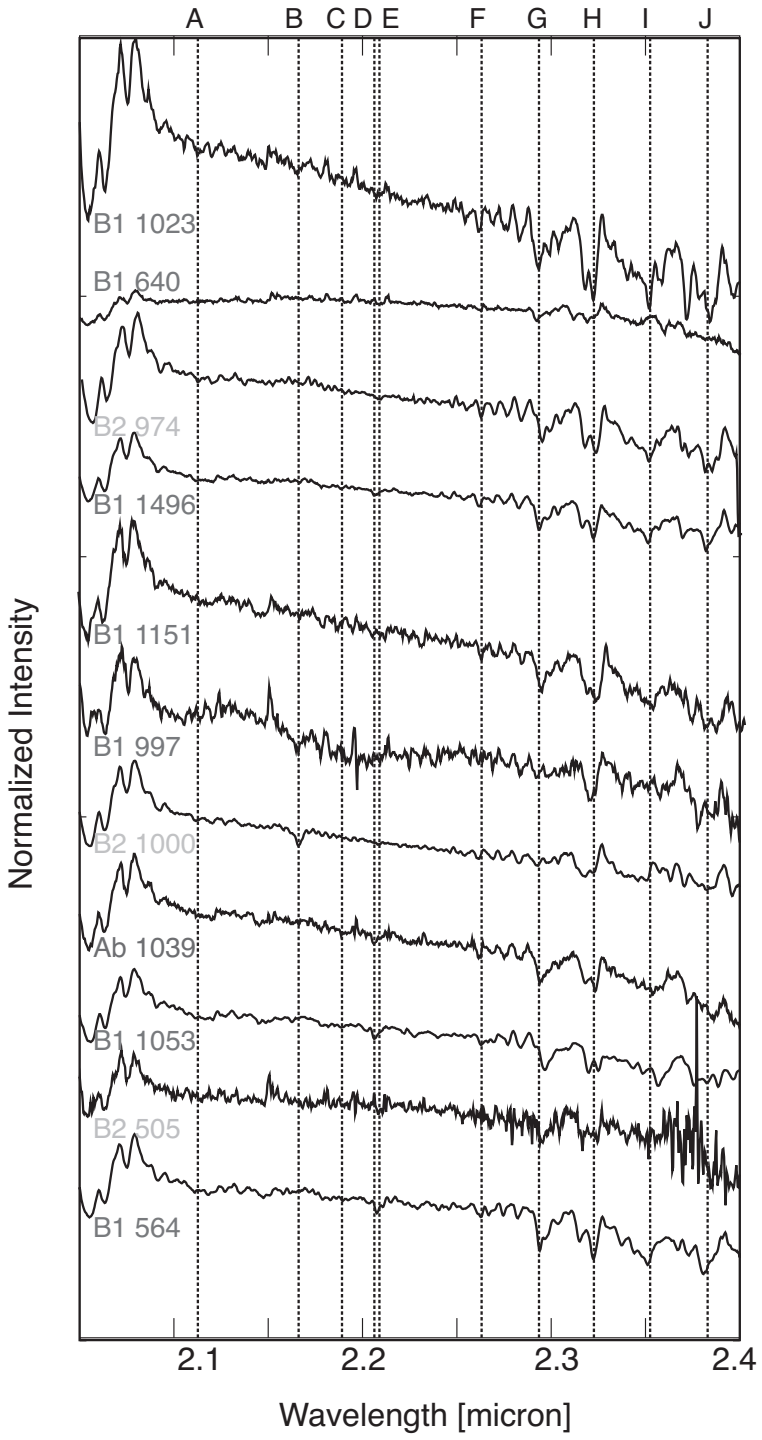

Figure 5.12: Normalized K_s-band spectra in mask R1. X-ray source numbers are given below each spectrum. The color of each number corresponds to group Ab, B1, and B2 in Chap. 6. The identification of features A–J is given in Table 5.4.

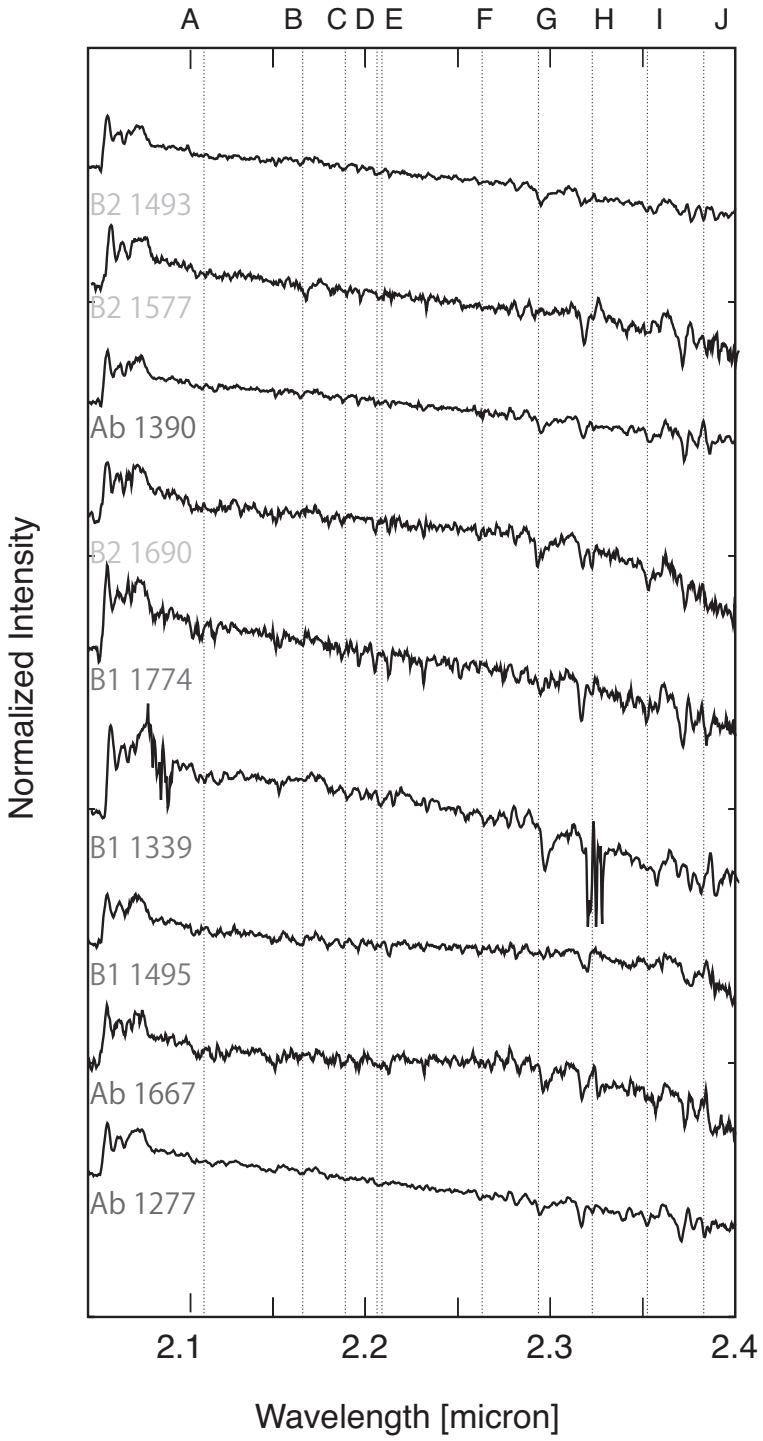

Figure 5.12: Extracted spectra in mask R2.

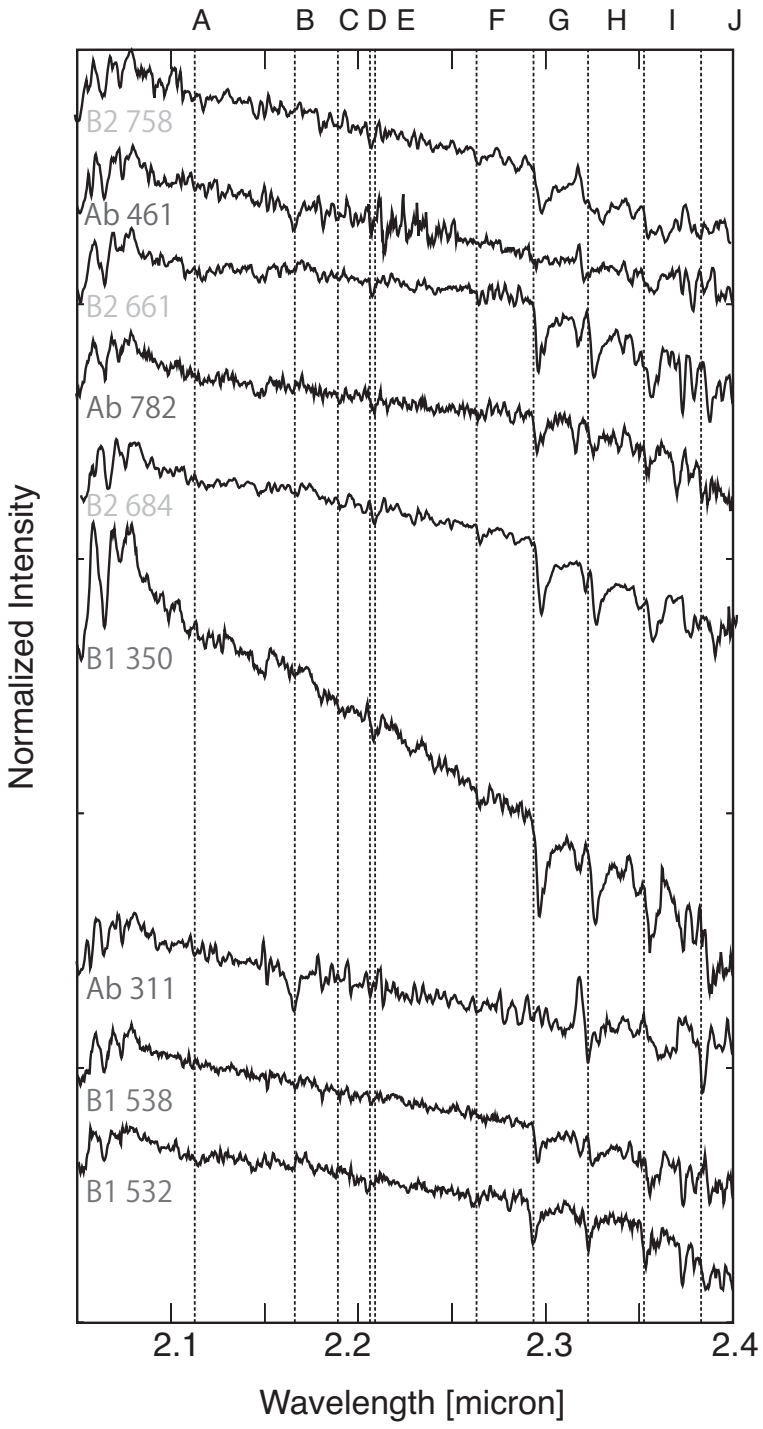

Figure 5.12: Extracted spectra in mask R3.

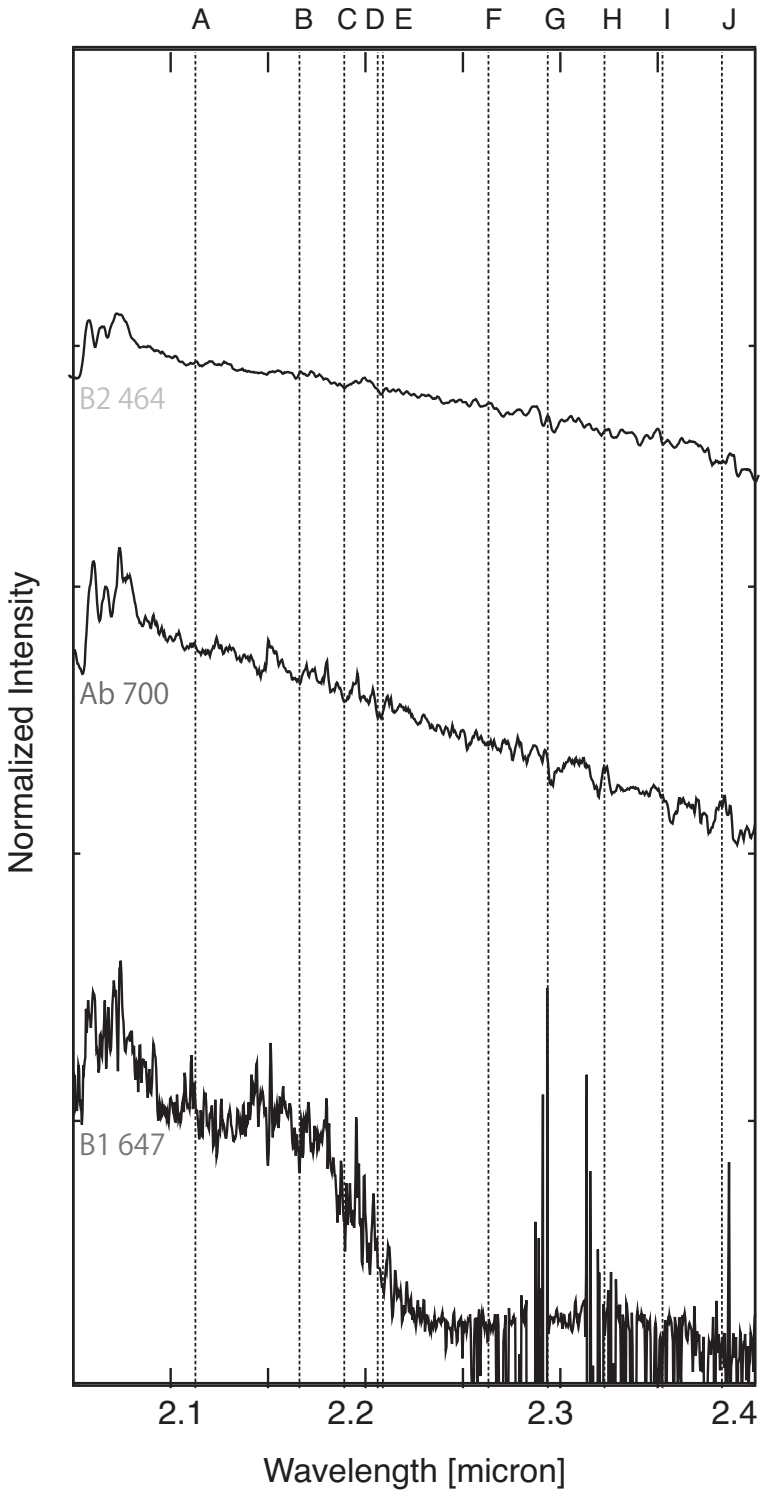

Figure 5.12: Extracted spectra in mask R4.

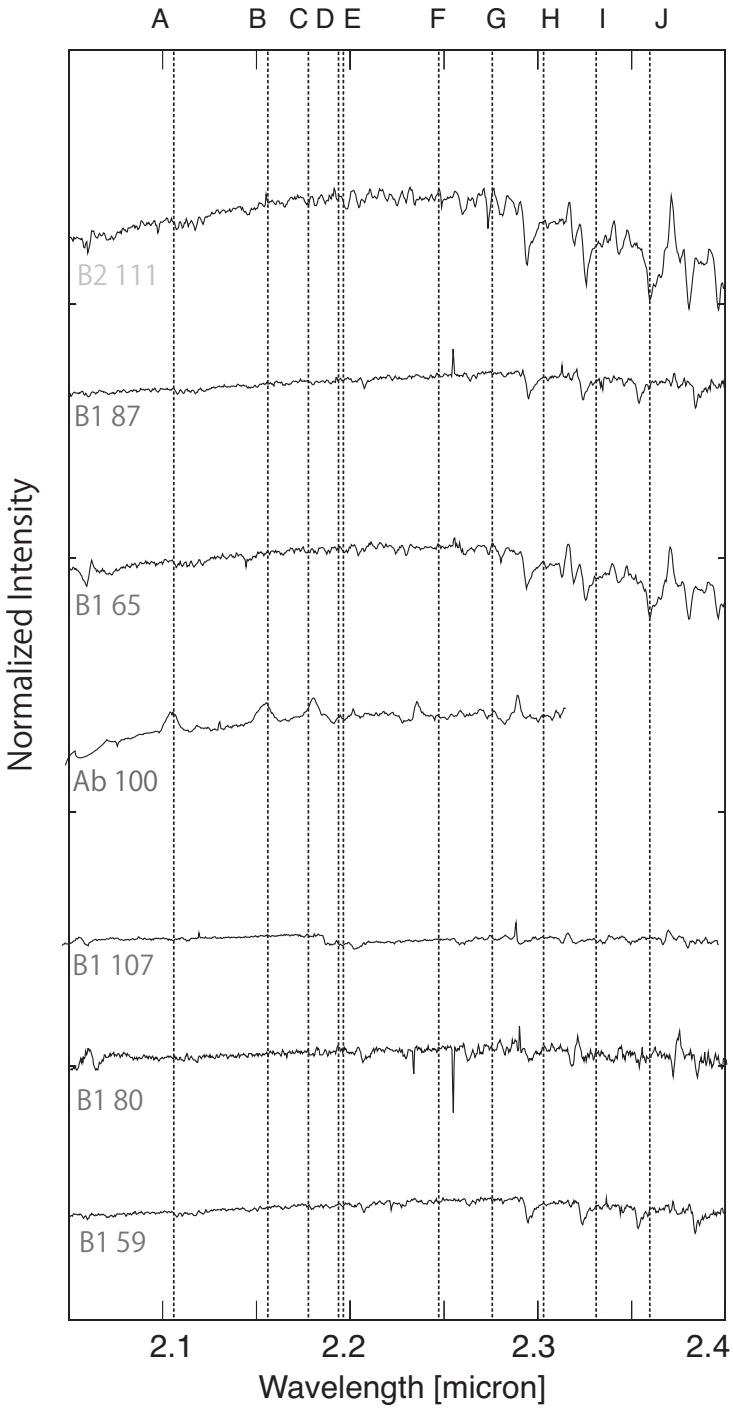

Figure 5.13: Example of normalized K_s-band spectra in the Ebisawa field. X-ray source numbers are given below each spectrum. The color of each number corresponds to group Ab, B1, and B2 in Chap. 6. The identification of features A–J is given in Table 5.4.

Table 5.4: List of K-band features

Element	Features [μm]	Correspondence with Figure 5.12
He_I	2.113	A
Mg_{II}	2.144	–
H_I	2.166	B
He_{II}	2.189	C
Na_I	2.206	D
Na_I	2.209	E
Ca_I	2.263	F
Ca_I	2.266	–
CO	2.293	G
CO	2.323	H
CO	2.352	I
CO	2.383	J

the sources in the Revnivtsev field. (1) Sources with Brγ and CO absorption features. (2) Sources only with CO absorption features. From these properties, (1) are G or K spectral type stars and (2) are M spectral type stars. In addition, some sources have metallic features (CaI, MgI and MgII). In the Ebisawa field, in addition to these two types, there are some sources that have emission features, which are likely to be CVs. Source classification based on NIR spectroscopic results is discussed in detail in § 6.3.

Chapter 6

Discussions

Contents

6.1 X-ray Properties of the Point Sources

6.1.1 Grouping by X-ray Colors

We first examine colors of all the X-ray point sources in the Revnivtsev field. As most of them have low photon statistics, we used a quantile analysis (Hong et al. 2004) to represent colors, which is effective in such a case. Using this method, we made a quantile color-color diagram (Figure 6.1). In the diagram, the quantile Q_x for each source is defined as

$$Q_x = \frac{E_{\rm x} - E_{\rm min}}{E_{\rm max} - E_{\rm min}}, \tag{6.1}$$

where $E_{\rm x}$ is the energy below which x % of the photons reside when sorted by energy, and $E_{\rm min} = 0.5$ keV and $E_{\rm max} = 8$ keV. For all the detected X-ray sources, we calculated Q_{50}, Q_{25}, and Q_{75} and used two combinations of these quantiles: q1 $= \log_{10} \frac{Q_{50}}{1-Q_{50}}$ and q2 $= \frac{3Q_{25}}{Q_{75}}$.

Regarding the Ebisawa field, we also made a quantile color-color diagram with the same method as the Revnivtsev field (Figure 6.2). On the diagram, the sources have almost the same distribution as in the Revnivtsev field. Thus, we applied the same criteria to separate all the detected X-ray point sources in the Ebisawa field. Hereafter, we mainly use the data of the Revnivtsev field because the Revnivtsev field is the deepest observation among the GRXE X-ray observations.

The q1 indicates the degree of photon spectrum being biased toward the harder (q1>0) or softer (q1<0) end, and the q2 indicates the degree of photon spectrum being less peaked (q2>1) or more peaked (q2<1). In order to put the diagram into a context, we simulated the quantiles for thermal and non-thermal spectra with different parameters. For the thermal spectra, we used an optically-thin thermal plasma model `brems` attenuated by the interstellar extinction model `tbabs` with the parameters in the ranges of $k_{\rm B}T = 0.5$–30 keV and $N_{\rm H} = 10^{20.5}$–10^{23} cm^{-2}. For the non-thermal spectra, we used a power-law model `pow` attenuated by the interstellar extinction model `tbabs` with the parameters in the ranges of $\Gamma = 1$–3 and $N_{\rm H} = 10^{20.5}$–10^{23} cm^{-2}.

In the plot, sources are distributed around (q1, q2) = (−0.5, 1.3). There are two branches extending up-and-leftward and up-and-rightward in the diagram. Based on this distribution, we define three groups of the sources: (A) q1 > -0.5, (B1) q1 ≤ -0.5 and q2 > 1.3, (B2) q1 ≤ -0.5 and q2 ≤ 1.3. Note that among the 21 bright sources of which spectra are studied individually, 18 sources are classified into group A while three are into group

B2. We then made a combined spectrum of each group using CIAO tool `combine_spectra` (Figure 6.3). This tool makes background-subtracted spectra, and photon counts-weighted ARFs and RMFs. It is noticeable that the spectra of group A and B2 show Fe K emission line feature in the 6–7 keV range, but B1 show hardly iron line emission. Existence of the Fe K feature in the combined spectrum of the group A apparently contradicts with the spectra of individual bright sources (Appendix B.1, C.1), in which almost no sources show significant Fe K emission. This strongly suggests that the Fe K emission feature depends on the source flux. We thus proceed to the flux-sorted spectra.

6.1.2 Grouping by X-ray Flux

In order to investigate contribution of the Fe K emission from the sources in the group A depending on the source fluxes, we separated the group A sources into three sub-groups by fluxes (bright, medium, and faint) so that each sub-group has almost the same total counts. The bright criterion is $> 6.8\times10^{-15}$ ergs cm^{-2} s^{-1}, the medium criterion is 6.8×10^{-15}–1.0×10^{-16}ergs cm^{-2} s^{-1}, and the faint criterion is $< 1.0\times10^{-16}$ ergs cm^{-2} s^{-1}. We then made a combined spectrum for each group. The spectra were normalized at 2.5 keV to facilitate comparison (Figure 6.4). We found that the fainter two sub-groups have obviously more significant Fe K line emission than the brightest sub-group. This suggests that the Fe K emission feature becomes more significant below a certain flux.

We then made combined spectra of the sources from the brightest one toward the faintest end by increasing the source number by 20 at each step. In other words, cumulative combined spectra were made above a certain threshold, and the threshold flux is gradually decreased. For each spectrum, we measured equivalent width (EW) of the Fe line. Figure 6.5 shows the EW value against the threshold flux. The EW starts to increase at around $F_{\rm X}$ $\sim6\times10^{-15}$ ergs cm^{-2} s^{-1}, indicating a new class of sources starts to dominate below this flux. We thus decided to separate the group A sources into two; sources with the fluxes above 6×10^{-15} ergs cm^{-2} s^{-1} (Aa) and those below this flux (Ab). Figure 6.6 shows distribution of the ME of each group. Sources in the group Aa and Ab have larger ME than those in B1 and B2, indicating that the sources in group A have harder spectra than the others.

We obtain fraction of the populations constituting the GRXE as follows (fraction in numbers and fluxes in 0.5–8 keV between 10^{-13} and 10^{-16} ergs cm^{-2} s^{-1}): Aa ($\sim$3%, $\sim$38%), Ab ($\sim$29%, $\sim$35%), B1 ($\sim$28%, $\sim$5%) and B2 ($\sim$40%, $\sim$22%).

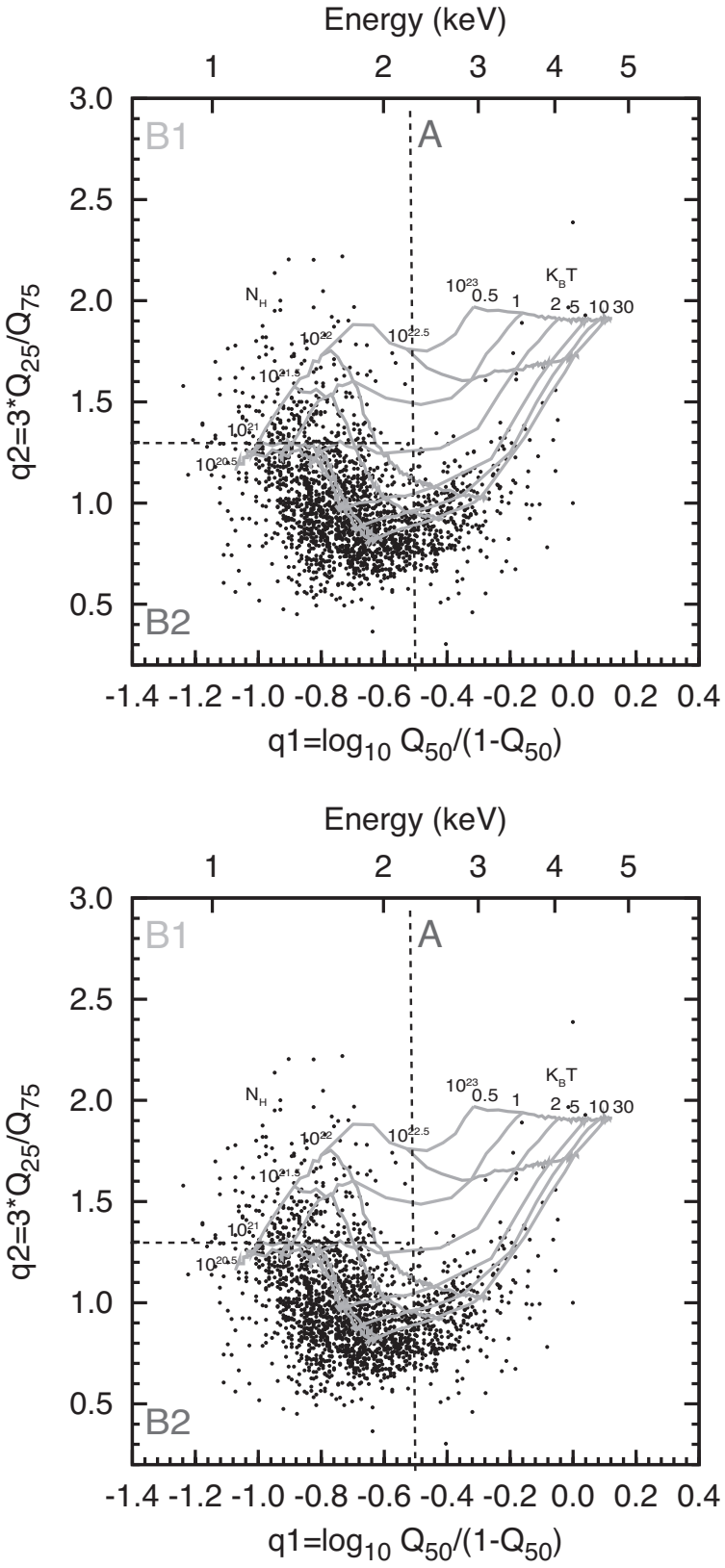

Figure 6.1: X-ray color-color diagrams of all the detected X-ray point sources in the Revnivtsev field. For reference, we plotted a grid of thermal spectra (top) and power-law spectra (bottom) attenuated by interstellar extinction with various parameter combinations. The labels indicate the values of $k_{\rm B}T$ (0.5, 1, 2, 5, 10, and 30 keV) and Γ (1, 1.5, 2.0, 2.5, and 3.0) and $N_{\rm H}$ ($10^{20.5}$, 10^{21}, $10^{21.5}$, 10^{22}, $10^{22.5}$, and 10^{23} cm^{-2}). We separate these sources into three groups (A, B1, and B2) by the values of q1 and q2.

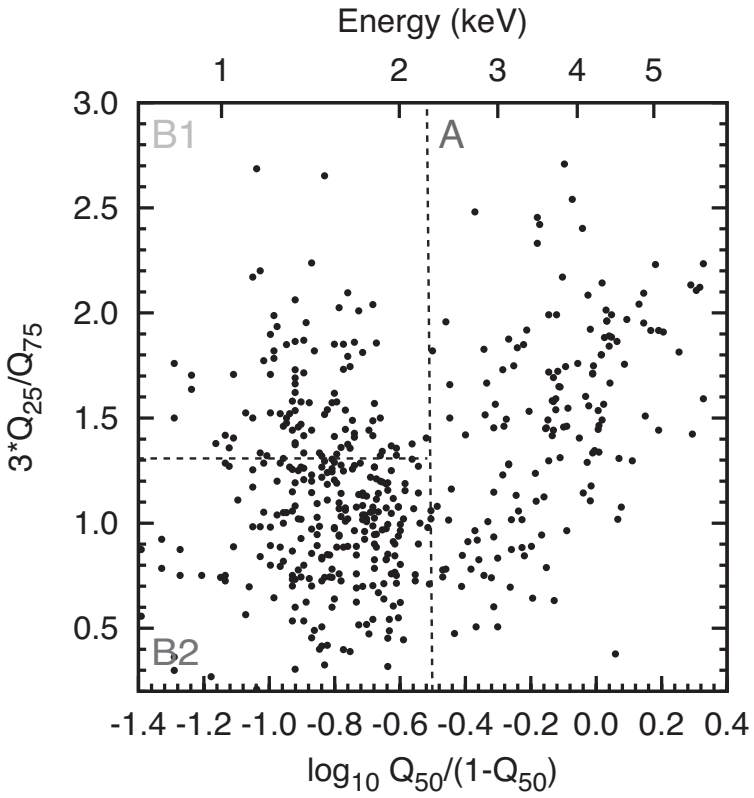

Figure 6.2: X-ray color-color diagrams of all the detected X-ray point sources in the Ebisawa field. We separated these sources into three groups (A, B1, and B2) by the same values of q1 and q2 as Figure 6.1.

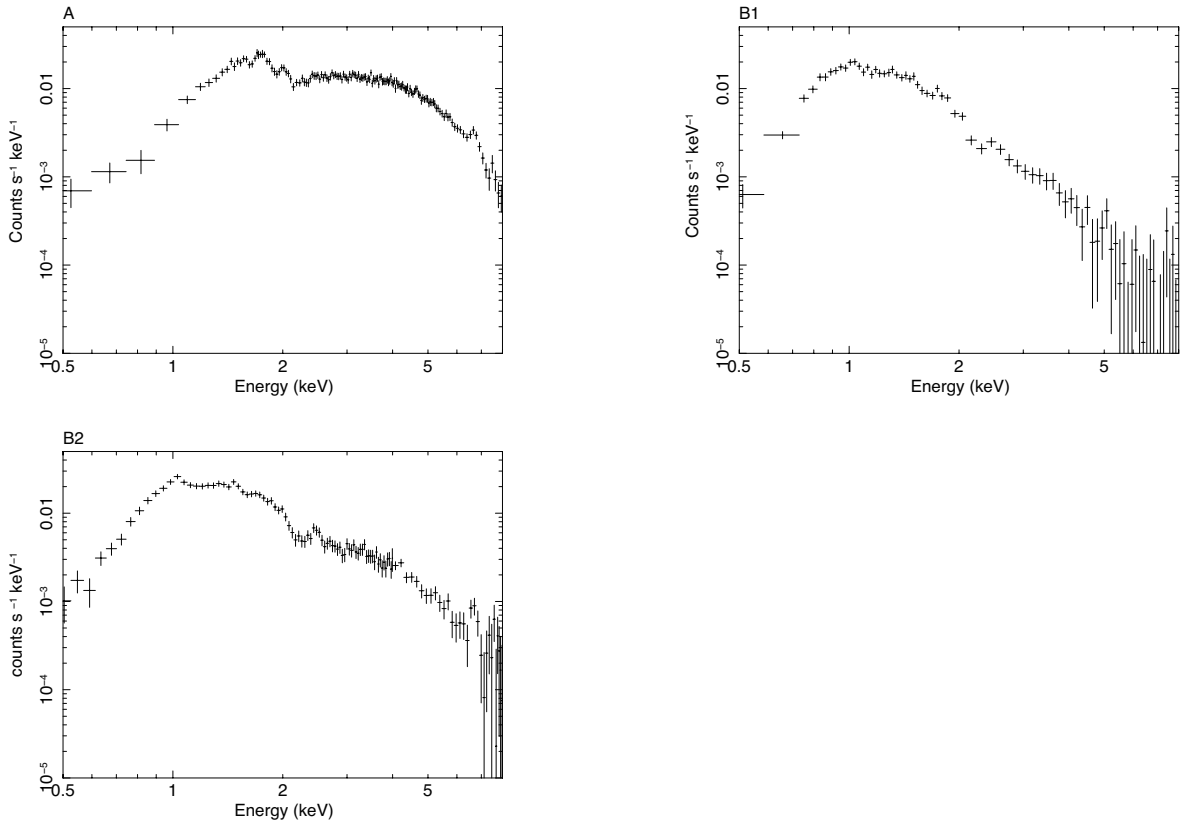

Figure 6.3: Combined spectra of X-ray point sources in group A (top left), B1 (top right), and B2 (down left).

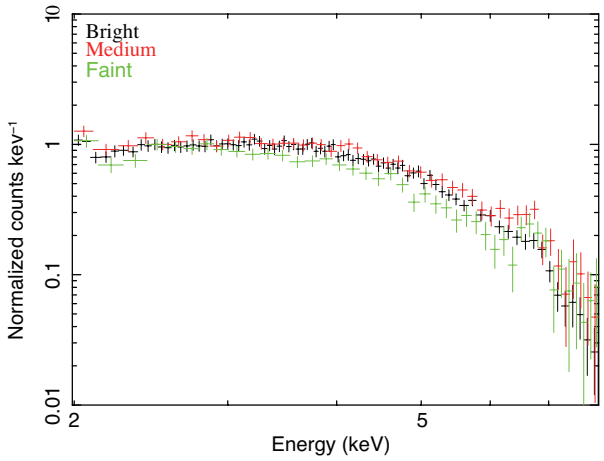

Figure 6.4: Combined spectra of different flux ranges: bright (black), medium (red), and faint (green). These spectra are normalized at 2.5 keV.

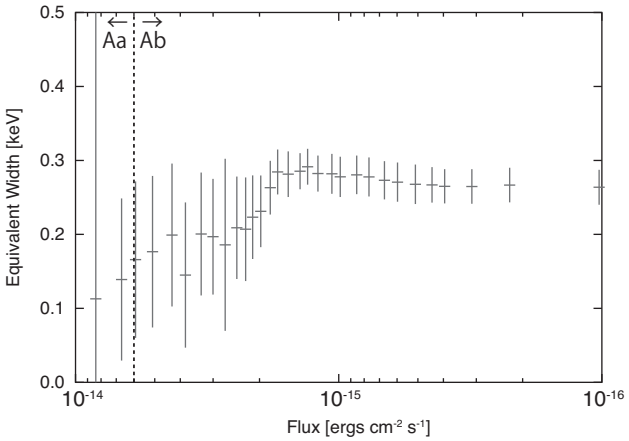

Figure 6.5: Equivalent width of the Fe K line of cumulatively combined spectra. Cross points show equivalent width at each flux. The error bars show a 1σ statistical uncertainty. The dashed line shows a boundary line between Aa and Ab.

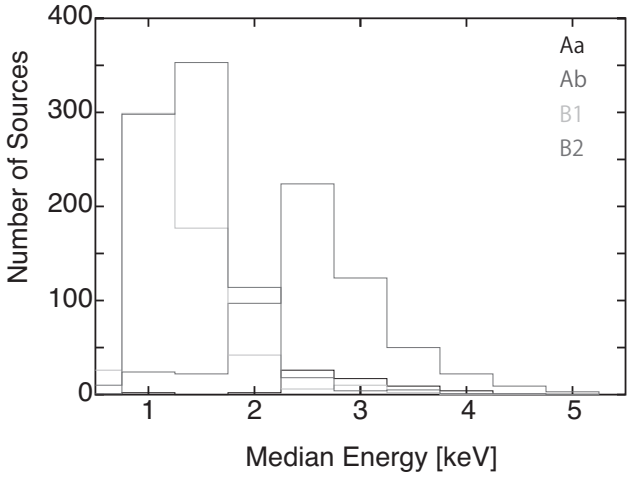

Figure 6.6: Histogram of the median energies of each group.

6.1.3 X-ray Photometric Properties

Source Variability

We plot X-ray variable sources in the quantile color-color diagram (Figure 6.7) made in the same manner as Figure 6.1. In this diagram, we plotted 101 variable sources selected in the KS test in § 5.1.3 with magenta. We found that more than half of the variable sources are in group B2. Fraction of the 101 variable sources in the four groups is the following: 6 (Aa), 21 (Ab), 18 (B1), and 56 (B2). The fraction of the variable sources in each group is 10±3 % (Aa), 4±2 % (Ab), 6±2 % (B1), and 13±4 % (B2), respectively.

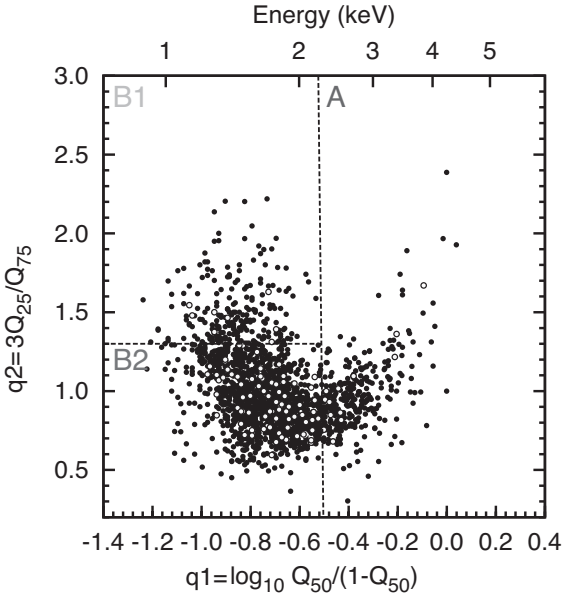

Figure 6.7: Quantile color-color diagrams of all the detected X-ray point sources, in which open circles show X-ray variable sources. Black circles show non-variable sources.

$\log N$–$\log S$ curve

We make the $\log N$–$\log S$ curve of X-ray point sources in the hard band (2–8 keV), separately for the group A, B1, B2, and total point sources (Figure 6.8). Note that the source detection efficiency is dependent on the off-axis angle (Figure 5.1), such that the sensitivity is the highest at around the image center. Also the $\log N$–$\log S$ curves are strongly affected by reduction of the detection rates in lower flux levels (Figure 5.2). Thus, below we make

fiducial discussion using the $\log N$–$\log S$ curves only above the flux level corresponding to the 100% detection rate.

In order to see the contribution of extra-galactic point sources, we compare our $\log N$–$\log S$ curve in the hard band with that of extra-galactic point sources detected in the same band by the *Chandra* Deep Field survey with a flux limit of 2.0×10^{-16} ergs cm^{-2} s^{-1} in 2–8 keV (Bauer et al. 2004). Since the extra-galactic sources are absorbed in the Revnivtsev field with a hydrogen column density of $N_{\rm H}\sim10^{22}$ cm^{-2} (Table 6.1), we take into account for this and use the $\log N$–$\log S$ curve with $N_{\rm H}\sim10^{22}$cm^{-2} in Bauer et al. (2004). As we show in Figure 6.8, the $\log N$–$\log S$ curve of the group A above 6×10^{-15} ergs cm^{-2} s^{-1} (which corresponds to Aa) is comparable with that of extra-galactic. Namely, number of the X-ray point sources in the group Aa is roughly the same as the number of the background AGNs. Below the threshold 6×10^{-15} ergs cm^{-2} s^{-1} and above the 100 % detection limit, the group A $\log N$–$\log S$ curve is much above the extra-galactic one, which indicates that Galactic sources dominate in the group Ab.

6.1.4 X-ray Spectroscopic Properties

Spectral Fitting

We make composite spectra for each group (Aa, Ab, B1, and B2) using the same method in § 6.1.1. It is noticable that Ab and B2 show a strong Fe line and Aa shows a weak Fe line (Figure 6.9). We now perform spectral fitting of the four composite spectra (Aa, Ab, B1, and B2) with more physically meaningful models in 0.5–8 keV. As we have shown in § 2.2, late-type stars, pre-CVs, and CVs have thermal spectra. Therefore, we first try two thermal models: a one-temperature plasma model and a two-temperature plasma model. We used the `apec` model as a thermal model in XSPEC. With a one-temperature plasma model, we could not fit any composite spectra. Then, using a two-temperature plasma model, we determined the best-fit model and parameters for Ab, B1, and B2 groups (Table 6.1). The composite spectra of the Ab, B1, and B2 are well fitted with a two-temperature thermal model. Comparing the best-fit parameters of Ab and B2, they have almost the same $k_{\rm B}T$, but the $N_{\rm H}$ values are different.

On the other hand, background AGNs have power-low spectra above $\sim$ 2 keV and an additional soft-excess component as we have shown in § 2.2. Therefore, for the Aa composite

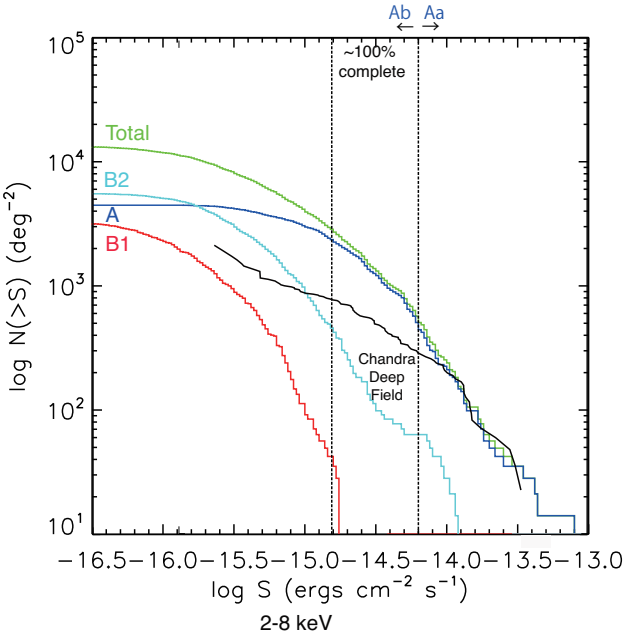

Figure 6.8: $\log N$–$\log S$ curve of the point sources detected in the Revnivtsev field in the hard band (2–8 keV). Green, blue, red, cyan solid curves correspond to the total, group A, group B1, and group B2 sources, respectively. On the diagrams, $\log N$–$\log S$ curve for extra-galactic sources with Galactic absorption ($N_{\rm H}$~10^{22} cm^{-2}) is shown in black for comparison (Bauer et al. 2004). The ~100% complete detection limit (§ 5.1.1) is shown as a vertical black dashed line. Flux boundary between the Aa sources and Ab sources is also indicated.

spectrum, we tried to fit with a one-temperature plasma model (for soft-excess) and a power-law model (Fe line is included). We used the `pow` model as a power-low model in XSPEC. We thus determined the best-fit model parameters for the Aa composite spectrum (Table 6.1).

In addition, we carried out spectral fitting of the composite spectra only in 4–8 keV with a power-law and a Gaussian model to precisely determine the iron line parameters and the underlying continuum (Table 6.2). Also in Table 6.2, we show contribution of each group to the total point-source continuum flux in 4–8 keV and the iron line flux. While Aa contributes to the continuum flux most, Ab, having the largest iron line EW, is the largest contributor to the iron line flux.

Furthermore, we have found that the bright individual sources with over 500 counts in the Aa group are successfully fitted with a power-law model in 0.5–8 keV without iron emission lines (Appendix C.1). The best-fit parameters of $N_{\rm H}$ and the photon index (Γ) are shown in Table 6.3.

Table 6.1: Best-fit parameters for spectral fittings

	Parameters	Aa	Ab	B1	B2
Two-temperature thermal model	$N_{\rm H}(10^{22}$ cm$^{-2})$		$1.93^{+0.85}_{-0.41}$	$0.69^{+0.06}_{-0.07}$	$0.79^{+0.19}_{-0.22}$
	$k_{\rm B}T_1$ (keV)		$0.20^{+0.12}_{-0.09}$	$0.61^{+0.03}_{-0.03}$	$0.96^{+0.09}_{-0.08}$
	$N_{\rm H}(10^{22}$ cm$^{-2})$		$1.99^{+0.28}_{-0.29}$	$1.04^{+0.25}_{-0.23}$	$0.14^{+0.05}_{-0.05}$
	$k_{\rm B}T_2$ (keV)		$10.47^{+2.46}_{-1.85}$	$1.93^{+0.37}_{-0.45}$	$9.55^{+3.30}_{-1.65}$
Thermal + Power-law model	$N_{\rm H}(10^{22}$ cm$^{-2})$	$0.07^{+0.27}_{-0.07}$			
	$k_{\rm B}T_1$ (keV)	$0.45^{+1.11}_{-0.45}$			
	$N_{\rm H}(10^{22}$ cm$^{-2})$	$1.79^{+0.77}_{-0.21}$			
	Photon index	$1.34^{+0.19}_{-0.09}$			
Reduced–χ^2		0.37	0.65	1.11	0.67

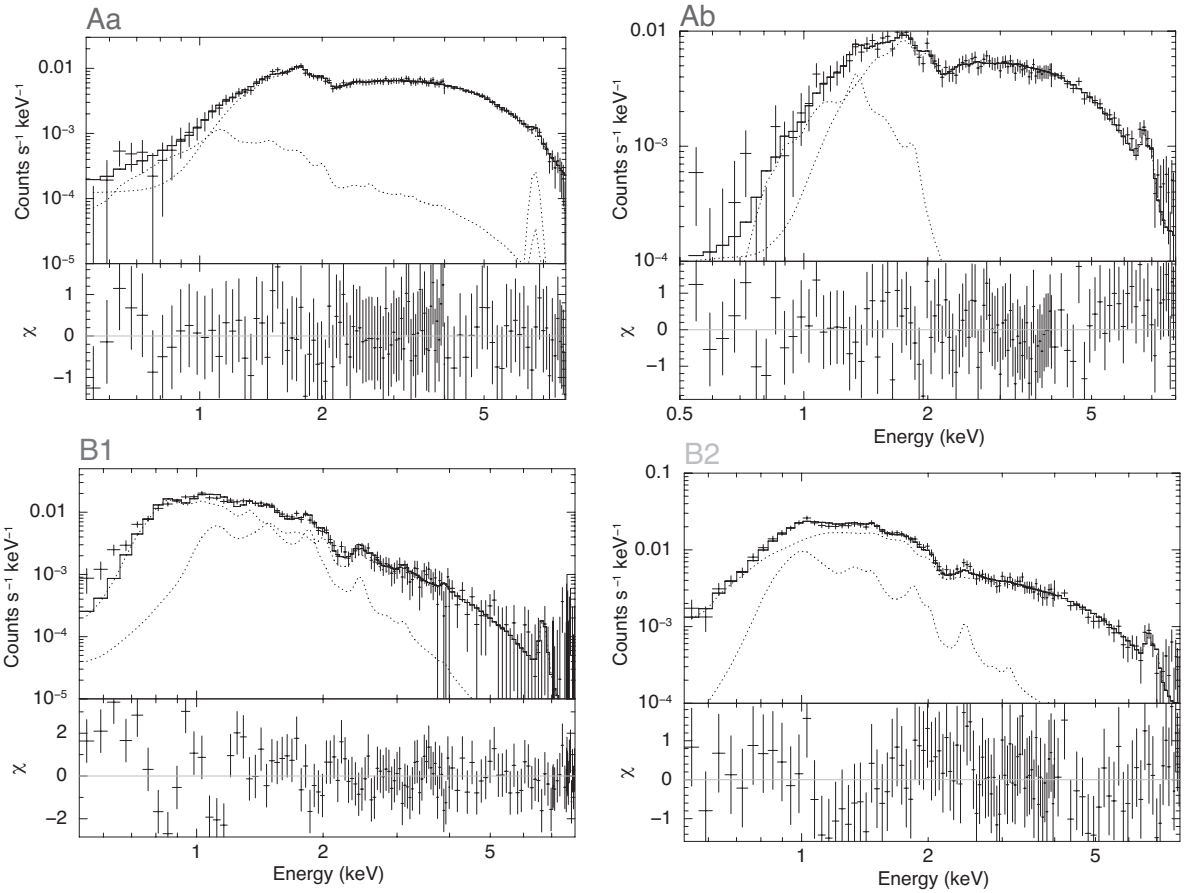

Figure 6.9: Composite spectra and model fitting for each spectrum in 0.5–8 keV. The model components are shown by dashed lines. The lower panel shows the residuals between the model and the data.

Table 6.2: Parameters of the composite spectra and total point-source spectrum in the iron energy band

Group	Line energy (keV)	EW[1] (eV)	$F_{\rm continuum}$[2] ($\times 10^{-13}$ ergs cm^{-2} s^{-1})	$f_{\rm continuum}$[3]	Line[4] flux (10^{-6} photons cm^{-2} s^{-1})	$f_{\rm Fe}$[5]
Aa	$6.75^{+0.10}_{-0.10}$	150^{+120}_{-105}	$6.4^{+0.4}_{-0.3}$	44%	$2.3^{+1.7}_{-1.4}$	18%
Ab	$6.72^{+0.05}_{-0.08}$	535^{+305}_{-230}	$5.5^{+0.4}_{-0.5}$	38%	$6.5^{+3.4}_{-2.7}$	52%
B2	$6.66^{+0.08}_{-0.08}$	340^{+200}_{-210}	$2.3^{+0.4}_{-0.3}$	16%	$3.7^{+2.0}_{-1.6}$	30%
B1	–	–	$0.3^{+0.1}_{-0.1}$	2%	–	–
Total point-source	$6.69^{+0.04}_{-0.04}$	321^{+121}_{-104}	$14.5^{+0.1}_{-0.1}$	–	$12.5^{+3.9}_{-3.5}$	–

[1] Equivalent width of the Fe K line.

[2] Continuum fluxes in 4–8 keV.

[3] Fraction to the total continuum.

[4] Fe K line fluxes.

[5] Fraction to the total point-source Fe K line flux.

Table 6.3: Power-law fitting of the group Aa bright sources

Seq. ID	$C_{\rm t,net}{}^{*}$	log $N_{\rm H}$ ($\rm cm^{-2}$)	Γ
33	1469.3	$22.4^{+0.09}_{-0.09}$	$1.7^{+0.3}_{-0.2}$
203†	670.9	$22.2^{+0.1}_{-0.2}$	$1.2^{+0.3}_{-0.3}$
371	783.6	$22.3^{+0.1}_{-0.1}$	$1.7^{+0.3}_{-0.3}$
385	633.8	$22.4^{+0.09}_{-0.09}$	$1.9^{+0.3}_{-0.3}$
438†	4325.4	$22.5^{+0.04}_{-0.04}$	$1.5^{+0.1}_{-0.1}$
888†	610.9	$22.1^{+0.1}_{-0.2}$	$1.4^{+0.3}_{-0.3}$
1083	643.2	$22.4^{+0.09}_{-0.09}$	$1.7^{+0.3}_{-0.3}$
1149†	2908.3	$22.4^{+0.06}_{-0.06}$	$1.3^{+0.1}_{-0.1}$
1207†	790.6	$22.2^{+0.1}_{-0.1}$	$1.5^{+0.3}_{-0.3}$
1252	1390.3	$22.1^{+0.08}_{-0.08}$	$1.6^{+0.2}_{-0.2}$
1320	509.6	$22.2^{+0.1}_{-0.1}$	$1.8^{+0.3}_{-0.3}$
1670	667.6	$22.2^{+0.1}_{-0.1}$	$1.6^{+0.3}_{-0.3}$
1732	704.5	$22.5^{+0.1}_{-0.1}$	$1.7^{+0.4}_{-0.4}$
1805	527.5	$22.5^{+0.1}_{-0.1}$	$2.0^{+0.4}_{-0.4}$
1831†	1447.3	$22.3^{+0.09}_{-0.10}$	$0.65^{+0.2}_{-0.2}$
1869†	1202.7	$22.4^{+0.1}_{-0.1}$	$1.0^{+0.3}_{-0.3}$
1893	561.9	$22.7^{+0.1}_{-0.2}$	$2.1^{\cdots}_{-0.5}$

*Source counts in 0.5–8 keV.

†Sources that are rejected to have an optically-thin thermal plasma spectrum are marked with †.

Summarizing the X-ray photometry and spectroscopy results of the point sources, the following are obtained:

X1: The 101 variable sources are divided into each group as 6(Aa), 21(Ab), 18(B1), and 56(B2). Fractions of the variable sources in each group is Aa (10±3%), Ab (4±2%), B1 (6±2%), and B2 (13±2%). Namely, B2 sources are most variable.

X2: The $\log N$–$\log S$ curve of the group Aa sources is comparable with that of the background AGNs considering the Galactic absorption (Figure 6.8). Namely, number of

the bright X-ray point sources in the group Aa is consistent with that expected for the background AGNs.

X3: The composite spectrum of the group Ab is represented with a two-temperature thermal plasma model with several keV and ∼10 keV (Figure 6.9). The spectrum also has a strong Fe emission line.

X4: The composite spectrum of the group B1 is represented with a two-temperature thermal plasma with low temperatures (Figure 6.9).

X5: The composite spectrum of the group B2 is represented with a two-temperature thermal plasma (low and high temperature; Figure 6.9). In addition, the spectrum has a strong Fe emission line.

X6: The best-fit parameters of $N_{\rm H}$ is different between Ab composite spectrum and B2 composite spectrum. The composite spectrum of Ab has larger $N_{\rm H}$ than B2, which suggests that sources in Ab tend to locate further than those in B2.

X7: Most bright sources in the group Aa have non-thermal spectra with very weak Fe K lines.

6.2 NIR Photometric Properties of the Point Sources

NIR Identification Fraction

We show the NIR identification fraction of each group in Table 6.4. Fractions of the group B1 and B2 are higher than those of the group Aa and Ab.

Table 6.4: NIR ID and unID fractions in each group

Group	Aa	Ab	B1	B2	Total
NIR identified	2	35	93	92	222
NIR unidentified	58	541	469	712	1780
Total	60	576	562	804	2002
ID fraction (%)	3	6	17	11	11

Color-Color Diagram

To better understand NIR properties of the sources, we made NIR color-color diagram (Figure 6.10). In the diagram, we plot Ab, B1, and B2 sources. There are no Aa sources on the diagram, because none are identified in the K_s-band. The intrinsic colors of dwarfs and giants are shown by the solid and dashed curves, respectively (Tokunaga 2000).

From Figure 6.10, we can see that most NIR-IDed X-ray sources in the group Ab have large extinction. The Ab sources gather around the position (H–K_s, J–H) = ($\sim$0.3, $\sim$1.2), which indicates that these sources are located rather at a large distance and intrinsically X-ray bright. They are likely to be accreting white dwarfs, which are known to be X-ray luminous relative to the NIR luminosities. On the other hand, NIR-IDed sources in the group B1 and B2 distribute over various extinctions. It suggests that these sources are located at various distances, including nearby late-type stars which are intrinsically X-ray faint.

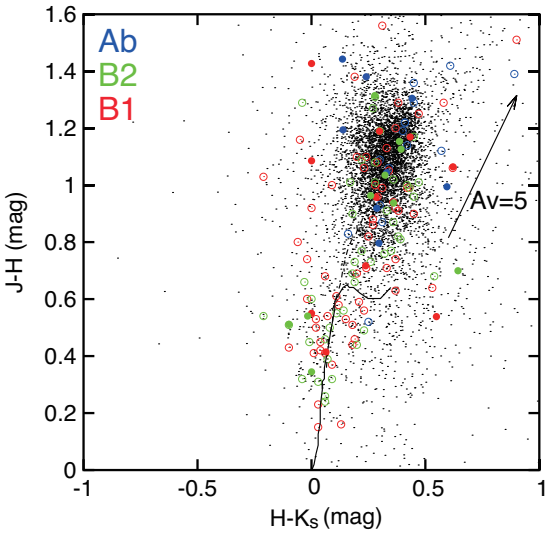

Figure 6.10: NIR color-color diagram of the NIR sources in J, H, and K_s-bands. Large open and filled circles show NIR IDed X-ray sources (blue: group Ab, green: group B1, and red: group B2 sources in § 6.1). Filled circles are sources we get NIR spectra in § 6.3. Small black dots show NIR sources without X-ray counterparts that include the SIRIUS and the 2MASS sources. Black solid and dashed curves represent the (evolutional) track of dwarfs and giants, respectively (Tokunaga 2000). Direction and amount of the extinction corresponding to $A_V = 5$ is shown with an arrow.

From the NIR imaging observations, the following results are obtained.

NP1: The NIR identification fraction is smaller in group A than in B1 and B2. It is the smallest in group Aa, and second smallest in group Ab.

NP2: Group Ab sources suffer large extinctions, which indicates that these sources are located at a large distance and intrinsically X-ray bright. These sources are likely to be accreting white dwarfs.

NP3: Most NIR IDed sources in the B1 and B2 groups distribute over various extinctions. This suggests that these sources are located at different distances, including nearby late-type stars which are intrinsically X-ray faint.

6.3 NIR Spectroscopic Properties of the Point Sources

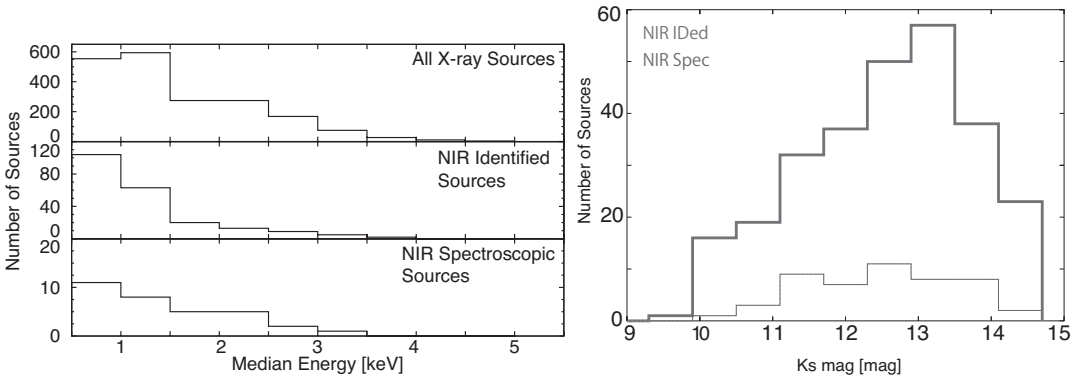

Figure 6.11: (Left) Histogram of the median energy of all the X-ray sources (top), NIR identified sources (middle), and NIR spectroscopic sources (bottom). (Right) Histogram of the K_s-band magnitude of NIR identified sources (thick line) and NIR spectroscopic sources (thin line) in the Revnivtsev field.

Before studying the NIR spectroscopic properties, we made histograms of the number of sources for median energies and K_s-band magnitudes. Figure 6.11 left shows histograms of the number of sources as a function of ME for all the X-ray sources, NIR IDed sources, and NIR spectroscopic sources. From the histograms, we can see that distribution of the sources are similar for each step (X-ray, NIR imaging, and NIR spectroscopy). For NIR spectroscopy, ME of the hardest source is about 3.5 keV. We made a histogram of the number of the K_s-band-detected SIRIUS sources and the Subaru spectroscopy sources at

each K_s-band magnitude in Figure 6.11 right. We see that NIR spectroscopic sources for the Subaru observations are almost uniformly distributed on K_s band from 10 to 15 mag.

In the Revnivtsev field, NIR spectra are mainly classified into the two classes; the spectra with type (1) HI (Brγ) absorption feature, type (2) HI (Brγ) and CO absorption features. The spectra of any group (Ab, B1, B2) are classified into these two classes. Type (1) sources are thought to be relatively earlier in the late-type stars (F- or G- or early K-type stars) and type (2) sources are thought to be relatively later in the late-type stars (mainly M-type) due to the CO absorption feature. All the sources in Ab, B1, and B2 are classified into type (1) or (2).

In the Ebisawa field, most NIR spectra are classified into types (1) and (2) above, but two sources are classified into type (3), indicating HI (Brγ) and HeII emission feature. These two sources are Seq ID 79,100 in Table 4.2, which are in group Ab. Type (3) is a signature of the CVs as we have shown in § 2.2.

From NP2 above, the Ab sources are considered to be accreting white dwarfs. The fact that only a small number of the Ab sources indicate the NIR signature of the CVs means that majority of the Ab sources are not CVs, but detached systems including white dwarfs without accretion disks (pre-CVs).

From the NIR spectroscopy (and NP2 above), the following results are revealed.

NS1: Most sources in the group Ab are type (1) or (2), and only 2 sources are type (3). From this, most sources in the group Ab are not CVs, but considered to be detached systems including white dwarfs (pre-CVs).

NS2: All the sources in the group B1 and B2 are type (1) or (2), which indicates that these sources are late-type stars.

6.4 Population of the Point Sources

In this section, we discuss origin of the X-ray point sources by using the results above. Table 6.5 shows that candidate populations for each group and evidences which are used for the classification. In Table 6.5, evidences with bold type are absolutely imperative to constrain populations. The evidences with regular type are supportive information.

Table 6.5: Classification of sources in each group. Here, the population indicates main population in each group. The evidences indicates the results to constrain each group population.

Group	Population[a]	Evidences[b]		
		X[c]	NP[c]	NS[c]
Aa	AGNs	**X2,X7**	**NP1**	
Ab	pre-CVs	**X3,X6**	**NP2**	**NS1**
	CVs	**X3.X6**	**NP2**	**NS1**
B1	Late-type stars (*quiescence*)	**X1,X4**	**NP3**	NS2
B2	Late-type stars (*flare*)	**X1,X5**	NP3	NS2

[a] Main population in each group.
[b] Evidences to constrain population.
[c] The labels in § 6.1, § 6.2, and § 6.3.

6.4.1 Group Aa sources

We propose that most sources in the group Aa are background AGNs due to the following reasons. First, in general, the AGNs have the power-law index $\Gamma \sim 1.7$ in the X-ray band regardless of their types and luminosity (Charles & Seward 1997). The X7 evidence is consistent with this.

Second, the X2 evidence indicates that the $\log N$–$\log S$ curve of the group Aa is comparable with that of the background AGNs considering the Galactic absorption.

Third, we use the NP1 evidence. Here, we examine the number of AGNs in our field by NIR observations. The number of galaxies (N) per square degree per magnitude at a certain K-band magnitude (K) is

$$\frac{dN}{dK} = 4000 \times 10^{\alpha(K-17)}, \tag{6.2}$$

where $\alpha = 0.67$ for $10 < K < 17$ mag (Tokunaga 2000). From this equation, the number of galaxies at $K_{\rm min} < K < K_{\rm max}$ is estimated by

$$\int_{K_{\rm min}}^{K_{\rm max}} \frac{dN}{dK} dK = \frac{4000}{\alpha \ln 10} (10^{\alpha(K_{\rm max}-17)} - 10^{\alpha(K_{\rm min}-17)}). \tag{6.3}$$

The interstellar extinction in the Revnivtsev field is $A_{\rm R} \sim 4$ (Revnivtsev et al. 2010), which corresponds to $A_{\rm K} \sim 1$. Thus, using the equation (6.3) with $K_{\rm min} = 10$ and $K_{\rm max} = 16$ and

considering the extinction, we can estimate number of the galaxies expected in our field of view. Thus, the estimated number of the galaxy is ∼10 in the *Chandra* FoV. This small number suggests that evidence NP1 is a consequence that Aa sources are mostly extra-galactic.

6.4.2 Group Ab sources

We consider that the group Ab sources are mainly pre-CVs, but including a small fraction of CVs, based on the following arguments. First, from the X3 evidence, the candidate sources of the group Ab are CVs (§ 2.2.2), pre-CVs (§ 2.2.3), and late-type stars (§ 2.2.1), because X-ray spectra of these populations have Fe K lines.

Second, from the X6 and NP2 evidences, the group Ab sources are located at large distances and intrinsically X-ray bright, which indicates that these sources are likely to be accreting white dwarfs. Therefore, we consider that CVs and pre-CVs are candidates of the group Ab sources.

Third, from the NP1 evidence, most group Ab sources have the NIR spectra of late-type stars except for the two CV-like spectra.

From these evidences, we consider that the group Ab sources are mainly pre-CVs, including a small fraction of CVs.

6.4.3 Group B1 sources

We consider that the group B1 sources are Galactic single or binary late-type stars on *quiescence* based on the following evidences.

First, from the X4 evidence, the group B1 source are considered to be late-type stars, because spectra from the late-type stars have low temperatures (a several keV; in § 2.2.1).

Second, from the X1 evidence, small fraction of the variable sources indicates that the group B1 sources are on *quiescence*.

Third, the NP3 evidence suggests that the group B1 sources include intrinsically X-ray faint late-type stars. In addition, the NS2 evidence supports that the B1 group sources are late-type stars.

From these evidences, we conclude that the group B1 sources are mostly late-type stars on *quiescence*.

6.4.4 Group B2 sources

We consider that the group B2 sources are Galactic single or binary late-type stars on *flare* based on the following evidences.

First, from the X5 evidence, the group B2 source candidates are CVs, pre-CVs, and late-type stars on *flare*, since spectra of these three populations have Fe K lines. However, the NP3 argument suggests that nearby X-ray dim sources are included in B2, which are likely to be late-type stars. From Table 6.2, the equivalent width of Fe K line of B2 corresponds to the equivalent width of late-type stars on *flare* within error ranges as we show in § 2.2.2.

Second, from the NS2 evidence, CVs are rejected. In addition, from the X1 argument, the group B2 sources are most variable, suggesting they are on *flare*.

We comment on the rather high temperature of 9.5 keV for the composite spectrum of B2 (Table 6.1). As we show in § 2.2.2, late-type stars are known to have higher temperature than several keV on *flare* such as UX Ari and II Peg. Thus, 9.5 keV is reasonable for the late-type stars on flare.

From these arguments, we consider that the group B2 sources are mostly late-type stars on *flare*.

Point Source Populations Constituting the GRXE

From X-ray and NIR studies above, we propose main population of each group as follows: Aa: background AGNs, Ab: mainly pre-CVs but a small fraction of CVs included, B1: late-type stars on *quiescence*, and B2: late-type stars on *flare*.

Chapter 7

Conclusions

In this thesis, we focused on revealing the nature of the Galactic X-ray point sources that primarily contribute to the GRXE Fe K-line emission. We carried out extensive X-ray and near-infrared (NIR) studies of the X-ray point sources constituting the GRXE. We have used the "Revnivtsev field" ($l = 0.^\circ1$, $b = -1.^\circ4$) and the "Ebisawa field" ($l = 28.^\circ5$, $b = 0.^\circ0$), but primarily the Revnivtsev field, since it is the most deeply exposed Galactic field by *Chandra X-ray Observatory* to date.

1. From the *Chandra X-ray Observatory* archive data in the Revnivtsev field, we detected 2,002 X-ray point sources in the 17×17 arcmin^2 Advanced CCD Imaging Spectrometer (ACIS)-I image. Our observation is complete down to $F_{\rm X}{\sim}10^{-15.2}$ ergs cm^{-2} s^{-1} in 0.5–8 keV with the faintest detected sources at $F_{\rm X}{\sim}10^{-16.2}$ ergs cm^{-2} s^{-1}. For bright sources (>100 counts), we studied individual X-ray spectra and source variability.

2. We divided all the detected sources into four sub-groups (Aa: hard and bright, Ab: hard and dim, B2: medium, and B1: soft) depending on their spectral colors and X-ray fluxes, and studied composite spectra of these groups. Most bright sources in the group Aa have non-thermal spectra with *very weak* Fe K line. Composite spectra of the group Ab and B2 have strong Fe K lines, whereas iron line emission is hardly seen in B1. We obtained fractions of each population to the total point-source flux in the iron K-band as follows (fractions to the 4–8 keV continuum and to the iron line): Aa (∼44%, ∼18%), Ab (∼38%, ∼52%), B1 (∼2%, ∼0%) and B2 (∼16%, ∼30%).

3. The fraction of the variable sources in group Aa, Ab, B1, and B2 is 10±3%, 4±2%,

6±2%, and 13±4%, respectively. Namely, B2 sources are most variable.

4. We conducted NIR imaging observations of the Revnivtsev field to identify X-ray sources using the Infra-Red Survey Facility 1.4 m telescope in South Africa. We obtained J- (1.25 μm), H-(1.65 μm), and $K_{\rm s}$-(2.14 μm) band Simultaneous Infra-Red Imager for Unbiased survey (SIRIUS) images to identify X-ray point sources in 7.7×7.7 arcmin^2 down to $K_{\rm s}$∼16 mag. Combining the 2MASS (Two Micron All Sky Survey) and our SIRIUS data, we identified the NIR counterparts for 222 X-ray sources (∼11% of the X-ray sources).

5. None of the group Aa sources have NIR counterparts in $K_{\rm s}$ band, which suggests that most of the group Aa sources are background AGNs attenuated by large Galactic extinction. In fact, the X-ray surface number density of Aa sources is consistent with that of the AGNs known in the high Galactic latitudes, considering the Galactic X-ray absorption. Most NIR identified sources in the group Ab have large extinction, which indicates that these sources are located rather at a large distance, suggesting that they are intrinsically X-ray bright. Hence, these sources are likely to be accreting white dwarfs, which are known to be X-ray luminous relative to NIR luminosity. On the other hand, NIR identified sources in the groups B1 and B2 show a wide range of extinction; this suggests that these sources are located at various distances, including nearby late-type stars that are intrinsically X-ray faint.

6. We performed follow-up NIR spectroscopic observations in the Revnivtsev field and the Ebisawa field for the 33 and 55 NIR identified sources, respectively, using the Subaru telescope. We obtained the NIR spectra of the sources in groups Ab, B1 and B2 in $K_{\rm s}$ band using the Multi-Object Infrared Camera and Spectrograph (MOIRCS). We found that these NIR spectra are classified into the following three types: (1) Spectra with HI (Brγ) and CO absorption lines, (2) Spectra with CO absorption lines, and (3) Spectra with HI (Brγ) and HeII emission lines. (1) and (2) are signatures of the late-type stars and type (3) is a signature of the accretion disk in CVs. Most Ab sources are type (1) or (2), and only 2 Ab sources are type (3). From this, we conclude that most sources in the group Ab are not CVs, but detached systems including a white dwarf which does not have NIR line emitting accretion disks (pre-CVs). All the sources in B1 and B2 are type (1) and (2), thus they are considered to be late-type stars.

7. From these X-ray and NIR studies, we propose the nature of the sources in each group as follows: The group Aa sources are considered to be mainly background AGNs. The

group Ab sources are mainly pre-CVs, but a small fraction of CVs are included. The group B2 sources are mainly late-type stars on *flare*, because of their time variability and high temperatures. At last, the group B1 sources are mainly late-type stars on *quiescence*.

8. We have confirmed that the GRXE is primarily explained with superposition of X-ray point sources. These point sources consists of background AGNs, CVs, detached systems including a white dwarf (pre-CVs), late-type stars on *flare*, and late-type stars on *quiescence*. Pre-CVs are the primary contributor to the GRXE iron line emission, and late-type stars on *flare* are the secondary. As opposed to what has been predicted, contributions from CVs (Yuasa 2011) or late-type stars on quiescence (Revnivtsev et al. 2006) to the GRXE iron line emission are not very significant.

Bibliography

Ali, B., Carr, J. S., Depoy, D. L., Frogel, J. A., & Sellgren, K. 1995, *Astronomical Journal*, 110, 2415

Anders, E. & Grevesse, N. 1989, *Geochimica et Cosmochimica Acta*, 53, 197

Awaki, H., Anabuki, N., Fukazawa, Y., et al. 2008, *Publication of Astronomical Society of Japan*, 60, 293

Baskill, D. S., Wheatley, P. J., & Osborne, J. P. 2005, *Monthly Notices of the Royal Astronomical Society*, 357, 626

Bauer, F. E., Alexander, D. M., Brandt, W. N., et al. 2004, *Astronomical Journal*, 128, 2048

Bertin, E. & Arnouts, S. 1996, *Astronomy & Astrophysics Supplement*, 117, 393

Brinkman, B. C., Gunsing, T., Kaastra, J. S., et al. 2000, in Society of Photo-Optical Instrumentation Engineers (SPIE) Conference Series, Vol. 4012, Society of Photo-Optical Instrumentation Engineers (SPIE) Conference Series, ed. J. E. Truemper & B. Aschenbach, 81–90

Broos, P. S., Townsley, L. K., Feigelson, E. D., et al. 2010, *Astrophysical Journal*, 714, 1582

Canizares, C. R., Davis, J. E., Dewey, D., et al. 2005, *Publication of Astronomical Society of Pacific*, 117, 1144

Charles, P. A. & Seward, F. D. 1997, Journal of the British Astronomical Association, 107, 44

Dhillon, V. S., Marsh, T. R., Duck, S. R., & Rosen, S. R. 1997, *Monthly Notices of the Royal Astronomical Society*, 285, 95

Ebisawa, K., Maeda, Y., Kaneda, H., & Yamauchi, S. 2001, Science, 293, 1633

Ebisawa, K., Tsujimoto, M., Paizis, A., et al. 2005, *Astrophysical Journal*, 635, 214

Ebisawa, K., Yamauchi, S., Tanaka, Y., et al. 2008, *Publication of Astronomical Society of Japan*, 60, 223

Ezuka, H. & Ishida, M. 1999, *Astrophysical Journal Supplement*, 120, 277

Garmire, G. P., Bautz, M. W., Ford, P. G., Nousek, J. A., & Ricker, Jr., G. R. 2003, in Society of Photo-Optical Instrumentation Engineers (SPIE) Conference Series, Vol. 4851, Society of Photo-Optical Instrumentation Engineers (SPIE) Conference Series, ed. J. E. Truemper & H. D. Tananbaum, 28–44

Güdel, M., Linsky, J. L., Brown, A., & Nagase, F. 1999, *Astrophysical Journal*, 511, 405

Hands, A. D. P., Warwick, R. S., Watson, M. G., & Helfand, D. J. 2004, *Monthly Notices of the Royal Astronomical Society*, 351, 31

Hellier, C. & Mukai, K. 2004, *Monthly Notices of the Royal Astronomical Society*, 352, 1037

Hoffmeister, C. & Kholopov, P. N. 1985, *Soviet Astronomy*, 29, 719

Hong, J., Schlegel, E. M., & Grindlay, J. E. 2004, *Astrophysical Journal*, 614, 508

Ichikawa, T., Suzuki, R., Tokoku, C., et al. 2006, in Presented at the Society of Photo-Optical Instrumentation Engineers (SPIE) Conference, Vol. 6269, Society of Photo-Optical Instrumentation Engineers (SPIE) Conference Series

Ivanov, V. D., Rieke, M. J., Engelbracht, C. W., et al. 2004, VizieR Online Data Catalog, 2151, 10387

Jerius, D. H., Gaetz, T. J., & Karovska, M. 2004, in Society of Photo-Optical Instrumentation Engineers (SPIE) Conference Series, Vol. 5165, Society of Photo-Optical Instrumentation Engineers (SPIE) Conference Series, ed. K. A. Flanagan & O. H. W. Siegmund, 433–444

Kashikawa, N., Aoki, K., Asai, R., et al. 2002, *Publication of Astronomical Society of Japan*, 54, 819

Kataza, H., Okamoto, Y., Takubo, S., et al. 2000, in Society of Photo-Optical Instrumentation Engineers (SPIE) Conference Series, Vol. 4008, Society of Photo-Optical Instrumentation Engineers (SPIE) Conference Series, ed. M. Iye & A. F. Moorwood, 1144–1152

Kimura, M., Maihara, T., Iwamuro, F., et al. 2010, *Publication of Astronomical Society of Japan*, 62, 1135

Kopal, Z. 1959, Close binary systems, ed. Kopal, Z.

Koyama, K. 1989a, *Publication of Astronomical Society of Japan*, 41, 665

Koyama, K. 1989b, *Publication of Astronomical Society of Japan*, 41, 665

Koyama, K., Awaki, H., Kunieda, H., Takano, S., & Tawara, Y. 1989, *Nature*, 339, 603

Koyama, K., Makishima, K., Tanaka, Y., & Tsunemi, H. 1986, *Publication of Astronomical Society of Japan*, 38, 121

Martin, E. L., Pavlenko, Y., & Rebolo, R. 1997, *Astronomy & Astrophysics*, 326, 731

Miyazaki, S., Komiyama, Y., Sekiguchi, M., et al. 2002, *Publication of Astronomical Society of Japan*, 54, 833

Murray, S. S., Austin, G. K., Chappell, J. H., et al. 2000, in Society of Photo-Optical Instrumentation Engineers (SPIE) Conference Series, Vol. 4012, Society of Photo-Optical Instrumentation Engineers (SPIE) Conference Series, ed. J. E. Truemper & B. Aschenbach, 68–80

Nagashima, C., Nagayama, T., Nakajima, Y., et al. 1999, in Star Formation 1999, ed. T. Nakamoto, 397–398

Nagayama, T., Nagashima, C., Nakajima, Y., et al. 2003, in Society of Photo-Optical Instrumentation Engineers (SPIE) Conference Series, Vol. 4841, Society of Photo-Optical Instrumentation Engineers (SPIE) Conference Series, ed. M. Iye & A. F. M. Moorwood, 459–464

Noguchi, K., Aoki, W., Kawanomoto, S., et al. 2002, *Publication of Astronomical Society of Japan*, 54, 855

Osten, R. A., Drake, S., Tueller, J., et al. 2007, *Astrophysical Journal*, 654, 1052

Pandey, J. C. & Singh, K. P. 2012, *Monthly Notices of the Royal Astronomical Society*, 419, 1219

Rana, V. R., Singh, K. P., Schlegel, E. M., & Barrett, P. E. 2006, Advances in Space Research, 38, 2847

Revnivtsev, M., Churazov, E., Postnov, K., & Tsygankov, S. 2009, *Astronomy & Astrophysics*, 507, 1211

Revnivtsev, M., Sazonov, S., Gilfanov, M., Churazov, E., & Sunyaev, R. 2006, *Astronomy & Astrophysics*, 452, 169

Revnivtsev, M., van den Berg, M., Burenin, R., et al. 2010, *Astronomy & Astrophysics*, 515, A49

Rousselot, P., Lidman, C., Cuby, J.-G., Moreels, G., & Monnet, G. 2000, *Astronomy & Astrophysics*, 354, 1134

Skrutskie, M. F., Cutri, R. M., Stiening, R., et al. 2006, *Astronomical Journal*, 131, 1163

Smith, R. K., Brickhouse, N. S., Liedahl, D. A., & Raymond, J. C. 2001, *Astrophysical Journal Issue* , 556, L91

Strassmeier, K. G., Hall, D. S., Fekel, F. C., & Scheck, M. 1993, *Astronomy & Astrophysics Supplement*, 100, 173

Sugizaki, M., Mitsuda, K., Kaneda, H., et al. 2001, *Astrophysical Journal Supplement*, 134, 77

Suzuki, R., Tokoku, C., Ichikawa, T., et al. 2008, *Publication of Astronomical Society of Japan*, 60, 1347

Tabur, V. 2007, *Publications of the Astronomical Society of Australia*, 24, 189

Tanaka, Y. 2002, *Astronomy & Astrophysics*, 382, 1052

Tanuma, S., Yokoyama, T., Kudoh, T., et al. 1999, *Publication of Astronomical Society of Japan*, 51, 161

Tappert, C., Gänsicke, B. T., Schmidtobreick, L., Mennickent, R. E., & Navarrete, F. P. 2007, *Astronomy & Astrophysics*, 475, 575

Tokunaga, A. T. 2000, Infrared Astronomy, ed. Cox, A. N., 143

Tokunaga, A. T., Kobayashi, N., Bell, J., et al. 1998, in Society of Photo-Optical Instrumentation Engineers (SPIE) Conference Series, Vol. 3354, Society of Photo-Optical Instrumentation Engineers (SPIE) Conference Series, ed. A. M. Fowler, 512–524

Tsuru, T., Makishima, K., Ohashi, T., et al. 1989, *Publication of Astronomical Society of Japan*, 41, 679

Verbunt, F., Bunk, W. H., Ritter, H., & Pfeffermann, E. 1997, *Astronomy & Astrophysics*, 327, 602

Warner, B. 1995, Cambridge Astrophysics Series, 28

Warwick, R. S., Turner, M. J. L., Watson, M. G., & Willingale, R. 1985, *Nature*, 317, 218

Weisskopf, M. C., Brinkman, B., Canizares, C., et al. 2002, *Publication of Astronomical Society of Pacific*, 114, 1

Wilms, J., Allen, A., & McCray, R. 2000, *Astrophysical Journal*, 542, 914

Worrall, D. M., Marshall, F. E., Boldt, E. A., & Swank, J. H. 1982, *Astrophysical Journal*, 255, 111

Yamasaki, N. Y., Ohashi, T., Takahara, F., et al. 1997, *Astrophysical Journal*, 481, 821

Yamauchi, S., Kawada, M., Koyama, K., Kunieda, H., & Tawara, Y. 1990, *Astrophysical Journal*, 365, 532

Yamauchi, S. & Koyama, K. 1993, *Astrophysical Journal*, 404, 620

Yuasa, T. 2011, Dissertation, The University of Tokyo

Yuasa, T., Nakazawa, K., Makishima, K., et al. 2010, *Astronomy & Astrophysics*, 520, A25

Appendix A

Chandra Sources List

Table A.1: *Chandra* source list

Source		Position				Extracted Counts							Characteristics				
Seq	CXOU J	R. A.	Decl.	Err	θ	$C_{\rm net}$	$\Delta C_{\rm net}$	$C'_{\rm bkg}$	$C_{\rm net,hard}$	PSF	PS	$P_{\rm B}$	Anom	Var	EffExp	$E_{\rm median}$	Photo $F_{\rm x}$
#		(deg)	(deg)	($''$)	($'$)						Frac				(ks)	(keV)	(ergs s^{-1} cm^{-2})
(1)	(2)	(3)	(4)	(5)	(6)	(7)	(8)	(9)	(10)	(11)	(12)	(13)	(14)	(15)	(16)	(17)	(18)
1	175044.88−292837.6	267.687010	-29.477113	0.4	11.6	78.4	23.5	437.6	29.2	0.89	3.3	-3.9	....	b	486.5	1.5	1.6×10^{-15}
2	175045.10−293431.4	267.687940	−29.575409	0.4	9.2	38.4	14.9	163.6	30.0	0.90	2.5	-2.7	g...	...	325.1	3.0	1.1×10^{-15}
3	175045.10−293240.5	267.687950	−29.544603	0.3	9.7	56.1	19.1	279.9	17.7	0.89	2.9	-3.3	g...	...	535.5	1.5	2.4×10^{-15}
4	175045.51−293222.4	267.689630	−29.539560	0.3	9.7	46.4	16.5	201.6	34.1	0.78	2.7	-3.1	g...	...	597.9	2.9	1.9×10^{-15}
5	175045.86−293503.5	267.691120	−29.584322	0.3	9.1	60.6	16.5	190.4	52.7	0.90	3.6	-5.0	g...	...	417.5	2.7	3.0×10^{-15}
6	175045.90−293208.7	267.691270	−29.535760	0.3	9.7	92.1	20.3	291.9	24.2	0.85	4.4	<-5	g...	...	639.9	1.4	1.5×10^{-15}
7	175046.03−293539.1	267.691800	−29.594220	0.4	9.0	40.2	15.5	179.8	10.7	0.90	2.5	-2.7	g...	...	387.2	1.8	1.3×10^{-15}
8	175046.07−293405.8	267.691960	−29.568297	0.3	9.2	69.0	19.2	270.0	46.8	0.90	3.5	-4.7	g...	...	570.4	2.4	2.0×10^{-15}
9	175046.25−292947.1	267.692710	−29.496437	0.3	10.7	60.1	17.6	224.9	51.2	0.69	3.3	-4.3	....	b	678.2	3.3	2.5×10^{-15}
10	175046.62−292935.0	267.694250	−29.493066	0.3	10.8	58.6	17.7	229.4	73.7	0.70	3.2	-4.1	....	b	677.5	5.2	3.9×10^{-15}
11	175047.08−293334.4	267.696170	−29.559558	0.3	9.1	48.4	19.9	316.6	8.2	0.90	2.4	-2.4	g...	...	679.6	1.2	6.3×10^{-16}
12	175047.51−293733.0	267.697980	−29.625834	0.3	9.0	51.4	17.4	226.6	42.1	0.90	2.9	-3.3	g...	...	519.2	2.8	2.0×10^{-15}
13	175048.28−293250.7	267.701180	−29.547440	0.2	9.0	148.7	22.4	321.3	125.7	0.90	6.5	<-5	....	a	714.8	3.5	4.8×10^{-15}
14	175048.39−292816.1	267.701660	−29.471139	0.4	11.3	71.4	20.2	304.6	47.4	0.90	3.5	-4.5	g...	...	386.5	2.4	3.1×10^{-15}
15	175048.54−293937.5	267.702280	−29.660423	0.3	9.5	102.3	19.1	235.7	82.1	0.90	5.2	<-5	g...	...	457.0	3.0	5.1×10^{-15}
16	175048.65−293538.6	267.702740	−29.594083	0.2	8.5	127.2	18.6	194.8	79.1	0.80	6.6	<-5	g...	...	734.4	3.6	4.8×10^{-15}
17	175048.86−293736.9	267.703620	−29.626938	0.3	8.8	73.8	20.0	296.2	30.3	0.90	3.6	-4.8	g...	...	698.8	1.9	1.4×10^{-15}
18	175048.91−292906.9	267.703810	−29.485275	0.3	10.6	124.8	25.5	482.2	45.0	0.90	4.8	<-5	....	a	668.0	1.6	1.9×10^{-15}
19	175048.95−293547.9	267.703980	−29.596661	0.2	8.5	82.7	16.4	165.3	51.4	0.76	4.9	<-5	....	a	752.1	2.5	2.1×10^{-15}
20	175049.07−293803.6	267.704500	−29.634354	0.3	8.8	82.8	20.6	312.2	13.8	0.90	3.9	<-5	g...	...	702.2	1.6	1.3×10^{-15}
21	175049.14−293346.2	267.704780	−29.562853	0.3	8.6	66.8	19.5	286.2	29.8	0.90	3.3	-4.2	....	a	722.0	1.9	1.2×10^{-15}
22	175049.30−293527.5	267.705420	−29.590998	0.2	8.4	141.8	20.9	264.2	67.8	0.88	6.6	<-5	....	a	766.0	1.7	2.1×10^{-15}
23	175049.37−294045.3	267.705740	−29.679276	0.3	9.9	56.8	18.9	274.2	47.6	0.90	2.9	-3.4	g...	...	488.4	3.0	2.5×10^{-15}
24	175049.58−293836.6	267.706600	−29.643509	0.2	8.9	132.0	21.7	309.0	19.7	0.90	5.9	<-5	g...	...	694.4	1.1	1.6×10^{-15}
25	175049.63−293025.2	267.706810	−29.507008	0.2	9.8	198.0	25.2	401.0	45.4	0.90	7.7	<-5	....	c	692.1	1.4	2.7×10^{-15}
26	175049.66−293913.2	267.706940	−29.653679	0.3	9.1	55.5	19.3	289.5	43.4	0.87	2.8	-3.1	g...	...	694.7	3.2	1.7×10^{-15}
27	175049.70−293222.6	267.707110	−29.539626	0.2	8.9	201.7	23.2	303.3	141.1	0.90	8.5	<-5	....	a	718.9	2.8	5.2×10^{-15}
28	175049.72−293116.2	267.707170	−29.521168	0.3	9.3	92.2	22.2	364.8	35.7	0.90	4.1	<-5	....	a	707.8	1.8	1.6×10^{-15}
29	175050.44−293713.8	267.710180	−29.620526	0.2	8.3	137.9	19.8	227.1	116.1	0.90	6.8	<-5	g...	...	642.8	3.5	5.5×10^{-15}
30	175050.52−293002.5	267.710500	−29.500698	0.3	9.8	109.7	23.0	384.3	41.1	0.90	4.7	<-5	....	a	683.5	1.5	1.6×10^{-15}
31	175050.54−294029.2	267.710610	−29.674795	0.3	9.6	131.1	21.3	292.9	44.1	0.86	6.0	<-5	g...	...	666.8	1.7	2.4×10^{-15}
32	175051.10−294235.8	267.712940	−29.709960	0.4	10.7	62.6	21.4	360.4	22.4	0.91	2.9	-3.2	....	a	471.8	1.8	1.5×10^{-15}
33	175051.16−293419.5	267.713170	−29.572106	0.1	8.1	1469.3	42.1	251.7	1106.7	0.90	34.5	<-5	....	a	785.9	2.9	3.6×10^{-14}
34	175051.21−293546.0	267.713390	−29.596137	0.3	8.0	46.6	18.2	259.4	0.0	0.90	2.5	-2.6	....	a	786.6	1.5	5.8×10^{-16}

(*cont.*)

Table A.1: *Chandra* source list

Source		Position				Extracted Counts				Characteristics							
Seq	CXOU J	R. A.	Decl.	Err	θ	$C_{\rm net}$	$\Delta C_{\rm net}$	$C'_{\rm bkg}$	$C_{\rm net,hard}$	PSF	PS	$P_{\rm B}$	Anom	Var	EffExp	$E_{\rm median}$	Photo $F_{\rm x}$
#		(deg)	(deg)	($''$)	($'$)						Frac				(ks)	(keV)	(ergs s^{-1} cm^{-2})
(1)	(2)	(3)	(4)	(5)	(6)	(7)	(8)	(9)	(10)	(11)	(12)	(13)	(14)	(15)	(16)	(17)	(18)
35	175051.24−293031.4	267.713500	−29.508729	0.2	9.4	146.0	23.3	361.0	37.6	0.90	6.1	<-5	....	b	693.5	1.6	2.3×10^{-15}
36	175051.49−293338.3	267.714550	−29.560646	0.2	8.1	114.8	19.9	251.2	78.9	0.90	5.6	<-5	....	b	783.4	2.9	2.8×10^{-15}
37	175051.59−294036.0	267.714980	−29.676687	0.3	9.5	96.6	19.2	244.4	70.0	0.84	4.9	<-5	g...	...	649.4	2.9	3.5×10^{-15}
38	175051.80−293834.5	267.715870	−29.642927	0.3	8.5	56.5	19.3	285.5	33.4	0.91	2.9	-3.2	g...	...	736.0	3.0	1.6×10^{-15}
39	175051.86−294311.3	267.716100	−29.719822	0.4	11.0	55.9	21.7	382.1	63.6	0.91	2.5	-2.6	g...	...	473.3	3.4	2.8×10^{-15}
40	175051.91−292813.7	267.716300	−29.470488	0.4	10.7	46.1	19.3	295.9	18.1	0.90	2.3	-2.3	g...	...	441.2	1.7	1.2×10^{-15}
41	175052.05−293502.7	267.716900	−29.584102	0.2	7.8	103.9	19.0	232.1	23.1	0.90	5.3	<-5	....	b	792.2	1.5	1.3×10^{-15}
42	175052.16−293404.1	267.717370	−29.567810	0.3	7.9	45.4	17.2	226.6	11.6	0.90	2.6	-2.8	....	b	789.3	1.5	5.6×10^{-16}
43	175052.17−293552.5	267.717380	−29.597921	0.2	7.8	134.3	19.9	235.7	96.6	0.89	6.6	<-5	....	a	790.7	2.9	3.3×10^{-15}
44	175052.27−293051.6	267.717830	−29.514360	0.3	9.0	70.9	21.0	338.1	10.1	0.90	3.3	-4.1	g...	...	744.0	1.2	8.2×10^{-16}
45	175052.43−293321.1	267.718460	−29.555883	0.2	8.0	98.3	18.8	227.7	43.6	0.90	5.1	<-5	....	a	762.7	1.8	1.5×10^{-15}
46	175052.60−293712.7	267.719200	−29.620215	0.3	7.9	51.7	16.5	197.3	26.9	0.88	3.0	-3.7	g...	...	702.2	3.8	2.0×10^{-15}
47	175052.62−293751.4	267.719260	−29.630946	0.2	8.0	110.1	19.4	239.9	40.3	0.89	5.5	<-5	....	c	771.3	1.8	1.7×10^{-15}
48	175052.71−294002.5	267.719660	−29.667371	0.3	8.9	82.1	20.7	313.9	42.6	0.90	3.9	<-5	g...	...	724.2	2.1	1.7×10^{-15}
49	175052.90−293133.3	267.720450	−29.525938	0.2	8.5	166.9	22.2	294.1	28.2	0.90	7.3	<-5	g...	...	766.8	1.3	1.9×10^{-15}
50	175052.95−293739.2	267.720660	−29.627567	0.2	7.9	81.0	18.5	235.0	60.5	0.89	4.3	<-5	....	b	770.0	2.9	2.1×10^{-15}
51	175052.97−293246.7	267.720710	−29.546322	0.2	8.0	180.5	21.0	233.5	77.4	0.91	8.4	<-5	....	a	774.2	1.7	2.6×10^{-15}
52	175053.04−293520.8	267.721000	−29.589137	0.2	7.6	55.3	17.2	216.7	6.6	0.90	3.1	-3.9	....	a	795.1	1.2	5.5×10^{-16}
53	175053.27−293641.7	267.721980	−29.611606	0.2	7.7	103.5	16.0	133.5	83.8	0.85	6.3	<-5	g...	...	633.1	2.9	3.4×10^{-15}
54	175053.37−293206.0	267.722380	−29.535005	0.2	8.2	134.1	20.2	245.9	63.2	0.90	6.5	<-5	g...	...	772.6	1.9	2.3×10^{-15}
55	175053.38−293921.6	267.722440	−29.656023	0.2	8.5	98.1	21.1	314.9	55.3	0.91	4.5	<-5	g...	...	759.6	2.8	2.5×10^{-15}
56	175053.51−293705.4	267.722970	−29.618180	0.2	7.7	132.0	18.4	183.0	27.7	0.89	7.0	<-5	g...	...	699.5	1.4	1.8×10^{-15}
57	175053.58−293648.6	267.723270	−29.613517	0.3	7.6	30.2	11.0	77.8	14.6	0.70	2.6	-3.1	g...	...	681.7	2.0	7.9×10^{-16}
58	175053.72−293726.8	267.723850	−29.624130	0.3	7.7	37.3	12.0	91.7	10.2	0.67	3.0	-3.7	....	b	775.5	1.3	5.9×10^{-16}
59	175053.73−293120.2	267.723880	−29.522304	0.2	8.5	224.1	23.2	283.9	43.5	0.90	9.4	<-5	g...	...	751.2	1.4	3.0×10^{-15}
60	175053.74−293409.0	267.723920	−29.569194	0.2	7.5	228.9	20.8	179.1	12.2	0.90	10.7	<-5	....	c	782.2	1.1	2.1×10^{-15}
61	175053.93−293036.6	267.724710	−29.510187	0.3	8.8	44.9	19.4	303.1	40.2	0.90	2.3	-2.2	....	a	747.0	2.5	9.9×10^{-16}
62	175053.96−294058.5	267.724840	−29.682930	0.3	9.2	58.0	20.5	329.0	30.1	0.90	2.8	-3.0	g...	...	730.9	3.0	1.7×10^{-15}
63	175053.98−293340.6	267.724920	−29.561305	0.2	7.6	87.1	17.1	180.9	76.2	0.90	5.0	<-5	....	c	784.8	3.7	2.7×10^{-15}
64	175053.99−293718.9	267.724970	−29.621943	0.2	7.6	194.6	19.4	158.4	20.2	0.83	9.8	<-5	....	c	766.8	1.1	2.0×10^{-15}
65	175054.03−293150.7	267.725130	−29.530767	0.2	8.2	88.5	19.0	246.5	66.0	0.90	4.5	<-5	g...	...	754.8	2.6	2.2×10^{-15}
66	175054.26−294327.4	267.726090	−29.724292	0.1	10.8	1600.2	46.2	470.8	1517.0	0.91	34.3	<-5	g...	...	618.0	4.0	7.7×10^{-14}
67	175054.28−293838.8	267.726170	−29.644118	0.2	8.0	75.9	19.0	259.1	26.6	0.90	3.9	<-5	....	b	769.8	1.4	8.2×10^{-16}
68	175054.28−292904.3	267.726190	−29.484530	0.3	9.7	57.6	21.2	359.4	16.3	0.90	2.7	-2.8	....	b	743.1	1.6	9.7×10^{-16}

(*cont.*)

Table A.1: *Chandra* source list

Source		Position				Extracted Counts				Characteristics							
Seq	CXOU J	R. A.	Decl.	Err	θ	$C_{\rm net}$	$\Delta C_{\rm net}$	$C'_{\rm bkg}$	$C_{\rm net,hard}$	PSF	PS	$P_{\rm B}$	Anom	Var	EffExp	$E_{\rm median}$	Photo $F_{\rm x}$
#		(deg)	(deg)	($''$)	($'$)						Frac				(ks)	(keV)	(ergs s^{-1} cm^{-2})
(1)	(2)	(3)	(4)	(5)	(6)	(7)	(8)	(9)	(10)	(11)	(12)	(13)	(14)	(15)	(16)	(17)	(18)
69	175054.35−292947.7	267.726500	−29.496604	0.3	9.2	69.1	16.5	180.9	31.3	0.75	4.1	<-5	....	a	751.3	1.9	1.4×10^{-15}
70	175054.47−293259.2	267.726980	−29.549782	0.3	7.7	50.4	16.0	184.6	29.5	0.90	3.0	-3.8	g...	...	768.4	2.6	1.2×10^{-15}
71	175054.52−293544.4	267.727190	−29.595674	0.2	7.3	51.0	16.4	194.0	19.9	0.90	3.0	-3.7	....	a	786.5	1.8	7.6×10^{-16}
72	175054.60−293136.5	267.727510	−29.526821	0.2	8.2	95.7	19.6	259.3	50.1	0.90	4.8	<-5	g...	...	758.8	2.0	1.8×10^{-15}
73	175054.69−293326.8	267.727890	−29.557464	0.3	7.5	31.8	9.4	46.2	16.1	0.55	3.2	-4.8	g...	...	766.1	2.1	9.6×10^{-16}
74	175054.90−293507.3	267.728790	−29.585381	0.2	7.2	106.7	17.3	168.3	96.2	0.90	6.0	<-5	....	a	786.7	3.6	3.2×10^{-15}
75	175054.98−294008.5	267.729120	−29.669039	0.2	8.6	282.9	24.8	296.1	175.8	0.90	11.2	<-5	....	a	755.8	2.7	6.9×10^{-15}
76	175055.22−293820.9	267.730110	−29.639148	0.3	7.7	39.1	16.7	215.9	22.1	0.90	2.3	-2.3	....	b	779.3	3.2	1.1×10^{-15}
77	175055.30−293324.7	267.730450	−29.556863	0.2	7.4	77.7	13.4	85.3	54.3	0.72	5.6	<-5	g...	...	746.9	2.6	2.4×10^{-15}
78	175055.36−294131.1	267.730670	−29.691983	0.2	9.3	670.4	32.7	352.6	499.1	0.90	20.2	<-5	....	b	736.5	3.0	1.9×10^{-14}
79	175055.39−293442.8	267.730800	−29.578572	0.2	7.1	56.1	15.0	148.9	30.1	0.90	3.6	<-5	g...	...	782.4	2.3	1.1×10^{-15}
80	175055.51−292949.1	267.731320	−29.496973	0.2	9.0	144.9	19.4	204.1	114.7	0.80	7.3	<-5	....	a	754.1	3.7	5.4×10^{-15}
81	175055.54−293637.6	267.731430	−29.610465	0.2	7.2	60.0	14.8	141.0	39.5	0.90	3.9	<-5	g...	...	612.2	3.3	2.2×10^{-15}
82	175055.56−293124.5	267.731510	−29.523478	0.1	8.1	443.8	27.1	254.2	374.2	0.90	16.1	<-5	....	a	779.0	3.3	1.2×10^{-14}
83	175055.60−293713.6	267.731680	−29.620467	0.2	7.3	70.0	16.1	167.0	22.6	0.88	4.2	<-5	g...	...	755.5	1.5	9.7×10^{-16}
84	175055.61−292930.2	267.731730	−29.491738	0.3	9.2	51.6	19.6	302.4	74.8	0.89	2.6	-2.7	g...	...	746.4	4.7	2.3×10^{-15}
85	175055.62−293216.2	267.731780	−29.537843	0.2	7.7	61.8	16.5	188.2	40.8	0.90	3.6	<-5	g...	...	780.2	2.5	1.4×10^{-15}
86	175055.65−293314.3	267.731880	−29.553980	0.2	7.4	221.4	19.9	148.6	170.0	0.90	10.9	<-5	g...	...	745.2	3.1	6.2×10^{-15}
87	175055.66−292805.5	267.731940	−29.468213	0.3	10.1	137.4	20.6	257.6	110.8	0.90	6.5	<-5	g...	...	484.3	3.4	7.3×10^{-15}
88	175055.76−293951.4	267.732350	−29.664287	0.3	8.3	47.5	18.9	282.5	15.4	0.91	2.4	-2.5	....	b	764.3	1.7	7.0×10^{-16}
89	175055.79−293840.2	267.732480	−29.644521	0.2	7.7	124.7	19.3	222.3	23.1	0.89	6.3	<-5	....	b	773.1	1.3	1.4×10^{-15}
90	175055.85−293204.3	267.732740	−29.534553	0.2	7.7	96.2	17.8	195.8	63.7	0.90	5.3	<-5	....	a	784.7	2.8	2.2×10^{-15}
91	175055.97−293515.6	267.733250	−29.587679	0.2	6.9	72.5	15.6	149.5	43.6	0.90	4.5	<-5	g...	...	779.0	2.5	1.6×10^{-15}
92	175056.07−293142.7	267.733630	−29.528547	0.3	7.8	40.1	17.0	225.9	40.3	0.90	2.3	-2.3	....	b	784.6	3.5	1.2×10^{-15}
93	175056.28−294209.2	267.734520	−29.702560	0.3	9.6	86.9	21.5	344.1	56.5	0.90	3.9	<-5	....	a	681.8	2.3	2.1×10^{-15}
94	175056.38−293715.8	267.734940	−29.621057	0.2	7.1	50.9	14.8	148.1	30.5	0.87	3.3	-4.6	....	b	763.8	2.5	1.1×10^{-15}
95	175056.55−293407.0	267.735660	−29.568635	0.2	6.9	162.1	17.7	130.9	9.7	0.90	8.9	<-5	g...	...	785.4	1.1	1.5×10^{-15}
96	175056.64−293051.0	267.736030	−29.514187	0.3	8.2	43.7	18.0	255.3	17.6	0.90	2.4	-2.4	g...	...	769.9	1.6	6.0×10^{-16}
97	175056.75−294327.1	267.736470	−29.724205	0.3	10.5	110.0	24.0	430.0	93.6	0.90	4.5	<-5	....	a	655.0	3.1	3.6×10^{-15}
98	175056.76−293928.7	267.736510	−29.657982	0.2	7.9	72.1	18.2	232.9	42.6	0.89	3.9	<-5	g...	...	756.4	2.8	1.8×10^{-15}
99	175056.81−293256.6	267.736710	−29.549069	0.3	7.2	34.7	14.1	144.3	22.5	0.90	2.4	-2.6	....	b	795.7	2.4	7.0×10^{-16}
100	175056.95−292922.0	267.737310	−29.489459	0.2	9.0	184.1	22.5	290.9	17.9	0.90	8.0	<-5	....	b	748.1	0.9	1.6×10^{-15}
101	175057.07−293505.2	267.737800	−29.584784	0.2	6.7	147.5	17.2	125.5	26.6	0.90	8.4	<-5	g...	...	785.1	1.3	1.7×10^{-15}
102	175057.14−294251.7	267.738110	−29.714373	0.3	10.0	69.9	21.8	373.1	20.4	0.90	3.1	-3.7	....	a	673.6	1.2	8.9×10^{-16}

(*cont.*)

Table A.1: *Chandra* source list

Source		Position				Extracted Counts							Characteristics				
Seq	CXOU J	R. A.	Decl.	Err	θ	$C_{\rm net}$	$\Delta C_{\rm net}$	$C'_{\rm bkg}$	$C_{\rm net,hard}$	PSF	PS	$P_{\rm B}$	Anom	Var	EffExp	$E_{\rm median}$	Photo $F_{\rm x}$
#		(deg)	(deg)	($''$)	($'$)						Frac				(ks)	(keV)	(ergs s^{-1} cm^{-2})
(1)	(2)	(3)	(4)	(5)	(6)	(7)	(8)	(9)	(10)	(11)	(12)	(13)	(14)	(15)	(16)	(17)	(18)
103	175057.18−293733.4	267.738280	−29.625958	0.2	7.0	106.3	17.2	165.7	54.5	0.90	6.0	<-5	....	c	764.0	2.0	1.9×10^{-15}
104	175057.23−293616.7	267.738470	−29.604666	0.2	6.7	105.7	14.7	92.3	55.7	0.86	7.0	<-5	g...	...	645.2	2.4	2.8×10^{-15}
105	175057.25−294128.2	267.738580	−29.691176	0.2	9.0	145.7	22.1	310.3	71.5	0.90	6.4	<-5	g...	...	743.5	2.0	2.8×10^{-15}
106	175057.28−293939.7	267.738690	−29.661041	0.2	7.9	49.4	17.0	215.6	8.1	0.88	2.8	-3.3	....	b	751.1	1.4	6.2×10^{-16}
107	175057.33−293813.6	267.738900	−29.637112	0.2	7.2	126.8	18.0	175.2	83.5	0.90	6.8	<-5	....	a	760.4	2.5	2.7×10^{-15}
108	175057.46−293119.3	267.739450	−29.522052	0.2	7.8	63.8	17.5	218.2	42.1	0.90	3.5	-4.9	....	a	782.5	3.2	1.8×10^{-15}
109	175057.54−293952.5	267.739790	−29.664597	0.3	8.0	52.2	17.4	224.8	15.8	0.90	2.9	-3.4	....	a	750.1	1.4	6.5×10^{-16}
110	175057.60−293633.6	267.740040	−29.609359	0.3	6.7	26.8	12.2	106.2	0.0	0.90	2.1	-2.1	g...	...	595.5	1.2	3.8×10^{-16}
111	175057.62−293620.7	267.740120	−29.605777	0.2	6.6	49.4	10.4	47.6	0.0	0.74	4.5	<-5	g...	...	557.3	1.2	9.0×10^{-16}
112	175057.66−293439.4	267.740250	−29.577629	0.2	6.6	45.9	13.3	114.1	16.1	0.90	3.3	-4.4	g...	...	796.1	1.7	6.8×10^{-16}
113	175057.76−294033.3	267.740680	−29.675927	0.2	8.3	259.8	23.4	255.2	138.6	0.91	10.9	<-5	g...	...	743.7	2.2	5.3×10^{-15}
114	175057.76−294155.7	267.740680	−29.698819	0.3	9.2	81.9	20.7	314.1	55.6	0.90	3.9	<-5	g...	...	709.0	2.7	2.2×10^{-15}
115	175057.83−293034.5	267.740970	−29.509603	0.3	8.1	57.7	17.7	229.3	24.9	0.90	3.2	-4.0	g...	...	773.0	1.7	9.0×10^{-16}
116	175057.85−293227.9	267.741050	−29.541093	0.2	7.2	216.0	19.6	143.0	173.6	0.90	10.8	<-5	....	b	796.9	3.4	6.1×10^{-15}
117	175058.05−292953.1	267.741880	−29.498097	0.2	8.5	133.6	20.5	256.4	46.8	0.90	6.4	<-5	....	c	765.7	1.5	1.8×10^{-15}
118	175058.22−293902.9	267.742610	−29.650809	0.2	7.4	108.5	18.1	193.5	31.6	0.90	5.8	<-5	....	b	758.4	1.4	1.3×10^{-15}
119	175058.38−293338.8	267.743260	−29.560785	0.2	6.6	68.4	14.1	112.6	48.7	0.90	4.7	<-5	....	b	807.0	3.0	1.7×10^{-15}
120	175058.60−293051.3	267.744180	−29.514250	0.3	7.8	59.6	17.1	207.4	45.8	0.90	3.4	-4.5	....	b	783.4	3.1	1.6×10^{-15}
121	175058.67−293025.2	267.744460	−29.507012	0.2	8.1	75.6	17.7	214.4	4.2	0.90	4.1	<-5	g...	...	778.2	1.0	6.7×10^{-16}
122	175058.78−293808.5	267.744920	−29.635707	0.2	6.9	196.3	19.3	150.7	9.4	0.90	9.9	<-5	g...	...	758.2	1.1	2.0×10^{-15}
123	175058.80−293414.6	267.745000	−29.570743	0.2	6.4	48.4	12.7	97.6	23.4	0.90	3.7	<-5	g...	...	810.3	2.0	8.2×10^{-16}
124	175059.04−293306.5	267.746010	−29.551820	0.2	6.7	67.4	13.5	97.6	48.0	0.87	4.8	<-5	....	a	815.3	2.9	1.6×10^{-15}
125	175059.04−293508.7	267.746020	−29.585773	0.2	6.3	56.5	13.1	98.5	33.8	0.89	4.2	<-5	....	a	810.6	2.5	1.2×10^{-15}
126	175059.11−293106.2	267.746330	−29.518400	0.3	7.6	54.7	16.2	186.3	63.8	0.90	3.3	-4.3	....	b	786.8	3.9	1.9×10^{-15}
127	175059.18−293452.8	267.746610	−29.581354	0.2	6.3	36.8	12.2	96.2	13.9	0.89	2.9	-3.6	....	a	814.8	1.9	5.8×10^{-16}
128	175059.26−293930.0	267.746920	−29.658341	0.2	7.5	87.6	17.1	183.4	42.8	0.90	5.0	<-5	g...	...	751.0	1.9	1.5×10^{-15}
129	175059.27−292906.7	267.746980	−29.485206	0.3	8.8	51.7	13.4	111.3	53.3	0.70	3.7	<-5	....	b	746.1	4.0	2.4×10^{-15}
130	175059.31−293433.6	267.747150	−29.576021	0.3	6.3	24.7	11.5	93.3	14.1	0.90	2.1	-2.1	....	a	819.4	2.8	5.5×10^{-16}
131	175059.32−293535.4	267.747170	−29.593172	0.2	6.2	37.4	12.4	101.6	1.7	0.89	2.9	-3.5	....	a	814.6	1.1	3.6×10^{-16}
132	175059.35−292858.1	267.747310	−29.482826	0.3	8.9	62.4	14.7	134.6	39.7	0.73	4.1	<-5	....	a	746.1	2.6	1.8×10^{-15}
133	175059.37−294029.6	267.747400	−29.674898	0.3	8.0	58.7	17.6	225.3	34.2	0.91	3.2	-4.1	g...	...	740.5	2.1	1.1×10^{-15}
134	175059.51−293310.6	267.747970	−29.552962	0.2	6.6	31.5	10.9	74.5	19.6	0.83	2.8	-3.4	....	b	805.8	2.2	6.2×10^{-16}
135	175059.52−294226.2	267.748010	−29.707299	0.3	9.3	139.2	21.4	289.8	114.4	0.90	6.3	<-5	....	c	666.7	3.6	5.6×10^{-15}
136	175059.52−294101.0	267.748020	−29.683634	0.2	8.3	218.5	22.2	242.5	153.0	0.91	9.6	<-5	....	a	736.2	2.9	5.0×10^{-15}

(*cont.*)

Table A.1: *Chandra* source list

Source		Position				Extracted Counts							Characteristics				
Seq	CXOU J	R. A.	Decl.	Err	θ	$C_{\rm net}$	$\Delta C_{\rm net}$	$C'_{\rm bkg}$	$C_{\rm net,hard}$	PSF	PS	$P_{\rm B}$	Anom	Var	EffExp	$E_{\rm median}$	Photo $F_{\rm x}$
#		(deg)	(deg)	($''$)	($'$)						Frac				(ks)	(keV)	(ergs s^{-1} cm^{-2})
(1)	(2)	(3)	(4)	(5)	(6)	(7)	(8)	(9)	(10)	(11)	(12)	(13)	(14)	(15)	(16)	(17)	(18)
137	175059.57−293038.4	267.748210	−29.510685	0.2	7.8	98.1	17.7	189.9	20.3	0.90	5.4	<-5	....	a	777.6	1.3	1.1×10^{-15}
138	175059.63−294007.9	267.748480	−29.668876	0.2	7.8	67.6	16.9	194.4	44.7	0.90	3.9	<-5	g...	...	741.6	2.7	1.7×10^{-15}
139	175059.69−293135.1	267.748730	−29.526426	0.2	7.2	142.3	17.7	149.7	27.4	0.89	7.8	<-5	....	a	796.1	1.3	1.6×10^{-15}
140	175059.74−292829.3	267.748940	−29.474830	0.3	9.2	100.5	20.7	296.5	63.7	0.90	4.7	<-5	....	c	749.2	2.6	2.3×10^{-15}
141	175059.76−293339.7	267.749000	−29.561034	0.1	6.4	176.9	17.1	94.1	31.0	0.90	10.1	<-5	....	a	815.7	1.4	1.9×10^{-15}
142	175059.96−293612.6	267.749870	−29.603517	0.2	6.1	68.0	12.9	82.0	36.6	0.90	5.1	<-5	g...	...	668.4	2.3	1.5×10^{-15}
143	175100.09−293650.6	267.750410	−29.614057	0.2	6.2	25.6	11.7	97.4	17.0	0.90	2.1	-2.1	g...	...	730.9	2.2	5.1×10^{-16}
144	175100.16−293205.3	267.750690	−29.534806	0.2	6.9	91.3	15.3	124.7	10.6	0.90	5.8	<-5	....	b	802.0	1.2	8.7×10^{-16}
145	175100.16−293331.7	267.750690	−29.558808	0.2	6.3	83.7	13.8	90.3	76.1	0.90	5.8	<-5	g...	...	786.5	3.6	2.6×10^{-15}
146	175100.17−293020.9	267.750730	−29.505828	0.3	7.9	77.7	17.0	189.3	13.2	0.90	4.4	<-5	g...	...	763.7	1.4	9.4×10^{-16}
147	175100.67−293413.0	267.752820	−29.570305	0.2	6.0	29.9	11.1	80.1	9.6	0.90	2.6	-3.0	....	a	819.0	1.1	2.8×10^{-16}
148	175100.69−293446.9	267.752910	−29.579703	0.2	5.9	31.7	11.1	77.3	8.9	0.90	2.7	-3.3	....	a	827.7	1.7	4.3×10^{-16}
149	175100.77−294304.9	267.753220	−29.718041	0.3	9.6	118.9	21.4	309.1	32.1	0.89	5.4	<-5	g...	...	654.9	1.2	1.6×10^{-15}
150	175100.79−293358.6	267.753310	−29.566303	0.2	6.1	58.9	12.3	78.1	18.8	0.90	4.6	<-5	....	a	821.5	1.5	7.3×10^{-16}
151	175100.92−293148.0	267.753860	−29.530021	0.2	6.9	62.2	14.3	122.8	11.1	0.90	4.2	<-5	....	a	785.0	1.2	6.3×10^{-16}
152	175100.97−293907.3	267.754070	−29.652034	0.2	6.9	103.9	15.6	119.1	44.9	0.84	6.5	<-5	....	b	798.3	1.8	1.6×10^{-15}
153	175100.99−294236.3	267.754130	−29.710098	0.2	9.2	204.3	22.7	277.7	159.6	0.90	8.8	<-5	g...	...	656.7	3.0	6.6×10^{-15}
154	175101.02−293501.2	267.754250	−29.583685	0.2	5.9	42.4	11.5	76.6	22.2	0.90	3.5	<-5	....	b	826.2	1.8	6.2×10^{-16}
155	175101.11−293139.0	267.754630	−29.527506	0.2	6.9	119.2	16.3	125.8	29.8	0.90	7.1	<-5	g...	...	777.9	1.2	1.3×10^{-15}
156	175101.21−293741.4	267.755060	−29.628190	0.2	6.2	62.0	13.7	109.0	21.4	0.89	4.4	<-5	....	a	821.3	1.8	9.1×10^{-16}
157	175101.23−293223.5	267.755160	−29.539871	0.2	6.5	112.0	15.2	102.0	75.8	0.90	7.1	<-5	g...	...	796.6	3.0	2.9×10^{-15}
158	175101.35−293750.2	267.755630	−29.630635	0.2	6.3	41.9	12.8	106.1	12.7	0.89	3.1	-4.0	....	a	820.8	1.7	5.6×10^{-16}
159	175101.41−293011.3	267.755880	−29.503146	0.2	7.8	88.0	17.0	177.0	51.9	0.90	5.0	<-5	....	b	780.3	2.6	1.9×10^{-15}
160	175101.45−293402.7	267.756060	−29.567430	0.2	5.9	110.9	14.1	72.1	23.5	0.90	7.6	<-5	....	b	817.5	1.4	1.3×10^{-15}
161	175101.50−293312.7	267.756260	−29.553536	0.2	6.1	35.7	11.5	83.3	24.9	0.90	3.0	-3.7	g...	...	807.9	3.9	1.2×10^{-15}
162	175101.60−294058.3	267.756680	−29.682873	0.2	8.0	68.3	17.6	216.7	74.9	0.90	3.8	<-5	....	a	770.5	3.8	2.2×10^{-15}
163	175101.66−293600.8	267.756920	−29.600226	0.2	5.7	27.2	10.9	78.8	15.6	0.90	2.4	-2.6	g...	...	801.5	2.2	5.0×10^{-16}
164	175101.66−293902.9	267.756940	−29.650810	0.2	6.8	87.7	14.1	95.3	76.9	0.81	6.0	<-5	....	a	809.1	3.8	3.0×10^{-15}
165	175101.66−293929.1	267.756950	−29.658086	0.2	7.0	88.6	16.5	162.4	53.4	0.90	5.2	<-5	....	b	803.2	2.4	1.7×10^{-15}
166	175101.76−293342.0	267.757360	−29.561680	0.2	5.9	45.3	9.7	37.7	9.9	0.77	4.4	<-5	....	b	810.3	1.4	5.8×10^{-16}
167	175101.88−293320.9	267.757860	−29.555817	0.2	6.0	27.3	10.7	74.7	12.6	0.90	2.4	-2.7	g...	...	783.7	1.9	4.6×10^{-16}
168	175102.04−293550.9	267.758540	−29.597476	0.2	5.6	22.8	10.5	74.2	2.8	0.90	2.1	-2.1	g...	...	821.9	1.3	2.4×10^{-16}
169	175102.12−292841.5	267.758840	−29.478207	0.3	8.7	70.4	18.3	237.6	33.5	0.90	3.7	<-5	g...	...	732.0	1.9	1.3×10^{-15}
170	175102.13−293137.5	267.758900	−29.527104	0.2	6.7	145.7	16.7	113.3	81.4	0.90	8.5	<-5	g...	...	796.2	2.3	2.9×10^{-15}

(*cont.*)

Table A.1: *Chandra* source list

Source		Position				Extracted Counts							Characteristics				
Seq	CXOU J	R. A.	Decl.	Err	θ	$C_{\rm net}$	$\Delta C_{\rm net}$	$C'_{\rm bkg}$	$C_{\rm net,hard}$	PSF	PS	$P_{\rm B}$	Anom	Var	EffExp	$E_{\rm median}$	Photo $F_{\rm x}$
#		(deg)	(deg)	($''$)	($'$)						Frac				(ks)	(keV)	(ergs s^{-1} cm^{-2})
(1)	(2)	(3)	(4)	(5)	(6)	(7)	(8)	(9)	(10)	(11)	(12)	(13)	(14)	(15)	(16)	(17)	(18)
171	175102.24−292807.0	267.759370	−29.468633	0.3	9.2	48.4	17.9	247.6	13.3	0.90	2.6	-2.8	g...	...	654.6	1.6	8.6×10^{-16}
172	175102.28−293343.1	267.759500	−29.561983	0.2	5.8	65.0	11.2	47.0	3.9	0.82	5.6	<-5	g...	...	802.4	1.0	6.1×10^{-16}
173	175102.35−294158.2	267.759830	−29.699526	0.2	8.6	213.1	22.6	267.9	151.9	0.91	9.2	<-5	....	b	740.4	2.7	5.2×10^{-15}
174	175102.54−293228.7	267.760620	−29.541313	0.2	6.2	37.1	11.6	83.9	25.8	0.90	3.1	-4.0	g...	...	796.4	3.0	9.9×10^{-16}
175	175102.61−293308.7	267.760910	−29.552432	0.2	5.9	25.6	10.6	74.4	5.4	0.90	2.3	-2.5	g...	...	797.3	1.3	2.8×10^{-16}
176	175102.70−293822.1	267.761280	−29.639480	0.2	6.2	38.7	10.6	61.3	31.1	0.77	3.5	<-5	....	b	821.5	3.7	1.3×10^{-15}
177	175102.71−294058.0	267.761300	−29.682798	0.3	7.8	45.7	16.2	193.3	36.0	0.89	2.7	-3.1	....	a	778.4	4.2	1.6×10^{-15}
178	175102.74−293941.3	267.761440	−29.661489	0.2	6.9	73.7	15.7	153.3	35.1	0.90	4.5	<-5	....	b	806.0	1.9	1.1×10^{-15}
179	175102.76−293816.8	267.761520	−29.638024	0.2	6.2	82.7	13.3	79.3	22.5	0.82	6.0	<-5	....	a	822.6	1.4	9.7×10^{-16}
180	175102.85−293413.0	267.761890	−29.570282	0.1	5.6	210.2	17.1	62.8	138.7	0.90	11.9	<-5	g...	...	805.5	2.8	5.1×10^{-15}
181	175102.89−293539.3	267.762080	−29.594255	0.2	5.4	33.9	10.0	55.1	26.7	0.86	3.2	-4.6	g...	...	816.9	3.4	1.1×10^{-15}
182	175102.92−293001.5	267.762180	−29.500417	0.2	7.6	331.1	22.7	156.9	224.4	0.90	14.3	<-5	g...	...	759.1	2.9	1.2×10^{-15}
183	175102.92−294020.3	267.762190	−29.672324	0.2	7.3	60.6	15.9	170.4	20.5	0.90	3.7	<-5	....	b	796.4	1.8	9.1×10^{-15}
184	175102.92−292924.5	267.762200	−29.490145	0.3	8.1	57.4	16.3	184.6	29.6	0.90	3.4	-4.7	g...	...	739.7	2.1	8.9×10^{-16}
185	175102.98−294038.9	267.762450	−29.677476	0.2	7.5	46.7	15.8	182.3	24.9	0.90	2.9	-3.4	....	b	791.2	2.1	8.2×10^{-16}
186	175102.99−293321.5	267.762500	−29.555994	0.2	5.8	95.2	13.4	68.8	9.8	0.90	6.8	<-5	g...	...	781.7	1.1	9.6×10^{-16}
187	175103.30−293119.3	267.763780	−29.522032	0.2	6.7	44.5	13.0	107.5	26.8	0.90	3.3	-4.4	g...	...	792.7	2.4	9.2×10^{-16}
188	175103.32−293900.4	267.763840	−29.650118	0.2	6.4	64.7	14.3	120.3	33.4	0.89	4.4	<-5	....	c	817.0	2.1	1.1×10^{-15}
189	175103.35−293444.3	267.763970	−29.578994	0.2	5.4	50.1	10.1	39.9	31.3	0.84	4.7	<-5	g...	...	806.2	2.8	1.3×10^{-15}
190	175103.36−293441.0	267.764010	−29.578056	0.3	5.4	12.8	6.0	17.2	2.8	0.62	1.9	-2.4	g...	...	804.4	1.4	1.7×10^{-15}
191	175103.36−293350.9	267.764040	−29.564163	0.2	5.6	66.2	11.9	61.8	42.1	0.90	5.3	<-5	g...	...	807.6	3.0	2.2×10^{-16}
192	175103.37−293326.3	267.764060	−29.557306	0.2	5.7	22.0	10.0	66.0	19.9	0.90	2.1	-2.2	g...	...	780.8	2.5	4.9×10^{-16}
193	175103.44−294147.1	267.764360	−29.696434	0.2	8.3	123.2	14.0	57.8	16.9	0.57	8.5	<-5	....	a	767.2	1.3	2.1×10^{-15}
194	175103.45−293741.5	267.764410	−29.628197	0.2	5.8	55.5	12.4	83.5	19.8	0.90	4.3	<-5	....	a	830.4	1.4	5.9×10^{-16}
195	175103.63−293651.8	267.765140	−29.614415	0.2	5.5	76.7	12.8	71.3	43.9	0.90	5.8	<-5	....	a	796.4	2.3	1.4×10^{-15}
196	175103.72−293149.7	267.765510	−29.530479	0.2	6.3	57.4	12.8	91.6	0.7	0.90	4.3	<-5	g...	...	799.3	0.9	4.5×10^{-16}
197	175103.84−294147.0	267.766030	−29.696390	0.2	8.2	39.8	8.9	29.2	6.4	0.44	4.2	<-5	....	a	770.2	1.1	8.1×10^{-16}
198	175103.86−293839.8	267.766110	−29.644413	0.2	6.2	113.1	15.1	95.9	79.9	0.89	7.3	<-5	....	b	822.9	3.0	2.7×10^{-15}
199	175103.90−293538.3	267.766260	−29.593996	0.1	5.2	109.3	13.5	56.7	68.3	0.90	7.8	<-5	g...	...	807.8	2.4	2.2×10^{-15}
200	175103.91−293013.5	267.766320	−29.503775	0.2	7.3	77.2	15.3	135.8	46.5	0.90	4.9	<-5	g...	...	759.8	2.6	1.9×10^{-15}
201	175103.92−293912.5	267.766340	−29.653475	0.2	6.5	35.0	13.0	118.0	15.9	0.89	2.6	-2.9	....	b	815.3	2.0	5.7×10^{-16}
202	175103.94−294114.5	267.766440	−29.687365	0.2	7.8	209.0	20.8	197.0	11.3	0.89	9.8	<-5	....	b	781.4	0.9	1.7×10^{-15}
203	175103.96−293431.0	267.766520	−29.575280	0.1	5.3	670.9	27.5	56.1	514.0	0.90	24.0	<-5	g...	...	814.5	3.1	1.8×10^{-14}
204	175103.98−293847.8	267.766590	−29.646612	0.2	6.2	69.5	13.6	99.5	34.3	0.89	4.9	<-5	....	b	821.1	2.1	1.2×10^{-15}

(*cont.*)

Table A.1: *Chandra* source list

Source		Position				Extracted Counts				Characteristics							
Seq	CXOU J	R. A.	Decl.	Err	θ	$C_{\rm net}$	$\Delta C_{\rm net}$	$C'_{\rm bkg}$	$C_{\rm net,hard}$	PSF	PS	$P_{\rm B}$	Anom	Var	EffExp	$E_{\rm median}$	Photo $F_{\rm x}$
#		(deg)	(deg)	($''$)	($'$)						Frac				(ks)	(keV)	(ergs s^{-1} cm^{-2})
(1)	(2)	(3)	(4)	(5)	(6)	(7)	(8)	(9)	(10)	(11)	(12)	(13)	(14)	(15)	(16)	(17)	(18)
205	175104.01−293552.6	267.766710	−29.597964	0.2	5.2	52.0	11.1	58.0	19.2	0.91	4.5	<-5	g...	...	807.6	1.5	6.6×10^{-16}
206	175104.08−294013.9	267.767010	−29.670542	0.3	7.1	28.5	9.8	55.5	0.2	0.68	2.8	-3.6	....	a	799.2	1.2	3.7×10^{-16}
207	175104.10−293643.0	267.767090	−29.611964	0.2	5.3	24.8	9.8	59.2	8.6	0.90	2.4	-2.8	g...	...	732.4	1.7	3.7×10^{-16}
208	175104.12−292748.9	267.767190	−29.463599	0.2	9.1	458.1	25.7	171.9	385.1	0.90	17.5	<-5	g...	...	487.5	3.5	2.2×10^{-14}
209	175104.12−294020.8	267.767200	−29.672471	0.2	7.2	85.3	15.2	126.7	21.0	0.86	5.4	<-5	....	b	797.6	1.4	1.0×10^{-15}
210	175104.13−293408.9	267.767230	−29.569157	0.1	5.3	161.3	15.3	55.7	99.3	0.90	10.2	<-5	....	a	816.4	2.3	3.0×10^{-15}
211	175104.15−293815.7	267.767300	−29.637709	0.1	5.9	347.5	21.4	87.5	203.7	0.90	15.8	<-5	....	a	828.0	2.4	6.6×10^{-15}
212	175104.17−293903.6	267.767400	−29.651016	0.2	6.3	76.0	14.3	111.0	60.1	0.90	5.1	<-5	....	a	817.8	3.4	2.1×10^{-15}
213	175104.18−294131.5	267.767430	−29.692106	0.3	8.0	37.9	11.2	73.1	0.0	0.62	3.2	-4.5	....	a	776.5	1.1	5.3×10^{-16}
214	175104.32−293356.0	267.768010	−29.565565	0.1	5.3	135.0	14.4	56.0	22.7	0.90	9.1	<-5	....	c	824.4	1.3	1.4×10^{-15}
215	175104.33−294313.2	267.768050	−29.720341	0.3	9.3	57.0	19.5	296.0	44.5	0.90	2.8	-3.2	....	a	685.1	3.2	1.8×10^{-15}
216	175104.36−294125.0	267.768170	−29.690300	0.2	7.9	44.8	11.0	64.2	25.3	0.61	3.9	<-5	....	b	779.1	2.6	1.5×10^{-15}
217	175104.52−294159.8	267.768850	−29.699965	0.2	8.3	92.8	13.3	69.2	55.0	0.57	6.7	<-5	....	c	758.0	2.3	2.0×10^{-15}
218	175104.52−293459.6	267.768870	−29.583233	0.1	5.1	97.6	12.7	50.4	65.3	0.90	7.4	<-5	....	b	813.5	2.6	2.9×10^{-15}
219	175104.55−293944.2	267.768960	−29.662299	0.2	6.7	61.5	14.0	117.5	23.3	0.89	4.2	<-5	....	a	808.5	1.8	9.0×10^{-16}
220	175104.56−293332.0	267.769020	−29.558901	0.2	5.4	53.2	11.0	55.8	17.7	0.90	4.6	<-5	g...	...	791.1	1.6	7.2×10^{-16}
221	175104.59−293537.4	267.769140	−29.593741	0.1	5.1	168.4	15.5	54.6	90.3	0.90	10.5	<-5	g...	...	804.0	2.3	3.2×10^{-15}
222	175104.66−293717.6	267.769440	−29.621575	0.2	5.4	33.0	10.9	72.0	33.4	0.90	2.9	-3.7	....	a	819.6	3.1	8.2×10^{-16}
223	175104.80−293753.9	267.770020	−29.631644	0.2	5.6	18.6	6.3	14.4	10.4	0.52	2.7	-4.5	....	b	820.6	2.4	6.2×10^{-16}
224	175104.88−293415.7	267.770350	−29.571052	0.2	5.1	54.7	10.6	46.3	27.1	0.90	4.9	<-5	....	a	828.0	1.9	8.2×10^{-16}
225	175104.95−294203.7	267.770640	−29.701040	0.3	8.3	67.0	14.1	114.0	23.4	0.70	4.6	<-5	....	a	751.5	1.5	1.2×10^{-15}
226	175104.99−293604.8	267.770830	−29.601353	0.2	5.0	28.9	8.2	29.1	2.8	0.85	3.3	<-5	g...	...	598.0	1.1	4.1×10^{-16}
227	175105.02−292926.7	267.770930	−29.490756	0.3	7.8	45.0	15.2	166.0	11.7	0.90	2.9	-3.4	....	c	792.6	1.5	5.6×10^{-16}
228	175105.04−293753.7	267.771000	−29.631611	0.2	5.6	19.9	6.7	18.1	13.4	0.58	2.7	-4.4	....	a	822.5	3.3	8.4×10^{-16}
229	175105.05−293201.3	267.771070	−29.533711	0.1	6.0	375.2	21.7	71.8	221.4	0.90	16.9	<-5	g...	...	796.1	2.5	8.3×10^{-15}
230	175105.09−293821.0	267.771230	−29.639188	0.2	5.8	29.4	9.0	40.6	21.3	0.74	3.1	-4.6	....	a	816.2	3.4	1.0×10^{-15}
231	175105.17−293052.0	267.771570	−29.514456	0.2	6.7	176.6	17.3	103.4	146.8	0.90	9.9	<-5	....	b	803.3	3.5	5.2×10^{-15}
232	175105.23−293344.9	267.771820	−29.562483	0.2	5.2	14.4	5.6	11.6	5.1	0.58	2.3	-3.6	g...	...	803.1	1.6	2.9×10^{-16}
233	175105.23−293647.8	267.771820	−29.613290	0.2	5.1	87.5	12.4	51.5	54.5	0.90	6.8	<-5	g...	...	772.0	2.4	1.8×10^{-15}
234	175105.24−293535.2	267.771870	−29.593123	0.2	4.9	32.7	9.6	49.3	13.4	0.90	3.2	-4.7	g...	...	815.3	1.5	4.2×10^{-16}
235	175105.26−292944.4	267.771950	−29.495676	0.2	7.5	174.7	18.6	149.3	135.3	0.90	9.1	<-5	....	b	795.5	3.3	4.9×10^{-15}
236	175105.26−293817.1	267.771950	−29.638105	0.2	5.7	32.5	8.6	32.5	22.1	0.67	3.6	<-5	....	a	818.1	3.2	1.1×10^{-15}
237	175105.27−292907.6	267.771980	−29.485471	0.3	8.0	46.5	15.7	179.5	23.2	0.90	2.9	-3.4	....	a	782.4	2.8	1.1×10^{-15}
238	175105.30−293709.7	267.772100	−29.619380	0.2	5.2	32.2	10.3	60.8	13.3	0.90	3.0	-4.0	g...	...	803.6	1.7	4.4×10^{-16}

(*cont.*)

Table A.1: *Chandra* source list

Source		Position				Extracted Counts							Characteristics				
Seq	CXOU J	R. A.	Decl.	Err	θ	$C_{\rm net}$	$\Delta C_{\rm net}$	$C'_{\rm bkg}$	$C_{\rm net,hard}$	PSF	PS	$P_{\rm B}$	Anom	Var	EffExp	$E_{\rm median}$	Photo $F_{\rm x}$
#		(deg)	(deg)	($''$)	($'$)						Frac				(ks)	(keV)	(ergs s^{-1} cm^{-2})
(1)	(2)	(3)	(4)	(5)	(6)	(7)	(8)	(9)	(10)	(11)	(12)	(13)	(14)	(15)	(16)	(17)	(18)
239	175105.38−294008.2	267.772420	−29.668966	0.2	6.8	33.9	13.2	124.1	3.4	0.90	2.5	-2.6	....	b	803.9	1.2	1.1×10^{-15}
240	175105.38−293031.0	267.772450	−29.508632	0.2	6.9	120.1	16.0	115.9	4.2	0.90	7.3	<-5	....	b	805.8	1.0	3.4×10^{-16}
241	175105.50−293135.4	267.772950	−29.526511	0.1	6.2	520.5	25.0	78.5	414.7	0.90	20.4	<-5	g...	...	807.3	3.0	1.3×10^{-14}
242	175105.51−293444.7	267.772990	−29.579096	0.2	4.9	30.5	9.3	44.5	2.1	0.90	3.1	-4.6	....	a	827.4	1.0	2.5×10^{-16}
243	175105.54−293345.9	267.773090	−29.562762	0.2	5.1	46.1	9.0	24.9	0.0	0.78	4.8	<-5	g...	...	810.7	1.1	5.0×10^{-16}
244	175105.55−293250.3	267.773130	−29.547331	0.3	5.5	19.6	9.1	52.4	17.2	0.90	2.0	-2.2	g...	...	810.0	2.8	4.8×10^{-16}
245	175105.57−293730.6	267.773220	−29.625181	0.2	5.3	26.3	9.9	59.7	24.4	0.90	2.5	-3.0	g...	...	798.6	3.6	7.8×10^{-16}
246	175105.63−293602.9	267.773480	−29.600822	0.2	4.9	38.5	9.2	36.5	2.9	0.90	3.9	<-5	g...	...	635.3	1.2	5.0×10^{-16}
247	175105.65−293433.1	267.773560	−29.575864	0.2	4.9	56.4	10.4	40.6	43.8	0.90	5.2	<-5	....	a	826.8	3.2	1.5×10^{-15}
248	175105.65−294041.0	267.773580	−29.678067	0.2	7.2	52.6	14.9	149.4	16.9	0.90	3.4	-4.8	....	a	795.9	1.5	6.3×10^{-16}
249	175105.69−293803.6	267.773730	−29.634354	0.2	5.5	64.0	12.0	67.0	38.1	0.90	5.1	<-5	g...	...	789.7	2.5	1.4×10^{-15}
250	175105.71−293331.5	267.773800	−29.558770	0.2	5.2	41.2	9.7	41.8	16.2	0.90	4.0	<-5	g...	...	783.2	1.7	6.4×10^{-16}
251	175105.73−293459.0	267.773890	−29.583064	0.2	4.8	17.1	8.3	42.9	8.9	0.89	1.9	-2.1	....	a	828.2	1.9	2.6×10^{-16}
252	175105.78−293315.4	267.774100	−29.554283	0.2	5.3	69.1	11.3	46.9	31.9	0.90	5.8	<-5	g...	...	813.6	2.0	1.1×10^{-15}
253	175105.78−293745.4	267.774100	−29.629285	0.2	5.4	48.2	10.7	53.8	32.5	0.88	4.3	<-5	g...	...	794.1	2.8	1.2×10^{-15}
254	175106.01−293320.7	267.775080	−29.555758	0.2	5.2	55.9	10.6	45.1	24.5	0.90	5.0	<-5	g...	...	821.8	1.6	7.5×10^{-16}
255	175106.05−293428.7	267.775230	−29.574664	0.2	4.8	23.7	8.3	35.3	14.9	0.90	2.7	-3.7	....	a	830.4	2.3	4.5×10^{-16}
256	175106.07−294355.4	267.775310	−29.732082	0.3	9.7	70.4	20.5	319.6	34.6	0.90	3.3	-4.2	....	a	684.3	2.1	1.4×10^{-15}
257	175106.10−293228.6	267.775420	−29.541301	0.2	5.6	82.2	12.4	57.8	20.7	0.90	6.4	<-5	g...	...	814.9	1.3	9.6×10^{-16}
258	175106.12−293405.7	267.775540	−29.568264	0.2	4.9	53.3	10.0	35.7	16.6	0.89	5.1	<-5	g...	...	825.2	1.6	7.5×10^{-16}
259	175106.24−293036.4	267.776000	−29.510121	0.2	6.7	48.4	12.8	98.6	36.3	0.90	3.6	<-5	....	a	808.1	2.9	1.2×10^{-15}
260	175106.35−293257.0	267.776470	−29.549187	0.2	5.3	23.6	9.0	47.4	10.2	0.90	2.5	-3.0	g...	...	817.9	1.7	3.5×10^{-16}
261	175106.37−293550.3	267.776560	−29.597328	0.2	4.7	17.3	8.4	43.7	6.8	0.90	1.9	-2.1	....	a	832.3	1.6	2.1×10^{-16}
262	175106.43−293916.6	267.776820	−29.654614	0.2	6.1	41.7	12.0	88.3	0.0	0.90	3.3	-4.6	g...	...	778.6	1.1	3.9×10^{-16}
263	175106.55−294205.2	267.777300	−29.701452	0.3	8.1	64.5	17.4	215.5	39.1	0.90	3.6	<-5	....	b	759.6	2.3	1.3×10^{-15}
264	175106.58−293521.8	267.777430	−29.589403	0.2	4.6	33.6	9.1	39.4	0.0	0.89	3.5	<-5	g...	...	834.6	1.0	2.8×10^{-16}
265	175106.67−294131.4	267.777800	−29.692083	0.2	7.7	73.8	16.7	181.2	29.7	0.90	4.3	<-5	....	a	782.0	1.8	1.1×10^{-15}
266	175106.68−293457.2	267.777870	−29.582570	0.1	4.6	62.4	10.5	36.6	19.2	0.90	5.7	<-5	....	b	838.2	1.5	7.3×10^{-16}
267	175106.78−293137.3	267.778250	−29.527042	0.2	5.9	45.4	11.4	70.6	26.1	0.90	3.8	<-5	g...	...	822.3	2.2	8.5×10^{-16}
268	175106.83−293516.1	267.778460	−29.587833	0.2	4.6	21.3	8.3	37.7	0.6	0.90	2.4	-3.0	....	b	842.9	1.1	1.8×10^{-16}
269	175106.91−293627.7	267.778810	−29.607721	0.1	4.7	176.6	15.0	33.4	12.0	0.90	11.4	<-5	g...	...	711.2	1.0	1.7×10^{-15}
270	175106.92−293654.6	267.778840	−29.615188	0.2	4.8	45.2	9.8	39.8	7.0	0.90	4.4	<-5	g...	...	795.9	1.3	4.9×10^{-16}
271	175106.94−294046.5	267.778930	−29.679589	0.2	7.0	164.2	17.4	117.8	86.2	0.87	9.2	<-5	....	a	781.3	2.3	3.3×10^{-15}
272	175106.96−293110.5	267.779040	−29.519607	0.3	6.2	30.1	10.9	74.9	5.2	0.89	2.6	-3.1	g...	...	808.3	1.1	2.9×10^{-16}

(*cont.*)

Table A.1: *Chandra* source list

Source		Position				Extracted Counts				Characteristics							
Seq	CXOU J	R. A.	Decl.	Err	θ	$C_{\rm net}$	$\Delta C_{\rm net}$	$C'_{\rm bkg}$	$C_{\rm net,hard}$	PSF	PS	$P_{\rm B}$	Anom	Var	EffExp	$E_{\rm median}$	Photo $F_{\rm x}$
#		(deg)	(deg)	($''$)	($'$)						Frac				(ks)	(keV)	(ergs s^{-1} cm^{-2})
(1)	(2)	(3)	(4)	(5)	(6)	(7)	(8)	(9)	(10)	(11)	(12)	(13)	(14)	(15)	(16)	(17)	(18)
273	175107.02−293254.1	267.779290	−29.548372	0.1	5.2	115.4	13.2	44.6	75.2	0.90	8.4	<-5	g...	...	825.7	2.6	2.5×10^{-15}
274	175107.06−293605.4	267.779430	−29.601520	0.2	4.6	22.0	7.6	28.0	2.6	0.90	2.7	-3.8	g...	...	548.2	1.5	3.9×10^{-16}
275	175107.14−293445.7	267.779790	−29.579376	0.1	4.6	109.2	12.4	31.8	77.3	0.90	8.4	<-5	g...	...	828.2	2.8	2.6×10^{-15}
276	175107.24−294256.6	267.780190	−29.715723	0.2	8.7	197.5	21.8	249.5	67.4	0.90	8.8	<-5	....	a	701.3	1.7	3.3×10^{-15}
277	175107.30−293810.1	267.780450	−29.636152	0.2	5.3	60.0	11.2	53.0	25.0	0.90	5.1	<-5	g...	...	794.9	1.8	9.1×10^{-16}
278	175107.32−293343.8	267.780530	−29.562189	0.2	4.8	31.4	8.6	33.6	17.1	0.90	3.4	<-5	g...	...	796.9	2.0	5.7×10^{-16}
279	175107.32−293632.9	267.780540	−29.609150	0.1	4.6	96.1	11.9	32.9	50.6	0.90	7.7	<-5	g...	...	722.6	2.1	1.9×10^{-15}
280	175107.37−293211.9	267.780710	−29.536642	0.1	5.5	172.9	15.8	58.1	104.1	0.90	10.6	<-5	g...	...	827.7	2.7	3.9×10^{-15}
281	175107.39−293836.6	267.780800	−29.643502	0.2	5.5	32.2	10.1	58.8	3.2	0.90	3.0	-4.1	g...	...	774.0	1.2	3.6×10^{-16}
282	175107.46−294049.1	267.781110	−29.680319	0.2	7.0	52.1	11.6	67.9	13.5	0.77	4.3	<-5	....	a	769.6	1.3	6.8×10^{-16}
283	175107.48−293513.0	267.781200	−29.586963	0.2	4.5	20.3	7.9	32.7	14.0	0.90	2.4	-3.1	g...	...	825.7	2.3	4.0×10^{-16}
284	175107.50−293532.0	267.781280	−29.592224	0.2	4.4	31.4	8.6	33.6	8.7	0.90	3.4	<-5	g...	...	832.3	1.4	3.7×10^{-16}
285	175107.57−293923.2	267.781580	−29.656467	0.2	6.0	89.8	13.5	77.2	44.1	0.90	6.4	<-5	g...	...	763.6	1.9	1.5×10^{-15}
286	175107.65−292949.5	267.781910	−29.497101	0.3	7.1	36.9	13.2	120.1	5.3	0.90	2.7	-3.1	g...	...	778.3	1.2	4.1×10^{-16}
287	175107.66−294037.3	267.781950	−29.677039	0.0	6.8	3252.3	58.6	114.7	834.6	0.90	55.1	<-5	g...	...	755.5	1.4	4.4×10^{-14}
288	175107.71−293406.8	267.782150	−29.568578	0.2	4.6	53.2	9.6	27.8	2.9	0.90	5.3	<-5	g...	...	824.0	1.2	5.7×10^{-16}
289	175107.73−293316.7	267.782230	−29.554659	0.2	4.9	33.1	8.9	35.9	18.5	0.90	3.5	<-5	g...	...	817.8	2.2	6.1×10^{-16}
290	175107.73−293947.2	267.782230	−29.663127	0.2	6.2	108.7	14.3	80.3	65.2	0.90	7.3	<-5	g...	...	764.8	2.5	2.5×10^{-15}
291	175107.78−293733.1	267.782420	−29.625864	0.2	4.9	32.6	9.2	42.4	2.5	0.90	3.3	<-5	....	a	821.6	1.0	2.7×10^{-16}
292	175107.81−293425.7	267.782580	−29.573829	0.1	4.5	60.0	9.9	27.0	49.2	0.90	5.8	<-5	g...	...	823.1	3.0	1.5×10^{-15}
293	175107.96−294321.1	267.783190	−29.722541	0.3	9.0	62.9	18.8	264.1	11.3	0.90	3.3	-4.1	....	a	687.5	1.7	1.0×10^{-15}
294	175108.01−293453.0	267.783390	−29.581400	0.1	4.4	161.8	14.3	27.2	108.8	0.90	10.9	<-5	g...	...	816.8	2.7	3.8×10^{-15}
295	175108.14−293520.2	267.783930	−29.588952	0.2	4.3	31.2	8.3	28.8	23.4	0.90	3.5	<-5	g...	...	818.1	3.0	8.4×10^{-16}
296	175108.19−294048.6	267.784160	−29.680184	0.2	6.9	107.4	15.7	118.6	46.6	0.90	6.6	<-5	g...	...	757.2	1.7	1.7×10^{-15}
297	175108.24−293937.0	267.784360	−29.660303	0.2	6.0	34.5	11.1	74.5	2.5	0.90	3.0	-3.9	g...	...	776.0	1.1	3.5×10^{-16}
298	175108.35−293822.9	267.784830	−29.639722	0.2	5.2	25.8	9.5	53.2	12.9	0.90	2.6	-3.2	g...	...	814.3	2.2	4.8×10^{-16}
299	175108.39−293946.8	267.784990	−29.663007	0.2	6.1	34.1	11.3	78.9	0.0	0.90	2.9	-3.6	g...	...	775.1	1.1	3.5×10^{-16}
300	175108.41−292959.0	267.785060	−29.499732	0.3	6.9	32.0	12.7	114.0	0.0	0.90	2.4	-2.6	....	a	799.7	1.1	3.0×10^{-16}
301	175108.45−293842.5	267.785210	−29.645154	0.2	5.4	30.8	10.2	61.2	19.0	0.90	2.9	-3.7	g...	...	804.8	2.4	6.2×10^{-16}
302	175108.53−293437.2	267.785560	−29.577006	0.1	4.3	50.9	9.2	24.1	25.6	0.90	5.2	<-5	g...	...	824.3	2.1	9.0×10^{-16}
303	175108.59−293914.6	267.785820	−29.654083	0.2	5.7	102.3	13.6	66.7	73.2	0.90	7.3	<-5	g...	...	801.0	3.0	2.7×10^{-15}
304	175108.68−293251.4	267.786200	−29.547620	0.1	4.9	183.7	15.3	33.3	69.0	0.88	11.6	<-5	g...	...	820.1	1.8	2.8×10^{-15}
305	175108.78−293654.8	267.786620	−29.615234	0.2	4.4	20.7	7.7	30.3	5.8	0.89	2.5	-3.3	g...	...	832.5	1.7	2.9×10^{-16}
306	175108.87−293138.4	267.786960	−29.527340	0.2	5.6	59.7	11.2	52.3	41.6	0.90	5.1	<-5	g...	...	806.7	2.6	1.4×10^{-15}

(*cont.*)

Table A.1: *Chandra* source list

Source		Position				Extracted Counts							Characteristics				
Seq	CXOU J	R. A.	Decl.	Err	θ	$C_{\rm net}$	$\Delta C_{\rm net}$	$C'_{\rm bkg}$	$C_{\rm net,hard}$	PSF	PS	$P_{\rm B}$	Anom	Var	EffExp	$E_{\rm median}$	Photo $F_{\rm x}$
#		(deg)	(deg)	($''$)	($'$)						Frac				(ks)	(keV)	(ergs s^{-1} cm^{-2})
(1)	(2)	(3)	(4)	(5)	(6)	(7)	(8)	(9)	(10)	(11)	(12)	(13)	(14)	(15)	(16)	(17)	(18)
307	175108.88−293332.1	267.787030	−29.558939	0.2	4.6	31.0	8.3	29.0	10.6	0.90	3.5	<-5	g...	...	810.7	1.8	4.8×10^{-16}
308	175108.98−293326.0	267.787440	−29.557228	0.1	4.6	109.6	12.3	29.4	18.2	0.90	8.5	<-5	g...	...	827.7	1.4	1.3×10^{-15}
309	175108.98−293739.1	267.787440	−29.627530	0.2	4.7	17.1	8.0	37.9	8.6	0.89	2.0	-2.2	g...	...	821.6	2.0	3.0×10^{-16}
310	175108.99−293305.1	267.787490	−29.551440	0.2	4.7	53.5	9.8	32.5	0.0	0.90	5.2	<-5	g...	...	834.0	1.1	5.1×10^{-16}
311	175109.08−293940.0	267.787840	−29.661134	0.2	5.9	60.1	12.1	71.9	42.6	0.90	4.8	<-5	....	a	796.3	2.6	1.3×10^{-15}
312	175109.09−293250.0	267.787900	−29.547233	0.1	4.8	68.3	10.1	22.7	7.9	0.82	6.4	<-5	g...	...	828.2	1.2	7.6×10^{-16}
313	175109.11−293454.1	267.787960	−29.581715	0.1	4.1	145.9	13.5	23.1	114.2	0.90	10.4	<-5	g...	...	827.7	3.3	4.1×10^{-15}
314	175109.47−292750.2	267.789490	−29.463965	0.3	8.5	61.3	16.8	196.7	42.4	0.90	3.5	-5.0	g...	...	692.9	2.5	1.5×10^{-15}
315	175109.51−293853.4	267.789650	−29.648193	0.2	5.3	26.8	9.8	57.2	26.5	0.90	2.6	-3.2	g...	...	815.8	4.8	1.1×10^{-15}
316	175109.52−293909.9	267.789680	−29.652772	0.2	5.5	33.3	10.3	60.7	10.5	0.91	3.1	-4.2	g...	...	816.1	1.4	4.0×10^{-16}
317	175109.54−293453.4	267.789750	−29.581524	0.1	4.0	133.3	13.0	22.7	77.5	0.90	9.8	<-5	g...	...	842.0	2.4	2.7×10^{-15}
318	175109.55−293834.1	267.789800	−29.642815	0.2	5.1	35.7	10.0	53.3	22.1	0.89	3.4	<-5	g...	...	813.5	2.8	8.4×10^{-16}
319	175109.58−293433.2	267.789930	−29.575908	0.1	4.1	53.0	9.3	24.0	10.9	0.90	5.4	<-5	g...	...	843.4	1.4	6.0×10^{-16}
320	175109.59−293526.0	267.789990	−29.590570	0.2	4.0	27.6	7.6	21.4	0.0	0.90	3.4	<-5	g...	...	836.3	1.1	2.6×10^{-16}
321	175109.66−292841.8	267.790290	−29.478280	0.3	7.8	35.6	15.1	170.4	0.0	0.90	2.3	-2.4	....	a	776.0	1.3	4.1×10^{-16}
322	175109.67−293822.2	267.790330	−29.639516	0.2	5.0	20.4	8.8	47.6	20.6	0.89	2.2	-2.4	g...	...	815.2	3.6	6.4×10^{-16}
323	175109.68−293140.1	267.790370	−29.527830	0.2	5.4	21.7	9.0	49.3	7.7	0.90	2.3	-2.6	....	a	837.3	1.7	3.0×10^{-16}
324	175109.75−293539.9	267.790630	−29.594425	0.2	4.0	15.3	7.1	26.7	10.9	0.90	2.0	-2.4	g...	...	838.2	2.9	3.6×10^{-16}
325	175109.77−293400.7	267.790730	−29.566866	0.2	4.2	14.0	6.8	25.0	7.9	0.90	1.9	-2.2	g...	...	841.6	2.2	2.4×10^{-16}
326	175109.78−293336.0	267.790790	−29.560010	0.1	4.4	74.8	10.6	26.2	57.1	0.90	6.7	<-5	g...	...	810.6	3.5	2.2×10^{-15}
327	175109.90−293527.5	267.791290	−29.590987	0.2	3.9	16.6	6.7	21.4	4.0	0.90	2.3	-3.0	g...	...	840.3	1.2	1.7×10^{-16}
328	175109.91−293706.7	267.791300	−29.618543	0.2	4.3	39.8	8.8	28.2	11.6	0.90	4.3	<-5	g...	...	833.8	1.5	4.8×10^{-16}
329	175109.97−293317.3	267.791560	−29.554809	0.1	4.4	144.3	13.7	29.7	98.5	0.90	10.1	<-5	g...	...	841.6	3.0	3.5×10^{-15}
330	175110.00−293157.8	267.791670	−29.532728	0.2	5.2	47.3	10.2	45.7	17.0	0.90	4.4	<-5	....	a	840.3	1.5	5.7×10^{-16}
331	175110.00−293206.4	267.791680	−29.535133	0.2	5.1	18.1	8.4	42.9	7.7	0.90	2.0	-2.2	....	a	842.0	2.8	3.9×10^{-16}
332	175110.01−293637.3	267.791720	−29.610384	0.1	4.1	55.0	9.5	25.0	21.9	0.90	5.5	<-5	g...	...	820.4	1.7	7.9×10^{-16}
333	175110.03−293505.7	267.791800	−29.584937	0.2	3.9	14.2	6.6	21.8	13.7	0.90	2.0	-2.4	....	a	854.7	3.7	4.1×10^{-16}
334	175110.03−293648.5	267.791800	−29.613493	0.2	4.1	17.9	7.0	24.1	5.0	0.90	2.4	-3.1	g...	...	840.4	1.1	3.0×10^{-16}
335	175110.03−293521.7	267.791830	−29.589381	0.2	3.9	20.9	7.0	20.1	9.3	0.90	2.8	-4.4	....	a	852.3	1.9	1.5×10^{-16}
336	175110.10−293227.2	267.792120	−29.540895	0.1	4.9	81.9	11.3	34.1	71.0	0.90	6.9	<-5	....	b	840.1	3.2	2.1×10^{-15}
337	175110.17−292828.1	267.792400	−29.474473	0.2	7.9	119.3	18.0	179.7	35.6	0.90	6.5	<-5	g...	...	765.0	1.4	1.5×10^{-15}
338	175110.23−294220.0	267.792660	−29.705572	0.3	7.9	52.6	12.2	81.4	39.1	0.71	4.1	<-5	g...	...	717.0	2.5	1.6×10^{-15}
339	175110.37−292812.3	267.793220	−29.470095	0.3	8.2	82.5	17.3	194.5	73.1	0.90	4.6	<-5	g...	...	758.9	3.4	2.6×10^{-15}
340	175110.37−293502.5	267.793230	−29.584042	0.1	3.8	54.1	9.1	19.9	36.5	0.90	5.6	<-5	....	a	857.1	2.5	1.1×10^{-15}

(*cont.*)

Table A.1: *Chandra* source list

Source		Position				Extracted Counts							Characteristics				
Seq	CXOU J	R. A.	Decl.	Err	θ	$C_{\rm net}$	$\Delta C_{\rm net}$	$C'_{\rm bkg}$	$C_{\rm net,hard}$	PSF	PS	$P_{\rm B}$	Anom	Var	EffExp	$E_{\rm median}$	Photo $F_{\rm x}$
#		(deg)	(deg)	($''$)	($'$)						Frac				(ks)	(keV)	(ergs s^{-1} cm^{-2})
(1)	(2)	(3)	(4)	(5)	(6)	(7)	(8)	(9)	(10)	(11)	(12)	(13)	(14)	(15)	(16)	(17)	(18)
341	175110.43−293332.8	267.793490	−29.559122	0.2	4.2	16.5	7.1	25.5	0.3	0.90	2.2	-2.7	g...	...	837.6	1.1	1.4×10^{-16}
342	175110.51−293656.5	267.793820	−29.615718	0.2	4.1	20.0	7.0	22.0	9.9	0.90	2.6	-3.9	g...	...	835.9	1.7	2.8×10^{-16}
343	175110.55−293348.6	267.793980	−29.563511	0.1	4.1	48.0	9.0	23.0	24.5	0.90	5.0	<-5	g...	...	822.5	2.0	7.9×10^{-16}
344	175110.57−294409.0	267.794050	−29.735848	0.2	9.5	191.7	22.4	278.3	67.9	0.90	8.4	<-5	g...	...	655.7	1.7	3.5×10^{-15}
345	175110.58−293832.7	267.794100	−29.642438	0.1	4.9	121.1	13.5	45.9	81.4	0.89	8.6	<-5	g...	...	817.8	2.7	2.8×10^{-15}
346	175110.64−293140.2	267.794350	−29.527847	0.2	5.3	21.8	8.8	46.2	2.1	0.90	2.3	-2.7	....	a	826.4	1.3	2.3×10^{-16}
347	175110.69−293741.9	267.794580	−29.628321	0.2	4.4	22.5	8.2	35.5	0.0	0.90	2.6	-3.4	g...	...	836.4	1.1	2.0×10^{-16}
348	175110.72−293441.1	267.794670	−29.578099	0.2	3.8	14.7	6.4	19.3	7.3	0.90	2.1	-2.7	....	c	854.3	2.2	2.5×10^{-16}
349	175110.73−293839.2	267.794720	−29.644239	0.1	5.0	72.8	11.4	45.2	33.4	0.89	6.1	<-5	g...	...	812.2	1.8	1.1×10^{-15}
350	175110.76−294142.1	267.794870	−29.695054	0.2	7.3	100.7	16.4	148.3	41.6	0.90	5.9	<-5	....	b	765.1	1.7	1.5×10^{-15}
351	175110.77−294115.5	267.794910	−29.687652	0.3	6.9	41.6	13.5	123.4	0.1	0.90	3.0	-3.6	g...	...	767.7	1.3	5.1×10^{-16}
352	175110.78−293947.0	267.794930	−29.663081	0.1	5.8	463.7	23.6	66.3	337.4	0.90	19.3	<-5	g...	...	801.7	3.0	1.2×10^{-14}
353	175110.82−293811.9	267.795090	−29.636648	0.2	4.7	26.7	9.0	43.3	4.1	0.90	2.8	-3.8	g...	...	826.0	1.5	3.3×10^{-16}
354	175110.87−292928.1	267.795330	−29.491166	0.3	7.0	25.9	9.6	54.1	9.4	0.69	2.6	-3.1	g...	...	788.8	1.3	3.8×10^{-16}
355	175110.93−294333.1	267.795550	−29.725874	0.3	8.9	72.6	18.4	240.4	0.0	0.90	3.8	<-5	g...	...	670.2	1.2	3.6×10^{-15}
356	175110.93−294216.1	267.795570	−29.704479	0.2	7.8	119.8	16.0	115.2	76.1	0.79	7.3	<-5	g...	...	730.9	2.8	9.4×10^{-16}
357	175111.00−293130.5	267.795850	−29.525158	0.2	5.4	30.7	9.4	46.3	18.4	0.90	3.1	-4.5	....	a	813.2	2.6	6.4×10^{-16}
358	175111.01−293408.3	267.795900	−29.568990	0.2	3.9	24.9	7.4	22.1	10.3	0.90	3.1	<-5	....	a	857.2	1.5	2.8×10^{-16}
359	175111.03−293118.8	267.795970	−29.521904	0.2	5.5	35.1	9.9	50.9	23.5	0.90	3.4	<-5	g...	...	814.0	2.8	8.0×10^{-16}
360	175111.04−292856.3	267.796040	−29.482308	0.3	7.4	47.0	14.3	138.0	52.1	0.90	3.2	-4.3	g...	...	776.1	4.7	1.9×10^{-15}
361	175111.07−292923.2	267.796160	−29.489792	0.3	7.0	30.0	9.9	57.0	20.9	0.73	2.9	-3.8	g...	...	789.1	2.6	8.4×10^{-16}
362	175111.18−293235.6	267.796590	−29.543232	0.2	4.6	21.4	7.7	29.6	13.0	0.90	2.6	-3.5	....	a	849.3	3.1	5.0×10^{-16}
363	175111.30−293054.0	267.797100	−29.515012	0.2	5.8	28.2	10.0	60.8	13.6	0.90	2.7	-3.3	....	b	811.5	1.9	4.3×10^{-16}
364	175111.34−293608.6	267.797260	−29.602395	0.2	3.7	11.8	5.6	13.2	4.2	0.90	1.9	-2.5	g...	...	531.9	1.8	8.6×10^{-16}
365	175111.34−293416.3	267.797290	−29.571196	0.1	3.8	47.6	8.7	19.4	26.1	0.90	5.1	<-5	g...	...	852.2	2.3	2.6×10^{-16}
366	175111.39−293200.3	267.797470	−29.533427	0.2	4.9	28.4	8.8	38.6	20.5	0.90	3.0	-4.5	g...	...	821.3	2.7	6.3×10^{-16}
367	175111.46−294016.1	267.797790	−29.671144	0.2	6.0	50.6	11.7	73.4	29.1	0.90	4.1	<-5	....	b	802.1	2.8	1.2×10^{-15}
368	175111.47−293140.2	267.797820	−29.527854	0.2	5.2	17.7	8.4	43.3	0.0	0.90	2.0	-2.1	g...	...	825.6	1.0	1.4×10^{-16}
369	175111.47−294243.9	267.797830	−29.712217	0.3	8.1	42.9	15.5	176.1	27.2	0.90	2.7	-3.1	g...	...	687.4	2.3	9.9×10^{-16}
370	175111.48−293148.7	267.797860	−29.530213	0.1	5.1	89.6	11.9	39.4	61.2	0.90	7.2	<-5	....	a	826.3	2.8	2.0×10^{-15}
371	175111.58−293532.6	267.798260	−29.592416	0.0	3.6	783.6	28.9	21.4	556.3	0.90	26.7	<-5	g...	...	857.0	2.8	1.7×10^{-14}
372	175111.59−293426.8	267.798320	−29.574114	0.2	3.7	24.0	7.0	17.0	7.7	0.90	3.2	<-5	g...	...	850.1	1.7	3.2×10^{-16}
373	175111.72−293613.0	267.798840	−29.603619	0.2	3.6	15.4	5.9	13.6	3.0	0.90	2.4	-3.6	g...	...	605.7	1.4	1.0×10^{-15}
374	175111.72−293132.1	267.798870	−29.525602	0.1	5.2	136.7	14.0	44.3	0.0	0.90	9.4	<-5	g...	...	822.3	0.9	2.3×10^{-16}

(*cont.*)

Table A.1: *Chandra* source list

Source		Position				Extracted Counts				Characteristics							
Seq	CXOU J	R. A.	Decl.	Err	θ	$C_{\rm net}$	$\Delta C_{\rm net}$	$C'_{\rm bkg}$	$C_{\rm net,hard}$	PSF	PS	$P_{\rm B}$	Anom	Var	EffExp	$E_{\rm median}$	Photo $F_{\rm x}$
#		(deg)	(deg)	($''$)	($'$)						Frac				(ks)	(keV)	(ergs s^{-1} cm^{-2})
(1)	(2)	(3)	(4)	(5)	(6)	(7)	(8)	(9)	(10)	(11)	(12)	(13)	(14)	(15)	(16)	(17)	(18)
375	175111.78−293502.6	267.799090	−29.584057	0.1	3.5	205.4	15.4	14.6	199.2	0.90	12.9	<-5	g...	...	856.0	3.6	5.9×10^{-15}
376	175111.81−293647.3	267.799220	−29.613150	0.2	3.8	20.6	7.0	20.4	0.0	0.90	2.8	-4.3	....	a	852.3	1.0	1.6×10^{-16}
377	175111.85−293259.8	267.799400	−29.549959	0.1	4.2	408.3	21.3	23.7	370.6	0.90	18.7	<-5	g...	...	832.3	4.1	1.3×10^{-14}
378	175111.86−293217.7	267.799430	−29.538265	0.1	4.7	64.6	10.4	32.4	34.1	0.90	5.9	<-5	....	a	832.5	2.0	1.0×10^{-15}
379	175111.90−293714.1	267.799620	−29.620610	0.1	3.9	119.2	12.4	21.8	24.4	0.90	9.2	<-5	....	b	849.4	1.4	1.2×10^{-15}
380	175111.90−294115.9	267.799620	−29.687760	0.1	6.8	262.7	20.1	116.3	200.6	0.90	12.8	<-5	g...	...	779.8	3.3	7.7×10^{-15}
381	175111.91−293435.9	267.799630	−29.576666	0.2	3.6	12.9	5.7	14.1	6.8	0.89	2.0	-2.8	g...	...	856.9	1.9	1.9×10^{-16}
382	175111.94−293651.7	267.799790	−29.614378	0.2	3.8	16.9	6.6	19.1	5.0	0.90	2.4	-3.4	....	a	852.0	1.8	2.4×10^{-16}
383	175111.98−293829.4	267.799950	−29.641523	0.2	4.6	31.3	9.0	39.7	20.1	0.90	3.3	<-5	g...	...	823.1	2.8	7.1×10^{-16}
384	175111.99−294105.1	267.799990	−29.684772	0.2	6.7	37.8	12.6	104.2	8.2	0.89	2.9	-3.5	....	c	789.0	1.5	4.9×10^{-16}
385	175112.04−293527.7	267.800170	−29.591031	0.0	3.5	633.8	26.1	19.2	431.9	0.90	23.8	<-5	g...	...	855.1	2.7	1.4×10^{-14}
386	175112.04−293535.6	267.800170	−29.593233	0.1	3.5	24.9	7.3	20.1	13.0	0.90	3.2	<-5	g...	...	855.2	2.0	4.0×10^{-16}
387	175112.12−293633.9	267.800540	−29.609431	0.1	3.6	41.8	8.3	18.2	19.8	0.90	4.7	<-5	....	b	851.5	1.9	6.1×10^{-16}
388	175112.16−294056.2	267.800700	−29.682286	0.2	6.5	40.3	12.3	95.7	28.7	0.89	3.1	-4.1	g...	...	790.4	3.0	1.1×10^{-15}
389	175112.18−294223.7	267.800770	−29.706597	0.2	7.7	88.8	16.4	159.2	57.5	0.90	5.2	<-5	g...	...	721.0	2.7	2.3×10^{-15}
390	175112.21−293939.3	267.800890	−29.660941	0.2	5.5	33.0	9.8	51.0	18.6	0.90	3.2	-4.7	g...	...	814.7	2.4	6.7×10^{-16}
391	175112.22−293130.7	267.800950	−29.525197	0.2	5.2	20.1	8.0	34.9	10.6	0.87	2.4	-2.9	....	a	841.3	2.6	4.3×10^{-16}
392	175112.25−293618.8	267.801070	−29.605247	0.2	3.5	13.6	5.8	14.4	4.8	0.90	2.1	-2.9	g...	...	726.7	1.5	1.8×10^{-16}
393	175112.32−292759.9	267.801350	−29.466645	0.3	8.1	39.5	14.0	137.5	28.7	0.82	2.7	-3.3	....	b	766.3	3.1	1.1×10^{-15}
394	175112.38−293243.8	267.801610	−29.545512	0.2	4.3	30.2	8.0	24.8	6.8	0.90	3.5	<-5	g...	...	838.5	1.3	3.0×10^{-16}
395	175112.40−293541.6	267.801680	−29.594891	0.2	3.4	17.8	6.3	15.2	4.7	0.90	2.6	-4.1	....	a	860.2	1.2	1.6×10^{-16}
396	175112.44−293141.6	267.801870	−29.528235	0.2	5.0	46.7	9.8	38.3	3.9	0.90	4.5	<-5	....	c	846.5	1.1	4.2×10^{-16}
397	175112.45−293044.1	267.801900	−29.512275	0.2	5.7	99.6	13.3	61.4	29.8	0.90	7.2	<-5	....	b	822.3	1.6	1.3×10^{-15}
398	175112.49−292732.7	267.802060	−29.459108	0.4	8.4	45.6	13.5	119.4	0.0	0.90	3.3	-4.2	g...	...	483.3	1.1	7.6×10^{-16}
399	175112.51−293353.8	267.802150	−29.564972	0.2	3.7	12.6	6.1	18.4	5.0	0.90	1.9	-2.3	g...	...	816.8	1.2	1.3×10^{-16}
400	175112.54−293331.1	267.802250	−29.558664	0.1	3.8	50.9	8.9	19.1	8.8	0.90	5.4	<-5	g...	...	834.5	1.3	5.4×10^{-16}
401	175112.59−293405.2	267.802470	−29.568135	0.2	3.6	16.9	6.4	17.1	6.3	0.90	2.4	-3.6	g...	...	848.1	1.5	2.0×10^{-16}
402	175112.64−293308.4	267.802680	−29.552345	0.2	4.0	13.2	6.4	20.8	1.5	0.90	1.9	-2.3	g...	...	844.7	1.5	1.5×10^{-16}
403	175112.67−293858.0	267.802830	−29.649448	0.2	4.9	40.5	9.6	40.5	3.8	0.90	4.0	<-5	....	a	834.5	1.3	4.1×10^{-16}
404	175112.68−293326.0	267.802840	−29.557227	0.2	3.8	24.2	7.1	18.8	0.0	0.90	3.2	<-5	g...	...	835.5	1.0	1.9×10^{-16}
405	175112.68−293623.7	267.802840	−29.606592	0.2	3.5	17.1	6.2	14.9	12.5	0.90	2.5	-4.0	g...	...	779.8	2.9	4.1×10^{-16}
406	175112.72−293214.4	267.803030	−29.537350	0.2	4.6	20.3	7.8	31.7	12.0	0.90	2.4	-3.1	....	b	855.0	3.1	4.8×10^{-16}
407	175112.75−293738.4	267.803140	−29.627351	0.2	4.0	13.9	6.9	26.1	4.5	0.90	1.9	-2.1	....	b	860.9	1.6	1.7×10^{-16}
408	175112.76−293447.9	267.803190	−29.579995	0.1	3.4	30.2	7.1	12.8	1.6	0.89	3.9	<-5	g...	...	852.8	1.2	2.9×10^{-16}

(*cont.*)

Table A.1: *Chandra* source list

Source		Position				Extracted Counts							Characteristics				
Seq	CXOU J	R. A.	Decl.	Err	θ	$C_{\rm net}$	$\Delta C_{\rm net}$	$C'_{\rm bkg}$	$C_{\rm net,hard}$	PSF	PS	$P_{\rm B}$	Anom	Var	EffExp	$E_{\rm median}$	Photo $F_{\rm x}$
#		(deg)	(deg)	($''$)	($'$)						Frac				(ks)	(keV)	(ergs s^{-1} cm^{-2})
(1)	(2)	(3)	(4)	(5)	(6)	(7)	(8)	(9)	(10)	(11)	(12)	(13)	(14)	(15)	(16)	(17)	(18)
409	175112.80−294038.5	267.803370	−29.677388	0.2	6.2	52.1	12.2	82.9	23.6	0.90	4.1	<-5	g...	...	793.3	1.9	8.7×10^{-16}
410	175112.82−293751.4	267.803420	−29.630961	0.1	4.1	37.5	8.8	30.5	17.2	0.89	4.0	<-5	....	a	856.1	1.9	5.4×10^{-16}
411	175112.83−293905.8	267.803460	−29.651615	0.2	4.9	21.5	8.4	39.5	14.8	0.90	2.4	-3.0	....	a	834.0	2.4	3.9×10^{-16}
412	175112.83−293434.6	267.803470	−29.576288	0.2	3.4	16.6	5.9	12.4	11.3	0.89	2.6	-4.3	g...	...	850.4	3.0	4.0×10^{-16}
413	175112.90−293645.5	267.803760	−29.612642	0.2	3.5	15.9	6.3	17.1	10.4	0.90	2.3	-3.3	....	b	862.4	2.5	3.0×10^{-16}
414	175112.97−293244.1	267.804050	−29.545603	0.2	4.2	28.3	7.7	22.7	23.7	0.90	3.4	<-5	....	a	854.7	3.0	6.5×10^{-16}
415	175112.98−293407.1	267.804120	−29.568644	0.2	3.5	12.0	5.8	16.0	4.3	0.90	1.9	-2.3	g...	...	838.6	1.6	1.5×10^{-16}
416	175113.04−293449.5	267.804340	−29.580419	0.2	3.3	15.6	5.8	12.4	7.8	0.89	2.4	-3.9	g...	...	843.3	2.3	2.9×10^{-16}
417	175113.11−293440.4	267.804660	−29.577902	0.1	3.3	83.9	10.3	12.1	48.4	0.90	7.7	<-5	g...	...	846.2	2.4	1.6×10^{-15}
418	175113.12−293503.7	267.804700	−29.584374	0.2	3.2	13.0	5.5	12.0	7.6	0.90	2.1	-3.1	g...	...	847.7	2.3	2.4×10^{-16}
419	175113.13−293351.8	267.804710	−29.564399	0.2	3.6	18.7	6.6	17.3	3.4	0.90	2.6	-4.1	g...	...	813.8	1.4	2.0×10^{-16}
420	175113.15−294224.3	267.804810	−29.706771	0.2	7.7	97.8	16.4	150.2	53.3	0.89	5.8	<-5	g...	...	730.3	2.1	1.9×10^{-15}
421	175113.21−292932.1	267.805050	−29.492260	0.2	6.7	61.2	13.4	101.8	43.1	0.90	4.4	<-5	....	b	805.6	2.9	1.5×10^{-15}
422	175113.25−293948.6	267.805220	−29.663512	0.2	5.4	53.7	10.9	52.3	7.9	0.90	4.7	<-5	....	b	819.7	1.2	5.1×10^{-16}
423	175113.30−293846.1	267.805430	−29.646153	0.1	4.6	58.8	10.5	39.2	39.2	0.90	5.4	<-5	....	a	844.7	2.9	1.3×10^{-15}
424	175113.31−294000.4	267.805480	−29.666789	0.2	5.6	16.3	5.8	11.7	7.2	0.52	2.5	-4.3	....	a	816.7	1.9	4.4×10^{-16}
425	175113.32−293610.9	267.805520	−29.603050	0.2	3.2	25.0	6.5	10.0	6.0	0.90	3.6	<-5	g...	...	616.5	1.6	4.2×10^{-16}
426	175113.47−293635.1	267.806130	−29.609754	0.1	3.4	91.3	10.9	15.7	71.2	0.90	8.0	<-5	....	b	869.8	3.4	2.3×10^{-15}
427	175113.52−293959.1	267.806340	−29.666417	0.2	5.6	24.4	6.5	10.6	14.0	0.53	3.5	<-5	....	a	819.9	2.2	7.3×10^{-16}
428	175113.56−292944.6	267.806510	−29.495744	0.2	6.5	92.9	14.2	92.1	67.1	0.90	6.3	<-5	....	c	813.4	2.7	2.0×10^{-15}
429	175113.56−293820.2	267.806530	−29.638970	0.1	4.3	48.1	9.8	36.9	24.1	0.90	4.7	<-5	....	a	855.2	2.0	7.4×10^{-16}
430	175113.58−293902.9	267.806590	−29.650823	0.2	4.8	29.6	8.7	36.4	26.9	0.90	3.2	<-5	....	a	841.2	3.9	7.3×10^{-16}
431	175113.58−293456.4	267.806600	−29.582344	0.1	3.2	34.9	7.3	11.1	20.7	0.90	4.4	<-5	....	a	849.0	2.7	9.0×10^{-16}
432	175113.59−294251.0	267.806640	−29.714184	0.3	8.0	60.4	16.0	174.6	7.9	0.90	3.6	<-5	....	a	699.4	1.4	8.2×10^{-16}
433	175113.60−293202.5	267.806670	−29.534043	0.2	4.6	29.6	8.5	33.4	10.0	0.90	3.3	<-5	g...	...	835.1	1.6	3.8×10^{-16}
434	175113.64−293527.0	267.806860	−29.590837	0.2	3.1	18.2	5.9	10.8	3.0	0.90	2.8	<-5	g...	...	841.9	1.4	2.0×10^{-16}
435	175113.68−293518.5	267.807000	−29.588498	0.1	3.1	29.7	6.9	10.3	9.4	0.90	4.0	<-5	g...	...	851.5	1.4	3.2×10^{-16}
436	175113.69−293851.5	267.807070	−29.647657	0.2	4.6	19.8	8.1	37.2	5.8	0.90	2.3	-2.7	....	c	844.9	1.5	3.8×10^{-16}
437	175113.69−293549.5	267.807080	−29.597105	0.2	3.2	11.8	5.2	10.2	11.1	0.90	2.0	-3.0	g...	...	654.5	3.1	2.2×10^{-16}
438	175113.70−293110.1	267.807110	−29.519476	0.0	5.2	4325.4	66.6	48.6	3523.3	0.90	64.4	<-5	....	c	826.2	3.4	1.2×10^{-13}
439	175113.73−292823.5	267.807240	−29.473214	0.2	7.7	104.5	16.8	156.5	14.2	0.90	6.0	<-5	....	b	787.4	1.3	1.1×10^{-15}
440	175113.79−293101.7	267.807480	−29.517163	0.2	5.3	25.2	9.4	51.8	5.5	0.90	2.5	-3.1	g...	...	824.8	1.1	2.2×10^{-16}
441	175113.84−294333.5	267.807690	−29.725981	0.3	8.6	99.7	19.0	233.3	67.0	0.91	5.1	<-5	g...	...	683.6	2.8	2.9×10^{-15}
442	175113.85−293651.5	267.807720	−29.614323	0.2	3.4	22.7	6.7	15.3	4.1	0.90	3.1	<-5	....	a	871.1	1.5	2.4×10^{-16}

(*cont.*)

Table A.1: *Chandra* source list

Source		Position				Extracted Counts				Characteristics							
Seq	CXOU J	R. A.	Decl.	Err	θ	$C_{\rm net}$	$\Delta C_{\rm net}$	$C'_{\rm bkg}$	$C_{\rm net,hard}$	PSF	PS	$P_{\rm B}$	Anom	Var	EffExp	$E_{\rm median}$	Photo $F_{\rm x}$
#		(deg)	(deg)	($''$)	($'$)						Frac				(ks)	(keV)	(ergs s^{-1} cm^{-2})
(1)	(2)	(3)	(4)	(5)	(6)	(7)	(8)	(9)	(10)	(11)	(12)	(13)	(14)	(15)	(16)	(17)	(18)
443	175113.89−293447.3	267.807900	−29.579814	0.0	3.1	268.3	17.2	11.7	203.4	0.89	15.1	<-5	....	a	860.2	3.2	6.5×10^{-15}
444	175113.91−293514.4	267.807960	−29.587347	0.1	3.1	86.5	10.4	10.5	25.3	0.90	7.9	<-5	g...	...	843.8	1.5	1.0×10^{-15}
445	175113.92−292905.1	267.808020	−29.484762	0.3	7.0	36.7	12.9	113.3	24.4	0.90	2.7	-3.2	....	a	806.3	2.3	6.7×10^{-16}
446	175113.95−293336.5	267.808160	−29.560139	0.1	3.5	28.5	7.3	16.5	16.1	0.90	3.7	<-5	....	a	860.6	2.2	4.7×10^{-16}
447	175113.96−293257.7	267.808200	−29.549387	0.1	3.9	48.9	8.9	21.1	40.5	0.90	5.2	<-5	....	a	858.5	3.9	1.4×10^{-15}
448	175113.98−293018.0	267.808270	−29.505011	0.2	5.9	37.4	10.8	66.6	18.1	0.90	3.3	-4.7	....	a	826.9	2.0	5.8×10^{-16}
449	175114.00−293743.2	267.808360	−29.628688	0.1	3.8	33.7	8.2	25.3	5.2	0.90	3.8	<-5	....	a	864.0	1.3	3.2×10^{-16}
450	175114.01−293314.6	267.808390	−29.554078	0.2	3.7	25.6	7.0	16.4	14.0	0.90	3.4	<-5	....	a	863.5	2.3	4.3×10^{-16}
451	175114.10−293529.3	267.808790	−29.591488	0.1	3.0	20.6	6.2	11.4	0.0	0.90	3.1	<-5	....	a	857.0	1.4	2.2×10^{-16}
452	175114.14−293821.2	267.808930	−29.639224	0.2	4.2	35.0	8.9	34.0	13.2	0.89	3.7	<-5	....	b	856.7	1.7	4.4×10^{-16}
453	175114.16−293505.6	267.809000	−29.584892	0.1	3.0	120.2	12.0	10.8	46.6	0.89	9.6	<-5	....	b	858.9	1.7	1.5×10^{-15}
454	175114.22−293223.9	267.809270	−29.539991	0.1	4.2	283.3	18.1	24.7	200.6	0.90	15.2	<-5	....	b	840.7	2.8	6.2×10^{-15}
455	175114.24−294008.0	267.809350	−29.668909	0.2	5.6	49.5	11.3	64.5	31.2	0.91	4.2	<-5	....	b	824.8	2.3	8.8×10^{-16}
456	175114.30−293711.2	267.809620	−29.619797	0.1	3.5	37.2	7.8	15.8	33.1	0.90	4.5	<-5	....	a	870.1	3.0	8.3×10^{-16}
457	175114.44−292746.2	267.810180	−29.462856	0.3	8.2	36.9	15.4	179.1	14.7	0.90	2.3	-2.4	g...	...	744.2	1.9	6.5×10^{-16}
458	175114.56−293755.8	267.810670	−29.632179	0.1	3.9	46.3	9.3	29.7	28.5	0.90	4.7	<-5	....	a	863.2	2.5	8.5×10^{-16}
459	175114.61−293512.4	267.810880	−29.586793	0.1	2.9	33.6	7.2	10.4	9.6	0.89	4.4	<-5	....	a	861.1	1.5	3.7×10^{-16}
460	175114.64−294310.7	267.811030	−29.719663	0.3	8.2	42.4	16.3	200.6	16.4	0.90	2.5	-2.7	....	a	695.9	1.8	7.7×10^{-16}
461	175114.68−293849.9	267.811190	−29.647214	0.1	4.5	53.1	9.1	20.9	36.6	0.81	5.5	<-5	....	c	851.6	3.0	1.3×10^{-15}
462	175114.69−293200.9	267.811210	−29.533607	0.2	4.4	35.3	8.4	26.7	22.3	0.90	3.9	<-5	g...	...	845.0	2.4	6.7×10^{-16}
463	175114.70−293549.4	267.811270	−29.597079	0.1	2.9	22.1	6.0	7.9	16.8	0.90	3.4	<-5	g...	...	620.8	3.6	8.6×10^{-16}
464	175114.79−293006.9	267.811640	−29.501944	0.1	6.0	229.1	17.9	70.9	20.1	0.90	12.4	<-5	....	b	826.5	1.3	2.4×10^{-15}
465	175114.86−293634.2	267.811940	−29.609510	0.1	3.1	36.8	7.6	13.2	21.5	0.90	4.5	<-5	....	a	863.1	2.5	6.7×10^{-16}
466	175114.95−293314.0	267.812300	−29.553900	0.1	3.5	103.2	11.4	14.8	63.4	0.89	8.7	<-5	....	b	856.1	2.4	1.9×10^{-15}
467	175114.95−293631.6	267.812320	−29.608805	0.1	3.0	21.3	6.3	11.7	9.2	0.89	3.1	<-5	....	a	851.7	1.6	2.5×10^{-16}
468	175114.95−293846.6	267.812320	−29.646285	0.1	4.4	87.5	11.3	27.5	68.0	0.86	7.4	<-5	....	a	853.1	3.2	2.2×10^{-15}
469	175114.96−293457.4	267.812370	−29.582627	0.1	2.9	28.0	6.7	10.0	12.2	0.89	3.9	<-5	....	a	857.2	1.9	4.0×10^{-16}
470	175115.02−293533.4	267.812620	−29.592624	0.2	2.8	13.3	5.4	10.7	4.1	0.89	2.2	-3.4	....	a	868.0	1.5	1.5×10^{-16}
471	175115.03−293908.8	267.812660	−29.652446	0.2	4.7	22.2	8.2	35.8	0.0	0.90	2.5	-3.3	....	a	845.3	0.9	1.5×10^{-16}
472	175115.06−293121.2	267.812760	−29.522577	0.1	4.9	109.2	12.7	38.8	47.4	0.90	8.2	<-5	....	a	856.1	1.7	1.4×10^{-15}
473	175115.09−293355.7	267.812880	−29.565494	0.1	3.2	140.6	12.9	13.4	95.0	0.89	10.5	<-5	g...	...	821.4	2.9	3.3×10^{-15}
474	175115.20−293702.8	267.813360	−29.617456	0.2	3.2	18.4	6.1	12.6	9.9	0.89	2.8	-4.9	....	a	851.5	2.0	2.8×10^{-16}
475	175115.20−293726.6	267.813370	−29.624069	0.2	3.4	12.0	5.8	15.0	9.9	0.89	1.9	-2.4	....	a	856.2	3.0	2.7×10^{-16}
476	175115.27−292910.0	267.813640	−29.486138	0.3	6.8	38.0	12.7	107.0	21.4	0.90	2.9	-3.5	g...	...	791.1	2.4	8.1×10^{-16}

(*cont.*)

Table A.1: *Chandra* source list

Source		Position				Extracted Counts							Characteristics				
Seq	CXOU J	R. A.	Decl.	Err	θ	$C_{\rm net}$	$\Delta C_{\rm net}$	$C'_{\rm bkg}$	$C_{\rm net,hard}$	PSF	PS	$P_{\rm B}$	Anom	Var	EffExp	$E_{\rm median}$	Photo $F_{\rm x}$
#		(deg)	(deg)	($''$)	($'$)						Frac				(ks)	(keV)	(ergs s^{-1} cm^{-2})
(1)	(2)	(3)	(4)	(5)	(6)	(7)	(8)	(9)	(10)	(11)	(12)	(13)	(14)	(15)	(16)	(17)	(18)
477	175115.28−293432.3	267.813680	−29.575639	0.2	2.9	10.2	5.1	10.8	4.9	0.89	1.8	-2.4	....	a	859.3	1.8	1.4×10^{-16}
478	175115.29−293822.5	267.813720	−29.639594	0.2	4.1	25.2	8.1	30.8	15.1	0.90	2.9	-4.4	....	a	858.8	2.7	5.1×10^{-16}
479	175115.37−293735.7	267.814050	−29.626594	0.2	3.5	21.1	6.8	17.9	22.4	0.89	2.9	-4.8	....	b	850.9	3.6	5.8×10^{-16}
480	175115.37−293927.3	267.814060	−29.657604	0.1	4.9	74.9	11.3	40.1	43.8	0.90	6.3	<-5	....	a	841.2	2.2	1.3×10^{-15}
481	175115.39−293903.5	267.814130	−29.650982	0.1	4.6	104.5	12.3	34.5	4.4	0.90	8.1	<-5	....	b	846.5	1.1	8.5×10^{-16}
482	175115.40−293325.1	267.814200	−29.556988	0.2	3.4	14.9	5.8	13.1	6.4	0.90	2.3	-3.5	....	a	862.7	1.5	1.7×10^{-16}
483	175115.42−293335.3	267.814260	−29.559827	0.2	3.3	14.1	5.7	12.9	3.4	0.90	2.2	-3.3	....	b	863.9	1.2	1.3×10^{-16}
484	175115.47−293707.6	267.814470	−29.618797	0.1	3.2	25.6	6.7	12.4	3.9	0.89	3.5	<-5	....	a	851.2	1.2	2.4×10^{-16}
485	175115.49−293527.4	267.814580	−29.590959	0.1	2.7	15.6	5.5	9.4	1.6	0.89	2.6	-4.6	....	a	866.6	1.5	1.7×10^{-16}
486	175115.66−293518.3	267.815290	−29.588440	0.1	2.7	18.5	5.7	8.5	11.0	0.89	2.9	<-5	....	c	863.3	2.3	3.2×10^{-16}
487	175115.75−293142.6	267.815650	−29.528514	0.2	4.5	20.0	6.2	12.0	12.8	0.69	3.0	<-5	....	a	860.2	2.9	5.8×10^{-16}
488	175115.79−293957.4	267.815810	−29.665947	0.2	5.3	43.6	10.3	51.4	17.7	0.90	4.0	<-5	....	b	833.1	1.8	6.2×10^{-16}
489	175115.81−293802.5	267.815880	−29.634043	0.2	3.7	18.3	7.1	24.7	7.0	0.90	2.4	-3.2	....	a	838.5	1.6	2.3×10^{-16}
490	175115.83−293753.0	267.815970	−29.631412	0.1	3.6	31.9	8.1	25.1	18.2	0.90	3.7	<-5	....	a	844.0	2.5	6.0×10^{-16}
491	175115.83−294216.4	267.815970	−29.704582	0.3	7.4	37.8	14.7	159.2	13.3	0.90	2.5	-2.7	....	a	781.6	1.7	5.4×10^{-16}
492	175115.87−293348.0	267.816150	−29.563349	0.1	3.1	32.7	7.2	11.3	14.7	0.90	4.2	<-5	g...	...	843.5	1.9	4.7×10^{-16}
493	175115.90−293215.5	267.816290	−29.537647	0.2	4.1	33.9	8.0	22.1	9.3	0.90	4.0	<-5	....	a	867.4	1.5	3.7×10^{-16}
494	175115.92−293315.1	267.816350	−29.554205	0.2	3.4	15.6	5.9	13.4	4.0	0.90	2.4	-3.7	....	a	877.3	1.5	1.7×10^{-16}
495	175115.94−293842.5	267.816430	−29.645165	0.1	4.2	44.8	9.2	29.2	17.4	0.90	4.6	<-5	....	a	825.5	1.8	6.5×10^{-16}
496	175115.95−293144.2	267.816480	−29.528945	0.2	4.5	19.8	5.9	9.2	12.2	0.65	3.1	<-5	....	a	854.9	2.4	5.0×10^{-16}
497	175115.95−293151.4	267.816490	−29.530955	0.1	4.4	116.8	12.5	27.2	120.5	0.90	8.9	<-5	....	a	858.8	4.4	3.9×10^{-15}
498	175115.99−293656.2	267.816650	−29.615612	0.1	3.0	26.2	6.7	11.8	17.4	0.90	3.6	<-5	....	a	854.5	2.8	5.4×10^{-16}
499	175116.02−293037.8	267.816790	−29.510502	0.2	5.4	46.2	10.5	51.8	34.8	0.90	4.2	<-5	g...	...	825.2	2.5	9.8×10^{-16}
500	175116.13−293951.0	267.817230	−29.664192	0.2	5.1	21.5	8.8	45.5	20.1	0.89	2.3	-2.7	....	b	837.9	4.1	2.8×10^{-16}
501	175116.13−293247.8	267.817240	−29.546616	0.2	3.6	24.5	7.0	17.5	6.4	0.90	3.2	<-5	....	a	874.1	1.5	6.9×10^{-16}
502	175116.16−293139.1	267.817350	−29.527537	0.2	4.5	32.3	8.4	28.7	18.9	0.90	3.6	<-5	....	a	849.6	2.4	6.2×10^{-16}
503	175116.19−293512.8	267.817460	−29.586899	0.1	2.6	19.0	5.7	8.0	2.4	0.89	3.0	<-5	....	a	869.0	1.1	1.6×10^{-16}
504	175116.21−293358.6	267.817580	−29.566289	0.1	2.9	17.8	5.8	10.2	12.5	0.89	2.8	<-5	....	b	846.7	2.6	3.5×10^{-16}
505	175116.31−293446.2	267.817970	−29.579525	0.1	2.6	24.3	6.3	8.7	13.4	0.89	3.6	<-5	....	b	881.7	2.2	3.9×10^{-16}
506	175116.31−293805.7	267.818000	−29.634925	0.2	3.7	24.6	7.5	23.4	0.0	0.90	3.1	<-5	....	a	827.1	1.3	2.5×10^{-16}
507	175116.36−293644.3	267.818170	−29.612310	0.2	2.9	9.9	4.9	9.1	3.4	0.89	1.8	-2.5	....	a	855.8	1.6	1.2×10^{-16}
508	175116.40−293516.8	267.818340	−29.588013	0.1	2.5	32.5	7.0	9.5	2.6	0.89	4.3	<-5	....	a	879.9	1.3	3.1×10^{-16}
509	175116.41−293846.0	267.818390	−29.646118	0.2	4.2	19.1	7.4	27.9	6.4	0.90	2.4	-3.1	....	a	829.3	1.6	2.4×10^{-16}
510	175116.45−294155.5	267.818570	−29.698761	0.3	7.0	33.2	13.7	135.8	11.6	0.90	2.3	-2.5	....	a	794.9	1.5	4.0×10^{-16}

(*cont.*)

Table A.1: *Chandra* source list

Source		Position				Extracted Counts				Characteristics							
Seq	CXOU J	R. A.	Decl.	Err	θ	$C_{\rm net}$	$\Delta C_{\rm net}$	$C'_{\rm bkg}$	$C_{\rm net,hard}$	PSF	PS	$P_{\rm B}$	Anom	Var	EffExp	$E_{\rm median}$	Photo $F_{\rm x}$
#		(deg)	(deg)	($''$)	($'$)						Frac				(ks)	(keV)	(ergs s^{-1} cm^{-2})
(1)	(2)	(3)	(4)	(5)	(6)	(7)	(8)	(9)	(10)	(11)	(12)	(13)	(14)	(15)	(16)	(17)	(18)
511	175116.53−293824.4	267.818910	−29.640136	0.2	3.9	22.6	7.6	26.4	11.9	0.90	2.8	-4.2	....	a	827.2	1.9	3.3×10^{-16}
512	175116.55−293756.7	267.818960	−29.632437	0.1	3.6	71.6	10.3	23.4	19.9	0.90	6.6	<-5	....	c	827.9	1.4	7.9×10^{-16}
513	175116.56−293007.0	267.819030	−29.501958	0.2	5.8	135.5	14.7	63.5	97.8	0.90	8.9	<-5	g...	...	809.6	3.0	3.5×10^{-15}
514	175116.58−294018.9	267.819090	−29.671920	0.2	5.5	77.3	12.1	54.7	45.5	0.89	6.1	<-5	....	a	823.4	2.4	1.9×10^{-16}
515	175116.58−293303.5	267.819100	−29.550997	0.2	3.4	19.2	6.3	13.8	1.9	0.90	2.8	-5.0	....	a	871.7	1.3	4.0×10^{-16}
516	175116.58−293813.4	267.819100	−29.637073	0.2	3.8	22.7	7.3	22.3	12.1	0.86	2.9	-4.7	....	a	824.7	2.1	1.5×10^{-15}
517	175116.59−293322.7	267.819130	−29.556308	0.1	3.2	21.5	6.3	11.5	16.4	0.90	3.1	<-5	....	a	878.0	3.1	4.9×10^{-16}
518	175116.61−293535.0	267.819220	−29.593069	0.1	2.5	13.4	5.2	8.6	3.7	0.89	2.3	-3.9	....	a	875.9	1.7	1.7×10^{-16}
519	175116.62−293934.0	267.819280	−29.659469	0.1	4.8	124.6	13.3	38.4	37.9	0.90	9.0	<-5	....	c	818.3	1.5	1.5×10^{-15}
520	175116.71−294013.4	267.819660	−29.670415	0.2	5.4	23.9	7.9	29.1	9.9	0.77	2.8	-4.2	....	a	822.0	1.7	3.7×10^{-16}
521	175116.73−293639.8	267.819730	−29.611082	0.2	2.7	15.4	5.4	8.6	6.7	0.89	2.6	-4.8	....	a	861.1	2.0	2.3×10^{-16}
522	175116.75−293616.9	267.819800	−29.604722	0.2	2.6	10.0	4.9	9.0	4.8	0.89	1.8	-2.5	g...	...	813.9	1.8	1.4×10^{-16}
523	175116.75−293816.2	267.819820	−29.637848	0.1	3.8	36.8	8.4	24.2	0.0	0.90	4.1	<-5	....	a	818.9	1.0	2.9×10^{-16}
524	175116.81−293940.0	267.820060	−29.661116	0.2	4.9	41.6	9.4	36.4	27.1	0.88	4.2	<-5	....	b	814.9	2.5	8.3×10^{-16}
525	175116.91−292946.0	267.820480	−29.496132	0.3	6.1	31.4	11.1	77.6	8.9	0.90	2.7	-3.3	....	b	806.1	1.7	4.5×10^{-16}
526	175116.92−293608.5	267.820520	−29.602388	0.1	2.5	24.5	6.2	7.5	8.6	0.90	3.6	<-5	g...	...	686.9	1.4	3.2×10^{-16}
527	175116.95−293915.2	267.820660	−29.654232	0.1	4.5	128.5	13.3	33.5	91.8	0.91	9.3	<-5	....	a	822.9	2.9	2.9×10^{-15}
528	175116.97−293141.1	267.820720	−29.528089	0.2	4.4	41.0	8.7	26.0	19.2	0.90	4.4	<-5	g...	...	840.8	1.9	6.5×10^{-16}
529	175117.00−293930.0	267.820840	−29.658337	0.1	4.7	83.5	11.5	35.5	61.4	0.90	7.0	<-5	....	a	817.5	2.8	1.8×10^{-15}
530	175117.01−294032.9	267.820910	−29.675819	0.2	5.7	22.1	9.1	50.9	11.5	0.85	2.3	-2.6	....	a	816.7	2.0	3.6×10^{-16}
531	175117.05−293046.7	267.821070	−29.512983	0.2	5.2	35.9	9.7	47.1	4.2	0.90	3.5	<-5	g...	...	823.5	1.1	3.5×10^{-16}
532	175117.08−294112.2	267.821180	−29.686726	0.2	6.3	82.0	13.8	92.0	32.9	0.90	5.7	<-5	....	b	805.7	1.9	1.2×10^{-15}
533	175117.10−293536.4	267.821260	−29.593451	0.2	2.4	9.1	4.7	7.9	0.4	0.89	1.7	-2.4	g...	...	825.7	1.3	9.7×10^{-17}
534	175117.12−293713.5	267.821360	−29.620430	0.2	3.0	11.9	5.4	12.1	4.6	0.90	2.0	-2.7	....	b	862.3	1.4	1.3×10^{-16}
535	175117.18−293158.3	267.821600	−29.532863	0.2	4.1	26.1	7.6	23.9	6.5	0.90	3.2	<-5	g...	...	844.9	1.7	3.6×10^{-16}
536	175117.20−293039.4	267.821690	−29.510972	0.1	5.3	119.7	13.5	48.3	111.6	0.90	8.5	<-5	g...	...	822.8	3.7	3.6×10^{-15}
537	175117.20−294219.6	267.821700	−29.705453	0.2	7.3	90.2	16.4	157.8	32.1	0.90	5.3	<-5	....	c	782.6	1.6	1.2×10^{-15}
538	175117.21−293822.9	267.821730	−29.639709	0.2	3.8	19.2	7.4	26.8	0.5	0.90	2.4	-3.2	....	a	848.4	1.1	1.6×10^{-16}
539	175117.22−293833.2	267.821790	−29.642568	0.1	3.9	98.8	11.9	29.2	60.1	0.90	8.0	<-5	....	c	843.4	2.5	1.9×10^{-15}
540	175117.28−293557.8	267.822000	−29.599393	0.2	2.4	11.6	4.7	5.4	2.2	0.90	2.2	-4.2	g...	...	488.0	1.4	2.1×10^{-16}
541	175117.37−293614.0	267.822380	−29.603897	0.1	2.4	24.5	6.2	7.5	3.5	0.89	3.6	<-5	g...	...	789.3	1.2	2.3×10^{-16}
542	175117.38−292928.1	267.822420	−29.491142	0.3	6.4	31.2	11.5	85.8	9.2	0.90	2.6	-3.0	....	a	805.5	1.3	3.4×10^{-16}
543	175117.38−293236.4	267.822420	−29.543472	0.2	3.6	16.2	6.3	16.8	10.1	0.90	2.4	-3.4	....	a	868.8	2.3	2.8×10^{-16}
544	175117.38−293711.4	267.822430	−29.619848	0.1	2.9	53.6	8.6	11.4	27.8	0.90	5.9	<-5	....	a	873.5	2.3	9.0×10^{-16}

(*cont.*)

Table A.1: *Chandra* source list

Source		Position				Extracted Counts							Characteristics				
Seq	CXOU J	R. A.	Decl.	Err	θ	$C_{\rm net}$	$\Delta C_{\rm net}$	$C'_{\rm bkg}$	$C_{\rm net,hard}$	PSF	PS	$P_{\rm B}$	Anom	Var	EffExp	$E_{\rm median}$	Photo $F_{\rm x}$
#		(deg)	(deg)	($''$)	($'$)						Frac				(ks)	(keV)	(ergs s^{-1} cm^{-2})
(1)	(2)	(3)	(4)	(5)	(6)	(7)	(8)	(9)	(10)	(11)	(12)	(13)	(14)	(15)	(16)	(17)	(18)
545	175117.41−293828.6	267.822570	−29.641303	0.2	3.8	17.4	7.3	27.6	9.8	0.90	2.2	-2.8	....	b	845.8	2.5	3.4×10^{-16}
546	175117.41−294033.6	267.822580	−29.676022	0.2	5.6	51.3	10.8	52.7	37.0	0.87	4.5	<-5	....	a	794.3	2.6	1.1×10^{-15}
547	175117.42−292811.8	267.822600	−29.469963	0.2	7.6	104.8	16.1	133.2	80.6	0.90	6.3	<-5	g...	...	701.0	3.0	3.1×10^{-15}
548	175117.43−293247.1	267.822650	−29.546427	0.2	3.5	13.7	5.9	15.3	4.7	0.90	2.1	-2.9	....	a	871.6	1.4	1.4×10^{-16}
549	175117.43−293323.7	267.822660	−29.556594	0.2	3.0	18.4	5.9	10.6	7.0	0.89	2.8	<-5	....	c	878.7	1.5	2.0×10^{-16}
550	175117.45−292939.6	267.822720	−29.494340	0.2	6.2	72.7	12.9	79.3	34.6	0.90	5.4	<-5	....	a	809.0	2.0	1.2×10^{-15}
551	175117.45−293936.7	267.822730	−29.660217	0.2	4.8	65.3	10.6	35.7	22.6	0.90	5.9	<-5	....	a	813.7	1.8	9.5×10^{-16}
552	175117.47−293007.3	267.822810	−29.502052	0.2	5.7	67.3	12.0	61.7	44.9	0.90	5.4	<-5	g...	...	810.3	3.3	1.9×10^{-15}
553	175117.51−293329.9	267.822960	−29.558314	0.2	3.0	9.7	5.0	10.3	5.7	0.89	1.7	-2.3	....	a	880.5	2.6	1.8×10^{-16}
554	175117.51−293438.5	267.822990	−29.577367	0.1	2.4	17.2	5.5	7.8	7.6	0.89	2.8	<-5	....	a	886.6	1.8	2.2×10^{-16}
555	175117.51−293822.1	267.823000	−29.639478	0.2	3.7	17.9	7.1	25.1	3.7	0.90	2.3	-3.1	....	b	843.3	1.6	2.1×10^{-16}
556	175117.52−293734.7	267.823030	−29.626322	0.1	3.1	54.4	9.0	17.6	19.4	0.90	5.7	<-5	....	a	873.2	1.6	6.3×10^{-16}
557	175117.56−294139.7	267.823170	−29.694388	0.2	6.7	86.6	15.0	118.4	73.8	0.90	5.6	<-5	....	b	794.2	3.7	1.0×10^{-14}
558	175117.56−292735.0	267.823180	−29.459739	0.2	8.1	371.3	22.9	125.7	200.0	0.90	15.9	<-5	g...	...	538.4	2.2	2.6×10^{-15}
559	175117.65−293621.6	267.823560	−29.606002	0.1	2.4	91.2	10.5	7.8	39.1	0.89	8.3	<-5	....	b	874.1	1.8	4.4×10^{-16}
560	175117.65−293130.8	267.823580	−29.525223	0.2	4.5	29.4	8.1	26.6	12.1	0.89	3.4	<-5	g...	...	833.2	1.8	1.2×10^{-15}
561	175117.69−293444.4	267.823720	−29.579014	0.1	2.3	16.5	5.4	7.5	5.4	0.90	2.8	<-5	....	a	885.9	1.7	2.0×10^{-16}
562	175117.70−293404.0	267.823750	−29.567791	0.2	2.6	10.4	4.8	7.6	2.3	0.89	1.9	-2.9	....	a	857.2	1.6	1.2×10^{-16}
563	175117.70−293726.9	267.823770	−29.624148	0.2	3.0	14.7	5.9	14.3	0.4	0.90	2.3	-3.3	....	a	875.3	1.5	1.6×10^{-16}
564	175117.73−293441.1	267.823910	−29.578095	0.1	2.3	34.7	7.0	7.3	9.7	0.90	4.6	<-5	....	c	884.0	1.8	4.6×10^{-16}
565	175117.74−293714.8	267.823930	−29.620793	0.1	2.9	26.1	6.6	10.9	8.1	0.90	3.6	<-5	....	a	877.8	1.7	3.2×10^{-16}
566	175117.80−293134.4	267.824180	−29.526248	0.2	4.4	26.4	7.8	25.6	15.8	0.90	3.2	<-5	g...	...	832.3	2.3	4.9×10^{-16}
567	175117.86−294301.6	267.824450	−29.717122	0.3	7.9	69.3	16.5	180.7	25.1	0.89	4.1	<-5	....	b	711.7	1.7	1.1×10^{-15}
568	175117.87−293415.6	267.824460	−29.571019	0.1	2.5	17.5	5.5	7.5	5.7	0.90	2.9	<-5	....	a	889.4	1.5	3.1×10^{-16}
569	175117.87−293158.5	267.824490	−29.532937	0.2	4.1	21.4	7.2	22.6	10.8	0.90	2.8	-4.2	g...	...	849.3	1.8	1.9×10^{-16}
570	175117.88−293038.5	267.824520	−29.510695	0.2	5.2	55.8	10.7	47.2	38.6	0.90	5.0	<-5	g...	...	818.9	2.8	1.3×10^{-15}
571	175117.89−293946.1	267.824580	−29.662807	0.2	4.9	16.8	8.0	38.2	0.5	0.90	2.0	-2.2	....	a	818.9	1.4	1.8×10^{-16}
572	175117.95−293356.4	267.824810	−29.565669	0.1	2.7	14.0	5.2	8.0	2.1	0.89	2.4	-4.3	g...	...	843.9	1.6	1.8×10^{-16}
573	175117.98−293214.0	267.824930	−29.537225	0.1	3.8	175.9	14.5	18.1	149.4	0.90	11.7	<-5	....	a	862.0	3.6	4.9×10^{-15}
574	175117.98−293716.3	267.824930	−29.621198	0.2	2.9	12.8	5.4	11.2	2.2	0.90	2.1	-3.1	....	a	877.6	1.4	1.3×10^{-16}
575	175118.00−293018.0	267.825020	−29.505026	0.2	5.5	29.5	9.7	53.5	2.0	0.90	2.9	-3.8	....	a	824.7	1.4	3.3×10^{-16}
576	175118.03−292758.5	267.825160	−29.466257	0.2	7.7	300.6	21.2	123.4	95.1	0.90	13.8	<-5	g...	...	587.6	1.6	6.3×10^{-15}
577	175118.11−293503.9	267.825500	−29.584433	0.2	2.2	9.3	4.5	6.7	4.4	0.90	1.8	-2.7	....	a	887.0	2.4	1.6×10^{-16}
578	175118.14−293523.8	267.825620	−29.589964	0.1	2.1	22.6	6.0	7.4	8.1	0.90	3.4	<-5	....	a	880.7	1.4	2.4×10^{-16}

(*cont.*)

Table A.1: *Chandra* source list

Source		Position				Extracted Counts							Characteristics				
Seq	CXOU J	R. A.	Decl.	Err	θ	$C_{\rm net}$	$\Delta C_{\rm net}$	$C'_{\rm bkg}$	$C_{\rm net,hard}$	PSF	PS	$P_{\rm B}$	Anom	Var	EffExp	$E_{\rm median}$	Photo $F_{\rm x}$
#		(deg)	(deg)	($''$)	($'$)						Frac				(ks)	(keV)	(ergs s^{-1} cm^{-2})
(1)	(2)	(3)	(4)	(5)	(6)	(7)	(8)	(9)	(10)	(11)	(12)	(13)	(14)	(15)	(16)	(17)	(18)
579	175118.16−293956.8	267.825690	−29.665793	0.1	5.0	305.4	19.1	38.6	187.9	0.89	15.6	<-5	....	a	818.5	2.4	5.9×10^{-15}
580	175118.18−293332.4	267.825780	−29.559023	0.1	2.8	70.2	9.5	9.8	13.2	0.89	7.0	<-5	....	c	881.9	1.3	6.9×10^{-16}
581	175118.20−293446.2	267.825870	−29.579516	0.1	2.2	10.8	4.8	7.2	4.4	0.90	2.0	-3.2	....	a	888.0	2.0	1.5×10^{-16}
582	175118.22−293348.5	267.825930	−29.563473	0.1	2.7	34.6	7.0	7.4	13.1	0.89	4.6	<-5	....	a	864.1	1.8	4.6×10^{-16}
583	175118.22−293547.9	267.825930	−29.596661	0.2	2.2	9.1	4.3	4.9	4.1	0.90	1.9	-3.1	g...	...	566.0	2.0	2.1×10^{-16}
584	175118.22−293753.4	267.825930	−29.631526	0.1	3.3	89.9	11.0	19.1	45.0	0.89	7.8	<-5	....	b	870.8	2.0	1.3×10^{-15}
585	175118.23−293832.2	267.825990	−29.642303	0.2	3.8	18.4	7.2	25.6	4.0	0.90	2.4	-3.1	....	a	852.6	1.2	1.6×10^{-16}
586	175118.25−293952.6	267.826080	−29.664627	0.1	4.9	76.4	10.1	14.6	9.5	0.71	7.2	<-5	....	b	818.9	1.3	9.8×10^{-16}
587	175118.29−292956.9	267.826240	−29.499139	0.3	5.8	23.3	10.0	64.7	4.4	0.90	2.2	-2.4	....	a	805.3	1.4	2.7×10^{-16}
588	175118.34−293624.3	267.826430	−29.606759	0.2	2.3	10.5	4.8	7.5	0.2	0.89	2.0	-3.0	....	a	882.4	1.5	1.1×10^{-16}
589	175118.36−293606.6	267.826520	−29.601854	0.2	2.2	9.5	4.4	5.5	3.1	0.90	1.9	-3.1	g...	...	699.4	1.8	1.6×10^{-16}
590	175118.36−294420.7	267.826530	−29.739104	0.4	9.1	33.1	14.4	153.9	0.0	0.85	2.2	-2.3	g...	...	510.0	1.2	5.7×10^{-16}
591	175118.41−293813.0	267.826720	−29.636950	0.1	3.5	25.9	7.5	22.1	3.1	0.90	3.2	<-5	....	b	866.6	1.5	2.9×10^{-16}
592	175118.42−293117.6	267.826750	−29.521561	0.2	4.6	63.4	10.1	27.6	52.4	0.89	6.0	<-5	g...	...	827.2	3.2	1.7×10^{-15}
593	175118.43−293943.6	267.826830	−29.662130	0.2	4.8	62.7	10.6	37.3	39.7	0.90	5.6	<-5	....	b	835.5	2.5	1.2×10^{-15}
594	175118.44−294123.1	267.826850	−29.689755	0.2	6.3	65.9	13.3	94.1	44.4	0.90	4.8	<-5	....	a	789.7	3.2	1.8×10^{-15}
595	175118.49−293321.5	267.827060	−29.555974	0.2	2.9	11.4	5.2	10.6	4.1	0.90	2.0	-2.8	....	b	871.8	1.5	1.3×10^{-16}
596	175118.49−293445.1	267.827080	−29.579205	0.1	2.2	14.1	5.1	6.9	1.6	0.90	2.5	-4.7	....	a	887.6	1.4	1.4×10^{-16}
597	175118.53−293732.7	267.827240	−29.625752	0.1	3.0	99.7	11.3	17.3	58.7	0.90	8.4	<-5	....	a	877.1	2.8	2.0×10^{-15}
598	175118.54−293412.8	267.827290	−29.570231	0.2	2.4	9.1	4.5	6.9	0.0	0.90	1.8	-2.6	....	a	885.1	1.3	8.6×10^{-17}
599	175118.57−293015.3	267.827390	−29.504261	0.2	5.5	53.3	10.9	52.7	19.8	0.90	4.7	<-5	....	c	809.0	1.7	7.4×10^{-16}
600	175118.57−293251.6	267.827400	−29.547683	0.2	3.2	13.9	5.8	14.1	7.0	0.90	2.2	-3.1	....	b	866.9	2.2	2.4×10^{-16}
601	175118.59−293006.4	267.827480	−29.501800	0.2	5.7	35.7	10.2	57.3	3.6	0.90	3.3	-4.9	g...	...	796.5	1.2	3.6×10^{-16}
602	175118.62−293027.1	267.827610	−29.507549	0.1	5.3	146.9	14.5	47.1	119.4	0.90	9.8	<-5	g...	...	818.1	3.0	3.7×10^{-15}
603	175118.63−293702.6	267.827660	−29.617398	0.1	2.6	14.0	5.4	10.0	3.5	0.90	2.3	-3.8	....	a	883.3	1.3	1.4×10^{-16}
604	175118.64−293515.4	267.827700	−29.587624	0.1	2.0	58.5	8.6	6.5	36.9	0.90	6.4	<-5	....	a	882.2	3.0	1.3×10^{-15}
605	175118.67−293317.3	267.827820	−29.554830	0.2	2.9	15.5	5.6	10.5	13.2	0.89	2.5	-4.3	....	a	872.6	3.6	4.3×10^{-16}
606	175118.68−293350.1	267.827840	−29.563941	0.1	2.6	27.8	6.4	7.2	15.3	0.89	4.0	<-5	g...	...	849.7	2.2	4.9×10^{-16}
607	175118.69−293641.7	267.827890	−29.611586	0.1	2.4	18.8	5.7	8.2	9.9	0.89	3.0	<-5	....	c	886.9	2.0	2.7×10^{-16}
608	175118.76−293645.4	267.828170	−29.612623	0.1	2.4	43.3	7.7	8.7	8.7	0.89	5.2	<-5	....	c	886.5	1.5	2.9×10^{-16}
609	175118.76−293339.4	267.828190	−29.560953	0.1	2.7	21.1	5.9	7.9	8.2	0.89	3.3	<-5	....	a	871.8	1.8	4.6×10^{-16}
610	175118.78−293811.3	267.828290	−29.636499	0.1	3.4	248.7	16.9	20.3	187.3	0.89	14.3	<-5	....	a	868.2	3.2	6.0×10^{-15}
611	175118.81−293739.7	267.828400	−29.627708	0.1	3.0	60.7	9.6	21.3	25.0	0.90	6.0	<-5	....	a	876.1	1.9	8.4×10^{-16}
612	175118.81−294404.9	267.828410	−29.734706	0.3	8.8	70.1	18.6	249.9	17.7	0.90	3.7	<-5	....	b	683.7	1.5	1.0×10^{-15}

(*cont.*)

Table A.1: *Chandra* source list

Source		Position				Extracted Counts							Characteristics				
Seq	CXOU J	R. A.	Decl.	Err	θ	$C_{\rm net}$	$\Delta C_{\rm net}$	$C'_{\rm bkg}$	$C_{\rm net,hard}$	PSF	PS	$P_{\rm B}$	Anom	Var	EffExp	$E_{\rm median}$	Photo $F_{\rm x}$
#		(deg)	(deg)	($''$)	($'$)						Frac				(ks)	(keV)	(ergs s^{-1} cm^{-2})
(1)	(2)	(3)	(4)	(5)	(6)	(7)	(8)	(9)	(10)	(11)	(12)	(13)	(14)	(15)	(16)	(17)	(18)
613	175118.83−293554.7	267.828470	−29.598549	0.2	2.1	9.7	4.3	4.3	4.5	0.90	2.0	-3.6	g...	...	493.2	1.9	2.3×10^{-16}
614	175118.91−293733.8	267.828810	−29.626070	0.1	2.9	50.3	8.8	17.7	21.8	0.90	5.4	<-5	....	a	877.5	1.7	6.3×10^{-16}
615	175118.91−293757.8	267.828820	−29.632733	0.2	3.2	13.3	6.2	18.7	3.1	0.89	2.0	-2.4	....	a	872.2	1.4	1.4×10^{-16}
616	175118.93−293547.2	267.828890	−29.596452	0.2	2.0	9.6	4.4	5.4	2.1	0.90	1.9	-3.2	g...	...	551.8	1.3	1.5×10^{-16}
617	175118.95−294105.9	267.828990	−29.684987	0.3	6.0	23.1	10.8	79.9	10.3	0.90	2.0	-2.1	....	a	805.5	1.7	3.1×10^{-16}
618	175119.01−294044.7	267.829240	−29.679089	0.2	5.7	29.4	10.4	65.6	5.4	0.90	2.7	-3.3	....	b	816.0	1.3	3.0×10^{-16}
619	175119.04−293613.7	267.829340	−29.603810	0.1	2.1	11.1	4.8	6.9	5.5	0.90	2.1	-3.4	....	b	852.8	2.0	1.7×10^{-16}
620	175119.06−293440.7	267.829440	−29.577992	0.1	2.1	12.5	4.9	6.5	4.8	0.90	2.3	-4.2	....	a	880.2	1.6	1.5×10^{-16}
621	175119.09−293345.3	267.829570	−29.562595	0.1	2.5	18.7	5.6	7.3	4.5	0.89	3.0	<-5	....	a	872.3	1.2	1.7×10^{-16}
622	175119.10−292956.3	267.829620	−29.498981	0.2	5.8	78.7	12.1	53.3	40.8	0.90	6.2	<-5	g...	...	687.7	2.3	1.9×10^{-15}
623	175119.13−293646.0	267.829720	−29.612804	0.1	2.4	33.9	7.0	8.1	10.1	0.89	4.5	<-5	....	a	887.2	1.6	3.9×10^{-16}
624	175119.14−293457.6	267.829760	−29.582672	0.1	2.0	9.5	4.5	6.5	3.6	0.90	1.9	-2.8	....	a	891.3	1.7	1.1×10^{-16}
625	175119.15−293551.5	267.829820	−29.597655	0.0	2.0	119.7	11.6	4.3	50.6	0.90	9.8	<-5	g...	...	512.9	1.7	2.5×10^{-15}
626	175119.17−293740.7	267.829880	−29.627976	0.0	3.0	365.9	20.2	20.1	255.9	0.90	17.7	<-5	....	b	876.5	3.2	8.3×10^{-16}
627	175119.17−293543.9	267.829910	−29.595533	0.1	2.0	61.2	8.7	5.8	14.3	0.90	6.6	<-5	g...	...	643.5	1.4	8.6×10^{-15}
628	175119.20−293411.5	267.830030	−29.569875	0.2	2.3	8.7	4.4	6.3	2.4	0.90	1.7	-2.6	g...	...	860.3	1.6	1.1×10^{-16}
629	175119.21−293801.2	267.830050	−29.633677	0.1	3.2	107.2	11.8	18.8	17.4	0.89	8.7	<-5	....	c	871.9	1.4	1.1×10^{-15}
630	175119.23−293322.2	267.830150	−29.556168	0.2	2.8	15.2	5.4	8.8	1.9	0.89	2.5	-4.6	g...	...	850.9	1.3	1.7×10^{-16}
631	175119.23−293917.4	267.830150	−29.654846	0.1	4.3	50.8	9.5	29.2	6.6	0.90	5.1	<-5	....	a	850.6	1.3	4.9×10^{-16}
632	175119.25−294246.3	267.830220	−29.712879	0.3	7.5	51.8	15.3	161.2	49.5	0.90	3.3	-4.4	....	a	704.3	4.0	1.9×10^{-15}
633	175119.31−293814.1	267.830470	−29.637252	0.1	3.4	26.0	7.6	23.0	13.4	0.90	3.2	<-5	....	a	869.0	2.0	5.2×10^{-16}
634	175119.31−293738.4	267.830480	−29.627342	0.1	2.9	44.8	8.5	18.2	14.4	0.87	5.0	<-5	....	c	877.2	1.5	3.8×10^{-16}
635	175119.34−293238.1	267.830620	−29.543929	0.1	3.3	35.4	7.5	13.6	0.0	0.90	4.4	<-5	g...	...	838.5	1.3	3.7×10^{-16}
636	175119.36−293317.8	267.830670	−29.554965	0.1	2.8	16.3	5.6	9.7	9.6	0.89	2.6	-4.8	g...	...	859.5	2.4	3.1×10^{-16}
637	175119.38−293711.1	267.830790	−29.619759	0.1	2.6	23.9	6.4	10.1	9.6	0.90	3.5	<-5	....	a	883.1	1.9	3.4×10^{-16}
638	175119.39−293624.3	267.830800	−29.606766	0.1	2.1	110.8	11.4	7.2	84.7	0.90	9.3	<-5	....	b	887.2	3.6	2.8×10^{-15}
639	175119.43−293608.4	267.830960	−29.602336	0.1	2.0	19.2	5.5	5.8	4.9	0.90	3.1	<-5	g...	...	756.6	1.6	2.2×10^{-16}
640	175119.43−293521.3	267.830990	−29.589276	0.1	1.9	11.9	4.8	6.1	7.7	0.90	2.2	-4.0	....	a	890.9	2.6	2.5×10^{-16}
641	175119.47−293659.4	267.831150	−29.616502	0.0	2.4	349.9	19.5	9.1	274.7	0.89	17.5	<-5	....	a	885.4	3.5	8.9×10^{-15}
642	175119.49−293734.3	267.831210	−29.626209	0.1	2.9	31.3	7.5	17.7	12.8	0.90	3.9	<-5	....	a	878.4	1.6	3.8×10^{-16}
643	175119.51−293118.0	267.831310	−29.521684	0.2	4.5	24.8	7.6	25.2	6.2	0.89	3.0	-4.9	g...	...	814.5	1.5	3.1×10^{-16}
644	175119.51−293935.8	267.831320	−29.659965	0.1	4.6	58.3	10.2	34.7	28.4	0.90	5.4	<-5	....	c	845.9	1.9	3.0×10^{-16}
645	175119.51−293256.6	267.831330	−29.549079	0.2	3.1	14.7	5.5	10.3	11.2	0.90	2.4	-4.0	g...	...	850.4	2.5	8.7×10^{-16}
646	175119.52−293127.8	267.831370	−29.524391	0.2	4.3	44.9	8.8	23.1	32.9	0.89	4.8	<-5	g...	...	824.4	3.0	1.1×10^{-15}

(*cont.*)

Table A.1: *Chandra* source list

Source		Position				Extracted Counts							Characteristics				
Seq	CXOU J	R. A.	Decl.	Err	θ	$C_{\rm net}$	$\Delta C_{\rm net}$	$C'_{\rm bkg}$	$C_{\rm net,hard}$	PSF	PS	$P_{\rm B}$	Anom	Var	EffExp	$E_{\rm median}$	Photo $F_{\rm x}$
#		(deg)	(deg)	($''$)	($'$)						Frac				(ks)	(keV)	(ergs s^{-1} cm^{-2})
(1)	(2)	(3)	(4)	(5)	(6)	(7)	(8)	(9)	(10)	(11)	(12)	(13)	(14)	(15)	(16)	(17)	(18)
647	175119.58−293952.9	267.831590	−29.664710	0.2	4.8	29.6	9.0	40.4	10.4	0.90	3.1	-4.7	....	b	837.9	1.1	2.0×10^{-16}
648	175119.58−293232.4	267.831620	−29.542358	0.2	3.4	21.4	6.5	13.6	0.0	0.90	3.1	<-5	g...	...	839.4	1.1	2.6×10^{-16}
649	175119.64−293051.2	267.831850	−29.514245	0.2	4.9	37.7	8.9	31.3	17.9	0.90	4.0	<-5	g...	...	751.3	2.0	6.8×10^{-16}
650	175119.66−293907.6	267.831920	−29.652136	0.2	4.1	18.5	7.2	25.5	5.5	0.89	2.4	-3.2	....	b	855.4	1.8	4.5×10^{-16}
651	175119.66−293142.9	267.831930	−29.528603	0.2	4.1	42.1	8.5	20.9	9.2	0.90	4.7	<-5	g...	...	827.4	1.3	2.6×10^{-16}
652	175119.69−293807.6	267.832060	−29.635457	0.1	3.3	22.1	7.0	19.9	6.8	0.89	2.9	-4.8	....	a	871.0	1.4	2.3×10^{-16}
653	175119.71−293249.8	267.832130	−29.547186	0.1	3.1	51.9	8.5	11.1	29.6	0.90	5.8	<-5	g...	...	843.9	2.6	1.1×10^{-15}
654	175119.72−293336.1	267.832190	−29.560048	0.1	2.5	18.7	5.7	8.3	8.0	0.89	3.0	<-5	g...	...	856.6	1.8	2.7×10^{-16}
655	175119.73−293352.8	267.832210	−29.564692	0.1	2.4	37.0	7.1	6.0	22.8	0.89	4.8	<-5	g...	...	835.4	2.5	7.5×10^{-16}
656	175119.75−293506.2	267.832300	−29.585069	0.1	1.8	15.5	5.2	6.5	4.4	0.90	2.7	<-5	....	c	881.8	1.6	1.9×10^{-16}
657	175119.79−293328.8	267.832490	−29.558027	0.1	2.6	64.5	9.0	7.5	14.4	0.89	6.8	<-5	g...	...	858.2	1.4	7.3×10^{-16}
658	175119.81−293240.0	267.832560	−29.544462	0.1	3.3	45.0	8.2	14.0	16.6	0.90	5.1	<-5	g...	...	849.1	1.7	6.0×10^{-16}
659	175119.81−294024.1	267.832580	−29.673387	0.2	5.3	32.0	9.9	54.0	17.8	0.90	3.1	-4.3	....	b	822.0	2.2	5.5×10^{-16}
660	175119.91−293321.3	267.832980	−29.555932	0.1	2.7	76.0	9.7	8.0	50.1	0.89	7.4	<-5	g...	...	854.8	2.6	1.6×10^{-15}
661	175119.94−294341.1	267.833120	−29.728085	0.2	8.4	90.9	14.7	106.1	21.8	0.70	6.0	<-5	....	c	691.1	1.3	1.4×10^{-15}
662	175119.95−293458.2	267.833160	−29.582860	0.0	1.8	172.8	13.9	6.2	94.8	0.90	12.0	<-5	g...	...	876.2	2.3	3.0×10^{-15}
663	175120.01−292841.9	267.833410	−29.478322	0.2	6.9	57.6	11.3	57.4	18.5	0.78	4.9	<-5	g...	...	730.2	1.4	8.4×10^{-16}
664	175120.01−293732.2	267.833410	−29.625615	0.1	2.8	20.8	6.5	15.2	0.0	0.90	2.9	<-5	....	a	879.6	1.1	1.7×10^{-16}
665	175120.08−294308.7	267.833680	−29.719096	0.2	7.8	139.8	18.4	176.2	146.7	0.90	7.4	<-5	....	a	705.6	4.8	6.3×10^{-15}
666	175120.10−293223.7	267.833780	−29.539930	0.2	3.4	22.9	6.6	14.1	0.0	0.90	3.2	<-5	g...	...	839.6	1.0	2.0×10^{-16}
667	175120.11−293250.8	267.833820	−29.547454	0.1	3.1	46.2	8.1	11.8	21.6	0.90	5.3	<-5	g...	...	857.9	1.7	6.2×10^{-16}
668	175120.16−293601.4	267.834000	−29.600393	0.2	1.8	8.6	4.3	5.4	0.0	0.90	1.8	-2.8	g...	...	622.0	1.5	3.8×10^{-16}
669	175120.16−293031.9	267.834020	−29.508863	0.3	5.2	15.4	7.4	30.6	7.5	0.90	1.9	-2.2	g...	...	589.5	2.0	1.3×10^{-16}
670	175120.19−293513.5	267.834140	−29.587097	0.1	1.7	9.8	4.4	5.2	6.8	0.90	2.0	-3.3	g...	...	872.9	2.4	1.8×10^{-16}
671	175120.22−293919.9	267.834280	−29.655532	0.1	4.3	89.8	11.3	26.2	46.4	0.89	7.6	<-5	....	a	852.5	2.1	1.4×10^{-15}
672	175120.25−293659.4	267.834390	−29.616509	0.1	2.3	15.8	5.4	8.2	4.2	0.89	2.6	<-5	....	a	886.9	1.8	2.1×10^{-16}
673	175120.25−293946.2	267.834400	−29.662835	0.2	4.7	23.4	8.4	37.6	1.3	0.90	2.6	-3.5	....	a	845.0	1.0	1.7×10^{-16}
674	175120.28−293453.5	267.834530	−29.581534	0.1	1.8	19.9	5.6	6.1	2.0	0.90	3.2	<-5	g...	...	874.6	1.0	1.5×10^{-16}
675	175120.29−292825.2	267.834570	−29.473667	0.2	7.2	78.1	14.7	119.9	45.4	0.90	5.1	<-5	....	c	773.7	2.7	1.8×10^{-15}
676	175120.30−293218.9	267.834590	−29.538603	0.1	3.5	72.9	9.9	15.1	26.8	0.90	7.0	<-5	g...	...	827.6	1.6	9.7×10^{-16}
677	175120.33−293503.4	267.834740	−29.584304	0.1	1.7	17.6	5.4	6.4	18.8	0.91	2.9	<-5	....	a	879.3	5.1	6.7×10^{-16}
678	175120.34−293320.4	267.834770	−29.555694	0.2	2.6	8.0	4.5	8.0	3.4	0.89	1.6	-2.0	g...	...	844.8	1.6	1.1×10^{-16}
679	175120.41−293812.0	267.835050	−29.636667	0.1	3.2	29.1	7.6	20.9	2.8	0.89	3.6	<-5	....	a	870.7	1.2	2.6×10^{-16}
680	175120.43−294156.2	267.835150	−29.698964	0.2	6.7	94.3	12.4	46.7	60.1	0.67	7.3	<-5	....	a	793.8	2.5	2.7×10^{-15}

(*cont.*)

Table A.1: *Chandra* source list

Source		Position				Extracted Counts							Characteristics				
Seq	CXOU J	R. A.	Decl.	Err	θ	$C_{\rm net}$	$\Delta C_{\rm net}$	$C'_{\rm bkg}$	$C_{\rm net,hard}$	PSF	PS	$P_{\rm B}$	Anom	Var	EffExp	$E_{\rm median}$	Photo $F_{\rm x}$
#		(deg)	(deg)	($''$)	($'$)						Frac				(ks)	(keV)	(ergs s^{-1} cm^{-2})
(1)	(2)	(3)	(4)	(5)	(6)	(7)	(8)	(9)	(10)	(11)	(12)	(13)	(14)	(15)	(16)	(17)	(18)
681	175120.43−294343.5	267.835150	−29.728752	0.2	8.4	111.1	13.8	62.9	32.6	0.58	7.8	<-5	....	a	694.6	1.7	2.7×10^{-15}
682	175120.47−293727.7	267.835330	−29.624386	0.1	2.6	80.9	10.2	12.1	15.0	0.90	7.6	<-5	....	b	881.2	1.3	7.7×10^{-16}
683	175120.49−292942.8	267.835400	−29.495223	0.3	5.9	31.4	10.0	56.6	11.9	0.90	3.0	-4.0	g...	...	683.0	1.5	4.6×10^{-16}
684	175120.51−293906.7	267.835460	−29.651877	0.2	4.0	17.0	6.9	23.0	12.2	0.90	2.3	-3.0	....	c	856.4	2.7	8.9×10^{-16}
685	175120.51−293840.6	267.835480	−29.644623	0.1	3.7	63.6	9.8	22.4	29.4	0.90	6.1	<-5	....	b	863.5	1.9	3.5×10^{-16}
686	175120.55−293331.7	267.835630	−29.558810	0.1	2.5	91.4	10.5	7.6	68.6	0.89	8.3	<-5	g...	...	848.6	2.6	2.0×10^{-15}
687	175120.61−293025.6	267.835890	−29.507130	0.3	5.2	25.4	8.1	30.6	9.8	0.90	3.0	-4.4	g...	...	597.9	1.7	4.9×10^{-16}
688	175120.62−293358.7	267.835930	−29.566332	0.2	2.2	9.9	4.5	6.1	2.6	0.90	1.9	-3.1	g...	...	809.5	1.7	8.8×10^{-16}
689	175120.62−293159.6	267.835950	−29.533226	0.1	3.8	45.8	8.4	16.2	22.0	0.90	5.1	<-5	g...	...	754.8	2.1	1.4×10^{-16}
690	175120.63−293306.1	267.835980	−29.551700	0.2	2.8	12.7	5.2	9.3	4.1	0.89	2.2	-3.5	g...	...	852.9	1.7	1.8×10^{-16}
691	175120.66−293259.7	267.836090	−29.549941	0.1	2.9	27.6	6.6	9.4	8.0	0.90	3.9	<-5	g...	...	844.8	1.4	3.2×10^{-16}
692	175120.73−293413.6	267.836400	−29.570467	0.2	2.0	7.2	4.2	5.8	2.6	0.90	1.5	-2.1	g...	...	842.0	1.1	6.6×10^{-17}
693	175120.74−294152.0	267.836430	−29.697805	0.2	6.7	26.6	6.9	14.4	18.0	0.45	3.6	<-5	....	b	796.1	2.4	1.1×10^{-15}
694	175120.75−292856.0	267.836490	−29.482243	0.3	6.6	49.8	12.8	98.2	22.7	0.90	3.7	<-5	....	b	793.5	1.9	7.5×10^{-16}
695	175120.75−293739.2	267.836490	−29.627560	0.1	2.7	108.1	11.7	16.9	47.2	0.90	8.8	<-5	....	a	879.0	1.9	1.5×10^{-15}
696	175120.76−293319.8	267.836500	−29.555511	0.1	2.6	15.4	5.4	8.6	9.3	0.89	2.6	-4.8	g...	...	861.0	2.6	3.2×10^{-16}
697	175120.78−293231.7	267.836590	−29.542146	0.1	3.3	21.5	6.5	13.5	5.9	0.90	3.1	<-5	g...	...	803.2	1.5	2.7×10^{-16}
698	175120.78−294106.4	267.836590	−29.685119	0.2	5.9	60.9	12.4	79.1	8.1	0.90	4.7	<-5	....	a	817.2	1.4	3.7×10^{-16}
699	175120.78−293516.9	267.836620	−29.588054	0.1	1.6	18.4	5.4	5.6	13.7	0.90	3.1	<-5	g...	...	867.1	2.6	6.8×10^{-16}
700	175120.80−292845.7	267.836690	−29.479363	0.2	6.8	105.2	14.4	85.8	66.2	0.85	7.0	<-5	....	c	798.5	2.4	2.2×10^{-15}
701	175120.80−293325.3	267.836690	−29.557037	0.1	2.5	15.2	5.3	7.8	6.3	0.89	2.6	-4.9	g...	...	863.4	1.9	2.3×10^{-16}
702	175120.84−293048.3	267.836850	−29.513419	0.3	4.9	15.0	6.5	20.0	4.4	0.86	2.1	-2.8	g...	...	594.2	1.4	2.6×10^{-16}
703	175120.85−294405.7	267.836900	−29.734939	0.2	8.7	160.2	20.6	234.8	130.4	0.90	7.6	<-5	....	a	669.5	3.1	4.8×10^{-15}
704	175120.89−293450.0	267.837050	−29.580568	0.1	1.6	9.3	4.4	5.7	0.0	0.90	1.9	-3.0	g...	...	850.5	1.0	7.7×10^{-17}
705	175120.91−294248.1	267.837160	−29.713384	0.2	7.5	116.1	17.1	154.9	72.7	0.90	6.6	<-5	....	a	718.3	2.6	2.8×10^{-15}
706	175120.93−293318.0	267.837240	−29.555008	0.1	2.6	37.5	7.3	8.5	19.2	0.89	4.8	<-5	g...	...	852.7	2.1	6.2×10^{-16}
707	175120.94−293855.1	267.837270	−29.648645	0.2	3.8	23.0	7.3	22.0	8.8	0.90	2.9	-4.8	....	a	860.0	1.7	3.0×10^{-16}
708	175121.09−292919.4	267.837890	−29.488725	0.2	6.3	52.1	12.1	79.9	19.1	0.90	4.1	<-5	....	b	806.1	1.5	6.4×10^{-16}
709	175121.12−293436.6	267.838040	−29.576848	0.1	1.7	26.0	6.2	6.0	14.9	0.90	3.9	<-5	g...	...	855.7	2.3	4.8×10^{-16}
710	175121.12−293728.1	267.838040	−29.624499	0.2	2.6	9.6	5.0	10.4	2.2	0.89	1.7	-2.2	....	a	864.4	1.2	9.1×10^{-17}
711	175121.15−293415.2	267.838140	−29.570903	0.1	1.9	10.2	4.5	5.8	0.0	0.90	2.0	-3.4	g...	...	841.8	1.3	1.1×10^{-16}
712	175121.16−293706.6	267.838170	−29.618524	0.1	2.3	13.3	5.1	7.7	5.6	0.89	2.3	-4.1	....	a	871.4	1.6	1.6×10^{-16}
713	175121.19−293442.4	267.838330	−29.578455	0.1	1.6	17.6	5.4	6.4	10.9	0.90	2.9	<-5	g...	...	859.6	2.3	3.2×10^{-16}
714	175121.20−293649.8	267.838370	−29.613836	0.1	2.1	9.8	4.7	7.2	3.6	0.90	1.9	-2.8	g...	...	868.8	1.8	1.4×10^{-16}

(*cont.*)

Table A.1: *Chandra* source list

Source		Position				Extracted Counts							Characteristics				
Seq	CXOU J	R. A.	Decl.	Err	θ	$C_{\rm net}$	$\Delta C_{\rm net}$	$C'_{\rm bkg}$	$C_{\rm net,hard}$	PSF	PS	$P_{\rm B}$	Anom	Var	EffExp	$E_{\rm median}$	Photo $F_{\rm x}$
#		(deg)	(deg)	($''$)	($'$)						Frac				(ks)	(keV)	(ergs s^{-1} cm^{-2})
(1)	(2)	(3)	(4)	(5)	(6)	(7)	(8)	(9)	(10)	(11)	(12)	(13)	(14)	(15)	(16)	(17)	(18)
715	175121.20−294147.3	267.838370	−29.696483	0.2	6.6	68.3	13.8	105.7	18.4	0.88	4.8	<-5	....	a	798.8	1.5	8.3×10^{-16}
716	175121.21−293559.5	267.838380	−29.599867	0.1	1.6	10.6	4.4	4.4	4.6	0.90	2.1	-4.1	g...	...	598.6	1.6	1.9×10^{-16}
717	175121.25−293011.4	267.838580	−29.503184	0.2	5.4	26.8	9.1	45.2	11.3	0.90	2.8	-3.7	g...	...	764.3	1.9	4.5×10^{-16}
718	175121.27−293717.0	267.838630	−29.621401	0.1	2.4	13.4	5.2	8.6	3.1	0.89	2.3	-3.9	....	b	867.4	1.7	1.7×10^{-16}
719	175121.28−293512.4	267.838670	−29.586787	0.1	1.5	24.9	6.1	6.1	4.8	0.90	3.7	<-5	g...	...	851.4	1.3	2.7×10^{-16}
720	175121.30−293429.4	267.838750	−29.574847	0.1	1.7	14.8	5.1	6.2	8.2	0.90	2.6	<-5	g...	...	848.2	2.4	2.9×10^{-16}
721	175121.30−293916.9	267.838770	−29.654715	0.2	4.1	19.4	7.3	25.6	2.8	0.89	2.5	-3.4	....	a	854.1	1.5	2.2×10^{-16}
722	175121.32−292937.0	267.838870	−29.493615	0.3	6.0	30.0	10.6	69.0	0.0	0.89	2.7	-3.3	....	b	813.0	1.3	3.1×10^{-16}
723	175121.32−293049.9	267.838870	−29.513874	0.2	4.8	30.2	7.8	21.8	8.4	0.86	3.6	<-5	g...	...	678.8	1.4	4.1×10^{-16}
724	175121.35−294052.6	267.838970	−29.681288	0.2	5.7	42.3	11.1	68.7	18.5	0.90	3.6	<-5	....	a	824.3	1.8	5.9×10^{-16}
725	175121.38−292830.8	267.839100	−29.475246	0.2	7.0	263.6	19.9	110.4	226.5	0.90	12.9	<-5	....	c	762.6	3.6	8.1×10^{-15}
726	175121.40−294016.9	267.839180	−29.671380	0.1	5.1	94.2	12.4	46.8	18.8	0.90	7.3	<-5	....	b	836.3	1.3	9.4×10^{-16}
727	175121.41−293618.7	267.839210	−29.605209	0.1	1.7	20.9	5.7	6.1	1.2	0.90	3.3	<-5	g...	...	841.0	1.3	2.2×10^{-16}
728	175121.46−292930.9	267.839430	−29.491923	0.3	6.0	31.7	10.9	73.3	7.2	0.89	2.8	-3.4	....	a	812.1	1.5	3.9×10^{-16}
729	175121.49−293407.5	267.839550	−29.568754	0.1	1.9	13.6	4.9	5.4	3.8	0.90	2.5	<-5	g...	...	818.7	1.4	1.6×10^{-16}
730	175121.50−293546.3	267.839600	−29.596217	0.1	1.5	45.5	7.5	3.5	37.6	0.90	5.6	<-5	g...	...	484.6	3.2	2.0×10^{-15}
731	175121.54−293822.5	267.839790	−29.639588	0.1	3.3	73.5	10.3	21.5	35.2	0.89	6.8	<-5	....	a	864.3	2.0	1.1×10^{-15}
732	175121.59−293151.7	267.839990	−29.531037	0.2	3.8	18.2	6.3	14.8	7.9	0.90	2.7	-4.4	g...	...	591.6	1.7	3.9×10^{-16}
733	175121.69−293856.4	267.840380	−29.649016	0.2	3.8	23.7	7.3	22.3	8.2	0.90	3.0	-5.0	....	b	860.1	1.8	3.3×10^{-16}
734	175121.70−293911.6	267.840420	−29.653237	0.2	4.0	16.1	7.0	24.9	1.5	0.90	2.1	-2.6	....	a	855.9	1.4	1.7×10^{-16}
735	175121.74−293501.8	267.840590	−29.583843	0.0	1.4	256.1	16.7	5.9	189.9	0.90	14.9	<-5	g...	...	847.7	3.0	6.3×10^{-15}
736	175121.74−293722.6	267.840610	−29.622965	0.1	2.4	12.9	5.2	9.1	3.2	0.89	2.2	-3.6	g...	...	861.9	1.6	1.7×10^{-16}
737	175121.75−293549.9	267.840660	−29.597202	0.1	1.5	15.6	4.9	3.4	2.6	0.90	2.9	<-5	g...	...	487.3	1.1	2.5×10^{-16}
738	175121.79−293551.7	267.840830	−29.597707	0.1	1.4	8.4	4.0	3.6	2.6	0.90	1.8	-3.3	g...	...	511.5	1.3	1.4×10^{-16}
739	175121.80−292818.8	267.840850	−29.471889	0.2	7.2	160.9	17.0	109.1	130.9	0.90	9.2	<-5	g...	...	683.8	3.2	5.1×10^{-15}
740	175121.80−293018.8	267.840870	−29.505229	0.1	5.3	144.8	14.3	43.2	121.7	0.90	9.8	<-5	....	b	823.0	3.6	4.3×10^{-15}
741	175121.80−293246.6	267.840870	−29.546291	0.1	3.0	32.9	6.9	8.1	5.3	0.90	4.4	<-5	g...	...	643.2	1.3	4.5×10^{-16}
742	175121.83−293315.6	267.840990	−29.554342	0.2	2.5	12.8	5.1	8.2	6.4	0.90	2.3	-3.8	g...	...	725.6	2.0	2.4×10^{-16}
743	175121.84−293333.5	267.841010	−29.559318	0.1	2.3	12.1	4.9	6.9	3.9	0.90	2.2	-3.8	g...	...	790.4	1.9	2.0×10^{-16}
744	175121.87−293751.6	267.841140	−29.631008	0.1	2.8	18.0	6.7	20.0	6.9	0.90	2.5	-3.5	g...	...	853.1	1.9	2.7×10^{-16}
745	175121.88−293437.4	267.841180	−29.577057	0.1	1.5	29.1	6.4	4.9	14.6	0.90	4.2	<-5	g...	...	841.1	2.0	4.7×10^{-16}
746	175121.89−293917.2	267.841210	−29.654797	0.2	4.1	40.7	8.7	25.3	6.0	0.90	4.4	<-5	....	c	854.4	1.4	4.2×10^{-16}
747	175121.91−294122.7	267.841320	−29.689659	0.2	6.1	56.1	12.8	91.9	29.5	0.90	4.2	<-5	....	a	814.1	2.2	9.9×10^{-16}
748	175121.92−293820.6	267.841360	−29.639062	0.0	3.2	284.9	18.0	20.1	180.6	0.90	15.4	<-5	g...	...	846.5	2.6	6.0×10^{-15}

(*cont.*)

Table A.1: *Chandra* source list

Source		Position				Extracted Counts							Characteristics				
Seq	CXOU J	R. A.	Decl.	Err	θ	$C_{\rm net}$	$\Delta C_{\rm net}$	$C'_{\rm bkg}$	$C_{\rm net,hard}$	PSF	PS	$P_{\rm B}$	Anom	Var	EffExp	$E_{\rm median}$	Photo $F_{\rm x}$
#		(deg)	(deg)	($''$)	($'$)						Frac				(ks)	(keV)	(ergs s^{-1} cm^{-2})
(1)	(2)	(3)	(4)	(5)	(6)	(7)	(8)	(9)	(10)	(11)	(12)	(13)	(14)	(15)	(16)	(17)	(18)
749	175121.95−293834.6	267.841470	−29.642954	0.1	3.4	28.8	7.5	19.2	5.3	0.89	3.6	<-5	g...	...	844.7	1.2	2.1×10^{-16}
750	175121.95−293351.2	267.841500	−29.564229	0.1	2.1	10.0	4.7	7.0	5.6	0.90	1.9	-2.9	g...	...	794.0	2.4	2.9×10^{-16}
751	175121.96−293707.7	267.841510	−29.618825	0.1	2.2	19.1	5.6	6.9	13.8	0.90	3.1	<-5	g...	...	829.4	2.4	4.0×10^{-16}
752	175121.96−293712.0	267.841520	−29.620013	0.1	2.2	13.5	5.1	7.5	0.5	0.89	2.4	-4.2	g...	...	830.8	1.2	1.4×10^{-16}
753	175122.02−293530.7	267.841770	−29.591882	0.1	1.4	8.4	4.1	4.6	0.6	0.90	1.8	-2.9	g...	...	716.9	1.2	1.0×10^{-16}
754	175122.05−293817.1	267.841880	−29.638109	0.1	3.2	26.8	7.2	17.2	9.5	0.88	3.5	<-5	g...	...	845.6	1.5	3.3×10^{-16}
755	175122.07−293413.6	267.841970	−29.570448	0.2	1.8	7.7	4.1	5.3	5.2	0.90	1.6	-2.4	g...	...	788.7	2.2	1.5×10^{-16}
756	175122.08−293344.2	267.842020	−29.562299	0.2	2.1	9.4	4.5	6.6	1.6	0.90	1.8	-2.8	g...	...	746.0	1.1	9.6×10^{-17}
757	175122.08−293735.9	267.842040	−29.626650	0.2	2.6	10.1	5.2	11.9	2.3	0.90	1.7	-2.2	g...	...	848.5	1.2	1.0×10^{-16}
758	175122.09−293943.0	267.842080	−29.661971	0.2	4.5	22.3	7.9	30.7	10.7	0.90	2.7	-3.7	....	a	847.0	2.0	3.5×10^{-16}
759	175122.10−293454.2	267.842120	−29.581726	0.1	1.4	13.0	4.9	6.0	8.0	0.90	2.4	-4.6	g...	...	847.6	2.3	2.4×10^{-16}
760	175122.10−293539.1	267.842120	−29.594205	0.1	1.4	11.3	4.4	3.7	3.5	0.90	2.3	-4.9	g...	...	588.2	1.4	1.8×10^{-16}
761	175122.11−293739.6	267.842150	−29.627694	0.1	2.6	20.1	6.4	13.9	8.2	0.90	2.9	<-5	g...	...	849.7	1.7	2.9×10^{-16}
762	175122.12−294146.8	267.842180	−29.696355	0.2	6.5	41.0	13.0	111.0	8.7	0.89	3.0	-3.8	....	a	805.6	1.8	5.9×10^{-16}
763	175122.16−293457.6	267.842370	−29.582684	0.1	1.4	18.4	5.4	5.6	6.2	0.90	3.1	<-5	g...	...	852.0	1.6	2.4×10^{-16}
764	175122.18−293819.4	267.842430	−29.638741	0.1	3.2	48.8	8.7	17.2	2.6	0.88	5.3	<-5	g...	...	849.3	1.3	5.0×10^{-16}
765	175122.19−293617.0	267.842470	−29.604735	0.1	1.6	22.5	5.8	5.5	8.0	0.90	3.5	<-5	g...	...	827.5	1.8	2.5×10^{-16}
766	175122.19−293427.8	267.842480	−29.574409	0.1	1.6	18.4	5.4	5.6	6.4	0.90	3.1	<-5	g...	...	820.8	1.7	3.3×10^{-16}
767	175122.23−293334.6	267.842660	−29.559619	0.2	2.2	7.2	4.2	5.8	1.2	0.90	1.5	-2.1	g...	...	686.3	1.4	1.0×10^{-16}
768	175122.32−293244.0	267.843040	−29.545578	0.1	2.9	21.9	6.0	8.1	7.5	0.90	3.3	<-5	g...	...	611.3	1.7	4.2×10^{-16}
769	175122.33−293609.4	267.843070	−29.602637	0.1	1.5	35.6	6.9	5.4	22.3	0.90	4.8	<-5	g...	...	785.9	3.6	1.5×10^{-16}
770	175122.33−293429.3	267.843080	−29.574833	0.1	1.5	13.6	4.9	5.4	1.5	0.90	2.5	<-5	g...	...	802.7	1.2	1.2×10^{-15}
771	175122.37−293601.7	267.843220	−29.600492	0.1	1.4	45.6	7.7	5.4	18.2	0.90	5.6	<-5	g...	...	693.1	1.8	8.0×10^{-16}
772	175122.40−293744.2	267.843360	−29.628951	0.1	2.6	33.4	7.5	14.6	5.6	0.90	4.2	<-5	g...	...	818.0	1.3	3.8×10^{-16}
773	175122.49−293333.2	267.843710	−29.559230	0.2	2.2	11.4	4.7	5.6	6.2	0.90	2.2	-4.0	g...	...	644.8	2.0	2.4×10^{-16}
774	175122.51−293425.2	267.843820	−29.573681	0.1	1.6	14.4	5.0	5.6	2.2	0.90	2.6	<-5	g...	...	781.3	1.5	1.8×10^{-16}
775	175122.52−292757.6	267.843850	−29.466000	0.3	7.5	70.0	14.4	118.0	45.2	0.90	4.7	<-5	g...	...	629.0	3.1	2.4×10^{-15}
776	175122.52−293405.3	267.843860	−29.568161	0.1	1.9	12.9	4.8	5.1	0.4	0.90	2.4	<-5	g...	...	682.6	1.0	1.3×10^{-16}
777	175122.54−294116.0	267.843950	−29.687792	0.2	6.0	58.4	12.6	85.6	7.5	0.90	4.4	<-5	....	a	816.8	1.1	4.9×10^{-16}
778	175122.55−293536.9	267.843960	−29.593595	0.1	1.3	8.4	4.0	3.6	2.6	0.90	1.8	-3.3	g...	...	615.1	1.3	1.2×10^{-16}
779	175122.56−293019.1	267.844010	−29.505311	0.2	5.2	33.8	9.1	39.2	29.7	0.90	3.5	<-5	g...	...	738.8	3.1	9.3×10^{-16}
780	175122.60−293429.2	267.844170	−29.574799	0.0	1.5	87.5	10.2	5.5	63.4	0.90	8.2	<-5	g...	...	775.4	2.9	2.2×10^{-15}
781	175122.64−293516.6	267.844360	−29.587957	0.1	1.2	10.4	4.1	2.6	7.0	0.79	2.2	<-5	g...	...	862.2	2.6	2.4×10^{-16}
782	175122.64−294254.8	267.844370	−29.715239	0.2	7.5	163.4	18.7	160.6	124.0	0.90	8.5	<-5	....	a	723.0	3.1	4.7×10^{-15}

(*cont.*)

Table A.1: *Chandra* source list

Source		Position				Extracted Counts							Characteristics				
Seq	CXOU J	R. A.	Decl.	Err	θ	$C_{\rm net}$	$\Delta C_{\rm net}$	$C'_{\rm bkg}$	$C_{\rm net,hard}$	PSF	PS	$P_{\rm B}$	Anom	Var	EffExp	$E_{\rm median}$	Photo $F_{\rm x}$
#		(deg)	(deg)	($''$)	($'$)						Frac				(ks)	(keV)	(ergs s^{-1} cm^{-2})
(1)	(2)	(3)	(4)	(5)	(6)	(7)	(8)	(9)	(10)	(11)	(12)	(13)	(14)	(15)	(16)	(17)	(18)
783	175122.66−293329.2	267.844440	−29.558125	0.2	2.3	7.3	4.2	5.7	2.3	0.89	1.5	-2.2	g...	...	618.4	1.4	1.1×10^{-16}
784	175122.69−293416.8	267.844550	−29.571339	0.1	1.7	9.8	4.4	5.2	0.3	0.90	2.0	-3.3	g...	...	700.2	1.1	1.0×10^{-16}
785	175122.70−293517.7	267.844610	−29.588256	0.1	1.2	24.5	5.9	4.5	22.2	0.87	3.8	<-5	g...	...	844.5	4.5	9.0×10^{-16}
786	175122.72−294018.8	267.844670	−29.671916	0.2	5.0	61.1	10.8	43.9	20.0	0.89	5.4	<-5	....	b	829.4	1.6	7.7×10^{-16}
787	175122.76−293002.6	267.844840	−29.500747	0.2	5.4	33.9	9.4	44.1	16.6	0.90	3.4	<-5	g...	...	677.0	2.0	6.8×10^{-16}
788	175122.76−293436.3	267.844840	−29.576769	0.0	1.4	224.8	15.7	5.2	181.3	0.90	13.9	<-5	g...	...	756.6	3.7	7.4×10^{-15}
789	175122.78−293704.3	267.844950	−29.617882	0.1	2.0	19.3	5.6	6.7	5.9	0.91	3.1	<-5	g...	...	837.0	1.8	2.8×10^{-16}
790	175122.83−292848.5	267.845130	−29.480139	0.2	6.6	93.8	13.8	81.2	62.8	0.90	6.5	<-5	g...	...	632.0	2.6	2.7×10^{-15}
791	175122.85−293202.5	267.845220	−29.534048	0.2	3.5	24.0	6.9	16.0	6.5	0.90	3.2	<-5	g...	...	779.9	1.1	2.3×10^{-16}
792	175122.85−293514.5	267.845220	−29.587380	0.1	1.2	53.1	8.1	4.9	5.1	0.90	6.1	<-5	g...	...	808.1	1.3	5.9×10^{-16}
793	175122.93−294010.1	267.845550	−29.669474	0.2	4.9	21.3	8.4	39.7	8.1	0.89	2.4	-2.9	....	a	825.5	1.4	2.3×10^{-16}
794	175122.94−293646.3	267.845600	−29.612864	0.1	1.8	12.0	4.9	7.0	1.7	0.90	2.2	-3.8	g...	...	821.3	1.2	1.2×10^{-16}
795	175122.99−293846.2	267.845830	−29.646173	0.2	3.5	28.4	7.3	17.6	7.1	0.90	3.6	<-5	g...	...	833.0	1.5	3.4×10^{-16}
796	175123.05−293404.4	267.846050	−29.567903	0.2	1.8	8.5	4.1	4.5	4.9	0.90	1.8	-3.0	g...	...	593.7	2.9	2.8×10^{-16}
797	175123.06−293735.9	267.846090	−29.626657	0.1	2.5	12.5	5.2	9.5	8.4	0.89	2.2	-3.3	g...	...	836.1	3.0	3.1×10^{-16}
798	175123.07−293127.5	267.846150	−29.524325	0.1	4.0	82.8	10.7	20.2	53.9	0.90	7.4	<-5	g...	...	753.9	2.4	1.7×10^{-15}
799	175123.09−293943.1	267.846210	−29.661985	0.1	4.4	63.0	10.1	29.0	55.2	0.90	5.9	<-5	g...	...	816.5	3.3	1.7×10^{-15}
800	175123.11−294320.6	267.846300	−29.722390	0.2	7.9	148.1	19.0	188.9	38.1	0.90	7.6	<-5	....	b	714.1	1.4	1.9×10^{-15}
801	175123.14−293723.6	267.846430	−29.623225	0.2	2.3	8.1	4.5	7.9	1.5	0.89	1.6	-2.1	g...	...	829.5	1.2	8.1×10^{-17}
802	175123.16−293705.7	267.846510	−29.618259	0.1	2.0	11.9	4.9	7.1	4.5	0.91	2.2	-3.7	g...	...	796.6	1.8	1.9×10^{-16}
803	175123.17−294214.6	267.846550	−29.704064	0.2	6.9	47.7	14.1	133.3	15.4	0.90	3.3	-4.5	....	a	779.2	1.7	2.3×10^{-16}
804	175123.17−293526.4	267.846560	−29.590671	0.1	1.1	20.2	5.5	4.8	2.5	0.90	3.3	<-5	g...	...	715.1	1.2	7.0×10^{-16}
805	175123.19−293047.5	267.846650	−29.513202	0.2	4.7	19.3	7.3	25.7	2.7	0.89	2.5	-3.3	g...	...	672.7	1.3	2.6×10^{-16}
806	175123.23−293749.2	267.846800	−29.630335	0.1	2.6	12.3	5.8	15.7	1.0	0.90	1.9	-2.4	g...	...	833.3	1.8	1.8×10^{-16}
807	175123.24−293242.4	267.846850	−29.545133	0.1	2.9	23.7	6.4	10.3	2.6	0.90	3.4	<-5	g...	...	733.5	1.7	3.5×10^{-16}
808	175123.24−293807.7	267.846850	−29.635479	0.1	2.9	36.0	8.1	21.0	18.4	0.90	4.2	<-5	g...	...	825.7	2.2	6.5×10^{-16}
809	175123.27−293342.7	267.846960	−29.561868	0.1	2.0	12.8	4.8	5.2	8.4	0.90	2.4	-4.9	g...	...	608.7	2.9	4.3×10^{-16}
810	175123.31−293603.7	267.847130	−29.601030	0.1	1.2	7.2	4.0	4.8	0.0	0.90	1.6	-2.3	g...	...	720.3	1.1	7.5×10^{-17}
811	175123.33−293954.1	267.847210	−29.665049	0.2	4.6	20.0	7.9	33.0	7.7	0.90	2.4	-3.0	g...	...	815.2	1.5	2.6×10^{-16}
812	175123.35−292817.5	267.847330	−29.471545	0.3	7.2	44.9	13.3	115.1	20.1	0.90	3.3	-4.2	g...	...	727.1	1.9	7.6×10^{-16}
813	175123.36−292727.0	267.847350	−29.457511	0.3	8.0	43.8	15.0	160.2	22.1	0.91	2.8	-3.4	g...	...	701.6	2.3	9.4×10^{-16}
814	175123.37−294114.2	267.847410	−29.687301	0.2	5.9	80.5	13.3	80.5	12.8	0.90	5.8	<-5	....	b	804.6	1.2	8.3×10^{-16}
815	175123.41−293356.8	267.847560	−29.565779	0.2	1.8	6.8	4.0	5.2	0.0	0.90	1.5	-2.1	g...	...	599.7	1.5	1.1×10^{-16}
816	175123.43−293646.2	267.847660	−29.612835	0.1	1.7	65.6	9.0	6.4	46.9	0.90	6.9	<-5	g...	...	832.3	2.8	1.4×10^{-15}

(*cont.*)

Table A.1: *Chandra* source list

Source		Position				Extracted Counts							Characteristics				
Seq	CXOU J	R. A.	Decl.	Err	θ	$C_{\rm net}$	$\Delta C_{\rm net}$	$C'_{\rm bkg}$	$C_{\rm net,hard}$	PSF	PS	$P_{\rm B}$	Anom	Var	EffExp	$E_{\rm median}$	Photo $F_{\rm x}$
#		(deg)	(deg)	($''$)	($'$)						Frac				(ks)	(keV)	(ergs s^{-1} cm^{-2})
(1)	(2)	(3)	(4)	(5)	(6)	(7)	(8)	(9)	(10)	(11)	(12)	(13)	(14)	(15)	(16)	(17)	(18)
817	175123.44−293254.8	267.847680	−29.548571	0.1	2.6	61.1	9.0	9.9	4.2	0.90	6.4	<-5	g...	...	726.4	1.0	5.8×10^{-16}
818	175123.46−293442.5	267.847780	−29.578489	0.1	1.3	14.0	4.8	4.0	3.8	0.90	2.6	<-5	g...	...	652.0	1.7	2.4×10^{-16}
819	175123.47−293222.7	267.847800	−29.539656	0.2	3.1	18.6	6.1	12.4	4.6	0.90	2.8	<-5	g...	...	768.1	1.5	2.4×10^{-16}
820	175123.50−293900.8	267.847920	−29.650250	0.2	3.7	16.6	6.5	18.4	2.3	0.90	2.4	-3.3	g...	...	780.9	1.1	1.7×10^{-16}
821	175123.57−293741.5	267.848210	−29.628210	0.1	2.5	21.0	6.2	11.0	1.4	0.89	3.1	<-5	g...	...	803.2	1.4	2.6×10^{-16}
822	175123.58−293421.3	267.848250	−29.572602	0.1	1.5	8.4	4.1	4.6	5.5	0.90	1.8	-2.9	g...	...	635.3	3.1	2.7×10^{-16}
823	175123.59−293623.8	267.848300	−29.606615	0.1	1.4	16.1	5.3	6.9	1.5	0.90	2.7	<-5	g...	...	801.8	1.5	2.1×10^{-16}
824	175123.59−293755.5	267.848330	−29.632087	0.0	2.7	291.0	18.0	16.0	211.2	0.90	15.7	<-5	g...	...	806.0	3.0	7.7×10^{-15}
825	175123.62−293232.3	267.848420	−29.542325	0.2	3.0	19.3	6.0	10.7	11.0	0.90	2.9	<-5	g...	...	748.5	2.2	3.8×10^{-16}
826	175123.65−293458.4	267.848560	−29.582915	0.1	1.1	12.1	4.5	3.9	1.7	0.90	2.4	<-5	g...	...	658.0	1.3	1.6×10^{-16}
827	175123.69−293036.2	267.848730	−29.510075	0.2	4.8	47.9	9.2	27.1	0.9	0.90	4.9	<-5	g...	...	659.5	0.9	4.4×10^{-16}
828	175123.70−293514.5	267.848780	−29.587387	0.1	1.0	8.7	4.1	4.3	3.4	0.90	1.8	-3.1	g...	...	712.4	1.9	1.5×10^{-16}
829	175123.72−293521.4	267.848850	−29.589297	0.1	1.0	9.0	4.3	5.0	2.3	0.90	1.9	-3.1	g...	...	691.8	1.8	1.6×10^{-16}
830	175123.75−293606.5	267.848970	−29.601818	0.1	1.2	13.3	4.9	5.7	5.2	0.90	2.4	-4.9	g...	...	736.8	1.8	2.1×10^{-16}
831	175123.76−293705.2	267.849030	−29.618123	0.1	1.9	18.3	5.5	6.7	8.9	0.91	3.0	<-5	g...	...	820.5	2.0	3.0×10^{-16}
832	175123.77−294019.0	267.849070	−29.671957	0.2	5.0	16.3	7.3	28.7	5.8	0.79	2.1	-2.5	g...	...	807.0	1.7	2.8×10^{-16}
833	175123.79−293308.0	267.849130	−29.552244	0.1	2.4	16.8	5.3	6.2	6.3	0.89	2.9	<-5	g...	...	722.2	1.7	2.6×10^{-16}
834	175123.79−293926.7	267.849140	−29.657437	0.2	4.1	46.1	8.9	22.9	10.5	0.90	4.9	<-5	g...	...	788.8	1.6	6.4×10^{-16}
835	175123.82−293602.6	267.849290	−29.600741	0.1	1.2	11.1	4.4	3.9	4.0	0.90	2.2	-4.7	g...	...	656.8	1.6	1.9×10^{-16}
836	175123.83−293844.0	267.849310	−29.645564	0.1	3.5	192.3	15.0	17.7	115.4	0.89	12.4	<-5	g...	...	806.0	2.5	4.2×10^{-15}
837	175123.84−292916.8	267.849340	−29.488027	0.2	6.2	163.4	15.9	70.6	21.2	0.90	10.0	<-5	g...	...	752.9	1.4	2.0×10^{-15}
838	175123.84−293530.7	267.849340	−29.591883	0.1	1.0	7.5	4.0	4.5	1.4	0.90	1.6	-2.5	g...	...	632.9	1.3	1.3×10^{-15}
839	175123.84−293202.0	267.849360	−29.533915	0.1	3.3	14.7	4.5	1.3	12.5	0.45	2.9	<-5	....	a	529.5	3.7	1.0×10^{-16}
840	175123.89−293807.1	267.849580	−29.635333	0.1	2.9	25.2	7.3	20.8	5.8	0.90	3.2	<-5	g...	...	807.4	1.3	2.9×10^{-16}
841	175123.91−293631.1	267.849630	−29.608660	0.1	1.5	31.6	6.7	6.4	1.0	0.90	4.4	<-5	g...	...	785.4	1.1	2.9×10^{-16}
842	175123.94−293202.6	267.849790	−29.534073	0.2	3.3	6.5	3.4	1.5	4.4	0.45	1.7	-3.7	....	b	528.5	3.2	5.2×10^{-16}
843	175123.96−293959.8	267.849840	−29.666630	0.2	4.7	23.9	8.3	35.1	0.0	0.90	2.7	-3.7	g...	...	799.1	1.0	2.2×10^{-16}
844	175124.02−293526.6	267.850110	−29.590729	0.1	1.0	13.1	4.7	3.9	6.6	0.90	2.5	<-5	g...	...	608.3	2.7	3.9×10^{-16}
845	175124.04−293216.9	267.850180	−29.538050	0.2	3.2	12.4	5.3	10.6	4.1	0.90	2.1	-3.1	g...	...	664.6	1.5	1.8×10^{-16}
846	175124.05−292852.9	267.850240	−29.481362	0.2	6.6	131.3	15.5	89.7	99.6	0.90	8.2	<-5	....	a	792.9	2.8	3.1×10^{-15}
847	175124.06−293648.8	267.850280	−29.613557	0.1	1.7	22.2	5.8	5.8	0.8	0.90	3.5	<-5	g...	...	774.9	1.2	2.1×10^{-16}
848	175124.06−293158.7	267.850290	−29.532992	0.2	3.4	12.9	5.7	13.1	4.5	0.90	2.1	-2.9	g...	...	655.4	1.6	2.4×10^{-16}
849	175124.06−294015.0	267.850290	−29.670846	0.2	4.9	39.9	8.9	30.1	6.6	0.81	4.2	<-5	g...	...	792.7	1.3	5.2×10^{-16}
850	175124.07−293444.0	267.850300	−29.578900	0.1	1.1	11.1	4.4	3.9	6.9	0.90	2.2	-4.6	g...	...	597.3	3.4	4.1×10^{-16}

(*cont.*)

Table A.1: *Chandra* source list

Source		Position				Extracted Counts				Characteristics							
Seq	CXOU J	R. A.	Decl.	Err	θ	$C_{\rm net}$	$\Delta C_{\rm net}$	$C'_{\rm bkg}$	$C_{\rm net,hard}$	PSF	PS	$P_{\rm B}$	Anom	Var	EffExp	$E_{\rm median}$	Photo $F_{\rm x}$
#		(deg)	(deg)	($''$)	($'$)						Frac				(ks)	(keV)	(ergs s^{-1} cm^{-2})
(1)	(2)	(3)	(4)	(5)	(6)	(7)	(8)	(9)	(10)	(11)	(12)	(13)	(14)	(15)	(16)	(17)	(18)
851	175124.09−293508.5	267.850380	−29.585703	0.1	1.0	14.8	4.9	4.2	2.5	0.90	2.7	<-5	g...	...	634.2	1.7	1.8×10^{-16}
852	175124.09−293314.1	267.850400	−29.553930	0.1	2.3	11.8	4.8	6.2	4.1	0.90	2.2	-3.9	g...	...	699.3	1.6	2.6×10^{-16}
853	175124.10−293015.8	267.850440	−29.504390	0.2	5.2	44.6	9.9	41.4	22.1	0.90	4.3	<-5	g...	...	742.9	1.9	7.3×10^{-16}
854	175124.13−293738.8	267.850560	−29.627463	0.0	2.4	444.4	21.8	9.6	322.4	0.89	19.9	<-5	g...	...	832.9	3.0	1.1×10^{-14}
855	175124.15−293653.4	267.850640	−29.614843	0.1	1.7	9.4	4.4	5.6	0.0	0.90	1.9	-3.0	g...	...	770.0	1.3	1.1×10^{-16}
856	175124.15−293756.4	267.850660	−29.632338	0.1	2.7	146.8	13.3	15.2	27.6	0.90	10.7	<-5	g...	...	833.5	1.3	1.5×10^{-15}
857	175124.16−293503.2	267.850700	−29.584248	0.1	1.0	8.5	4.0	3.5	3.9	0.90	1.8	-3.4	g...	...	606.4	1.7	1.5×10^{-16}
858	175124.19−293413.4	267.850800	−29.570393	0.1	1.5	22.0	5.7	5.0	0.3	0.90	3.5	<-5	g...	...	619.0	1.4	3.1×10^{-16}
859	175124.21−293545.4	267.850890	−29.595956	0.2	1.0	7.6	3.7	2.4	3.3	0.90	1.8	-3.5	g...	...	386.2	1.7	2.2×10^{-16}
860	175124.22−293659.2	267.850940	−29.616469	0.1	1.8	16.1	5.2	5.9	9.8	0.90	2.8	<-5	g...	...	764.6	2.8	4.1×10^{-16}
861	175124.29−292901.6	267.851210	−29.483782	0.2	6.4	139.9	15.6	85.1	27.3	0.90	8.7	<-5	....	b	809.4	1.3	1.5×10^{-15}
862	175124.29−293128.3	267.851210	−29.524550	0.2	3.9	18.9	6.6	17.1	9.4	0.90	2.7	-4.2	g...	...	693.7	2.0	3.5×10^{-16}
863	175124.33−293322.7	267.851390	−29.556333	0.1	2.1	12.7	4.9	6.3	2.0	0.90	2.3	-4.3	g...	...	702.3	1.3	1.5×10^{-16}
864	175124.37−293237.7	267.851560	−29.543808	0.2	2.8	14.8	5.2	7.2	5.6	0.89	2.6	-5.0	g...	...	658.6	1.6	2.4×10^{-16}
865	175124.39−293653.8	267.851650	−29.614969	0.1	1.7	18.6	5.4	5.4	1.7	0.90	3.1	<-5	g...	...	740.7	1.3	2.2×10^{-16}
866	175124.39−293749.3	267.851660	−29.630374	0.1	2.6	15.6	5.8	12.4	7.6	0.90	2.4	-3.9	g...	...	820.9	1.7	2.2×10^{-16}
867	175124.40−293049.5	267.851670	−29.513772	0.1	4.6	83.9	11.2	29.1	61.2	0.90	7.2	<-5	g...	...	762.7	2.9	2.0×10^{-15}
868	175124.45−293225.2	267.851880	−29.540340	0.2	3.0	13.7	5.3	9.3	6.8	0.90	2.3	-3.8	g...	...	675.0	2.0	2.6×10^{-16}
869	175124.47−293329.2	267.851980	−29.558132	0.1	2.0	23.2	5.9	5.8	13.0	0.90	3.6	<-5	g...	...	691.6	2.3	4.9×10^{-16}
870	175124.51−293941.6	267.852140	−29.661573	0.2	4.4	20.0	7.6	29.0	7.6	0.90	2.5	-3.2	g...	...	788.6	1.6	2.8×10^{-16}
871	175124.52−294055.3	267.852200	−29.682029	0.2	5.5	30.6	10.0	58.4	18.2	0.90	2.9	-3.8	g...	...	755.8	2.0	5.6×10^{-16}
872	175124.55−294356.7	267.852310	−29.732422	0.3	8.5	64.5	17.6	221.5	49.3	0.91	3.6	-4.9	....	b	680.8	2.9	1.8×10^{-15}
873	175124.57−293234.5	267.852400	−29.542933	0.2	2.8	8.4	4.7	8.6	2.2	0.89	1.6	-2.1	g...	...	688.1	1.6	1.3×10^{-16}
874	175124.58−292931.3	267.852420	−29.492049	0.2	5.9	47.0	11.3	68.0	30.9	0.90	4.0	<-5	....	b	824.0	2.1	7.9×10^{-16}
875	175124.63−293123.4	267.852660	−29.523177	0.2	4.1	17.7	6.7	20.3	6.6	0.90	2.4	-3.4	g...	...	759.9	1.8	2.7×10^{-16}
876	175124.66−294113.7	267.852760	−29.687153	0.2	5.8	58.7	11.8	67.3	6.7	0.90	4.7	<-5	g...	...	748.0	1.1	1.6×10^{-16}
877	175124.66−293432.5	267.852770	−29.575705	0.1	1.1	15.2	4.9	3.8	0.0	0.90	2.8	<-5	g...	...	608.2	1.0	5.8×10^{-16}
878	175124.67−293655.8	267.852800	−29.615527	0.1	1.7	47.0	7.7	5.0	7.0	0.90	5.7	<-5	g...	...	682.5	1.3	3.9×10^{-15}
879	175124.67−292654.8	267.852830	−29.448559	0.5	8.1	23.5	8.3	36.5	26.0	0.90	2.7	-3.5	g...	...	169.3	3.8	6.2×10^{-16}
880	175124.71−293143.9	267.852990	−29.528886	0.2	3.7	16.3	6.2	15.7	5.0	0.89	2.4	-3.6	g...	...	752.4	1.4	2.0×10^{-16}
881	175124.73−293045.6	267.853060	−29.512669	0.2	4.7	27.9	8.3	32.1	16.9	0.90	3.1	-5.0	....	c	817.6	2.5	5.5×10^{-16}
882	175124.75−293202.6	267.853130	−29.534082	0.2	3.4	10.4	5.5	13.6	5.3	0.90	1.7	-2.1	g...	...	732.9	2.1	1.9×10^{-16}
883	175124.76−293418.6	267.853190	−29.571842	0.1	1.2	13.0	4.8	5.0	4.6	0.90	2.4	<-5	g...	...	633.3	1.7	2.3×10^{-16}
884	175124.80−293800.6	267.853370	−29.633511	0.1	2.7	24.1	6.7	13.9	7.9	0.90	3.3	<-5	g...	...	777.0	1.8	3.8×10^{-16}

(*cont.*)

Table A.1: *Chandra* source list

Source		Position				Extracted Counts							Characteristics				
Seq	CXOU J	R. A.	Decl.	Err	θ	$C_{\rm net}$	$\Delta C_{\rm net}$	$C'_{\rm bkg}$	$C_{\rm net,hard}$	PSF	PS	$P_{\rm B}$	Anom	Var	EffExp	$E_{\rm median}$	Photo $F_{\rm x}$
#		(deg)	(deg)	($''$)	($'$)						Frac				(ks)	(keV)	(ergs s^{-1} cm^{-2})
(1)	(2)	(3)	(4)	(5)	(6)	(7)	(8)	(9)	(10)	(11)	(12)	(13)	(14)	(15)	(16)	(17)	(18)
885	175124.83−293830.5	267.853470	−29.641831	0.1	3.2	44.9	8.5	19.1	32.9	0.90	4.9	<-5	g...	...	817.6	2.8	1.0×10^{-15}
886	175124.87−293850.1	267.853640	−29.647274	0.2	3.5	15.2	6.1	15.8	2.2	0.90	2.3	-3.2	g...	...	828.0	1.5	1.8×10^{-16}
887	175124.96−293444.1	267.854010	−29.578934	0.1	0.9	12.5	4.7	4.5	1.6	0.90	2.4	<-5	g...	...	641.1	1.3	1.6×10^{-16}
888	175125.00−293016.1	267.854180	−29.504480	0.1	5.2	610.9	26.2	46.1	399.2	0.90	22.9	<-5	....	b	844.4	2.7	1.3×10^{-14}
889	175125.00−293159.4	267.854180	−29.533176	0.1	3.4	33.3	7.5	14.7	7.0	0.90	4.2	<-5	g...	...	792.4	1.5	4.1×10^{-16}
890	175125.08−293430.7	267.854540	−29.575210	0.1	1.0	13.2	4.7	3.8	1.0	0.90	2.5	<-5	g...	...	638.1	1.3	1.7×10^{-16}
891	175125.10−293323.4	267.854590	−29.556501	0.1	2.0	13.1	4.9	5.9	10.1	0.90	2.4	-4.7	g...	...	709.9	3.1	3.6×10^{-16}
892	175125.12−292749.2	267.854700	−29.463674	0.1	7.6	443.1	25.0	152.9	365.9	0.90	17.4	<-5	....	a	791.0	3.5	1.3×10^{-14}
893	175125.12−293611.8	267.854700	−29.603298	0.1	1.1	22.1	5.5	2.9	7.7	0.90	3.6	<-5	g...	...	468.2	1.5	5.0×10^{-16}
894	175125.20−293606.1	267.855040	−29.601695	0.1	1.0	8.4	3.9	2.6	0.9	0.90	1.9	-3.9	g...	...	428.3	1.5	2.3×10^{-16}
895	175125.32−293456.0	267.855500	−29.582241	0.2	0.7	5.6	3.5	3.4	0.0	0.89	1.4	-2.0	g...	...	620.4	1.2	7.0×10^{-17}
896	175125.36−293827.6	267.855690	−29.641014	0.2	3.1	18.9	6.6	18.1	11.0	0.90	2.6	-4.1	g...	...	754.6	2.3	4.0×10^{-16}
897	175125.41−293742.0	267.855880	−29.628336	0.1	2.4	27.0	6.3	6.0	0.0	0.89	4.0	<-5	g...	...	560.0	1.3	1.2×10^{-16}
898	175125.41−293459.9	267.855910	−29.583330	0.1	0.7	10.8	4.3	3.2	1.8	0.89	2.2	-4.9	g...	...	621.3	1.1	4.7×10^{-16}
899	175125.44−294041.5	267.856030	−29.678221	0.2	5.3	19.6	5.6	6.4	6.4	0.46	3.2	<-5	g...	...	760.7	1.8	6.3×10^{-16}
900	175125.47−293843.0	267.856150	−29.645285	0.2	3.3	23.6	6.6	13.4	5.3	0.89	3.3	<-5	g...	...	752.6	1.2	2.6×10^{-16}
901	175125.48−293528.8	267.856170	−29.591353	0.1	0.7	11.4	4.3	2.6	7.2	0.90	2.3	<-5	g...	...	423.7	3.4	6.0×10^{-16}
902	175125.49−294107.2	267.856230	−29.685343	0.1	5.7	178.2	16.3	67.8	91.8	0.90	10.6	<-5	g...	...	756.8	2.1	3.2×10^{-16}
903	175125.49−293852.0	267.856250	−29.647800	0.2	3.5	18.8	6.3	14.2	6.3	0.90	2.8	-4.7	g...	...	747.5	1.8	3.5×10^{-15}
904	175125.51−294048.9	267.856330	−29.680264	0.2	5.4	34.1	10.1	55.9	20.0	0.90	3.2	-4.6	g...	...	761.1	2.8	8.6×10^{-16}
905	175125.58−293430.1	267.856610	−29.575051	0.1	1.0	13.6	4.8	4.4	2.6	0.90	2.6	<-5	g...	...	711.7	1.3	1.6×10^{-16}
906	175125.59−293444.4	267.856650	−29.579013	0.1	0.8	9.5	4.3	4.5	2.5	0.90	2.0	-3.5	g...	...	715.0	1.3	1.1×10^{-16}
907	175125.60−294038.8	267.856690	−29.677470	0.2	5.2	31.3	6.9	8.7	16.5	0.48	4.2	<-5	g...	...	770.0	2.2	1.2×10^{-15}
908	175125.61−293311.7	267.856720	−29.553271	0.1	2.2	24.0	6.2	8.0	9.6	0.90	3.6	<-5	g...	...	821.7	1.6	3.0×10^{-16}
909	175125.62−293806.5	267.856790	−29.635157	0.1	2.7	29.3	6.9	10.7	7.7	0.90	4.0	<-5	g...	...	566.2	1.5	5.7×10^{-16}
910	175125.64−293603.5	267.856850	−29.600994	0.1	0.9	53.6	8.1	3.4	3.8	0.90	6.2	<-5	g...	...	509.4	1.1	8.0×10^{-16}
911	175125.67−292929.0	267.856960	−29.491410	0.2	5.9	45.1	11.1	64.9	31.7	0.90	3.9	<-5	....	b	825.1	2.9	1.0×10^{-15}
912	175125.67−293142.6	267.856990	−29.528525	0.1	3.7	85.2	10.7	18.8	7.4	0.90	7.6	<-5	....	b	863.7	1.1	7.3×10^{-16}
913	175125.72−293134.5	267.857180	−29.526264	0.2	3.9	30.8	7.5	18.2	18.2	0.90	3.8	<-5	....	a	858.6	2.4	5.6×10^{-16}
914	175125.81−293832.5	267.857570	−29.642379	0.2	3.1	17.0	5.9	12.0	7.2	0.90	2.6	-4.5	g...	...	575.0	1.7	3.7×10^{-16}
915	175125.83−293016.7	267.857660	−29.504660	0.2	5.2	22.8	7.0	19.2	5.4	0.73	3.0	<-5	....	a	840.2	1.4	3.0×10^{-16}
916	175125.85−293629.8	267.857740	−29.608302	0.1	1.3	10.1	4.1	2.9	3.1	0.90	2.1	-4.7	g...	...	483.5	1.2	1.8×10^{-16}
917	175125.86−293505.3	267.857780	−29.584827	0.1	0.6	20.0	5.4	4.0	10.8	0.89	3.3	<-5	g...	...	716.2	2.7	4.8×10^{-16}
918	175125.97−292939.8	267.858220	−29.494413	0.2	5.8	61.2	11.7	61.8	43.7	0.90	5.0	<-5	....	b	825.8	2.8	1.4×10^{-15}

(*cont.*)

Table A.1: *Chandra* source list

Source		Position				Extracted Counts							Characteristics				
Seq	CXOU J	R. A.	Decl.	Err	θ	$C_{\rm net}$	$\Delta C_{\rm net}$	$C'_{\rm bkg}$	$C_{\rm net,hard}$	PSF	PS	$P_{\rm B}$	Anom	Var	EffExp	$E_{\rm median}$	Photo $F_{\rm x}$
#		(deg)	(deg)	($''$)	($'$)						Frac				(ks)	(keV)	(ergs s^{-1} cm^{-2})
(1)	(2)	(3)	(4)	(5)	(6)	(7)	(8)	(9)	(10)	(11)	(12)	(13)	(14)	(15)	(16)	(17)	(18)
919	175125.99−292816.3	267.858310	−29.471208	0.3	7.1	40.6	13.3	118.4	32.3	0.90	2.9	-3.5	....	b	801.2	3.0	1.0×10^{-15}
920	175125.99−293430.1	267.858310	−29.575048	0.0	1.0	97.5	10.7	5.5	85.3	0.90	8.7	<-5	g...	...	803.8	3.5	2.7×10^{-15}
921	175126.04−293641.0	267.858520	−29.611399	0.1	1.5	23.3	5.7	3.7	2.8	0.90	3.7	<-5	g...	...	507.6	1.2	3.9×10^{-16}
922	175126.11−293454.8	267.858800	−29.581913	0.1	0.7	58.3	8.5	4.7	17.4	0.89	6.5	<-5	g...	...	791.3	1.5	6.9×10^{-16}
923	175126.13−293541.7	267.858880	−29.594922	0.1	0.6	7.5	3.7	2.5	3.1	0.90	1.8	-3.4	g...	...	447.5	1.3	1.4×10^{-16}
924	175126.14−293324.3	267.858940	−29.556761	0.1	2.0	37.8	7.2	7.2	7.7	0.90	4.9	<-5	....	c	886.9	1.4	2.5×10^{-16}
925	175126.14−293157.8	267.858950	−29.532742	0.2	3.5	17.1	6.3	15.9	7.2	0.89	2.5	-3.8	....	a	873.2	1.9	3.9×10^{-16}
926	175126.17−293244.8	267.859050	−29.545779	0.1	2.7	62.9	9.1	11.1	32.5	0.89	6.5	<-5	....	a	884.7	2.1	9.6×10^{-16}
927	175126.18−293204.5	267.859090	−29.534589	0.2	3.4	21.1	6.6	15.9	0.0	0.90	2.9	<-5	....	b	874.9	1.1	1.6×10^{-16}
928	175126.19−293925.4	267.859160	−29.657060	0.1	4.0	57.9	9.2	17.1	53.5	0.90	5.9	<-5	g...	...	622.3	4.1	2.8×10^{-15}
929	175126.26−293225.3	267.859440	−29.540382	0.1	3.0	45.8	8.1	12.2	16.8	0.90	5.3	<-5	....	a	880.0	1.7	5.5×10^{-16}
930	175126.28−293153.0	267.859530	−29.531405	0.2	3.5	17.6	6.5	17.4	8.3	0.90	2.5	-3.8	....	a	871.9	2.0	2.6×10^{-16}
931	175126.29−293933.3	267.859550	−29.659256	0.1	4.2	197.5	15.2	18.5	115.8	0.90	12.5	<-5	g...	...	630.1	2.5	1.9×10^{-16}
932	175126.29−294146.7	267.859560	−29.696330	0.3	6.4	36.2	12.0	93.8	23.5	0.90	2.9	-3.5	g...	...	754.1	2.4	5.7×10^{-15}
933	175126.29−293135.8	267.859580	−29.526619	0.2	3.8	16.5	6.4	17.5	9.1	0.90	2.4	-3.4	....	a	867.4	1.6	8.2×10^{-16}
934	175126.31−293946.7	267.859630	−29.662993	0.1	4.4	71.4	10.3	23.6	29.3	0.90	6.6	<-5	g...	...	668.7	1.9	1.4×10^{-15}
935	175126.36−293434.5	267.859840	−29.576264	0.1	0.9	11.1	4.5	4.9	3.2	0.90	2.2	-4.1	....	b	841.7	1.6	1.4×10^{-16}
936	175126.39−293123.9	267.859980	−29.523327	0.2	4.0	27.4	7.5	20.6	11.3	0.90	3.4	<-5	....	a	864.2	1.8	3.7×10^{-16}
937	175126.41−293217.2	267.860050	−29.538120	0.2	3.1	18.0	6.2	14.0	4.7	0.90	2.7	-4.4	....	a	877.9	1.5	1.9×10^{-16}
938	175126.41−293414.6	267.860070	−29.570733	0.1	1.3	22.7	5.9	6.3	8.2	0.90	3.5	<-5	....	a	839.7	1.7	2.9×10^{-16}
939	175126.48−293905.2	267.860340	−29.651461	0.1	3.7	43.9	7.9	10.1	0.0	0.90	5.2	<-5	g...	...	447.0	1.1	8.7×10^{-16}
940	175126.50−294109.1	267.860430	−29.685877	0.2	5.8	53.7	11.7	69.3	18.9	0.90	4.4	<-5	g...	...	759.6	1.6	7.4×10^{-16}
941	175126.51−293511.5	267.860460	−29.586549	0.1	0.5	47.2	7.7	4.8	12.3	0.89	5.7	<-5	g...	...	823.6	1.4	5.3×10^{-16}
942	175126.60−293425.1	267.860840	−29.573652	0.1	1.1	12.6	4.9	6.4	1.3	0.90	2.3	-4.2	....	a	872.6	1.6	1.5×10^{-16}
943	175126.66−293502.3	267.861090	−29.583980	0.1	0.6	8.0	4.1	5.0	2.5	0.89	1.7	-2.6	....	a	858.9	1.4	8.1×10^{-17}
944	175126.67−293611.2	267.861140	−29.603138	0.1	0.9	10.5	4.4	4.5	4.6	0.90	2.1	-4.0	g...	...	738.1	1.8	1.4×10^{-16}
945	175126.67−293402.6	267.861150	−29.567391	0.1	1.4	17.4	5.4	6.6	3.0	0.90	2.9	<-5	....	a	869.5	1.1	1.7×10^{-16}
946	175126.74−293543.2	267.861450	−29.595346	0.1	0.6	6.5	3.7	3.5	5.8	0.90	1.5	-2.4	g...	...	533.9	3.2	2.5×10^{-16}
947	175126.79−292905.5	267.861660	−29.484888	0.2	6.3	157.8	15.9	76.2	146.0	0.90	9.6	<-5	....	a	815.3	4.2	5.3×10^{-15}
948	175126.82−293321.7	267.861770	−29.556053	0.1	2.1	17.0	5.6	9.0	5.0	0.90	2.8	<-5	....	a	891.3	1.6	1.9×10^{-16}
949	175126.82−293515.5	267.861770	−29.587647	0.1	0.4	43.6	7.4	4.4	22.5	0.90	5.5	<-5	g...	...	818.0	2.0	6.9×10^{-16}
950	175126.84−293406.2	267.861850	−29.568401	0.1	1.4	12.6	4.9	6.4	6.0	0.90	2.3	-4.3	....	...	861.8	1.9	1.7×10^{-16}
951	175126.86−293552.3	267.861940	−29.597879	0.1	0.6	15.9	5.0	4.1	7.6	0.89	2.9	<-5	g...	...	637.2	1.8	2.4×10^{-15}
952	175126.86−293228.3	267.861950	−29.541216	0.1	2.9	100.7	11.1	10.3	80.4	0.90	8.7	<-5	....	a	880.2	3.3	2.9×10^{-16}

(*cont.*)

Table A.1: *Chandra* source list

Source		Position				Extracted Counts							Characteristics				
Seq	CXOU J	R. A.	Decl.	Err	θ	$C_{\rm net}$	$\Delta C_{\rm net}$	$C'_{\rm bkg}$	$C_{\rm net,hard}$	PSF	PS	$P_{\rm B}$	Anom	Var	EffExp	$E_{\rm median}$	Photo $F_{\rm x}$
#		(deg)	(deg)	($''$)	($'$)						Frac				(ks)	(keV)	(ergs s^{-1} cm^{-2})
(1)	(2)	(3)	(4)	(5)	(6)	(7)	(8)	(9)	(10)	(11)	(12)	(13)	(14)	(15)	(16)	(17)	(18)
953	175126.89−293451.3	267.862070	−29.580944	0.1	0.7	11.9	4.7	5.1	4.5	0.89	2.3	-4.4	....	a	886.8	1.6	1.4×10^{-16}
954	175126.89−293627.8	267.862080	−29.607738	0.1	1.1	7.7	4.0	4.3	1.6	0.90	1.7	-2.7	g...	...	721.5	1.2	8.6×10^{-17}
955	175126.98−293420.3	267.862420	−29.572307	0.1	1.1	16.9	5.3	6.1	5.6	0.90	2.9	<-5	....	c	862.9	1.6	3.0×10^{-16}
956	175126.98−292959.7	267.862440	−29.499931	0.3	5.4	21.9	9.0	49.1	9.4	0.90	2.3	-2.6	....	b	837.5	1.8	2.0×10^{-16}
957	175127.00−293706.7	267.862520	−29.618552	0.0	1.7	194.3	14.6	4.7	145.7	0.90	12.8	<-5	g...	...	640.7	3.2	6.4×10^{-15}
958	175127.06−293654.1	267.862750	−29.615044	0.1	1.5	16.1	5.1	4.9	10.4	0.90	2.8	<-5	g...	...	677.2	3.4	5.6×10^{-16}
959	175127.08−293127.6	267.862870	−29.524340	0.2	4.0	17.4	6.7	20.6	13.1	0.90	2.4	-3.3	....	a	864.6	2.4	3.1×10^{-16}
960	175127.08−293214.9	267.862870	−29.537491	0.1	3.2	22.2	6.5	12.8	8.6	0.90	3.2	<-5	....	a	876.7	1.9	3.1×10^{-16}
961	175127.13−293135.9	267.863070	−29.526657	0.1	3.8	183.5	14.8	19.5	17.3	0.90	12.0	<-5	....	a	866.7	1.1	1.6×10^{-15}
962	175127.16−293837.9	267.863190	−29.643886	0.2	3.3	23.2	6.5	11.8	0.9	0.90	3.3	<-5	g...	...	481.2	1.3	4.3×10^{-16}
963	175127.20−293115.4	267.863340	−29.520958	0.2	4.2	30.5	8.0	24.5	32.5	0.90	3.6	<-5	....	a	861.2	4.7	1.1×10^{-15}
964	175127.20−293154.9	267.863340	−29.531924	0.2	3.5	22.8	6.8	16.2	6.9	0.90	3.1	<-5	....	a	871.6	1.6	2.7×10^{-16}
965	175127.21−293523.8	267.863400	−29.589953	0.1	0.4	8.1	4.0	3.9	0.6	0.90	1.8	-3.0	g...	...	712.0	1.3	9.8×10^{-17}
966	175127.24−294205.1	267.863510	−29.701442	0.2	6.7	119.4	15.5	102.6	29.4	0.90	7.4	<-5	g...	...	692.9	1.4	1.7×10^{-15}
967	175127.26−293243.6	267.863590	−29.545452	0.1	2.7	117.6	11.8	9.4	94.0	0.89	9.6	<-5	....	a	883.4	3.8	3.3×10^{-15}
968	175127.28−293710.7	267.863680	−29.619650	0.1	1.8	76.8	9.6	5.2	7.2	0.90	7.6	<-5	g...	...	678.8	1.2	9.9×10^{-16}
969	175127.29−293258.6	267.863740	−29.549633	0.1	2.4	10.6	4.9	8.4	0.0	0.89	1.9	-2.9	....	a	886.7	1.2	9.2×10^{-17}
970	175127.31−293918.9	267.863820	−29.655263	0.3	4.0	10.7	5.6	14.3	9.6	0.90	1.8	-2.1	g...	...	462.5	2.8	4.6×10^{-16}
971	175127.37−293234.4	267.864070	−29.542912	0.2	2.8	10.6	5.1	10.4	4.5	0.90	1.9	-2.6	....	b	881.1	1.8	1.4×10^{-16}
972	175127.38−293750.2	267.864090	−29.630638	0.2	2.5	10.9	4.9	8.1	4.5	0.90	2.0	-3.0	g...	...	650.0	1.8	2.0×10^{-16}
973	175127.40−293629.6	267.864180	−29.608234	0.1	1.1	11.5	4.5	4.5	2.7	0.90	2.3	-4.5	g...	...	827.7	1.4	1.3×10^{-16}
974	175127.41−293349.9	267.864240	−29.563872	0.1	1.6	66.3	9.1	6.7	7.8	0.90	6.9	<-5	....	c	890.1	1.2	5.9×10^{-16}
975	175127.50−294006.4	267.864590	−29.668455	0.1	4.8	113.8	12.2	21.2	82.3	0.90	9.0	<-5	g...	...	423.6	2.9	2.8×10^{-16}
976	175127.50−293323.8	267.864600	−29.556624	0.1	2.0	16.7	5.5	8.3	13.4	0.90	2.7	<-5	....	a	889.9	2.3	5.9×10^{-15}
977	175127.58−292915.7	267.864940	−29.487709	0.2	6.1	44.2	11.4	71.8	11.2	0.90	3.7	<-5	....	a	823.1	1.1	3.8×10^{-16}
978	175127.63−292851.3	267.865140	−29.480929	0.2	6.6	80.3	13.5	86.7	55.4	0.90	5.7	<-5	....	a	812.3	2.9	1.8×10^{-15}
979	175127.64−293737.0	267.865180	−29.626965	0.1	2.2	10.2	4.7	6.8	0.0	0.90	1.9	-3.0	g...	...	716.6	1.1	4.3×10^{-16}
980	175127.64−293128.4	267.865200	−29.524561	0.2	3.9	22.8	7.1	20.2	13.0	0.90	3.0	-5.0	....	a	864.4	2.5	1.1×10^{-16}
981	175127.65−294046.4	267.865220	−29.679580	0.3	5.4	31.7	8.6	33.3	13.6	0.90	3.5	<-5	g...	...	449.4	1.8	1.0×10^{-15}
982	175127.70−294223.8	267.865430	−29.706619	0.2	7.0	80.6	14.5	110.4	28.1	0.90	5.4	<-5	g...	...	631.0	1.8	4.9×10^{-16}
983	175127.70−293223.7	267.865440	−29.539928	0.1	3.0	37.8	7.5	11.2	12.2	0.90	4.7	<-5	....	b	878.2	1.8	1.6×10^{-15}
984	175127.72−293209.1	267.865530	−29.535883	0.2	3.3	18.9	6.2	13.1	5.5	0.90	2.8	-5.0	....	b	874.6	1.6	2.2×10^{-16}
985	175127.74−294330.4	267.865600	−29.725130	0.3	8.0	39.7	15.1	167.3	15.6	0.90	2.5	-2.8	g...	...	623.7	1.8	8.4×10^{-16}
986	175127.79−293556.5	267.865820	−29.599043	0.1	0.6	15.6	5.0	4.4	8.2	0.89	2.8	<-5	g...	...	767.1	2.1	2.7×10^{-16}

(*cont.*)

Table A.1: *Chandra* source list

Source		Position				Extracted Counts							Characteristics				
Seq	CXOU J	R. A.	Decl.	Err	θ	$C_{\rm net}$	$\Delta C_{\rm net}$	$C'_{\rm bkg}$	$C_{\rm net,hard}$	PSF	PS	$P_{\rm B}$	Anom	Var	EffExp	$E_{\rm median}$	Photo $F_{\rm x}$
#		(deg)	(deg)	($''$)	($'$)						Frac				(ks)	(keV)	(ergs s^{-1} cm^{-2})
(1)	(2)	(3)	(4)	(5)	(6)	(7)	(8)	(9)	(10)	(11)	(12)	(13)	(14)	(15)	(16)	(17)	(18)
987	175127.79−294238.0	267.865830	−29.710580	0.3	7.3	39.0	13.4	122.0	6.0	0.90	2.8	-3.3	g...	...	626.7	1.4	6.0×10^{-16}
988	175127.83−294256.0	267.865980	−29.715558	0.3	7.5	33.4	13.0	118.6	15.3	0.89	2.5	-2.7	g...	...	587.2	1.8	7.5×10^{-16}
989	175127.88−293757.7	267.866200	−29.632713	0.2	2.6	11.2	5.2	10.8	1.7	0.90	1.9	-2.7	g...	...	742.8	1.6	1.6×10^{-16}
990	175127.90−293510.4	267.866280	−29.586245	0.0	0.4	64.0	8.8	5.0	30.1	0.89	6.8	<-5	g...	...	827.4	1.9	9.5×10^{-16}
991	175127.94−293300.6	267.866420	−29.550188	0.1	2.4	21.1	5.9	7.9	15.0	0.89	3.3	<-5	....	a	884.1	2.9	4.5×10^{-16}
992	175127.94−293638.2	267.866450	−29.610619	0.1	1.2	8.4	4.1	4.6	4.7	0.90	1.8	-2.9	g...	...	838.0	2.1	1.4×10^{-16}
993	175127.95−293508.5	267.866480	−29.585722	0.0	0.4	237.7	16.1	5.3	185.9	0.89	14.3	<-5	....	b	853.5	3.3	6.0×10^{-15}
994	175127.99−293410.5	267.866640	−29.569608	0.1	1.3	16.7	5.3	6.3	4.2	0.90	2.8	<-5	....	a	848.2	1.6	2.0×10^{-16}
995	175128.00−293634.6	267.866700	−29.609622	0.1	1.2	9.5	4.3	4.5	3.7	0.90	2.0	-3.5	g...	...	844.5	1.9	1.4×10^{-16}
996	175128.02−293908.7	267.866770	−29.652437	0.1	3.8	88.2	10.7	15.8	60.6	0.90	7.8	<-5	g...	...	617.2	3.0	3.0×10^{-15}
997	175128.03−293452.7	267.866820	−29.581325	0.1	0.6	27.6	6.3	5.4	0.4	0.89	4.1	<-5	....	a	860.8	1.2	2.4×10^{-16}
998	175128.03−293725.9	267.866830	−29.623878	0.2	2.0	8.6	4.5	7.4	4.9	0.90	1.7	-2.3	....	a	858.0	2.6	1.7×10^{-16}
999	175128.04−294034.7	267.866870	−29.676318	0.2	5.2	75.4	10.9	32.6	30.8	0.90	6.6	<-5	g...	...	485.7	1.9	1.9×10^{-15}
1000	175128.13−293703.7	267.867210	−29.617717	0.1	1.7	35.9	7.0	6.1	2.9	0.90	4.8	<-5	....	a	858.1	1.1	2.9×10^{-16}
1001	175128.15−293650.6	267.867320	−29.614066	0.1	1.4	67.3	9.1	5.7	51.1	0.90	7.0	<-5	g...	...	848.4	2.7	1.4×10^{-15}
1002	175128.17−292748.9	267.867410	−29.463604	0.3	7.6	35.0	13.7	135.0	20.9	0.90	2.5	-2.7	....	b	769.2	2.0	5.9×10^{-16}
1003	175128.20−294013.8	267.867520	−29.670517	0.2	4.9	34.1	8.2	24.9	14.2	0.90	3.9	<-5	g...	...	529.6	1.8	5.9×10^{-16}
1004	175128.20−293347.0	267.867530	−29.563064	0.1	1.7	31.6	6.7	6.4	21.8	0.90	4.4	<-5	....	b	879.5	2.6	8.0×10^{-16}
1005	175128.21−293110.2	267.867580	−29.519510	0.2	4.2	35.3	8.3	24.7	12.1	0.90	4.0	<-5	....	a	859.1	1.7	4.5×10^{-16}
1006	175128.25−293248.3	267.867730	−29.546774	0.2	2.6	8.8	4.8	9.2	5.8	0.89	1.6	-2.1	....	a	881.6	2.4	1.5×10^{-16}
1007	175128.27−292951.8	267.867800	−29.497736	0.2	5.5	30.7	9.6	50.3	0.0	0.90	3.0	-4.2	....	a	835.5	0.9	2.2×10^{-16}
1008	175128.32−293426.3	267.868020	−29.573997	0.1	1.1	10.5	4.5	5.5	1.4	0.89	2.1	-3.6	....	a	849.0	1.8	1.4×10^{-16}
1009	175128.34−294000.8	267.868120	−29.666891	0.2	4.6	34.8	8.2	24.2	14.3	0.90	4.0	<-5	g...	...	577.7	1.8	8.0×10^{-16}
1010	175128.35−293621.5	267.868140	−29.605985	0.1	0.9	13.5	4.9	5.5	5.0	0.89	2.5	<-5	....	a	868.8	1.8	1.8×10^{-16}
1011	175128.36−293714.7	267.868170	−29.620765	0.1	1.9	11.9	4.9	7.1	4.0	0.90	2.2	-3.7	....	a	866.5	1.7	1.5×10^{-16}
1012	175128.37−293735.9	267.868250	−29.626643	0.2	2.2	8.2	4.5	7.8	2.3	0.90	1.6	-2.1	....	a	865.6	1.7	1.1×10^{-16}
1013	175128.38−293438.2	267.868290	−29.577295	0.1	0.9	11.7	4.7	5.3	2.4	0.89	2.2	-4.3	....	b	853.2	1.4	1.2×10^{-16}
1014	175128.39−293215.4	267.868330	−29.537623	0.2	3.2	12.7	5.4	11.3	9.7	0.89	2.1	-3.1	....	a	873.1	2.6	2.5×10^{-16}
1015	175128.39−293303.9	267.868330	−29.551089	0.2	2.4	9.3	4.7	7.7	4.1	0.89	1.8	-2.5	....	a	884.8	1.9	1.3×10^{-16}
1016	175128.44−293901.7	267.868520	−29.650473	0.1	3.6	34.5	7.7	16.5	14.5	0.90	4.2	<-5	g...	...	725.5	1.9	6.1×10^{-16}
1017	175128.46−293733.0	267.868590	−29.625836	0.1	2.2	15.6	5.3	7.4	9.3	0.90	2.6	<-5	....	b	865.7	2.2	1.1×10^{-16}
1018	175128.46−293445.8	267.868610	−29.579406	0.1	0.8	10.4	4.5	5.6	2.2	0.90	2.0	-3.5	....	a	852.9	1.5	2.6×10^{-16}
1019	175128.48−293625.0	267.868680	−29.606965	0.1	1.0	18.6	5.4	5.4	0.1	0.89	3.1	<-5	....	a	877.1	1.0	1.4×10^{-16}
1020	175128.52−293328.7	267.868870	−29.557981	0.0	2.0	106.0	11.1	7.0	20.4	0.91	9.1	<-5	....	b	870.5	1.3	1.0×10^{-15}

(*cont.*)

Table A.1: *Chandra* source list

Source		Position				Extracted Counts							Characteristics				
Seq	CXOU J	R. A.	Decl.	Err	θ	$C_{\rm net}$	$\Delta C_{\rm net}$	$C'_{\rm bkg}$	$C_{\rm net,hard}$	PSF	PS	$P_{\rm B}$	Anom	Var	EffExp	$E_{\rm median}$	Photo $F_{\rm x}$
#		(deg)	(deg)	($''$)	($'$)						Frac				(ks)	(keV)	(ergs s^{-1} cm^{-2})
(1)	(2)	(3)	(4)	(5)	(6)	(7)	(8)	(9)	(10)	(11)	(12)	(13)	(14)	(15)	(16)	(17)	(18)
1021	175128.55−293158.6	267.868990	−29.532949	0.1	3.4	30.4	7.2	14.6	20.4	0.90	3.9	<-5	....	a	868.6	2.5	5.8×10^{-16}
1022	175128.57−293220.9	267.869060	−29.539158	0.2	3.1	16.0	5.7	11.0	4.3	0.90	2.5	-4.4	....	a	875.1	1.3	1.6×10^{-16}
1023	175128.60−293630.8	267.869200	−29.608556	0.1	1.1	62.7	8.8	5.3	8.0	0.89	6.7	<-5	....	c	888.3	1.4	6.1×10^{-16}
1024	175128.61−293555.1	267.869220	−29.598649	0.1	0.6	6.9	3.9	4.1	2.5	0.90	1.6	-2.4	g...	...	780.9	1.0	5.0×10^{-15}
1025	175128.61−293059.7	267.869230	−29.516586	0.1	4.4	238.1	16.8	25.9	153.6	0.88	13.8	<-5	....	a	855.8	2.7	5.8×10^{-17}
1026	175128.62−293746.2	267.869280	−29.629513	0.1	2.4	28.8	6.7	9.2	30.2	0.90	4.0	<-5	g...	...	854.7	4.3	9.6×10^{-16}
1027	175128.66−293205.2	267.869440	−29.534789	0.1	3.3	13.6	4.5	2.4	8.0	0.46	2.7	<-5	....	a	871.1	3.0	6.0×10^{-16}
1028	175128.69−293639.8	267.869550	−29.611069	0.1	1.3	8.4	4.3	5.6	11.1	0.90	1.7	-2.6	....	...	889.2	3.8	2.3×10^{-16}
1029	175128.74−293552.1	267.869790	−29.597821	0.1	0.6	17.4	5.1	3.6	4.8	0.90	3.1	<-5	g...	...	727.0	1.5	2.3×10^{-16}
1030	175128.75−292943.5	267.869800	−29.495427	0.3	5.7	25.0	9.6	55.0	20.5	0.90	2.5	-3.0	....	b	826.9	3.8	7.4×10^{-16}
1031	175128.75−293545.5	267.869820	−29.595995	0.1	0.5	7.7	3.9	3.3	1.0	0.90	1.7	-3.0	g...	...	607.1	1.2	7.2×10^{-16}
1032	175128.75−293206.0	267.869830	−29.535013	0.1	3.3	16.2	4.9	2.8	13.8	0.50	3.0	<-5	....	a	871.4	3.3	1.0×10^{-16}
1033	175128.82−293236.2	267.870090	−29.543404	0.1	2.8	30.9	6.9	9.1	14.7	0.89	4.2	<-5	....	b	877.6	2.0	4.6×10^{-16}
1034	175128.82−293501.7	267.870100	−29.583821	0.1	0.6	15.6	5.1	5.4	3.1	0.90	2.7	<-5	....	a	854.6	1.4	1.7×10^{-16}
1035	175128.85−293058.7	267.870250	−29.516319	0.1	4.4	77.4	10.3	17.6	13.2	0.82	7.2	<-5	....	a	855.2	1.4	9.0×10^{-16}
1036	175128.87−293131.2	267.870300	−29.525361	0.2	3.9	28.9	7.5	19.1	25.8	0.90	3.6	<-5	....	a	861.8	4.1	8.9×10^{-16}
1037	175128.90−294349.2	267.870440	−29.730351	0.3	8.4	56.1	15.0	149.9	24.6	0.90	3.6	<-5	g...	...	474.6	2.0	1.7×10^{-15}
1038	175128.94−293412.3	267.870600	−29.570103	0.0	1.3	123.1	11.8	4.9	87.5	0.90	10.0	<-5	g...	...	837.6	2.8	2.6×10^{-15}
1039	175128.95−293444.1	267.870640	−29.578926	0.1	0.8	22.9	5.8	5.1	13.7	0.89	3.6	<-5	....	c	852.6	2.8	4.9×10^{-16}
1040	175128.96−293603.8	267.870700	−29.601064	0.1	0.7	8.9	4.3	5.1	2.3	0.89	1.8	-3.0	....	a	883.6	1.7	1.1×10^{-16}
1041	175128.97−293500.6	267.870730	−29.583501	0.1	0.6	19.9	5.5	5.1	5.3	0.89	3.3	<-5	....	b	859.1	1.5	2.3×10^{-16}
1042	175129.03−293315.2	267.870980	−29.554242	0.1	2.2	10.5	4.7	6.5	1.8	0.90	2.0	-3.2	....	a	855.9	1.1	8.6×10^{-17}
1043	175129.04−293236.8	267.871030	−29.543581	0.1	2.8	15.7	5.5	9.3	0.0	0.90	2.6	-4.7	....	b	861.3	1.2	1.5×10^{-16}
1044	175129.14−293012.7	267.871450	−29.503553	0.1	5.2	277.6	18.5	43.4	87.7	0.90	14.6	<-5	....	c	836.4	1.6	3.4×10^{-15}
1045	175129.16−292924.3	267.871540	−29.490096	0.1	6.0	293.4	19.5	64.6	241.0	0.89	14.7	<-5	....	a	811.6	3.5	8.4×10^{-15}
1046	175129.18−293256.6	267.871610	−29.549064	0.1	2.5	13.8	5.2	8.2	7.2	0.89	2.4	-4.2	....	a	853.2	2.0	2.1×10^{-16}
1047	175129.20−293117.5	267.871690	−29.521533	0.1	4.1	66.1	9.9	21.9	7.7	0.90	6.3	<-5	....	b	858.4	1.1	5.3×10^{-16}
1048	175129.22−293541.0	267.871790	−29.594729	0.0	0.5	79.9	9.6	3.1	59.8	0.90	7.9	<-5	g...	...	592.7	2.6	2.4×10^{-15}
1049	175129.23−292936.2	267.871820	−29.493391	0.1	5.8	818.9	30.1	58.1	393.4	0.90	26.7	<-5	....	c	817.4	2.0	1.3×10^{-14}
1050	175129.23−293605.2	267.871830	−29.601467	0.1	0.8	8.1	4.1	4.9	0.0	0.89	1.7	-2.7	....	a	882.3	1.2	7.4×10^{-17}
1051	175129.25−293849.7	267.871910	−29.647166	0.2	3.4	27.9	7.2	16.1	14.0	0.89	3.6	<-5	....	a	845.7	2.1	4.5×10^{-16}
1052	175129.30−293756.0	267.872100	−29.632231	0.1	2.5	14.2	5.6	11.8	9.7	0.89	2.3	-3.5	....	a	873.3	2.4	2.6×10^{-16}
1053	175129.33−293746.3	267.872210	−29.629531	0.2	2.4	11.8	5.1	9.2	5.9	0.90	2.1	-3.1	....	a	876.6	2.0	1.7×10^{-16}
1054	175129.34−293126.4	267.872270	−29.524012	0.2	4.0	12.7	6.4	21.3	5.7	0.90	1.8	-2.1	....	a	860.7	2.1	2.0×10^{-16}

(*cont.*)

Table A.1: *Chandra* source list

Source		Position				Extracted Counts							Characteristics				
Seq	CXOU J	R. A.	Decl.	Err	θ	$C_{\rm net}$	$\Delta C_{\rm net}$	$C'_{\rm bkg}$	$C_{\rm net,hard}$	PSF	PS	$P_{\rm B}$	Anom	Var	EffExp	$E_{\rm median}$	Photo $F_{\rm x}$
#		(deg)	(deg)	($''$)	($'$)						Frac				(ks)	(keV)	(ergs s^{-1} cm^{-2})
(1)	(2)	(3)	(4)	(5)	(6)	(7)	(8)	(9)	(10)	(11)	(12)	(13)	(14)	(15)	(16)	(17)	(18)
1055	175129.38−292950.9	267.872430	−29.497482	0.2	5.6	28.3	8.5	33.7	11.8	0.82	3.1	-4.9	....	b	824.5	1.7	4.1×10^{-16}
1056	175129.38−293233.6	267.872430	−29.542684	0.2	2.9	13.1	5.2	8.9	0.0	0.89	2.3	-3.7	....	a	849.1	1.1	2.5×10^{-16}
1057	175129.38−293033.4	267.872440	−29.509289	0.2	4.9	22.5	8.1	34.5	9.8	0.90	2.6	-3.5	....	a	842.1	1.5	2.0×10^{-16}
1058	175129.38−293210.8	267.872450	−29.536338	0.2	3.3	17.2	5.9	11.8	5.7	0.90	2.6	-4.6	....	a	851.4	1.6	1.1×10^{-16}
1059	175129.41−293446.5	267.872580	−29.579585	0.0	0.8	370.5	19.9	5.5	246.3	0.90	18.1	<-5	....	b	869.4	2.6	7.3×10^{-15}
1060	175129.42−292946.3	267.872590	−29.496212	0.1	5.6	131.3	14.1	52.7	20.9	0.89	9.0	<-5	....	b	820.1	1.3	1.3×10^{-15}
1061	175129.45−293920.3	267.872740	−29.655663	0.1	4.0	43.0	8.5	21.0	14.5	0.90	4.7	<-5	g...	...	793.6	1.7	5.2×10^{-16}
1062	175129.45−293340.7	267.872750	−29.561310	0.1	1.8	36.6	7.1	6.4	14.9	0.90	4.8	<-5	g...	...	839.8	1.8	5.9×10^{-16}
1063	175129.46−293838.6	267.872790	−29.644077	0.2	3.3	17.9	6.7	20.1	0.4	0.89	2.5	-3.5	....	a	857.4	1.0	1.4×10^{-16}
1064	175129.47−293520.2	267.872800	−29.588966	0.1	0.5	8.1	4.0	3.9	1.6	0.89	1.8	-3.0	g...	...	690.5	1.2	9.1×10^{-17}
1065	175129.48−293331.1	267.872870	−29.558642	0.1	2.0	34.0	6.9	6.0	15.8	0.87	4.6	<-5	....	a	846.5	1.8	4.7×10^{-16}
1066	175129.55−294017.1	267.873130	−29.671424	0.2	4.9	81.4	11.4	35.6	3.2	0.90	6.8	<-5	g...	...	720.8	1.1	8.2×10^{-16}
1067	175129.56−293602.7	267.873180	−29.600776	0.1	0.7	47.9	7.8	5.1	20.8	0.89	5.7	<-5	g...	...	862.5	1.8	6.8×10^{-16}
1068	175129.57−293713.1	267.873240	−29.620314	0.1	1.9	36.4	7.2	7.6	10.5	0.90	4.7	<-5	....	a	884.9	1.8	4.7×10^{-16}
1069	175129.58−293137.1	267.873280	−29.526983	0.2	3.8	15.4	6.5	19.6	5.1	0.90	2.2	-2.9	....	a	851.1	1.8	2.1×10^{-16}
1070	175129.59−293406.5	267.873320	−29.568491	0.1	1.4	8.2	4.3	5.8	2.0	0.90	1.7	-2.5	....	a	843.3	1.2	7.3×10^{-17}
1071	175129.62−293331.2	267.873440	−29.558684	0.1	2.0	88.6	10.3	7.4	82.4	0.90	8.2	<-5	g...	...	838.8	3.6	2.4×10^{-15}
1072	175129.63−293334.2	267.873490	−29.559501	0.1	1.9	14.0	5.1	7.0	10.7	0.91	2.5	-4.6	g...	...	839.7	3.8	4.1×10^{-16}
1073	175129.65−293616.3	267.873550	−29.604529	0.1	0.9	17.6	5.3	5.4	9.3	0.89	3.0	<-5	g...	...	865.2	2.1	6.8×10^{-17}
1074	175129.65−293436.4	267.873560	−29.576796	0.1	1.0	7.0	4.0	5.0	0.7	0.89	1.5	-2.2	....	a	875.9	1.3	2.8×10^{-16}
1075	175129.79−293905.6	267.874160	−29.651558	0.2	3.7	23.2	7.1	19.8	16.9	0.90	3.0	<-5	....	c	849.9	3.4	6.2×10^{-16}
1076	175129.83−293321.4	267.874310	−29.555960	0.1	2.2	65.7	9.1	7.3	29.6	0.90	6.8	<-5	g...	...	837.4	1.9	9.6×10^{-16}
1077	175129.85−294307.9	267.874410	−29.718876	0.1	7.6	824.9	31.3	117.1	143.2	0.90	26.0	<-5	g...	...	495.1	1.3	1.6×10^{-14}
1078	175129.88−292949.8	267.874540	−29.497167	0.3	5.6	19.3	9.1	52.7	11.5	0.90	2.0	-2.1	....	a	808.9	2.3	3.6×10^{-16}
1079	175129.93−293206.7	267.874740	−29.535216	0.2	3.4	18.7	6.1	12.3	11.9	0.90	2.8	<-5	....	a	833.7	2.4	3.4×10^{-16}
1080	175129.97−293300.3	267.874890	−29.550107	0.1	2.5	57.4	8.6	7.6	13.0	0.89	6.3	<-5	g...	...	833.9	1.4	6.3×10^{-16}
1081	175129.99−292956.4	267.874960	−29.499006	0.2	5.5	26.9	9.3	49.1	18.0	0.90	2.7	-3.5	....	b	811.3	3.5	7.4×10^{-16}
1082	175130.01−293456.8	267.875070	−29.582462	0.1	0.8	42.9	7.5	6.1	1.1	0.89	5.3	<-5	....	a	889.3	1.2	3.6×10^{-16}
1083	175130.06−293613.4	267.875290	−29.603734	0.0	0.9	643.2	26.0	5.8	470.2	0.89	24.3	<-5	g...	...	863.5	2.9	1.4×10^{-14}
1084	175130.07−294046.0	267.875320	−29.679448	0.2	5.4	27.0	9.6	54.0	0.0	0.90	2.7	-3.3	g...	...	716.1	1.0	2.6×10^{-16}
1085	175130.08−293349.8	267.875370	−29.563858	0.1	1.7	26.2	6.2	5.8	5.3	0.90	3.9	<-5	....	a	865.9	1.4	2.8×10^{-16}
1086	175130.09−292838.3	267.875390	−29.477329	0.3	6.8	54.7	12.8	93.3	29.5	0.90	4.1	<-5	....	a	801.8	2.2	9.8×10^{-16}
1087	175130.11−294216.4	267.875500	−29.704583	0.3	6.9	54.9	13.5	110.1	2.1	0.90	3.9	<-5	g...	...	654.9	1.4	8.0×10^{-16}
1088	175130.12−293711.7	267.875540	−29.619925	0.1	1.9	20.7	5.8	7.3	14.4	0.90	3.3	<-5	....	a	875.0	3.7	5.8×10^{-16}

(*cont.*)

Table A.1: *Chandra* source list

Source		Position				Extracted Counts							Characteristics				
Seq	CXOU J	R. A.	Decl.	Err	θ	$C_{\rm net}$	$\Delta C_{\rm net}$	$C'_{\rm bkg}$	$C_{\rm net,hard}$	PSF	PS	$P_{\rm B}$	Anom	Var	EffExp	$E_{\rm median}$	Photo $F_{\rm x}$
#		(deg)	(deg)	($''$)	($'$)						Frac				(ks)	(keV)	(ergs s^{-1} cm^{-2})
(1)	(2)	(3)	(4)	(5)	(6)	(7)	(8)	(9)	(10)	(11)	(12)	(13)	(14)	(15)	(16)	(17)	(18)
1089	175130.14−293144.0	267.875590	−29.528908	0.1	3.8	40.8	8.2	17.2	18.3	0.90	4.7	<-5	....	a	828.9	1.9	6.0×10^{-16}
1090	175130.15−293633.3	267.875660	−29.609261	0.1	1.3	15.5	5.1	5.5	0.3	0.90	2.7	<-5	g...	...	856.1	1.2	1.5×10^{-16}
1091	175130.19−293636.7	267.875820	−29.610207	0.1	1.3	7.7	4.1	5.3	5.3	0.90	1.6	-2.4	g...	...	854.4	3.1	1.9×10^{-16}
1092	175130.23−293133.1	267.876000	−29.525872	0.1	3.9	50.3	8.9	19.7	23.4	0.90	5.3	<-5	....	a	823.6	1.8	6.9×10^{-16}
1093	175130.39−293220.4	267.876660	−29.539020	0.1	3.2	21.6	6.1	9.4	2.4	0.90	3.2	<-5	g...	...	824.7	1.3	2.2×10^{-16}
1094	175130.44−293500.2	267.876840	−29.583416	0.1	0.8	16.4	5.3	6.6	2.0	0.90	2.8	<-5	....	a	884.3	1.0	1.2×10^{-16}
1095	175130.49−293712.4	267.877050	−29.620122	0.1	1.9	24.3	6.1	6.7	11.9	0.90	3.7	<-5	g...	...	850.6	1.9	3.6×10^{-16}
1096	175130.51−292724.0	267.877160	−29.456690	0.3	8.0	31.7	14.9	170.3	25.5	0.90	2.1	-2.0	....	b	763.9	4.6	1.2×10^{-15}
1097	175130.51−293200.0	267.877160	−29.533335	0.1	3.5	32.3	7.4	14.7	14.1	0.90	4.1	<-5	....	a	820.1	1.9	4.8×10^{-16}
1098	175130.60−293306.2	267.877520	−29.551744	0.1	2.4	11.7	5.0	8.3	2.3	0.89	2.1	-3.3	....	a	864.5	1.1	9.9×10^{-17}
1099	175130.62−293227.7	267.877590	−29.541043	0.0	3.1	290.2	17.8	9.8	4.2	0.90	15.8	<-5	....	a	838.1	0.9	2.0×10^{-15}
1100	175130.62−293504.8	267.877590	−29.584693	0.1	0.8	13.1	4.9	5.9	0.0	0.89	2.4	-4.6	....	a	847.6	0.8	8.2×10^{-17}
1101	175130.63−293600.3	267.877640	−29.600084	0.1	0.9	11.3	4.5	4.7	3.6	0.89	2.2	-4.3	g...	...	816.3	1.3	1.3×10^{-16}
1102	175130.67−293429.2	267.877800	−29.574801	0.1	1.2	21.0	5.7	6.0	4.0	0.89	3.3	<-5	....	a	862.3	1.3	2.1×10^{-16}
1103	175130.67−293441.5	267.877800	−29.578217	0.1	1.0	10.8	4.5	5.2	2.2	0.89	2.1	-3.8	....	...	884.6	1.4	1.1×10^{-16}
1104	175130.67−293632.1	267.877810	−29.608933	0.1	1.3	31.6	6.6	5.4	17.1	0.89	4.4	<-5	g...	...	825.6	2.3	6.2×10^{-16}
1105	175130.71−293120.3	267.878000	−29.522313	0.2	4.2	15.9	6.6	20.1	4.4	0.90	2.2	-3.0	....	a	817.0	1.4	1.8×10^{-16}
1106	175130.72−293323.0	267.878030	−29.556396	0.1	2.2	19.0	5.7	8.0	1.3	0.90	3.0	<-5	....	b	873.7	1.3	1.8×10^{-16}
1107	175130.73−293232.5	267.878080	−29.542376	0.0	3.0	453.0	22.0	10.0	325.1	0.90	20.1	<-5	....	a	845.9	3.0	1.0×10^{-14}
1108	175130.74−294111.7	267.878110	−29.686594	0.2	5.8	33.8	10.8	70.2	21.2	0.90	3.0	-3.9	g...	...	733.1	2.1	6.2×10^{-16}
1109	175130.77−293742.4	267.878230	−29.628459	0.1	2.4	10.9	4.9	8.1	3.0	0.90	2.0	-3.0	g...	...	843.8	1.8	1.6×10^{-16}
1110	175130.79−293908.8	267.878300	−29.652468	0.2	3.8	31.0	7.7	20.0	7.4	0.90	3.8	<-5	....	a	857.4	1.4	3.2×10^{-16}
1111	175130.80−293736.5	267.878370	−29.626817	0.0	2.3	722.1	27.5	7.9	387.1	0.90	25.8	<-5	g...	...	834.9	2.1	1.2×10^{-14}
1112	175130.85−293204.1	267.878550	−29.534478	0.2	3.5	12.5	5.5	12.5	5.0	0.90	2.0	-2.8	....	a	819.2	1.8	1.8×10^{-16}
1113	175130.87−293620.5	267.878630	−29.605711	0.1	1.2	13.5	4.8	4.5	1.6	0.89	2.5	<-5	g...	...	821.2	1.2	1.5×10^{-16}
1114	175130.87−293627.1	267.878650	−29.607541	0.1	1.2	13.1	4.8	4.9	6.3	0.89	2.5	<-5	g...	...	792.5	1.8	2.2×10^{-16}
1115	175130.89−293915.9	267.878740	−29.654432	0.2	3.9	12.5	6.4	21.5	4.7	0.90	1.8	-2.1	....	a	855.9	1.5	1.4×10^{-16}
1116	175130.93−293508.1	267.878900	−29.585597	0.1	0.8	24.2	6.0	5.8	9.3	0.89	3.7	<-5	g...	...	803.8	1.6	3.2×10^{-16}
1117	175130.97−294000.5	267.879060	−29.666809	0.2	4.7	27.6	8.6	36.4	7.9	0.90	3.0	-4.5	....	c	836.6	1.3	2.9×10^{-16}
1118	175130.98−293921.7	267.879120	−29.656039	0.1	4.0	106.6	11.9	22.4	0.0	0.90	8.6	<-5	....	a	854.3	1.0	8.3×10^{-16}
1119	175131.00−293932.4	267.879170	−29.659023	0.2	4.2	39.7	8.6	25.3	9.0	0.90	4.3	<-5	....	b	850.6	1.7	5.2×10^{-16}
1120	175131.01−293335.7	267.879230	−29.559942	0.1	2.0	18.7	5.7	8.3	5.4	0.91	3.0	<-5	....	b	885.7	1.7	2.3×10^{-16}
1121	175131.02−293430.5	267.879270	−29.575161	0.1	1.2	12.2	4.8	5.8	5.2	0.89	2.3	-4.3	....	a	865.5	1.9	1.8×10^{-16}
1122	175131.04−293718.5	267.879370	−29.621814	0.1	2.0	13.9	5.0	6.1	1.2	0.90	2.5	<-5	g...	...	839.0	0.9	9.9×10^{-17}

(*cont.*)

Table A.1: *Chandra* source list

Source		Position				Extracted Counts							Characteristics				
Seq	CXOU J	R. A.	Decl.	Err	θ	$C_{\rm net}$	$\Delta C_{\rm net}$	$C'_{\rm bkg}$	$C_{\rm net,hard}$	PSF	PS	$P_{\rm B}$	Anom	Var	EffExp	$E_{\rm median}$	Photo $F_{\rm x}$
#		(deg)	(deg)	($''$)	($'$)						Frac				(ks)	(keV)	(ergs s^{-1} cm^{-2})
(1)	(2)	(3)	(4)	(5)	(6)	(7)	(8)	(9)	(10)	(11)	(12)	(13)	(14)	(15)	(16)	(17)	(18)
1123	175131.08−293216.9	267.879510	−29.538050	0.1	3.2	126.7	12.2	10.3	40.2	0.89	9.9	<-5	....	a	840.9	1.6	1.6×10^{-15}
1124	175131.10−293318.4	267.879610	−29.555121	0.1	2.2	28.3	6.5	7.7	10.4	0.90	4.0	<-5	....	a	877.9	1.6	3.3×10^{-16}
1125	175131.11−293311.2	267.879660	−29.553121	0.1	2.4	13.5	5.1	7.5	6.7	0.89	2.4	-4.2	....	b	874.1	2.2	2.2×10^{-16}
1126	175131.12−293510.1	267.879680	−29.586144	0.1	0.8	14.5	5.0	5.5	5.6	0.90	2.6	<-5	g...	...	762.1	1.5	1.9×10^{-16}
1127	175131.17−293833.5	267.879890	−29.642642	0.2	3.2	12.0	6.2	20.0	2.8	0.89	1.8	-2.0	....	a	850.2	1.3	1.2×10^{-16}
1128	175131.23−293443.4	267.880140	−29.578737	0.1	1.1	33.0	6.8	6.0	23.1	0.89	4.5	<-5	....	a	883.5	2.6	6.3×10^{-16}
1129	175131.27−293408.9	267.880310	−29.569140	0.1	1.5	10.3	4.5	5.7	0.0	0.90	2.0	-3.4	....	a	864.0	1.2	8.8×10^{-17}
1130	175131.32−292743.6	267.880510	−29.462122	0.3	7.7	50.7	10.7	52.3	17.5	0.64	4.5	<-5	....	a	778.9	1.7	1.0×10^{-15}
1131	175131.34−293521.9	267.880600	−29.589419	0.1	0.8	18.3	5.2	3.7	10.7	0.89	3.2	<-5	g...	...	649.7	2.7	5.0×10^{-16}
1132	175131.35−293703.9	267.880640	−29.617764	0.1	1.8	19.9	5.5	5.1	8.2	0.90	3.3	<-5	g...	...	791.1	1.6	2.8×10^{-16}
1133	175131.36−292907.9	267.880680	−29.485554	0.2	6.4	139.8	15.3	76.2	99.1	0.90	8.8	<-5	....	a	793.7	3.0	3.5×10^{-15}
1134	175131.37−293303.7	267.880750	−29.551031	0.1	2.5	49.1	8.1	7.9	13.5	0.89	5.7	<-5	....	c	880.5	1.5	5.2×10^{-16}
1135	175131.42−293446.5	267.880930	−29.579611	0.0	1.1	64.2	8.9	5.8	14.3	0.89	6.8	<-5	....	a	880.8	1.4	6.4×10^{-16}
1136	175131.43−294033.2	267.880980	−29.675906	0.2	5.2	25.1	9.5	53.9	14.0	0.90	2.5	-3.0	....	a	826.1	2.3	4.7×10^{-16}
1137	175131.46−294335.1	267.881090	−29.726442	0.3	8.1	24.2	8.3	34.8	8.9	0.50	2.8	-3.8	g...	...	620.7	1.6	8.1×10^{-16}
1138	175131.50−293536.1	267.881250	−29.593387	0.1	0.9	8.0	3.9	3.0	0.0	0.90	1.8	-3.4	g...	...	630.0	1.3	1.1×10^{-16}
1139	175131.53−293339.5	267.881410	−29.560997	0.1	2.0	12.8	5.1	8.2	2.5	0.91	2.2	-3.7	....	a	878.3	1.0	9.3×10^{-17}
1140	175131.53−293559.8	267.881410	−29.599947	0.1	1.0	20.0	5.4	4.0	4.6	0.89	3.3	<-5	g...	...	798.4	1.5	2.7×10^{-16}
1141	175131.53−293613.5	267.881410	−29.603767	0.1	1.2	11.3	4.5	4.7	0.5	0.89	2.2	-4.3	g...	...	820.7	1.3	1.2×10^{-16}
1142	175131.55−293623.6	267.881490	−29.606575	0.1	1.3	7.8	4.1	5.2	1.5	0.89	1.7	-2.5	g...	...	829.9	1.4	9.4×10^{-17}
1143	175131.57−292855.4	267.881570	−29.482076	0.3	6.6	34.3	11.7	87.7	25.0	0.90	2.8	-3.4	....	b	786.1	2.7	7.6×10^{-16}
1144	175131.59−293647.6	267.881630	−29.613249	0.1	1.6	17.1	5.3	5.9	11.3	0.90	2.9	<-5	g...	...	831.2	2.7	1.2×10^{-16}
1145	175131.59−293632.2	267.881640	−29.608957	0.1	1.4	11.4	4.7	5.6	0.0	0.90	2.2	-4.0	g...	...	832.6	1.3	3.8×10^{-16}
1146	175131.60−293038.4	267.881700	−29.510677	0.2	4.9	61.6	10.3	33.4	48.1	0.90	5.7	<-5	g...	...	789.8	3.0	1.5×10^{-15}
1147	175131.63−293205.1	267.881820	−29.534765	0.1	3.4	29.4	7.0	12.6	10.1	0.90	3.9	<-5	....	b	826.0	1.7	3.9×10^{-16}
1148	175131.66−293450.0	267.881940	−29.580569	0.1	1.1	17.6	5.3	5.4	11.3	0.89	3.0	<-5	....	a	882.3	2.3	2.9×10^{-16}
1149	175131.68−292957.0	267.882010	−29.499183	0.0	5.6	2908.3	54.9	51.7	2276.9	0.90	52.5	<-5	....	b	793.8	3.3	7.9×10^{-14}
1150	175131.69−293224.1	267.882050	−29.540051	0.1	3.1	42.1	7.7	9.9	22.2	0.90	5.1	<-5	....	a	851.6	2.0	6.5×10^{-16}
1151	175131.76−293350.4	267.882350	−29.564023	0.1	1.8	29.3	6.5	6.7	12.9	0.90	4.1	<-5	....	b	881.8	1.9	3.9×10^{-16}
1152	175131.77−293459.9	267.882400	−29.583329	0.1	1.0	19.3	5.5	5.7	3.2	0.89	3.2	<-5	....	a	876.3	1.1	1.6×10^{-16}
1153	175131.78−293723.3	267.882440	−29.623147	0.1	2.2	22.8	5.9	6.2	2.8	0.90	3.5	<-5	g...	...	794.7	1.2	2.5×10^{-16}
1154	175131.80−293909.2	267.882520	−29.652564	0.2	3.9	16.0	6.5	19.0	8.0	0.90	2.3	-3.1	g...	...	811.8	1.9	2.6×10^{-16}
1155	175131.82−293757.3	267.882620	−29.632584	0.2	2.7	13.9	5.2	8.1	5.9	0.90	2.4	-4.3	g...	...	805.2	1.9	2.3×10^{-16}
1156	175131.84−293420.8	267.882670	−29.572471	0.1	1.4	10.3	4.5	5.7	9.0	0.90	2.0	-3.4	....	a	845.7	4.0	3.1×10^{-16}

(*cont.*)

Table A.1: *Chandra* source list

Source		Position				Extracted Counts							Characteristics				
Seq	CXOU J	R. A.	Decl.	Err	θ	$C_{\rm net}$	$\Delta C_{\rm net}$	$C'_{\rm bkg}$	$C_{\rm net,hard}$	PSF	PS	$P_{\rm B}$	Anom	Var	EffExp	$E_{\rm median}$	Photo $F_{\rm x}$
#		(deg)	(deg)	($''$)	($'$)						Frac				(ks)	(keV)	(ergs s^{-1} cm^{-2})
(1)	(2)	(3)	(4)	(5)	(6)	(7)	(8)	(9)	(10)	(11)	(12)	(13)	(14)	(15)	(16)	(17)	(18)
1157	175131.84−293601.6	267.882690	−29.600448	0.1	1.1	9.4	4.1	3.6	0.7	0.89	2.0	-3.9	g...	...	840.8	1.5	1.2×10^{-16}
1158	175131.86−294331.0	267.882770	−29.725295	0.3	8.1	40.1	9.2	34.9	24.7	0.51	4.1	<-5	g...	...	604.0	2.5	2.8×10^{-15}
1159	175131.86−293750.8	267.882780	−29.630784	0.1	2.6	106.4	11.2	7.6	70.2	0.89	9.1	<-5	g...	...	799.6	2.9	2.0×10^{-15}
1160	175131.87−293211.3	267.882830	−29.536498	0.1	3.3	23.3	6.4	10.7	7.6	0.90	3.4	<-5	....	a	844.2	1.7	3.1×10^{-16}
1161	175131.89−293109.3	267.882880	−29.519263	0.2	4.4	15.2	6.7	22.8	6.4	0.89	2.1	-2.6	....	a	818.6	1.6	1.9×10^{-16}
1162	175131.93−293816.2	267.883070	−29.637847	0.2	3.0	12.3	5.6	13.7	3.2	0.90	2.0	-2.6	g...	...	804.7	1.7	1.9×10^{-16}
1163	175131.96−293151.0	267.883190	−29.530835	0.2	3.7	16.1	6.1	14.9	2.1	0.90	2.4	-3.6	....	b	843.9	1.3	1.6×10^{-16}
1164	175131.97−293935.1	267.883220	−29.659760	0.1	4.3	61.9	10.0	28.1	27.6	0.90	5.9	<-5	g...	...	817.5	1.8	1.8×10^{-16}
1165	175131.97−293522.2	267.883230	−29.589519	0.1	0.9	6.5	3.7	3.5	3.6	0.90	1.5	-2.4	g...	...	623.4	2.6	9.3×10^{-16}
1166	175131.99−293345.1	267.883320	−29.562553	0.1	1.9	12.3	5.0	7.7	8.7	0.91	2.2	-3.7	....	a	881.3	2.3	2.0×10^{-16}
1167	175132.04−294109.7	267.883500	−29.686041	0.2	5.8	34.1	11.0	73.9	3.4	0.90	3.0	-3.8	....	a	812.0	1.4	3.8×10^{-16}
1168	175132.05−292746.0	267.883560	−29.462789	0.3	7.7	65.5	12.8	82.5	49.5	0.76	4.9	<-5	....	a	758.7	2.7	1.8×10^{-15}
1169	175132.07−294118.7	267.883650	−29.688544	0.3	6.0	22.5	10.7	79.5	4.3	0.90	2.0	-2.0	....	a	809.1	1.8	3.2×10^{-16}
1170	175132.08−293418.3	267.883680	−29.571773	0.1	1.5	18.6	5.5	6.4	0.0	0.90	3.1	<-5	....	a	842.4	1.0	1.4×10^{-16}
1171	175132.10−293252.1	267.883770	−29.547810	0.1	2.7	18.3	5.8	9.7	10.7	0.89	2.9	<-5	....	a	853.7	3.0	4.2×10^{-16}
1172	175132.11−293011.0	267.883820	−29.503082	0.2	5.3	21.1	8.8	45.9	5.3	0.90	2.3	-2.6	....	b	805.0	1.5	2.6×10^{-16}
1173	175132.12−294059.0	267.883870	−29.683069	0.1	5.7	147.7	15.3	69.3	133.5	0.90	9.3	<-5	....	a	815.6	4.1	4.8×10^{-15}
1174	175132.15−293629.3	267.883990	−29.608147	0.1	1.4	9.0	4.3	5.0	4.6	0.90	1.9	-3.1	g...	...	821.7	2.7	2.1×10^{-16}
1175	175132.17−294000.8	267.884070	−29.666889	0.2	4.7	22.3	7.8	29.7	6.4	0.87	2.7	-3.8	....	b	816.5	1.5	2.9×10^{-16}
1176	175132.20−292732.8	267.884170	−29.459136	0.3	7.9	18.7	8.6	45.3	6.9	0.60	2.0	-2.2	....	a	750.5	1.6	4.0×10^{-16}
1177	175132.28−293307.4	267.884520	−29.552069	0.1	2.5	13.0	5.1	8.0	4.2	0.89	2.3	-3.9	....	b	857.1	1.3	1.3×10^{-16}
1178	175132.28−293914.1	267.884530	−29.653930	0.2	4.0	23.5	7.2	20.5	6.2	0.90	3.0	<-5	g...	...	795.6	1.4	2.8×10^{-16}
1179	175132.32−293454.7	267.884670	−29.581884	0.0	1.2	195.3	14.7	6.7	130.9	0.89	12.8	<-5	....	a	880.6	2.7	3.9×10^{-15}
1180	175132.33−292818.6	267.884710	−29.471840	0.3	7.2	52.6	13.5	112.4	32.7	0.89	3.8	<-5	....	a	750.8	2.6	1.2×10^{-15}
1181	175132.33−294138.1	267.884710	−29.693926	0.2	6.3	68.1	13.2	90.9	3.0	0.90	5.0	<-5	....	b	800.6	1.3	7.4×10^{-16}
1182	175132.37−293246.8	267.884900	−29.546337	0.1	2.8	33.0	7.0	9.0	16.8	0.89	4.4	<-5	....	a	847.7	2.0	5.0×10^{-16}
1183	175132.38−294230.6	267.884950	−29.708515	0.2	7.2	88.0	16.0	147.0	63.9	0.90	5.3	<-5	....	a	754.6	2.9	2.2×10^{-15}
1184	175132.40−293405.7	267.885010	−29.568258	0.1	1.7	7.9	4.3	6.1	1.2	0.90	1.6	-2.3	....	a	863.5	1.1	6.6×10^{-17}
1185	175132.40−293740.6	267.885030	−29.627963	0.1	2.5	15.0	5.2	7.0	3.5	0.89	2.6	<-5	g...	...	836.9	1.4	1.8×10^{-16}
1186	175132.41−293329.3	267.885080	−29.558164	0.1	2.2	10.9	4.8	7.1	4.7	0.90	2.0	-3.3	....	a	868.0	1.7	1.3×10^{-16}
1187	175132.42−293357.0	267.885100	−29.565836	0.1	1.8	8.8	4.5	7.2	2.9	0.90	1.7	-2.4	....	a	862.6	1.4	3.6×10^{-16}
1188	175132.42−292944.3	267.885120	−29.495647	0.2	5.8	28.5	9.8	56.5	8.5	0.89	2.8	-3.5	....	b	788.0	1.5	9.5×10^{-17}
1189	175132.44−293253.7	267.885200	−29.548264	0.1	2.7	40.2	7.5	8.8	25.1	0.89	5.0	<-5	....	a	848.0	2.3	7.0×10^{-16}
1190	175132.50−293112.1	267.885420	−29.520037	0.2	4.3	31.6	8.0	23.4	24.9	0.89	3.7	<-5	....	a	851.3	3.3	8.0×10^{-16}

(*cont.*)

Table A.1: *Chandra* source list

Source		Position				Extracted Counts							Characteristics				
Seq	CXOU J	R. A.	Decl.	Err	θ	$C_{\rm net}$	$\Delta C_{\rm net}$	$C'_{\rm bkg}$	$C_{\rm net,hard}$	PSF	PS	$P_{\rm B}$	Anom	Var	EffExp	$E_{\rm median}$	Photo $F_{\rm x}$
#		(deg)	(deg)	($''$)	($'$)						Frac				(ks)	(keV)	(ergs s^{-1} cm^{-2})
(1)	(2)	(3)	(4)	(5)	(6)	(7)	(8)	(9)	(10)	(11)	(12)	(13)	(14)	(15)	(16)	(17)	(18)
1191	175132.50−293421.5	267.885450	−29.572661	0.1	1.5	12.0	4.8	6.0	4.0	0.90	2.2	-4.1	....	a	844.2	1.6	1.5×10^{-16}
1192	175132.52−293636.2	267.885540	−29.610076	0.0	1.6	256.4	16.7	6.6	94.8	0.90	14.9	<-5	g...	...	864.5	1.7	3.4×10^{-15}
1193	175132.60−293349.5	267.885840	−29.563756	0.1	1.9	25.7	6.3	7.3	13.0	0.91	3.8	<-5	....	a	869.5	2.0	6.6×10^{-15}
1194	175132.60−294000.8	267.885850	−29.666897	0.2	4.7	23.2	8.0	31.8	8.8	0.90	2.7	-3.8	g...	...	774.1	1.7	3.7×10^{-16}
1195	175132.60−293131.1	267.885860	−29.525308	0.1	4.0	338.0	19.4	20.0	208.8	0.90	16.9	<-5	....	b	856.5	2.6	3.8×10^{-16}
1196	175132.70−293207.5	267.886280	−29.535431	0.2	3.5	16.8	5.9	12.2	4.0	0.90	2.6	-4.4	....	a	841.3	1.5	1.9×10^{-16}
1197	175132.74−293834.2	267.886450	−29.642834	0.2	3.4	16.3	6.5	18.7	4.9	0.89	2.3	-3.2	g...	...	803.6	1.4	2.0×10^{-16}
1198	175132.82−293314.9	267.886750	−29.554163	0.1	2.4	10.5	4.8	7.5	2.0	0.89	2.0	-3.0	....	a	843.3	1.2	9.9×10^{-17}
1199	175132.83−293546.2	267.886830	−29.596172	0.1	1.2	11.0	4.4	4.0	8.6	0.90	2.2	-4.5	g...	...	707.4	3.9	4.1×10^{-16}
1200	175132.95−293953.8	267.887320	−29.664960	0.2	4.6	48.6	9.6	32.4	25.5	0.90	4.8	<-5	g...	...	785.8	2.0	8.8×10^{-16}
1201	175132.96−293850.4	267.887350	−29.647350	0.2	3.6	11.8	6.0	18.2	0.0	0.90	1.8	-2.1	g...	...	805.9	1.4	3.0×10^{-15}
1202	175132.96−292734.1	267.887360	−29.459483	0.3	8.0	83.2	15.1	124.8	83.5	0.83	5.3	<-5	....	a	736.9	3.8	1.4×10^{-16}
1203	175132.97−292639.2	267.887390	−29.444233	0.4	8.6	61.6	11.7	61.4	14.3	0.90	5.0	<-5	g...	...	223.4	1.5	3.7×10^{-15}
1204	175132.97−293821.0	267.887400	−29.639178	0.2	3.2	14.1	5.8	13.9	3.0	0.89	2.2	-3.2	g...	...	819.5	1.4	1.6×10^{-16}
1205	175132.99−293436.8	267.887460	−29.576915	0.1	1.4	11.6	4.7	5.4	3.1	0.90	2.2	-4.1	....	a	865.0	1.4	1.2×10^{-16}
1206	175133.00−292854.9	267.887540	−29.481931	0.3	6.6	29.8	11.6	90.2	0.2	0.90	2.5	-2.7	....	a	767.5	1.2	2.9×10^{-16}
1207	175133.05−294247.6	267.887720	−29.713229	0.1	7.5	790.6	31.5	165.4	536.7	0.90	24.7	<-5	....	c	759.5	2.8	2.9×10^{-16}
1208	175133.05−293154.0	267.887740	−29.531694	0.1	3.7	35.2	7.6	14.8	2.3	0.90	4.3	<-5	....	b	857.9	1.1	1.9×10^{-14}
1209	175133.07−293527.9	267.887820	−29.591105	0.1	1.2	7.1	3.9	3.9	3.8	0.90	1.6	-2.5	g...	...	652.3	2.2	1.6×10^{-16}
1210	175133.11−292949.8	267.888000	−29.497184	0.2	5.7	47.5	10.8	56.5	31.8	0.90	4.2	<-5	....	a	801.2	2.4	9.3×10^{-16}
1211	175133.14−293535.7	267.888090	−29.593269	0.1	1.3	28.5	6.2	3.5	9.0	0.90	4.2	<-5	g...	...	648.4	1.6	4.7×10^{-16}
1212	175133.22−294158.5	267.888420	−29.699596	0.2	6.7	76.2	12.1	55.8	57.8	0.74	6.1	<-5	....	a	781.3	3.5	5.6×10^{-16}
1213	175133.22−293426.3	267.888430	−29.573990	0.1	1.6	61.2	8.7	5.8	5.9	0.90	6.6	<-5	g...	...	821.2	1.2	1.8×10^{-16}
1214	175133.22−293458.2	267.888440	−29.582838	0.1	1.3	16.0	5.1	5.0	2.0	0.90	2.8	<-5	....	a	841.9	1.5	2.8×10^{-15}
1215	175133.24−293718.4	267.888530	−29.621801	0.0	2.2	408.7	20.9	7.3	169.3	0.90	19.1	<-5	g...	...	853.8	1.8	5.7×10^{-15}
1216	175133.25−293630.6	267.888570	−29.608501	0.1	1.6	26.9	6.3	6.1	1.7	0.90	3.9	<-5	g...	...	840.4	1.1	1.2×10^{-16}
1217	175133.25−293243.0	267.888580	−29.545294	0.2	3.0	12.8	5.2	9.2	3.8	0.89	2.2	-3.5	....	a	852.0	1.3	2.5×10^{-16}
1218	175133.29−293508.7	267.888710	−29.585756	0.1	1.2	19.2	5.5	5.8	8.3	0.90	3.2	<-5	g...	...	725.6	1.9	1.5×10^{-16}
1219	175133.29−293722.9	267.888710	−29.623036	0.1	2.3	23.1	6.1	7.9	8.2	0.90	3.5	<-5	g...	...	853.1	1.7	3.2×10^{-16}
1220	175133.29−293046.6	267.888720	−29.512948	0.2	4.8	14.5	7.2	29.5	2.1	0.90	1.9	-2.1	....	a	822.2	1.3	3.2×10^{-16}
1221	175133.31−293430.8	267.888810	−29.575239	0.0	1.5	200.7	14.9	5.3	179.1	0.90	13.0	<-5	....	a	833.8	3.6	5.6×10^{-15}
1222	175133.38−293924.9	267.889120	−29.656944	0.1	4.2	70.2	10.3	24.8	46.8	0.90	6.5	<-5	g...	...	790.8	2.6	1.7×10^{-15}
1223	175133.41−293620.4	267.889220	−29.605676	0.0	1.5	108.2	11.2	6.8	13.1	0.90	9.2	<-5	g...	...	854.3	1.1	9.7×10^{-16}
1224	175133.46−294040.7	267.889430	−29.677996	0.1	5.4	176.8	15.8	54.2	95.9	0.90	10.9	<-5	g...	...	767.3	2.2	2.0×10^{-15}

(*cont.*)

Table A.1: *Chandra* source list

Source		Position				Extracted Counts							Characteristics				
Seq	CXOU J	R. A.	Decl.	Err	θ	$C_{\rm net}$	$\Delta C_{\rm net}$	$C'_{\rm bkg}$	$C_{\rm net,hard}$	PSF	PS	$P_{\rm B}$	Anom	Var	EffExp	$E_{\rm median}$	Photo $F_{\rm x}$
#		(deg)	(deg)	($''$)	($'$)						Frac				(ks)	(keV)	(ergs s^{-1} cm^{-2})
(1)	(2)	(3)	(4)	(5)	(6)	(7)	(8)	(9)	(10)	(11)	(12)	(13)	(14)	(15)	(16)	(17)	(18)
1225	175133.46−293400.8	267.889440	−29.566895	0.0	1.9	151.5	13.1	7.5	63.5	0.91	11.1	<-5	....	c	850.0	1.7	3.7×10^{-15}
1226	175133.52−294150.9	267.889700	−29.697484	0.2	6.6	102.6	13.3	58.4	79.3	0.77	7.4	<-5	g...	...	768.1	3.1	3.3×10^{-15}
1227	175133.53−293515.5	267.889740	−29.587646	0.1	1.3	54.7	8.2	4.3	2.5	0.89	6.3	<-5	g...	...	645.8	1.1	6.0×10^{-16}
1228	175133.58−293825.9	267.889920	−29.640543	0.1	3.3	53.4	8.8	14.6	41.3	0.90	5.7	<-5	g...	...	816.4	3.8	1.8×10^{-15}
1229	175133.60−293134.5	267.890030	−29.526267	0.0	4.0	379.5	20.6	23.5	262.5	0.90	18.0	<-5	....	b	836.5	3.0	8.7×10^{-15}
1230	175133.65−293516.5	267.890210	−29.587919	0.1	1.3	6.6	3.9	4.4	1.6	0.89	1.5	-2.2	g...	...	648.6	1.0	6.6×10^{-15}
1231	175133.65−293313.1	267.890230	−29.553655	0.0	2.6	318.8	18.6	8.2	195.6	0.89	16.7	<-5	....	a	864.4	2.8	6.6×10^{-17}
1232	175133.66−293708.0	267.890290	−29.618894	0.1	2.2	7.8	4.4	7.2	3.3	0.90	1.6	-2.1	g...	...	838.5	1.9	1.3×10^{-16}
1233	175133.68−293955.2	267.890350	−29.665341	0.2	4.7	19.5	7.8	32.5	10.9	0.90	2.3	-2.9	g...	...	771.0	2.0	3.8×10^{-16}
1234	175133.68−294022.0	267.890350	−29.672789	0.2	5.1	35.2	9.5	44.8	1.4	0.90	3.5	<-5	g...	...	782.6	1.2	3.9×10^{-16}
1235	175133.69−293804.7	267.890380	−29.634644	0.1	3.0	44.0	7.9	11.0	21.1	0.89	5.2	<-5	g...	...	839.4	2.0	7.2×10^{-16}
1236	175133.72−293744.9	267.890520	−29.629165	0.1	2.7	17.6	5.6	8.4	8.9	0.89	2.8	<-5	g...	...	851.5	2.0	2.8×10^{-16}
1237	175133.74−293308.9	267.890620	−29.552489	0.1	2.6	68.7	9.3	8.3	42.4	0.90	7.0	<-5	....	a	844.8	2.3	1.2×10^{-15}
1238	175133.76−293442.5	267.890700	−29.578489	0.1	1.5	29.6	6.5	6.4	12.9	0.90	4.2	<-5	....	c	869.8	1.9	4.2×10^{-16}
1239	175133.78−293652.4	267.890770	−29.614565	0.1	2.0	26.3	6.3	6.7	5.9	0.90	3.9	<-5	g...	...	854.6	1.4	3.0×10^{-16}
1240	175133.81−293109.5	267.890890	−29.519327	0.2	4.4	17.1	7.1	25.9	3.2	0.90	2.2	-2.8	....	a	829.9	1.2	1.6×10^{-16}
1241	175133.82−293423.0	267.890940	−29.573063	0.1	1.7	14.7	5.0	5.3	8.2	0.90	2.6	<-5	g...	...	810.5	2.0	2.3×10^{-16}
1242	175133.82−293431.6	267.890950	−29.575466	0.1	1.6	66.2	9.0	5.8	44.0	0.90	6.9	<-5	g...	...	822.2	2.5	1.3×10^{-15}
1243	175133.84−293201.5	267.891040	−29.533761	0.1	3.6	29.3	7.1	13.7	8.7	0.90	3.8	<-5	....	c	839.7	1.4	3.1×10^{-16}
1244	175133.96−292754.3	267.891540	−29.465108	0.1	7.6	406.3	24.4	158.7	297.0	0.90	16.3	<-5	....	b	772.6	3.2	1.1×10^{-14}
1245	175133.98−293550.2	267.891610	−29.597303	0.1	1.5	21.4	5.6	4.6	9.3	0.90	3.5	<-5	g...	...	784.9	1.9	3.5×10^{-16}
1246	175134.00−293338.6	267.891670	−29.560734	0.1	2.2	13.7	5.1	7.3	1.7	0.90	2.4	-4.4	....	a	852.7	1.5	1.5×10^{-16}
1247	175134.00−293634.7	267.891680	−29.609649	0.1	1.8	8.9	4.4	6.1	4.1	0.90	1.8	-2.7	g...	...	858.9	2.0	1.4×10^{-16}
1248	175134.01−293900.1	267.891710	−29.650031	0.1	3.8	87.2	10.9	20.8	60.4	0.90	7.6	<-5	g...	...	810.9	2.7	2.0×10^{-15}
1249	175134.03−293826.3	267.891810	−29.640644	0.1	3.3	84.3	10.5	15.7	52.0	0.90	7.6	<-5	g...	...	838.3	2.7	1.8×10^{-15}
1250	175134.04−292834.4	267.891840	−29.476235	0.2	7.0	67.1	13.9	109.9	44.0	0.90	4.6	<-5	....	c	794.3	2.7	1.5×10^{-15}
1251	175134.05−292928.6	267.891910	−29.491303	0.3	6.1	24.3	10.2	66.7	16.8	0.89	2.3	-2.5	....	a	795.6	2.2	4.4×10^{-16}
1252	175134.06−293103.9	267.891940	−29.517762	0.0	4.6	1390.3	38.2	26.7	840.8	0.90	36.0	<-5	....	c	823.2	2.5	2.8×10^{-14}
1253	175134.09−293752.7	267.892060	−29.631318	0.2	2.8	16.8	5.6	9.2	2.7	0.89	2.7	<-5	g...	...	834.5	1.5	2.2×10^{-16}
1254	175134.09−294200.8	267.892060	−29.700227	0.2	6.8	97.8	14.7	101.2	58.4	0.88	6.4	<-5	g...	...	743.7	2.6	2.6×10^{-15}
1255	175134.10−293416.9	267.892090	−29.571382	0.1	1.8	18.3	5.4	5.7	9.0	0.90	3.1	<-5	....	a	839.4	1.7	2.4×10^{-16}
1256	175134.15−292713.8	267.892330	−29.453844	0.3	8.3	52.5	16.1	185.5	34.0	0.90	3.2	-4.0	g...	...	690.5	2.4	1.2×10^{-15}
1257	175134.17−293909.0	267.892410	−29.652507	0.1	4.0	95.0	11.5	25.0	24.9	0.90	7.9	<-5	g...	...	809.0	1.4	1.2×10^{-15}
1258	175134.19−293018.5	267.892460	−29.505158	0.2	5.3	30.2	9.3	44.8	19.4	0.90	3.1	-4.5	....	a	805.8	2.5	6.2×10^{-16}

(*cont.*)

Table A.1: *Chandra* source list

Source		Position				Extracted Counts							Characteristics				
Seq	CXOU J	R. A.	Decl.	Err	θ	$C_{\rm net}$	$\Delta C_{\rm net}$	$C'_{\rm bkg}$	$C_{\rm net,hard}$	PSF	PS	$P_{\rm B}$	Anom	Var	EffExp	$E_{\rm median}$	Photo $F_{\rm x}$
#		(deg)	(deg)	($''$)	($'$)						Frac				(ks)	(keV)	(ergs s^{-1} cm^{-2})
(1)	(2)	(3)	(4)	(5)	(6)	(7)	(8)	(9)	(10)	(11)	(12)	(13)	(14)	(15)	(16)	(17)	(18)
1259	175134.22−293639.1	267.892590	−29.610865	0.1	1.9	26.1	6.3	6.9	11.0	0.90	3.8	<-5	g...	...	850.6	1.8	3.7×10^{-16}
1260	175134.27−293738.7	267.892800	−29.627436	0.1	2.6	17.0	5.5	8.0	12.8	0.89	2.8	<-5	g...	...	830.1	3.1	4.6×10^{-16}
1261	175134.29−293448.8	267.892890	−29.580244	0.1	1.6	9.3	4.3	4.7	2.5	0.90	1.9	-3.3	....	a	862.9	1.8	1.2×10^{-16}
1262	175134.38−293858.5	267.893250	−29.649584	0.1	3.9	39.5	8.2	19.5	12.0	0.89	4.5	<-5	g...	...	807.0	1.6	2.7×10^{-16}
1263	175134.38−293339.1	267.893280	−29.560879	0.1	2.3	25.6	6.3	7.4	6.8	0.90	3.8	<-5	....	a	870.7	1.4	5.7×10^{-16}
1264	175134.39−293057.8	267.893320	−29.516070	0.1	4.7	69.3	10.4	27.7	17.7	0.90	6.3	<-5	....	b	827.8	1.5	8.4×10^{-16}
1265	175134.41−293936.5	267.893410	−29.660163	0.2	4.4	24.0	7.8	28.0	6.2	0.90	2.9	-4.4	g...	...	810.4	1.7	3.5×10^{-16}
1266	175134.43−293312.9	267.893460	−29.553596	0.1	2.6	35.6	7.2	9.4	4.2	0.89	4.6	<-5	....	a	852.0	1.1	4.1×10^{-16}
1267	175134.43−293154.3	267.893480	−29.531768	0.1	3.8	31.9	7.5	16.1	11.5	0.90	4.0	<-5	....	c	836.7	1.6	2.9×10^{-16}
1268	175134.45−293716.1	267.893560	−29.621151	0.2	2.4	7.9	4.5	8.1	4.4	0.90	1.6	-2.0	g...	...	849.4	2.3	1.5×10^{-16}
1269	175134.47−293239.0	267.893640	−29.544176	0.1	3.1	81.6	10.2	11.4	54.4	0.89	7.6	<-5	....	a	849.6	2.8	1.8×10^{-15}
1270	175134.51−294042.4	267.893800	−29.678451	0.2	5.5	59.2	11.3	55.8	26.1	0.90	5.0	<-5	g...	...	792.9	1.9	9.9×10^{-16}
1271	175134.52−293351.5	267.893870	−29.564326	0.1	2.2	24.7	6.2	7.3	12.5	0.90	3.7	<-5	....	a	868.4	2.3	4.2×10^{-16}
1272	175134.52−293820.5	267.893870	−29.639040	0.2	3.3	10.4	5.5	13.6	8.5	0.89	1.7	-2.1	g...	...	824.6	2.6	2.3×10^{-16}
1273	175134.54−293407.4	267.893920	−29.568732	0.1	2.0	22.8	6.0	7.2	1.5	0.91	3.5	<-5	....	a	862.3	1.2	2.1×10^{-16}
1274	175134.55−293458.3	267.893980	−29.582862	0.1	1.6	14.7	5.1	6.3	4.9	0.90	2.6	<-5	g...	...	793.2	1.7	2.0×10^{-16}
1275	175134.61−293202.9	267.894220	−29.534147	0.1	3.7	29.3	7.2	14.7	14.2	0.90	3.8	<-5	....	a	844.2	1.9	4.2×10^{-16}
1276	175134.63−293733.7	267.894310	−29.626046	0.1	2.6	48.9	8.1	8.1	16.7	0.89	5.7	<-5	g...	...	850.2	1.7	6.5×10^{-16}
1277	175134.64−293609.4	267.894360	−29.602633	0.1	1.7	37.4	7.1	5.6	23.2	0.90	4.9	<-5	....	a	855.9	3.5	1.0×10^{-15}
1278	175134.64−293858.6	267.894360	−29.649625	0.2	3.9	22.6	7.1	20.4	4.6	0.88	3.0	-4.9	g...	...	832.4	1.5	2.9×10^{-16}
1279	175134.65−294144.3	267.894400	−29.695660	0.3	6.5	39.5	12.1	92.5	30.2	0.90	3.1	-4.1	g...	...	758.4	3.7	1.3×10^{-15}
1280	175134.69−293337.9	267.894570	−29.560545	0.1	2.3	27.4	6.4	6.6	9.0	0.87	4.0	<-5	....	a	859.6	1.6	3.1×10^{-15}
1281	175134.69−293118.9	267.894580	−29.521926	0.1	4.4	296.9	18.4	22.1	58.6	0.89	15.7	<-5	....	c	834.1	1.4	3.3×10^{-16}
1282	175134.70−293633.7	267.894620	−29.609375	0.1	1.9	11.3	4.8	6.7	2.1	0.90	2.1	-3.6	g...	...	839.7	1.2	1.1×10^{-16}
1283	175134.73−293826.3	267.894750	−29.640649	0.1	3.4	230.3	16.2	14.7	6.0	0.89	13.8	<-5	g...	...	826.9	1.0	1.9×10^{-15}
1284	175134.77−293035.7	267.894900	−29.509935	0.3	5.1	15.9	7.9	37.1	11.4	0.90	1.9	-2.0	....	a	824.5	2.8	3.5×10^{-16}
1285	175134.80−294214.1	267.895020	−29.703933	0.3	7.0	44.7	13.8	128.3	37.4	0.90	3.1	-4.2	g...	...	749.2	3.0	1.3×10^{-15}
1286	175134.81−293339.6	267.895060	−29.561010	0.1	2.3	35.8	7.1	7.2	12.5	0.87	4.7	<-5	....	a	861.3	1.8	4.8×10^{-16}
1287	175134.82−293243.0	267.895110	−29.545287	0.2	3.1	13.4	5.4	10.6	0.0	0.89	2.2	-3.5	....	a	848.8	1.4	1.4×10^{-16}
1288	175134.83−293211.9	267.895150	−29.536654	0.2	3.6	10.0	5.3	13.0	0.3	0.90	1.7	-2.1	....	a	850.4	1.2	9.0×10^{-17}
1289	175134.84−293127.2	267.895200	−29.524233	0.1	4.2	108.1	11.9	21.9	56.2	0.89	8.7	<-5	....	a	837.3	2.2	1.9×10^{-15}
1290	175134.85−293809.7	267.895230	−29.636039	0.0	3.2	243.5	16.5	11.5	200.0	0.89	14.3	<-5	g...	...	832.8	3.2	6.6×10^{-15}
1291	175134.86−293541.0	267.895260	−29.594736	0.1	1.6	8.8	4.3	5.2	3.7	0.90	1.8	-2.9	g...	...	656.9	1.6	1.4×10^{-16}
1292	175134.87−293327.8	267.895330	−29.557723	0.2	2.5	8.6	4.7	8.4	5.5	0.89	1.6	-2.2	....	a	857.7	3.2	2.1×10^{-16}

(*cont.*)

Table A.1: *Chandra* source list

Source		Position				Extracted Counts							Characteristics				
Seq	CXOU J	R. A.	Decl.	Err	θ	$C_{\rm net}$	$\Delta C_{\rm net}$	$C'_{\rm bkg}$	$C_{\rm net,hard}$	PSF	PS	$P_{\rm B}$	Anom	Var	EffExp	$E_{\rm median}$	Photo $F_{\rm x}$
#		(deg)	(deg)	($''$)	($'$)						Frac				(ks)	(keV)	(ergs s^{-1} cm^{-2})
(1)	(2)	(3)	(4)	(5)	(6)	(7)	(8)	(9)	(10)	(11)	(12)	(13)	(14)	(15)	(16)	(17)	(18)
1293	175134.89−293848.2	267.895380	−29.646744	0.1	3.7	47.5	8.8	20.5	32.0	0.90	5.1	<-5	g...	...	821.8	2.5	1.6×10^{-15}
1294	175134.89−293721.4	267.895410	−29.622632	0.1	2.5	66.9	9.2	9.1	48.1	0.89	6.8	<-5	g...	...	840.7	2.9	1.0×10^{-15}
1295	175134.90−293414.7	267.895430	−29.570750	0.2	2.0	7.4	4.3	6.6	0.5	0.91	1.5	-2.1	....	a	842.9	1.2	6.7×10^{-17}
1296	175134.91−293616.0	267.895470	−29.604455	0.1	1.8	9.8	4.5	6.2	2.0	0.90	1.9	-3.0	....	a	855.9	1.4	1.1×10^{-16}
1297	175134.92−293430.2	267.895530	−29.575079	0.1	1.8	33.1	6.9	6.9	22.6	0.90	4.5	<-5	g...	...	805.1	2.9	7.7×10^{-16}
1298	175134.93−293735.3	267.895560	−29.626490	0.2	2.7	12.6	5.2	9.4	5.2	0.89	2.2	-3.4	g...	...	842.4	1.9	1.9×10^{-16}
1299	175134.94−293451.9	267.895600	−29.581085	0.1	1.7	16.0	5.2	6.0	5.3	0.90	2.8	<-5	....	c	864.1	1.6	3.8×10^{-16}
1300	175134.94−293228.9	267.895620	−29.541364	0.1	3.3	27.7	6.8	11.3	8.7	0.89	3.8	<-5	....	b	856.2	1.8	1.9×10^{-16}
1301	175134.97−293233.0	267.895720	−29.542519	0.1	3.3	38.5	7.5	10.5	18.1	0.89	4.8	<-5	....	a	857.0	1.9	5.5×10^{-16}
1302	175135.00−293652.3	267.895860	−29.614550	0.1	2.1	11.7	4.9	7.3	3.7	0.90	2.1	-3.6	g...	...	843.7	1.2	1.1×10^{-16}
1303	175135.00−293937.9	267.895870	−29.660545	0.2	4.5	23.6	7.9	29.4	5.6	0.90	2.8	-4.1	g...	...	799.4	1.3	2.6×10^{-16}
1304	175135.11−293806.1	267.896310	−29.635038	0.1	3.1	30.2	7.0	11.8	27.9	0.90	4.0	<-5	g...	...	841.1	3.4	8.3×10^{-16}
1305	175135.14−293231.7	267.896440	−29.542149	0.2	3.3	18.9	6.0	11.1	11.7	0.89	2.9	<-5	....	a	852.7	2.1	3.0×10^{-16}
1306	175135.20−293429.8	267.896700	−29.574955	0.1	1.9	69.3	9.2	6.7	37.7	0.90	7.1	<-5	g...	...	822.6	2.1	1.1×10^{-15}
1307	175135.23−293054.4	267.896810	−29.515113	0.2	4.8	29.4	8.3	29.6	10.0	0.91	3.3	<-5	....	a	814.1	1.4	3.2×10^{-16}
1308	175135.27−293452.9	267.896960	−29.581382	0.1	1.7	20.1	5.7	6.9	5.9	0.90	3.2	<-5	....	b	830.1	1.6	2.5×10^{-16}
1309	175135.34−293508.6	267.897280	−29.585731	0.1	1.7	15.0	5.0	5.0	3.5	0.90	2.7	<-5	g...	...	626.9	1.2	1.8×10^{-16}
1310	175135.39−293358.2	267.897490	−29.566185	0.1	2.2	32.6	6.9	7.4	6.6	0.90	4.4	<-5	....	a	860.8	1.6	3.9×10^{-16}
1311	175135.41−293846.0	267.897570	−29.646120	0.2	3.8	22.6	7.1	20.4	8.9	0.90	2.9	-4.9	g...	...	827.3	1.7	3.2×10^{-16}
1312	175135.42−293355.3	267.897590	−29.565368	0.1	2.3	29.3	6.5	6.7	11.0	0.90	4.1	<-5	....	a	866.0	1.6	3.4×10^{-16}
1313	175135.42−293749.2	267.897590	−29.630336	0.2	2.9	16.5	5.6	9.5	8.8	0.89	2.7	-5.0	g...	...	832.0	2.3	3.1×10^{-16}
1314	175135.45−293415.1	267.897720	−29.570870	0.1	2.1	10.8	4.8	7.2	0.0	0.91	2.0	-3.2	....	a	840.6	1.2	9.8×10^{-17}
1315	175135.49−293559.8	267.897910	−29.599963	0.0	1.8	98.9	10.8	7.1	58.8	0.90	8.7	<-5	....	b	840.5	2.4	1.9×10^{-15}
1316	175135.54−293931.4	267.898110	−29.658742	0.2	4.4	35.0	8.6	30.0	21.5	0.90	3.8	<-5	g...	...	807.3	2.5	7.6×10^{-16}
1317	175135.57−294206.6	267.898220	−29.701852	0.1	6.9	463.2	24.8	121.8	327.0	0.90	18.3	<-5	g...	...	761.5	2.8	1.2×10^{-14}
1318	175135.58−293823.7	267.898260	−29.639936	0.1	3.4	22.9	6.7	15.1	10.0	0.90	3.2	<-5	g...	...	835.7	1.7	1.1×10^{-15}
1319	175135.58−293538.5	267.898290	−29.594030	0.1	1.8	34.5	6.9	6.5	24.1	0.90	4.6	<-5	g...	...	678.8	3.4	3.1×10^{-16}
1320	175135.60−293754.8	267.898340	−29.631890	0.0	3.0	509.6	23.3	10.4	310.5	0.89	21.4	<-5	g...	...	831.6	2.4	1.0×10^{-14}
1321	175135.61−293620.9	267.898390	−29.605821	0.1	1.9	17.4	5.5	7.6	3.3	0.90	2.9	<-5	....	b	846.8	1.5	2.0×10^{-16}
1322	175135.65−293542.7	267.898570	−29.595215	0.1	1.8	13.0	5.0	7.0	4.8	0.90	2.3	-4.2	g...	...	704.7	1.5	1.8×10^{-16}
1323	175135.71−293359.1	267.898810	−29.566418	0.1	2.3	12.7	5.0	7.3	9.9	0.89	2.3	-4.0	....	...	865.1	3.5	3.3×10^{-16}
1324	175135.75−293329.8	267.898980	−29.558281	0.1	2.6	14.7	5.3	8.3	4.9	0.89	2.5	-4.5	....	a	864.3	1.7	1.9×10^{-16}
1325	175135.77−293200.2	267.899070	−29.533396	0.1	3.8	50.7	8.7	16.3	10.9	0.90	5.5	<-5	....	a	845.6	1.3	4.9×10^{-16}
1326	175135.81−293808.0	267.899240	−29.635569	0.2	3.2	13.5	5.4	10.5	6.1	0.88	2.3	-3.5	g...	...	823.8	1.8	2.0×10^{-16}

(*cont.*)

Table A.1: *Chandra* source list

Source		Position				Extracted Counts							Characteristics				
Seq	CXOU J	R. A.	Decl.	Err	θ	$C_{\rm net}$	$\Delta C_{\rm net}$	$C'_{\rm bkg}$	$C_{\rm net,hard}$	PSF	PS	$P_{\rm B}$	Anom	Var	EffExp	$E_{\rm median}$	Photo $F_{\rm x}$
#		(deg)	(deg)	($''$)	($'$)						Frac				(ks)	(keV)	(ergs s^{-1} cm^{-2})
(1)	(2)	(3)	(4)	(5)	(6)	(7)	(8)	(9)	(10)	(11)	(12)	(13)	(14)	(15)	(16)	(17)	(18)
1327	175135.83−292834.1	267.899310	−29.476146	0.3	7.1	45.1	13.3	113.9	23.7	0.89	3.3	-4.3	....	a	789.9	2.1	7.9×10^{-16}
1328	175135.92−292844.9	267.899670	−29.479148	0.2	6.9	67.0	13.8	106.0	12.3	0.90	4.7	<-5	....	b	795.7	1.3	7.0×10^{-16}
1329	175135.96−293819.1	267.899840	−29.638657	0.1	3.4	61.2	9.1	12.8	4.4	0.89	6.3	<-5	g...	...	808.7	1.3	6.6×10^{-16}
1330	175135.97−293717.7	267.899900	−29.621588	0.2	2.6	12.0	5.2	10.0	0.0	0.89	2.1	-3.1	....	a	843.2	1.2	1.1×10^{-16}
1331	175136.00−293423.0	267.900020	−29.573069	0.1	2.1	12.5	4.9	6.5	5.5	0.90	2.3	-4.2	....	a	824.0	1.8	1.7×10^{-16}
1332	175136.02−293549.9	267.900120	−29.597211	0.1	1.9	27.2	6.4	7.8	11.6	0.90	3.9	<-5	g...	...	798.3	1.8	4.0×10^{-16}
1333	175136.03−293647.8	267.900140	−29.613296	0.2	2.3	8.6	4.5	7.4	1.5	0.90	1.7	-2.3	....	a	834.9	1.1	7.5×10^{-17}
1334	175136.05−293241.0	267.900220	−29.544737	0.1	3.3	22.0	6.3	11.0	0.1	0.89	3.2	<-5	....	c	842.8	1.1	1.9×10^{-16}
1335	175136.14−293135.7	267.900620	−29.526590	0.1	4.2	56.7	9.3	20.3	23.9	0.90	5.8	<-5	....	b	815.9	1.8	8.3×10^{-16}
1336	175136.16−292903.5	267.900700	−29.484310	0.1	6.6	292.2	20.2	92.8	211.5	0.90	14.1	<-5	....	a	803.4	2.9	6.9×10^{-15}
1337	175136.17−293124.8	267.900710	−29.523581	0.1	4.4	114.9	12.3	23.1	61.8	0.89	9.0	<-5	g...	...	811.7	2.3	2.2×10^{-15}
1338	175136.18−293100.3	267.900770	−29.516759	0.2	4.8	15.7	7.4	30.3	2.5	0.90	2.0	-2.3	....	a	823.9	1.1	1.4×10^{-16}
1339	175136.21−293216.7	267.900910	−29.537989	0.1	3.6	59.5	9.1	13.5	28.4	0.90	6.2	<-5	....	c	847.2	1.9	8.7×10^{-16}
1340	175136.24−293646.9	267.901020	−29.613042	0.1	2.3	12.0	5.0	8.0	6.2	0.90	2.2	-3.5	....	b	850.7	2.1	1.9×10^{-16}
1341	175136.30−292932.3	267.901280	−29.492326	0.3	6.2	27.0	10.4	68.0	7.3	0.89	2.5	-2.9	....	a	811.8	1.6	3.5×10^{-16}
1342	175136.31−293445.5	267.901330	−29.579330	0.1	2.0	71.7	9.4	7.3	43.7	0.90	7.2	<-5	....	a	869.3	2.8	1.5×10^{-15}
1343	175136.32−293800.6	267.901360	−29.633526	0.1	3.2	30.5	7.0	11.5	15.9	0.90	4.0	<-5	....	a	830.3	2.1	4.9×10^{-16}
1344	175136.33−292813.4	267.901400	−29.470391	0.3	7.4	50.6	14.7	147.4	37.5	0.90	3.3	-4.6	....	a	783.8	3.2	1.3×10^{-15}
1345	175136.34−294053.6	267.901420	−29.681568	0.1	5.8	179.0	16.1	62.0	123.9	0.88	10.8	<-5	g...	...	783.0	2.6	4.2×10^{-15}
1346	175136.39−293323.9	267.901650	−29.556646	0.1	2.8	28.0	6.6	9.0	10.4	0.89	3.9	<-5	....	a	868.3	1.5	1.8×10^{-16}
1347	175136.39−293250.9	267.901660	−29.547474	0.1	3.2	26.9	6.8	12.1	0.0	0.89	3.7	<-5	....	b	852.0	0.9	3.1×10^{-16}
1348	175136.39−293403.6	267.901660	−29.567690	0.1	2.3	18.2	5.6	7.8	7.1	0.89	2.9	<-5	....	a	870.1	1.8	2.5×10^{-16}
1349	175136.40−293747.4	267.901690	−29.629839	0.1	3.0	164.7	13.7	10.3	78.5	0.88	11.5	<-5	....	b	820.5	2.0	2.6×10^{-15}
1350	175136.44−293208.9	267.901870	−29.535811	0.2	3.8	23.5	6.7	14.5	11.2	0.90	3.2	<-5	g...	...	815.7	1.9	3.6×10^{-16}
1351	175136.47−293602.3	267.901970	−29.600666	0.1	2.0	18.4	5.6	7.6	6.2	0.90	3.0	<-5	....	a	856.9	1.5	2.1×10^{-16}
1352	175136.47−293744.5	267.901990	−29.629044	0.0	3.0	181.4	14.4	10.6	113.4	0.88	12.2	<-5	g...	...	819.3	2.8	4.1×10^{-15}
1353	175136.48−293033.5	267.902030	−29.509318	0.1	5.2	223.1	16.8	41.9	4.2	0.90	12.9	<-5	....	b	830.1	0.9	1.6×10^{-15}
1354	175136.58−293710.8	267.902440	−29.619683	0.2	2.6	14.2	5.3	8.8	1.4	0.89	2.4	-4.2	....	a	839.2	1.3	1.4×10^{-16}
1355	175136.59−293633.7	267.902460	−29.609378	0.1	2.2	29.4	6.6	7.6	11.4	0.90	4.1	<-5	....	a	858.6	1.7	5.0×10^{-16}
1356	175136.59−293400.8	267.902500	−29.566912	0.1	2.4	40.4	7.5	8.6	10.1	0.89	5.0	<-5	....	a	871.2	1.7	3.8×10^{-16}
1357	175136.60−293904.2	267.902510	−29.651193	0.2	4.1	31.5	8.3	28.5	11.3	0.90	3.6	<-5	g...	...	797.2	1.5	4.0×10^{-16}
1358	175136.61−294057.0	267.902550	−29.682514	0.2	5.9	30.1	9.4	47.9	21.9	0.81	3.0	-4.3	g...	...	782.9	3.8	1.8×10^{-16}
1359	175136.61−293054.4	267.902580	−29.515112	0.2	4.9	18.7	7.9	35.3	0.4	0.91	2.2	-2.6	....	a	821.8	1.2	1.2×10^{-15}
1360	175136.66−294340.6	267.902750	−29.727968	0.3	8.3	33.5	7.4	13.5	4.3	0.40	4.2	<-5	g...	...	515.8	1.2	1.2×10^{-15}

(*cont.*)

Table A.1: *Chandra* source list

Source		Position				Extracted Counts							Characteristics				
Seq	CXOU J	R. A.	Decl.	Err	θ	$C_{\rm net}$	$\Delta C_{\rm net}$	$C'_{\rm bkg}$	$C_{\rm net,hard}$	PSF	PS	$P_{\rm B}$	Anom	Var	EffExp	$E_{\rm median}$	Photo $F_{\rm x}$
#		(deg)	(deg)	($''$)	($'$)						Frac				(ks)	(keV)	(ergs s^{-1} cm^{-2})
(1)	(2)	(3)	(4)	(5)	(6)	(7)	(8)	(9)	(10)	(11)	(12)	(13)	(14)	(15)	(16)	(17)	(18)
1361	175136.70−294241.1	267.902950	−29.711419	0.2	7.5	202.1	19.6	157.9	153.6	0.90	10.0	<-5	g...	...	742.0	3.1	6.1×10^{-15}
1362	175136.80−293238.3	267.903370	−29.543993	0.1	3.4	28.3	6.9	11.7	22.0	0.90	3.8	<-5	....	b	830.5	3.3	7.4×10^{-16}
1363	175136.81−294336.4	267.903410	−29.726800	0.3	8.2	28.3	6.9	11.7	10.9	0.40	3.8	<-5	g...	...	439.0	1.6	1.6×10^{-15}
1364	175136.91−293352.9	267.903810	−29.564721	0.1	2.5	16.7	5.5	8.3	7.2	0.89	2.7	<-5	....	a	865.2	1.8	2.3×10^{-16}
1365	175136.93−292926.1	267.903900	−29.490610	0.2	6.3	34.3	8.2	23.7	7.8	0.58	3.9	<-5	....	a	811.5	1.5	6.5×10^{-16}
1366	175136.98−292902.2	267.904090	−29.483946	0.3	6.7	29.4	11.8	95.6	0.6	0.90	2.4	-2.6	....	b	802.6	0.9	2.2×10^{-16}
1367	175136.98−293712.5	267.904110	−29.620162	0.1	2.7	20.6	6.1	10.4	8.6	0.89	3.1	<-5	....	a	849.6	1.5	2.3×10^{-16}
1368	175137.03−293131.0	267.904310	−29.525302	0.2	4.4	16.6	6.9	23.4	1.3	0.89	2.2	-2.9	....	a	817.1	1.1	1.5×10^{-16}
1369	175137.07−293458.2	267.904460	−29.582838	0.1	2.1	25.8	6.2	6.2	8.7	0.90	3.8	<-5	g...	...	745.7	1.4	3.2×10^{-16}
1370	175137.08−293706.1	267.904510	−29.618377	0.1	2.6	13.2	5.3	9.8	5.8	0.89	2.2	-3.6	....	a	845.2	1.7	1.7×10^{-16}
1371	175137.13−294104.0	267.904730	−29.684467	0.2	6.0	139.8	15.4	80.2	107.5	0.90	8.8	<-5	g...	...	782.4	3.5	4.2×10^{-15}
1372	175137.15−293918.8	267.904810	−29.655241	0.2	4.4	16.8	7.5	31.2	6.8	0.90	2.1	-2.4	g...	...	804.4	1.4	2.0×10^{-16}
1373	175137.18−293122.9	267.904920	−29.523039	0.1	4.5	102.0	11.9	26.0	56.7	0.89	8.2	<-5	....	c	843.8	2.4	1.8×10^{-15}
1374	175137.19−293639.1	267.904990	−29.610876	0.1	2.4	17.8	5.6	8.2	9.1	0.90	2.9	<-5	....	a	865.3	2.2	2.9×10^{-16}
1375	175137.28−293702.3	267.905340	−29.617327	0.0	2.6	146.4	13.0	9.6	99.9	0.89	10.8	<-5	....	b	845.6	2.9	3.2×10^{-15}
1376	175137.30−294113.7	267.905440	−29.687152	0.2	6.2	106.9	14.3	80.1	53.2	0.90	7.2	<-5	....	a	778.6	2.0	1.9×10^{-15}
1377	175137.31−293409.6	267.905480	−29.569355	0.1	2.4	72.8	9.5	8.2	23.1	0.89	7.2	<-5	....	a	849.3	1.7	9.4×10^{-16}
1378	175137.32−292930.4	267.905500	−29.491790	0.2	6.3	83.0	11.7	41.0	8.5	0.74	6.8	<-5	....	a	811.9	1.2	9.8×10^{-16}
1379	175137.32−293511.0	267.905500	−29.586402	0.1	2.1	32.1	6.7	5.9	10.8	0.91	4.4	<-5	g...	...	642.5	1.3	4.0×10^{-16}
1380	175137.32−293927.7	267.905540	−29.657707	0.2	4.6	34.4	8.8	32.6	5.4	0.90	3.7	<-5	....	b	804.6	1.5	4.2×10^{-16}
1381	175137.33−292940.3	267.905560	−29.494554	0.2	6.1	66.9	12.2	67.1	4.4	0.89	5.3	<-5	....	a	813.1	1.0	5.2×10^{-16}
1382	175137.39−293620.7	267.905810	−29.605755	0.1	2.3	11.9	5.0	8.1	5.1	0.90	2.1	-3.4	....	a	866.1	1.3	1.2×10^{-16}
1383	175137.41−293558.2	267.905910	−29.599513	0.1	2.2	13.2	5.2	8.8	6.2	0.90	2.3	-3.7	....	a	865.0	1.6	1.5×10^{-16}
1384	175137.42−294150.9	267.905950	−29.697496	0.2	6.8	200.2	18.1	106.8	154.3	0.90	10.7	<-5	g...	...	765.2	3.3	6.1×10^{-15}
1385	175137.44−293450.6	267.906010	−29.580750	0.1	2.2	11.6	4.9	7.4	1.4	0.90	2.1	-3.5	....	a	821.1	1.7	1.5×10^{-16}
1386	175137.44−293641.0	267.906020	−29.611396	0.2	2.5	10.6	4.9	8.4	0.8	0.89	1.9	-2.8	....	a	865.2	1.4	1.1×10^{-16}
1387	175137.45−293034.2	267.906050	−29.509513	0.2	5.3	31.7	7.3	14.3	4.2	0.63	4.0	<-5	....	a	815.2	1.1	4.2×10^{-16}
1388	175137.46−293251.2	267.906090	−29.547559	0.1	3.3	22.2	6.4	11.8	3.1	0.89	3.2	<-5	....	a	832.3	1.0	1.8×10^{-16}
1389	175137.47−293749.5	267.906150	−29.630441	0.1	3.2	65.7	9.4	13.3	26.3	0.89	6.6	<-5	....	a	833.3	1.8	9.4×10^{-16}
1390	175137.47−294049.6	267.906150	−29.680448	0.2	5.8	83.5	13.3	77.5	55.3	0.90	6.0	<-5	....	a	785.7	3.3	2.3×10^{-15}
1391	175137.48−293125.9	267.906200	−29.523887	0.2	4.5	17.8	6.2	14.2	6.3	0.79	2.6	-4.3	....	a	843.6	1.7	2.6×10^{-16}
1392	175137.49−293218.7	267.906210	−29.538542	0.1	3.8	28.3	7.1	14.7	13.7	0.90	3.7	<-5	....	a	828.5	1.9	4.3×10^{-16}
1393	175137.49−293515.3	267.906220	−29.587606	0.0	2.1	239.8	16.2	7.2	230.8	0.90	14.3	<-5	g...	...	699.7	4.4	9.7×10^{-15}
1394	175137.53−293602.6	267.906410	−29.600729	0.0	2.2	230.7	16.0	8.3	15.5	0.90	14.0	<-5	....	a	865.4	1.1	1.8×10^{-15}

(*cont.*)

Table A.1: *Chandra* source list

Source		Position				Extracted Counts							Characteristics				
Seq	CXOU J	R. A.	Decl.	Err	θ	$C_{\rm net}$	$\Delta C_{\rm net}$	$C'_{\rm bkg}$	$C_{\rm net,hard}$	PSF	PS	$P_{\rm B}$	Anom	Var	EffExp	$E_{\rm median}$	Photo $F_{\rm x}$
#		(deg)	(deg)	($''$)	($'$)						Frac				(ks)	(keV)	(ergs s^{-1} cm^{-2})
(1)	(2)	(3)	(4)	(5)	(6)	(7)	(8)	(9)	(10)	(11)	(12)	(13)	(14)	(15)	(16)	(17)	(18)
1395	175137.54−293824.9	267.906420	−29.640259	0.2	3.7	11.2	5.9	16.8	4.1	0.89	1.8	-2.1	....	a	832.9	1.6	1.4×10^{-16}
1396	175137.55−293145.5	267.906480	−29.529320	0.2	4.2	14.5	6.6	21.5	2.3	0.90	2.0	-2.5	....	a	847.7	0.9	9.9×10^{-17}
1397	175137.57−294236.7	267.906580	−29.710217	0.2	7.5	112.1	16.3	133.9	35.8	0.85	6.7	<-5	g...	...	743.9	1.5	1.7×10^{-15}
1398	175137.62−293941.7	267.906770	−29.661585	0.2	4.8	19.3	8.0	35.7	4.2	0.90	2.3	-2.7	....	a	798.7	1.8	2.9×10^{-16}
1399	175137.64−293305.3	267.906840	−29.551492	0.1	3.2	47.2	8.1	10.8	5.2	0.89	5.4	<-5	....	a	831.6	1.1	4.0×10^{-16}
1400	175137.65−293601.2	267.906880	−29.600352	0.1	2.2	88.1	10.3	7.9	62.6	0.89	8.1	<-5	....	b	865.9	2.8	1.8×10^{-15}
1401	175137.65−293726.9	267.906910	−29.624166	0.2	3.0	14.3	5.5	10.7	5.7	0.89	2.3	-3.8	....	a	841.9	1.5	1.6×10^{-16}
1402	175137.66−293951.8	267.906940	−29.664393	0.2	4.9	17.7	8.1	38.3	9.4	0.90	2.1	-2.3	g...	...	793.0	2.0	3.1×10^{-16}
1403	175137.67−293503.2	267.906990	−29.584230	0.1	2.2	12.6	4.8	5.4	1.3	0.91	2.4	-4.7	g...	...	645.6	1.2	1.6×10^{-16}
1404	175137.69−293337.4	267.907050	−29.560413	0.2	2.8	12.6	5.1	8.4	4.1	0.89	2.2	-3.6	....	a	841.2	1.3	1.3×10^{-16}
1405	175137.71−293036.4	267.907140	−29.510113	0.1	5.3	51.6	8.8	16.4	2.8	0.68	5.5	<-5	....	b	818.2	1.3	6.8×10^{-16}
1406	175137.81−293102.2	267.907560	−29.517291	0.1	4.9	77.2	11.1	34.8	50.2	0.90	6.6	<-5	....	a	823.5	2.9	1.7×10^{-15}
1407	175137.86−293026.6	267.907790	−29.507416	0.2	5.4	80.4	11.9	47.6	63.8	0.90	6.5	<-5	....	b	805.1	3.3	2.2×10^{-15}
1408	175137.90−293034.3	267.907940	−29.509542	0.2	5.3	15.7	7.1	26.3	4.3	0.79	2.1	-2.5	....	b	804.6	1.4	2.1×10^{-16}
1409	175137.90−293857.1	267.907950	−29.649221	0.1	4.2	60.8	10.0	29.2	28.8	0.90	5.8	<-5	....	a	816.0	1.9	9.1×10^{-16}
1410	175137.91−293515.0	267.907970	−29.587505	0.1	2.2	18.2	5.5	6.8	0.2	0.90	3.0	<-5	g...	...	699.2	0.9	1.5×10^{-16}
1411	175137.91−293904.2	267.907980	−29.651167	0.2	4.3	24.6	8.1	32.4	0.6	0.90	2.8	-4.1	....	a	821.1	1.1	2.0×10^{-16}
1412	175138.00−293816.7	267.908340	−29.637981	0.2	3.6	10.6	5.7	15.4	1.6	0.89	1.7	-2.0	....	a	842.9	1.4	1.1×10^{-16}
1413	175138.07−293021.7	267.908660	−29.506041	0.1	5.5	172.5	15.4	48.5	148.0	0.90	10.8	<-5	....	a	800.4	3.6	5.1×10^{-15}
1414	175138.09−293716.6	267.908710	−29.621299	0.1	2.9	23.8	6.5	12.2	6.2	0.89	3.4	<-5	....	a	861.4	1.5	2.7×10^{-16}
1415	175138.10−294105.3	267.908760	−29.684815	0.1	6.1	263.5	19.2	84.5	25.2	0.90	13.3	<-5	....	a	773.3	1.2	2.8×10^{-15}
1416	175138.11−293749.8	267.908820	−29.630507	0.2	3.3	20.4	6.3	12.6	8.7	0.90	3.0	<-5	....	a	847.0	1.7	2.7×10^{-16}
1417	175138.12−293451.8	267.908870	−29.581075	0.1	2.3	14.0	5.1	7.0	7.5	0.89	2.5	-4.7	g...	...	786.8	2.1	2.4×10^{-16}
1418	175138.15−293418.8	267.909000	−29.571907	0.1	2.5	17.2	5.5	7.8	4.3	0.89	2.8	<-5	....	a	840.6	1.1	1.5×10^{-16}
1419	175138.17−293658.8	267.909060	−29.616347	0.1	2.8	88.4	10.5	10.6	14.1	0.89	8.0	<-5	....	a	861.9	1.3	8.8×10^{-16}
1420	175138.25−293433.7	267.909390	−29.576036	0.1	2.4	12.1	4.9	6.9	6.0	0.89	2.2	-3.9	g...	...	807.8	1.8	9.0×10^{-16}
1421	175138.25−293107.1	267.909410	−29.518653	0.2	4.9	39.8	9.1	32.2	28.2	0.91	4.2	<-5	....	a	809.9	2.8	1.8×10^{-16}
1422	175138.28−293320.0	267.909540	−29.555564	0.2	3.1	11.2	5.1	9.8	4.0	0.89	2.0	-2.8	....	a	833.3	1.5	1.4×10^{-16}
1423	175138.29−293456.1	267.909550	−29.582276	0.1	2.3	17.9	5.5	7.1	4.5	0.89	2.9	<-5	g...	...	712.3	1.7	2.8×10^{-16}
1424	175138.32−293741.2	267.909690	−29.628121	0.2	3.2	16.4	6.0	13.6	4.9	0.89	2.5	-3.9	....	a	855.2	1.6	1.9×10^{-16}
1425	175138.33−294240.3	267.909750	−29.711208	0.1	7.6	614.2	28.4	160.8	273.1	0.89	21.2	<-5	g...	...	747.9	1.8	1.0×10^{-14}
1426	175138.35−294026.5	267.909820	−29.674034	0.2	5.5	23.2	9.9	63.8	0.0	0.90	2.2	-2.4	....	a	795.3	0.9	2.1×10^{-15}
1427	175138.35−293330.1	267.909830	−29.558373	0.1	3.0	78.1	9.9	9.9	61.5	0.90	7.5	<-5	....	a	836.0	3.4	1.7×10^{-16}
1428	175138.36−293309.1	267.909860	−29.552533	0.1	3.2	162.1	13.7	10.9	15.9	0.89	11.4	<-5	....	b	843.1	1.2	1.5×10^{-15}

(*cont.*)

Table A.1: *Chandra* source list

Source		Position				Extracted Counts							Characteristics				
Seq	CXOU J	R. A.	Decl.	Err	θ	$C_{\rm net}$	$\Delta C_{\rm net}$	$C'_{\rm bkg}$	$C_{\rm net,hard}$	PSF	PS	$P_{\rm B}$	Anom	Var	EffExp	$E_{\rm median}$	Photo $F_{\rm x}$
#		(deg)	(deg)	($''$)	($'$)						Frac				(ks)	(keV)	(ergs s^{-1} cm^{-2})
(1)	(2)	(3)	(4)	(5)	(6)	(7)	(8)	(9)	(10)	(11)	(12)	(13)	(14)	(15)	(16)	(17)	(18)
1429	175138.39−294013.2	267.909960	−29.670360	0.2	5.3	35.7	10.1	55.3	21.7	0.90	3.3	-5.0	....	a	792.9	2.2	6.5×10^{-16}
1430	175138.40−293158.1	267.910030	−29.532823	0.2	4.1	20.3	7.0	21.7	4.9	0.90	2.7	-4.0	....	a	833.2	1.3	2.1×10^{-16}
1431	175138.40−293458.2	267.910040	−29.582854	0.1	2.3	34.6	6.9	6.4	20.7	0.89	4.6	<-5	g...	...	682.7	2.2	7.2×10^{-16}
1432	175138.44−293042.1	267.910180	−29.511700	0.2	5.2	23.0	8.7	43.0	13.9	0.90	2.5	-3.1	....	a	804.9	2.5	4.6×10^{-16}
1433	175138.44−293543.9	267.910190	−29.595545	0.1	2.4	16.2	5.5	8.8	4.3	0.89	2.7	<-5	g...	...	789.8	1.7	2.2×10^{-16}
1434	175138.49−293605.2	267.910400	−29.601460	0.1	2.4	26.6	6.6	10.4	1.7	0.89	3.7	<-5	....	b	862.2	1.2	2.5×10^{-16}
1435	175138.53−293146.9	267.910570	−29.529714	0.2	4.3	13.6	6.2	18.4	4.2	0.86	2.0	-2.5	g...	...	813.0	1.3	1.5×10^{-16}
1436	175138.57−293722.8	267.910710	−29.623026	0.1	3.1	59.0	9.1	14.0	30.6	0.89	6.1	<-5	....	a	858.2	2.4	1.1×10^{-15}
1437	175138.58−293738.7	267.910770	−29.627421	0.1	3.2	23.2	6.6	13.8	19.7	0.89	3.2	<-5	....	b	854.1	4.2	7.3×10^{-16}
1438	175138.58−293901.5	267.910770	−29.650435	0.2	4.3	23.2	7.6	26.8	3.4	0.87	2.8	-4.3	....	a	831.8	1.5	2.8×10^{-16}
1439	175138.59−293214.4	267.910800	−29.537343	0.2	3.9	13.5	6.3	19.5	0.4	0.90	2.0	-2.4	....	a	828.5	1.2	1.3×10^{-16}
1440	175138.59−293517.4	267.910810	−29.588176	0.0	2.4	167.7	13.7	7.3	108.8	0.90	11.8	<-5	g...	...	711.5	2.5	3.9×10^{-15}
1441	175138.66−293711.1	267.911100	−29.619765	0.1	3.0	40.6	7.8	12.4	13.7	0.89	4.9	<-5	....	b	859.5	1.6	4.9×10^{-16}
1442	175138.73−292940.7	267.911410	−29.494655	0.1	6.2	462.6	23.6	70.4	441.1	0.90	19.2	<-5	....	c	792.4	4.0	1.6×10^{-14}
1443	175138.76−293150.6	267.911540	−29.530749	0.2	4.3	14.5	6.2	17.5	0.0	0.85	2.1	-2.9	....	a	821.3	1.1	1.4×10^{-16}
1444	175138.77−293116.0	267.911560	−29.521135	0.2	4.8	15.5	7.4	31.5	4.7	0.90	1.9	-2.2	....	a	810.0	1.7	2.1×10^{-16}
1445	175138.77−293519.5	267.911560	−29.588752	0.1	2.4	34.3	7.0	7.7	11.8	0.89	4.5	<-5	g...	...	735.9	1.6	4.7×10^{-16}
1446	175138.80−293500.8	267.911700	−29.583573	0.2	2.4	8.0	4.3	6.0	1.7	0.89	1.6	-2.3	g...	...	631.6	1.5	1.3×10^{-16}
1447	175138.81−292912.4	267.911750	−29.486781	0.2	6.6	34.5	9.3	41.5	7.8	0.74	3.5	<-5	....	a	779.0	1.4	5.2×10^{-16}
1448	175138.82−293005.3	267.911770	−29.501478	0.2	5.8	78.0	12.0	53.0	73.3	0.89	6.2	<-5	....	a	792.0	4.2	2.8×10^{-15}
1449	175138.84−293903.6	267.911840	−29.651011	0.1	4.4	79.6	10.9	28.4	35.6	0.88	6.9	<-5	....	a	830.7	1.8	3.4×10^{-16}
1450	175138.84−293853.0	267.911870	−29.648079	0.2	4.2	24.2	7.9	28.8	10.9	0.90	2.9	-4.3	....	a	830.6	1.8	1.2×10^{-15}
1451	175138.85−293301.1	267.911890	−29.550318	0.2	3.4	12.5	5.6	13.5	1.3	0.90	2.0	-2.7	....	a	844.0	0.9	8.6×10^{-17}
1452	175138.88−293409.3	267.912040	−29.569265	0.1	2.7	52.1	8.3	8.9	28.9	0.89	5.9	<-5	g...	...	813.8	2.3	9.8×10^{-16}
1453	175138.90−293319.9	267.912120	−29.555555	0.2	3.2	13.9	5.5	11.1	3.0	0.89	2.3	-3.5	....	a	845.6	1.6	1.8×10^{-16}
1454	175138.92−293326.8	267.912200	−29.557460	0.2	3.1	15.1	5.5	9.9	0.0	0.89	2.5	-4.3	....	a	836.5	0.9	1.1×10^{-16}
1455	175138.93−293230.7	267.912240	−29.541866	0.1	3.8	56.0	9.0	16.0	4.5	0.90	5.9	<-5	....	a	823.9	1.2	5.5×10^{-16}
1456	175138.94−293547.9	267.912270	−29.596650	0.1	2.5	19.9	6.0	10.1	1.9	0.89	3.0	<-5	....	b	839.0	1.1	1.7×10^{-16}
1457	175138.99−293722.5	267.912490	−29.622931	0.2	3.1	17.6	6.2	14.4	12.8	0.89	2.6	-4.2	....	a	856.3	2.5	3.4×10^{-16}
1458	175139.02−293139.1	267.912600	−29.527535	0.1	4.5	149.2	13.8	25.8	10.4	0.89	10.4	<-5	....	a	814.1	1.1	1.4×10^{-15}
1459	175139.08−293438.1	267.912840	−29.577254	0.2	2.6	8.1	4.5	7.9	1.6	0.89	1.6	-2.1	g...	...	788.3	1.6	1.1×10^{-16}
1460	175139.11−293351.5	267.912980	−29.564319	0.1	2.9	26.4	6.6	10.6	11.4	0.89	3.7	<-5	g...	...	826.8	1.9	4.1×10^{-16}
1461	175139.19−293640.1	267.913310	−29.611164	0.2	2.8	10.2	5.0	9.8	2.8	0.89	1.8	-2.5	....	a	860.8	1.4	1.0×10^{-16}
1462	175139.19−293803.7	267.913330	−29.634377	0.1	3.6	25.9	7.1	17.1	12.1	0.89	3.4	<-5	....	c	849.0	1.8	3.6×10^{-16}

(*cont.*)

Table A.1: *Chandra* source list

Source		Position				Extracted Counts							Characteristics				
Seq	CXOU J	R. A.	Decl.	Err	θ	$C_{\rm net}$	$\Delta C_{\rm net}$	$C'_{\rm bkg}$	$C_{\rm net,hard}$	PSF	PS	$P_{\rm B}$	Anom	Var	EffExp	$E_{\rm median}$	Photo $F_{\rm x}$
#		(deg)	(deg)	($''$)	($'$)						Frac				(ks)	(keV)	(ergs s^{-1} cm^{-2})
(1)	(2)	(3)	(4)	(5)	(6)	(7)	(8)	(9)	(10)	(11)	(12)	(13)	(14)	(15)	(16)	(17)	(18)
1463	175139.21−292825.6	267.913380	−29.473783	0.3	7.4	37.7	12.9	111.3	20.8	0.86	2.8	-3.3	....	b	759.2	2.3	7.9×10^{-16}
1464	175139.22−293541.8	267.913430	−29.594959	0.1	2.5	39.0	7.5	10.0	30.8	0.90	4.8	<-5	g...	...	775.2	3.1	9.9×10^{-16}
1465	175139.23−293354.8	267.913460	−29.565227	0.1	2.9	11.8	4.4	3.2	0.0	0.59	2.4	<-5	g...	...	821.1	1.1	1.5×10^{-16}
1466	175139.23−293506.7	267.913500	−29.585214	0.1	2.5	14.6	5.1	6.4	1.1	0.89	2.6	<-5	g...	...	632.6	1.4	2.2×10^{-16}
1467	175139.24−293851.2	267.913540	−29.647565	0.2	4.2	25.2	8.0	29.8	20.7	0.90	3.0	-4.5	....	b	838.1	2.7	5.2×10^{-16}
1468	175139.27−293651.9	267.913640	−29.614427	0.2	2.9	10.6	5.2	11.4	1.0	0.89	1.8	-2.4	....	a	859.2	1.2	9.5×10^{-17}
1469	175139.28−293705.7	267.913700	−29.618259	0.1	3.0	21.5	6.3	11.5	14.2	0.89	3.2	<-5	....	a	856.1	3.3	5.5×10^{-16}
1470	175139.29−293034.2	267.913730	−29.509509	0.2	5.4	50.4	10.4	46.6	24.6	0.90	4.6	<-5	....	c	802.0	1.9	2.6×10^{-15}
1471	175139.29−293027.2	267.913750	−29.507562	0.1	5.6	133.9	14.1	49.1	79.1	0.90	9.2	<-5	....	a	799.0	2.3	8.2×10^{-16}
1472	175139.29−293356.3	267.913750	−29.565649	0.1	2.9	24.8	6.0	5.2	12.1	0.69	3.8	<-5	g...	...	822.0	2.0	5.2×10^{-16}
1473	175139.32−293333.0	267.913840	−29.559178	0.1	3.1	28.0	6.8	11.0	8.6	0.89	3.8	<-5	....	b	826.8	1.5	3.3×10^{-16}
1474	175139.34−293454.8	267.913930	−29.581900	0.1	2.5	37.5	7.2	6.5	0.7	0.89	4.9	<-5	g...	...	670.2	1.1	7.3×10^{-16}
1475	175139.34−293050.1	267.913940	−29.513941	0.2	5.2	36.6	9.5	42.4	25.4	0.90	3.7	<-5	....	c	814.8	2.5	4.2×10^{-16}
1476	175139.39−293713.5	267.914140	−29.620427	0.2	3.1	14.4	5.8	13.6	6.8	0.89	2.2	-3.3	....	a	854.2	1.3	1.4×10^{-16}
1477	175139.42−292916.2	267.914270	−29.487846	0.2	6.6	100.6	13.6	69.4	1.3	0.85	7.1	<-5	....	b	770.8	0.9	8.0×10^{-16}
1478	175139.44−292750.5	267.914360	−29.464029	0.3	8.0	43.6	14.4	143.4	3.4	0.84	2.9	-3.7	....	a	754.4	1.2	5.1×10^{-16}
1479	175139.44−293816.9	267.914360	−29.638042	0.2	3.8	28.4	7.5	19.6	3.0	0.90	3.5	<-5	....	a	846.3	1.4	2.9×10^{-16}
1480	175139.46−293130.8	267.914450	−29.525226	0.2	4.7	33.3	8.5	29.7	11.1	0.90	3.7	<-5	g...	...	813.2	1.5	4.2×10^{-16}
1481	175139.49−293223.7	267.914570	−29.539938	0.2	4.0	14.8	6.6	21.2	2.1	0.90	2.1	-2.6	....	a	830.0	1.7	1.9×10^{-16}
1482	175139.52−293252.1	267.914690	−29.547831	0.1	3.6	23.7	6.8	15.3	5.3	0.90	3.2	<-5	g...	...	817.0	1.5	3.0×10^{-16}
1483	175139.52−293344.6	267.914700	−29.562415	0.1	3.1	18.3	5.9	10.7	7.3	0.89	2.8	<-5	....	b	832.7	1.8	2.6×10^{-16}
1484	175139.54−293359.7	267.914750	−29.566593	0.2	2.9	9.6	5.0	10.4	2.1	0.89	1.7	-2.2	....	b	829.7	1.7	1.3×10^{-16}
1485	175139.56−294135.2	267.914850	−29.693122	0.3	6.7	32.6	12.7	111.4	11.7	0.90	2.5	-2.7	....	b	775.3	1.6	8.2×10^{-16}
1486	175139.56−292842.0	267.914870	−29.478361	0.2	7.2	78.9	14.6	116.1	11.7	0.89	5.2	<-5	g...	...	763.7	1.2	4.7×10^{-16}
1487	175139.58−292636.5	267.914930	−29.443486	0.4	9.0	47.5	14.1	132.5	36.0	0.90	3.3	-4.5	g...	...	397.3	2.6	2.2×10^{-15}
1488	175139.59−293503.5	267.914960	−29.584308	0.1	2.6	26.8	6.4	7.2	1.8	0.89	3.9	<-5	g...	...	611.5	1.1	3.3×10^{-16}
1489	175139.64−293202.9	267.915200	−29.534144	0.2	4.2	16.3	6.8	22.7	2.1	0.89	2.2	-2.9	....	a	823.9	1.4	1.8×10^{-16}
1490	175139.66−292719.7	267.915280	−29.455493	0.3	8.5	115.1	19.0	220.9	112.9	0.90	5.9	<-5	....	a	752.1	4.4	4.6×10^{-15}
1491	175139.66−293621.4	267.915290	−29.605962	0.1	2.7	16.5	5.8	11.5	10.8	0.89	2.6	-4.4	....	a	858.6	4.3	5.4×10^{-16}
1492	175139.70−293811.5	267.915430	−29.636545	0.1	3.8	169.3	14.2	18.7	105.5	0.89	11.5	<-5	....	b	845.9	2.5	3.3×10^{-15}
1493	175139.75−293316.8	267.915630	−29.554673	0.1	3.4	24.3	6.6	12.7	9.8	0.89	3.4	<-5	....	b	822.4	1.7	3.3×10^{-16}
1494	175139.77−293547.0	267.915730	−29.596389	0.1	2.6	104.8	11.2	9.2	2.0	0.89	8.9	<-5	....	a	836.1	1.1	9.0×10^{-16}
1495	175139.78−293710.5	267.915780	−29.619584	0.1	3.1	71.5	9.8	14.5	6.4	0.90	6.9	<-5	....	a	855.2	1.1	6.0×10^{-16}
1496	175139.88−293750.1	267.916190	−29.630587	0.1	3.6	136.6	12.9	17.4	108.0	0.90	10.2	<-5	....	b	849.1	3.3	3.4×10^{-15}

(*cont.*)

Table A.1: *Chandra* source list

Source		Position				Extracted Counts							Characteristics				
Seq	CXOU J	R. A.	Decl.	Err	θ	$C_{\rm net}$	$\Delta C_{\rm net}$	$C'_{\rm bkg}$	$C_{\rm net,hard}$	PSF	PS	$P_{\rm B}$	Anom	Var	EffExp	$E_{\rm median}$	Photo $F_{\rm x}$
#		(deg)	(deg)	($''$)	($'$)						Frac				(ks)	(keV)	(ergs s^{-1} cm^{-2})
(1)	(2)	(3)	(4)	(5)	(6)	(7)	(8)	(9)	(10)	(11)	(12)	(13)	(14)	(15)	(16)	(17)	(18)
1497	175139.89−292817.1	267.916240	−29.471419	0.3	7.6	33.3	14.3	152.7	20.1	0.90	2.2	-2.3	g...	...	763.9	2.4	7.1×10^{-16}
1498	175139.90−294008.0	267.916280	−29.668907	0.2	5.4	75.7	12.4	63.3	58.1	0.90	5.9	<-5	....	a	811.3	3.7	2.2×10^{-15}
1499	175139.96−293357.9	267.916510	−29.566087	0.1	3.0	30.7	6.9	10.3	9.3	0.89	4.1	<-5	g...	...	823.2	1.6	3.9×10^{-16}
1500	175139.99−292831.8	267.916630	−29.475501	0.3	7.4	44.2	12.9	106.8	19.8	0.85	3.3	-4.3	....	c	766.8	1.9	7.7×10^{-16}
1501	175140.02−293442.4	267.916780	−29.578453	0.1	2.7	14.6	5.3	8.4	1.1	0.89	2.5	-4.5	g...	...	763.7	1.5	1.9×10^{-16}
1502	175140.05−293814.7	267.916900	−29.637425	0.1	3.9	46.0	8.7	21.0	29.5	0.90	5.0	<-5	....	b	846.0	2.6	9.2×10^{-16}
1503	175140.08−293000.7	267.917020	−29.500220	0.2	6.0	31.7	10.1	59.3	8.8	0.89	3.0	-4.0	....	b	783.7	1.4	3.9×10^{-16}
1504	175140.12−293854.3	267.917170	−29.648438	0.2	4.4	38.8	9.1	33.2	13.8	0.90	4.0	<-5	....	a	838.0	1.7	5.2×10^{-16}
1505	175140.14−293515.5	267.917280	−29.587658	0.2	2.7	10.7	4.9	8.3	4.3	0.89	2.0	-2.9	g...	...	714.9	1.4	1.4×10^{-16}
1506	175140.17−293915.0	267.917400	−29.654184	0.2	4.7	19.7	8.3	40.3	3.2	0.90	2.2	-2.6	....	a	833.1	1.6	2.4×10^{-16}
1507	175140.20−293108.8	267.917530	−29.519132	0.2	5.0	29.0	8.7	37.0	4.5	0.90	3.1	-4.8	....	a	812.0	1.3	3.0×10^{-16}
1508	175140.21−293641.5	267.917570	−29.611555	0.1	3.0	21.6	6.3	11.4	1.3	0.89	3.2	<-5	....	b	856.4	1.3	2.2×10^{-16}
1509	175140.22−293033.3	267.917600	−29.509256	0.2	5.6	22.6	9.1	50.4	0.0	0.90	2.3	-2.7	....	b	786.2	0.8	1.6×10^{-16}
1510	175140.23−293459.8	267.917650	−29.583299	0.2	2.7	12.6	5.0	7.4	7.7	0.90	2.3	-3.9	g...	...	583.3	2.2	3.2×10^{-16}
1511	175140.23−293619.8	267.917660	−29.605515	0.1	2.9	14.9	5.6	11.1	11.8	0.89	2.4	-3.9	....	a	856.7	3.5	4.0×10^{-16}
1512	175140.25−293233.7	267.917720	−29.542709	0.2	3.9	21.2	7.0	19.8	5.0	0.91	2.8	-4.6	....	b	835.9	1.4	1.4×10^{-16}
1513	175140.25−293223.0	267.917730	−29.539726	0.2	4.1	16.2	6.7	21.8	0.8	0.90	2.2	-2.9	....	a	838.2	1.1	2.3×10^{-16}
1514	175140.27−293319.3	267.917830	−29.555375	0.1	3.4	36.8	7.6	13.2	13.7	0.89	4.5	<-5	....	b	825.6	1.7	5.0×10^{-16}
1515	175140.28−293605.1	267.917860	−29.601440	0.1	2.8	41.3	7.8	11.7	24.2	0.89	4.9	<-5	....	b	855.7	2.4	7.6×10^{-16}
1516	175140.31−292751.5	267.917960	−29.464308	0.3	8.0	70.2	14.6	124.8	40.2	0.81	4.6	<-5	....	b	762.3	2.3	1.6×10^{-15}
1517	175140.34−293253.2	267.918090	−29.548136	0.2	3.7	12.6	5.8	15.4	0.0	0.89	2.0	-2.5	....	b	841.7	1.4	1.4×10^{-16}
1518	175140.35−294002.7	267.918130	−29.667433	0.2	5.4	49.8	11.0	59.2	22.5	0.90	4.3	<-5	....	a	818.6	1.9	3.3×10^{-16}
1519	175140.35−293323.8	267.918140	−29.556623	0.2	3.4	18.6	6.2	13.4	8.4	0.90	2.7	-4.8	....	b	830.4	2.2	7.4×10^{-16}
1520	175140.37−293733.6	267.918230	−29.626027	0.2	3.5	16.8	6.3	16.2	0.7	0.89	2.4	-3.7	....	a	851.2	1.5	1.9×10^{-16}
1521	175140.42−293432.0	267.918420	−29.575578	0.2	2.9	12.1	5.2	9.9	9.9	0.89	2.1	-3.1	g...	...	806.5	2.4	2.3×10^{-16}
1522	175140.48−293304.3	267.918700	−29.551197	0.1	3.6	32.5	7.4	14.5	10.2	0.90	4.1	<-5	....	a	845.0	1.7	4.2×10^{-16}
1523	175140.52−293054.0	267.918860	−29.515019	0.2	5.3	22.0	8.5	41.0	17.2	0.90	2.4	-3.0	g...	...	786.2	2.4	4.5×10^{-16}
1524	175140.55−294134.1	267.918960	−29.692809	0.2	6.7	70.9	14.2	113.1	13.2	0.89	4.8	<-5	....	a	779.0	1.1	4.3×10^{-16}
1525	175140.55−293340.5	267.918990	−29.561268	0.1	3.3	35.2	7.4	11.8	6.0	0.89	4.4	<-5	....	c	844.3	1.6	6.9×10^{-16}
1526	175140.56−293603.3	267.919010	−29.600930	0.1	2.9	35.3	7.4	11.7	3.2	0.89	4.5	<-5	....	b	856.7	1.1	3.0×10^{-16}
1527	175140.58−294234.8	267.919120	−29.709673	0.2	7.7	339.9	23.6	187.1	248.5	0.90	14.1	<-5	....	a	757.1	3.0	9.0×10^{-15}
1528	175140.61−293132.9	267.919230	−29.525827	0.2	4.8	16.7	7.7	33.3	6.6	0.90	2.0	-2.3	....	a	815.4	1.9	2.6×10^{-16}
1529	175140.61−293910.1	267.919250	−29.652832	0.2	4.7	40.6	9.6	41.4	22.6	0.90	4.0	<-5	....	a	832.0	2.9	9.1×10^{-16}
1530	175140.63−292953.3	267.919300	−29.498165	0.2	6.2	82.3	12.8	65.7	61.6	0.90	6.2	<-5	g...	...	780.3	3.1	2.2×10^{-15}

(*cont.*)

Table A.1: *Chandra* source list

Source		Position				Extracted Counts							Characteristics				
Seq	CXOU J	R. A.	Decl.	Err	θ	$C_{\rm net}$	$\Delta C_{\rm net}$	$C'_{\rm bkg}$	$C_{\rm net,hard}$	PSF	PS	$P_{\rm B}$	Anom	Var	EffExp	$E_{\rm median}$	Photo $F_{\rm x}$
#		(deg)	(deg)	($''$)	($'$)						Frac				(ks)	(keV)	(ergs s^{-1} cm^{-2})
(1)	(2)	(3)	(4)	(5)	(6)	(7)	(8)	(9)	(10)	(11)	(12)	(13)	(14)	(15)	(16)	(17)	(18)
1531	175140.67−293624.4	267.919490	−29.606794	0.1	3.0	17.3	5.8	10.7	10.9	0.89	2.7	-5.0	....	b	855.1	2.5	3.3×10^{-16}
1532	175140.68−293525.7	267.919530	−29.590487	0.2	2.9	10.4	4.9	8.6	2.9	0.89	1.9	-2.8	g...	...	670.3	1.3	5.9×10^{-16}
1533	175140.68−293346.0	267.919540	−29.562782	0.1	3.3	37.9	7.6	12.1	19.3	0.89	4.6	<-5	....	b	851.2	2.0	1.4×10^{-16}
1534	175140.72−292801.7	267.919680	−29.467162	0.3	7.9	53.1	13.7	115.9	21.6	0.81	3.7	<-5	....	b	765.4	1.9	9.7×10^{-16}
1535	175140.77−293540.3	267.919880	−29.594529	0.2	2.9	11.8	5.1	9.2	1.7	0.89	2.1	-3.2	g...	...	770.2	1.5	1.5×10^{-16}
1536	175140.79−293831.1	267.919990	−29.641976	0.1	4.2	175.3	14.8	27.7	123.4	0.90	11.5	<-5	....	a	840.7	3.0	4.0×10^{-15}
1537	175140.82−293736.7	267.920120	−29.626877	0.1	3.6	170.7	14.2	17.3	122.3	0.89	11.6	<-5	....	a	849.7	2.8	3.6×10^{-15}
1538	175140.88−294144.0	267.920360	−29.695562	0.2	6.9	181.0	18.2	129.0	133.6	0.90	9.7	<-5	....	a	777.5	3.1	4.7×10^{-15}
1539	175140.92−292738.7	267.920510	−29.460765	0.2	8.3	108.4	18.5	209.6	26.2	0.90	5.7	<-5	....	c	753.5	1.4	1.3×10^{-15}
1540	175140.93−293430.0	267.920580	−29.575016	0.1	3.0	16.1	5.8	11.9	3.5	0.89	2.5	-4.2	....	a	820.8	1.4	1.7×10^{-16}
1541	175141.03−293353.3	267.920960	−29.564827	0.1	3.3	50.4	8.5	12.6	3.6	0.90	5.6	<-5	....	b	849.0	1.3	5.0×10^{-16}
1542	175141.05−293512.5	267.921060	−29.586831	0.1	2.9	21.6	6.1	9.4	8.8	0.89	3.2	<-5	g...	...	711.9	1.9	3.9×10^{-16}
1543	175141.05−294116.0	267.921060	−29.687800	0.2	6.5	65.1	13.8	107.9	41.6	0.90	4.6	<-5	....	a	783.4	2.6	1.4×10^{-15}
1544	175141.07−293752.7	267.921140	−29.631310	0.2	3.8	20.4	7.0	20.6	12.9	0.90	2.7	-4.2	....	a	846.5	2.2	3.4×10^{-16}
1545	175141.11−293318.8	267.921310	−29.555247	0.2	3.6	13.8	6.0	16.2	0.0	0.90	2.1	-2.8	....	a	845.0	1.2	1.3×10^{-16}
1546	175141.11−293445.9	267.921310	−29.579417	0.1	2.9	22.0	6.3	11.0	4.7	0.89	3.2	<-5	g...	...	752.7	1.4	2.6×10^{-16}
1547	175141.12−293314.4	267.921370	−29.554021	0.2	3.6	18.7	6.5	16.3	6.2	0.90	2.7	-4.3	....	b	844.7	1.2	1.7×10^{-16}
1548	175141.24−293901.3	267.921860	−29.650374	0.2	4.6	22.8	8.5	39.2	6.7	0.90	2.5	-3.2	....	b	829.8	1.1	2.0×10^{-16}
1549	175141.25−293829.2	267.921910	−29.641469	0.2	4.2	22.1	7.6	26.9	3.5	0.90	2.7	-4.0	....	a	837.9	1.1	2.0×10^{-16}
1550	175141.26−293400.7	267.921920	−29.566864	0.2	3.3	11.6	5.6	13.4	4.4	0.89	1.9	-2.5	....	b	851.0	1.5	1.1×10^{-15}
1551	175141.26−293310.4	267.921950	−29.552905	0.1	3.7	52.9	8.8	16.1	35.8	0.89	5.6	<-5	....	a	839.1	2.6	1.3×10^{-16}
1552	175141.27−293220.6	267.921980	−29.539058	0.2	4.2	16.8	6.9	23.2	0.0	0.90	2.3	-2.9	....	a	821.5	1.2	1.6×10^{-16}
1553	175141.31−294006.8	267.922140	−29.668569	0.2	5.5	30.4	10.5	66.6	19.1	0.90	2.8	-3.4	....	a	811.7	2.9	7.0×10^{-16}
1554	175141.37−293542.4	267.922400	−29.595132	0.1	3.0	52.7	8.5	10.3	25.7	0.89	5.9	<-5	g...	...	792.9	2.0	8.7×10^{-16}
1555	175141.40−294305.2	267.922520	−29.718124	0.2	8.2	169.3	20.6	227.7	134.9	0.90	8.0	<-5	....	b	738.4	3.3	6.0×10^{-16}
1556	175141.40−293112.2	267.922540	−29.520076	0.2	5.1	52.3	10.1	38.7	4.7	0.90	4.9	<-5	g...	...	794.5	1.3	5.1×10^{-15}
1557	175141.44−293508.4	267.922670	−29.585668	0.1	3.0	22.0	6.2	10.0	5.8	0.89	3.3	<-5	g...	...	711.3	1.1	2.3×10^{-16}
1558	175141.45−293456.9	267.922720	−29.582492	0.2	3.0	13.7	5.4	10.3	5.3	0.90	2.3	-3.6	g...	...	614.0	1.0	1.5×10^{-16}
1559	175141.48−293950.1	267.922860	−29.663933	0.2	5.3	39.2	10.3	55.8	28.6	0.90	3.6	<-5	....	b	815.4	2.5	8.1×10^{-16}
1560	175141.53−293928.2	267.923070	−29.657841	0.2	5.0	32.6	9.5	47.4	6.9	0.90	3.2	-4.8	....	c	821.4	1.6	2.4×10^{-16}
1561	175141.53−293432.1	267.923080	−29.575605	0.2	3.1	13.5	5.5	11.5	8.4	0.89	2.2	-3.3	....	a	818.3	2.2	4.2×10^{-16}
1562	175141.60−293720.2	267.923350	−29.622279	0.2	3.6	12.5	5.9	16.5	2.9	0.90	1.9	-2.4	....	a	848.7	1.6	1.6×10^{-16}
1563	175141.64−293710.1	267.923510	−29.619480	0.1	3.5	46.7	8.3	14.3	27.1	0.90	5.3	<-5	....	a	849.5	2.6	9.1×10^{-16}
1564	175141.68−293350.8	267.923700	−29.564119	0.1	3.4	32.6	7.4	14.4	10.2	0.89	4.1	<-5	....	a	843.5	1.8	4.6×10^{-16}

(*cont.*)

Table A.1: *Chandra* source list

Source		Position				Extracted Counts							Characteristics				
Seq	CXOU J	R. A.	Decl.	Err	θ	$C_{\rm net}$	$\Delta C_{\rm net}$	$C'_{\rm bkg}$	$C_{\rm net,hard}$	PSF	PS	$P_{\rm B}$	Anom	Var	EffExp	$E_{\rm median}$	Photo $F_{\rm x}$
#		(deg)	(deg)	($''$)	($'$)						Frac				(ks)	(keV)	(ergs s^{-1} cm^{-2})
(1)	(2)	(3)	(4)	(5)	(6)	(7)	(8)	(9)	(10)	(11)	(12)	(13)	(14)	(15)	(16)	(17)	(18)
1565	175141.71−293333.7	267.923810	−29.559363	0.1	3.6	29.3	7.3	15.7	10.6	0.90	3.8	<-5	....	a	833.2	1.6	3.7×10^{-16}
1566	175141.71−293550.9	267.923810	−29.597486	0.1	3.1	17.4	5.9	11.6	5.8	0.89	2.7	-4.7	....	a	841.3	1.8	2.4×10^{-16}
1567	175141.74−293401.3	267.923920	−29.567049	0.2	3.3	13.7	5.7	13.3	4.1	0.90	2.2	-3.1	....	a	845.2	1.2	1.3×10^{-16}
1568	175141.82−293030.0	267.924290	−29.508349	0.2	5.8	26.2	9.7	55.8	4.1	0.89	2.6	-3.1	g...	...	787.4	1.5	3.4×10^{-16}
1569	175141.84−293110.0	267.924350	−29.519465	0.1	5.2	207.4	16.3	39.6	57.6	0.90	12.4	<-5	g...	...	796.0	1.5	2.7×10^{-15}
1570	175141.86−293728.9	267.924440	−29.624718	0.2	3.7	13.8	6.2	18.2	8.9	0.90	2.0	-2.6	....	a	844.8	4.1	4.4×10^{-16}
1571	175141.89−293211.8	267.924550	−29.536620	0.2	4.4	31.4	8.0	23.6	16.5	0.89	3.7	<-5	....	c	803.9	2.0	5.2×10^{-16}
1572	175141.93−292926.1	267.924740	−29.490588	0.1	6.7	216.3	18.1	88.7	125.6	0.90	11.7	<-5	....	a	775.3	2.4	4.5×10^{-15}
1573	175141.94−293528.8	267.924770	−29.591351	0.1	3.2	53.5	8.5	9.5	29.8	0.89	5.9	<-5	g...	...	643.4	2.4	1.4×10^{-15}
1574	175142.01−294002.9	267.925050	−29.667474	0.2	5.6	100.5	13.6	67.5	12.2	0.91	7.1	<-5	....	b	811.4	1.2	9.8×10^{-16}
1575	175142.03−293232.3	267.925160	−29.542318	0.1	4.2	73.6	10.3	22.4	32.4	0.90	6.8	<-5	g...	...	802.9	1.8	1.1×10^{-15}
1576	175142.05−293402.1	267.925210	−29.567269	0.1	3.4	121.4	12.1	13.6	96.0	0.90	9.6	<-5	....	a	838.8	3.5	3.4×10^{-15}
1577	175142.06−293610.7	267.925250	−29.602973	0.1	3.2	18.6	6.3	14.4	9.9	0.89	2.7	-4.6	....	b	840.2	2.1	1.8×10^{-16}
1578	175142.06−293536.4	267.925290	−29.593461	0.2	3.2	16.0	5.6	10.0	1.8	0.89	2.6	-4.6	g...	...	715.5	1.2	3.1×10^{-16}
1579	175142.11−293308.2	267.925470	−29.552288	0.2	3.9	21.7	6.9	18.3	2.3	0.91	2.9	-4.9	....	a	820.4	1.0	1.8×10^{-16}
1580	175142.12−293330.3	267.925530	−29.558444	0.1	3.7	74.2	10.1	16.8	22.2	0.90	7.0	<-5	....	c	824.1	1.3	7.7×10^{-16}
1581	175142.17−293058.2	267.925750	−29.516190	0.2	5.4	64.6	11.0	43.4	34.0	0.90	5.6	<-5	g...	...	797.2	2.4	1.3×10^{-15}
1582	175142.22−292800.1	267.925940	−29.466714	0.3	8.0	55.7	16.4	191.3	0.0	0.90	3.3	-4.3	....	a	744.6	1.2	6.0×10^{-16}
1583	175142.24−294015.5	267.926010	−29.670979	0.1	5.8	145.8	15.5	75.2	84.3	0.90	9.1	<-5	....	a	808.3	2.2	1.2×10^{-16}
1584	175142.24−293630.2	267.926020	−29.608398	0.2	3.3	11.1	5.6	13.9	1.1	0.90	1.8	-2.3	....	b	839.3	1.4	2.6×10^{-15}
1585	175142.26−294214.5	267.926110	−29.704040	0.3	7.5	23.1	8.9	45.9	3.1	0.56	2.5	-3.0	....	a	775.1	1.1	3.5×10^{-16}
1586	175142.32−293321.3	267.926360	−29.555944	0.2	3.8	12.4	6.0	17.6	3.2	0.90	1.9	-2.3	....	a	820.0	1.8	1.8×10^{-16}
1587	175142.37−294148.7	267.926550	−29.696872	0.2	7.1	61.8	15.1	147.2	37.2	0.90	4.0	<-5	....	a	783.2	2.4	1.2×10^{-15}
1588	175142.38−293622.6	267.926600	−29.606302	0.1	3.3	22.9	6.6	14.1	0.0	0.90	3.2	<-5	g...	...	831.9	1.0	1.8×10^{-16}
1589	175142.41−294207.6	267.926740	−29.702136	0.3	7.4	30.2	9.0	39.8	11.2	0.57	3.2	-4.9	....	b	776.9	1.6	6.3×10^{-16}
1590	175142.43−293335.7	267.926800	−29.559919	0.1	3.7	89.8	10.9	17.2	44.4	0.90	7.9	<-5	....	a	822.0	1.9	3.2×10^{-16}
1591	175142.43−293012.8	267.926820	−29.503565	0.3	6.1	22.2	10.0	65.8	7.5	0.90	2.1	-2.2	g...	...	784.3	1.7	1.5×10^{-16}
1592	175142.43−293259.6	267.926820	−29.549904	0.2	4.0	14.9	6.4	19.1	4.8	0.90	2.1	-2.8	....	b	804.9	1.2	1.4×10^{-15}
1593	175142.44−293440.2	267.926860	−29.577834	0.1	3.2	71.0	9.7	13.0	10.7	0.89	6.9	<-5	g...	...	751.9	1.3	7.9×10^{-16}
1594	175142.47−293232.3	267.926960	−29.542314	0.2	4.3	24.0	7.4	23.0	6.1	0.90	3.0	-4.9	g...	...	805.2	1.2	2.5×10^{-16}
1595	175142.47−293717.8	267.926970	−29.621629	0.2	3.7	20.0	6.6	16.0	5.8	0.90	2.8	-4.8	....	a	830.5	1.4	2.2×10^{-16}
1596	175142.48−293901.9	267.927040	−29.650541	0.2	4.8	47.8	10.1	42.2	16.8	0.89	4.5	<-5	....	b	823.6	1.6	6.2×10^{-16}
1597	175142.51−293251.1	267.927130	−29.547539	0.2	4.1	20.9	7.0	21.1	3.7	0.90	2.8	-4.3	g...	...	806.8	0.9	1.5×10^{-16}
1598	175142.55−293646.2	267.927320	−29.612861	0.2	3.5	14.0	5.9	15.0	3.3	0.89	2.2	-3.0	....	c	834.6	1.4	1.5×10^{-16}

(*cont.*)

Table A.1: *Chandra* source list

Source		Position				Extracted Counts							Characteristics				
Seq	CXOU J	R. A.	Decl.	Err	θ	$C_{\rm net}$	$\Delta C_{\rm net}$	$C'_{\rm bkg}$	$C_{\rm net,hard}$	PSF	PS	$P_{\rm B}$	Anom	Var	EffExp	$E_{\rm median}$	Photo $F_{\rm x}$
#		(deg)	(deg)	($''$)	($'$)						Frac				(ks)	(keV)	(ergs s^{-1} cm^{-2})
(1)	(2)	(3)	(4)	(5)	(6)	(7)	(8)	(9)	(10)	(11)	(12)	(13)	(14)	(15)	(16)	(17)	(18)
1599	175142.59−293511.9	267.927480	−29.586651	0.1	3.2	50.1	8.5	12.9	41.0	0.90	5.6	<-5	g...	...	768.7	3.1	1.3×10^{-15}
1600	175142.62−293331.6	267.927600	−29.558802	0.1	3.7	53.9	9.0	17.1	15.8	0.90	5.7	<-5	....	b	815.6	1.5	6.5×10^{-16}
1601	175142.67−293200.8	267.927800	−29.533563	0.2	4.7	21.8	7.8	30.2	7.5	0.90	2.6	-3.6	....	a	806.7	1.3	2.3×10^{-16}
1602	175142.70−293555.9	267.927940	−29.598878	0.2	3.3	16.6	6.2	15.4	13.9	0.89	2.5	-3.7	....	b	837.1	2.9	3.8×10^{-16}
1603	175142.79−292716.3	267.928310	−29.454541	0.3	8.8	43.9	17.8	246.1	0.0	0.89	2.4	-2.5	....	b	734.0	1.0	4.0×10^{-16}
1604	175142.83−293435.1	267.928500	−29.576434	0.2	3.4	19.0	6.4	15.0	10.4	0.90	2.7	-4.6	g...	...	783.6	2.5	4.0×10^{-16}
1605	175142.84−293802.3	267.928510	−29.633982	0.1	4.2	40.5	8.6	24.5	10.1	0.90	4.4	<-5	....	a	820.9	1.5	5.0×10^{-16}
1606	175142.85−292636.5	267.928550	−29.443486	0.4	9.3	33.2	15.1	174.8	27.4	0.90	2.1	-2.1	....	a	434.7	5.4	2.7×10^{-15}
1607	175142.89−294206.9	267.928710	−29.701929	0.3	7.5	25.8	12.0	102.2	22.5	0.79	2.1	-2.1	....	a	775.7	3.0	7.4×10^{-16}
1608	175142.92−293443.6	267.928840	−29.578787	0.1	3.3	77.3	10.0	12.7	51.1	0.90	7.3	<-5	g...	...	705.4	2.7	4.3×10^{-16}
1609	175142.92−293127.1	267.928860	−29.524211	0.2	5.1	23.3	8.6	40.7	13.2	0.90	2.6	-3.3	....	a	797.5	2.2	1.9×10^{-15}
1610	175142.94−293924.6	267.928920	−29.656861	0.2	5.2	28.5	9.6	52.5	8.7	0.90	2.8	-3.7	....	a	818.6	1.6	3.6×10^{-16}
1611	175143.04−294328.3	267.929340	−29.724554	0.3	8.6	55.9	16.2	185.1	53.2	0.90	3.3	-4.5	g...	...	550.4	3.5	4.4×10^{-16}
1612	175143.04−293947.8	267.929350	−29.663291	0.2	5.5	23.7	7.3	21.3	9.4	0.69	3.0	<-5	....	a	814.1	1.8	2.4×10^{-15}
1613	175143.06−293902.3	267.929450	−29.650646	0.2	4.9	18.9	8.7	46.1	0.6	0.90	2.1	-2.2	....	a	818.6	1.2	1.8×10^{-16}
1614	175143.17−293436.0	267.929880	−29.576691	0.2	3.4	18.2	6.3	14.8	4.5	0.90	2.7	-4.4	g...	...	751.5	1.2	2.0×10^{-16}
1615	175143.18−293402.6	267.929940	−29.567413	0.1	3.6	148.8	13.3	15.2	71.4	0.90	10.7	<-5	g...	...	800.9	1.9	2.3×10^{-15}
1616	175143.19−293943.4	267.929980	−29.662083	0.2	5.5	37.7	8.8	29.3	17.9	0.77	4.1	<-5	....	b	815.0	1.9	6.7×10^{-16}
1617	175143.24−293121.2	267.930170	−29.522560	0.2	5.3	46.5	10.0	41.5	2.2	0.90	4.4	<-5	g...	...	790.8	1.0	4.1×10^{-16}
1618	175143.24−293514.8	267.930200	−29.587460	0.1	3.4	117.4	12.0	13.6	57.5	0.90	9.4	<-5	g...	...	755.5	1.9	1.9×10^{-15}
1619	175143.36−293003.4	267.930700	−29.500955	0.3	6.3	31.7	11.1	77.3	16.3	0.90	2.7	-3.3	....	a	780.5	2.4	6.2×10^{-16}
1620	175143.38−293504.0	267.930760	−29.584449	0.1	3.4	196.1	15.0	12.9	127.2	0.90	12.7	<-5	g...	...	696.9	2.7	5.1×10^{-15}
1621	175143.38−293601.4	267.930780	−29.600416	0.1	3.4	21.0	6.6	16.0	4.2	0.89	2.9	<-5	....	a	832.2	1.6	2.7×10^{-16}
1622	175143.46−293915.9	267.931090	−29.654429	0.2	5.1	25.9	9.0	45.1	14.5	0.87	2.7	-3.5	....	a	812.3	2.1	4.4×10^{-16}
1623	175143.57−293148.6	267.931550	−29.530189	0.1	5.0	318.1	19.3	34.9	221.8	0.91	16.0	<-5	g...	...	792.1	3.0	8.1×10^{-15}
1624	175143.59−294237.6	267.931660	−29.710462	0.2	8.0	73.1	13.0	80.9	45.0	0.67	5.4	<-5	....	b	759.7	2.6	2.3×10^{-15}
1625	175143.61−293933.0	267.931740	−29.659189	0.1	5.4	115.6	13.7	56.4	50.3	0.90	8.1	<-5	....	a	810.9	1.9	1.8×10^{-15}
1626	175143.63−293224.6	267.931800	−29.540168	0.1	4.6	356.6	20.1	26.4	27.3	0.89	17.3	<-5	g...	...	795.0	1.0	3.0×10^{-15}
1627	175143.64−293325.4	267.931870	−29.557065	0.1	4.0	50.8	9.0	20.2	8.3	0.90	5.3	<-5	g...	...	787.9	1.5	6.7×10^{-16}
1628	175143.64−293355.2	267.931870	−29.565347	0.2	3.8	18.3	6.6	17.7	1.9	0.90	2.6	-3.9	g...	...	796.0	1.6	2.6×10^{-16}
1629	175143.66−293810.3	267.931950	−29.636198	0.2	4.4	26.8	8.0	28.2	2.6	0.90	3.1	<-5	....	a	817.2	1.2	2.6×10^{-16}
1630	175143.69−293300.6	267.932050	−29.550172	0.2	4.2	19.4	7.0	21.6	9.1	0.90	2.6	-3.8	g...	...	802.8	1.5	2.6×10^{-16}
1631	175143.72−294045.4	267.932180	−29.679287	0.2	6.4	36.4	12.4	102.6	7.7	0.90	2.8	-3.3	....	a	795.0	1.5	4.4×10^{-16}
1632	175143.75−293610.7	267.932300	−29.602977	0.1	3.5	25.6	7.1	17.4	18.8	0.90	3.3	<-5	....	a	828.0	3.4	7.2×10^{-16}

(*cont.*)

Table A.1: *Chandra* source list

Source		Position				Extracted Counts							Characteristics				
Seq	CXOU J	R. A.	Decl.	Err	θ	$C_{\rm net}$	$\Delta C_{\rm net}$	$C'_{\rm bkg}$	$C_{\rm net,hard}$	PSF	PS	$P_{\rm B}$	Anom	Var	EffExp	$E_{\rm median}$	Photo $F_{\rm x}$
#		(deg)	(deg)	($''$)	($'$)						Frac				(ks)	(keV)	(ergs s^{-1} cm^{-2})
(1)	(2)	(3)	(4)	(5)	(6)	(7)	(8)	(9)	(10)	(11)	(12)	(13)	(14)	(15)	(16)	(17)	(18)
1633	175143.77−293243.5	267.932390	−29.545419	0.1	4.4	83.2	10.9	23.8	40.9	0.89	7.3	<-5	g...	...	793.4	1.9	4.1×10^{-16}
1634	175143.77−293425.6	267.932400	−29.573778	0.2	3.6	13.6	6.1	17.4	9.9	0.90	2.0	-2.6	g...	...	798.4	4.6	1.4×10^{-15}
1635	175143.77−293052.2	267.932410	−29.514508	0.2	5.7	37.6	10.0	51.4	10.2	0.89	3.6	<-5	....	b	792.1	1.3	5.3×10^{-16}
1636	175143.78−293659.9	267.932440	−29.616649	0.2	3.8	19.1	6.7	18.9	3.3	0.90	2.6	-4.0	....	a	828.7	1.5	2.4×10^{-16}
1637	175143.82−292709.5	267.932610	−29.452661	0.3	9.0	112.7	20.2	266.3	36.1	0.90	5.4	<-5	....	a	731.6	1.3	1.3×10^{-15}
1638	175143.85−293534.5	267.932730	−29.592940	0.2	3.5	18.1	6.3	14.9	10.3	0.90	2.6	-4.3	g...	...	702.1	2.7	4.6×10^{-16}
1639	175143.86−293322.1	267.932760	−29.556157	0.1	4.1	60.4	9.7	22.6	54.1	0.90	5.9	<-5	g...	...	797.4	3.1	4.2×10^{-16}
1640	175143.86−292933.5	267.932790	−29.492649	0.3	6.8	32.9	12.1	98.1	0.9	0.90	2.6	-3.0	....	a	776.6	1.5	1.6×10^{-15}
1641	175143.94−293317.7	267.933100	−29.554932	0.1	4.1	98.1	11.5	22.9	92.0	0.90	8.1	<-5	g...	...	798.4	4.1	3.5×10^{-15}
1642	175143.97−293213.8	267.933240	−29.537167	0.1	4.7	85.7	11.4	31.3	61.4	0.91	7.2	<-5	g...	...	793.4	2.8	2.0×10^{-15}
1643	175143.99−293915.0	267.933320	−29.654179	0.2	5.2	46.5	10.5	51.5	19.6	0.90	4.2	<-5	....	b	807.2	1.8	6.8×10^{-16}
1644	175144.06−293351.0	267.933590	−29.564184	0.2	3.9	28.3	7.4	18.7	8.8	0.90	3.6	<-5	g...	...	792.1	1.6	3.9×10^{-16}
1645	175144.09−293135.7	267.933740	−29.526604	0.1	5.2	218.0	16.7	42.0	27.8	0.90	12.7	<-5	....	c	800.3	1.2	2.1×10^{-15}
1646	175144.15−293254.9	267.933970	−29.548597	0.2	4.4	13.3	6.6	22.7	0.0	0.89	1.9	-2.2	g...	...	792.5	1.2	1.4×10^{-16}
1647	175144.24−294005.0	267.934340	−29.668083	0.2	5.9	82.5	13.3	77.5	36.4	0.90	6.0	<-5	g...	...	789.8	1.9	1.4×10^{-15}
1648	175144.25−294253.3	267.934410	−29.714823	0.2	8.3	224.8	22.5	251.2	162.7	0.90	9.8	<-5	....	c	753.6	3.1	6.0×10^{-15}
1649	175144.26−294235.3	267.934430	−29.709817	0.2	8.0	254.3	21.6	182.7	182.0	0.86	11.5	<-5	....	b	759.0	3.1	1.3×10^{-15}
1650	175144.26−293321.4	267.934450	−29.555948	0.1	4.1	45.0	8.9	24.0	37.6	0.90	4.8	<-5	g...	...	792.6	3.4	7.1×10^{-15}
1651	175144.29−293617.8	267.934560	−29.604955	0.1	3.7	49.2	8.9	20.8	18.9	0.90	5.2	<-5	....	b	809.9	1.8	7.4×10^{-16}
1652	175144.35−293848.7	267.934810	−29.646888	0.2	5.0	28.7	9.0	42.3	21.5	0.90	3.0	-4.3	....	a	810.0	3.5	2.0×10^{-15}
1653	175144.35−293531.2	267.934830	−29.592010	0.1	3.7	42.8	8.1	14.2	43.2	0.90	5.0	<-5	g...	...	643.9	4.1	8.5×10^{-16}
1654	175144.40−293944.4	267.935000	−29.662358	0.2	5.6	47.2	11.5	70.8	42.0	0.90	3.9	<-5	....	b	798.2	4.2	1.7×10^{-15}
1655	175144.44−293439.5	267.935200	−29.577654	0.2	3.7	19.4	6.3	13.6	0.0	0.90	2.8	<-5	g...	...	685.9	1.1	2.0×10^{-16}
1656	175144.47−293301.6	267.935320	−29.550458	0.2	4.3	13.6	6.7	23.4	2.9	0.90	1.9	-2.2	g...	...	796.8	1.6	1.8×10^{-16}
1657	175144.51−293812.8	267.935470	−29.636891	0.2	4.6	18.3	7.8	33.7	5.3	0.90	2.2	-2.6	....	a	819.7	1.1	1.7×10^{-16}
1658	175144.54−293840.1	267.935620	−29.644492	0.1	4.9	87.4	11.8	39.6	62.0	0.90	7.1	<-5	....	a	814.9	2.8	2.0×10^{-15}
1659	175144.60−292733.8	267.935850	−29.459395	0.2	8.7	252.8	23.1	249.2	173.9	0.89	10.7	<-5	....	a	753.0	3.0	6.7×10^{-15}
1660	175144.62−294010.5	267.935930	−29.669607	0.2	6.0	74.0	12.8	74.0	10.1	0.87	5.6	<-5	....	c	785.8	1.4	4.3×10^{-16}
1661	175144.62−293656.9	267.935950	−29.615833	0.2	4.0	24.0	7.3	22.0	11.1	0.90	3.1	<-5	....	a	810.6	2.2	8.9×10^{-16}
1662	175144.76−293211.2	267.936510	−29.536466	0.1	4.9	72.7	10.9	34.3	38.3	0.90	6.4	<-5	g...	...	800.3	2.1	1.3×10^{-15}
1663	175144.77−292949.4	267.936560	−29.497064	0.2	6.7	68.2	13.5	96.8	10.4	0.90	4.9	<-5	....	b	787.2	1.4	7.8×10^{-16}
1664	175144.80−293142.4	267.936680	−29.528458	0.2	5.2	41.3	9.9	44.7	28.4	0.90	4.0	<-5	g...	...	802.0	2.8	9.7×10^{-16}
1665	175144.81−293408.1	267.936730	−29.568926	0.2	3.9	13.2	6.3	19.8	1.0	0.90	1.9	-2.3	g...	...	787.3	1.7	2.0×10^{-16}
1666	175144.82−293602.7	267.936750	−29.600757	0.1	3.8	111.8	12.0	20.2	31.0	0.90	8.9	<-5	g...	...	791.2	1.6	1.6×10^{-15}

(*cont.*)

Table A.1: *Chandra* source list

Source		Position				Extracted Counts							Characteristics				
Seq	CXOU J	R. A.	Decl.	Err	θ	$C_{\rm net}$	$\Delta C_{\rm net}$	$C'_{\rm bkg}$	$C_{\rm net,hard}$	PSF	PS	$P_{\rm B}$	Anom	Var	EffExp	$E_{\rm median}$	Photo $F_{\rm x}$
#		(deg)	(deg)	($''$)	($'$)						Frac				(ks)	(keV)	(ergs s^{-1} cm^{-2})
(1)	(2)	(3)	(4)	(5)	(6)	(7)	(8)	(9)	(10)	(11)	(12)	(13)	(14)	(15)	(16)	(17)	(18)
1667	175144.82−293710.9	267.936760	−29.619706	0.1	4.1	82.7	10.8	22.3	35.2	0.90	7.3	<-5	....	c	809.7	1.7	1.2×10^{-15}
1668	175144.85−293743.0	267.936910	−29.628618	0.1	4.4	84.9	11.3	31.1	25.6	0.90	7.2	<-5	....	b	822.8	1.4	9.7×10^{-16}
1669	175144.97−292747.1	267.937390	−29.463093	0.3	8.5	82.5	17.2	191.5	45.0	0.85	4.6	<-5	....	b	757.6	2.5	1.9×10^{-15}
1670	175144.97−293802.0	267.937390	−29.633890	0.0	4.6	667.6	27.0	33.4	436.8	0.90	24.3	<-5	....	a	823.7	2.7	1.4×10^{-14}
1671	175144.98−294002.9	267.937440	−29.667478	0.1	5.9	261.8	19.1	80.2	169.5	0.90	13.4	<-5	....	a	791.1	2.6	5.9×10^{-15}
1672	175145.02−292824.7	267.937620	−29.473545	0.2	7.9	79.4	13.1	76.6	51.5	0.69	5.8	<-5	....	a	769.3	2.4	2.1×10^{-15}
1673	175145.06−293013.7	267.937760	−29.503823	0.2	6.4	89.8	13.8	83.2	75.0	0.90	6.3	<-5	....	a	794.7	3.5	1.7×10^{-15}
1674	175145.06−292635.1	267.937780	−29.443104	0.4	9.5	43.6	11.1	65.4	19.6	0.64	3.8	<-5	....	a	435.0	1.9	2.6×10^{-15}
1675	175145.11−293825.7	267.937960	−29.640486	0.1	4.8	93.3	12.0	36.7	0.3	0.90	7.5	<-5	....	b	820.6	0.9	5.4×10^{-16}
1676	175145.11−292915.9	267.937990	−29.487764	0.2	7.2	62.9	14.3	123.1	0.8	0.89	4.2	<-5	....	b	782.5	1.0	6.6×10^{-16}
1677	175145.15−292701.5	267.938160	−29.450417	0.3	9.2	49.2	18.8	274.8	23.7	0.90	2.6	-2.7	....	a	694.8	1.6	7.7×10^{-16}
1678	175145.17−292850.4	267.938250	−29.480687	0.3	7.6	50.0	13.6	117.0	49.2	0.83	3.5	-4.9	....	a	776.4	3.2	1.4×10^{-15}
1679	175145.22−293102.1	267.938430	−29.517250	0.2	5.8	34.5	10.1	55.5	5.0	0.89	3.2	-4.7	....	b	799.9	1.5	4.4×10^{-16}
1680	175145.31−293858.1	267.938800	−29.649490	0.2	5.2	73.3	11.6	47.7	35.3	0.90	6.1	<-5	....	a	810.5	2.0	1.2×10^{-15}
1681	175145.33−293739.1	267.938900	−29.627532	0.2	4.4	15.2	7.1	26.8	7.7	0.89	2.0	-2.3	g...	...	789.0	2.4	3.1×10^{-16}
1682	175145.36−293528.4	267.939040	−29.591244	0.2	3.9	21.6	6.5	13.4	12.0	0.90	3.1	<-5	g...	...	613.5	2.2	5.7×10^{-16}
1683	175145.37−294323.1	267.939060	−29.723097	0.2	8.7	164.0	19.8	203.0	108.0	0.90	8.1	<-5	g...	...	561.0	2.9	6.2×10^{-15}
1684	175145.42−293637.6	267.939290	−29.610459	0.2	4.0	34.9	8.0	21.1	6.6	0.90	4.1	<-5	g...	...	778.6	1.2	3.8×10^{-16}
1685	175145.44−293405.0	267.939370	−29.568062	0.1	4.1	248.8	17.0	23.2	13.0	0.90	14.2	<-5	g...	...	803.2	1.0	2.0×10^{-15}
1686	175145.44−294234.9	267.939370	−29.709716	0.2	8.1	100.9	18.7	224.1	69.8	0.90	5.2	<-5	....	a	749.8	2.8	2.5×10^{-15}
1687	175145.60−292826.1	267.940040	−29.473927	0.3	8.0	58.3	12.0	70.7	0.0	0.66	4.7	<-5	....	a	768.3	1.3	8.6×10^{-16}
1688	175145.60−294008.6	267.940040	−29.669069	0.2	6.1	126.1	15.2	85.9	97.0	0.89	8.0	<-5	....	b	792.9	2.9	3.0×10^{-15}
1689	175145.61−293552.9	267.940050	−29.598048	0.2	3.9	11.6	6.0	18.4	3.8	0.90	1.8	-2.0	g...	...	765.7	1.0	1.3×10^{-15}
1690	175145.61−292836.5	267.940060	−29.476815	0.3	7.8	54.0	16.0	181.0	34.5	0.90	3.3	-4.3	....	a	771.5	2.9	1.1×10^{-16}
1691	175145.66−293300.0	267.940280	−29.550000	0.2	4.6	14.9	7.1	28.1	1.1	0.89	1.9	-2.2	....	a	814.5	1.4	1.7×10^{-16}
1692	175145.72−293333.3	267.940520	−29.559252	0.2	4.3	18.7	7.1	24.3	5.5	0.90	2.4	-3.3	....	a	812.2	1.6	2.5×10^{-16}
1693	175145.75−293649.8	267.940630	−29.613861	0.2	4.2	16.8	6.9	23.2	18.8	0.90	2.3	-2.9	g...	...	771.0	4.1	6.1×10^{-16}
1694	175145.83−293726.2	267.940960	−29.623951	0.2	4.4	33.1	8.3	26.9	34.2	0.90	3.7	<-5	g...	...	781.8	4.2	1.2×10^{-15}
1695	175145.87−293139.9	267.941150	−29.527771	0.2	5.4	69.4	11.5	50.6	8.4	0.90	5.8	<-5	....	a	808.4	1.3	7.6×10^{-16}
1696	175145.90−293224.6	267.941250	−29.540175	0.2	5.0	30.6	9.0	40.4	6.5	0.90	3.2	-4.9	....	b	814.3	1.2	3.0×10^{-16}
1697	175145.90−294205.7	267.941270	−29.701609	0.2	7.8	94.3	17.5	189.7	18.5	0.90	5.2	<-5	....	a	754.1	1.3	6.0×10^{-16}
1698	175145.90−293424.7	267.941280	−29.573535	0.2	4.1	37.5	8.5	25.5	17.7	0.90	4.2	<-5	g...	...	808.5	1.9	1.1×10^{-15}
1699	175145.94−293457.7	267.941420	−29.582719	0.2	4.0	24.9	6.8	14.1	1.9	0.89	3.4	<-5	g...	...	609.4	1.1	3.4×10^{-16}
1700	175145.95−292855.0	267.941460	−29.481970	0.3	7.6	31.2	11.8	93.8	29.2	0.79	2.5	-2.8	....	b	776.0	3.2	9.4×10^{-16}

(*cont.*)

Table A.1: *Chandra* source list

Source		Position				Extracted Counts							Characteristics				
Seq	CXOU J	R. A.	Decl.	Err	θ	$C_{\rm net}$	$\Delta C_{\rm net}$	$C'_{\rm bkg}$	$C_{\rm net,hard}$	PSF	PS	$P_{\rm B}$	Anom	Var	EffExp	$E_{\rm median}$	Photo $F_{\rm x}$
#		(deg)	(deg)	($''$)	($'$)						Frac				(ks)	(keV)	(ergs s^{-1} cm^{-2})
(1)	(2)	(3)	(4)	(5)	(6)	(7)	(8)	(9)	(10)	(11)	(12)	(13)	(14)	(15)	(16)	(17)	(18)
1701	175145.95−293453.3	267.941470	−29.581497	0.2	4.0	12.8	5.7	14.2	2.3	0.90	2.0	-2.7	g...	...	560.0	1.4	2.5×10^{-16}
1702	175146.02−292640.8	267.941750	−29.444681	0.3	9.5	69.5	13.4	92.5	40.9	0.72	5.0	<-5	....	a	426.1	2.2	3.0×10^{-15}
1703	175146.02−294042.1	267.941790	−29.678378	0.2	6.6	70.7	14.1	111.3	10.9	0.90	4.8	<-5	....	b	784.8	1.4	8.0×10^{-16}
1704	175146.05−293552.3	267.941880	−29.597885	0.1	4.0	127.4	12.6	18.6	84.8	0.90	9.7	<-5	g...	...	742.4	3.0	3.8×10^{-15}
1705	175146.06−293340.8	267.941940	−29.561359	0.2	4.3	25.3	7.6	24.7	8.5	0.89	3.1	<-5	....	a	812.5	1.5	3.1×10^{-16}
1706	175146.17−293255.7	267.942390	−29.548826	0.2	4.7	16.7	7.8	35.3	0.0	0.90	2.0	-2.2	....	a	818.9	1.1	1.5×10^{-16}
1707	175146.24−294022.1	267.942690	−29.672819	0.1	6.4	191.0	17.5	96.0	109.9	0.90	10.6	<-5	....	a	785.2	2.4	9.4×10^{-16}
1708	175146.24−293745.6	267.942700	−29.629343	0.2	4.6	41.2	9.1	30.8	26.4	0.90	4.3	<-5	g...	...	774.4	2.5	3.9×10^{-15}
1709	175146.28−293716.9	267.942870	−29.621365	0.2	4.4	22.9	7.6	26.1	11.7	0.90	2.8	-4.2	g...	...	768.5	2.0	4.0×10^{-16}
1710	175146.35−293508.3	267.943130	−29.585661	0.2	4.1	24.9	7.3	20.1	4.4	0.90	3.2	<-5	g...	...	701.5	1.6	4.2×10^{-16}
1711	175146.36−293841.4	267.943170	−29.644858	0.2	5.2	56.0	10.7	47.0	38.3	0.90	5.0	<-5	g...	...	769.7	3.1	1.5×10^{-15}
1712	175146.36−293932.2	267.943200	−29.658955	0.2	5.8	94.0	13.6	76.0	63.4	0.90	6.6	<-5	....	a	780.8	2.7	2.1×10^{-15}
1713	175146.44−293751.9	267.943530	−29.631111	0.2	4.7	21.8	7.6	28.2	10.7	0.87	2.7	-3.8	g...	...	766.0	2.0	4.0×10^{-16}
1714	175146.46−293123.2	267.943620	−29.523116	0.2	5.7	48.0	10.8	57.0	5.1	0.89	4.2	<-5	....	a	808.8	1.1	4.1×10^{-16}
1715	175146.50−293219.2	267.943750	−29.538682	0.1	5.1	475.8	23.4	45.2	255.2	0.90	19.9	<-5	....	b	817.4	2.2	8.3×10^{-15}
1716	175146.50−293325.4	267.943780	−29.557071	0.2	4.5	46.3	9.2	28.7	8.4	0.89	4.7	<-5	....	b	819.9	1.4	5.2×10^{-16}
1717	175146.51−293619.8	267.943810	−29.605513	0.2	4.2	29.7	7.7	21.3	2.8	0.90	3.6	<-5	g...	...	721.1	1.0	3.1×10^{-16}
1718	175146.54−293214.2	267.943940	−29.537302	0.2	5.2	43.8	9.9	43.2	0.0	0.90	4.2	<-5	....	b	817.5	1.1	4.0×10^{-16}
1719	175146.58−293802.5	267.944100	−29.634044	0.2	4.9	22.6	8.3	37.4	11.8	0.90	2.5	-3.3	g...	...	765.2	2.0	4.0×10^{-16}
1720	175146.64−292833.8	267.944340	−29.476081	0.3	8.0	40.2	16.2	198.8	20.5	0.90	2.4	-2.5	....	a	766.5	2.0	6.7×10^{-16}
1721	175146.69−293510.8	267.944570	−29.586337	0.2	4.1	15.5	6.6	21.5	9.7	0.90	2.2	-2.8	g...	...	696.3	2.2	3.6×10^{-16}
1722	175146.69−293640.1	267.944580	−29.611162	0.2	4.3	21.0	7.3	24.0	8.2	0.90	2.7	-3.9	g...	...	714.5	1.8	4.0×10^{-16}
1723	175146.71−293008.6	267.944650	−29.502404	0.3	6.7	34.1	12.2	98.9	2.4	0.90	2.7	-3.1	....	b	791.8	1.3	3.6×10^{-16}
1724	175146.71−293554.9	267.944650	−29.598597	0.2	4.1	29.1	7.6	19.9	25.9	0.90	3.6	<-5	g...	...	713.7	4.7	1.5×10^{-15}
1725	175146.71−293856.9	267.944660	−29.649142	0.2	5.4	32.8	9.8	52.2	7.7	0.90	3.2	-4.6	g...	...	771.0	1.4	4.0×10^{-16}
1726	175146.72−293546.8	267.944670	−29.596356	0.2	4.1	23.3	7.0	18.7	3.3	0.90	3.1	<-5	g...	...	721.4	1.2	3.0×10^{-16}
1727	175146.76−294129.2	267.944850	−29.691463	0.2	7.3	178.2	19.0	158.8	121.6	0.90	9.1	<-5	....	a	764.9	2.8	4.3×10^{-15}
1728	175146.77−293540.5	267.944880	−29.594610	0.2	4.1	20.8	6.8	18.2	8.9	0.90	2.8	-4.6	g...	...	702.5	1.3	3.1×10^{-16}
1729	175146.78−293400.3	267.944920	−29.566763	0.2	4.4	39.0	8.7	27.0	9.9	0.90	4.2	<-5	....	b	820.0	1.1	3.6×10^{-16}
1730	175146.78−293752.8	267.944950	−29.631337	0.2	4.8	32.9	8.4	29.1	10.7	0.87	3.7	<-5	g...	...	768.2	1.6	5.1×10^{-16}
1731	175146.86−293521.3	267.945280	−29.589254	0.2	4.2	25.6	7.2	18.4	13.4	0.90	3.3	<-5	g...	...	577.0	2.3	7.7×10^{-16}
1732	175146.92−294304.3	267.945540	−29.717862	0.1	8.7	704.5	31.8	264.5	559.6	0.90	21.8	<-5	....	b	728.9	3.2	2.0×10^{-14}
1733	175146.97−293424.6	267.945740	−29.573519	0.2	4.3	44.6	9.0	27.4	15.3	0.90	4.7	<-5	....	a	813.7	1.6	5.7×10^{-16}
1734	175146.98−292801.0	267.945790	−29.466948	0.3	8.5	60.7	17.6	223.3	40.7	0.88	3.4	-4.4	....	b	749.7	3.3	1.8×10^{-15}

(*cont.*)

Table A.1: *Chandra* source list

Source		Position				Extracted Counts				Characteristics							
Seq	CXOU J	R. A.	Decl.	Err	θ	$C_{\rm net}$	$\Delta C_{\rm net}$	$C'_{\rm bkg}$	$C_{\rm net,hard}$	PSF	PS	$P_{\rm B}$	Anom	Var	EffExp	$E_{\rm median}$	Photo $F_{\rm x}$
#		(deg)	(deg)	($''$)	($'$)						Frac				(ks)	(keV)	(ergs s^{-1} cm^{-2})
(1)	(2)	(3)	(4)	(5)	(6)	(7)	(8)	(9)	(10)	(11)	(12)	(13)	(14)	(15)	(16)	(17)	(18)
1735	175147.05−293001.0	267.946050	−29.500303	0.2	6.8	51.7	13.3	107.3	11.1	0.90	3.8	<-5	....	b	788.4	1.5	6.5×10^{-16}
1736	175147.08−293957.5	267.946200	−29.665992	0.3	6.2	25.4	11.4	89.6	5.1	0.90	2.1	-2.2	g...	...	747.4	1.4	3.3×10^{-16}
1737	175147.09−293535.0	267.946240	−29.593076	0.2	4.2	29.3	7.6	19.7	6.9	0.90	3.6	<-5	g...	...	681.0	1.6	5.1×10^{-16}
1738	175147.12−293908.7	267.946340	−29.652432	0.2	5.6	64.7	11.7	59.3	19.3	0.90	5.3	<-5	g...	...	765.1	1.5	8.5×10^{-16}
1739	175147.19−293030.5	267.946640	−29.508490	0.3	6.5	36.1	11.7	86.9	12.9	0.90	2.9	-3.7	....	a	795.2	1.7	7.1×10^{-15}
1740	175147.19−292710.4	267.946650	−29.452899	0.2	9.2	275.2	24.8	302.8	194.6	0.90	10.9	<-5	....	a	722.2	2.8	5.0×10^{-16}
1741	175147.20−293834.1	267.946680	−29.642812	0.2	5.3	46.0	10.3	49.0	23.5	0.90	4.2	<-5	g...	...	766.9	2.1	8.6×10^{-16}
1742	175147.21−293331.7	267.946730	−29.558817	0.2	4.6	19.6	7.7	31.4	0.9	0.90	2.4	-3.0	....	c	821.5	1.7	2.7×10^{-16}
1743	175147.23−293505.5	267.946810	−29.584863	0.2	4.2	35.2	8.6	28.8	18.3	0.90	3.9	<-5	g...	...	775.0	1.9	5.8×10^{-16}
1744	175147.28−293811.2	267.947010	−29.636465	0.2	5.1	42.8	9.6	38.2	12.1	0.90	4.2	<-5	g...	...	742.9	1.5	6.3×10^{-16}
1745	175147.45−293305.6	267.947740	−29.551564	0.2	4.9	50.7	10.2	42.3	23.2	0.90	4.7	<-5	....	b	819.4	1.9	7.5×10^{-16}
1746	175147.46−294215.1	267.947760	−29.704212	0.2	8.1	306.6	23.4	211.4	211.5	0.90	12.8	<-5	....	b	743.9	3.0	8.1×10^{-15}
1747	175147.51−293856.6	267.947960	−29.649076	0.2	5.6	20.4	9.2	53.6	0.5	0.90	2.1	-2.3	g...	...	759.1	1.1	2.1×10^{-16}
1748	175147.56−293233.2	267.948170	−29.542567	0.1	5.2	137.6	14.4	53.4	92.5	0.90	9.2	<-5	....	b	815.8	2.5	2.8×10^{-15}
1749	175147.56−294244.5	267.948190	−29.712363	0.2	8.5	194.5	16.4	56.5	42.3	0.54	11.5	<-5	....	b	730.8	1.4	4.2×10^{-15}
1750	175147.72−293106.1	267.948860	−29.518371	0.3	6.1	21.4	10.3	71.6	6.3	0.89	2.0	-2.0	....	a	799.0	1.7	3.0×10^{-16}
1751	175147.79−293400.8	267.949150	−29.566901	0.2	4.6	18.4	7.8	33.6	3.8	0.90	2.2	-2.6	....	a	821.5	1.2	1.8×10^{-16}
1752	175147.88−294238.8	267.949520	−29.710779	0.2	8.5	154.7	14.6	43.3	96.0	0.50	10.2	<-5	....	a	735.6	2.7	6.9×10^{-15}
1753	175148.05−293738.8	267.950230	−29.627450	0.2	4.9	59.7	10.2	33.3	13.4	0.90	5.6	<-5	g...	...	693.9	1.4	1.0×10^{-15}
1754	175148.07−294304.1	267.950300	−29.717811	0.3	8.8	93.4	19.1	244.6	11.9	0.87	4.8	<-5	....	a	704.9	1.4	1.3×10^{-15}
1755	175148.13−293150.1	267.950550	−29.530589	0.2	5.7	23.4	9.7	59.6	8.5	0.90	2.3	-2.5	....	b	806.9	1.7	3.3×10^{-16}
1756	175148.15−293517.6	267.950640	−29.588225	0.1	4.5	113.8	12.5	28.2	80.6	0.89	8.8	<-5	g...	...	644.6	2.8	3.3×10^{-15}
1757	175148.18−292930.2	267.950770	−29.491731	0.3	7.4	30.9	13.0	120.1	6.0	0.85	2.3	-2.4	....	b	771.3	1.1	3.1×10^{-16}
1758	175148.20−293338.9	267.950840	−29.560831	0.2	4.8	34.2	9.1	38.8	24.9	0.90	3.5	<-5	....	a	818.8	3.2	8.8×10^{-16}
1759	175148.23−293831.9	267.950990	−29.642211	0.2	5.4	88.7	12.1	44.3	53.0	0.90	7.0	<-5	g...	...	675.2	2.6	2.9×10^{-15}
1760	175148.33−293208.3	267.951400	−29.535654	0.2	5.5	25.0	7.9	29.0	6.3	0.73	3.0	-4.5	....	b	810.0	1.6	3.8×10^{-16}
1761	175148.34−294115.1	267.951420	−29.687544	0.2	7.4	139.7	17.0	129.3	51.1	0.88	8.0	<-5	g...	...	732.3	1.7	2.3×10^{-15}
1762	175148.36−293315.7	267.951540	−29.554364	0.2	5.0	54.3	10.5	44.7	22.6	0.90	4.9	<-5	....	b	816.7	1.8	7.9×10^{-16}
1763	175148.37−293647.9	267.951570	−29.613315	0.2	4.7	35.0	8.8	32.0	0.0	0.90	3.8	<-5	g...	...	736.0	1.2	4.3×10^{-16}
1764	175148.38−294129.8	267.951600	−29.691613	0.3	7.6	38.3	12.1	92.7	14.8	0.78	3.0	-3.9	g...	...	725.8	1.6	7.0×10^{-16}
1765	175148.42−293205.5	267.951780	−29.534885	0.2	5.6	16.7	6.1	14.3	1.2	0.57	2.5	-3.9	....	a	809.5	1.6	3.5×10^{-16}
1766	175148.60−293112.8	267.952530	−29.520245	0.2	6.2	41.2	11.4	75.8	0.3	0.90	3.4	<-5	....	b	798.6	1.1	3.7×10^{-16}
1767	175148.65−293558.8	267.952720	−29.599671	0.2	4.6	26.8	8.3	33.2	12.0	0.90	3.0	-4.6	g...	...	792.0	1.7	4.0×10^{-16}
1768	175148.70−293858.8	267.952940	−29.649672	0.3	5.8	30.9	9.8	53.1	18.8	0.90	3.0	-4.1	g...	...	667.2	2.6	1.0×10^{-15}

(*cont.*)

Table A.1: *Chandra* source list

Source		Position				Extracted Counts							Characteristics				
Seq	CXOU J	R. A.	Decl.	Err	θ	$C_{\rm net}$	$\Delta C_{\rm net}$	$C'_{\rm bkg}$	$C_{\rm net,hard}$	PSF	PS	$P_{\rm B}$	Anom	Var	EffExp	$E_{\rm median}$	Photo $F_{\rm x}$
#		(deg)	(deg)	($''$)	($'$)						Frac				(ks)	(keV)	(ergs s^{-1} cm^{-2})
(1)	(2)	(3)	(4)	(5)	(6)	(7)	(8)	(9)	(10)	(11)	(12)	(13)	(14)	(15)	(16)	(17)	(18)
1769	175148.77−293404.2	267.953220	−29.567856	0.1	4.8	61.7	9.9	25.3	30.2	0.82	5.9	<-5	....	c	814.3	2.0	1.1×10^{-15}
1770	175148.79−293008.8	267.953300	−29.502468	0.3	7.0	45.2	13.2	111.8	18.5	0.90	3.3	-4.4	....	a	777.5	1.6	6.1×10^{-16}
1771	175148.82−292856.0	267.953450	−29.482236	0.3	7.9	33.0	15.5	187.0	31.8	0.90	2.1	-2.0	....	a	745.1	3.2	9.2×10^{-16}
1772	175148.85−294121.5	267.953550	−29.689307	0.2	7.5	110.4	15.7	117.6	17.4	0.85	6.8	<-5	g...	...	719.2	1.3	3.7×10^{-16}
1773	175148.85−293641.1	267.953560	−29.611426	0.2	4.8	31.9	8.8	36.1	2.9	0.90	3.4	<-5	g...	...	772.7	1.3	1.4×10^{-15}
1774	175148.91−293409.3	267.953800	−29.569276	0.2	4.8	30.3	7.8	22.7	9.2	0.81	3.6	<-5	....	b	813.9	1.7	4.6×10^{-16}
1775	175148.91−293505.6	267.953810	−29.584895	0.0	4.6	1779.1	43.2	39.9	398.4	0.89	40.7	<-5	g...	...	759.2	1.4	2.2×10^{-14}
1776	175149.04−293220.9	267.954370	−29.539158	0.2	5.5	43.9	11.0	65.1	19.1	0.90	3.8	<-5	....	a	807.5	1.9	6.8×10^{-16}
1777	175149.07−293651.7	267.954500	−29.614373	0.2	4.9	34.0	9.0	37.0	23.2	0.89	3.6	<-5	g...	...	778.8	2.7	8.1×10^{-16}
1778	175149.09−293123.1	267.954550	−29.523100	0.2	6.1	63.4	12.3	73.6	6.1	0.89	4.9	<-5	....	a	798.3	1.1	6.0×10^{-16}
1779	175149.10−293802.1	267.954600	−29.633932	0.2	5.3	45.6	10.2	46.4	20.7	0.90	4.3	<-5	g...	...	739.5	1.7	7.6×10^{-16}
1780	175149.12−293352.6	267.954700	−29.564635	0.2	4.9	40.4	9.7	42.6	28.0	0.91	4.0	<-5	....	a	812.5	2.4	7.8×10^{-16}
1781	175149.23−293938.8	267.955160	−29.660784	0.2	6.3	74.9	12.8	74.1	59.0	0.90	5.6	<-5	g...	...	666.0	2.6	2.4×10^{-15}
1782	175149.33−293228.8	267.955550	−29.541349	0.2	5.5	36.9	10.7	64.1	0.6	0.90	3.3	-4.8	....	b	802.1	1.0	5.1×10^{-16}
1783	175149.33−293030.1	267.955560	−29.508362	0.3	6.8	32.0	7.8	21.0	8.8	0.53	3.8	<-5	....	a	780.1	1.1	3.0×10^{-16}
1784	175149.40−292738.6	267.955860	−29.460735	0.2	9.1	217.9	23.3	293.1	180.2	0.90	9.1	<-5	....	a	736.0	3.3	6.4×10^{-15}
1785	175149.45−292812.1	267.956080	−29.470039	0.3	8.6	88.6	19.2	252.4	50.2	0.90	4.5	<-5	....	a	745.0	2.3	1.8×10^{-15}
1786	175149.51−293147.8	267.956320	−29.529954	0.2	5.9	40.9	11.1	68.1	3.2	0.89	3.5	<-5	....	a	798.5	1.1	3.6×10^{-16}
1787	175149.55−294040.0	267.956470	−29.677790	0.2	7.1	92.8	15.1	117.2	29.0	0.90	5.9	<-5	g...	...	661.7	1.7	1.9×10^{-15}
1788	175149.57−294253.4	267.956550	−29.714834	0.3	8.9	125.0	20.7	274.0	4.2	0.91	5.9	<-5	g...	...	683.9	1.0	1.4×10^{-15}
1789	175149.59−293215.2	267.956630	−29.537571	0.2	5.7	21.3	10.1	67.7	18.5	0.90	2.0	-2.1	....	a	799.2	3.8	6.7×10^{-16}
1790	175149.59−293801.1	267.956660	−29.633640	0.2	5.4	27.7	9.2	46.3	11.4	0.87	2.9	-3.9	g...	...	766.5	1.5	3.9×10^{-16}
1791	175149.61−293034.7	267.956730	−29.509650	0.2	6.8	56.9	9.7	27.1	21.1	0.62	5.6	<-5	....	a	780.4	1.7	1.2×10^{-15}
1792	175149.72−293736.6	267.957170	−29.626854	0.2	5.2	60.5	11.1	49.5	36.2	0.89	5.2	<-5	g...	...	779.1	2.5	1.4×10^{-15}
1793	175149.77−293544.8	267.957400	−29.595793	0.2	4.8	39.3	9.5	40.7	6.7	0.90	3.9	<-5	....	b	800.6	1.2	4.1×10^{-16}
1794	175149.81−293657.8	267.957560	−29.616077	0.2	5.0	30.8	9.3	44.2	21.9	0.90	3.1	-4.6	....	c	802.6	2.8	7.3×10^{-16}
1795	175149.89−293454.0	267.957900	−29.581681	0.2	4.8	17.5	8.3	41.5	2.9	0.90	2.0	-2.2	g...	...	734.4	1.4	2.1×10^{-16}
1796	175149.90−293040.4	267.957930	−29.511233	0.2	6.7	32.2	8.7	33.8	8.0	0.67	3.5	<-5	....	c	766.9	1.3	4.8×10^{-16}
1797	175149.91−294003.1	267.957970	−29.667545	0.2	6.7	69.4	13.6	99.6	18.6	0.90	4.9	<-5	g...	...	688.6	1.7	4.6×10^{-15}
1798	175149.91−293844.3	267.957990	−29.645664	0.1	5.9	158.0	15.5	65.0	116.6	0.90	9.9	<-5	g...	...	756.1	3.2	1.3×10^{-15}
1799	175149.96−293204.9	267.958190	−29.534698	0.2	5.9	28.0	10.5	69.0	4.4	0.89	2.5	-3.0	....	b	798.6	1.6	3.6×10^{-16}
1800	175150.02−294232.3	267.958450	−29.708990	0.3	8.6	93.6	19.1	242.4	6.3	0.91	4.8	<-5	g...	...	670.0	1.3	1.3×10^{-15}
1801	175150.05−293903.5	267.958560	−29.650986	0.2	6.1	64.4	12.3	71.6	14.0	0.90	5.0	<-5	g...	...	755.0	1.4	8.6×10^{-16}
1802	175150.10−293112.9	267.958770	−29.520252	0.3	6.4	28.4	11.5	89.6	9.8	0.90	2.4	-2.6	....	a	779.9	1.8	4.3×10^{-16}

(*cont.*)

Table A.1: *Chandra* source list

Source		Position				Extracted Counts							Characteristics				
Seq	CXOU J	R. A.	Decl.	Err	θ	$C_{\rm net}$	$\Delta C_{\rm net}$	$C'_{\rm bkg}$	$C_{\rm net,hard}$	PSF	PS	$P_{\rm B}$	Anom	Var	EffExp	$E_{\rm median}$	Photo $F_{\rm x}$
#		(deg)	(deg)	($''$)	($'$)						Frac				(ks)	(keV)	(ergs s^{-1} cm^{-2})
(1)	(2)	(3)	(4)	(5)	(6)	(7)	(8)	(9)	(10)	(11)	(12)	(13)	(14)	(15)	(16)	(17)	(18)
1803	175150.10−293913.6	267.958780	−29.653779	0.2	6.2	34.5	11.0	72.5	18.4	0.89	3.0	-3.9	g...	...	752.2	1.8	5.7×10^{-16}
1804	175150.18−292940.0	267.959090	−29.494449	0.3	7.5	40.2	14.5	149.8	0.0	0.90	2.7	-3.1	....	b	758.8	1.2	4.3×10^{-16}
1805	175150.23−293143.7	267.959320	−29.528814	0.1	6.1	527.5	25.1	75.5	382.1	0.90	20.6	<-5	....	b	785.5	2.8	1.2×10^{-14}
1806	175150.27−293445.4	267.959500	−29.579300	0.2	4.9	18.5	7.9	34.5	23.1	0.90	2.2	-2.6	g...	...	634.9	4.9	9.5×10^{-16}
1807	175150.28−293738.5	267.959510	−29.627369	0.2	5.4	26.0	9.6	55.0	5.4	0.89	2.6	-3.1	....	a	797.5	1.1	2.3×10^{-16}
1808	175150.33−293540.5	267.959740	−29.594598	0.2	4.9	26.4	8.8	40.6	10.9	0.90	2.8	-3.9	....	b	797.4	1.8	4.1×10^{-16}
1809	175150.35−293456.2	267.959830	−29.582280	0.2	4.9	25.1	8.8	42.9	14.2	0.90	2.7	-3.5	g...	...	758.9	2.1	4.8×10^{-16}
1810	175150.40−293601.0	267.960030	−29.600297	0.2	5.0	55.1	10.4	40.9	9.1	0.90	5.1	<-5	g...	...	798.2	1.4	6.6×10^{-16}
1811	175150.45−293944.7	267.960230	−29.662441	0.2	6.6	40.8	12.6	101.2	17.5	0.90	3.1	-4.0	g...	...	749.1	1.8	6.6×10^{-16}
1812	175150.47−292859.0	267.960320	−29.483061	0.2	8.1	116.5	18.7	208.5	65.6	0.90	6.1	<-5	....	a	758.2	2.2	2.2×10^{-15}
1813	175150.52−293701.6	267.960500	−29.617113	0.2	5.2	26.2	9.5	53.8	18.6	0.90	2.6	-3.2	g...	...	792.8	2.6	4.9×10^{-16}
1814	175150.52−293532.2	267.960540	−29.592292	0.2	5.0	28.9	8.8	39.1	14.0	0.90	3.1	-4.6	g...	...	758.8	1.8	5.9×10^{-16}
1815	175150.54−293612.4	267.960600	−29.603461	0.2	5.0	65.2	10.8	39.8	29.6	0.90	5.7	<-5	....	c	798.9	1.9	1.0×10^{-15}
1816	175150.59−293732.7	267.960830	−29.625770	0.2	5.4	75.3	12.3	61.7	38.2	0.90	5.9	<-5	....	a	793.4	2.1	1.3×10^{-15}
1817	175150.61−293317.2	267.960890	−29.554794	0.1	5.4	162.8	15.4	56.2	28.7	0.90	10.2	<-5	....	b	806.5	1.3	1.7×10^{-15}
1818	175150.66−293414.1	267.961110	−29.570585	0.1	5.1	380.2	21.4	53.8	65.8	0.91	17.4	<-5	....	a	807.4	1.3	4.0×10^{-15}
1819	175150.74−293807.1	267.961440	−29.635313	0.1	5.7	223.4	17.6	67.6	47.9	0.90	12.3	<-5	....	c	787.9	1.5	2.8×10^{-15}
1820	175150.81−292731.2	267.961720	−29.458692	0.3	9.3	150.5	22.7	329.5	37.9	0.90	6.5	<-5	....	a	716.9	1.5	2.2×10^{-15}
1821	175150.84−292702.3	267.961840	−29.450658	0.2	9.7	401.9	28.4	366.1	107.5	0.90	13.9	<-5	....	c	699.4	1.5	5.7×10^{-15}
1822	175150.90−293618.2	267.962090	−29.605065	0.1	5.1	130.6	13.7	42.4	93.1	0.90	9.2	<-5	g...	...	789.4	3.0	3.4×10^{-15}
1823	175150.93−293005.5	267.962240	−29.501542	0.1	7.3	297.8	21.5	138.2	24.6	0.90	13.5	<-5	....	b	766.0	1.1	2.9×10^{-15}
1824	175150.95−294045.5	267.962300	−29.679310	0.3	7.3	45.8	14.8	152.2	35.6	0.90	3.0	-3.8	g...	...	725.5	2.8	3.7×10^{-16}
1825	175150.95−293257.2	267.962320	−29.549234	0.2	5.6	14.3	5.2	7.7	4.8	0.43	2.5	-4.5	....	b	802.2	1.5	1.3×10^{-15}
1826	175151.08−293258.8	267.962870	−29.549691	0.2	5.6	27.9	6.6	9.1	6.1	0.47	3.9	<-5	....	b	787.5	1.5	6.6×10^{-16}
1827	175151.09−292928.2	267.962890	−29.491167	0.2	7.8	180.1	19.6	177.9	110.1	0.90	9.0	<-5	....	a	758.5	2.4	3.8×10^{-15}
1828	175151.17−292802.0	267.963240	−29.467238	0.2	9.0	188.5	21.9	259.5	22.4	0.88	8.4	<-5	....	b	722.7	1.2	2.2×10^{-15}
1829	175151.18−293015.9	267.963290	−29.504424	0.2	7.2	87.8	14.0	92.2	55.7	0.82	6.0	<-5	....	b	773.2	2.7	2.2×10^{-15}
1830	175151.22−293848.3	267.963450	−29.646759	0.3	6.1	24.3	11.0	83.7	17.8	0.90	2.1	-2.2	....	a	778.7	3.3	6.9×10^{-16}
1831	175151.29−293310.3	267.963710	−29.552867	0.0	5.6	1447.3	39.4	62.7	1225.1	0.90	36.3	<-5	....	b	794.1	3.6	4.3×10^{-14}
1832	175151.35−293642.9	267.964000	−29.611940	0.2	5.3	37.4	9.9	48.6	25.4	0.89	3.6	<-5	g...	...	791.6	3.1	1.0×10^{-15}
1833	175151.54−293723.0	267.964790	−29.623081	0.2	5.5	34.5	10.7	67.5	0.0	0.90	3.1	-4.1	....	b	788.6	1.1	3.1×10^{-16}
1834	175151.62−294141.0	267.965100	−29.694724	0.2	8.1	226.6	21.3	198.4	153.3	0.90	10.4	<-5	g...	...	705.7	2.9	6.8×10^{-15}
1835	175151.66−293336.5	267.965250	−29.560154	0.2	5.5	31.1	10.1	59.9	13.3	0.90	2.9	-3.8	....	a	794.3	1.8	5.6×10^{-16}
1836	175151.66−293151.0	267.965280	−29.530840	0.2	6.3	27.6	11.5	89.4	19.5	0.90	2.3	-2.5	....	a	779.7	2.4	4.6×10^{-16}

(*cont.*)

Table A.1: *Chandra* source list

Source		Position				Extracted Counts							Characteristics				
Seq	CXOU J	R. A.	Decl.	Err	θ	$C_{\rm net}$	$\Delta C_{\rm net}$	$C'_{\rm bkg}$	$C_{\rm net,hard}$	PSF	PS	$P_{\rm B}$	Anom	Var	EffExp	$E_{\rm median}$	Photo $F_{\rm x}$
#		(deg)	(deg)	($''$)	($'$)						Frac				(ks)	(keV)	(ergs s^{-1} cm^{-2})
(1)	(2)	(3)	(4)	(5)	(6)	(7)	(8)	(9)	(10)	(11)	(12)	(13)	(14)	(15)	(16)	(17)	(18)
1837	175151.73−293732.3	267.965560	−29.625659	0.1	5.6	157.4	15.7	70.6	113.5	0.90	9.7	<-5	....	b	789.8	2.9	3.8×10^{-15}
1838	175151.81−293639.1	267.965880	−29.610869	0.1	5.4	113.9	13.5	54.1	45.2	0.90	8.1	<-5	g...	...	784.4	1.8	1.8×10^{-15}
1839	175151.82−293203.5	267.965940	−29.534313	0.3	6.2	27.6	11.2	83.4	25.6	0.87	2.4	-2.6	....	a	780.2	3.7	8.9×10^{-16}
1840	175151.89−294122.2	267.966240	−29.689521	0.2	7.9	327.8	23.2	182.2	30.9	0.90	13.8	<-5	g...	...	717.3	1.1	3.6×10^{-15}
1841	175152.05−293805.1	267.966880	−29.634751	0.1	5.9	157.0	16.1	82.0	96.3	0.90	9.5	<-5	....	a	782.7	2.5	3.3×10^{-15}
1842	175152.06−293547.7	267.966920	−29.596608	0.2	5.3	74.4	11.7	48.6	62.2	0.90	6.1	<-5	g...	...	782.0	3.3	2.1×10^{-15}
1843	175152.20−293348.3	267.967520	−29.563441	0.2	5.5	32.7	10.4	62.3	18.4	0.90	3.0	-4.0	....	b	789.6	2.4	6.5×10^{-16}
1844	175152.27−292810.0	267.967820	−29.469468	0.3	9.0	81.4	17.3	194.6	48.8	0.81	4.6	<-5	....	a	721.6	2.9	2.4×10^{-15}
1845	175152.28−292830.6	267.967860	−29.475167	0.3	8.7	112.6	20.1	264.4	77.2	0.90	5.5	<-5	....	a	724.2	3.1	3.2×10^{-15}
1846	175152.32−293202.5	267.968010	−29.534043	0.2	6.3	60.9	12.9	90.1	17.1	0.90	4.5	<-5	....	c	779.5	1.3	6.7×10^{-16}
1847	175152.41−293244.9	267.968400	−29.545815	0.1	6.0	476.0	24.1	79.0	341.7	0.89	19.3	<-5	....	a	784.0	2.9	1.1×10^{-14}
1848	175152.46−294214.4	267.968610	−29.704017	0.2	8.7	328.3	24.9	260.7	274.3	0.91	12.9	<-5	g...	...	704.0	3.7	1.2×10^{-14}
1849	175152.49−292908.7	267.968710	−29.485766	0.2	8.2	192.6	20.3	191.4	123.3	0.88	9.3	<-5	....	b	730.1	2.6	4.7×10^{-15}
1850	175152.54−293415.4	267.968950	−29.570960	0.2	5.5	24.6	9.7	57.4	17.5	0.90	2.4	-2.8	g...	...	756.0	2.9	6.3×10^{-16}
1851	175152.55−293452.9	267.968990	−29.581370	0.1	5.4	289.1	19.1	53.9	202.1	0.90	14.8	<-5	....	b	762.0	2.8	6.9×10^{-15}
1852	175152.56−292957.0	267.969030	−29.499191	0.3	7.7	42.6	15.1	164.4	9.2	0.90	2.7	-3.2	....	b	740.2	1.5	5.6×10^{-16}
1853	175152.59−292712.9	267.969160	−29.453593	0.2	9.8	68.8	11.6	52.2	53.6	0.46	5.7	<-5	....	a	713.8	3.2	3.9×10^{-15}
1854	175152.60−294101.6	267.969170	−29.683803	0.3	7.8	51.5	16.2	188.5	6.8	0.90	3.1	-3.9	g...	...	719.1	1.4	6.8×10^{-16}
1855	175152.63−293750.8	267.969310	−29.630786	0.2	5.9	47.5	12.0	82.5	18.6	0.90	3.8	<-5	g...	...	765.4	1.8	7.9×10^{-16}
1856	175152.64−293813.6	267.969340	−29.637119	0.2	6.1	32.8	11.3	81.2	11.8	0.88	2.8	-3.4	g...	...	765.5	1.7	8.1×10^{-16}
1857	175152.64−292920.2	267.969350	−29.488971	0.2	8.1	69.9	14.2	113.1	3.7	0.78	4.8	<-5	....	a	734.4	1.1	7.3×10^{-15}
1858	175152.64−293051.8	267.969360	−29.514389	0.1	7.1	260.7	20.1	120.3	205.0	0.90	12.6	<-5	....	a	761.1	3.2	5.3×10^{-16}
1859	175152.69−293214.9	267.969580	−29.537482	0.2	6.3	42.1	8.2	16.9	30.3	0.53	4.8	<-5	....	a	778.9	2.8	1.7×10^{-15}
1860	175152.78−293309.2	267.969950	−29.552556	0.2	5.9	30.9	10.9	75.1	26.4	0.89	2.7	-3.3	....	a	782.9	3.2	8.2×10^{-16}
1861	175152.83−293934.9	267.970130	−29.659705	0.2	6.9	54.6	14.4	133.4	36.1	0.90	3.7	<-5	g...	...	758.3	2.7	1.4×10^{-15}
1862	175152.91−293216.7	267.970470	−29.537983	0.2	6.3	44.4	8.3	16.6	17.4	0.53	5.0	<-5	....	a	781.6	1.8	1.1×10^{-15}
1863	175152.96−294124.3	267.970680	−29.690092	0.2	8.1	115.9	18.3	195.1	43.7	0.89	6.2	<-5	g...	...	713.4	1.7	2.0×10^{-15}
1864	175152.99−293453.8	267.970820	−29.581615	0.2	5.5	43.5	10.7	58.5	27.8	0.89	3.9	<-5	g...	...	755.3	2.5	9.8×10^{-16}
1865	175153.09−294037.4	267.971220	−29.677082	0.2	7.6	186.5	19.8	180.5	113.9	0.90	9.2	<-5	....	a	749.0	2.4	4.1×10^{-15}
1866	175153.10−292719.9	267.971290	−29.455536	0.3	9.8	51.5	10.8	52.5	44.3	0.45	4.6	<-5	....	b	716.9	3.5	3.4×10^{-15}
1867	175153.30−293415.8	267.972120	−29.571074	0.2	5.6	43.2	9.9	42.8	14.7	0.82	4.2	<-5	g...	...	718.6	1.7	7.4×10^{-16}
1868	175153.31−293658.7	267.972160	−29.616331	0.2	5.8	34.7	11.2	76.3	7.3	0.90	3.0	-3.8	g...	...	783.8	1.3	3.9×10^{-16}
1869	175153.33−294245.0	267.972220	−29.712512	0.1	9.2	1202.7	39.6	313.3	985.9	0.90	30.0	<-5	g...	...	686.0	3.5	5.5×10^{-16}
1870	175153.33−293535.5	267.972250	−29.593206	0.2	5.6	50.4	11.2	61.6	6.3	0.89	4.3	<-5	....	b	786.1	1.3	4.2×10^{-14}

(*cont.*)

Table A.1: *Chandra* source list

Source		Position				Extracted Counts							Characteristics				
Seq	CXOU J	R. A.	Decl.	Err	θ	$C_{\rm net}$	$\Delta C_{\rm net}$	$C'_{\rm bkg}$	$C_{\rm net,hard}$	PSF	PS	$P_{\rm B}$	Anom	Var	EffExp	$E_{\rm median}$	Photo $F_{\rm x}$
#		(deg)	(deg)	($''$)	($'$)						Frac				(ks)	(keV)	(ergs s^{-1} cm^{-2})
(1)	(2)	(3)	(4)	(5)	(6)	(7)	(8)	(9)	(10)	(11)	(12)	(13)	(14)	(15)	(16)	(17)	(18)
1871	175153.38−293813.6	267.972430	−29.637133	0.2	6.2	57.4	13.0	94.6	18.0	0.89	4.3	<-5	g...	...	766.5	1.7	1.5×10^{-15}
1872	175153.38−293734.8	267.972450	−29.626347	0.2	6.0	126.5	15.2	85.5	13.7	0.90	8.1	<-5	g...	...	774.1	1.3	8.8×10^{-16}
1873	175153.44−293639.2	267.972700	−29.610908	0.2	5.7	78.2	12.6	65.8	43.7	0.87	6.0	<-5	....	b	791.8	2.4	1.6×10^{-15}
1874	175153.54−293411.8	267.973090	−29.569959	0.2	5.7	53.5	10.3	40.5	35.3	0.78	5.0	<-5	g...	...	747.8	2.6	1.4×10^{-15}
1875	175153.58−293053.9	267.973290	−29.514998	0.2	7.2	244.7	19.9	126.3	24.2	0.89	12.0	<-5	....	a	755.1	1.3	2.9×10^{-15}
1876	175153.60−293416.0	267.973340	−29.571128	0.2	5.7	29.5	7.5	18.5	13.0	0.66	3.7	<-5	g...	...	707.2	1.9	7.1×10^{-16}
1877	175153.60−293621.3	267.973370	−29.605941	0.2	5.7	55.8	11.6	64.2	6.4	0.87	4.6	<-5	g...	...	786.8	1.1	5.7×10^{-16}
1878	175153.71−293531.6	267.973830	−29.592125	0.2	5.6	50.8	11.3	64.2	31.0	0.89	4.3	<-5	....	b	781.2	2.5	1.1×10^{-15}
1879	175153.80−293915.5	267.974170	−29.654308	0.2	6.8	96.6	15.6	128.4	0.0	0.90	6.0	<-5	g...	...	749.7	1.2	1.7×10^{-15}
1880	175153.80−293844.2	267.974190	−29.645631	0.2	6.6	166.3	17.4	114.7	18.5	0.90	9.3	<-5	g...	...	765.0	1.2	1.1×10^{-15}
1881	175153.83−293823.2	267.974300	−29.639792	0.2	6.4	48.9	13.0	104.1	37.3	0.90	3.6	<-5	g...	...	766.3	2.7	1.2×10^{-15}
1882	175153.84−293518.0	267.974350	−29.588342	0.2	5.7	38.9	10.3	56.1	14.6	0.90	3.6	<-5	g...	...	646.5	1.7	6.5×10^{-16}
1883	175153.84−293859.4	267.974370	−29.649835	0.2	6.7	117.8	16.1	120.2	27.8	0.90	7.1	<-5	g...	...	761.9	1.4	1.5×10^{-15}
1884	175153.90−293641.8	267.974600	−29.611629	0.1	5.8	312.8	20.4	79.2	223.9	0.90	15.0	<-5	....	b	786.4	2.9	7.6×10^{-15}
1885	175154.02−292643.5	267.975100	−29.445441	0.3	10.4	79.5	22.1	373.5	52.3	0.90	3.5	-4.5	g...	...	594.9	2.8	2.7×10^{-15}
1886	175154.05−293622.2	267.975220	−29.606192	0.2	5.8	48.1	11.5	70.9	20.9	0.88	4.0	<-5	....	a	780.8	1.7	7.1×10^{-16}
1887	175154.18−293744.4	267.975760	−29.629014	0.1	6.2	181.3	17.5	102.7	56.5	0.90	10.1	<-5	....	a	778.6	1.6	2.6×10^{-15}
1888	175154.21−293353.7	267.975890	−29.564934	0.2	5.9	29.0	11.0	78.0	4.9	0.89	2.5	-2.9	....	a	770.4	1.3	3.2×10^{-16}
1889	175154.25−293009.8	267.976080	−29.502730	0.3	7.8	35.0	15.4	181.0	25.1	0.90	2.2	-2.2	....	b	762.6	3.4	1.0×10^{-15}
1890	175154.34−293028.4	267.976420	−29.507897	0.2	7.6	97.7	17.0	169.3	69.1	0.91	5.6	<-5	....	b	765.9	2.7	2.2×10^{-15}
1891	175154.40−294131.1	267.976680	−29.691979	0.3	8.4	74.4	19.1	263.6	30.2	0.91	3.8	<-5	....	a	725.0	1.8	1.3×10^{-15}
1892	175154.43−293328.1	267.976830	−29.557814	0.2	6.1	33.8	11.6	87.2	9.1	0.89	2.8	-3.4	....	b	769.0	1.6	4.7×10^{-16}
1893	175154.54−294006.3	267.977260	−29.668418	0.1	7.5	561.9	27.8	178.1	458.5	0.90	19.8	<-5	g...	...	743.0	3.2	1.7×10^{-14}
1894	175154.56−293146.6	267.977370	−29.529634	0.2	6.9	44.3	13.3	115.7	21.5	0.89	3.2	-4.1	....	b	770.7	1.9	7.2×10^{-16}
1895	175154.71−292806.1	267.977960	−29.468370	0.1	9.4	6440.6	83.0	352.4	4336.1	0.90	77.1	<-5	....	c	722.4	2.7	1.6×10^{-13}
1896	175154.90−293827.6	267.978790	−29.641025	0.2	6.6	165.4	17.6	122.6	22.1	0.90	9.1	<-5	....	a	776.5	1.2	1.8×10^{-15}
1897	175154.94−293101.6	267.978950	−29.517130	0.2	7.4	142.3	17.5	141.7	98.7	0.90	7.9	<-5	....	a	767.5	3.0	3.6×10^{-15}
1898	175154.99−293710.4	267.979150	−29.619571	0.2	6.2	39.2	12.5	101.8	20.6	0.90	3.0	-3.8	....	b	766.3	2.1	7.0×10^{-16}
1899	175155.03−293305.7	267.979330	−29.551591	0.2	6.4	44.0	12.7	102.0	18.9	0.90	3.3	-4.5	....	c	771.2	1.9	7.4×10^{-16}
1900	175155.03−293616.5	267.979330	−29.604589	0.2	6.0	60.9	12.6	83.1	17.3	0.90	4.6	<-5	g...	...	752.2	1.5	7.9×10^{-16}
1901	175155.13−293650.9	267.979740	−29.614143	0.2	6.1	40.7	12.5	100.3	2.5	0.90	3.1	-4.0	....	a	767.6	1.1	4.0×10^{-16}
1902	175155.14−293408.6	267.979780	−29.569064	0.3	6.1	24.4	11.0	82.6	10.9	0.89	2.1	-2.2	g...	...	745.7	2.2	4.7×10^{-16}
1903	175155.29−292953.1	267.980400	−29.498097	0.2	8.1	159.6	19.9	209.4	104.1	0.90	7.8	<-5	....	b	747.4	2.6	3.8×10^{-15}
1904	175155.33−292747.1	267.980580	−29.463098	0.2	9.7	92.7	13.1	64.3	73.1	0.48	6.8	<-5	....	b	716.8	3.3	5.3×10^{-15}

(*cont.*)

Table A.1: *Chandra* source list

Source		Position				Extracted Counts							Characteristics				
Seq	CXOU J	R. A.	Decl.	Err	θ	$C_{\rm net}$	$\Delta C_{\rm net}$	$C'_{\rm bkg}$	$C_{\rm net,hard}$	PSF	PS	$P_{\rm B}$	Anom	Var	EffExp	$E_{\rm median}$	Photo $F_{\rm x}$
#		(deg)	(deg)	($''$)	($'$)						Frac				(ks)	(keV)	(ergs s^{-1} cm^{-2})
(1)	(2)	(3)	(4)	(5)	(6)	(7)	(8)	(9)	(10)	(11)	(12)	(13)	(14)	(15)	(16)	(17)	(18)
1905	175155.40−293356.6	267.980840	−29.565731	0.2	6.2	30.8	11.7	92.2	10.0	0.89	2.5	-2.8	....	b	774.8	1.5	4.0×10^{-16}
1906	175155.47−293907.8	267.981140	−29.652184	0.2	7.1	121.8	17.2	152.2	54.6	0.90	6.9	<-5	....	a	764.4	1.9	2.0×10^{-15}
1907	175155.69−293113.9	267.982060	−29.520530	0.2	7.4	125.8	16.9	139.2	49.0	0.89	7.2	<-5	....	a	761.7	1.8	2.0×10^{-15}
1908	175155.70−293303.0	267.982100	−29.550835	0.2	6.5	57.2	13.6	109.8	5.6	0.89	4.1	<-5	....	c	774.5	1.1	5.5×10^{-16}
1909	175155.75−294019.4	267.982300	−29.672081	0.2	7.8	85.0	18.0	215.0	48.4	0.89	4.6	<-5	....	c	749.8	2.4	1.8×10^{-15}
1910	175155.80−293733.6	267.982530	−29.626002	0.2	6.5	36.3	12.5	103.7	8.2	0.87	2.8	-3.3	....	b	754.5	1.5	5.0×10^{-16}
1911	175155.93−293555.1	267.983050	−29.598658	0.2	6.1	131.9	15.4	87.1	86.8	0.90	8.3	<-5	....	a	760.4	2.6	3.1×10^{-15}
1912	175156.01−292755.1	267.983400	−29.465323	0.2	9.7	140.7	16.5	111.3	87.6	0.59	8.3	<-5	....	a	721.1	2.6	5.0×10^{-15}
1913	175156.06−293544.2	267.983600	−29.595615	0.2	6.2	57.4	12.7	88.6	63.5	0.90	4.3	<-5	....	b	770.3	4.9	2.5×10^{-15}
1914	175156.20−293518.2	267.984180	−29.588413	0.3	6.2	27.0	10.9	79.0	12.7	0.89	2.4	-2.6	g...	...	665.4	2.0	5.5×10^{-16}
1915	175156.21−293742.0	267.984240	−29.628337	0.3	6.6	30.6	10.1	60.4	18.5	0.74	2.9	-3.7	....	a	743.8	3.1	1.0×10^{-15}
1916	175156.25−293031.1	267.984380	−29.508639	0.2	7.9	247.6	21.6	190.4	57.5	0.90	11.2	<-5	....	c	751.8	1.5	3.3×10^{-15}
1917	175156.27−293733.7	267.984490	−29.626044	0.2	6.6	65.3	12.7	80.7	7.3	0.80	4.9	<-5	....	b	754.1	1.3	8.2×10^{-16}
1918	175156.37−293007.6	267.984880	−29.502112	0.2	8.2	198.1	19.7	165.9	119.8	0.84	9.8	<-5	....	b	748.9	2.4	4.6×10^{-15}
1919	175156.55−293226.0	267.985640	−29.540562	0.2	6.9	66.5	14.5	125.5	27.9	0.89	4.4	<-5	....	a	765.5	1.7	9.9×10^{-16}
1920	175156.57−293939.2	267.985720	−29.660913	0.3	7.6	48.8	16.4	197.2	18.4	0.90	2.9	-3.4	g...	...	733.0	1.5	6.7×10^{-16}
1921	175156.59−293417.3	267.985820	−29.571480	0.3	6.3	39.5	11.7	83.5	26.7	0.90	3.2	-4.4	g...	...	611.2	2.9	1.3×10^{-15}
1922	175156.61−294239.4	267.985880	−29.710950	0.3	9.6	131.4	21.8	310.6	80.6	0.85	5.9	<-5	....	a	700.8	2.9	3.9×10^{-15}
1923	175156.63−293306.6	267.985980	−29.551838	0.2	6.7	63.3	14.0	115.7	40.7	0.90	4.3	<-5	....	c	766.8	2.9	1.6×10^{-15}
1924	175156.65−294222.9	267.986060	−29.706375	0.3	9.4	59.3	16.7	197.7	36.5	0.73	3.4	-4.7	....	a	712.7	2.6	1.8×10^{-15}
1925	175156.67−293018.8	267.986160	−29.505229	0.3	8.1	42.2	11.7	80.8	29.8	0.68	3.4	-5.0	....	a	751.0	2.8	1.3×10^{-15}
1926	175156.81−293716.8	267.986740	−29.621352	0.2	6.6	30.1	13.2	127.9	0.2	0.89	2.2	-2.2	g...	...	756.0	1.0	2.7×10^{-16}
1927	175156.91−293433.6	267.987130	−29.576020	0.2	6.4	82.7	12.5	58.3	20.0	0.79	6.4	<-5	g...	...	690.4	1.4	1.3×10^{-15}
1928	175157.05−293442.2	267.987730	−29.578395	0.2	6.4	98.7	13.5	68.3	45.0	0.80	7.0	<-5	....	b	761.1	1.9	1.8×10^{-15}
1929	175157.27−293823.8	267.988650	−29.639971	0.2	7.1	79.6	16.0	155.4	64.5	0.90	4.8	<-5	....	c	751.5	3.3	2.3×10^{-15}
1930	175157.50−293258.0	267.989590	−29.549446	0.2	6.9	59.0	14.3	128.0	39.7	0.90	4.0	<-5	....	b	762.5	2.8	1.4×10^{-15}
1931	175157.51−293754.1	267.989640	−29.631704	0.2	6.9	93.2	16.5	157.8	32.2	0.90	5.5	<-5	....	a	754.5	1.6	1.3×10^{-15}
1932	175157.60−294148.7	267.990010	−29.696877	0.2	9.1	306.0	26.5	359.0	22.6	0.90	11.3	<-5	....	b	708.5	1.3	3.8×10^{-15}
1933	175157.61−293721.9	267.990060	−29.622774	0.2	6.8	49.1	12.2	84.9	15.7	0.78	3.9	<-5	....	b	761.5	1.6	7.8×10^{-16}
1934	175157.65−293731.8	267.990210	−29.625507	0.2	6.8	88.6	14.8	113.4	29.8	0.84	5.8	<-5	....	b	760.4	1.4	1.2×10^{-15}
1935	175157.78−293122.1	267.990760	−29.522823	0.2	7.7	82.4	16.7	173.6	1.8	0.90	4.8	<-5	....	b	756.7	1.2	8.4×10^{-16}
1936	175157.79−293047.0	267.990810	−29.513080	0.2	8.0	261.8	22.2	200.2	48.3	0.90	11.6	<-5	....	c	753.3	1.3	3.0×10^{-15}
1937	175157.79−293431.6	267.990810	−29.575445	0.2	6.6	54.1	13.4	108.9	7.4	0.90	3.9	<-5	g...	...	681.8	1.3	6.9×10^{-16}
1938	175157.90−294112.4	267.991290	−29.686791	0.2	8.7	206.8	20.7	194.2	68.1	0.79	9.8	<-5	....	c	709.4	1.6	3.4×10^{-15}

(*cont.*)

Table A.1: *Chandra* source list

Source		Position				Extracted Counts							Characteristics				
Seq	CXOU J	R. A.	Decl.	Err	θ	$C_{\rm net}$	$\Delta C_{\rm net}$	$C'_{\rm bkg}$	$C_{\rm net,hard}$	PSF	PS	$P_{\rm B}$	Anom	Var	EffExp	$E_{\rm median}$	Photo $F_{\rm x}$
#		(deg)	(deg)	($''$)	($'$)						Frac				(ks)	(keV)	(ergs s^{-1} cm^{-2})
(1)	(2)	(3)	(4)	(5)	(6)	(7)	(8)	(9)	(10)	(11)	(12)	(13)	(14)	(15)	(16)	(17)	(18)
1939	175157.94−293219.3	267.991420	−29.538711	0.1	7.2	304.7	21.8	145.3	234.5	0.90	13.6	<-5	....	a	761.7	3.3	8.8×10^{-15}
1940	175158.08−293915.3	267.992010	−29.654264	0.3	7.6	39.6	16.2	200.4	28.7	0.90	2.4	-2.5	....	a	740.8	2.8	1.0×10^{-15}
1941	175158.10−293523.5	267.992100	−29.589880	0.3	6.6	36.0	12.8	112.0	18.5	0.90	2.7	-3.1	....	c	744.3	2.1	6.8×10^{-16}
1942	175158.23−293140.7	267.992630	−29.527984	0.3	7.6	39.7	15.2	171.3	30.4	0.90	2.5	-2.8	....	b	755.9	2.7	9.3×10^{-16}
1943	175158.34−293349.2	267.993100	−29.563682	0.2	6.8	90.2	15.7	134.8	50.3	0.90	5.6	<-5	....	a	765.2	2.4	1.8×10^{-15}
1944	175158.45−294119.9	267.993550	−29.688880	0.2	8.9	178.2	20.2	201.8	120.9	0.79	8.6	<-5	....	a	712.4	3.3	6.2×10^{-15}
1945	175158.55−293437.8	267.993990	−29.577187	0.2	6.7	49.9	13.9	125.1	20.6	0.90	3.5	<-5	g...	...	743.6	1.8	8.1×10^{-16}
1946	175158.61−293814.5	267.994210	−29.637363	0.2	7.3	107.9	17.6	178.1	94.2	0.90	6.0	<-5	....	c	754.7	3.6	3.4×10^{-15}
1947	175158.66−292918.0	267.994440	−29.488346	0.3	9.1	62.3	17.9	232.7	29.7	0.89	3.4	-4.4	g...	...	613.7	2.0	1.4×10^{-15}
1948	175158.70−293124.5	267.994600	−29.523482	0.2	7.8	123.3	18.2	184.7	25.4	0.90	6.6	<-5	....	a	750.9	1.4	1.5×10^{-15}
1949	175158.82−293453.4	267.995100	−29.581516	0.3	6.8	46.0	13.2	112.0	7.8	0.86	3.4	-4.5	g...	...	715.3	1.2	5.4×10^{-16}
1950	175158.84−292937.0	267.995170	−29.493616	0.3	8.9	97.8	18.8	229.2	66.1	0.90	5.1	<-5	g...	...	630.8	3.0	3.0×10^{-15}
1951	175158.85−294207.1	267.995230	−29.701990	0.3	9.5	69.7	22.7	408.3	8.6	0.90	3.0	-3.4	....	a	697.9	1.3	9.1×10^{-16}
1952	175158.95−293957.1	267.995660	−29.665876	0.2	8.2	203.6	22.4	265.4	17.9	0.91	8.9	<-5	....	c	728.7	1.1	2.1×10^{-15}
1953	175159.02−293526.6	267.995930	−29.590741	0.3	6.8	30.5	13.1	123.5	6.5	0.90	2.2	-2.3	....	b	753.2	1.6	4.2×10^{-16}
1954	175159.13−294100.2	267.996380	−29.683395	0.2	8.8	400.1	27.7	328.9	222.1	0.90	14.2	<-5	....	a	718.3	2.3	8.5×10^{-15}
1955	175159.20−293538.9	267.996680	−29.594151	0.3	6.8	31.2	13.3	128.8	0.0	0.90	2.3	-2.3	g...	...	755.0	1.0	2.8×10^{-16}
1956	175159.24−293135.5	267.996870	−29.526530	0.2	7.8	127.3	14.5	66.7	60.0	0.66	8.5	<-5	....	a	751.3	1.9	2.9×10^{-15}
1957	175159.42−293106.4	267.997620	−29.518466	0.2	8.1	132.4	17.6	155.6	65.5	0.85	7.3	<-5	....	a	722.2	2.0	2.5×10^{-15}
1958	175159.44−293451.4	267.997700	−29.580957	0.3	6.9	35.0	13.4	126.0	37.1	0.89	2.5	-2.7	g...	...	723.8	4.1	1.4×10^{-15}
1959	175159.50−293056.0	267.997950	−29.515569	0.3	8.2	65.8	14.0	112.2	49.4	0.78	4.5	<-5	g...	...	697.5	3.1	2.2×10^{-15}
1960	175159.62−293145.9	267.998450	−29.529418	0.2	7.8	230.6	19.7	134.4	173.8	0.84	11.4	<-5	....	b	747.8	3.1	6.8×10^{-15}
1961	175159.63−293634.2	267.998460	−29.609526	0.1	7.0	407.7	24.2	150.3	254.3	0.90	16.5	<-5	g...	...	755.1	2.6	9.7×10^{-15}
1962	175159.66−293414.3	267.998610	−29.570664	0.2	7.0	84.8	14.9	119.2	10.6	0.90	5.5	<-5	g...	...	593.5	1.2	1.2×10^{-15}
1963	175159.71−293307.1	267.998800	−29.551983	0.3	7.3	30.4	14.0	147.6	18.8	0.89	2.1	-2.1	....	b	756.6	4.3	1.2×10^{-15}
1964	175159.90−293157.9	267.999590	−29.532757	0.3	7.8	59.8	13.4	102.2	29.7	0.77	4.3	<-5	....	a	744.2	2.0	1.2×10^{-15}
1965	175200.01−293335.7	268.000080	−29.559917	0.3	7.2	45.4	14.7	150.6	3.5	0.89	3.0	-3.8	....	b	758.8	1.4	5.5×10^{-16}
1966	175200.13−293619.9	268.000580	−29.605539	0.2	7.1	122.0	17.2	153.0	77.9	0.90	6.9	<-5	g...	...	750.7	2.6	2.9×10^{-15}
1967	175200.16−293401.6	268.000680	−29.567136	0.2	7.2	96.4	16.2	146.6	12.1	0.90	5.7	<-5	g...	...	686.1	1.1	1.1×10^{-15}
1968	175200.26−293509.6	268.001100	−29.586010	0.3	7.1	66.7	14.1	115.3	42.6	0.90	4.6	<-5	g...	...	592.9	2.7	2.2×10^{-15}
1969	175200.33−293735.9	268.001410	−29.626660	0.2	7.4	53.4	16.3	188.6	11.1	0.90	3.2	-4.1	....	a	747.6	1.4	6.5×10^{-16}
1970	175200.43−294237.6	268.001830	−29.710460	0.3	10.1	178.3	26.0	455.7	129.4	0.90	6.7	<-5	....	a	657.0	3.0	5.4×10^{-15}
1971	175200.47−293438.5	268.001990	−29.577365	0.3	7.1	30.6	14.4	158.4	2.1	0.90	2.0	-2.0	....	a	749.8	1.3	3.7×10^{-16}
1972	175200.63−294106.9	268.002650	−29.685258	0.3	9.1	98.2	22.2	360.8	64.2	0.90	4.3	<-5	....	a	713.6	2.9	2.7×10^{-15}

(*cont.*)

Table A.1: *Chandra* source list

Source		Position				Extracted Counts				Characteristics							
Seq	CXOU J	R. A.	Decl.	Err	θ	$C_{\rm net}$	$\Delta C_{\rm net}$	$C'_{\rm bkg}$	$C_{\rm net,hard}$	PSF	PS	$P_{\rm B}$	Anom	Var	EffExp	$E_{\rm median}$	Photo $F_{\rm x}$
#		(deg)	(deg)	($''$)	($'$)						Frac				(ks)	(keV)	(ergs s^{-1} cm^{-2})
(1)	(2)	(3)	(4)	(5)	(6)	(7)	(8)	(9)	(10)	(11)	(12)	(13)	(14)	(15)	(16)	(17)	(18)
1973	175200.64−293242.8	268.002680	−29.545234	0.2	7.6	81.6	16.6	170.4	46.1	0.90	4.8	<-5	....	b	736.3	2.1	1.6×10^{-15}
1974	175200.77−293155.5	268.003250	−29.532088	0.2	7.9	219.6	20.3	166.4	190.5	0.90	10.6	<-5	g...	...	635.8	3.6	8.1×10^{-15}
1975	175200.86−294007.3	268.003590	−29.668698	0.2	8.6	151.9	21.8	291.1	27.1	0.89	6.8	<-5	....	c	728.8	1.4	1.9×10^{-15}
1976	175200.94−293344.2	268.003940	−29.562297	0.3	7.4	38.0	14.9	165.0	17.7	0.89	2.5	-2.7	....	a	734.6	1.8	6.1×10^{-16}
1977	175201.05−293625.2	268.004400	−29.607007	0.1	7.3	446.2	25.2	158.8	57.4	0.89	17.4	<-5	....	a	746.2	1.2	4.9×10^{-15}
1978	175201.46−293739.4	268.006090	−29.627620	0.3	7.7	42.5	13.3	116.5	23.1	0.77	3.1	-3.9	....	c	740.8	2.3	1.0×10^{-15}
1979	175201.47−293815.3	268.006160	−29.637594	0.2	7.9	168.9	20.8	236.1	27.6	0.90	7.9	<-5	g...	...	735.3	1.3	2.1×10^{-15}
1980	175201.63−293629.6	268.006820	−29.608228	0.2	7.4	89.5	15.4	128.5	11.5	0.82	5.6	<-5	g...	...	736.9	1.3	1.2×10^{-15}
1981	175201.67−293750.6	268.006990	−29.630731	0.2	7.8	61.6	14.8	138.4	37.7	0.80	4.0	<-5	....	b	738.8	2.5	1.6×10^{-15}
1982	175201.68−293452.8	268.007000	−29.581351	0.2	7.4	214.2	19.7	148.8	119.2	0.88	10.6	<-5	g...	...	677.7	2.4	5.2×10^{-15}
1983	175201.80−294216.7	268.007510	−29.704639	0.3	10.1	109.1	25.6	502.9	28.5	0.90	4.2	<-5	....	b	688.8	1.5	1.6×10^{-15}
1984	175202.01−293404.0	268.008380	−29.567780	0.3	7.5	54.7	14.8	144.3	30.4	0.90	3.6	<-5	g...	...	568.9	2.2	1.5×10^{-15}
1985	175202.05−294010.9	268.008560	−29.669706	0.3	8.8	74.7	20.3	307.3	8.4	0.89	3.6	-4.8	....	b	716.9	1.2	8.5×10^{-16}
1986	175202.29−293502.2	268.009580	−29.583959	0.2	7.5	161.0	18.1	145.0	88.1	0.89	8.6	<-5	g...	...	590.0	2.1	4.2×10^{-15}
1987	175202.39−293539.5	268.010000	−29.594308	0.2	7.5	119.2	18.0	181.8	78.2	0.89	6.4	<-5	....	a	741.0	2.9	3.1×10^{-15}
1988	175203.00−293749.8	268.012530	−29.630515	0.3	8.0	42.5	17.5	237.5	12.7	0.90	2.4	-2.4	g...	...	727.3	1.5	5.9×10^{-16}
1989	175203.30−293603.1	268.013760	−29.600865	0.2	7.7	176.0	20.0	198.0	28.9	0.90	8.6	<-5	g...	...	711.1	1.2	2.0×10^{-15}
1990	175203.37−294233.4	268.014050	−29.709291	0.3	10.5	102.2	18.3	207.8	28.7	0.68	5.4	<-5	g...	...	610.2	1.7	2.8×10^{-15}
1991	175203.86−293938.8	268.016120	−29.660797	0.2	8.9	159.8	20.1	216.2	44.1	0.82	7.8	<-5	g...	...	698.1	1.4	2.6×10^{-15}
1992	175203.89−294010.8	268.016240	−29.669667	0.3	9.2	107.6	21.8	334.4	24.6	0.89	4.8	<-5	g...	...	689.7	1.4	1.5×10^{-15}
1993	175204.01−294030.7	268.016720	−29.675198	0.2	9.4	222.5	25.0	365.5	147.2	0.90	8.7	<-5	g...	...	680.1	2.5	5.7×10^{-15}
1994	175204.27−294219.5	268.017810	−29.705436	0.2	10.4	266.9	26.4	391.1	200.8	0.84	9.9	<-5	....	a	622.0	3.3	1.0×10^{-14}
1995	175204.56−293911.5	268.019020	−29.653209	0.2	8.8	270.4	24.9	315.6	172.8	0.90	10.6	<-5	g...	...	698.7	2.9	1.4×10^{-15}
1996	175204.56−293709.3	268.019040	−29.619252	0.3	8.2	65.8	17.3	209.2	18.5	0.90	3.7	<-5	g...	...	620.1	1.9	7.7×10^{-15}
1997	175204.69−293935.8	268.019570	−29.659968	0.3	9.0	106.3	19.3	237.7	43.0	0.83	5.4	<-5	g...	...	687.4	1.8	2.1×10^{-15}
1998	175205.04−294056.0	268.021030	−29.682223	0.2	9.7	132.4	20.8	270.6	105.2	0.81	6.2	<-5	g...	...	635.7	3.2	5.4×10^{-15}
1999	175205.41−294039.6	268.022550	−29.677689	0.3	9.6	47.5	15.3	165.5	37.6	0.69	3.0	-3.8	....	a	640.4	3.9	2.6×10^{-15}
2000	175206.24−294013.2	268.026010	−29.670345	0.3	9.6	108.2	21.6	324.8	97.9	0.90	4.9	<-5	g...	...	569.6	3.5	4.7×10^{-15}
2001	175206.36−293841.6	268.026520	−29.644900	0.4	8.9	47.7	14.0	129.3	30.3	0.90	3.3	-4.6	g...	...	296.9	2.5	3.1×10^{-15}
2002	175206.49−294131.1	268.027060	−29.691998	0.3	10.3	72.3	24.0	465.7	16.4	0.90	2.9	-3.3	g...	...	594.9	1.5	1.3×10^{-15}

(1) X-ray catalog sequence number, sorted by R. A. (2) IAU designation. (3),(4) R. A. and Decl. in the equinox J2000.0. (5) Estimated standard deviation of the randam component of the posittion error. (6) Off-axis angle. (7),(8) Estimated net counts extracted in 0.5–8.0 keV;average of the upper and lower 1 σ errors on

column 6. (9) Background counts expected in the source extraction region (total band). (10) Estimated net counts extracted in the hard band (2.0–8.0 keV). (11) Fraction of the PSF (at 1.497 keV) enclosed within the extraction region. A reduced PSF fraction (significantly below 90%) may indicate that the source is in a crowded region. (12) Photometric significance. (13) Logarithmic probability that extracted counts (0.5–8.0 keV) are solely from background. (14)Source anomalies: g = fractional time that source was on a detector (FRACEXPO from *mkarf*) is < 0.9 (15) Variability characterization based on K-S statistic (0.5–8.0 keV): a = no evidence for variability ($0.05 < P_{KS}$); b = possibly variable ($0.005 < P_{KS} < 0.05$); c = definitely variable ($P_{KS} < 0.005$). No value is reported for sources in chip gaps or on field edges. (16) Effective exposure time: approximate time the source would have to be observed on-axis to obtain the reported number of counts. (17) Background-corrected median photon energy (0.5–8.0 keV). (18) Photometric flux estimate in the 0.5–8.0 keV band.

Appendix B

Thermal Spectral Fitting

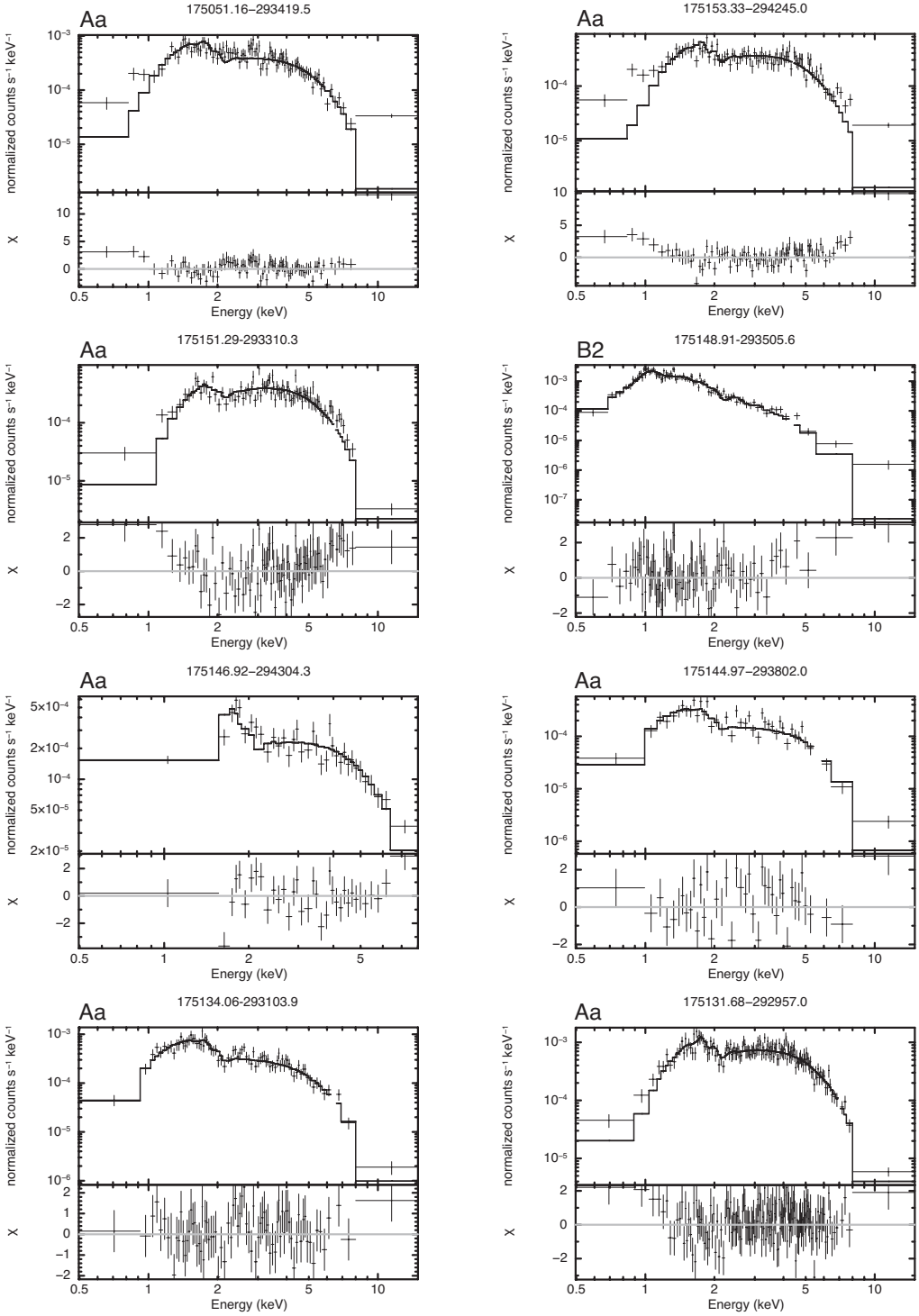

Figure B.1: Thermal spectral fittings for X-ray sources, which have source counts over 500.

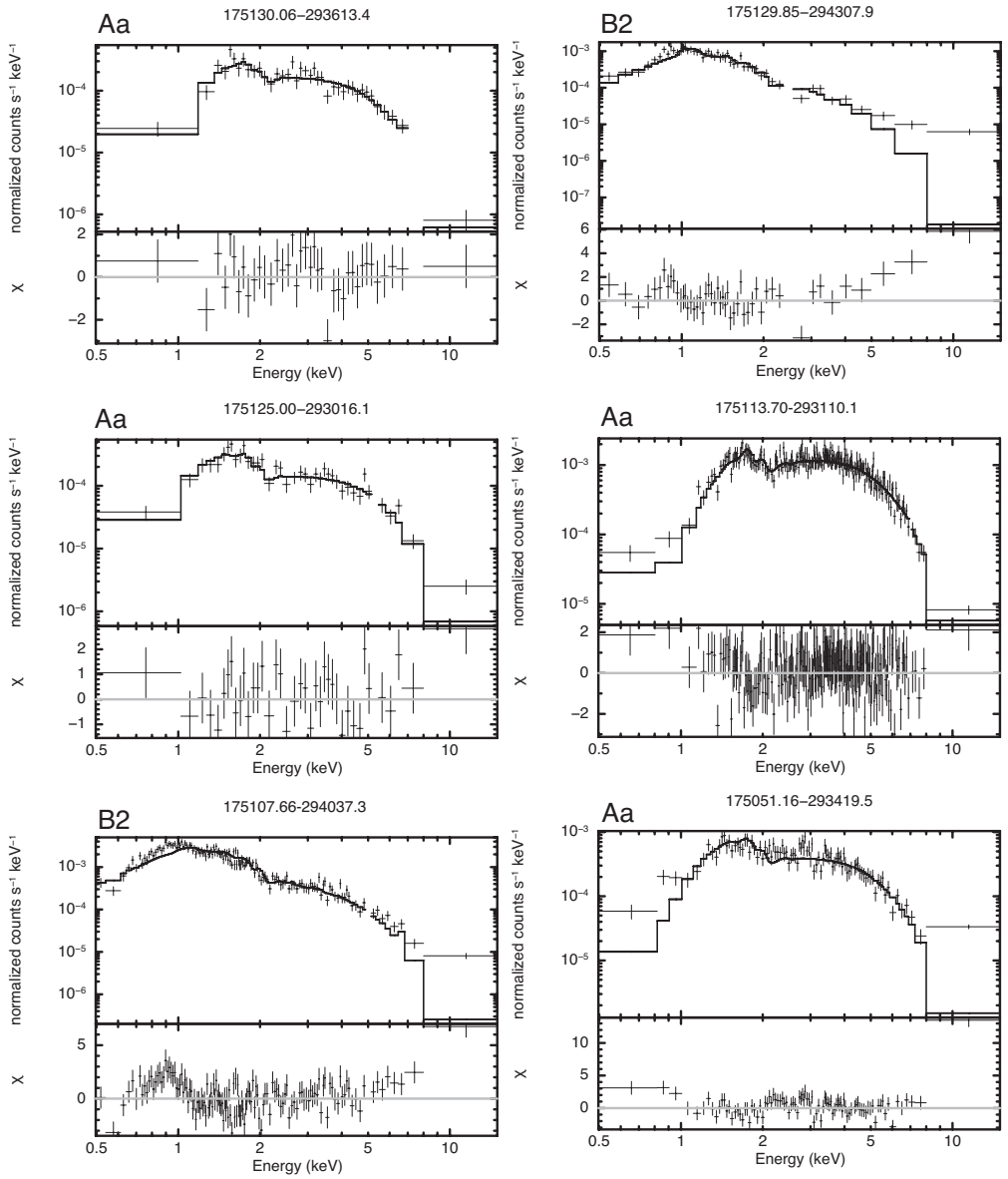

Figure B.1: Continued.

Appendix C

Power-law Spectral Fitting

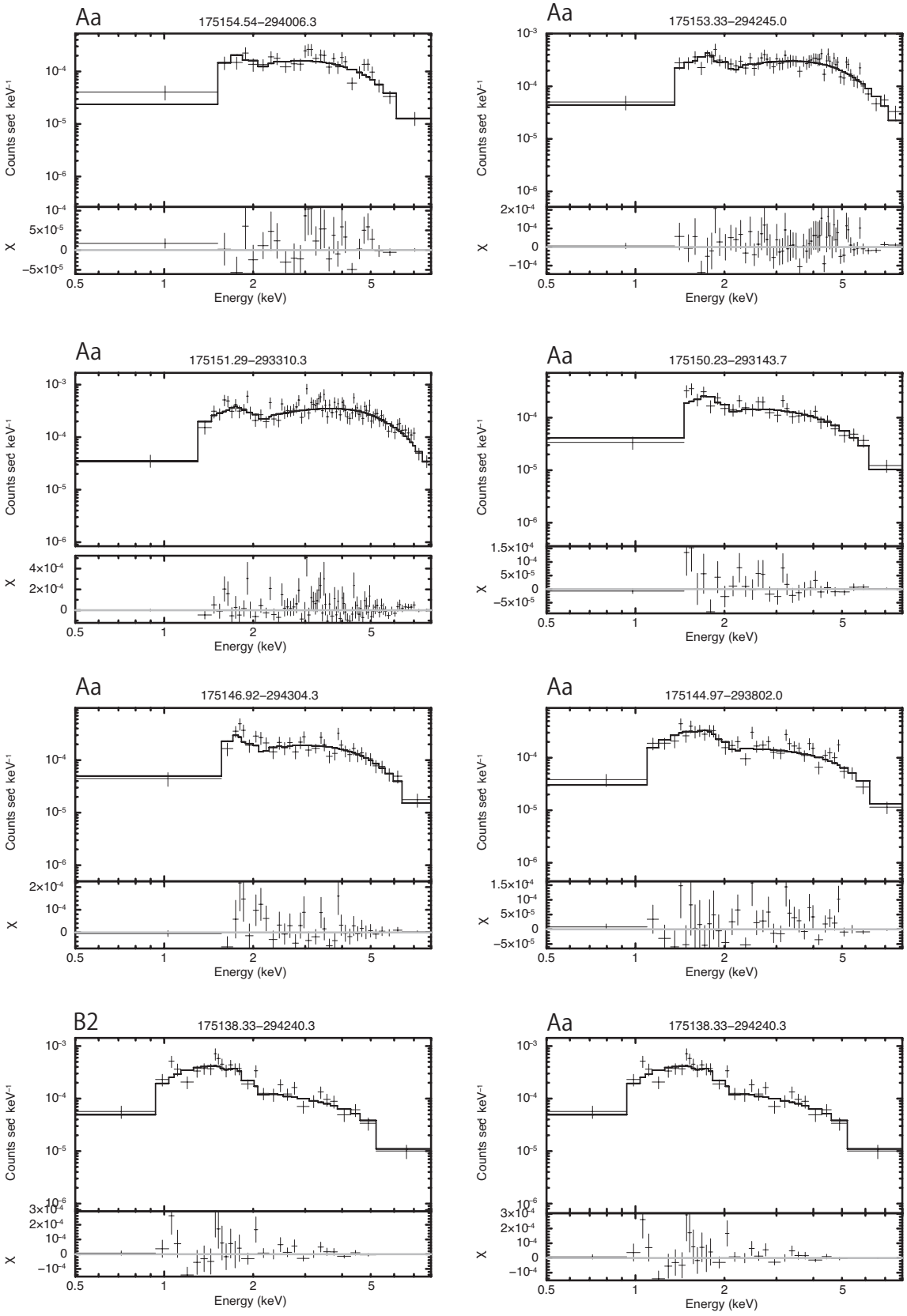

Figure C.1: Power-law spectral fittings for X-ray sources, which have source counts over 500.

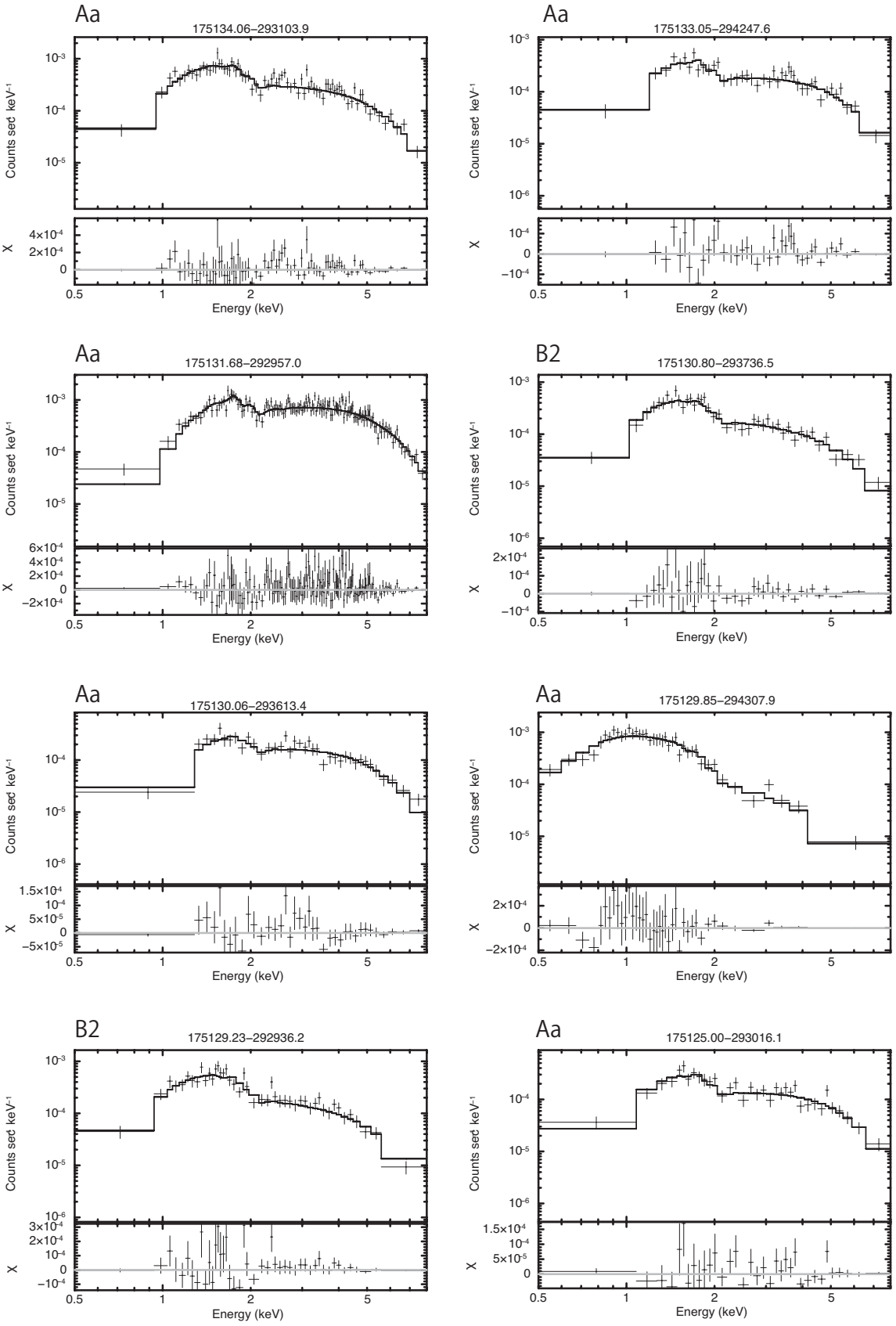

Figure C.1: Continued.

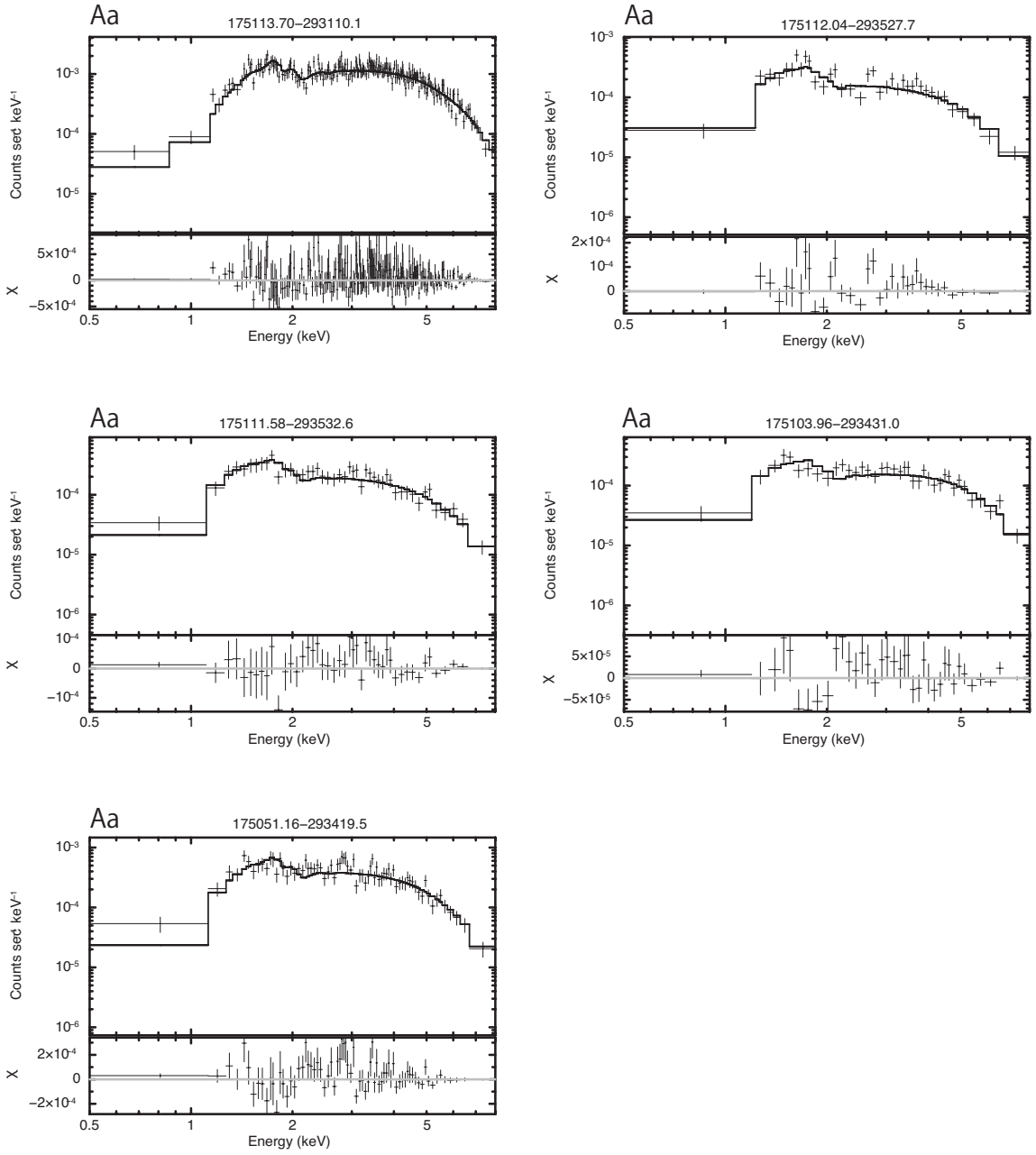

Figure C.1: Continued.

Appendix D

X-ray Light curves of Variable Sources

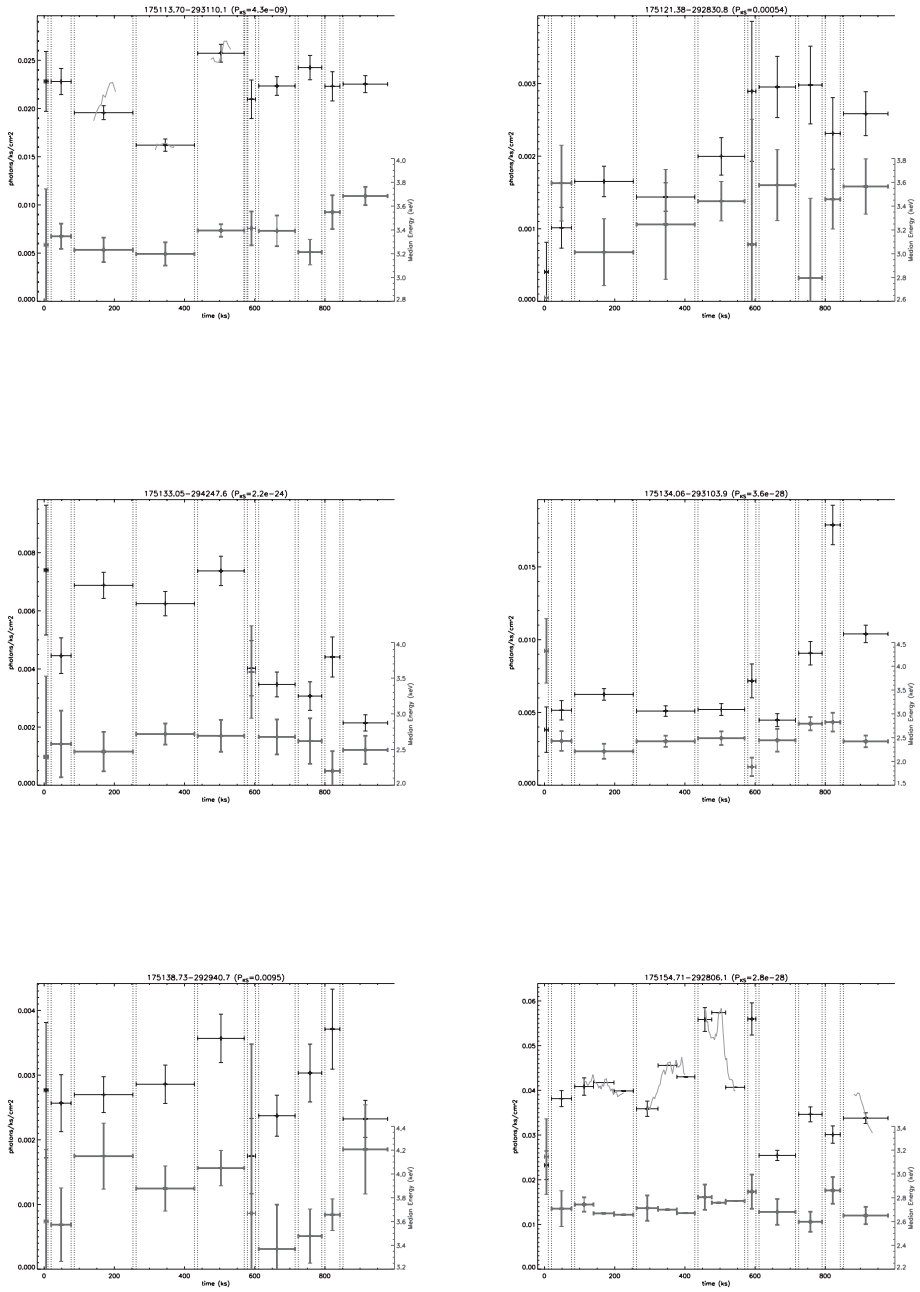

Figure D.1: Concatenated light curves for variable ($P_{\rm KS} < 5 \times 10^{-3}$) and bright (more than 1000 counts) sources. The light curves show variations in count rate (black thin histograms are binned and blue adaptively smoothed curve) and black thick histogram shows variations in median energy. Time intervals between observations are indicated by black dotted vertical lines.

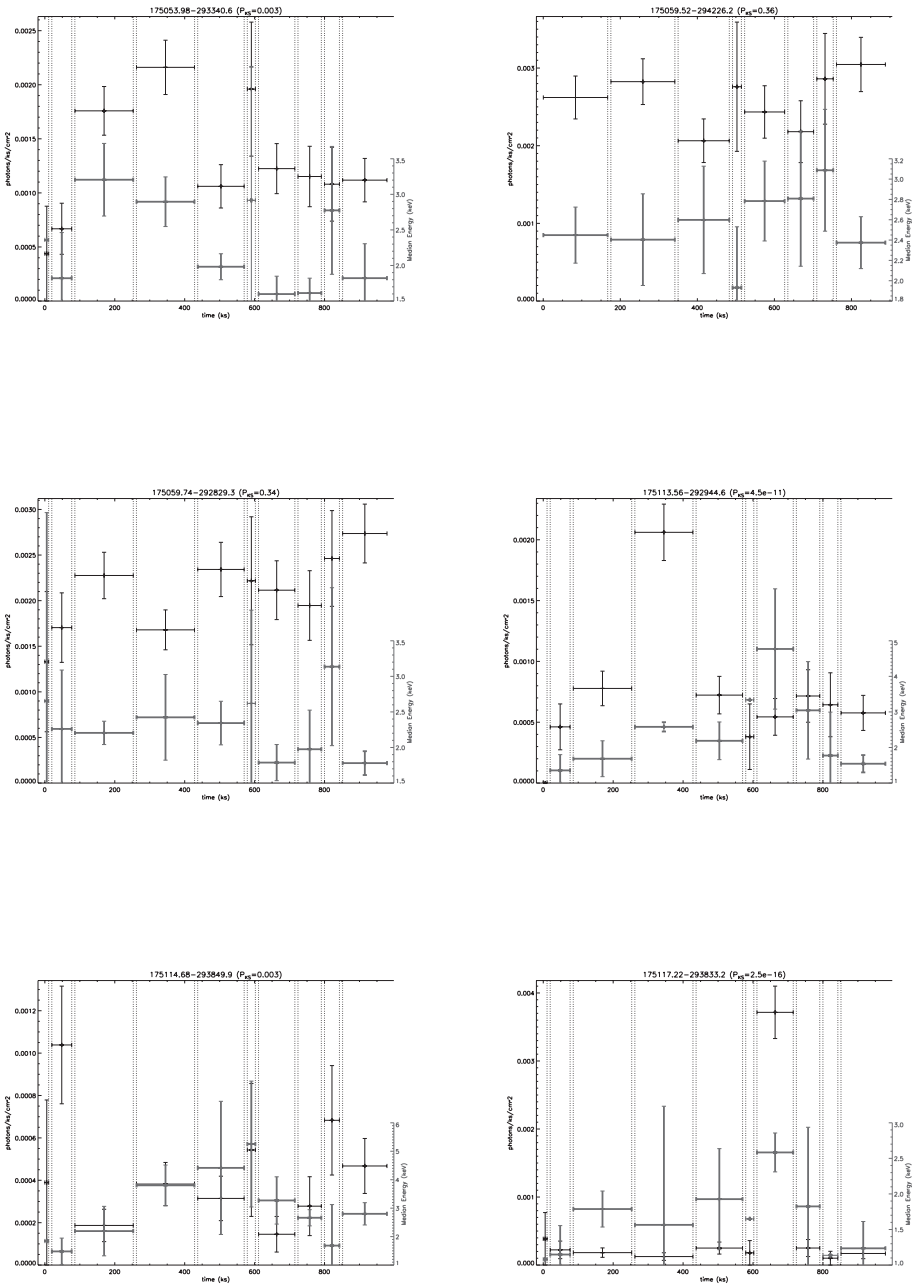

Figure D.1: Light curves of variable sources in the group Ab.

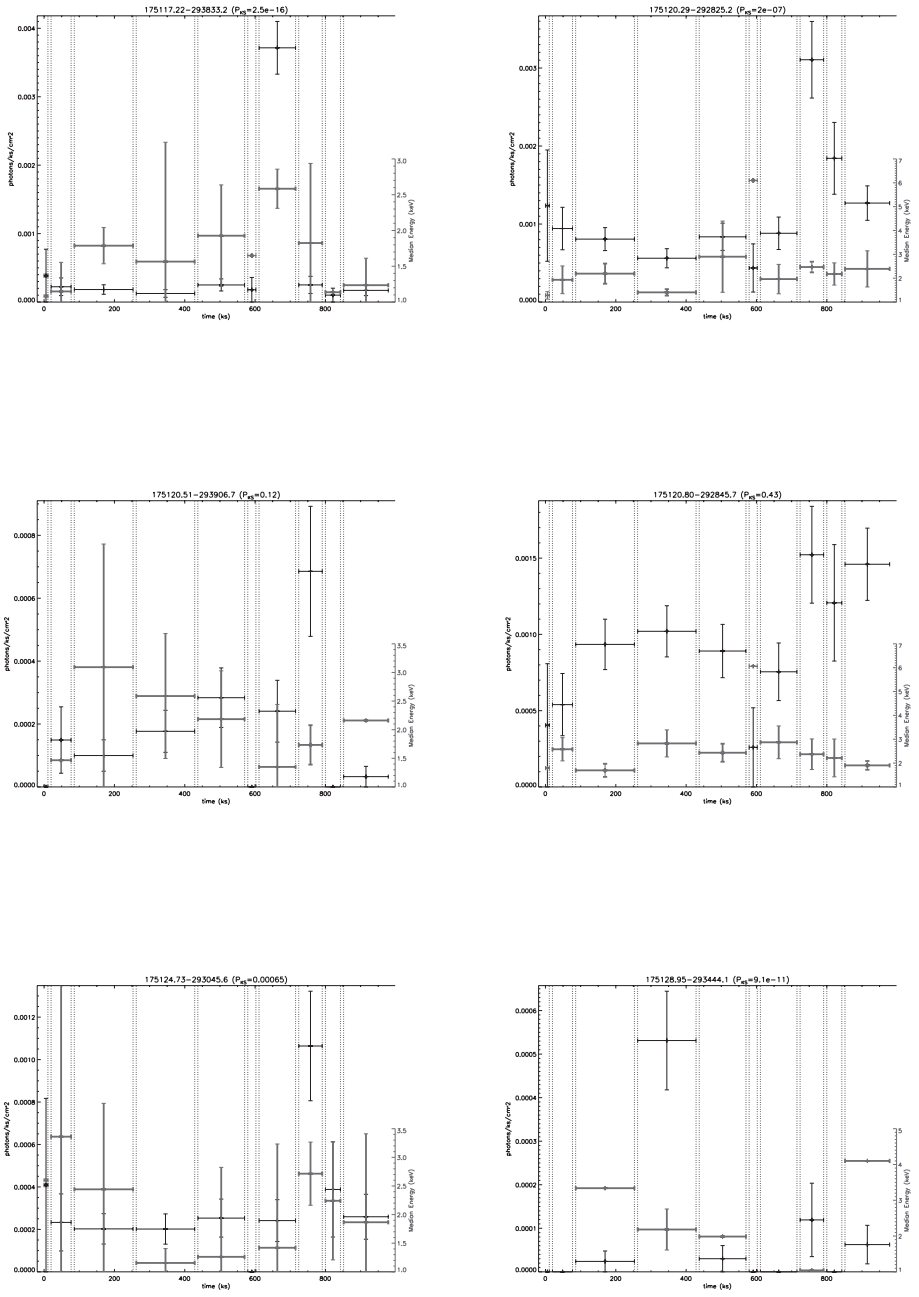

Figure D.1: Light curves of variable sources in the group Ab.

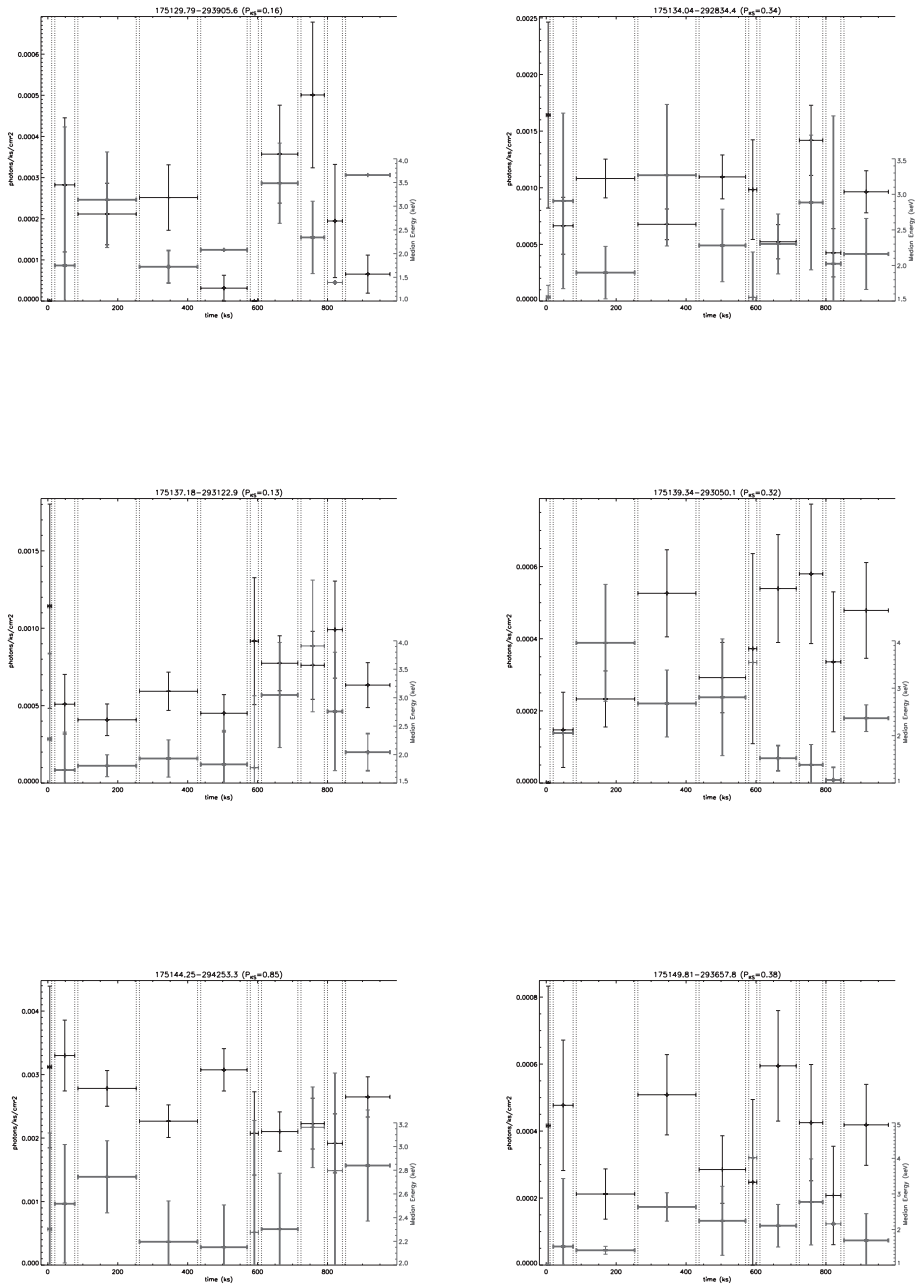

Figure D.1: Light curves of variable sources in the group Ab.

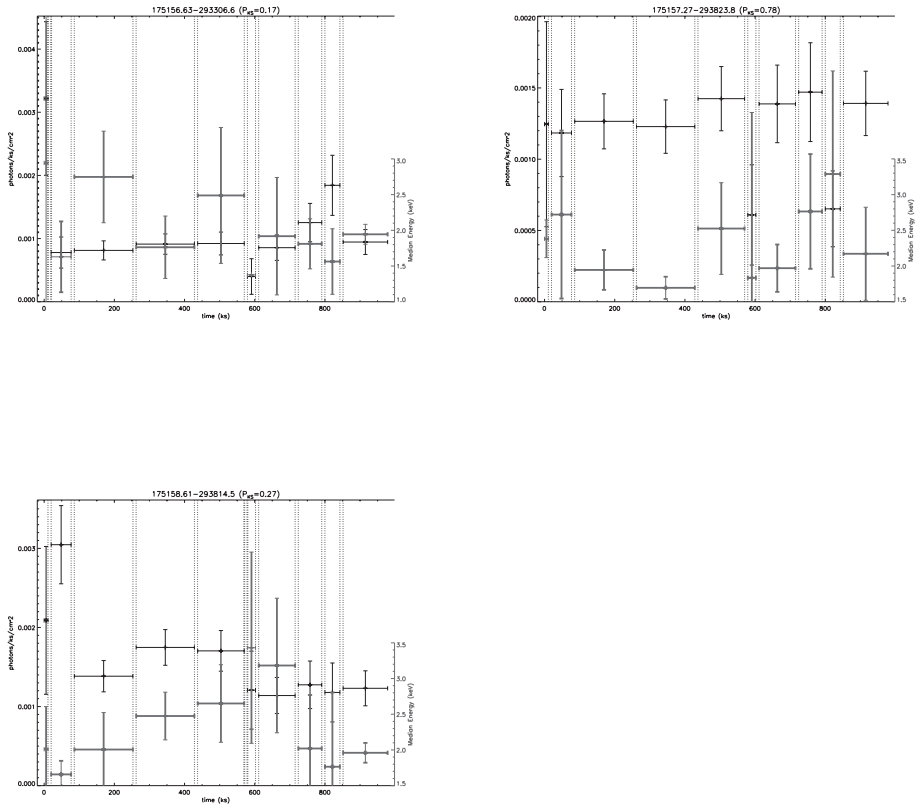

Figure D.1: Light curves of variable sources in the group Ab.

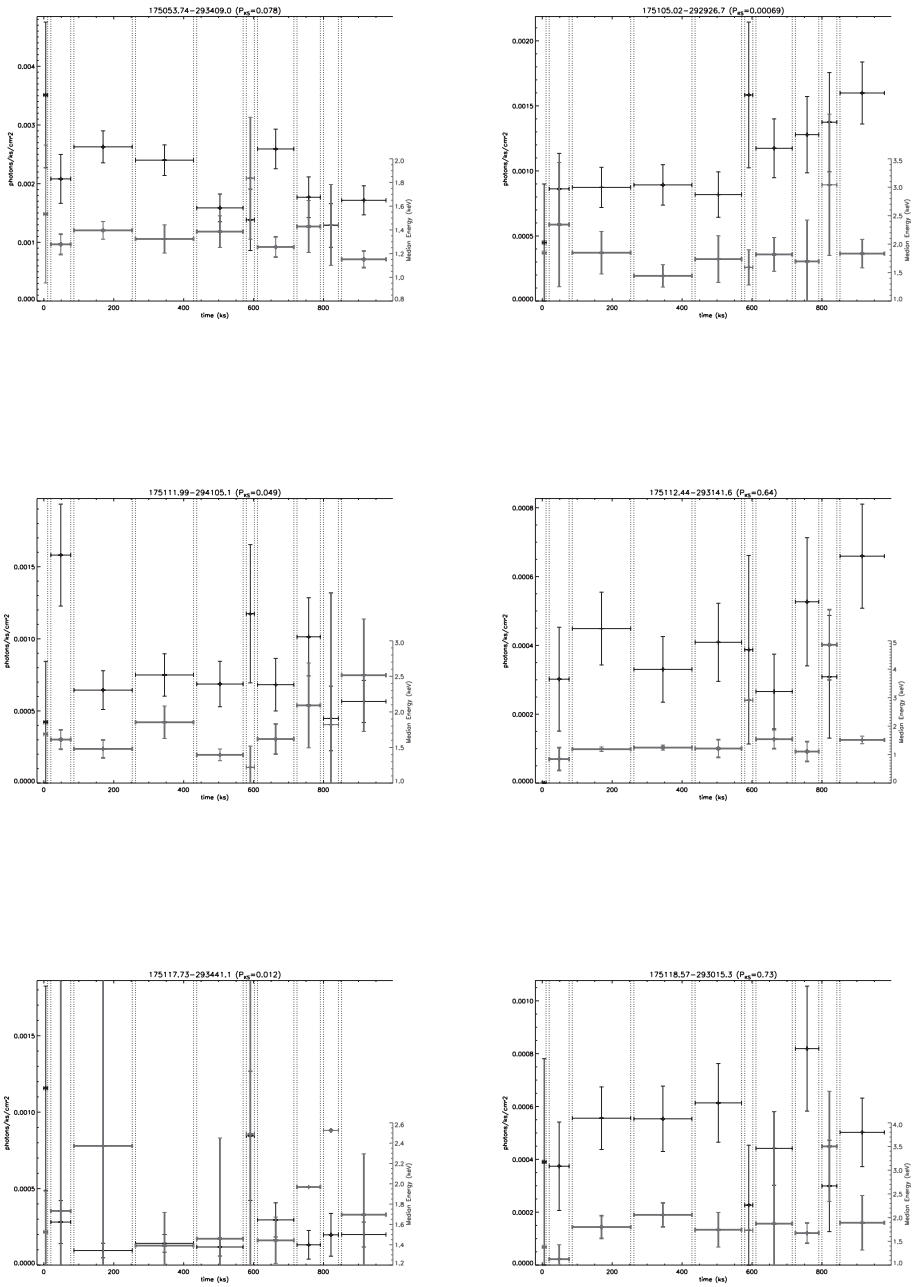

Figure D.1: Light curves of variable sources in the group B1.

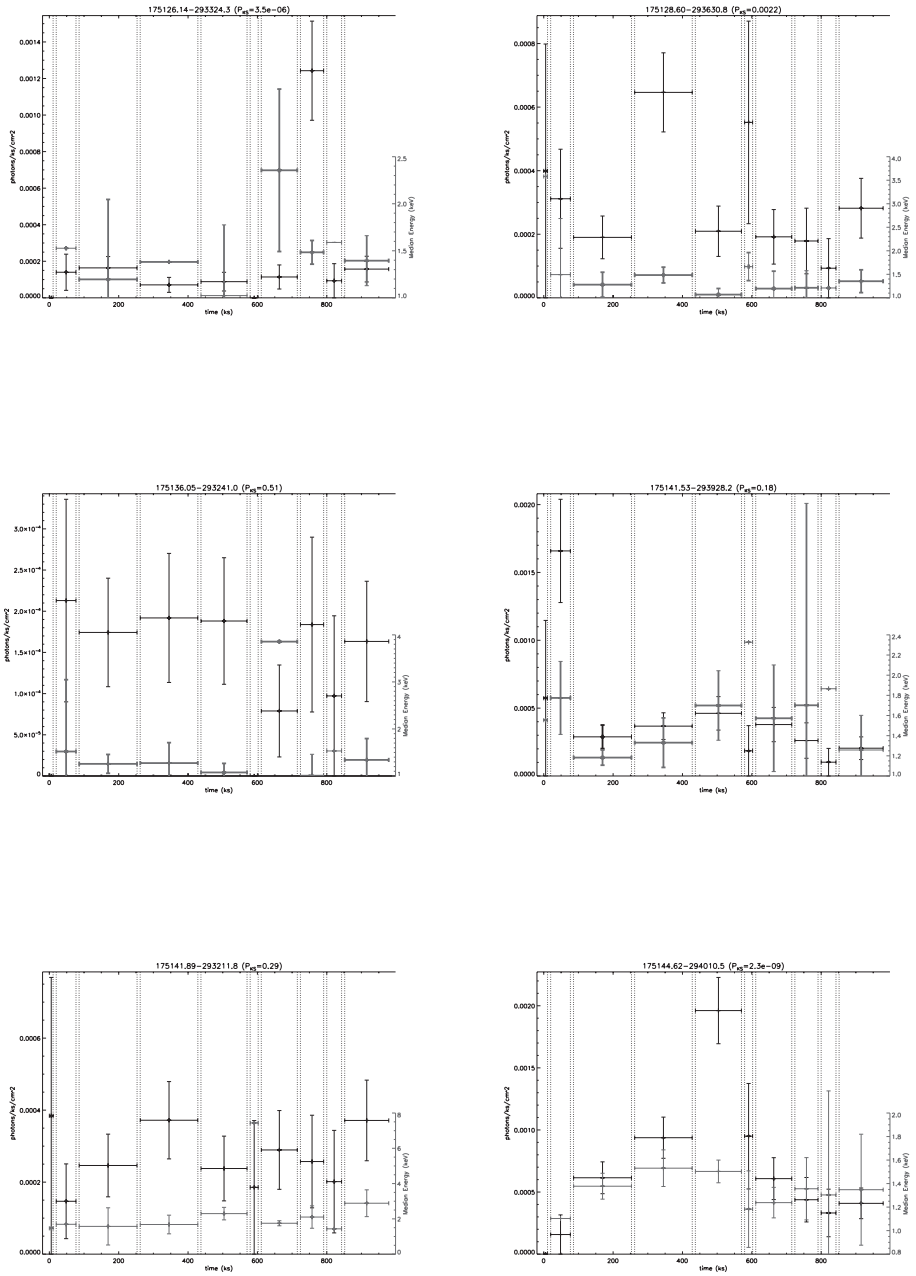

Figure D.1: Light curves of variable sources in the group B1.

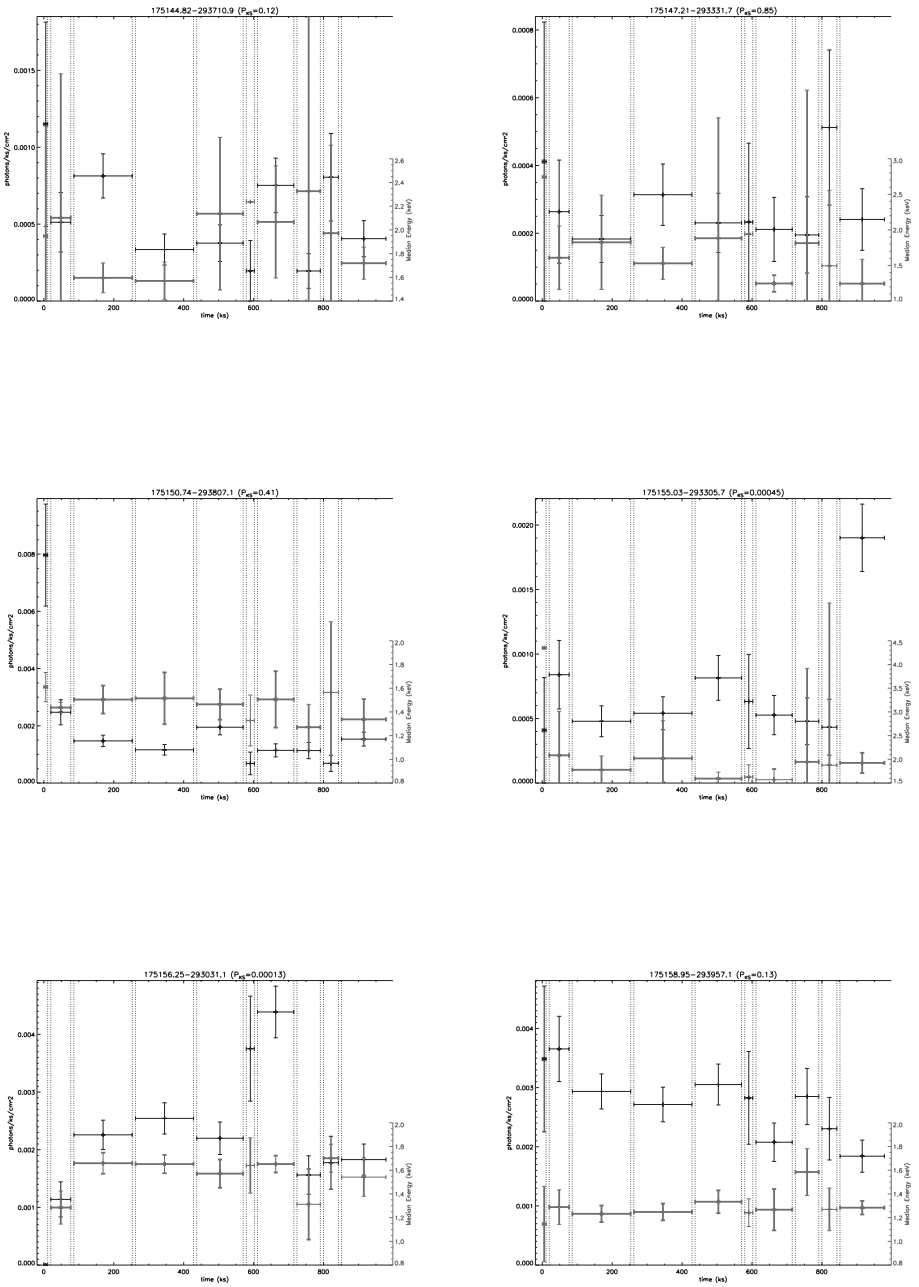

Figure D.1: Light curves of variable sources in the group B1.

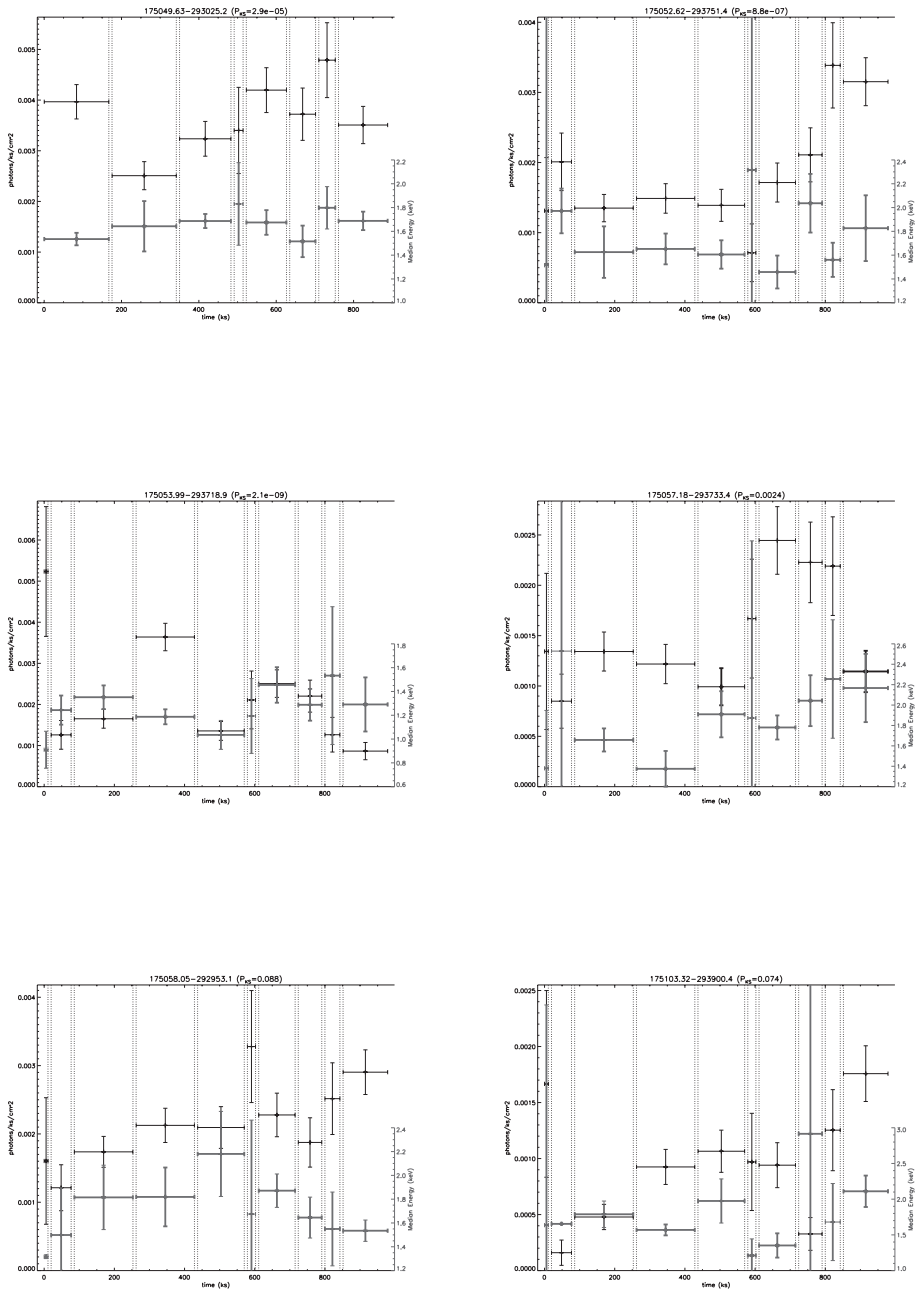

Figure D.1: Light curves of variable sources in the group B2.

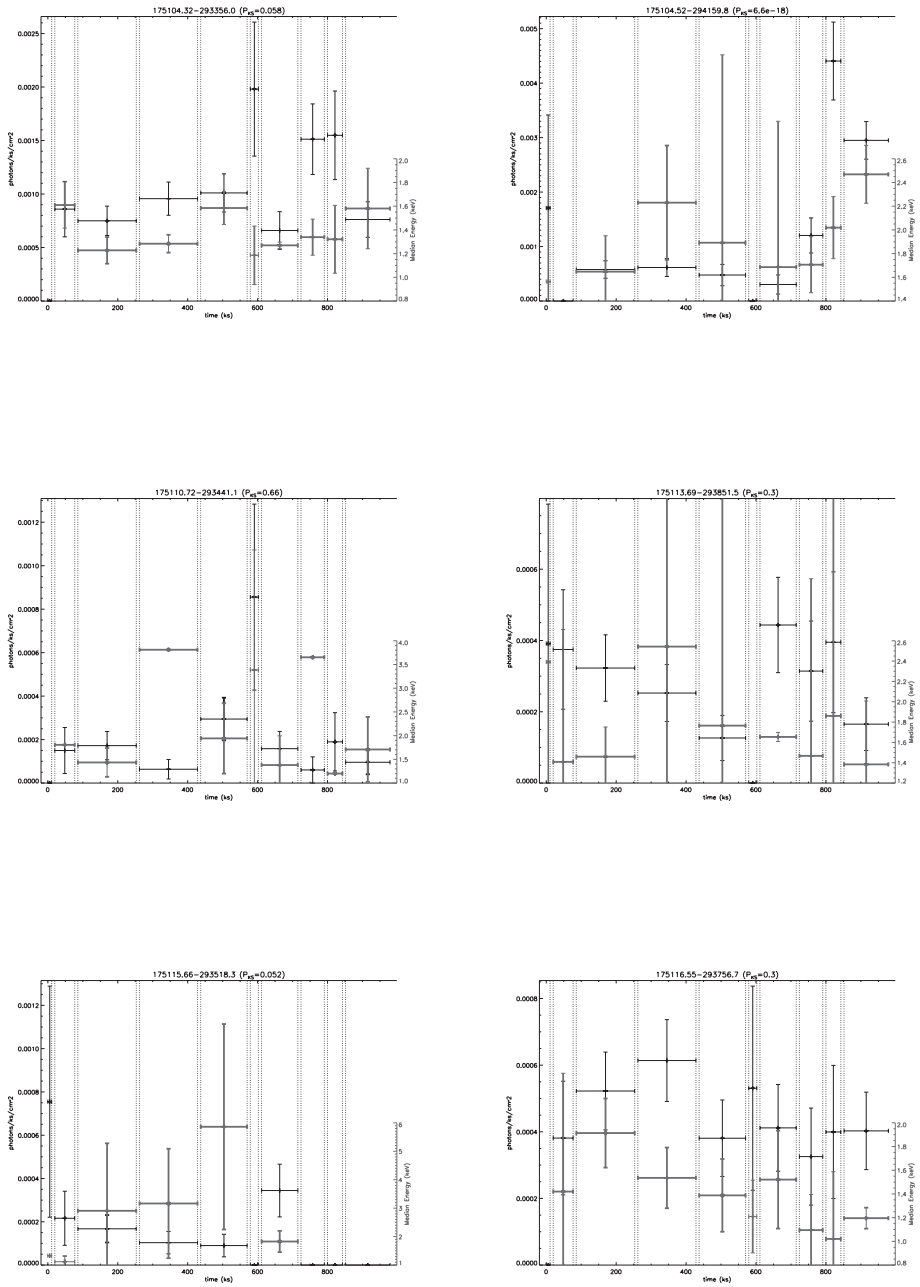

Figure D.1: Light curves of variable sources in the group B2.

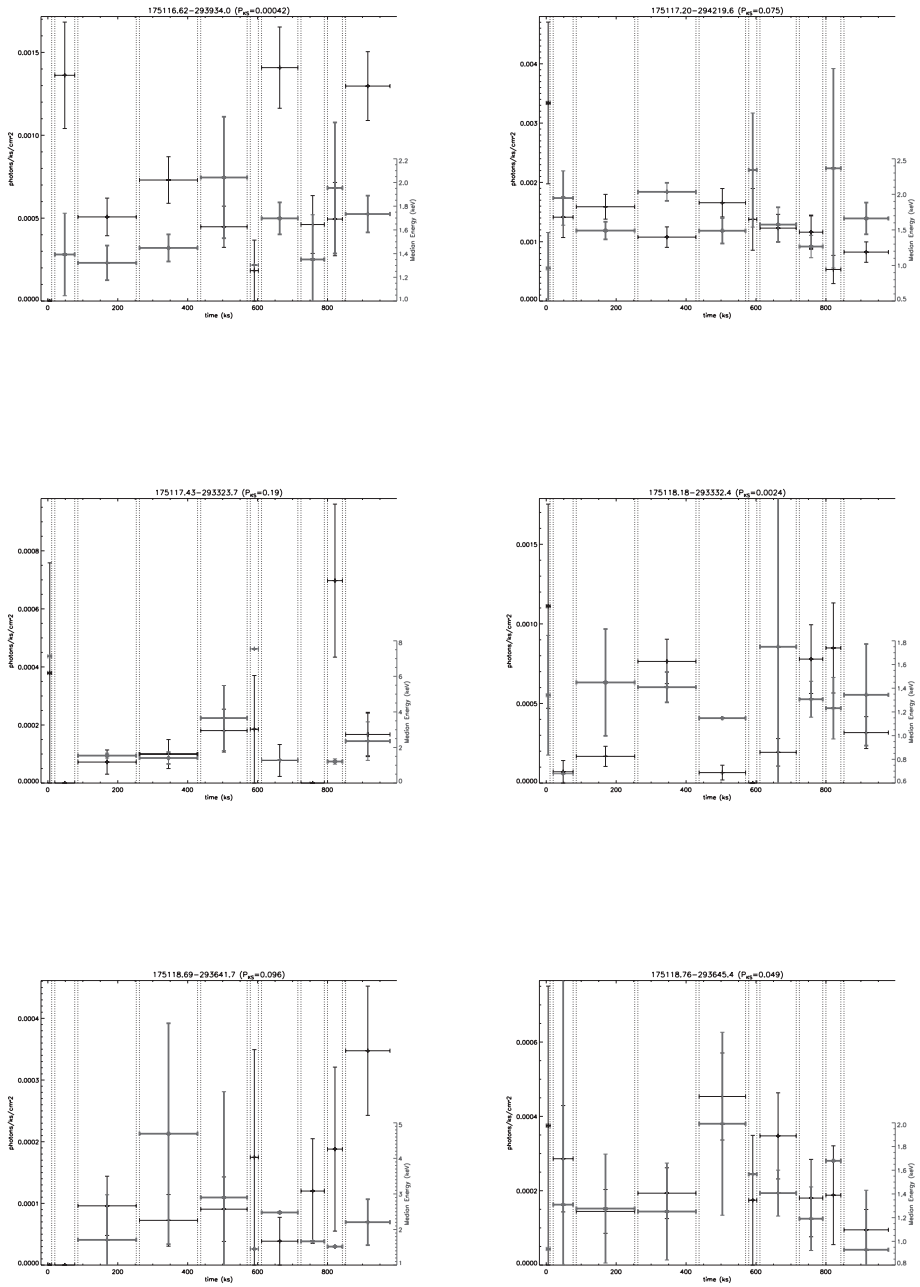

Figure D.1: Light curves of variable sources in the group B2.

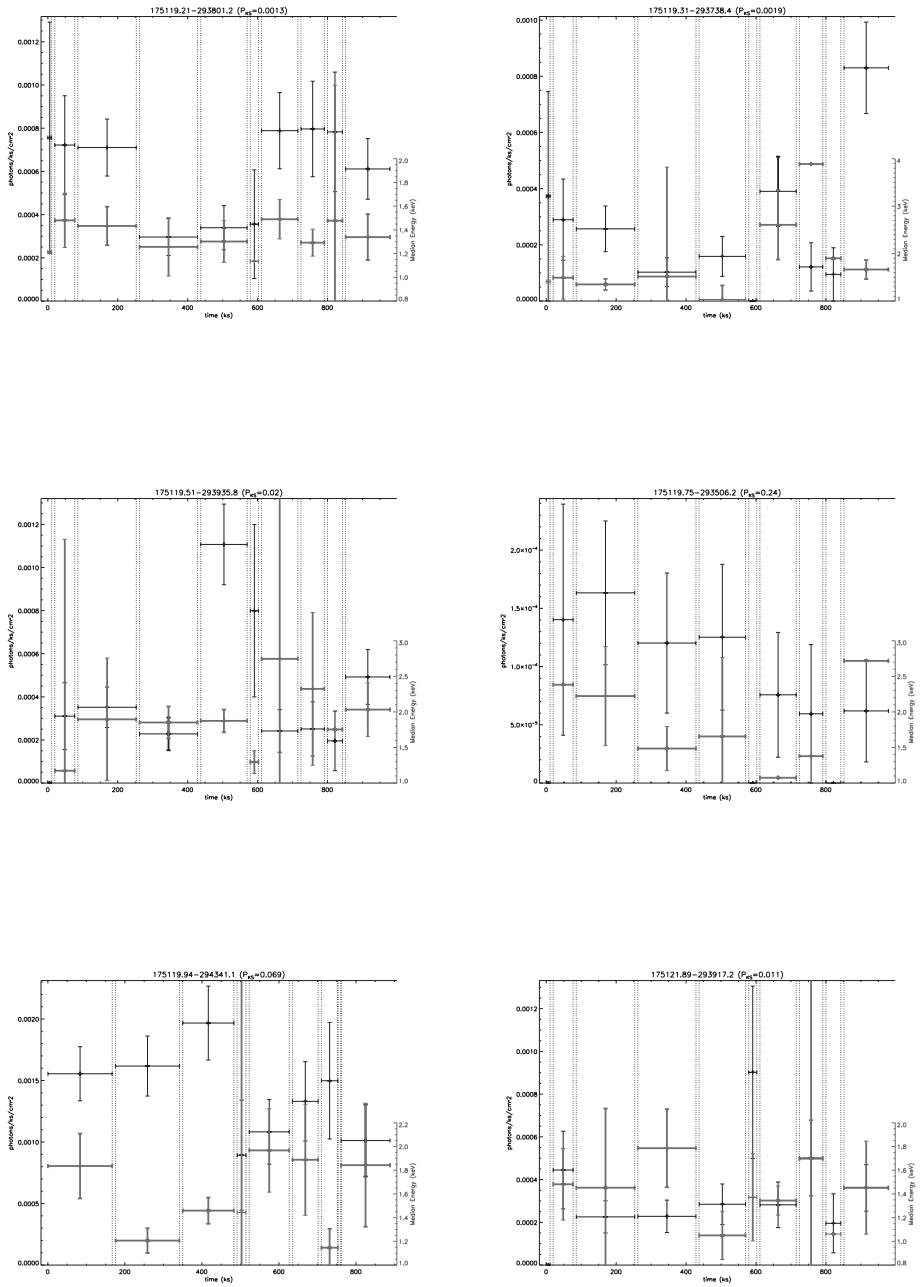

Figure D.1: Light curves of variable sources in the group B2.

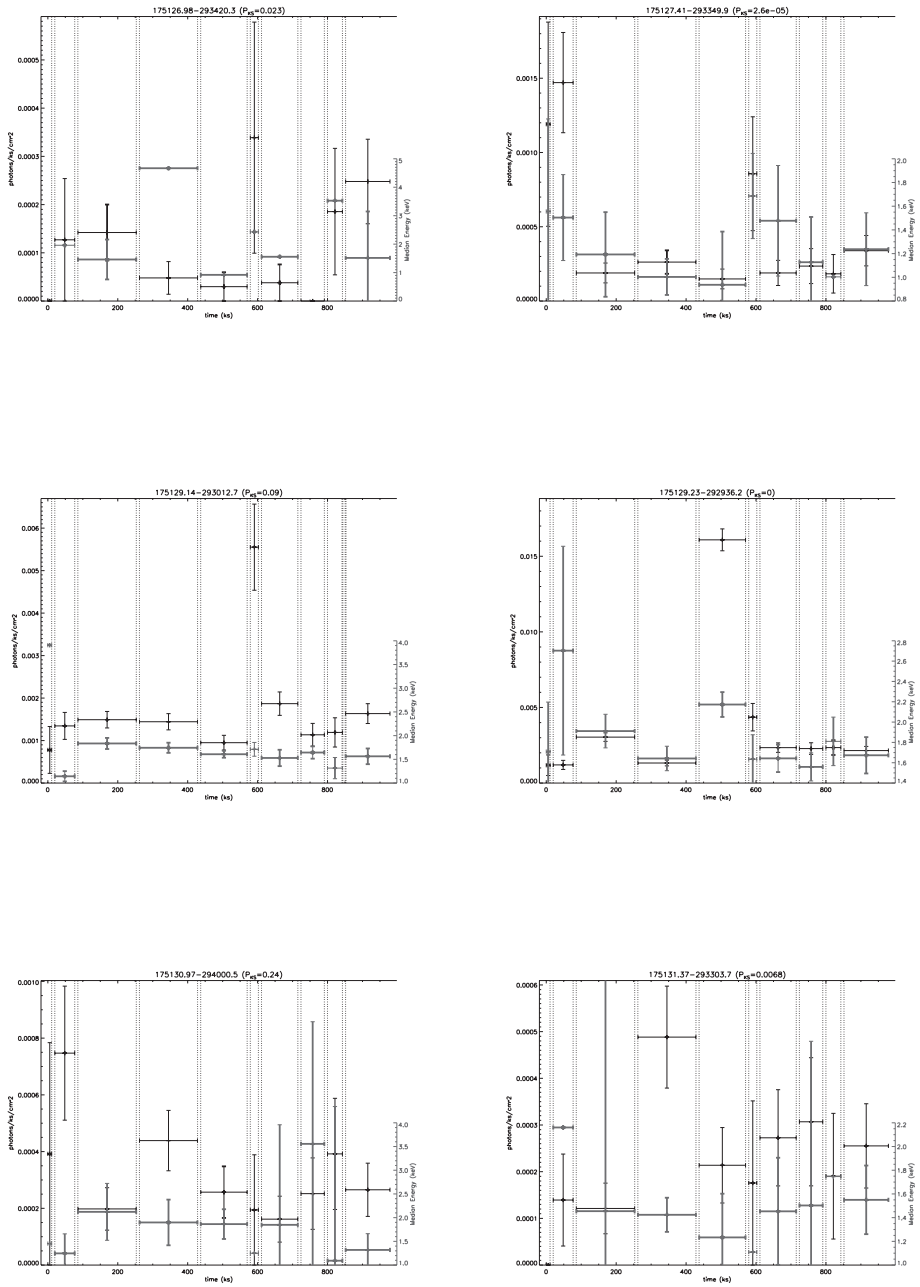

Figure D.1: Light curves of variable sources in the group B2.

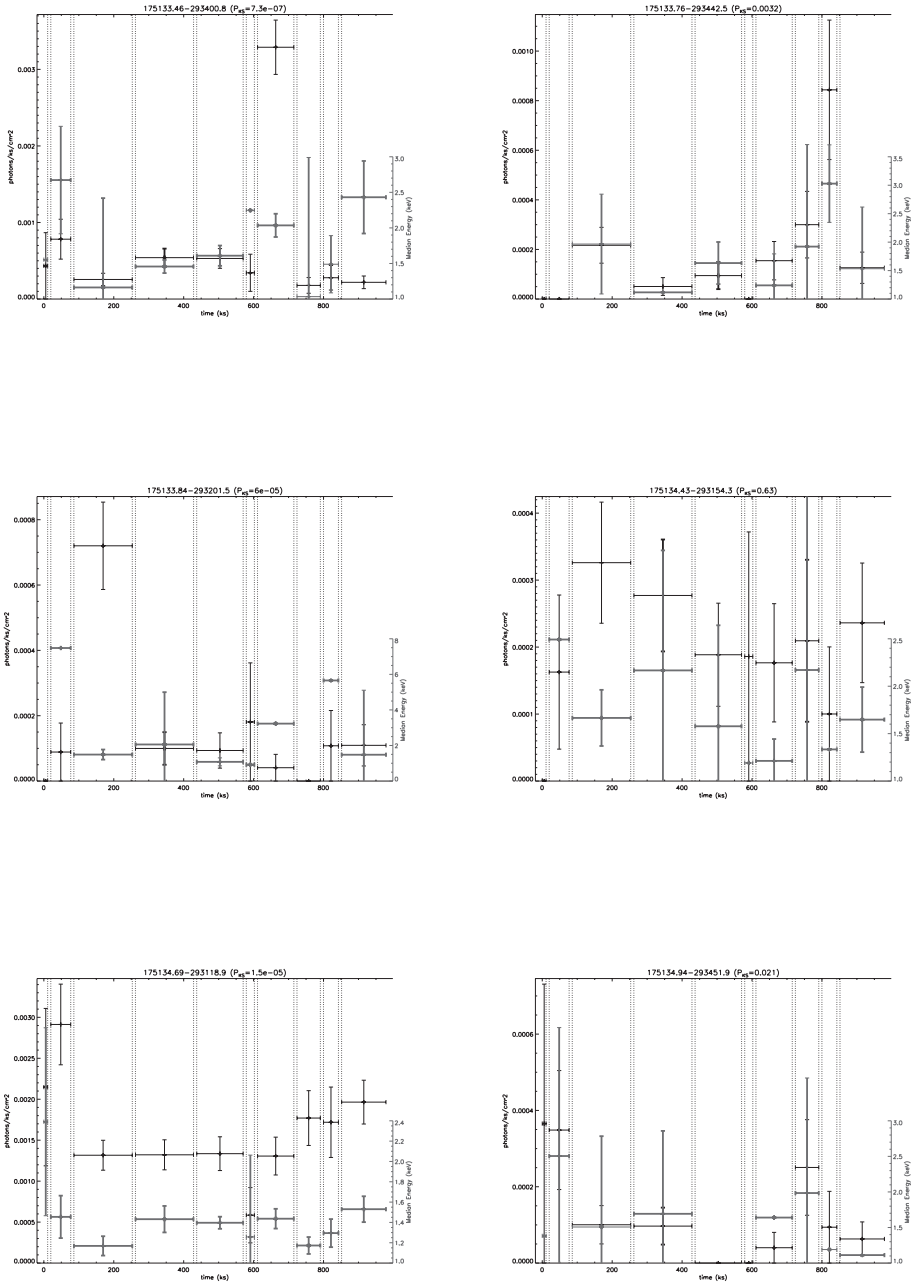

Figure D.1: Light curves of variable sources in the group B2.

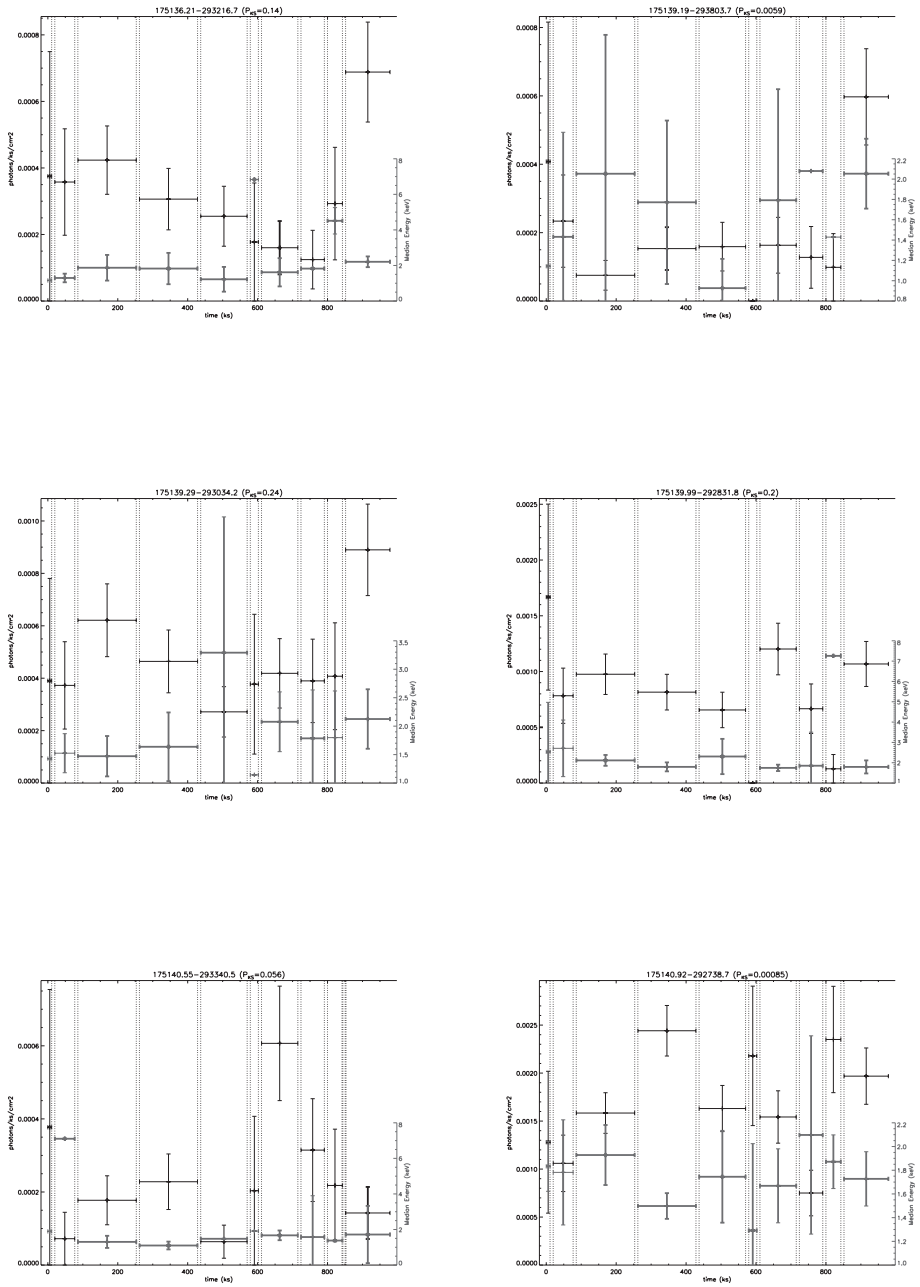

Figure D.1: Light curves of variable sources in the group B2.

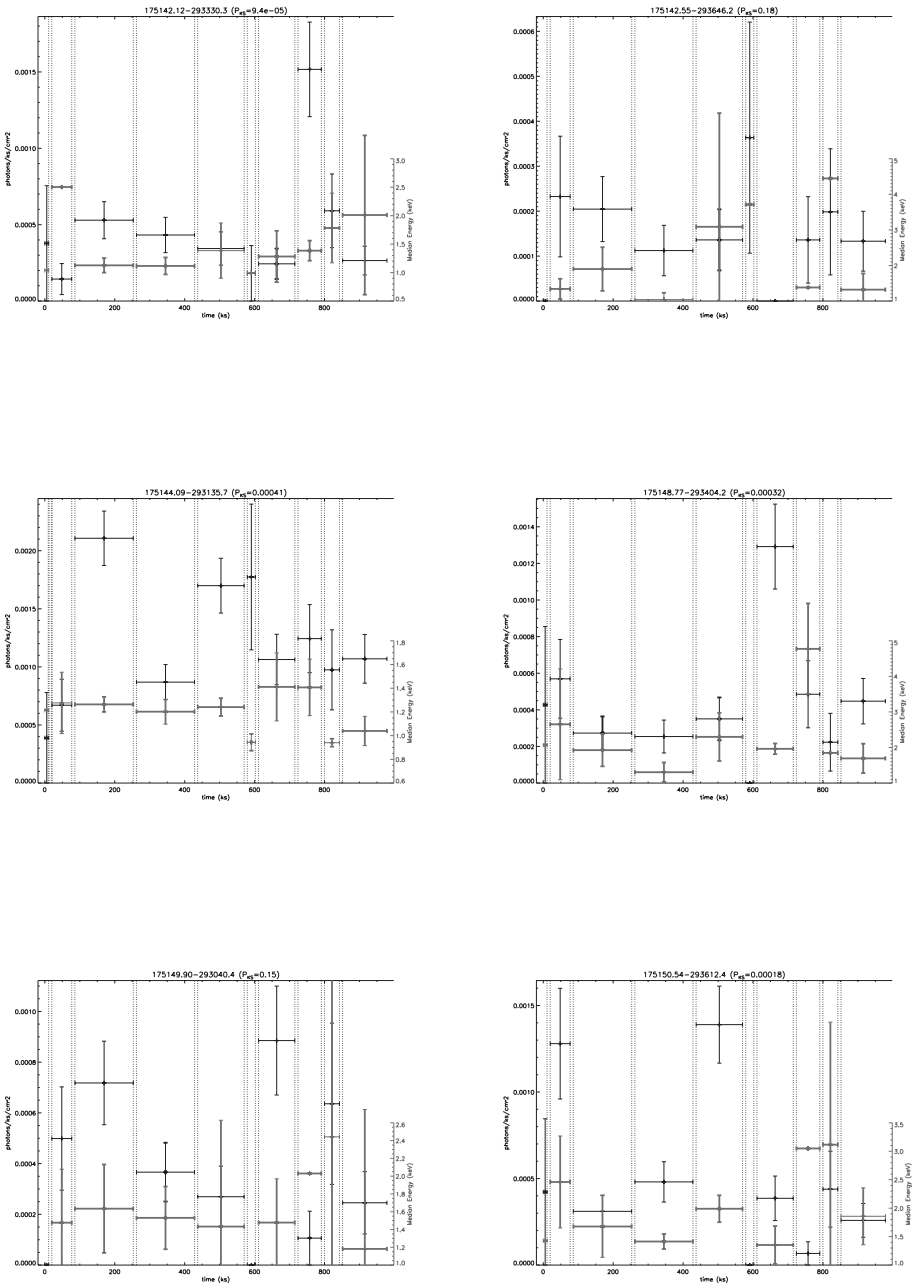

Figure D.1: Light curves of variable sources in the group B2.

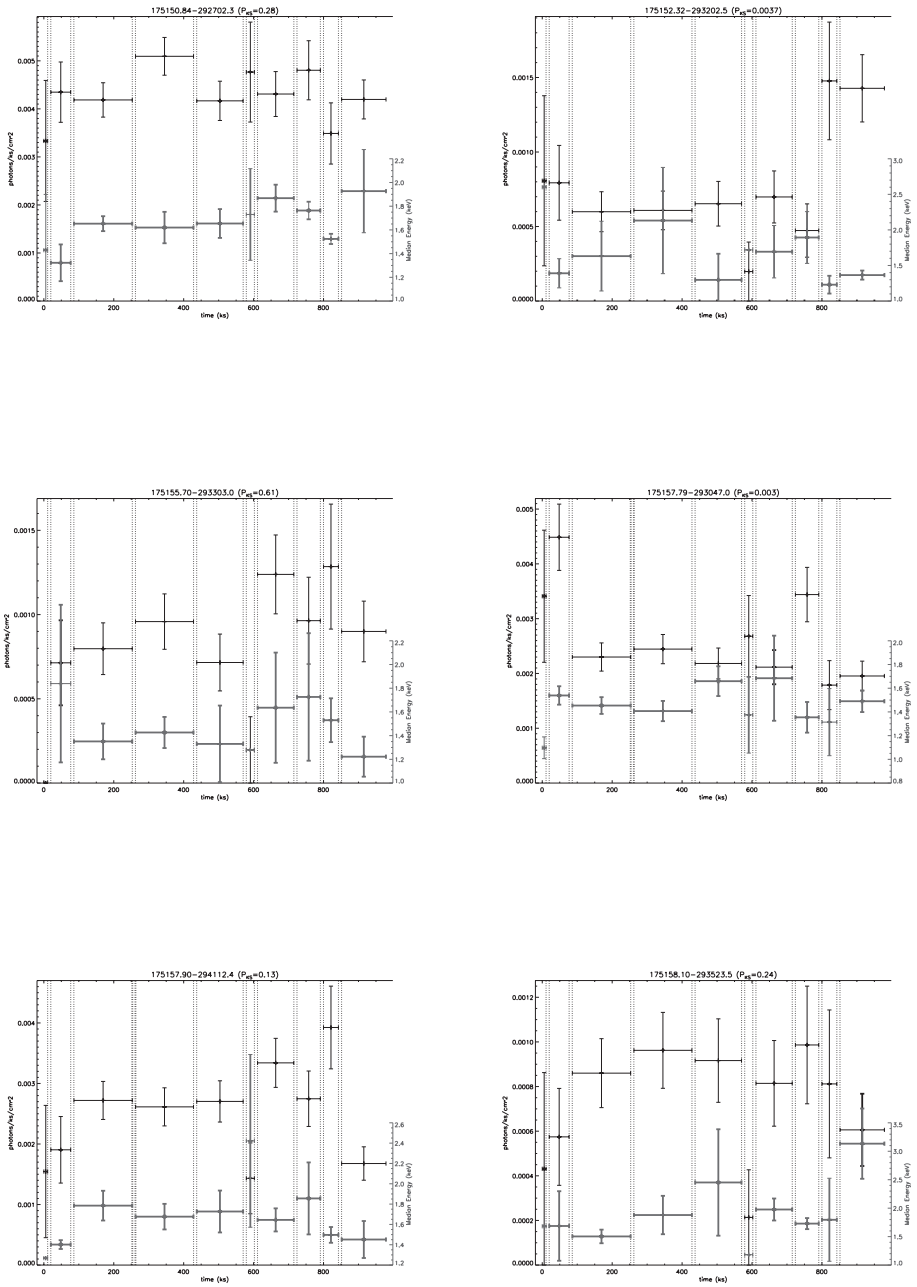

Figure D.1: Light curves of variable sources in the group B2.

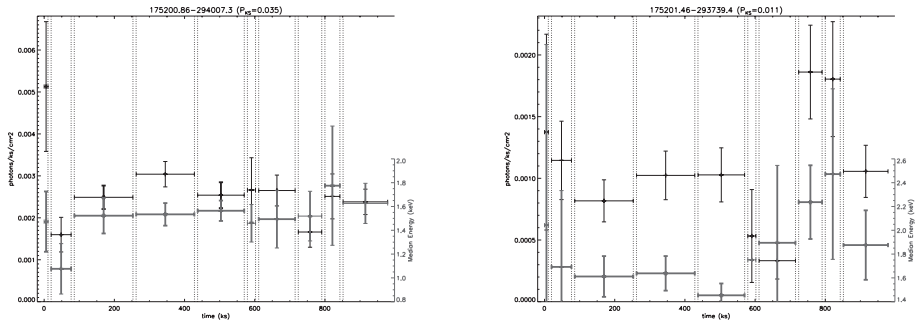

Figure D.1: Light curves of variable sources in the group B2.

Appendix E

Chandra–SIRIUS Counterpart Sources list

Table E.1: *Chandra*-SIRIUS counterpartpairs

Seq	R.A.	Decl.	ΔR	J mag	$\Delta Jmag$	H mag	$\Delta Hmag$	K_s mag	$\Delta Kmag$
#	(J2000.0)	(J2000.0)	(arcsec)	(mag)	(mag)	(mag)	(mag)	(mag)	(mag)
(1)	(2)	(3)	(4)	(5)	(6)	(7)	(8)	(9)	(10)
9	267.6925	−29.4965	1.1	...	...	...	...	13.73	0.11
13	267.7012	−29.5476	0.9	12.02	0.01	10.58	0.01	...	...
21	267.7048	−29.5628	0.3	14.36	0.08	...	...	12.83	0.06
30	267.7105	−29.5007	0.2	15.46	0.10	14.45	0.10	14.28	0.12
41	267.7168	−29.5841	0.7	12.61	0.01	...	...	12.06	0.02
43	267.7174	−29.5981	1.1	13.33	0.03	12.29	0.04	...	...
49	267.7206	−29.5261	1.2	11.50	0.01	...	...	...	...
51	267.7207	−29.5464	0.4	11.03	0.01	...	...	...	...
59	267.7240	−29.5224	1.1	11.37	0.01	10.91	0.01	...	...
66	267.7258	−29.7242	1.2	15.48	0.12	14.36	0.11	...	...
68	267.7264	−29.6441	1.2	13.28	0.03	12.26	0.03	...	...
72	267.7276	−29.5267	0.9	15.36	0.14	...	...	13.76	0.11
88	267.7323	−29.6641	0.6	16.30	0.13	15.23	0.16	...	...
101	267.7379	−29.5846	1.0	13.96	0.05	...	...	12.41	0.03
111	267.7400	−29.6057	1.0	14.81	0.11	...	...	13.54	0.08
115	267.7411	−29.5095	1.2	...	...	13.66	0.05	13.21	0.05
122	267.7450	−29.6358	0.4	14.54	0.05	13.90	0.10	13.37	0.06
135	267.7482	−29.6836	1.0	...	...	...	...	13.30	0.07
141	267.7491	−29.5610	0.6	13.70	0.05	...	...	...	...
144	267.7506	−29.5347	0.6	13.98	0.05	13.49	0.11	13.26	0.07
146	267.7507	−29.5057	0.9	13.71	0.04	...	...	...	...
155	267.7546	−29.5276	0.8	15.68	0.11	15.12	0.13	...	...
167	267.7580	−29.5559	0.9	...	...	...	...	14.89	0.16
168	267.7585	−29.5975	0.2	13.85	0.05	...	...	12.47	0.04
194	267.7643	−29.6281	1.1	14.32	0.07	13.03	0.06	13.07	0.07
199	267.7663	−29.5941	0.9	11.27	0.01	...	...	...	...
202	267.7664	−29.6873	0.4	11.53	0.01	11.16	0.01	11.07	0.01
206	267.7667	−29.6705	1.0	11.18	0.01	...	...	...	...
213	267.7673	−29.6919	0.8	11.49	0.01	10.88	0.01	...	...
220	267.7692	−29.5588	1.1	13.04	0.02	...	...	...	...
235	267.7719	−29.4958	1.0	15.81	0.18	...	...	...	...
243	267.7731	−29.5628	0.4	11.38	0.01	...	...	...	...
249	267.7737	−29.6345	1.0	10.23	0.01	...	...	...	...
276	267.7801	−29.7156	0.5	13.85	0.05	12.98	0.04	12.62	0.04
288	267.7821	−29.5686	0.1	14.83	0.08	...	...	14.32	0.12

(*cont.*)

Table E.1: *Chandra*-SIRIUS counterpartpairs

Seq	R.A.	Decl.	ΔR	J mag	$\Delta Jmag$	H mag	$\Delta Hmag$	K_s mag	$\Delta Kmag$
#	(J2000.0)	(J2000.0)	(arcsec)	(mag)	(mag)	(mag)	(mag)	(mag)	(mag)
(1)	(2)	(3)	(4)	(5)	(6)	(7)	(8)	(9)	(10)
296	267.7841	−29.6803	1.1	12.72	0.01	11.81	0.01	11.48	0.01
304	267.7863	−29.5475	0.9	12.34	0.02	11.32	0.02	10.96	0.02
312	267.7878	−29.5471	0.7	14.46	0.09	13.43	0.07	13.64	0.11
319	267.7899	−29.5759	0.3	14.16	0.08	...	...	13.70	0.13
320	267.7899	−29.5906	0.4	12.58	0.02	11.95	0.04	11.58	0.03
328	267.7914	−29.6184	1.1	14.42	0.04	13.74	0.09	13.20	0.07
332	267.7919	−29.6103	1.1	...	...	...	...	14.69	0.14
361	267.7963	−29.4897	1.1	15.55	0.09	14.33	0.07	13.92	0.06
372	267.7984	−29.5742	0.5	14.26	0.06	13.27	0.05	12.85	0.05
372	267.7984	−29.5742	0.6	14.34	0.05	13.44	0.08	12.99	0.05
379	267.7996	−29.6207	0.9	14.09	0.04	13.32	0.03	13.10	0.04
395	267.8017	−29.5949	0.4	15.12	0.09	15.20	0.12	...	...
404	267.8027	−29.5572	1.0	14.01	0.04	13.51	0.04	13.49	0.06
408	267.8033	−29.5799	1.1	...	...	15.41	0.14	...	...
449	267.8082	−29.6288	1.2	13.84	0.04	...	...	...	...
460	267.8109	−29.7196	0.8	14.02	0.03	12.94	0.02	12.65	0.03
466	267.8124	−29.5539	0.5	11.60	0.01	...	...	...	...
467	267.8124	−29.6087	0.6	13.83	0.05	12.82	0.04	12.35	0.04
484	267.8144	−29.6189	0.8	...	...	12.20	0.02	12.13	0.03
492	267.8162	−29.5633	0.4	...	...	13.47	0.06	...	...
500	267.8171	−29.5468	1.2	15.29	0.10	...	...	...	...
503	267.8173	−29.5869	0.7	14.64	0.08	14.47	0.11	...	...
505	267.8180	−29.5794	0.9	15.58	0.12	14.27	0.09	13.99	0.10
519	267.8193	−29.6595	0.1	...	...	14.73	0.12	...	...
527	267.8206	−29.6542	0.3	11.32	0.01	...	...	...	...
532	267.8211	−29.6866	0.7	15.19	0.09	14.13	0.09	13.51	0.08
533	267.8211	−29.5935	0.8	...	...	13.60	0.06	13.40	0.07
535	267.8215	−29.5328	0.8	...	...	13.67	0.08	13.34	0.08
538	267.8217	−29.6398	0.8	12.47	0.01	12.06	0.02	12.00	0.03
558	267.8233	−29.6944	0.6	15.54	0.12	14.45	0.09	14.23	0.10
568	267.8245	−29.5329	0.5	...	...	15.53	0.19	...	...
589	267.8267	−29.6018	0.9	15.38	0.11	14.39	0.09	13.96	0.10
599	267.8274	−29.5042	0.6	12.35	0.01	11.43	0.01	11.06	0.01
609	267.8281	−29.6126	0.7	13.91	0.05	13.15	0.04	12.83	0.05
611	267.8284	−29.6278	0.6	14.30	0.07	13.53	0.07	13.18	0.07

(*cont.*)

Table E.1: *Chandra*-SIRIUS counterpartpairs

Seq	R.A.	Decl.	ΔR	J mag	$\Delta Jmag$	H mag	$\Delta Hmag$	K_s mag	$\Delta Kmag$
#	(J2000.0)	(J2000.0)	(arcsec)	(mag)	(mag)	(mag)	(mag)	(mag)	(mag)
(1)	(2)	(3)	(4)	(5)	(6)	(7)	(8)	(9)	(10)
625	267.8298	−29.5976	0.3	13.69	0.07	12.50	0.06	12.20	0.06
630	267.8301	−29.5562	0.4	15.44	0.12	14.28	0.10	14.33	0.17
631	267.8301	−29.6549	0.8	15.12	0.06	13.56	0.04	13.25	0.07
647	267.8317	−29.5423	0.3	14.31	0.07	13.80	0.09	13.90	0.12
671	267.8343	−29.6557	1.1	...	...	12.11	0.01	11.77	0.02
674	267.8344	−29.5815	0.6	12.27	0.01	11.95	0.01	11.99	0.01
683	267.8356	−29.4952	1.2	13.93	0.04	...	...	...	...
697	267.8366	−29.5422	0.3	14.02	0.03	12.73	0.02	12.35	0.02
699	267.8364	−29.6852	1.1	13.41	0.04	12.32	0.03	12.02	0.03
720	267.8386	−29.5749	1.0	...	...	15.19	0.11	14.95	0.16
723	267.8388	−29.5139	0.4	...	...	...	...	13.22	0.07
737	267.8408	−29.5972	0.7	13.44	0.02	12.90	0.05	13.11	0.07
750	267.8414	−29.6429	0.7	14.21	0.07	13.34	0.06	13.03	0.07
765	267.8425	−29.5744	0.2	...	...	15.17	0.14	14.83	0.15
771	267.8433	−29.6004	0.8	10.44	0.01	...	...	...	...
792	267.8452	−29.5874	0.3	15.58	0.17	14.85	0.13	...	...
795	267.8457	−29.6462	1.1	16.49	0.10	13.38	0.05	...	...
814	267.8474	−29.6873	0.3	14.83	0.07	14.39	0.10	14.19	0.11
816	267.8476	−29.6129	0.7	10.93	0.01	...	...	...	...
817	267.8477	−29.5486	0.2	14.57	0.09	13.86	0.09	13.53	0.11
822	267.8484	−29.5727	0.8	...	...	14.02	0.07	...	...
827	267.8486	−29.5100	0.9	12.09	0.01	11.86	0.01	11.83	0.01
839	267.8494	−29.5919	0.3	14.62	0.08	13.33	0.06	12.88	0.06
840	267.8496	−29.6352	1.0	...	...	...	...	14.10	0.15
841	267.8496	−29.6086	0.5	14.42	0.06	13.32	0.06	13.12	0.07
846	267.8504	−29.4813	1.0	14.01	0.03	12.65	0.03	12.20	0.03
872	267.8522	−29.7323	1.1	13.95	0.05	12.89	0.03	12.55	0.04
874	267.8525	−29.4921	0.6	13.89	0.05	12.51	0.04	12.32	0.04
876	267.8527	−29.5757	0.4	14.37	0.07	13.77	0.07	13.77	0.09
887	267.8540	−29.5788	0.8	14.69	0.08	13.63	0.07	13.40	0.08
890	267.8544	−29.5753	1.1	14.43	0.08	14.00	0.10	14.10	0.14
907	267.8566	−29.6775	0.8	15.36	0.10	14.19	0.08	13.74	0.08
915	267.8577	−29.5048	1.0	13.17	0.02	...	...	12.71	0.05
921	267.8585	−29.6114	0.5	14.72	0.06	14.18	0.08	14.11	0.11
927	267.8591	−29.5346	0.1	10.96	0.01	...	...	...	...

(*cont.*)

Table E.1: *Chandra*-SIRIUS counterpartpairs

Seq	R.A.	Decl.	ΔR	J mag	$\Delta Jmag$	H mag	$\Delta Hmag$	K_s mag	$\Delta Kmag$
#	(J2000.0)	(J2000.0)	(arcsec)	(mag)	(mag)	(mag)	(mag)	(mag)	(mag)
(1)	(2)	(3)	(4)	(5)	(6)	(7)	(8)	(9)	(10)
934	267.8597	−29.6628	1.0	...	...	12.63	0.05	12.32	0.06
944	267.8611	−29.5673	0.5	12.74	0.01	12.35	0.02	12.28	0.03
976	267.8647	−29.6685	0.9	11.38	0.01	...	...	...	...
980	267.8653	−29.6269	0.9	12.92	0.02	12.09	0.02	11.93	0.03
989	267.8662	−29.6328	0.5	15.35	0.11	14.15	0.09	13.78	0.09
997	267.8668	−29.5813	0.3	...	...	...	...	13.51	0.07
999	267.8668	−29.6764	0.9	13.24	0.02	12.28	0.02	11.83	0.02
1000	267.8673	−29.6176	1.0	11.26	0.01	10.95	0.01	10.92	0.01
1003	267.8675	−29.5631	0.2	10.86	0.01	...	...	...	...
1007	267.8677	−29.4977	0.7	12.61	0.01	12.35	0.03	12.29	0.03
1010	267.8681	−29.6061	0.8	15.12	0.10	14.20	0.12	14.20	0.14
1019	267.8686	−29.6069	0.5	13.71	0.03	12.66	0.02	12.32	0.02
1034	267.8700	−29.5838	0.8	15.21	0.09	14.53	0.10	14.47	0.12
1044	267.8714	−29.5037	0.9	14.34	0.06	13.68	0.07	13.71	0.11
1047	267.8716	−29.5215	0.3	14.80	0.05	13.86	0.07	13.50	0.05
1049	267.8718	−29.4934	0.4	15.71	0.10	...	...	14.21	0.09
1061	267.8727	−29.5614	0.9	15.16	0.10	14.17	0.09	13.74	0.08
1066	267.8732	−29.6714	0.2	...	...	14.46	0.14	14.21	0.10
1079	267.8746	−29.5353	0.8	15.45	0.16	14.60	0.16	...	...
1082	267.8750	−29.5825	0.3	15.61	0.13	14.92	0.13	14.72	0.14
1084	267.8754	−29.6794	0.4	11.72	0.01	10.86	0.01	10.59	0.01
1092	267.8760	−29.5259	0.2	15.13	0.11	...	...	13.79	0.09
1094	267.8768	−29.5834	0.4	12.06	0.01	11.37	0.01	11.19	0.01
1099	267.8776	−29.5411	0.4	10.79	0.01	...	...	...	...
1100	267.8775	−29.5847	0.6	10.82	0.01	...	...	...	...
1118	267.8790	−29.6560	0.7	12.36	0.01	11.75	0.01	11.64	0.01
1121	267.8793	−29.5751	0.5	14.90	0.11	13.77	0.08	13.44	0.09
1151	267.8824	−29.5641	0.7	13.97	0.04	13.01	0.03	12.72	0.04
1159	267.8828	−29.7252	0.8	13.36	0.02	12.22	0.01	11.80	0.01
1165	267.8831	−29.6597	0.8	15.75	0.13	14.56	0.09	14.16	0.10
1171	267.8838	−29.5478	0.3	14.38	0.09	13.45	0.07	13.15	0.07
1178	267.8845	−29.6539	0.2	13.77	0.03	13.21	0.04	13.07	0.04
1185	267.8852	−29.6279	0.9	15.42	0.09	14.32	0.06	14.08	0.07
1203	267.8872	−29.4441	1.1	11.34	0.01	...	...	...	...
1212	267.8885	−29.5739	0.9	13.47	0.04	12.35	0.03	11.78	0.03

(*cont.*)

Table E.1: *Chandra*-SIRIUS counterpartpairs

Seq	R.A.	Decl.	ΔR	J mag	$\Delta Jmag$	H mag	$\Delta Hmag$	K_s mag	$\Delta Kmag$
#	(J2000.0)	(J2000.0)	(arcsec)	(mag)	(mag)	(mag)	(mag)	(mag)	(mag)
(1)	(2)	(3)	(4)	(5)	(6)	(7)	(8)	(9)	(10)
1216	267.8888	−29.5453	1.1	...	...	14.95	0.13	...	...
1217	267.8884	−29.6086	1.1	14.59	0.10	13.77	0.08	13.39	0.10
1223	267.8890	−29.6057	1.1	13.52	0.04	13.07	0.05	13.08	0.06
1239	267.8908	−29.6146	0.3	14.48	0.08	13.66	0.09	13.41	0.10
1245	267.8916	−29.5973	0.3	14.75	0.10	13.48	0.07	13.21	0.07
1280	267.8946	−29.5219	0.2	12.45	0.01	11.94	0.02	11.76	0.02
1283	267.8947	−29.6407	0.4	12.78	0.01	12.36	0.02	12.32	0.03
1299	267.8956	−29.5413	0.2	...	...	14.80	0.13	14.92	0.13
1325	267.8990	−29.5334	0.3	13.90	0.04	13.35	0.04	13.24	0.05
1330	267.8999	−29.6216	0.3	15.67	0.13	...	...	...	...
1337	267.9008	−29.5237	1.1	13.95	0.06	...	...	...	...
1346	267.9017	−29.5473	1.2	13.50	0.02	...	...	...	...
1353	267.9020	−29.5093	0.2	11.84	0.01	11.28	0.01	11.05	0.01
1360	267.9027	−29.7281	1.0	12.78	0.01	11.53	0.01	11.06	0.01
1368	267.9042	−29.5253	0.5	13.59	0.02	12.78	0.02	12.39	0.02
1369	267.9045	−29.5829	0.2	...	...	14.17	0.11	...	...
1377	267.9055	−29.5694	0.1	...	...	...	...	14.66	0.19
1388	267.9059	−29.5476	1.2	13.92	0.04	...	...	13.62	0.07
1399	267.9069	−29.5515	0.6	12.48	0.02	11.77	0.01	11.53	0.02
1410	267.9078	−29.5876	1.0	14.96	0.11	14.36	0.09	14.38	0.11
1415	267.9087	−29.6848	0.6	12.29	0.02	11.66	0.02	12.86	0.05
1424	267.9099	−29.6282	1.1	14.41	0.05	13.42	0.04	13.11	0.04
1425	267.9097	−29.7112	0.3	13.99	0.04	13.26	0.04	13.07	0.05
1454	267.9120	−29.5575	1.1	10.73	0.01	...	...	...	...
1456	267.9122	−29.5967	0.4	15.17	0.09	14.17	0.10	14.08	0.11
1469	267.9136	−29.6182	0.8	14.67	0.08	14.15	0.11	13.90	0.12
1473	267.9137	−29.5593	1.2	14.04	0.04	13.03	0.03	12.75	0.04
1477	267.9142	−29.4879	0.6	11.18	0.01	10.68	0.01	10.60	0.01
1478	267.9142	−29.4641	1.1	15.43	0.10	...	...	14.02	0.09
1483	267.9145	−29.5623	1.2	...	...	...	...	13.27	0.09
1488	267.9150	−29.5843	0.5	13.26	0.03	12.94	0.04	12.85	0.05
1494	267.9157	−29.5964	0.4	15.22	0.10	14.77	0.11	14.73	0.15
1495	267.9157	−29.6196	0.5	13.80	0.04	13.27	0.05	13.25	0.05
1503	267.9170	−29.5003	0.8	14.65	0.07	13.65	0.08	13.23	0.06
1509	267.9176	−29.5094	0.9	13.03	0.02	12.50	0.03	12.35	0.03

(*cont.*)

Table E.1: *Chandra*-SIRIUS counterpartpairs

Seq	R.A.	Decl.	ΔR	J mag	$\Delta Jmag$	H mag	$\Delta Hmag$	K_s mag	$\Delta Kmag$
#	(J2000.0)	(J2000.0)	(arcsec)	(mag)	(mag)	(mag)	(mag)	(mag)	(mag)
(1)	(2)	(3)	(4)	(5)	(6)	(7)	(8)	(9)	(10)
1519	267.9183	−29.6675	1.1	...	...	14.46	0.11	14.37	0.12
1525	267.9190	−29.6928	0.0	...	...	...	...	14.26	0.16
1532	267.9194	−29.5629	0.9	15.32	0.11	14.24	0.09	13.96	0.10
1557	267.9226	−29.5857	0.6	15.88	0.14	...	...	...	...
1572	267.9247	−29.4906	0.5	...	...	14.37	0.15	13.90	0.11
1577	267.9253	−29.5935	0.4	13.64	0.03	13.18	0.03	13.12	0.04
1579	267.9255	−29.5524	0.6	13.53	0.03	13.09	0.04	12.91	0.06
1582	267.9260	−29.4666	0.9	14.62	0.08	...	...	...	...
1582	267.9260	−29.4666	1.2	...	...	13.77	0.06	...	...
1603	267.9282	−29.4546	0.6	13.48	0.03	13.32	0.03	13.19	0.04
1603	267.9282	−29.4546	0.6	13.74	0.02	13.28	0.05	13.09	0.03
1666	267.9368	−29.6008	0.3	14.32	0.06	13.58	0.05	13.21	0.06
1667	267.9367	−29.6199	1.1	14.10	0.09	...	...	...	...
1669	267.9374	−29.4631	0.2	14.37	0.10	...	...	...	...
1677	267.9382	−29.4503	1.0	11.69	0.01	...	...	...	...
1684	267.9391	−29.6104	0.6	...	...	12.04	0.02	11.97	0.04
1685	267.9393	−29.5681	0.5	14.89	0.13	14.09	0.12	14.15	0.16
1687	267.9402	−29.4739	0.9	14.18	0.07	...	...	...	...
1706	267.9425	−29.5488	0.4	14.48	0.11	...	...	...	...
1717	267.9439	−29.6054	0.7	13.26	0.02	...	...	...	...
1729	267.9448	−29.5668	0.7	14.54	0.07	13.64	0.04	13.46	0.07
1740	267.9467	−29.5084	0.9	15.97	0.15	14.55	0.10	13.94	0.09
1763	267.9516	−29.6134	0.6	14.06	0.07	...	...	...	...
1771	267.9534	−29.4823	0.4	13.10	0.02	11.88	0.02	11.47	0.01
1774	267.9539	−29.5692	1.0	13.91	0.07	...	...	...	...
1775	267.9538	−29.5849	0.4	12.00	0.01	11.34	0.01	11.15	0.01
1809	267.9597	−29.5822	0.4	14.91	0.14	13.91	0.09	13.63	0.12
1810	267.9599	−29.6001	0.9	...	...	13.74	0.05	13.39	0.06
1817	267.9608	−29.5548	0.3	...	...	14.74	0.12	...	...
1818	267.9610	−29.5706	0.6	...	...	14.45	0.09	...	...
1820	267.9618	−29.4586	0.7	...	...	14.09	0.10	13.89	0.10
1823	267.9622	−29.5017	1.1	13.18	0.03	12.60	0.04	12.48	0.04
1832	267.9639	−29.6120	0.8	14.25	0.10	...	...	...	...
1833	267.9646	−29.6231	0.8	13.20	0.03	12.79	0.03	12.78	0.05
1845	267.9678	−29.4753	0.9	10.89	0.01	...	...	...	...

(*cont.*)

Table E.1: *Chandra*-SIRIUS counterpartpairs

Seq	R.A.	Decl.	ΔR	J mag	$\Delta Jmag$	H mag	$\Delta Hmag$	$K_{\rm s}$ mag	$\Delta Kmag$
#	(J2000.0)	(J2000.0)	(arcsec)	(mag)	(mag)	(mag)	(mag)	(mag)	(mag)
(1)	(2)	(3)	(4)	(5)	(6)	(7)	(8)	(9)	(10)
1846	267.9681	−29.5342	1.2	14.02	0.03	...	...	...	...
1855	267.9692	−29.6309	1.0	14.70	0.08	13.82	0.06	13.55	0.11
1856	267.9693	−29.4891	1.1	12.28	0.01	11.54	0.01	11.56	0.01
1869	267.9720	−29.5931	1.2	...	...	11.61	0.01	...	...
1879	267.9740	−29.6457	1.1	...	...	10.97	0.01	10.61	0.01
1905	267.9808	−29.5657	0.5	14.40	0.09	13.46	0.06	...	...
1916	267.9843	−29.5087	0.6	13.19	0.02	12.60	0.02	12.39	0.03
1934	267.9900	−29.6254	1.0	...	...	13.07	0.05	12.33	0.04
1969	268.0015	−29.6267	0.8	14.57	0.08	...	...	...	...
1977	268.0045	−29.6070	0.6	10.47	0.01	...	...	...	...
1978	268.0060	−29.6275	0.2	...	...	14.70	0.11	...	...
1986	268.0096	−29.5839	0.6	10.28	0.01	...	...	...	...

(1) X-ray catalog sequence number, sorted by R. A. (2),(3) NIR source position. (4) The distance between X-ray source and NIR source. (5),(7),(9) J ,H ,$K_{\rm s}$ magnitude. (6),(8),(10) J ,H ,$K_{\rm s}$ -magnitude errors.

Acknowledgements

This PhD thesis was completed by supports from many people. I am grateful to professor Ken Ebisawa who gave me an opportunity to study at ISAS. He gave me many advice about the Galactic Ridge X-ray Emission. I also appreciate to professor Masayuki Itoh who introduced me to X-ray astronomy and advised me to study at ISAS when I was the master's course at Kobe University.

I appreciate vary much to assistant professor Masahiro Tsujimoto. He always gave me many advice about my study and many knowledge which are X-ray and NIR astronomy and astrophysics, space-based and ground-based observations, presentation skills, and mental attitude to carry out my research. Moreover, when I felt down, he cheered me up and made me laugh with some jokes of Kansai dialect. It's not too much to say that this thesis could not have completed without him. Moreover, Dr. Takahiro Nagayama helped my observation using IRSF at the South African Astronomical Observatory.

I am oblige to Dr. Tessei Yoshida for giving me advice about my thesis and teaching me many things including logical thinking, basic astronomy and astrophysics, and how to write papers.

I appreciate all the members of the ISAS X-ray group. I especially thank to Ikuyuki Mitsuishi, Kentaro Someya, Hiroshi Yoshitake, Takayoshi Hayashi, Takehiro Miyakawa, Kei Saitou, Takahisa Fujinaga and Naoki Iso. Thanks to them, I spend happy time at ISAS.

Finally, I appreciate to my parents for supporting me. They helped me and understood my research life.

This work is based on data collected with IRSF telescope and Subaru telescope. The former is operated by Nagoya University and the South African Astronomical Observatory. The latter is operated by the National Astronomical Observatory of Japan. The *Chandra* data were obtained through *Chandra* X-ray Observatory Science Center (CXC) operated for NASA by the Smithsonian Astrophysical Observatory. This thesis makes use of data products from Two Micron All Sky Survey. In addition, we used IRAF which is distributed by the National Optical Astronomy Observatory.